# Elemental and isotopic geochemistry of crystal-melt systems: Elucidating the construction and evolution of silicic magmas in the shallow crust, using examples from southeast Iceland and southwest USA

By

Abraham De Jesus Padilla

Dissertation

Submitted to the Faculty of the

Graduate School of Vanderbilt University

in partial fulfillment of the requirements

for the degree of

DOCTOR OF PHILOSOPHY

in

Environmental Engineering

August, 2015

Nashville, Tennessee

Approved:

Calvin F. Miller, Ph.D.
Guilherme A.R. Gualda, Ph.D.
David J. Furbish, Ph.D.
James H. Clarke, Ph.D.
George M. Hornberger, Ph.D.

Para mi mamá y mi papá

Por introducirme a un mundo con amor incondicional.

# ACKNOWLEDGEMENTS

I owe an immense and very special thank you to Calvin Miller and Guilherme Gualda. I could not have asked for better mentors. They challenged me to see the world from a different perspective, and provided the necessary guidance to help me succeed along this path in science. Without them, many of my accomplishments would not have been possible.

I am incredibly grateful to have the unconditional support of my family in every endeavor of life. Thank you for being a never-ending source of encouragement and inspiration.

I thank my best friend, Beverly Walker, who has been there with me every step of the way. If not for her company, encouragement, and support, I may have lost my mind long ago.

Life and work at Vanderbilt would not have been as enjoyable were it not for my EES colleagues and new Nashville family. Special thanks to my Ph.D. committee, David Furbish, Jim Clarke, and George Hornberger, for their guidance, Tenley Banik and Tamara Carley for helping drive Team Iceland research, Teri Pugh for always adding a spark to my days, Aaron Covey for his master-of-all-trades support, and to my fellow graduate students for making life great.

Many collaborators contributed a great deal of time and expertise to my work. I thank, in particular Rita Economos (UCLA/SMU), who opened the doors that led me on this scientific quest. I am glad I can continue calling her a mentor, a colleague, and a friend. I also thank Axel Schmitt (UCLA), Joe Wooden and Matt Cobble (Stanford-USGS), Ilya Bindeman (U. of Oregon), and Chris Fisher (WSU) for their extensive help with analytical work.

This research would not have been possible without the financial support of the National Science Foundation (grants NSF-EAR-1220523, Iceland Zircon; NSF-EAR-07-39496, Peach Spring Tuff), the Vanderbilt University Discovery Grant Program (awarded to G. Gualda), and Vanderbilt's Department of Earth and Environmental Sciences.

# TABLE OF CONTENTS

Page

Chapter

Appendix

# LIST OF TABLES

Table Page

CHAPTER II

CHAPTER III

CHAPTER V

# LIST OF FIGURES

Figure Page

CHAPTER II

CHAPTER III

CHAPTER IV

CHAPTER V

# CHAPTER I

## Introduction

Silicic magmatism is fundamentally important on two levels: on a human timescale, silicic magmas (>65 wt.% $SiO_2$) generate the most explosive volcanic eruptions on the planet (e.g. Bryan *et al.*, 2010; Miller & Wark, 2008; Bindeman, 2006). Not only are such eruptions instantaneously devastating to their surroundings, they also have longer-term global climatic effects that greatly affect and can threaten human civilization (e.g. Thordarson & Self, 2003; Robock, 2002; Rampino & Ambrose, 2000). On a geologic timescale, silicic rocks make up a major fraction of the continental crust, and thus silicic magmatism plays an integral role in creating permanent crust and continental landmasses (e.g. Hawkesworth & Kemp, 2006; Rudnick, 1995). It is therefore important to investigate how silicic magmatic systems evolve in order to gain a better understanding of the processes that control whether these explosive magmas remain trapped within the Earth's crust, solidifying into silicic plutons, or whether they ultimately reach the Earth's surface, culminating in violent volcanic eruptions, often with catastrophic results.

Of particular interest to my research are magmatic systems in the shallow crust, where buoyant silicic magmas commonly accumulate, regularly stalling, cooling, and evolving over hundreds of thousands to millions of years. Because they often form part of large, complex, inter-connected systems that involve both intrusive (plutonic) complexes as well as active extrusive (volcanic) centers, these silicic magmas are frequently rejuvenated, remobilized, and incorporated by younger, hotter magmas as they make their way to the Earth's surface for eruption (e.g. Claiborne *et al.*, 2010b; Fohey-Breting *et al.*, 2010; Shane *et al.*, 2008; Lipman, 2007; Walker *et al.*, 2007). Many investigators have suggested that such magmatic recharge events play a vital role not only in the longevity of magmatic systems but also in the eruptive behavior of their associated volcanic centers (e.g. Ruprecht & Bachmann, 2010; Wiebe & Hawkins, 2004; Wark *et al.*, 2007; Sparks *et al.*, 1977). Complex magmatic interactions are commonly preserved in solidified intrusions (e.g. Harper *et al.*, 2004; Frost & Mahood, 1987; Marshall & Sparks, 1984), and can reveal a wealth of information about the different processes involved in their formation. With the proper tools, we can investigate and begin to decipher the complex stories written in these composite intrusions, and assess their importance in the formation of highly destructive eruptible magmas, as well as permanent continental crust. This idea forms the fundamental motivation for the research that I present in this dissertation.

## 1. **Crystal-Melt Systems**

As magmatic systems evolve, they inevitably reach a point at which they begin to cool, and thus to crystallize mineral phases. The crystallization assemblage of a magmatic system, and in turn the geochemical composition of those minerals, is not only dependent on the geochemical composition of the source magmas and the physical conditions (e.g. pressure and temperature) under which they exist, but importantly also on the different processes that influence the system as it evolves (e.g. rapid decompression, crustal contamination, fractional crystallization, etc.). As minerals grow throughout the life of a system, they have the ability record information related to their crystallizing conditions and to those processes that influence the system at different stages of magma evolution. The crystallization of different mineral phases, in turn, modifies the composition of their coexisting melt, and consequently can affect the geochemical evolution of the whole system. Thus, crystals and their chemistry are fundamental tools that can help us better understand the major processes that influence how magmatic systems evolve, and in particular what factors drive magmas toward more evolved (silicic) compositions in in different crustal environments (e.g. Wiebe *et al.*, 2007; Marsh, 2006; Loomis & Welber, 1987).

An important aspect of interpreting the information found in minerals is to understand the way geochemical elements behave in different magmatic systems, and, importantly, how they are partitioned between coexisting phases, solid and liquid alike. The behavior of trace elements, such as the rare earth elements (REE), is of major interest, as their abundance or scarcity can inform us about the crystallization of accessory minerals, the main repositories for elements that behave incompatibly in all other major mineral phases, from which we can extract information regarding their conditions of crystallization and magmatic evolution. The refractory nature of many accessory minerals makes them ideal for preserving information about magmatic processes (*cf.* Robinson & Miller, 1999). Among them, zircon has been widely recognized as a valuable tool for elucidating both the environmental and the temporal record of the magmatic system(s) from which it crystallizes (Fig. 4). Though it is a minor constituent, it is present in most rocks and sediment in and on the Earth's crust. Its low solubility in almost all melt and fluid compositions, its stability at Earth’s surface, and its physical durability during transport enable it to survive many crustal processes during which most or all other minerals are destroyed. In addition, elemental diffusion in zircon is extremely slow (Cherniak & Watson, 2003), which allows it to retain its geochemical composition and zoning patterns far longer than any other mineral phase. Importantly, because it incorporates abundant U and Th during crystallization, age information is also preserved allowing us to determine temporal relationships pertaining to those processes and environments it records (e.g. Hoskin and Schaltegger, 2003).

In my dissertation research, I utilized a range of crystal-melt geochemical systems (elemental and isotopic alike, particularly in zircon) to address the primary aims of my research regarding the role of crystals in their parental magmatic systems:

1) *In what ways does the crystallization of particular mineral phases (e.g. accessory minerals) influence the geochemical evolution of the magma(s) from which they crystallize?*
2) *Can we distinguish the signature of magmatic events from post-magmatic events in crystals from the same magmatic system using various geochemical characteristics?*
3) *How robust is the zircon geochemical fingerprint for deciphering and interpreting the evolution of composite magmatic systems?*

While the geochemical characteristics of minerals can tell us a lot about the magmatic processes they experienced, it is important to note that looking at products of volcanic eruptions may yield information that is different from what is preserved in intrusive rocks. Namely, crystals in volcanic rocks may preserve information more pertinent to eruptive timescales (*cf.* Pamukcu *et al.*, 2012; Wark *et al.*, 2007; Bindeman, 2006) that is absent in their intrusive counterparts, though crystals from intrusive rocks are likely to yield a longer and more complete geochemical record of their magmatic system as a whole (magmatic timescales; e.g., Wiebe *et al.*, 2007). Thus, it is important to pay attention to both systems, as they provide complementary information about magmatic processes in general (e.g. Bachmann *et al.*, 2005), and the overarching topic they seek to address remain fundamentally the same: *How do large volumes of explosive (silicic) and eruptible magmas originate, evolve, and accumulate in the shallow crust, and how long do they last?*

## 2. **Dissertation Components**

In the following chapters, I present the results of my dissertation research, encompassing two diverse projects investigating complementary aspects of silicic magmatism, one utilizing the record of silicic volcanic products in northern Arizona, and the other that of silicic intrusive rocks in Iceland. Within each chapter, I address the different research objectives of each individual study, as well as the relevance and importance of my results toward better understanding silicic magmatic systems. The four components of this dissertation work are:

Chapter II: *Crystal-melt elemental partitioning in silicic magmatic systems: an example from the Peach Spring Tuff high-silica rhyolite, N. Arizona*

Chapter III: *Elucidating the complex magmatic history of the Austurhorn Silicic Intrusive Complex (SE Iceland) using zircon elemental and isotopic geochemistry and geochronology*

Chapter IV: *Generating the world's lowest magmatic $\delta^{18}O$ zircon signature: melting of intensely hydrothermally altered crust beneath the Austurhorn magmatic system, SE Iceland*

Chapter V: *The varied personalities of silicic intrusions in Iceland: a spatial and temporal comparison of shallow magmatic systems preserved in the zircon geochemical record*

In Chapter II, I present a focused geochemical study of the crystal cargo in one of the most evolved pumice samples from The Peach Spring Tuff (PST), a well-studied Miocene high-silica rhyolite eruption in southern Nevada, USA (Pamukcu *et al.*, 2013, 2015; Colombini *et al.*, 2011; Gualda *et al.*, 2010). The well-preserved pumice glass (groundmass) in the PST allowed for measurements of what we believe to be the most representative composition of the melt with which its crystalline cargo coexisted at the time of the eruption. Coupled with the composition of crystal rims, the glass compositions permitted the calculation of partition coefficients ($K_d$) for high-$SiO_2$ rhyolites from the PST system, presenting an excellent opportunity to directly and quantitatively address the effect that each crystallizing mineral phase had, relative to the rest of the mineral assemblage, on the abundance and distribution of elements in silicic magmas within the PST magmatic system. I present an extensive high-quality and internally consistent $K_d$ dataset that accurately represents the PST magmatic system at or near the time of eruption, and provide a thorough assessment of the crystallographic controls that each mineral phase exerts on the distribution of dispersed elements in their parental melt.

Chapter III is the first of three related studies investigating the zircon geochemical record in silicic and composite intrusions of Iceland. In her dissertation research investigating Icelandic silicic rocks, Carley (Vanderbilt, 2014) found that zircon populations in volcanic rocks are typically sparse, despite the abundance of highly evolved rock compositions. In contrast, most intrusive rocks of all compositions typically contain vastly more abundant zircon populations. Thus, it is likely that silicic intrusions are the dominant repository for zircons in the Icelandic crust, and as such, intrusive zircons should provide a much more complete geochemical record of the dominant magmatic processes related to the generation of silicic magmas in the Icelandic crust. However, there have been few investigations of zircon in Icelandic rocks (e.g. Bindeman *et al.*, 2012; Martin *et al.*, 2011; Carley *et al.*, 2011), and almost none focusing on intrusive rocks. In this chapter, as an effort to thoroughly characterize what we believe to be the dominant Icelandic zircon population, I present an in-depth zircon investigation of rocks from the mafic-felsic composite zone (MSCZ) at the Austurhorn Intrusive Complex (AIC; Furman *et al.*, 1992a,b; Mattson *et al.*, 1986; Blake, 1966), in SE Iceland, the first detailed geochemical study of intrusive Icelandic zircons. The AIC presents a suite of rocks that best exemplifies the complex array of mafic-felsic magmatic interactions typical of silicic systems in Iceland, providing an ideal location to investigate the importance of magma recharge and mixing events in the evolution of silicic systems, and importantly to assess the extent to which those events can be preserved in the zircon geochemical record. Using a combination of zircon elemental and isotopic geochemistry and geochronology, along with supporting field observations and whole-rock geochemistry, I demonstrate that MSCZ zircons clearly preserve a record of open system magmatic processes, as well as evidence, in their isotopic compositions, for crustal recycling and mixing of mantle components in the production and accumulation of their parental silicic magmas within the Austurhorn magmatic system.

In Chapter IV, I present a focused study of the oxygen isotopic ($\delta^{18}O$, ‰) variability in different mineral phases from rocks of the Austurhorn Intrusive Complex. This study is a continuation of the work presented in Chapter III, but the focus is largely on a unique subset of samples that preserve geochemical characteristics that are not commonplace across the MSCZ. Namely, I report zircons from two very fine-grained high-silica granophyres (~78 wt.% $SiO_2$) that preserve geochemical compositions that fall outside the fields for the typical composition of Austurhorn zircons, and Icelandic zircons in general, including the lowest oxygen isotopic values yet measured in primary (magmatic) zircons from any rocks in Iceland or the rest of the world, extending to as low as –11.3 ‰. In magmatic products, such low oxygen isotopic compositions are typically indicative of extensive recycling of intensely hydrothermally (meteoric) altered low-$\delta^{18}O$ crust. Using the oxygen isotopic compositions of primary minerals (quartz, feldspar) from the same samples along with supporting field evidence, I demonstrate that these low-$\delta^{18}O$ zircons are indeed preserving a magmatic signature, rather than secondary alteration, and thus represent products of partial melting of variably altered crust. In addition, based on the extreme $\delta^{18}O$ variability in these zircons, the greater $\delta^{18}O$ homogeneity of coexisting major minerals and whole-rocks, and the disequilibrium between major minerals and zircons, I conclude that the parental magmas for these samples were amalgamated from multiple batches of melts with extremely diverse oxygen compositions. This focused study provides a unique example of the geochemical record for one of the end-member processes by which silicic magmas are generated in the Earth's crust: pure partial-melting of altered pre-existing crust.

Lastly, in Chapter V, I present an overview of the geochemistry of six different silicic and composite Icelandic intrusions, spanning nearly 10 M.y. of Icelandic magmatic history, from ~2 Ma to ~12 Ma: the Lýsuskarð intrusion in western Iceland, the Sandfell laccolith in eastern Iceland, and the Austurhorn, Reyðarártindur, Slaufrudalur, and Vesturhorn intrusions in southeastern Iceland. Though each has some unique attributes, certain shared characteristics among most of these intrusions make them ideal candidates for investigating systematic processes related to the generation of silicic magmas in the shallow Icelandic crust: voluminous silicic material, an associated mafic intrusive complex, and composite zones displaying intimate association (mixing and mingling) of mafic and silicic magmas. In this study, I use a similar approach as that presented in Chapter III and compare the elemental and isotopic geochemical signatures of zircons from a range of rock compositions in each intrusion. I present a general assessment of how silicic composite magmatic systems have varied in the shallow Icelandic crust through space and time.

# CHAPTER II

## Crystal-Melt Elemental Partitioning in Silicic Magmatic Systems: an Example from the Peach Spring Tuff High-Silica Rhyolite, Southwest USA

### Abstract

Partition coefficients ($K_d$) are critical for the quantitative modeling of the evolution of magmatic systems. High-silica rhyolites (HSR) are characterized by saturation in numerous phases, such that a comprehensive $K_d$ database is necessary. While there exists a large body of published $K_d$ values, various methods have been used and studies focus on different compositions and conditions, and most studies are limited to small suites of elements (e.g. rare earth elements - REE) typically in few (2-3) mineral phases. In this study, we present $K_d$ values for a suite of 45 elements in 8 mineral phases from a HSR of the Peach Spring Tuff (PST): sanidine, plagioclase, biotite, amphibole, titanite, apatite, zircon, and chevkinite.

We determine $K_d$ by measuring crystal rim compositions and unaltered glass from a single volcanic sample, which reflect equilibration between crystals and melt in the system at or near the time of eruption. We measure compositions using a combination of SEM-EDS and LA-ICP-MS analysis.

We show that titanite strongly partitions REE from the melt, with a significant preference for middle (MREE) over light (LREE) and heavy-REE (HREE). Apatite and amphibole share a similar MREE-enriched pattern, though with absolute $K_d$ values more than an order of magnitude lower than titanite; while apatite displays a slight preference for LREE over HREE, amphibole shows a higher affinity for HREE than LREE. Zircon strongly partitions HREE, Hf, and U, with little affinity for LREE. Chevkinite concentrates LREE and Th significantly more than any other

phase we analyzed. Biotite $K_d$ are generally low (<10), with the highest values for transition metals and Ba. Sanidine and plagioclase display a strong preference for Sr, Ba, and Eu.

Our dataset is largely consistent with published studies that use similar (*in situ*) techniques in samples of similar composition (HSR). We observe a large variation in other studies that we attribute in part to contamination from inclusions in crystals, particularly when measuring compositions by whole-crystal methods. Our dataset suggests that accessory minerals play a dominant role in the partitioning of trace elements. They collectively control the distribution of REE and high field strength elements (HFSE) in the system. On the other hand, large ion lithophile elements (LILE) are most dominantly influenced by feldspars, but, if abundant, phases such as biotite and apatite may also influence the partitioning of LILE from the melt.

We analyze our data in light of the theoretical crystal lattice strain model (LSM), by fitting our data to curves that have the expected form in Ln($K_d$) versus ionic radius space (*Onuma* diagrams). The fact that we are successful in finding good fits for much of our data, especially the REE, reinforces the idea that mineral-melt equilibrium was attained and analytical data are of appropriate quality. Additionally, we use the fitted curves to estimate $Ce^{3+}$/Ce and $Eu^{2+}$/Eu ratios in the melt, which are controlled by the oxidation state of the magma. We estimate that >97% of all Ce in the PST melt existed as $Ce^{3+}$. The proportion of $Eu^{2+}$ in the melt is not as well constrained; we estimate $Eu^{2+}$ ranges mainly from ~10 to ~50% of the total Eu.

# 1. **Introduction**

Partition coefficients ($K_d$) are widely used in quantitative modeling of the evolution of magmatic systems (e.g. Bea *et al.*, 1994; Dall'Agnol *et al.*, 1999; Deering and Bachmann, 2010; Halliday *et al.*, 1991; Mahood and Hildreth, 1983; Miller and Mittlefehldt, 1984; many others). Of particular interest is the highly debated petrogenesis of high-silica rhyolites, whether by fractional crystallization of mafic parental magmas or partial melting of pre-existing crust, a subject that has been the focus of many recent studies (e.g. Bachmann and Bergantz, 2004; Bachmann and Bergantz, 2008; Glazner *et al.*, 2008; Michael, 1983; Miller and Mittlefehldt, 1984; Streck, 2002; many others). Having a good understanding of the way elements are partitioned among coexisting phases in a magma is essential for any quantitative model.

Over the years, there have been major efforts by many investigators to determine partition coefficients for diverse systems, spanning a wide range of compositions and tectonic settings, employing both controlled experiments (e.g. Blundy *et al.*, 1998; Gaetani and Grove, 1995; Prowatke and Klemme, 2006; Watson, 1976; Watson, 1980; many others) and measurements in natural samples by both bulk crystal or whole-crystal analysis (e.g. Bacon and Druitt, 1988; Luhr and Carmichael, 1980; Mahood and Hildreth, 1983; Nagasawa, 1970; many others) and *in situ* techniques (e.g. Anderson *et al.*, 2000; Bachmann *et al.*, 2005; Bea *et al.*, 1994; Colombini *et al.*, 2011; Sano *et al.*, 2002; Severs *et al.*, 2009; many others). However, because of the difficulty, complexity, and the high cost associated with many approaches, studies have been generally limited to small suites of elements (e.g. REEs, HFSEs) in few (2-3) mineral phases. An additional common obstacle is the lack of a corresponding “melt” composition for the natural system under study: unaltered glass (closest to a “melt” composition) is commonly unavailable, crystalline groundmass in volcanic and rapidly quenched intrusive rocks is not typically a reliable representation of host melt, and whole-rock compositions of plutonic rocks are even less likely to reflect melt compositions. As a result, many published $K_d$ datasets are likely not representative of natural magmatic systems, and much less of equilibrium conditions between crystals and their host melt.

In this study, we use a systematic approach and relatively fast method to measure compositions and calculate partition coefficients for a large number of elements and several mineral phases in a single volcanic rock. We focus on a high-silica rhyolite from the Peach Spring Tuff, a well-studied Miocene volcanic deposit in southwestern USA (Colombini *et al.*, 2011; Gualda *et al.*, 2010; Pamukcu *et al.*, 2013, 2015). Our approach involves measuring as many elements as possible with a combination of laser ablation ICP mass spectrometry (LA-ICP-MS) and quantitative energy-dispersive spectrometry (EDS) analysis on an analytical scanning electron microscope (SEM) in unaltered glass and in as many mineral phases as we could identify and separate from a single PST pumice sample. While there is some uncertainty regarding the exact conditions of crystallization (Pamukcu *et al.*, 2015), partition coefficients measured in this way correspond to conditions that are relevant for natural systems and avoid some of the problems typically encountered in experimental studies related to slow kinetics of growth and equilibration in highly silicic melt, particularly for accessory minerals.

## 2. **Background & Methods**

### 2.1. Sample Used

We used crystal separates from a single, non-welded, high-silica rhyolite pumice clast from the Peach Spring Tuff (PST, sample KPST01A) collected from a distal outflow outcrop near Kingman, AZ (see Gualda *et al.*, 2010; Pamukcu *et al.*, 2013, 2015). This pumice clast is among the most evolved PST samples studied by Pamukcu *et al.* (2013). It is relatively dense (1.41 g·cm$^{-3}$), with a phenocryst assemblage that consists of sanidine, plagioclase, quartz, titanite, biotite, amphibole, Fe-Ti oxides (mostly magnetite), apatite, allanite, chevkinite, and zircon. Estimates for the system conditions of the Kingman distal outflow magma prior to eruption are on the order of ~220 MPa of pressure (full range of 185-230 MPa; these are thoroughly discussed by Pamukcu *et al.*, 2015), and Zr-in-titanite temperatures fall in the range of 760º to 779ºC (see Pamukcu *et al.*, 2013, for detailed discussion). Though little work has been done toward estimating redox conditions of the magma, it can be generally constrained by the phase assemblage of the PST to the QTMAI (quartz-titanite-magnetite-amphibole-ilmenite) buffer (Wones, 1989), closely above the FMQ buffer, indicating relatively oxidizing conditions. Pamukcu *et al.* (2013) report whole-rock (75.3 wt.% $SiO_2$, anhydrous basis) and glass (76.7 wt.% $SiO_2$, anhydrous basis) compositions for KPST01, as well as compositions of titanite and zircon measured using the SHRIMP-RG. In addition, Colombini *et al.* (2011) report separate zircon, titanite, and glass compositions (accessory minerals also measured by SHRIMP-RG; glass by LA-ICP-MS) from the same pumice sample (KPST01), and discuss derived partition coefficients for zircon and titanite. We compare our own $K_d$ results to those of Colombini *et al.* (2011), and expand on that dataset by including $K_d$ for all phases (except Fe-Ti oxides and allanite, as we were unable to find allanite in our crystal separates) measured with LA-ICP-MS and EDS.

### 2.2. Sample preparation

We obtained crystal separates by lightly crushing the sample using a baseball bat, followed by sieving, with additional crushing and sieving until all material had been crushed to sizes that would clear a 2 mm sieve. Crystals were then separated from glass fragments by winnowing in water and then by heavy liquid separation using methylene iodide (MEI), followed by magnetic separation using a small hand-held magnet (Gualda *et al.*, 2004; Pamukcu *et al.*, 2013).

Using a stereomicroscope, we hand-picked individual crystals for each mineral phase found in the crystal-rich fractions (both heavy and light fraction of MEI separation), as well as PST glass pieces from the glass-rich fraction. To the extent possible, we picked crystals with glass attached to their edges so as to better ensure that these were phases growing in the melt rather than as inclusions within larger crystals, which is particularly important in the case of the smaller accessory phases. We obtained grains from seven different mineral phases: titanite, chevkinite, zircon, amphibole, biotite, sanidine, and plagioclase; although we weren't able to separate apatite crystals, we later found apatite as large inclusions within biotite crystals during LA-ICP-MS analysis.

Lastly, we mounted all the separated crystals, along with large glass particles, in epoxy, polished them by hand to expose the grain interiors, and imaged them using reflected light with a Zeiss Stemi 2000-C microscope with an attached Zeiss AxioCam MRc 5 camera at Vanderbilt University.

### 2.3. SEM analysis

With the goal of documenting variations in the abundances of Na, K, and Ca for some of the major minerals (sanidine, plagioclase, and amphibole), we obtained analyses for major elements in these phases by quantitative EDS analysis using a $LaB_6$ Tescan Vega 3 LM variable pressure SEM equipped with an Oxford X-max 50 $mm^2$ EDS system installed at Vanderbilt University (see Table 1).

**Table 1**. Average concentrations ($\bar{c}$) and partition coefficients ($K_d$)[1] for sample KPST01A[2].

| **Phase →** | **Glass** | **Titanite** | | **Chevkinite** | | **Zircon** | | **Apatite** | |
|---|---|---|---|---|---|---|---|---|---|
| **Element ↓** | $\bar{c}_m$ (ppm) | $\bar{c}_s$ (ppm) | $K_d$ | $\bar{c}_s$ (ppm) | $K_d$ | $\bar{c}_s$ (ppm) | $K_d$ | $\bar{c}_s$ (ppm) | $K_d$ |
| **Li**$^{1+}$ | 14 | 20 | 1.41 | | | | | 3984 | 277 |
| **B**$^{3+}$ | 50 | 141 | 2.82 | | | | | | |
| **Na**$^{1+}$ | 18597 | 406 | 0.022 | 69 | 0.004 | | | 156606 | 8.42 |
| **Mg**$^{2+}$ | 539 | 614 | 1.14 | $5226^{\#}$ | 9.70 | | | 3303300* | |
| **Al**$^{3+}$ | 50701 | 8318 | 0.164 | 14862 | 0.293 | 2086 | 0.041 | 1599830* | |
| **Si**$^{4+\&}$ | 359928 | $142008^{\#\&}$ | 0.395 | $93488^{\#\&}$ | 0.260 | $147571^{\#\&}$ | 0.410 | 3387040* | |
| **K**$^{1+}$ | 59870 | | | | | | | 2270994* | |
| **Ca**$^{2+}$ | 2452 | $192500^{\#\&}$ | 79 | 44595 | 18 | | | $393086^{\#\&}$ | 160 |
| **Sc**$^{3+}$ | 2.52 | 47 | 19 | 2429 | 964 | 296 | 117 | 383 | 152 |
| **Ti**$^{4+}$ | 722 | $181600^{\#\&}$ | 251 | $119023^{\#}$ | 165 | 1485 | 2.06 | 415278 | 575 |
| **V**$^{5+}$ | 1.14 | 244 | 214 | 218 | 192 | | | 1035 | 909 |
| **Mn**$^{2+}$ | 341 | 2133 | 6.26 | 1948 | 5.72 | | | 111035* | |
| **Co**$^{2+}$ | 0.460 | | | | | | | 517* | |
| **Ni**$^{2+}$ | 3.99 | | | | | | | 643* | |
| **Cu**$^{2+}$ | 11 | | | 7.54 | 0.705 | | | 367* | |
| **Zn**$^{2+}$ | 43 | 119 | 2.75 | 61 | 1.42 | | | 17934* | |
| **Ga**$^{3+}$ | 20 | 12 | 0.598 | 21 | 1.05 | | | 891 | 45 |
| **Ge**$^{4+}$ | 1.93 | 30 | 15 | 118 | 61 | | | | |
| **Rb**$^{1+}$ | 252 | 3.74 | 0.015 | | | | | 12491* | |
| **Sr**$^{2+}$ | 3.72 | 3.36 | 0.904 | 32 | 8.62 | | | 213 | 57 |
| **Y**$^{3+}$ | 19 | 6499 | 344 | 2646 | 140 | 1508 | 80 | 2550 | 135 |
| **Zr**$^{4+}$ | 118 | 1022 | 8.66 | 6775 | 57 | $431400^{\#\&}$ | 3653 | 192 | 1.62 |
| **Nb**$^{5+}$ | 33 | 2033 | 61 | 700 | 21 | 8.90 | 0.267 | 1793 | 54 |
| **Cs**$^{1+}$ | 3.88 | | | | | | | 326 | 84 |
| **Ba**$^{2+}$ | 4.91 | 45 | 9.08 | 652 | 133 | 1.02 | 0.207 | 2404 | 489 |
| **La**$^{3+}$ | 45 | 3386 | 75 | $156926^{\#}$ | 3484 | 3.38 | 0.075 | 4928 | 109 |
| **Ce**$^{3+}$ | 79 | 12681 | 160 | $261983^{\#}$ | 3310 | 56 | 0.703 | 10508 | 133 |
| **Pr**$^{3+}$ | 6.97 | 2004 | 288 | 14110 | 2025 | | | 1179 | 169 |
| **Nd**$^{3+}$ | 20 | 8839 | 438 | 46887 | 2326 | 6.86 | 0.340 | 4824 | 239 |
| **Sm**$^{3+}$ | 2.85 | 2089 | 733 | 4576 | 1607 | 9.30 | 3.26 | 721 | 253 |
| **Eu**$^{3+}$ | 0.277 | 153 | 551 | 285 | 1028 | 2.43 | 8.75 | 42 | 152 |
| **Gd**$^{3+}$ | 2.57 | 1534 | 596 | 2132 | 829 | 29 | 11 | 592 | 230 |
| **Tb**$^{3+}$ | 0.353 | 256 | 727 | 184 | 523 | 10 | 29 | 99 | 280 |
| **Dy**$^{3+}$ | 2.14 | 1401 | 655 | 754 | 352 | 127 | 59 | 497 | 232 |
| **Ho**$^{3+}$ | 0.601 | 262 | 437 | 112 | 186 | 48 | 80 | 101 | 168 |
| **Er**$^{3+}$ | 1.76 | 634 | 361 | 275 | 157 | 215 | 122 | 194 | 111 |
| **Tm**$^{3+}$ | 0.337 | 77 | 229 | 40 | 120 | 43 | 128 | 27 | 80 |
| **Yb**$^{3+}$ | 2.35 | 430 | 183 | 371 | 158 | 391 | 166 | 181 | 77 |
| **Lu**$^{3+}$ | 0.364 | 46 | 126 | 73 | 200 | 75 | 207 | 15 | 42 |
| **Hf** $^{4+}$ | 4.00 | 64 | 16 | 416 | 104 | 9278 | 2317 | | |
| **Ta**$^{5+}$ | 1.55 | 118 | 76 | 20 | 13 | 1.62 | 1.05 | 23 | 15 |
| **Tl**$^{3+}$ | 1.50 | | | | | | | 96 | 64 |
| **Pb**$^{2}$+ | 32 | 4.61 | 0.143 | 30 | 0.916 | 3.88 | 0.120 | 173 | 5.36 |
| **Th**$^{4+}$ | 29 | 262 | 9.08 | $7826^{\#}$ | 271 | 212 | 7.33 | 148 | 5.13 |
| **U**$^{4+}$ | 6.31 | 23 | 3.65 | 43 | 6.82 | 139 | 22 | 13 | 2.07 |

---

[1] $K_d = \frac{\bar{c_s}}{\bar{c_m}}$, where $\bar{c_s}$ and $\overline{c_m}$ denote average concentration in the solid (*s*) and melt (*m*) phases, respectively

[2] Note: essential structural constituents (ESCs) for each phase are denoted by $^{\#}$; values constrained by stoichiometry are denoted by $^{\&}$; ESCs in biotite are omitted from apatite $K_d$, denoted by *, as these are likely problematic due to their enriched concentrations in biotite and our non-conventional method of obtaining apatite data

**Table 1**. Continued[3]

| **Phase →** | **Amphibole** | | **Biotite** | | **Sanidine** | | **Plagioclase** | |
|---|---|---|---|---|---|---|---|---|
| **Element ↓** | $\overline{c}_s$ (ppm) | $K_d$ | $\overline{c}_s$ (ppm) | $K_d$ | $\overline{c}_s$ (ppm) | $K_d$ | $\overline{c}_s$ (ppm) | $K_d$ |
| **Li$^{1+}$** | 20 | 1.40 | 90 | 6.30 | 1.99 | 0.139 | 4.80 | 0.334 |
| **B$^{3+}$** | | | | | | | | |
| **Na$^{1+}$** | 14600$^{\%}$ | 0.785 | 4046 | 0.218 | 35700$^{\%}$ | 1.92 | 65529$^{\%\#}$ | 3.52 |
| **Mg$^{2+}$** | | 162 | 140200.0$^{\&\#}$ | 260 | 5.70 | 0.011 | 43 | 0.079 |
| **Al$^{3+}$** | 32600$^{\%\#}$ | 0.643 | 61619$^{\#}$ | 1.22 | 102200$^{\%\#}$ | 2.02 | 129757$^{\%\#}$ | 2.56 |
| **Si$^{4+\&}$** | 224800$^{\%\#}$ | 0.625 | 194361$^{\&\#}$ | 0.540 | 306700$^{\%\#}$ | 0.852 | 346900$^{\%\#}$ | 0.964 |
| **K$^{1+}$** | 6000$^{\%}$ | 0.100 | 82249$^{\#}$ | 1.37 | 80400$^{\%\#}$ | 1.34 | 13543$^{\%}$ | 0.226 |
| **Ca$^{2+}$** | 86500$^{\%\#}$ | 35 | 673 | 0.274 | 3400$^{\%}$ | 1.39 | 26629$^{\%\#}$ | 11 |
| **Sc$^{3+}$** | 198 | 79 | 16 | 6.34 | 1.35 | 0.537 | 1.17 | 0.466 |
| **Ti$^{4+}$** | 8500$^{\%}$ | 12 | 17694 | 24 | 100 | 0.138 | 92 | 0.127 |
| **V$^{5+}$** | 35 | 31 | 46 | 40 | | | 0.320 | 0.281 |
| **Mn$^{2+}$** | 2600$^{\%}$ | 7.64 | 4440 | 13 | 1.33 | 0.004 | 15 | 0.043 |
| **Co$^{2+}$** | 11 | 25 | 19 | 41 | | | | |
| **Ni$^{2+}$** | | | 16 | 3.88 | | | | |
| **Cu$^{2+}$** | | | 3.72 | 0.348 | | | 0.610 | 0.057 |
| **Zn$^{2+}$** | 563 | 13 | 790 | 18 | | | 6.68 | 0.155 |
| **Ga$^{3+}$** | 16 | 0.832 | 39 | 1.98 | 19 | 0.960 | 26 | 1.31 |
| **Ge$^{4+}$** | 5.58 | 2.89 | 2.79 | 1.44 | 1.22 | 0.629 | 0.966 | 0.500 |
| **Rb$^{1+}$** | 2.93 | 0.012 | 395 | 1.57 | 98 | 0.391 | 4.43 | 0.018 |
| **Sr$^{2+}$** | 1.64 | 0.442 | 1.14 | 0.307 | 21 | 5.60 | 52 | 14 |
| **Y$^{3+}$** | 127 | 6.72 | 0.889 | 0.047 | | | 0.212 | 0.011 |
| **Zr$^{4+}$** | 47 | 0.397 | 6.20 | 0.052 | 0.544 | 0.005 | 0.487 | 0.004 |
| **Nb$^{5+}$** | 36 | 1.07 | 52 | 1.56 | | | | |
| **Cs$^{1+}$** | | | 1.67 | 0.430 | 0.049 | 0.013 | 0.065 | 0.017 |
| **Ba$^{2+}$** | 2.33 | 0.475 | 46 | 9.44 | 59 | 12 | 22 | 4.50 |
| **La$^{3+}$** | 47 | 1.04 | 0.944 | 0.021 | 3.71 | 0.082 | 14 | 0.307 |
| **Ce$^{3+}$** | 158 | 1.99 | 2.57 | 0.032 | 2.45 | 0.031 | 15 | 0.189 |
| **Pr$^{3+}$** | 25 | 3.53 | 0.247 | 0.036 | 0.097 | 0.014 | 0.828 | 0.119 |
| **Nd$^{3+}$** | 104 | 5.16 | 2.38 | 0.118 | 0.510 | 0.025 | 1.85 | 0.092 |
| **Sm$^{3+}$** | 23 | 8.10 | | | | | | |
| **Eu$^{3+}$** | 1.75 | 6.32 | | | 0.645 | 2.33 | 0.932 | 3.36 |
| **Gd$^{3+}$** | 19 | 7.33 | | | | | | |
| **Tb$^{3+}$** | 3.43 | 9.74 | | | | | | |
| **Dy$^{3+}$** | 23 | 11 | 1.29 | 0.603 | | | | |
| **Ho$^{3+}$** | 4.36 | 7.26 | | | | | | |
| **Er$^{3+}$** | 11 | 6.52 | | | | | | |
| **Tm$^{3+}$** | 1.73 | 5.13 | | | | | | |
| **Yb$^{3+}$** | 11 | 4.60 | | | | | | |
| **Lu$^{3+}$** | 1.53 | 4.21 | | | | | | |
| **Hf$^{4+}$** | 3.29 | 0.821 | | | | | | |
| **Ta$^{5+}$** | 0.661 | 0.427 | 0.690 | 0.445 | | | | |
| **Tl$^{3+}$** | | | 1.52 | 1.01 | 0.354 | 0.236 | | |
| **Pb$^{2}$+** | 2.13 | 0.066 | 4.91 | 0.152 | 32 | 0.988 | 20 | 0.620 |
| **Th$^{4+}$** | 1.03 | 0.036 | 0.460 | 0.016 | | | | |
| **U$^{4+}$** | 0.460 | 0.073 | | | | | | |

---

[3] Note: values constrained by quantitative SEM-EDS analysis are denoted by $^{\%}$

We analyzed small areas on rims of grains of each mineral, under conditions of 15 kV electron beam acceleration and maximum beam intensity, resulting in absorbed currents of ~10 nA. Data acquisition and processing was performed with the Oxford software Aztec. Values determined using SEM-EDS are indicated in Table 1; because these elements are essential structural constituents (ESC) of these phases, which control the stability of the said phases, the reported $K_d$ values are of more limited use.

### 2.4. LA-ICP-MS analysis

We determined concentrations of dispersed elements (those found in trace amounts) in glass and minerals by LA-ICP-MS using a New Wave/Merchant UP-213 nm Laser Ablation unit connected to a PerkinElmer Elan 6100 DRC II ICP-MS installed at Vanderbilt University. We set the laser settings to yield a fluence of 4.8-5.0 J/cm$^2$, at a repetition rate of 5 Hz, with He (0.9 min$^{-1}$) as the carrier gas. Each analysis began with 30 s of blank acquisition, followed by 60 s of ablation and 30 s of wash-out time to allow the measured values to return to blank levels.

We measured a total of 54 analytes (Table 1; Fig. 1) during each analysis. For every 10-20 measurements of unknowns, we analyzed 3-5 primary (for calibration) and secondary (treated as unknowns) standards to evaluate the precision and accuracy of the results (see Appendix A). We used *NIST 610* and *NIST 612* glasses (Pearce *et al.*, 1997) as the primary and secondary standards, respectively, for analyses done with a laser spot size of 20 µm (titanite, chevkinite, zircon), 40 µm (amphibole, apatite), and 80 µm (glass, biotite), and *NIST 612* and *NIST 614* (Kurosawa *et al.*, 2002) glasses for analyses with a spot size of 120 µm (sanidine, plagioclase). We chose Si as the internal standard for glass and minerals, with the exception of apatite (for which we used Ca). We selected the laser spot sizes according to the size of the grains for each mineral phase (smaller for accessory minerals, larger for major minerals), and analyzed glass with all laser spot sizes to find the best balance between measuring low-concentration elements (e.g. HREE) and avoiding crystals within the glass (Fig. 2). We analyzed all mineral phases at or as near as possible to the rim of the grains.

During biotite analyses we identified ablation intervals over which the measured Si and K concentrations were abnormally low, and Ca and P concentrations were uncharacteristically high. We identified these intervals as large apatite inclusions within biotite. For some analyses these intervals were long enough to permit quantitative analysis of apatite. Our apatite data are reliable only for elements with high concentration in apatite and low concentration in biotite, due to the memory effect resulting from long wash-out times in the instrument used. We omitted all analyses in which we encountered apatite inclusions from our biotite dataset when calculating average elemental concentrations for biotite, such that we are confident our biotite dataset has not been affected by any inclusions.

### 2.5. Data reduction

We used *Glitter* (Griffin *et al.*, 2008) to reduce the LA-ICP-MS data. To the extent possible, we also removed analyses that appeared contaminated by inclusions, which we typically identified by spikes in non-essential elements during the course of ablation. Lastly, we reviewed the data for each analyte in each phase to identify and remove analyses that were clear outliers; we then averaged remaining values to yield our best value for the concentration of each element in each phase. In addition, we note that, because measurements of essential structural constituents by LA-ICP-MS are often not reliable, we either (1) use ideal values constrained by stoichiometry for the essential structural constituents in some of our mineral phases; or (2) use results from quantitative SEM-EDS analyses (identified in Table 1).

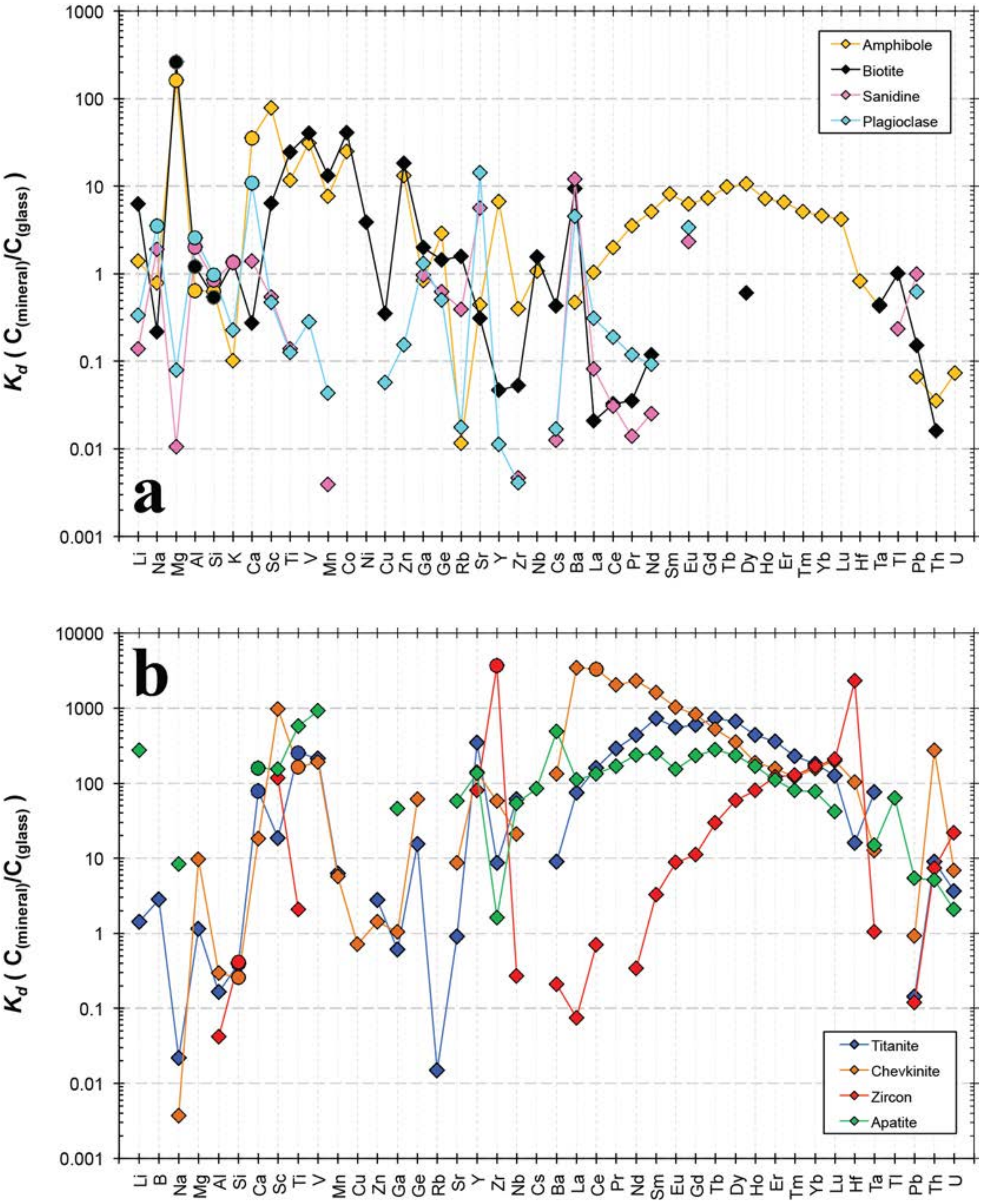

**Figure 1.**

Partition coefficients ($K_d$) measured in minerals from sample KPST01A. Essential structural components (ESC) for each mineral are denoted by circular symbols, whereas diamonds represent dispersed elements. **(a)** Major minerals (amphibole, biotite, sanidine, plagioclase). **(b)** Accessory minerals (titanite, chevkinite, zircon, apatite).

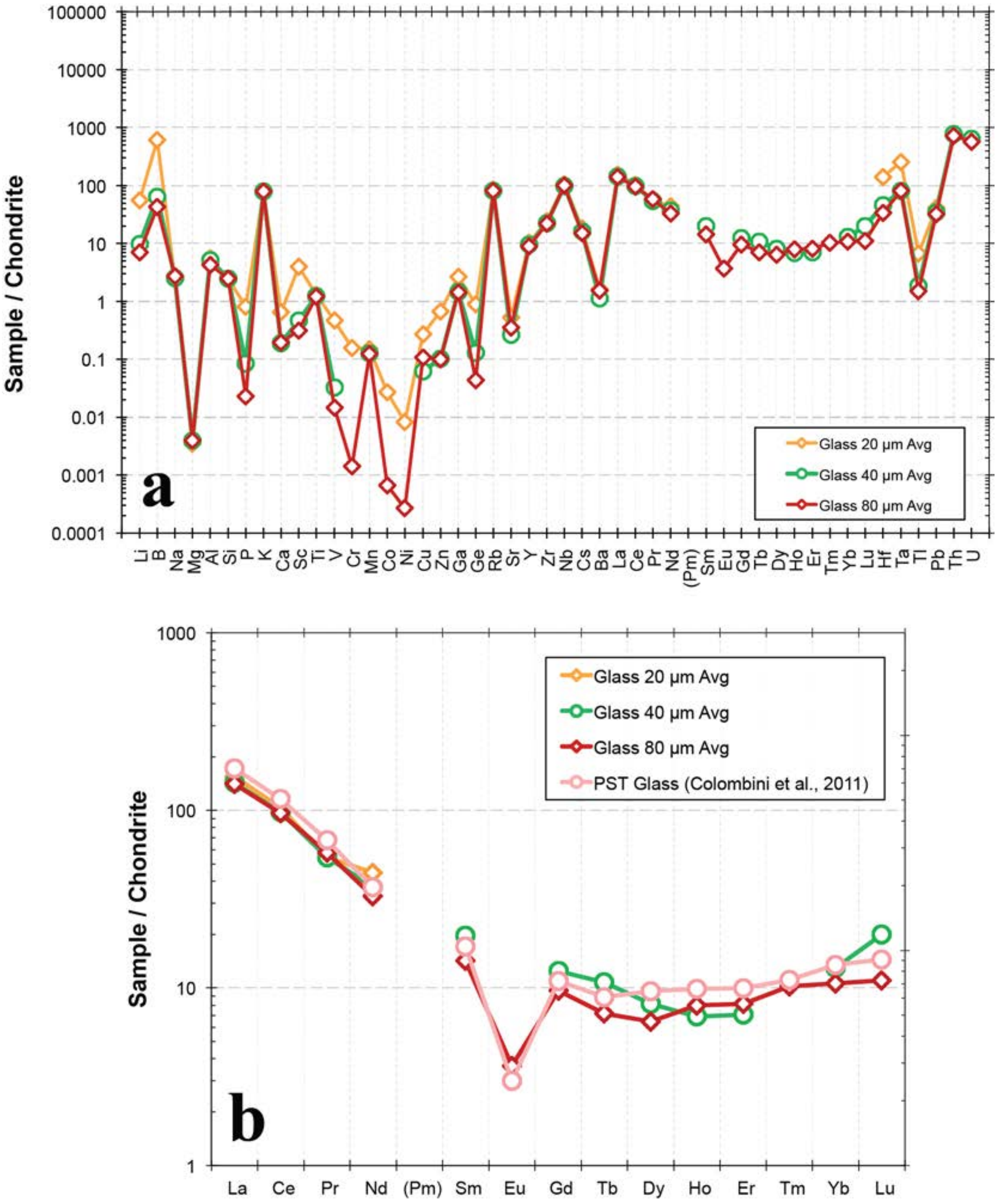

**Figure 2**

Chondrite-normalized elemental concentrations in KPST01A glass, measured with different laser spot sizes (20, 40, and 80 µm) to assess the accuracy and reproducibility of each laser spot size. **(a)** All elements measured. **(b)** REE elements only; values from Colombini *et al.* (2011) are also shown. Values for HREE using a 20 µm beam are below detection.

The concentrations ($\bar{c}$) used for partition coefficient calculation correspond to averages of at least 3 and up to 25 individual measurements per element. We calculated an average glass composition using our 80 µm measurements, as it was the most consistent, reliable, and extensive of our glass datasets (see Fig. 2; note in particular that, for some elements, the 20 µm dataset deviates significantly from the rest, especially for HREE; this is a result of attempting to measure glass concentrations that are lower than the detection limit of LA-ICP-MS analyses using a 20 µm spot). The partition coefficients ($K_d$) for each element are then calculated by dividing the average element concentration in each mineral phase by the average concentration of that element in the glass.

## 3. **Results**

We compare our calculated $K_d$ values for each mineral phase with those of previously published studies available in the *Geochemical Earth Reference Model* ("GERM") partition coefficient database ([earthref.org/kdd], see Appendix A.5-A.6; Bacon and Druitt, 1988; Bea *et al.*, 1994; Ewart and Griffin, 1994; Leeman and Phelps, 1981; Mahood and Hildreth, 1983; Nagasawa, 1970; Nash and Crecraft, 1985; Schnetzler and Philpotts, 1970; Sisson, 1994; Stix and Gorton, 1990; Streck and Grunder, 1997) as well as some values not currently listed on *GERM* (Anderson *et al.*, 2000; Bachmann *et al.*, 2005; Colombini *et al.*, 2011; Sano *et al.*, 2002; Troll *et al.*, 2003). For simplicity, we collectively refer to all published studies as the "literature data." In addition, because the focus of our study is the Peach Spring Tuff, a high-silica rhyolite (HSR), we have primarily selected studies that investigated natural systems of similar character (rhyolite and HSR) for comparison. At first glance, we note that other published studies reporting partition coefficients typically focus on fewer mineral phases (2-3 at most) or a smaller array of studied elements.

### 3.1. Titanite

The $K_d$ patterns that we observe in titanite are generally in agreement with those of literature data (Fig. 3). In particular, the REE are highly concentrated in titanite, and they display their typical higher affinity for middle REE (MREE), relative to light and heavy REE (LREE and HREE, respectively), observed by others (e.g. Bachmann *et al.*, 2005; Colombini *et al.*, 2011); our $K_d$ values are on the same order of magnitude as other published $K_d$ values. We note that Troll *et al.* (2003) report lower values for the REE, but they display the same overall pattern, and we attribute the differences in these values to the different rock compositions used in their study (peralkaline rhyolite). For other elements (non-REE), $K_d$ values from the literature data are generally within a half order of magnitude of our reported values.

### 3.2. Chevkinite

Notably, and to the best of our knowledge, the only published study that reports partition coefficients for chevkinite is that of Troll *et al.* (2003), though they report only a small suite of elements (Fig. 4). We point out the agreement in the $K_d$ pattern for the LREE and MREE, displaying a strong preference for LREE over HREE. As we previously noted, the contrast in rock composition (peralkaline rhyolite) likely accounts for the half order of magnitude difference between our $K_d$ values and those of Troll *et al.* (2003).

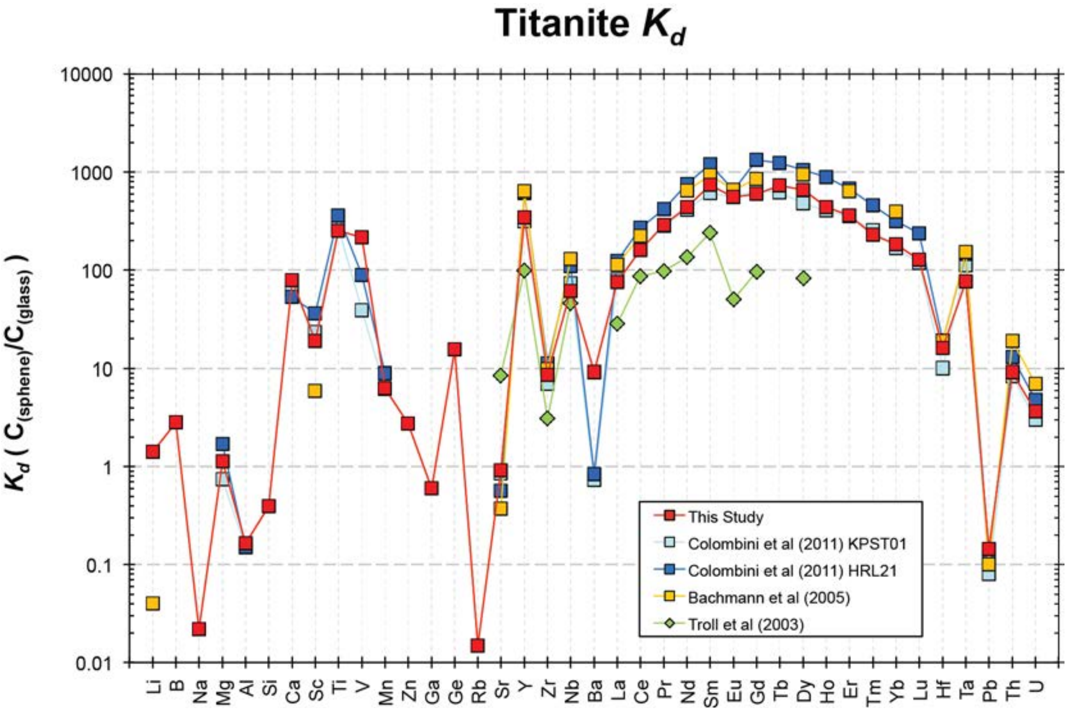

**Figure 3**

Comparison plot of partition coefficients ($K_d$) calculated for titanite vs. published literature data: Colombini *et al.* (2011), Bachmann *et al.* (2005), and Troll *et al.* (2003). Data symbols correspond to the studied rock type as follows: square = high-silica rhyolite; diamond = rhyolite.

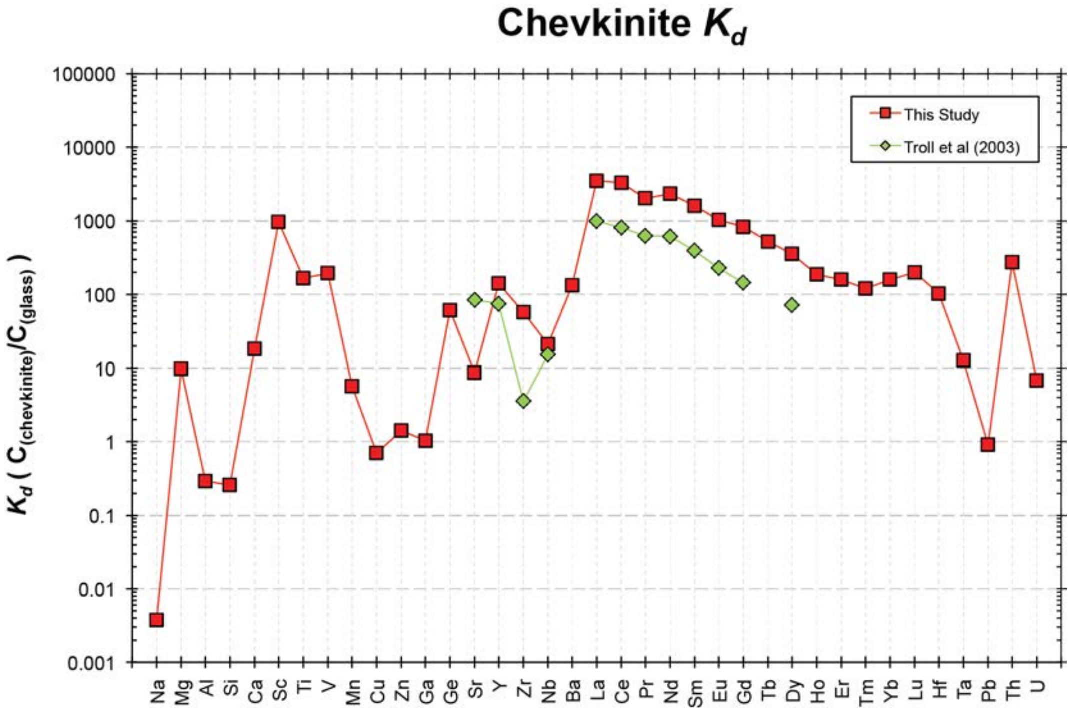

**Figure 4**

Comparison plot of partition coefficients ($K_d$) calculated for chevkinite vs. published literature data: Troll *et al.* (2003). Data symbols correspond to the studied rock type as follows: square = high-silica rhyolite; diamond = rhyolite.

### 3.3. Zircon

For the most part, our zircon $K_d$ values are in good agreement with those reported in the literature, and in particular with other studies that focused on high-silica rhyolite compositions (e.g. Bachmann *et al.*, 2005; Colombini *et al.*, 2011). Zircon displays a high affinity for Zr, Hf, and MREE and especially HREE (Fig. 5). Most of our values are within an order of magnitude or less of the values reported in other studies. The most notable difference is in the range of $K_d$ values for the LREE (La-Sm). Some studies report significantly lower $K_d$ values for La and more pronounced Ce and Eu anomalies than ours. We note, in particular, that the LREE $K_d$ patterns reported by Mahood and Hildreth (1983) and Bea *et al.* (1994) are significantly higher than the results of other studies, displaying a more linear trend than what is typically observed, of increasing $K_d$ values with increasing atomic number. These inconsistencies are likely the result of glass or LREE-rich inclusions in zircon (e.g. chevkinite, allanite, xenotime), which even if small in size can significantly affect concentrations, and therefore $K_d$ values. Lanthanum concentrations in zircon are likely <100 ppb (see Colombini *et al.*, 2011), which is many orders of magnitude lower than the 1,000-100,000 ppm concentrations observed in other accessory minerals such as apatite, chevkinite, and titanite (see Table 1); even rhyolite melt, with 20-100 ppm La, is much enriched (2-3 orders of magnitude) in LREE over zircon. It follows that even minute inclusions of such LREE-rich phases would affect measurements of La (and other LREE) in zircon (Colombini *et al.*, 2011; Michael, 1988). This is consistent with the fact that SHRIMP results for zircon from the same PST HSR presented by Colombini *et al.* (2011) show lower concentration and $K_d$ for the LREE than what we obtain; because SHRIMP produces much shallower analyzed pits than our LA-ICP-MS spots, this technique is much less likely to encounter inclusions. Results presented here suggest that caution needs to be exercised with

LREE values in zircon obtained via LA-ICPMS; this is particularly important when quantitatively determining the magnitude of the Ce anomaly (Ce/Ce*), which has been suggested as a proxy for the oxidation state of magmas (Trail *et al.*, 2011, 2012, 2015). We find it difficult to fully assess the quality of our non-REE $K_d$ values due to the scarcity of published data for these, but we note that the overall patterns remain in general agreement.

### 3.4. Apatite

Though there are a number of published studies reporting $K_d$ values for apatite, few report data from natural samples and the available data are essentially limited to the REE. The general patterns observed in our data are similar to those for literature data, but the range in $K_d$ values extends over more than an order of magnitude (Fig. 6). We point out that the pattern observed in our data, displaying slightly higher affinity for MREE than for LREE or HREE, best agrees with the data reported by Sano *et al.* (2002), with our values being less than half an order of magnitude higher. In contrast, the values reported by Bea *et al.* (1994) are higher, especially for HREE, and display a more linear trend for the HREE, which, similar to high LREE in zircon, may be the result of HREE-rich inclusions in their samples (see Michael, 1988). We emphasize that our data for apatite come from inclusions within biotite crystals exposed during ablation, so we urge some caution in the interpretation of these $K_d$ values. Accordingly, we have omitted from our dataset any elements that are typically enriched in biotite (e.g. K, Si, Al, Mg, Co, Ni, Cu, and Zn); on the other hand, we expect our results to be reliable for elements that are more abundant in apatite than in biotite (e.g. REE).

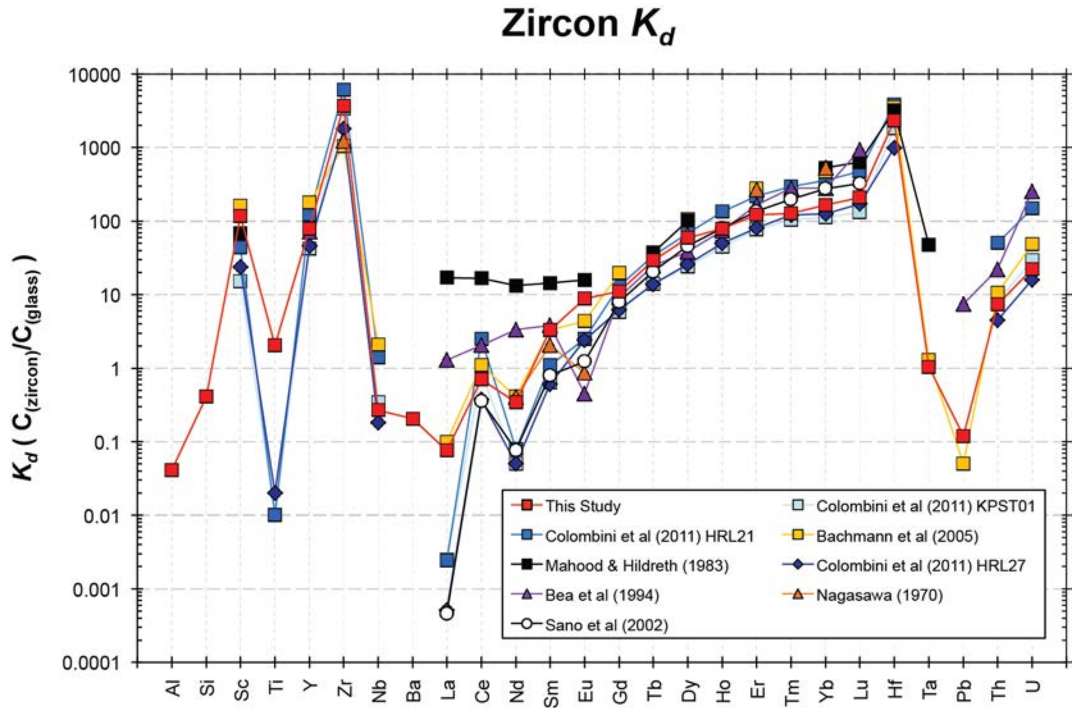

**Figure 5**

Comparison plot of partition coefficients ($K_d$) calculated for zircon vs. published literature data: Colombini *et al.* (2011); Bachmann *et al.* (2005); Mahood & Hildreth (1983); Bea *et al.* (1994); Nagasawa (1970); and Sano *et al.* (2002). Data symbols correspond to the studied rock type as follows: square = high-silica rhyolite; diamond = rhyolite; triangle = granite; circle = dacite.

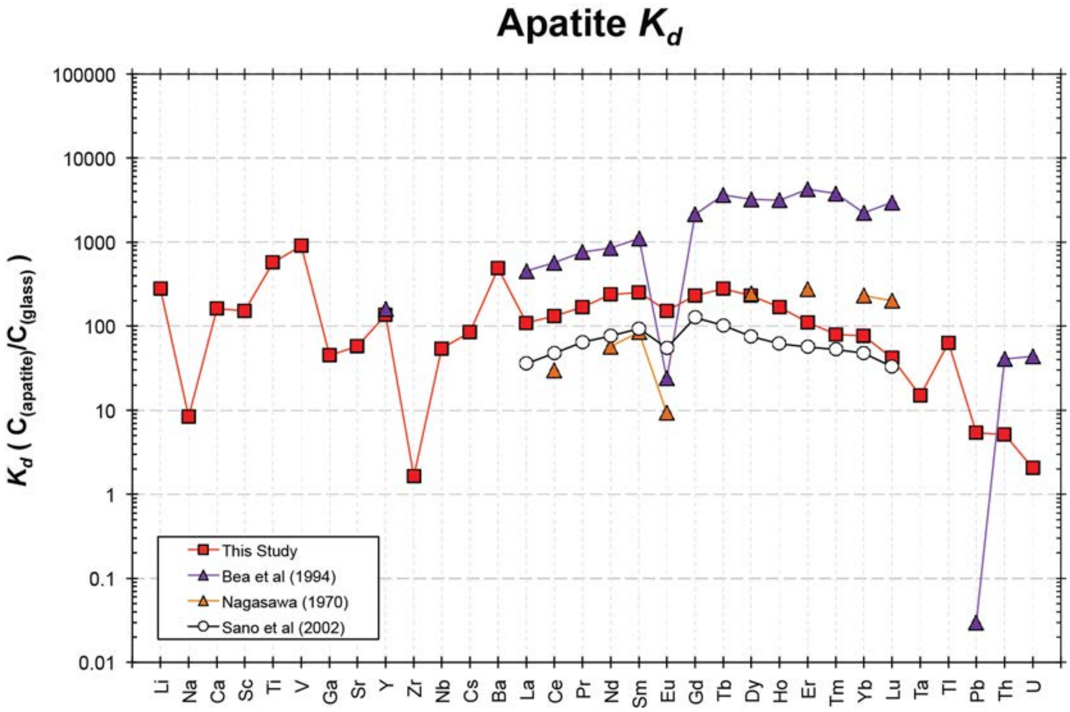

**Figure 6**

Comparison plot of partition coefficients ($K_d$) calculated for apatite vs. published literature data: Bea *et al.* (1994); Nagasawa (1970); and Sano *et al.* (2002). Data symbols correspond to the studied rock type as follows: square = high-silica rhyolite; triangle = granite; circle = dacite.

### 3.5. Amphibole (Hornblende)

The $K_d$ values for amphibole in literature data show some scatter; yet, our $K_d$ values generally fall within half an order of magnitude of literature values (Fig. 7). The overall pattern for the REE, displaying a stronger affinity for MREE and for HREE than for LREE, similar to that observed for titanite, is consistent across all studies. We note, in particular, that our data are most similar to those of Bachmann *et al.* (2005) and Sisson (1994).

### 3.6. Biotite

Large inclusions of other minerals in biotite are very common and, as we discovered during our analyses, can be very difficult to avoid, especially when the data are collected using a relatively large spot size to improve the quality of the data for elements in low concentrations. Thus, we suspect that a large portion of published $K_d$ values for biotite may be unreliable (see Michael, 1988). To the extent possible, we have filtered our own dataset to exclude any analyses with suspected "contamination" from inclusions, identified chiefly by spikes of non-essential elements in biotite during the course of each analysis, and here we report only what we consider our most reliable $K_d$ values. We observe a large amount of variability in both literature values and our own dataset (Fig. 8), with no evident patterns in any of the studies. We urge caution in the use or interpretation of these values, in particular when considering datasets displaying high REE (especially LREE) $K_d$ values, as these may reflect the occurrence of accessory mineral inclusions (e.g. Mahood and Hildreth, 1983; Nash and Crecraft, 1985).

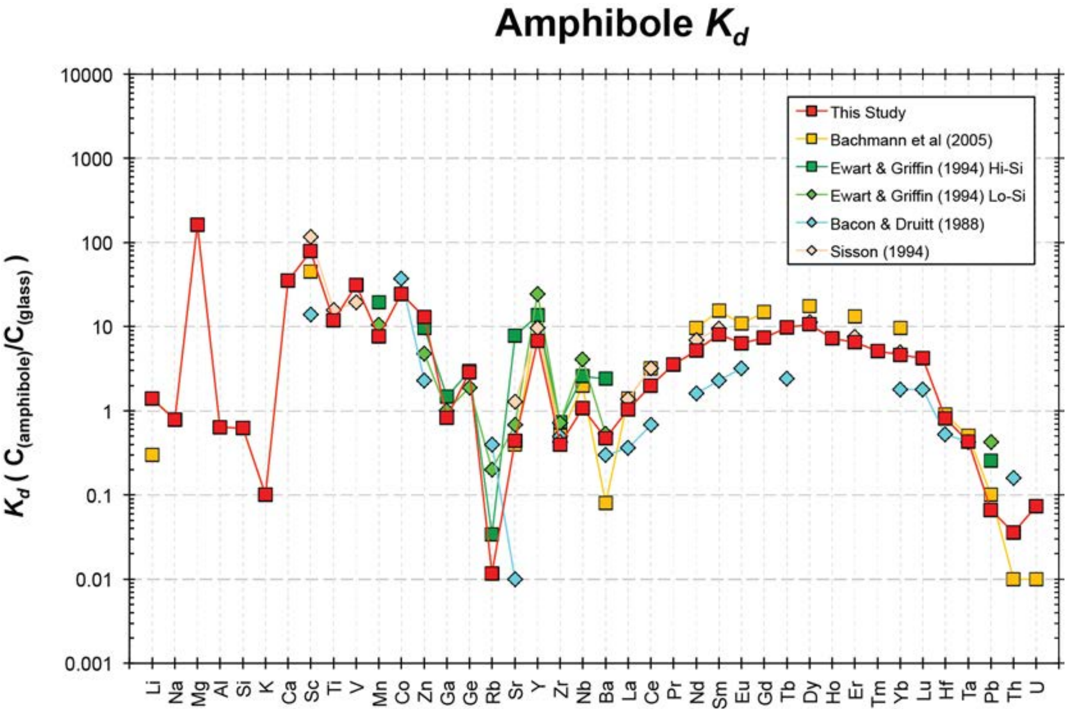

**Figure 7**

Comparison plot of partition coefficients ($K_d$) calculated for amphibole vs. published literature data: Bachmann *et al.* (2005); Ewart & Griffin (1994); Bacon & Druitt (1988); and Sisson (1994). Data symbols correspond to the studied rock type as follows: square = high-silica rhyolite; diamond = rhyolite.

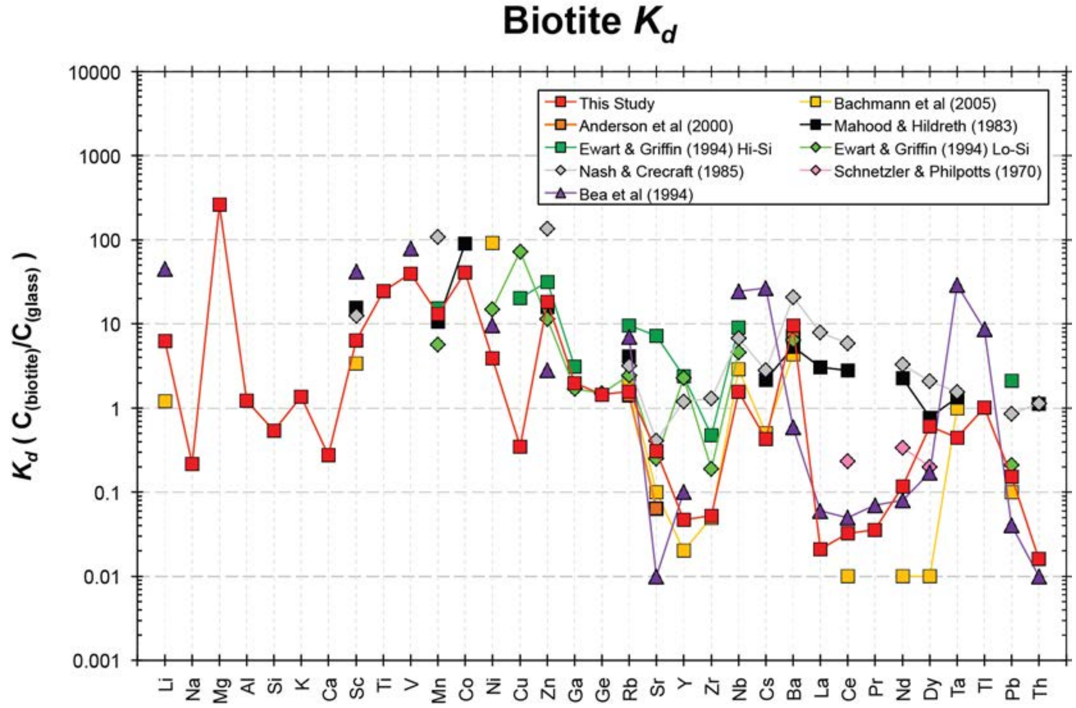

**Figure 8**

Comparison plot of partition coefficients ($K_d$) calculated for biotite vs. published literature data: Bachmann *et al.* (2005); Mahood & Hildreth (1983); Bea *et al.* (1994); Ewart & Griffin (1994); Schnetzler & Philpotts (1970); Nash & Crecraft (1985); and Anderson *et al.* (2001). Data symbols correspond to the studied rock type as follows: square = high-silica rhyolite; diamond = rhyolite; triangle = granite.

### 3.7. Sanidine

Despite the scarcity of data for alkali-feldspar, there is general agreement between literature data and our data, especially for Rb, Sr, Ba and, to a lesser extent, Eu (Fig. 9). There is particularly good agreement between our values and those of Bachmann *et al.* (2005) and Anderson *et al.* (2000), the latter of which were obtained by ion microprobe. Though we were able to measure concentrations of some REE in sanidine, we point out that most of our measurements were of sub-ppm concentrations and all were near the detection limit, and thus we suggest caution in the use and interpretation of these values.

### 3.8. Plagioclase

The literature dataset for plagioclase displays a large amount of scatter, with $K_d$ for most elements varying over 1-2 orders of magnitude with few noticeable patterns, save for spikes in Sr, Ba, and Eu observed in most studies (Fig. 10). Notably, our data is in best agreement with that of Bachmann *et al.* (2005), save for large differences in Ba and the HREE (Dy-Yb); our data also agree well with those of Anderson *et al.* (2000); it is generally also in good agreement with most other literature values for elements that are strongly partitioned into plagioclase (e.g. Sr, Eu). The elevated $K_d$ values for REE reported by Bea *et al.* (1994) are likely the result of REE-rich accessory mineral inclusions in plagioclase, and we point out that, similarly to sanidine, all of our measurements in plagioclase yielded sub-ppm REE concentrations (except for Eu), near the detection limit of our instrument, and readers should be cautious in interpreting these values.

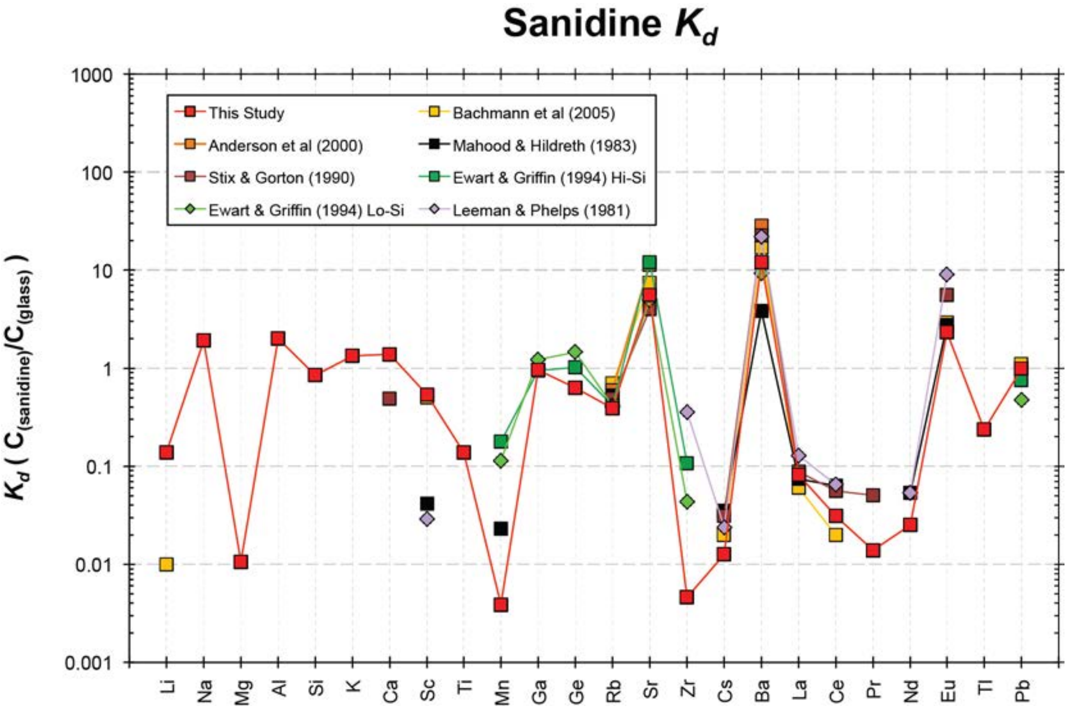

**Figure 9**

Comparison plot of partition coefficients ($K_d$) calculated for sanidine vs. published literature data: Bachmann *et al.* (2005); Mahood & Hildreth (1983); Ewart & Griffin (1994); Stix & Gorton (1990); Leeman & Phelps (1981); and Anderson *et al.* (2001). Data symbols correspond to the studied rock type as follows: square = high-silica rhyolite; diamond = rhyolite.

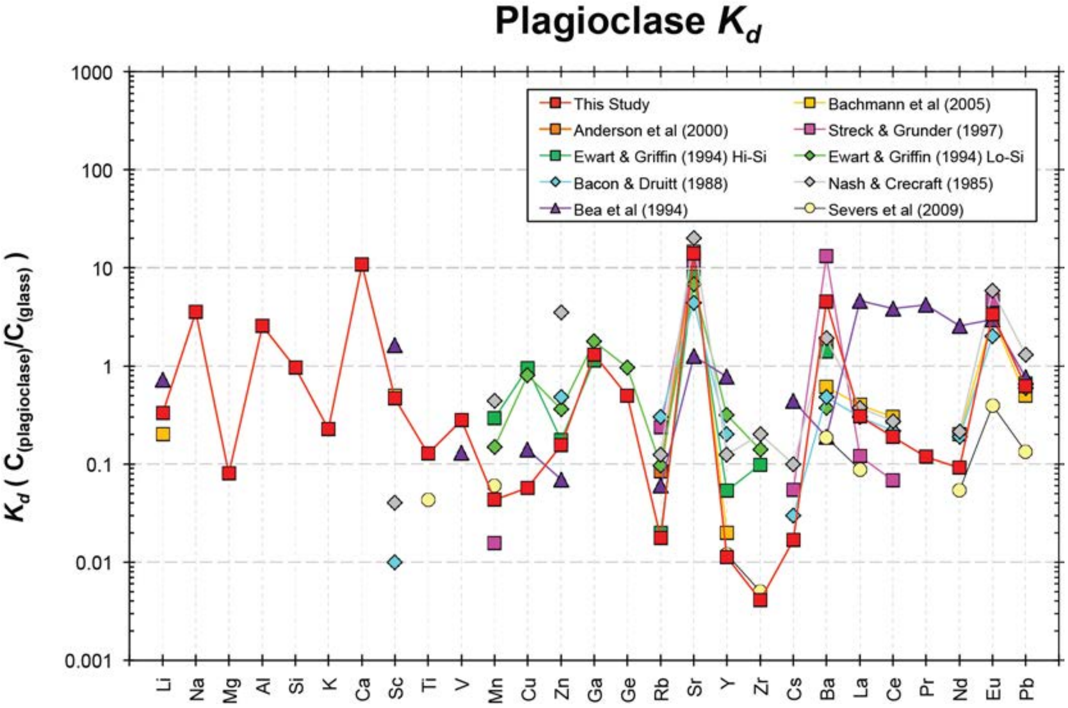

**Figure 10**

Comparison plot of partition coefficients ($K_d$) calculated for plagioclase vs. published literature data: Bachmann *et al.* (2005); Bea *et al.* (1994); Ewart & Griffin (1994); Bacon & Druitt (1988); Nash & Crecraft (1985); Streck & Grunder (1997); and Anderson *et al.* (2000). Data symbols correspond to the studied rock type as follows: square = high-silica rhyolite; diamond = rhyolite; triangle = granite.

# 4. **Discussion**

## 4.1. Controls on REE distribution

Based on our results, it is evident that accessory minerals (titanite, chevkinite, zircon, and apatite) collectively control the partitioning of all rare earth elements in the PST melt (Fig. 11a; e.g. Arth, 1976; Wark and Miller, 1993). Of the major minerals, amphibole has the highest partition coefficients for REE, though Eu is also partitioned strongly by the feldspars. Since $K_d$ values for amphibole are 1-2 orders of magnitude lower than most accessory minerals, amphibole abundances would have to be higher by that same amount in order for it to play an equal role in REE partitioning (e.g. amphibole would need to be ~80 times more abundant to exert the same control on MREE as titanite). Chevkinite displays the highest affinity for the LREE, with $K_d$ values that are over an order of magnitude higher than any other mineral, particularly for La and Ce. Though it is scarce, chevkinite likely plays the dominant role on the partitioning of LREE, while titanite, which also displays a high affinity for LREE, plays a strong secondary role. It is evident, however, that titanite, which preferentially incorporates MREE over other REE, takes on the primary role of fractionating MREE from the melt, due to its abundance in the PST system coupled with its high MREE $K_d$ values. Interestingly, apatite and amphibole share a similar REE $K_d$ pattern to titanite, displaying a higher affinity (though much lower in magnitude) for MREE; these MREE-rich phases, along with chevkinite, also contribute to fractionating MREE from the melt. In rocks where titanite is absent, amphibole and apatite would have the strongest influence on the partitioning of MREE. Zircon plays a significant role in the partitioning of the HREE, with contributions from titanite, chevkinite, and apatite, which all have similar $K_d$ values for the HREE. While zircon is a ubiquitous phase, it is also not very abundant; in the PST case, titanite, being by far the most abundant REE-rich accessory, controls the behavior of the HREE.

## 4.2. Controls on high field strength element (HFSE) distribution (Th, U, Nb, Hf)

Our data suggest that, despite its low abundance, chevkinite holds the primary control on the distribution of Th in the PST. The Th $K_d$ values for titanite and zircon are more than an order of magnitude lower than that for chevkinite (Fig. 11b); but, given the higher abundance of both titanite and zircon, they may also play significant roles in fractionating Th in the PST. These roles are slightly reversed when it comes to the partitioning of U, in which zircon takes on the primary role, with titanite, and to a lesser extent chevkinite, also contributing significantly.

Notably, titanite, apatite, and chevkinite all display a higher affinity for the highly incompatible Nb than the other mineral phases, though titanite, being considerably more abundant, is likely the dominant control on its distribution (Fig. 11b). In contrast, the distribution of Hf is entirely controlled by zircon, which is abundant and whose $K_d$ is more than an order of magnitude larger than for any other mineral phase in the PST (Fig. 11b).

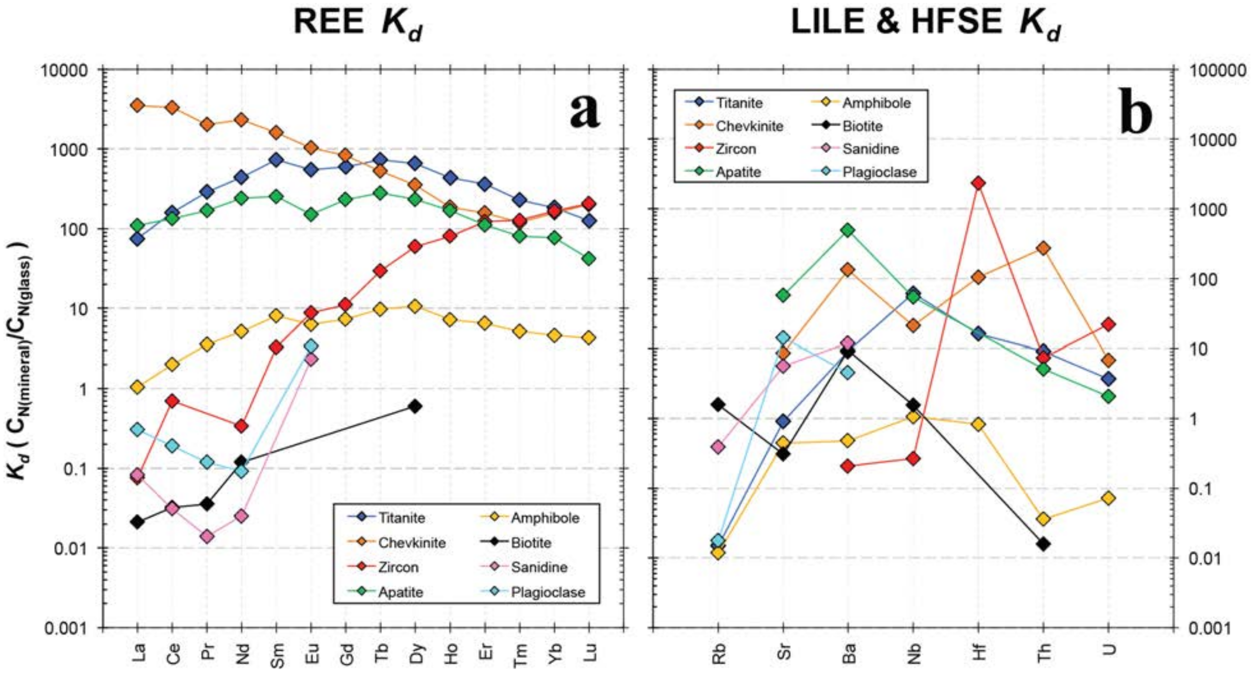

**Figure 11**

Comparison plot of partition coefficients ($K_d$) calculated for all mineral phases of the Peach Spring Tuff high silica rhyolite (sample KPST01A). **(a)** Rare Earth Elements (REE: La-Lu). **(b)** Large ion lithophile elements (LILE: Rb, Sr, Ba) and high field strength elements (HFSE: Nb, Hf, Th, U).

### 4.3. Controls on large ion lithophile element (LILE) distribution (Rb, Sr, Ba)

The distribution of Rb, Sr, and Ba in the PST melt, as expected, appears to be largely controlled by feldspar crystallization (sanidine and plagioclase alike; see Fig. 11b), but accessory minerals can play an important role. We find that Sr and Ba are partitioned on roughly the same magnitude by both feldspars, with a slight preference for Sr in plagioclase and for Ba in sanidine (Fig. 11b). The $K_d$ for Sr in apatite and Ba in both apatite and chevkinite are substantially higher than those for feldspars. Yet, the abundance of the feldspars is much greater than that of apatite or chevkinite, such that feldspars should play the dominant role in the behavior of Sr and Ba. The $K_d$ value for Rb in sanidine is more than an order of magnitude greater than that for plagioclase, though substantially <1; the $K_d$ for Rb in biotite is ~4x larger than the $K_d$ in sanidine, such that sanidine and biotite should both control the distribution of Rb.

### 4.4. Crystallographic controls on partitioning

We interpret the partition coefficient dataset in light of the theoretical considerations of crystal lattice strain by Blundy and Wood (1994, 2003), which predict that cations substituting into a particular crystallographic site will conform to a parabola-like function due to the mismatch in size and valence state between the cations and the site. We fit our data to this function in the form of $y = ax^3 + bx^2 + c$, where $y$ represents $K_d$ in log space (that is, $Ln[K_d]$) and $x$ is the ionic radius; we use a least squares difference method to perform the fitting, and we plot them on *Onuma* diagrams (plots of ionic radius versus $Ln[K_d]$; Figs. 12-19; Onuma *et al.*, 1968) in order to assess how groups of elements partition into various sites within each mineral. We select each group of elements based on their charge and the coordination site they are most likely to occupy within the mineral structure (see Table 2). Using *Onuma* diagrams and best-fit curves calculated from a minimum of 4 cations per group, we are able to constrain the families of cations that are most likely to occupy each site, as well as predict the ideal radius of each crystallographic site, which occurs at the apex of their respective best-fit curves. This type of analysis not only illustrates the crystallographic controls on element partitioning, but it also constitutes an effective test of the quality of the $K_d$ values presented here, and it allows prediction of $K_d$ values for non-analyzed elements; further, we demonstrate that we can calculate the relative abundance of different valence states for some elements, notably Ce and Eu (Colombini *et al.*, 2011).

For some families of cations, we do not have sufficient data to obtain a proper fit, in large part due to their relatively low abundance in some mineral phases (e.g. REE in feldspars), but also because of their relative scarcity in nature (e.g. $1^+$ and $5^+$ cations). In general, we find well-constrained fits with at least 5 cations of a given valence in a given crystallographic site. In some cases, when a single cation (or two cations of very similar size) is much more abundant than other cations in the mineral (e.g. $Zr^{4+}$, $Hf^{4+}$ in zircon), we can force the apex of the parabola-like function to occur at the ionic radius for such cation. This is especially useful for estimating expected concentrations (or $K_d$ values) of cations that are of particular interest in studies of silicic magmas, such as Eu and Ce (see additional discussion below; section *4.4.c*). Fits calculated by this method are denoted in our figures by a dashed line. For a more detailed description of this method, see Appendix A.7.

**Table 2**. Coordination (*Cr.*) and corresponding ionic radii (*R* in Å)[4] used for each cation in *Onuma* diagrams (Figs. 12-22).

| **Phase →** | **Titanite** | | **Chevkinite** | | **Zircon** | | **Apatite** | | **Amphibole** | | **Biotite** | | **Sanidine** | | **Plagioclase** | |
|---|---|---|---|---|---|---|---|---|---|---|---|---|---|---|---|---|
| **Element ↓** | *Cr.* | *R* (Å) | *Cr.* | *R* (Å) | *Cr.* | *R* (Å) | *Cr.* | *R* (Å) | *Cr.* | *R* (Å) | *Cr.* | *R* (Å) | *Cr.* | *R* (Å) | *Cr.* | *R* (Å) |
| **Li**$^{1+}$ | VI | 0.760 | -- | -- | -- | -- | IV | 0.590 | VI | 0.760 | VI | 0.760 | IV | 0.590 | IV | 0.590 |
| **B**$^{3+}$ | IV | 0.110 | -- | -- | -- | -- | -- | -- | -- | -- | -- | -- | -- | -- | -- | -- |
| **Na**$^{1+}$ | VII | 1.12 | VIII | 1.18 | -- | -- | IX | 1.24 | XII | 1.39 | XII | 1.39 | IX | 1.24 | IX | 1.24 |
| **Mg**$^{2+}$ | VII | 0.805 | VI | 0.720 | -- | -- | -- | -- | VI | 0.720 | VI | 0.720 | IX | 0.975 | IX | 0.975 |
| **Al**$^{3+}$ | VI | 0.535 | VI | 0.535 | IV | 0.390 | -- | -- | IV | 0.390 | IV | 0.390 | IV | 0.390 | IV | 0.390 |
| **Si**$^{4+}$ | IV | 0.260 | IV | 0.260 | IV | 0.260 | -- | -- | IV | 0.260 | IV | 0.260 | IV | 0.260 | IV | 0.260 |
| **K**$^{1+}$ | -- | -- | -- | -- | -- | -- | -- | -- | XII | 1.64 | XII | 1.64 | IX | 1.55 | IX | 1.55 |
| **Ca**$^{2+}$ | VII | 1.06 | X | 1.23 | -- | -- | IX | 1.18 | VIII | 1.12 | XII | 1.34 | IX | 1.18 | IX | 1.18 |
| **Sc**$^{3+}$ | VII | 0.808 | VI | 0.745 | VIII | 0.870 | VII | 0.808 | VI | 0.745 | VI | 0.745 | IX | 0.933 | IX | 0.933 |
| **Ti**$^{4+}$ | VI | 0.605 | VI | 0.605 | IV | 0.420 | IV | 0.420 | VI | 0.605 | VI | 0.605 | IV | 0.420 | IV | 0.420 |
| **V**$^{5+}$ | VI | 0.540 | VI | 0.540 | -- | -- | IV | 0.355 | VI | 0.540 | VI | 0.540 | -- | -- | IV | 0.355 |
| **Mn**$^{2+}$ | VII | 0.900 | VI | 0.830 | -- | -- | -- | -- | VI | 0.830 | VI | 0.830 | IX | 1.03 | IX | 1.03 |
| **Co**$^{2+}$ | VII | 0.823 | -- | -- | -- | -- | -- | -- | VI | 0.745 | VI | 0.745 | -- | -- | -- | -- |
| **Ni**$^{2+}$ | -- | -- | -- | -- | -- | -- | -- | -- | -- | -- | VI | 0.690 | -- | -- | -- | -- |
| **Cu**$^{2+}$ | -- | -- | VI | 0.730 | -- | -- | -- | -- | -- | -- | VI | 0.730 | -- | -- | IV | 0.570 |
| **Zn**$^{2+}$ | VII | 0.820 | VI | 0.740 | -- | -- | -- | -- | VI | 0.740 | VI | 0.740 | -- | -- | IX | 0.980 |
| **Ga**$^{3+}$ | VI | 0.620 | VI | 0.620 | -- | -- | VII | 0.697 | VI | 0.620 | VI | 0.620 | IV | 0.470 | IV | 0.470 |
| **Ge**$^{4+}$ | VI | 0.530 | IV | 0.390 | -- | -- | -- | -- | VI | 0.530 | VI | 0.530 | IV | 0.390 | IV | 0.390 |
| **Rb**$^{1+}$ | VII | 1.56 | -- | -- | -- | -- | -- | -- | XII | 1.72 | XII | 1.72 | IX | 1.63 | IX | 1.63 |
| **Sr**$^{2+}$ | VII | 1.21 | X | 1.36 | -- | -- | IX | 1.31 | VIII | 1.26 | XII | 1.44 | IX | 1.31 | IX | 1.31 |
| **Y**$^{3+}$ | VII | 0.960 | VIII | 1.02 | VIII | 1.02 | VII | 0.960 | VIII | 1.02 | VI | 0.900 | -- | -- | IX | 1.08 |
| **Zr**$^{4+}$ | VII | 0.780 | VI | 0.720 | VIII | 0.840 | VII | 0.780 | VII | 0.780 | VI | 0.720 | IV | 0.590 | IV | 0.590 |
| **Nb**$^{5+}$ | VII | 0.690 | VIII | 0.740 | VIII | 0.740 | VII | 0.690 | VIII | 0.740 | VI | 0.640 | -- | -- | -- | -- |
| **Cs**$^{1+}$ | -- | -- | -- | -- | -- | -- | IX | 1.78 | -- | -- | XII | 1.88 | IX | 1.78 | IX | 1.78 |
| **Ba**$^{2+}$ | VII | 1.38 | X | 1.52 | VIII | 1.42 | IX | 1.47 | VIII | 1.42 | XII | 1.61 | IX | 1.47 | IX | 1.47 |
| **La**$^{3+}$ | VII | 1.10 | VIII | 1.16 | VIII | 1.16 | VII | 1.10 | VIII | 1.16 | VI | 1.03 | IX | 1.22 | IX | 1.22 |
| **Ce**$^{3+}$ | VII | 1.07 | VIII | 1.14 | VIII | 1.14 | VII | 1.07 | VIII | 1.14 | VI | 1.01 | IX | 1.20 | IX | 1.20 |
| **Pr**$^{3+}$ | VII | 1.06 | VIII | 1.13 | | | VII | 1.06 | VIII | 1.13 | VI | 0.990 | IX | 1.18 | IX | 1.18 |
| **Nd**$^{3+}$ | VII | 1.05 | VIII | 1.11 | VIII | 1.11 | VII | 1.05 | VIII | 1.11 | VI | 0.983 | IX | 1.16 | IX | 1.16 |
| **Sm**$^{3+}$ | VII | 1.02 | VIII | 1.08 | VIII | 1.08 | VII | 1.02 | VIII | 1.08 | -- | -- | -- | -- | -- | -- |
| **Eu**$^{3+}$ | VII | 1.01 | VIII | 1.07 | VIII | 1.07 | VII | 1.01 | VIII | 1.07 | -- | -- | IX | 1.12 | IX | 1.12 |
| **Gd**$^{3+}$ | VII | 1.00 | VIII | 1.05 | VIII | 1.05 | VII | 1.00 | -- | -- | -- | -- | -- | -- | -- | -- |
| **Tb**$^{3+}$ | VII | 0.980 | VIII | 1.04 | VIII | 1.04 | VII | 0.980 | -- | -- | -- | -- | -- | -- | -- | -- |
| **Dy**$^{3+}$ | VII | 0.970 | VIII | 1.03 | VIII | 1.03 | VII | 0.970 | -- | -- | VI | 0.912 | -- | -- | -- | -- |
| **Ho**$^{3+}$ | VII | 0.958 | VIII | 1.02 | VIII | 1.02 | VII | 0.958 | -- | -- | -- | -- | -- | -- | -- | -- |
| **Er**$^{3+}$ | VII | 0.945 | VIII | 1.00 | VIII | 1.00 | VII | 0.945 | -- | -- | -- | -- | -- | -- | -- | -- |
| **Tm**$^{3+}$ | VII | 0.937 | VI | 0.880 | VIII | 0.994 | VII | 0.937 | -- | -- | -- | -- | -- | -- | -- | -- |
| **Yb**$^{3+}$ | VII | 0.925 | VI | 0.868 | VIII | 0.985 | VII | 0.925 | -- | -- | -- | -- | -- | -- | -- | -- |
| **Lu**$^{3+}$ | VII | 0.919 | VI | 0.861 | VIII | 0.977 | VII | 0.919 | -- | -- | -- | -- | -- | -- | -- | -- |
| **Hf**$^{4+}$ | VII | 0.760 | VI | 0.710 | VIII | 0.830 | -- | -- | -- | -- | -- | -- | -- | -- | -- | -- |
| **Ta**$^{5+}$ | VII | 0.690 | VIII | 0.740 | VIII | 0.740 | VII | 0.690 | -- | -- | VI | 0.640 | -- | -- | -- | -- |
| **Tl**$^{3+}$ | -- | -- | -- | -- | -- | -- | IX | 1.04 | -- | -- | VI | 0.885 | IX | 1.04 | -- | -- |
| **Pb**$^{2}$+ | VII | 1.23 | X | 1.40 | VIII | 1.29 | IX | 1.35 | VIII | 1.29 | XII | 1.49 | IX | 1.35 | IX | 1.35 |
| **Th**$^{4+}$ | VII | 0.995 | VI | 0.940 | VIII | 1.05 | VII | 0.995 | VII | 0.995 | -- | -- | -- | -- | -- | -- |
| **U**$^{4+}$ | VII | 0.950 | VI | 0.890 | VIII | 1.00 | VII | 0.950 | VII | 0.950 | -- | -- | -- | -- | -- | -- |

---

[4] *Ionic radii* (R) obtained at [http://abulafia.mt.ic.ac.uk/shannon/radius.php], taken from "Revised Effective Ionic Radii and Systematic Studies of Interatomic Distances in Halides and Chalcogenides" (Shannon, 1976)

### *4.4.a. <u>Rare Earth Elements (REE) Fits</u>*

For the most part, REE elements in accessory minerals and amphibole conform very well to an *Onuma* curve (Figs. 12-16, 20). For some cation groups (e.g. $3^+$ cations in zircon and biotite), the REE only define one limb of the parabola, though we point out that the zircon fit is particularly good. The low abundance of REE in sanidine and plagioclase yields incomplete datasets for which true fits cannot be calculated.

Of the few elements that do not conform to the fits, some are easily explained. For example, the low $K_d$ values for Eu (e.g. for titanite, apatite, and amphibole) result from the coexistence of divalent and trivalent Eu ($Eu^{2+}$ and $Eu^{3+}$, respectively) and the relatively high $Eu^{2+}/Eu^{3+}$ ratio in silicic magmas. Our $K_d$ reflect total Eu in the melt, and any minerals that preferentially incorporate $Eu^{3+}$ over $Eu^{2+}$ (e.g. titanite) will be deficient in total Eu relative to other REE. The opposite is true for minerals preferentially incorporating $Eu^{2+}$, which results in enriched total Eu relative to the other REE as can be observed in the feldspars (Fig. 18-19). Similarly, anomalies observed in Ce $K_d$ result from the coexistence of $Ce^{3+}$ and $Ce^{4+}$. However, with the exception of zircon, which readily accommodates $Ce^{4+}$ in the Zr site because of their chemical similarities, Ce anomalies are typically very small or absent. This suggests that $Ce^{3+}$ largely dominates Ce abundances in magmatic systems (see additional discussion below).

Surprisingly, La does not conform to the REE fits in titanite, zircon, or apatite, resulting in apparent positive La anomalies. In addition, amphibole displays a positive Dy anomaly. Previous researchers have also noted similar misfits for some REE in accessory phases (e.g. Colombini *et al.*, 2011). We suggest these misfits are the result of REE-rich micro inclusions in those phases. For example, if we consider the *Onuma* fit for REE in zircon (Fig. 14), the predicted $K_d$ for La would be 0.0026, from which we deduce that the amount of La that can be accommodated in zircon is on the order of ~100 ppb, which contrasts with the measured 3.4 ppm concentration and resulting $K_d = 0.075$. A small-volume LREE-rich inclusion can easily account for the ~3 ppm of La we measure in zircon. In this context, it becomes clear that the sub-ppm intrinsic abundance of La in zircon presents a substantial obstacle to accurate determination of La concentrations, given that the measurements will invariably be affected by inclusions, particularly for determinations using LA-ICP-MS, which make use of relatively large analyzed volumes. This has important implications for the determination of Ce anomalies in zircon and any derived estimates of oxidation state that make use of such anomalies (Trail *et al.*, 2011, 2012, 2015).

Interestingly, Gd is systematically low in the *Onuma* fits for all REE-rich phases except chevkinite (i.e. titanite, zircon, apatite, amphibole). Similarly, despite having a radius nearly identical to that of Ho, Y, which, along with Sc, is typically associated with the REE due to its chemical similarity, is also systematically low in most phases. We note that Gd concentrations in glass appear to be high in our chondrite-normalized REE pattern (see Fig. 2b). It is thus possible that our $K_d$ for Gd are slightly underestimated, as a consequence. In addition, Pr in chevkinite and biotite as well as Sm in apatite plot below the best-fit curves. The reasons for these misfits are not immediately clear to us, as these elements do not exist in other valence states and cannot be explained by REE-enriched inclusions.

Notably, our data suggest that the REE in chevkinite are partitioned between two crystallographic sites with different coordination (Fig. 13). As expected, the LREE conform to a fit for the $(La,Ce)^{[VIII]}$ site in chevkinite, but the heaviest REE (Tm-Lu) and Sc, in contrast, occupy the $(Ti)^{[VI]}$ site along with the HFSE.

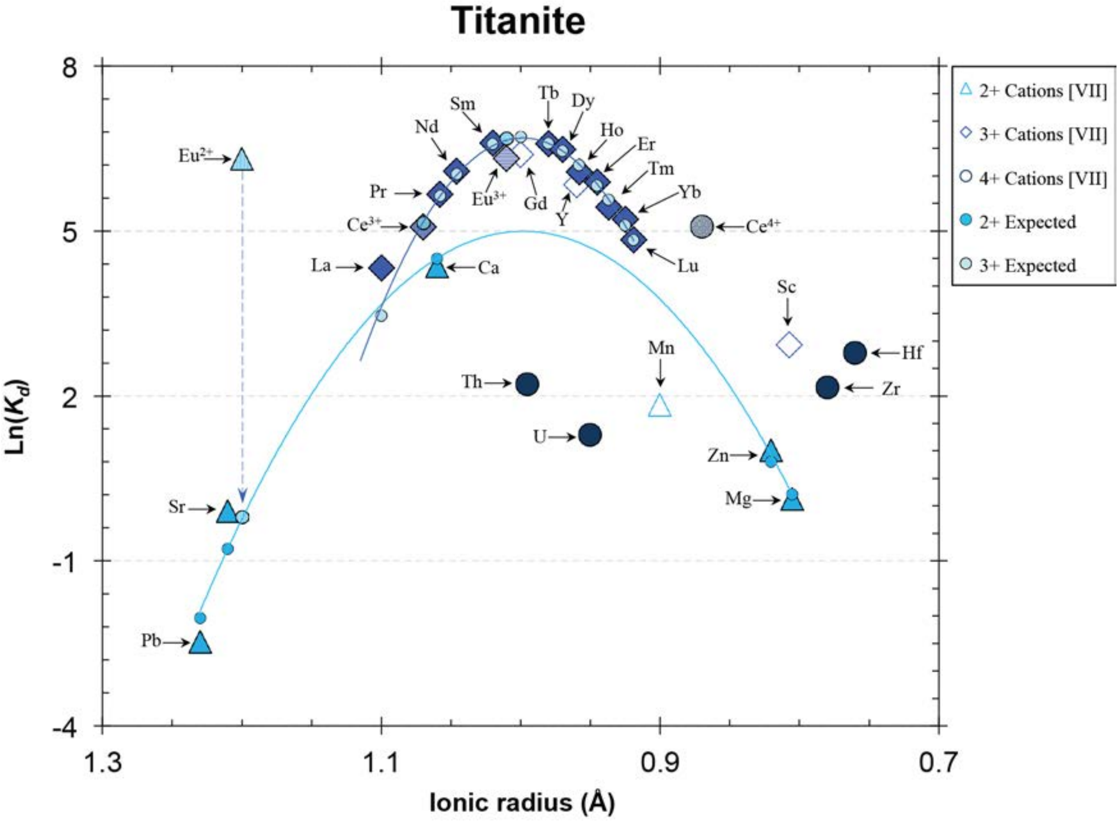

**Figure 12**

Onuma plot (Ln($K_d$) vs. ionic radius) for titanite. For each group of cations, only filled symbols are included in the determination of a best-fit curve (Eu$^{3+}$ is excluded from the REE fit). The corresponding expected Ln($K_d$) values for each cation are plotted as small filled circles. Where the differences are large, vertical dashed arrows connect measured to expected Ln($K_d$) values. Roman numerals indicate the coordination of the site that each group of cations occupies.

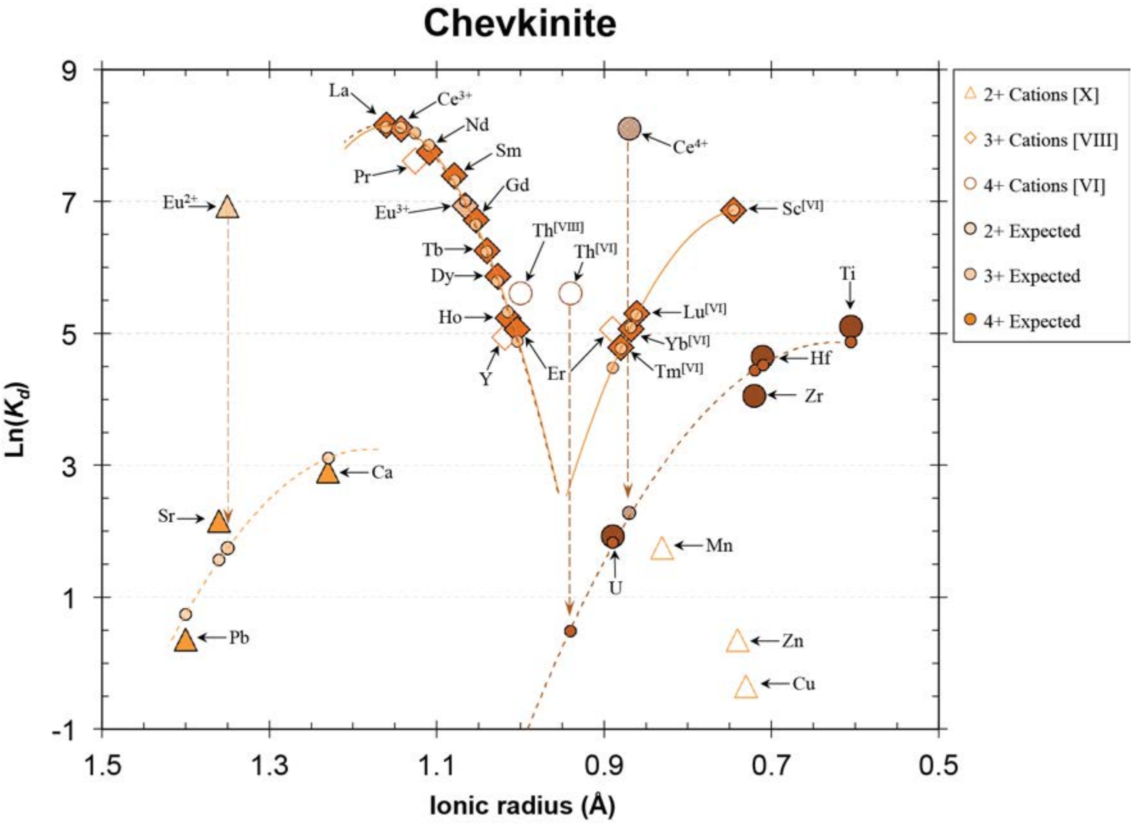

**Figure 13**

Onuma plot (Ln($K_d$) vs. ionic radius) for chevkinite. For each group of cations, only filled symbols are included in the determination of a best-fit curve. The corresponding expected Ln($K_d$) values for each cation are plotted as small filled circles. Where the differences are large, vertical dashed arrows connect measured to expected Ln($K_d$) values. Roman numerals indicate the coordination of the site that each group of cations occupies. For cation groups that do not conform to a best-fit curve, an assumed fit is calculated (see section 4.4 for details) and plotted as a dashed curve (e.g. HFSE, LILE).

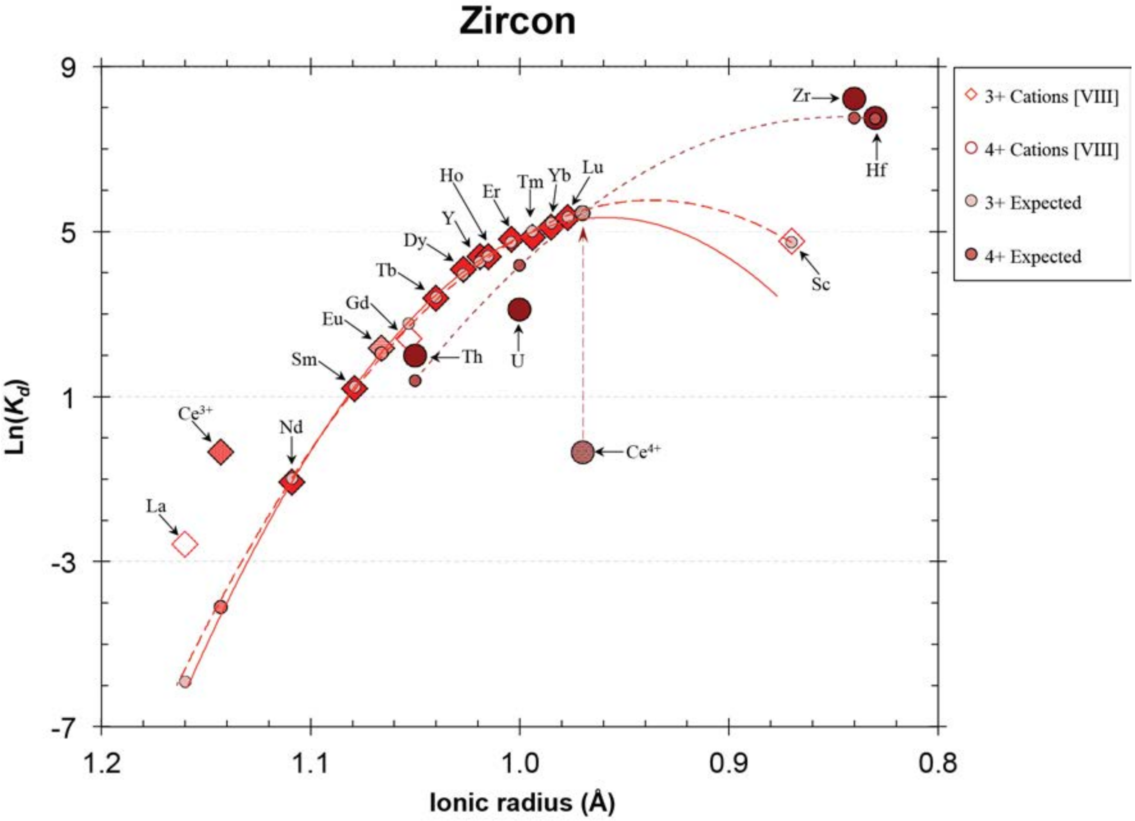

**Figure 14**

Onuma plot (Ln($K_d$) vs. ionic radius) for zircon. For each group of cations, only filled symbols are included in the determination of a best-fit curve (Ce$^{3+}$ is excluded from the REE fit). The corresponding expected Ln($K_d$) values for each cation are plotted as small filled circles. Where the differences are large, vertical dashed arrows connect measured to expected Ln($K_d$) values. Roman numerals indicate the coordination of the site that each group of cations occupies. For cation groups that do not conform to a best-fit curve, an assumed fit is calculated (see section 4.4 for details) and plotted as a dashed curve (e.g. HFSE).

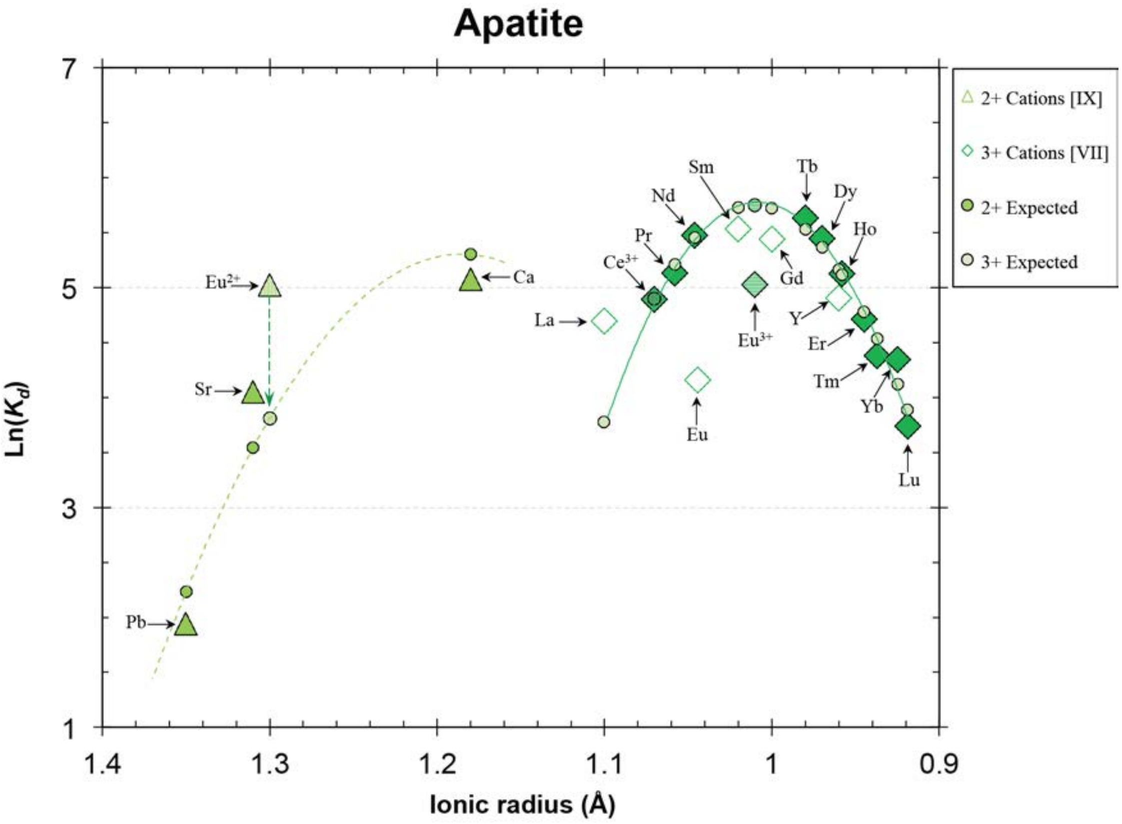

**Figure 15**

Onuma plot (Ln($K_d$) vs. ionic radius) for apatite. For each group of cations, only filled symbols are included in the determination of a best-fit curve ($Eu^{3+}$ is excluded from the REE fit). The corresponding expected Ln($K_d$) values for each cation are plotted as small filled circles. Roman numerals indicate the coordination of the site that each group of cations occupies. For cation groups that do not conform to a best-fit curve, an assumed fit is calculated (see section 4.4 for details) and plotted as a dashed curve (e.g. LILE).

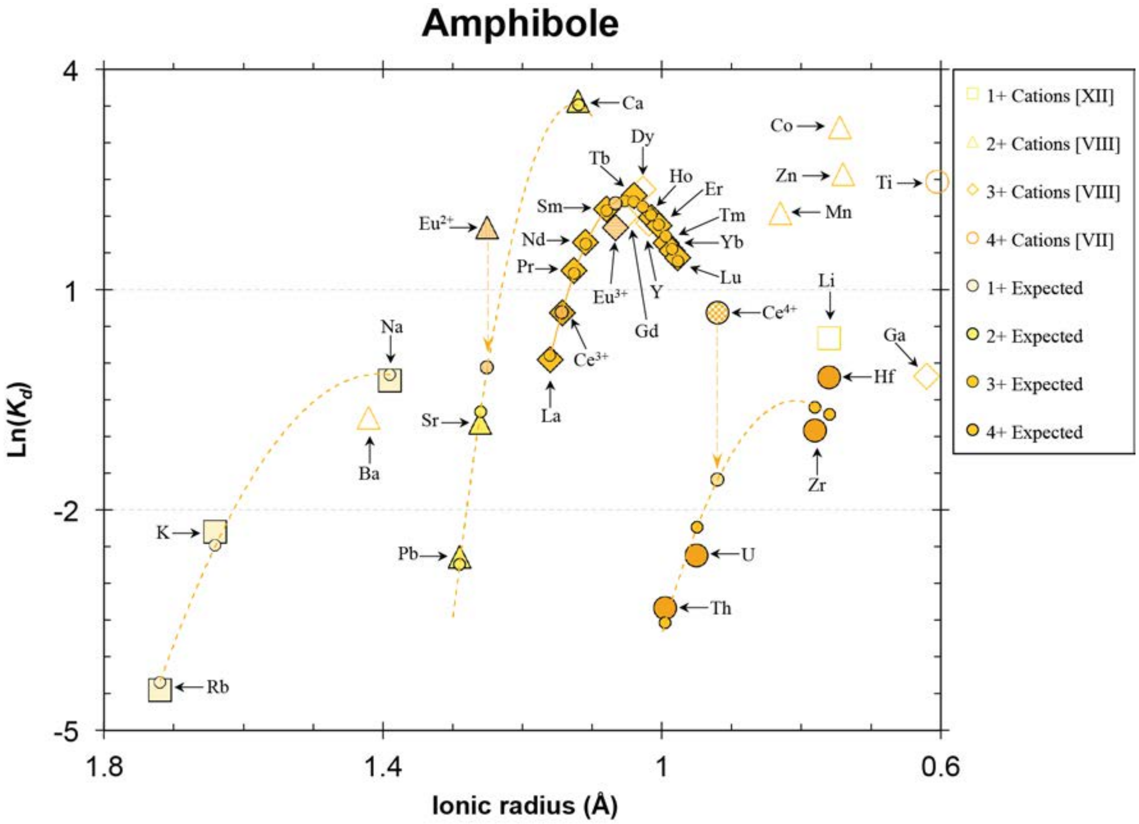

**Figure 16**

Onuma plot (Ln($K_d$) vs. ionic radius) for amphibole. For each group of cations, only filled symbols are included in the determination of a best-fit curve (Eu$^{3+}$ is excluded from the REE fit). The corresponding expected Ln($K_d$) values for each cation are plotted as small filled circles. Where the differences are large, vertical dashed arrows connect measured to expected Ln($K_d$) values. Roman numerals indicate the coordination of the site that each group of cations occupies. For cation groups that do not conform to a best-fit curve, an assumed fit is calculated (see section 4.4 for details) and plotted as a dashed curve (e.g. HFSE, LILE).

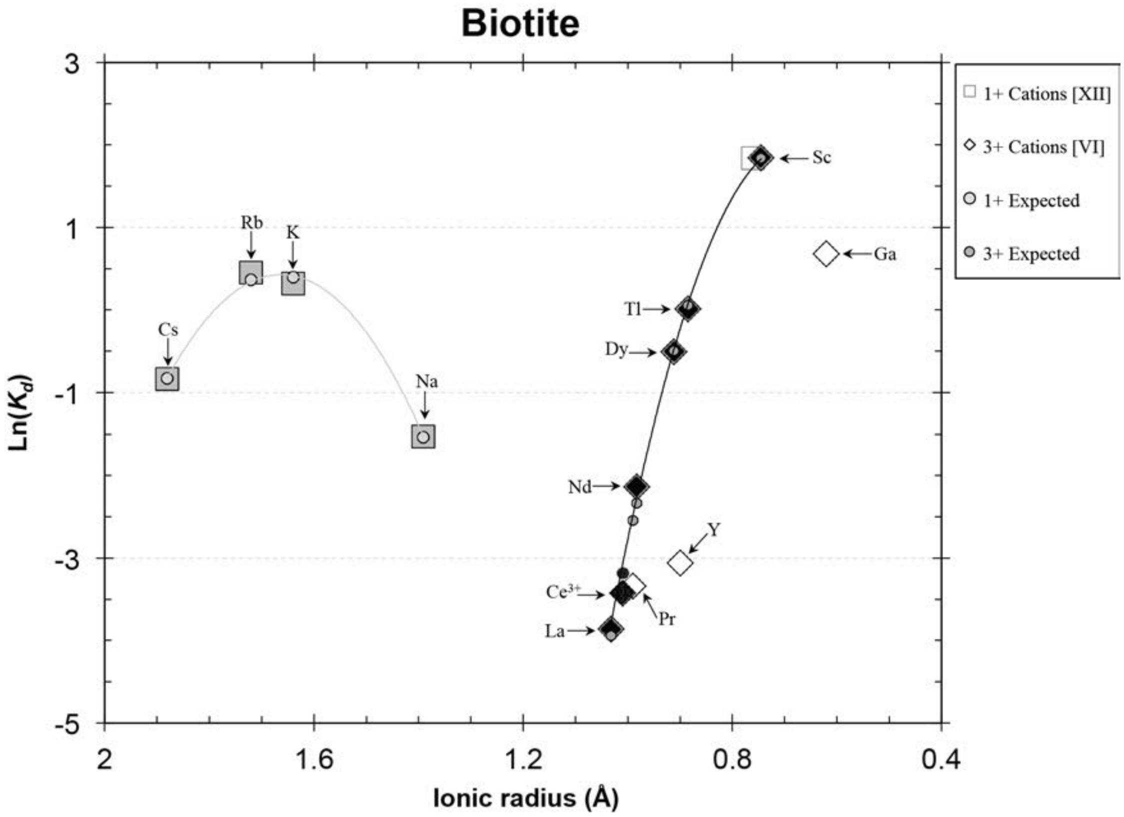

**Figure 17**

Onuma plot (Ln($K_d$) vs. ionic radius) for biotite. For each group of cations, only filled symbols are included in the determination of a best-fit curve. The corresponding expected Ln($K_d$) values for each cation are plotted as small filled circles. Roman numerals indicate the coordination of the site that each group of cations occupies.

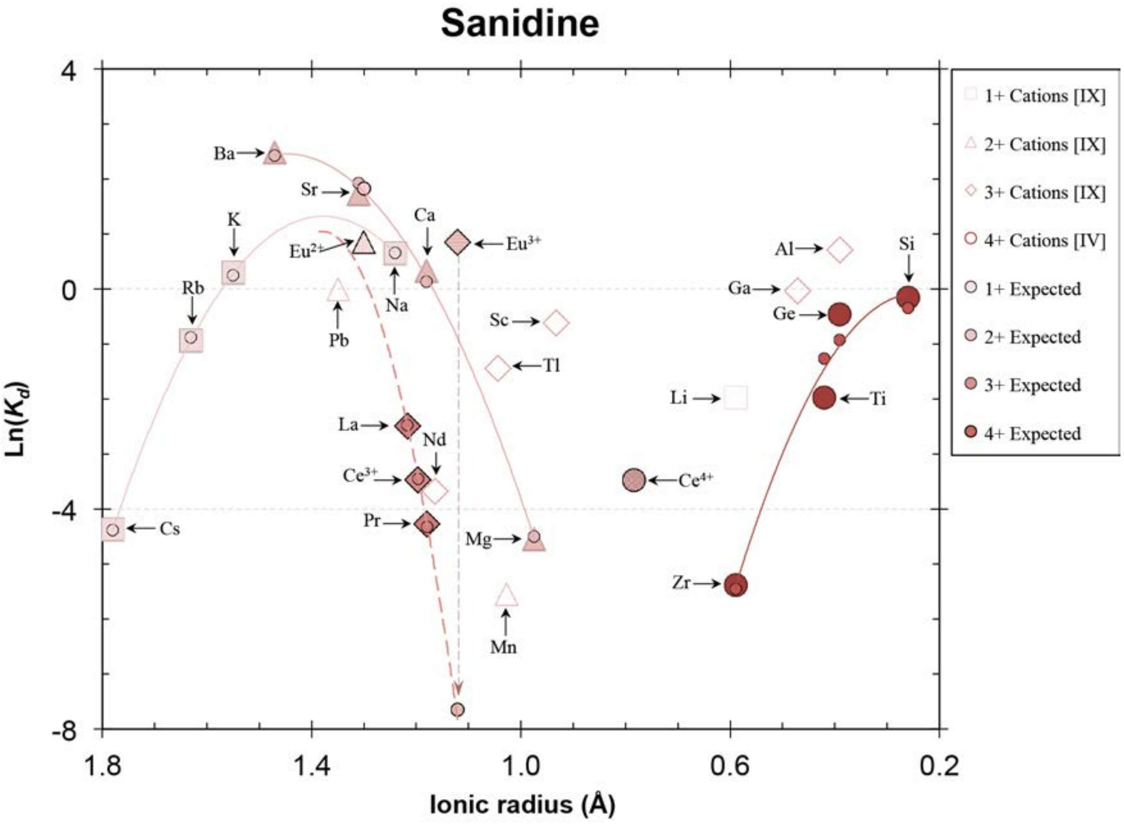

**Figure 18**

Onuma plot (Ln($K_d$) vs. ionic radius) for sanidine. For each group of cations, only filled symbols are included in the determination of a best-fit curve ($Eu^{3+}$ is excluded from the REE fit). The corresponding expected Ln($K_d$) values for each cation are plotted as small filled circles. Where the differences are large, vertical dashed arrows connect measured to expected Ln($K_d$) values. Roman numerals indicate the coordination of the site that each group of cations occupies. For cation groups that do not conform to a best-fit curve, an assumed fit is calculated (see section 4.4 for details) and plotted as a dashed curve (e.g. REE).

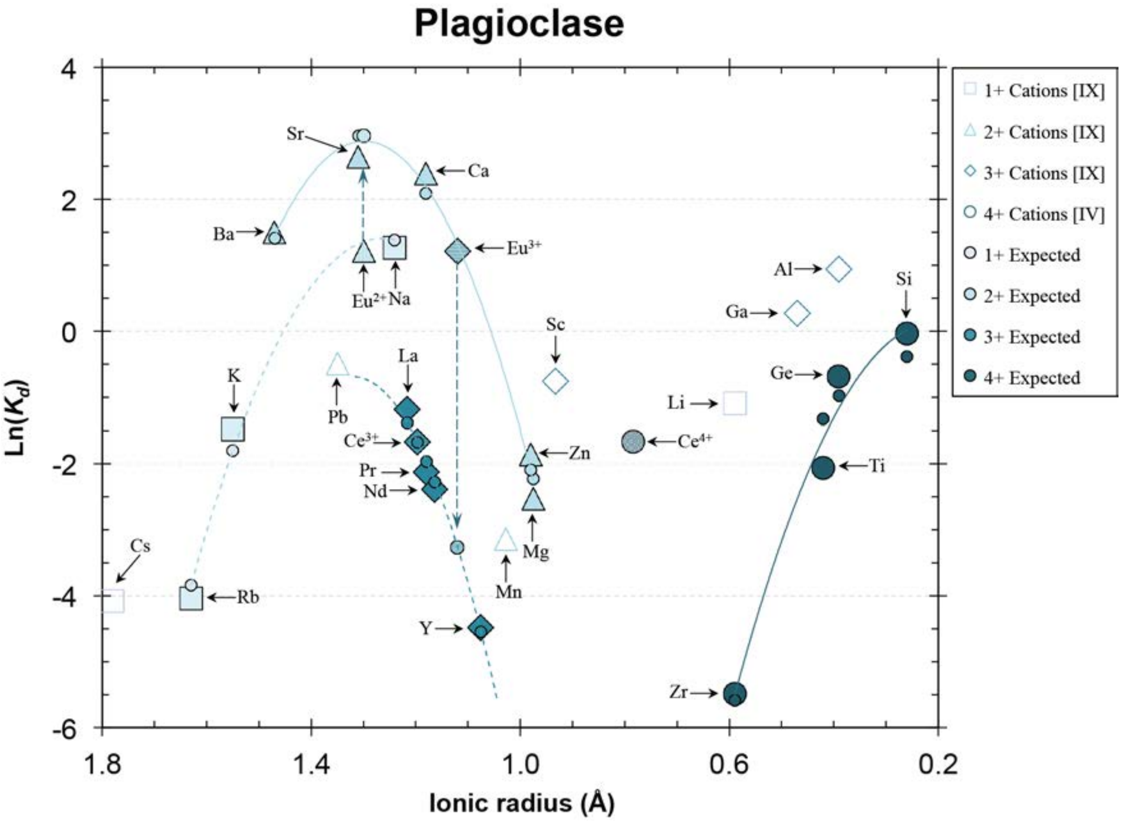

**Figure 19**

Onuma plot (Ln($K_d$) vs. ionic radius) for plagioclase. For each group of cations, only filled symbols are included in the determination of a best-fit curve ($Eu^{3+}$ is excluded from the REE fit). The corresponding expected Ln($K_d$) values for each cation are plotted as small filled circles. Where the differences are large, vertical dashed arrows connect measured to expected Ln($K_d$) values. Roman numerals indicate the coordination of the site that each group of cations occupies. For cation groups that do not conform to a best-fit curve, an assumed fit is calculated (see section 4.4 for details) and plotted as a dashed curve (e.g. REE, LILE).

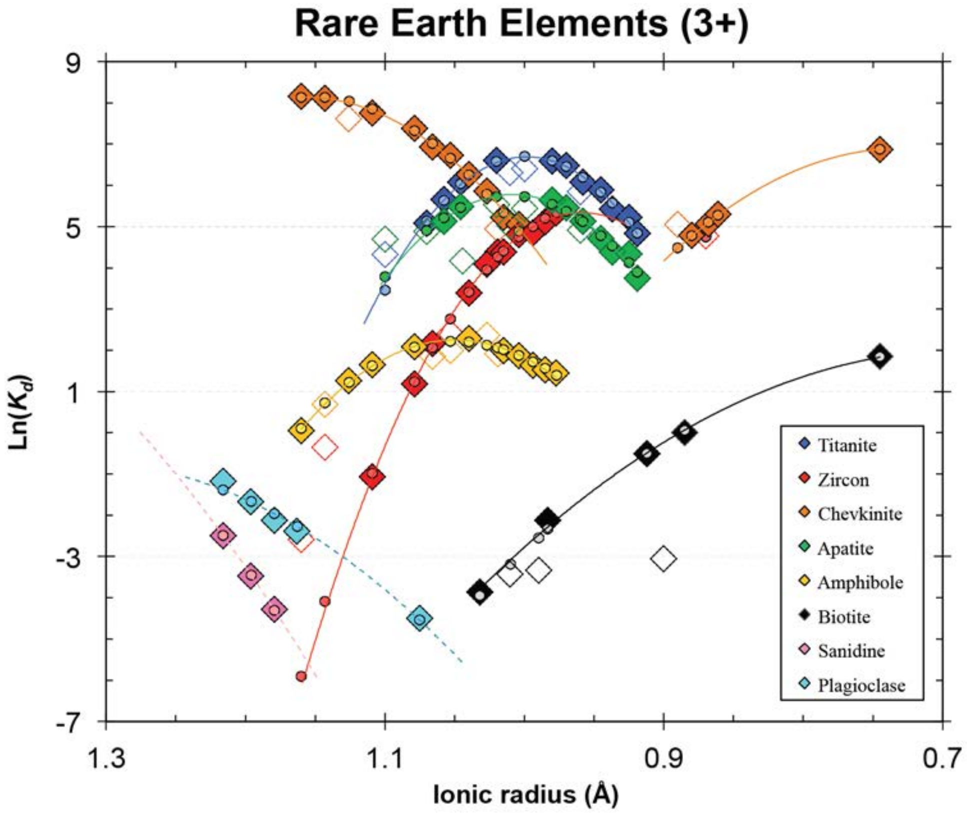

**Figure 20**

Onuma plot (Ln($K_d$) vs. ionic radius) for rare earth elements (REE) in all mineral phases. Only filled symbols are included in the determination of a best-fit curve. The corresponding expected Ln($K_d$) values for each cation are plotted as small filled circles. Dashed curves indicate an assumed fit (see section 4.4 for details).

### 4.4.b. Large Ion Lithophile Elements (LILE), High Field Strength Elements (HFSE), and other Onuma fits

Because of the limited number of HFSE and LILE that exist in any given valence state, it is difficult to obtain sufficient data to calculate true Onuma fits in most minerals. In many cases, divalent LILE share a crystallographic site with smaller $2^+$ cations, making it possible to calculate an Onuma fit for that group of cations. We see some relatively good fits for groups of $2^+$ cations, though such fits are largely limited to the major mineral phases (Fig. 21), as expected since their mineral structures can more readily accommodate LILE, particularly when a dedicated alkali or alkaline earth metal site is present. However, in most phases LILE occupy larger sites than other cations in the same valence (e.g. transition metals), or the phases simply cannot simultaneously accommodate LILE and smaller cations resulting in very low concentrations of one or both groups (e.g. in zircon). We encounter the same issue with HFSE, as few phases can accommodate these in the same site as smaller $4^+$ cations (e.g. the Si site), or concentrate enough HFSE to define a proper *Onuma* fit (see Fig. 22). Notably, we can approximate HFSE fits for chevkinite, zircon, and amphibole by forcing the curves to fit the radius of their host cations (see Figs. 13-14, 16, 22), as previously discussed, but we are unable to do the same for other accessory phases despite the fact that most have relatively elevated concentrations of a sufficient number of HFSE (typically Zr, Hf, Th, and U). The misfit of Th in chevkinite (Fig. 13) suggests that it is partitioned into the larger $(La,Ce)^{[VIII]}$ site along with the REE, while U is partitioned into the smaller $(Ti)^{[VI]}$ site with Zr and Hf. This may explain why Th is enriched in chevkinite relative to other accessory minerals. In the same way we do for the HFSE, we can also approximate fits for some groups of $2^+$ cations in accessory phases (e.g. chevkinite, see Fig. 13; apatite, see Fig. 15). The value of these forced fits is further discussed below (see section *4.4.c*).

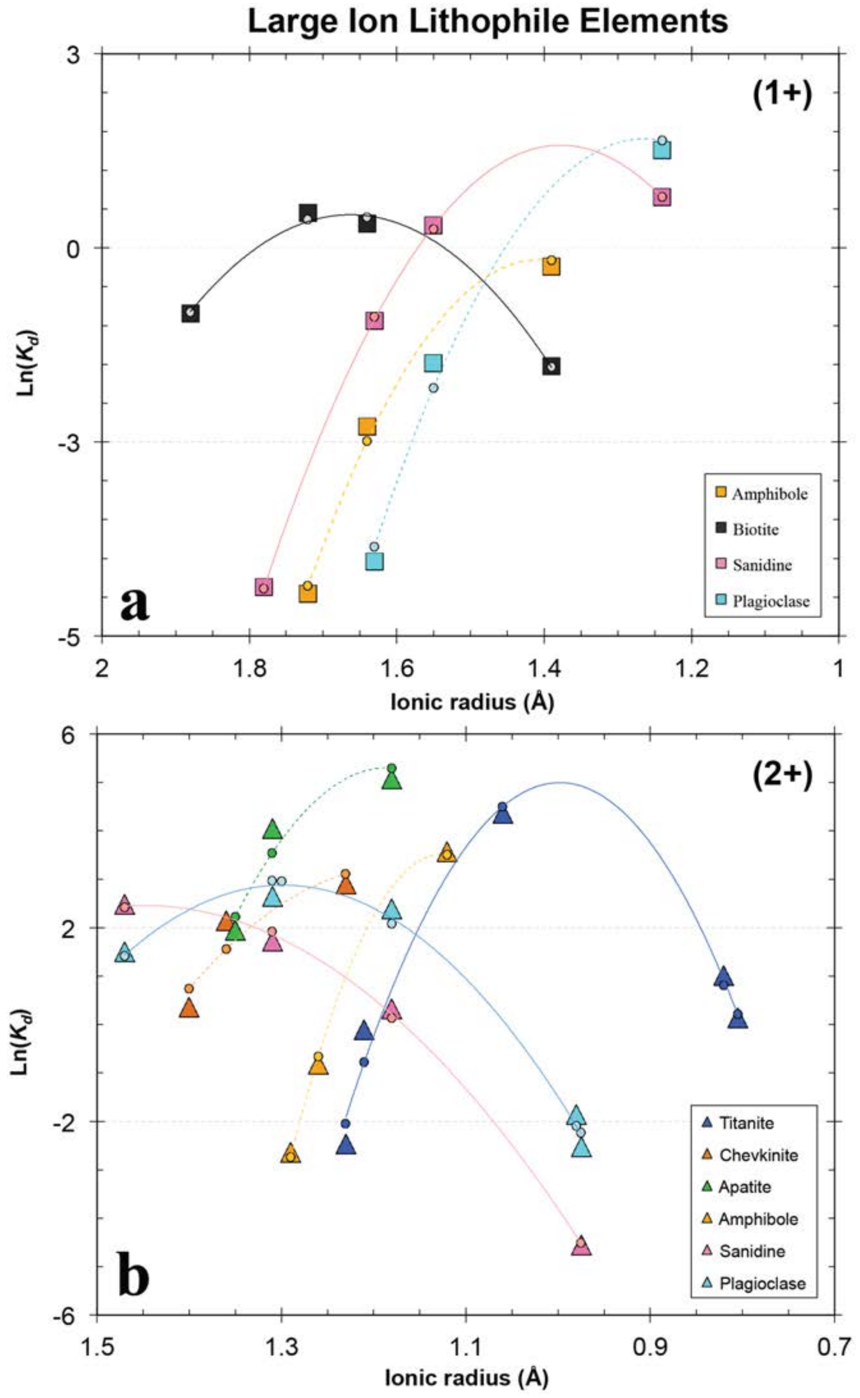

**Figure 21**

Onuma plot (Ln($K_d$) vs. ionic radius) for large ion lithophile elements (LILE) in all mineral phases. The corresponding expected Ln($K_d$) values for each cation are plotted as small filled circles. Dashed curves indicate an assumed fit (see section 4.4 for details). **(a)** monovalent LILE. **(b)** divalent LILE.

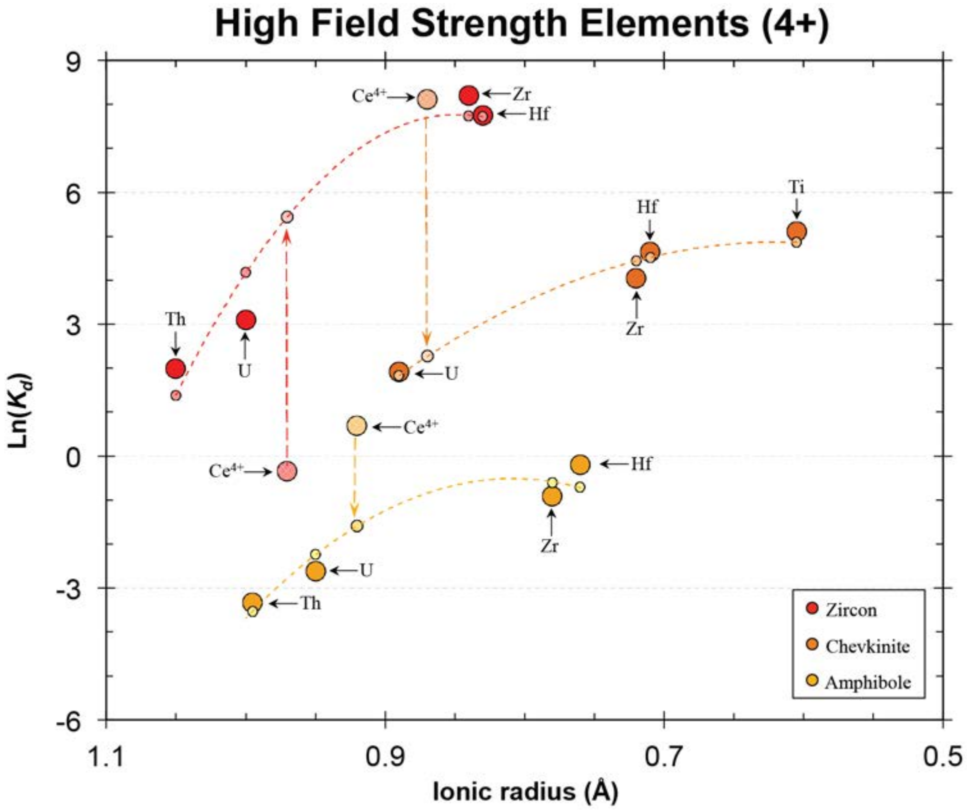

**Figure 22**

Onuma plot (Ln($K_d$) vs. ionic radius) for assumed HFSE fits in zircon, chevkinite, and amphibole (see section 4.4 for details). The corresponding expected Ln($K_d$) values for each cation are plotted as small filled circles. Vertical dashed arrows connect measured to expected $Ce^{4+}$ Ln($K_d$) values in their respective curves for each mineral phase.

We note that the apex of the best-fit curve for 9-fold coordinated $2^+$ cations in plagioclase is more closely aligned with the radius of $Eu^{2+[IX]}$ and $Sr^{2+[IX]}$, rather than that of $Ca^{2+}$ (Fig. 19), illustrating the strong affinity and consequent large $K_d$ for $Eu^{2+}$ in plagioclase. Interestingly, we also observe a similar shift for the $1^+$ cations curve in sanidine, whose apex is shifted toward a smaller size than the expected $K^{1+[IX]}$ radius, and for the $2^+$ and $3^+$ curves in titanite whose apexes are aligned at approximately the same radius, though shifted toward a smaller size than the expected $Ca^{2+[VII]}$ radius, and perhaps suggesting that REE are abundant enough in titanite such that the $Ca^{2+[VII]}$ site is truly a $(Ca+REE)^{[VII]}$ site.

With the exception of feldspars, we find that Ba is systematically off in all our mineral datasets, and does not conform to the fit in any group of $2^+$ cations in the same coordination to which it should theoretically belong. The reason for this misfit is not immediately clear to us. In contrast, when present in measurable concentrations (such as in major phases), Rb and Sr appear to conform well to best-fit curves with other LILE in their respective valence (e.g. $K^+$ and $Na^+$ for $Rb^+$; $Ca^{2+}$ and $Pb^{2+}$ for $Sr^{2+}$).

### 4.4.c. Estimating $Ce^{4+}$ and $Eu^{2+}$ proportions in silicic melts

Previous researchers have suggested that $Ce^{4+}$ and $Eu^{2+}$ can be used as indicators of oxidizing (indicated by the existence of $Ce^{4+}$) vs. reducing (existence of $Eu^{2+}$) conditions in magmas (e.g. Trail *et al.*, 2011). However, the occurrence of both Ce and Eu anomalies in PST phases is a clear indication that $Eu^{2+}$, $Eu^{3+}$, $Ce^{3+}$, and $Ce^{4+}$ all coexist in the PST melt, particularly in phases like apatite, which contains anomalies in both species. Additional knowledge about the coexistence, and relative proportions, of these species could shed light about their dependence on, or effect of, the oxidation state of their parental magma. With this in mind, from the mathematical definition of partition coefficients and the calculation of expected partition coefficients from Onuma fits (see above), Colombini *et al.* (2011) derived the following expression to estimate the relative proportion of $Ce^{3+}$ ($X_{Melt}^{Ce^{3+}}$) to total Ce ($Ce^{tot}$) in silicate melts:

$$X_{Melt}^{Ce^{3+}} = ({K_d}^{Ce^{tot}} - {K_d}^{Ce^{4+}})/({K_d}^{Ce^{3+}} - {K_d}^{Ce^{4+}})$$

where ${K_d}^{Ce^{3+}}$ and ${K_d}^{Ce^{4+}}$ represent the calculated expected $K_d$ for $Ce^{3+}$ and $Ce^{4+}$, respectively, and ${K_d}^{Ce^{tot}}$ represents the measured $K_d$ for Ce. This equation can also be used to estimate the relative proportion of $Eu^{2+}$ ($X_{Melt}^{Eu^{2+}}$) to total Eu ($Eu^{tot}$) in the melt. Using the same approach and the equation above, we calculated the relative proportions of $Ce^{3+}$ and $Eu^{2+}$ for the Peach Spring Tuff (Table 3). We note that these values are best estimated for phases in which we have good fits for both the REE and $4^+$ cations (to estimate Ce proportions) or $2^+$ cations (to estimate Eu proportions), such that we can accurately calculate the ideal $K_d$ values for both valences. However, as previously discussed (see section *4.4.a*), fits for some of the $4^+$ and $2^+$ groups of cations require additional assumptions regarding the ionic radius at which the apex in $K_d$ occurs. Nonetheless, reasonable estimates for, ${K_d}^{Ce^{4+}}$ and ${K_d}^{Eu^{2+}}$ can be obtained in some cases, especially when the expected $Eu^{2+}$ or $Ce^{4+}$ values fall between those of other $2^+$ or $4^+$ cations occupying the same site and coordination. Estimated values for ${K_d}^{Ce^{3+}}$ and ${K_d}^{Eu^{3+}}$ are less problematic, given that the REE usually sufficiently constrain the Onuma fits.

**Table 3**. Abundances of $Eu^{2+}$ and $Ce^{3+}$ relative to total Eu and Ce, estimated from $K_d$ values and *Onuma* curves.

| | **Phase →** | **Titanite** | **Chevkinite** | **Zircon** | **Apatite** | **Amphibole** | **Sanidine** | **Plagioclase** |
|---|---|---|---|---|---|---|---|---|
| **$LnK_d$ ($Eu^{Tot}$)** | | 6.31 | 6.9 | -- | 5.0 | 1.8 | 0.8 | 1.2 |
| $Eu^{2+}$ | Coordination | VII | X | -- | VIII | VIII | IX | IX |
| | Radius | 1.20 | 1.35 | -- | 1.25 | 1.25 | 1.30 | 1.30 |
| | $Y_{Expected}$ | -0.21 | 1.7 | -- | 3.2 | -0.1 | 1.8 | 3.0 |
| $Eu^{3+}$ | Coordination | VII | VIII | -- | VIII | VIII | IX | IX |
| | Radius | 1.01 | 1.07 | -- | 1.07 | 1.07 | 1.12 | 1.12 |
| | $Y_{Expected}$ | 6.67 | 7.0 | -- | 5.6 | 2.2 | -7.6 | -3.3 |
| | **$Eu^{2+}/Eu^{Tot}$** | **0.303** | **0.067** | **--** | **0.525** | **0.312** | **0.376** | **0.173** |
| **$LnK_d$ ($Ce^{Tot}$)** | | -- | 8.1 | -0.4 | -- | 0.7 | -- | -- |
| $Ce^{3+}$ | Coordination | -- | VIII | VIII | -- | VIII | -- | -- |
| | Radius | -- | 1.14 | 1.14 | -- | 1.14 | -- | -- |
| | $Y_{Expected}$ | -- | 8.1 | -4.1 | -- | 0.7 | -- | -- |
| $Ce^{4+}$ | Coordination | -- | VI | VIII | -- | VII | -- | -- |
| | Radius | -- | 0.87 | 0.97 | -- | 0.92 | -- | -- |
| | $Y_{Expected}$ | -- | 2.3 | 5.4 | -- | -1.6 | -- | -- |
| | **$Ce^{3+}/Ce^{Tot}$** | **--** | **0.978** | **0.997** | **--** | **0.968** | **--** | **--** |

Based on our HFSE fits for zircon, chevkinite, and amphibole, we calculate that almost all Ce exists in the trivalent state (see Table 3, Fig. 22; estimates range from ~97 to ~99% $Ce^{3+}$), in agreement with estimates of ~99% previously obtained for zircon fits by Colombini *et al.* (2011). In contrast, our estimates for the proportion of $Eu^{2+}$ stretch over a wider range, from ~10 to ~50%, with the majority of phases indicating $Eu^{2+}$ abundances of ~30%. While these first order estimates may vary, they are not inconsistent with each other. One of the many benefits of having extensive $K_d$ datasets such as the one we present here, with as many phases and elements as possible analyzed, is the ability to obtain significantly better constraints on these types of relationships, which would allow us to make useful comparisons between different magmatic systems, and help advance our understanding of their dependence on oxidation conditions and their influence on overall magmatic evolution.

## 5. **Conclusions**

We present an extensive dataset of partition coefficients for a high-silica rhyolite from the Peach Spring Tuff. We use the same analytical techniques (LA-ICP-MS for minor and dispersed elements, quantitative SEM-EDS for select essential structural constituents) to measure the concentrations of 54 elements in glass and 7 mineral phases from the same pumice sample (Fig. 1; Table 1). This makes the derived dataset of $K_d$ unique and it provides a high degree of internal consistency between the $K_d$ values for the various minerals present. Our approach is similar to that of Colombini *et al.* (2011) and Bachmann *et al.* (2005), and our results are largely in agreement with those, but we present data for a larger number of elements in a larger number of phases. We believe that coupling compositions of crystal rims with glass compositions from the same sample is likely to yield very reliable partition coefficients that reflect equilibration between crystals and melt in the volcanic system at or near the time of eruption. In addition, analyzing *in situ* concentrations helps minimize contamination from inclusions, especially in minerals that are commonly hosts to abundant inclusions (e.g. biotite, amphibole, and feldspars). We emphasize, as has been previously noted (e.g. Michael, 1988), that, because of the inability to avoid inclusions, whole-crystal dissolution (e.g. ID-MS) and bulk analysis (e.g. INAA) methods are likely to yield unreliable concentrations, and therefore unreliable $K_d$ values. We highlight that our LA-ICP-MS analyses are very consistent with analyses done on the same sample by other high-precision methods (e.g. Colombini *et al.*, 2011: zircon and titanite data collected by SHRIMP-RG; Sano *et al.*, 2002: zircon and apatite data collected by SHRIMP). Our approach carries the advantage of faster and significantly less expensive analyses, thereby allowing us to analyze a broader suite of elements in more mineral phases and put together an extensive dataset.

We found that, while we were able to obtain good quality data for a large suite of dispersed elements, there are some elements that cannot be reliably measured by the LA-ICP-MS instrumentation we used. In general, the quality of our data is best for the rare earth elements (La-Lu, Y), a majority of high field strength elements (e.g. U, Th, Pb, Nb, Hf, Zr), and large ion lithophile elements (Rb, Sr). In contrast, some important elements (e.g. Fe, Ti and other transition metals) are more difficult to quantify due to isobaric interferences.

For a majority of cation groups in every mineral phase we are able to fit our data to *Onuma* curves (ionic radius vs. $Ln[K_d]$) that conform to the theoretical crystal lattice strain model of Blundy and Wood (1994, 2003). Our fits are particularly good for the REE. For other groups of cations (e.g. HFSE) we can calculate the theoretical fit that would conform to our data fairly well. This approach is especially useful in estimating the expected total concentrations of multivalent cations that are selectively incorporated by certain phases, resulting in elemental anomalies, as is the case for Eu and Ce. The simultaneous occurrence of Eu and Ce anomalies in some phases of the PST (e.g. apatite) is an indication that both elements coexisted in all valence states in the parental melt. We offer a mathematical expression for estimating the relative proportions of each of these valence species. Our results indicate that >97% of total Ce exists in the $Ce^{3+}$ valence, whereas the relative proportions of Eu species are not as well constrained, with the calculated proportion of $Eu^{2+}$ mainly ranging from ~10 to ~50%.

Lastly, we conclude that, in the PST system, the distribution of REE and HFSE is collectively controlled by chevkinite (LREE, Th), titanite (MREE, Nb), and zircon (HREE, Hf, U), while LILE are mainly partitioned into sanidine (Rb, Sr, Ba) and plagioclase (Sr, Ba), with some likely significant contribution from biotite (Rb, Ba) and apatite (MREE, Nb, Sr, Ba).

Additional datasets like the one presented here would allow better assessment of the potential limitations and caveats of this dataset. More importantly, perhaps, they would very likely provide critical data to enhance our understanding of the effects of composition and crystallization conditions on elemental partitioning. One key component that is missing is the quantitative assessment of mineral abundances, which would allow for computation of bulk distribution coefficients and would make it possible to more rigorously evaluate the relative contributions of the various phases present.

# CHAPTER III

## Elucidating the magmatic history of the Austurhorn Silicic Intrusive Complex (SE Iceland) using zircon elemental and isotopic geochemistry and geochronology

### Abstract

The Austurhorn Intrusive Complex (AIC) in SE Iceland comprises large bodies of granophyre, gabbro, and a mafic-silicic composite zone (MSCZ) that exemplifies magmatic interactions common in Icelandic silicic systems. However, despite being one of Iceland's best-studied intrusions, few studies have included detailed analyses of zircon, a mineral widely recognized as a valuable tracer of the history and evolution of its parental magma(s). In this study, we employ *in situ* zircon elemental and isotopic (hafnium and oxygen) geochemistry, as well as U-Pb geochronology, as tools for elucidating the complex construction and magmatic evolution of Austurhorn's MSCZ.

The trace element compositions of AIC zircons form a broad but coherent array partly overlapping with the zircon geochemical signature for Icelandic silicic volcanic rocks. Hafnium concentrations are low (less than 10,000 ppm), typical of Icelandic zircon, and Ti concentrations range from ~5 to 40 ppm (Ti-in-zircon model temperatures = 750-990°C). Zircon $\delta^{18}O$ values vary from +2.2 to +4.8 ‰, consistent with magmatic zircon from other Icelandic silicic rocks and preserving evidence for recycling of hydrothermally altered crust as a significant contributor in the generation of silicic magmas within the Austurhorn system. Zircon epsilon-Hf values generally range from +11 to +15. This range overlaps with that of Icelandic basalts from off-rift settings as well as the least depleted rift basalts, suggesting that the Austurhorn magmatic system developed within a transitional rift environment.

*In situ* zircon U-Pb ages (SHRIMP-RG) yield a mean of 6.52 ±0.03 Ma for the entire complex, but span a range of ~300 k.y., from 6.35 ±0.08 to 6.67 ±0.06 Ma (2σ SE). Gabbros and the most silicic units (high-$SiO_2$ granophyres) fall on the older end of this range, while granophyres and intermediate units make up the younger part of the complex. We interpret this to represent the approximate timescale of magmatic construction of the MSCZ, consistent with field evidence suggesting multiple short-lived magmatic intrusion events occurring closely spaced in time, allowing periodic re-melting and rejuvenation of mush-like material and a prolonged lifetime for the complex.

# 1. **Introduction**

Silicic rocks make up an estimated 10-13% of Icelandic exposures (Jónasson, 2007; Gunnarsson *et al.*, 1998; Walker, 1966), the largest known concentration in a modern oceanic setting. The petrogenesis of these rocks has received considerable attention, but most investigations have focused on volcanism (e.g. Gunnarsson *et al.*, 1998; Martin and Sigmarsson, 2007; Carley *et al.*, 2011, 2014; Bindeman *et al.*, 2012); less attention has been paid to the more sparsely exposed silicic intrusive rocks. In particular, there has been no detailed study to date of zircon in any Icelandic intrusion. Because of its low solubility in almost all melt and fluid compositions, its stability and resistance to alteration at Earth's surface, and extremely slow elemental diffusion within its crystal lattice at magmatic temperatures (e.g. Cherniak *et al.*, 1997a,b; Watson and Cherniak, 1997; Cherniak and Watson, 2000, 2007), zircon can retain valuable geochemical information about the environments in which it grew, including crystallization temperature, the composition of the melt(s) from which it crystallized, and elapsed time since crystallization (age), making it a powerful tool for investigating the evolution of silicic magmatic systems.

We have selected the relatively well-studied Austurhorn intrusive complex (Blake, 1966; Gale *et al.*, 1966; Mattson *et al.*, 1986; Furman *et al.*, 1992a, 1992b; Thorarinsson and Tegner, 2009) for the first detailed study of zircon from an Icelandic intrusion. In combination with supporting field investigation, petrography, and whole-rock elemental and isotopic geochemistry, we use zircon trace element and U-Pb, Hf, and O isotopic analyses to investigate the petrogenesis of the Austurhorn intrusive complex. In particular, we aim to elucidate (1) the nature of zircon in the rock types commonly associated with shallow Icelandic intrusions, (2) emplacement and magmatic processes within the Austurhorn chamber, and (3) the origin(s) of the AIC magma(s). We present clear geochemical evidence, and supporting field observations, for open-system processes in the Austurhorn magmatic system, including physical exchange of zircons among magmas of contrasting compositions, consistent with previous interpretations based on field relationships (e.g. Furman *et al.,* 1992b; Mattson *et al.,* 1986). We observe varying characteristics in whole-rock as well as zircon elemental and isotopic geochemistry that indicate repeated magmatic input from variable sources into the Austurhorn system. Finally, based on our dataset and observations, we propose that silicic magmas at Austurhorn were generated by assimilation and fractional crystallization (AFC) processes in which a significant portion of the crustal assimilant was generated by partial melting of hydrothermally-altered crust (e.g. Sigmarsson *et al.*, 1991).

## 2. **Geological Background**

### 2.1. The Austurhorn Intrusive Complex, SE Iceland

The Austurhorn intrusive complex (AIC) is a small, Late Miocene composite intrusion located along the coast of southeastern Iceland (Fig. 1). Cropping out over an area of 15 km$^2$, the AIC is equivalent in dimension and in diversity and abundance of rock types to modern and Neogene Icelandic central volcanoes. The exposed portion of the AIC (Fig. 2) is surrounded by a ~1 km wide metamorphic thermal areole that includes roof and wall contacts in several locations, where the AIC intrudes predominantly west-dipping basaltic lavas and tuffs from the Álftafjördur and Lón Late-Miocene central volcanoes (Blake, 1970, 1966; Ross & Mussett, 1976). The intrusion comprises granophyre, gabbro, minor felsite, and an extensive mafic-silicic composite zone (MSCZ – previously referred to as the "net-veined complex;" e.g. Furman *et al.*, 1992; Mattson *et al.*, 1986; Blake, 1966) in which there is abundant evidence for open system behavior, including chamber replenishment by dense basaltic and buoyant silicic magmas indicated by commingling textures (Fig. 3; Mattson et al, 1986; Furman, 1992). The exposed gabbro is largely restricted to the peaks Hvalnesfjall and Þúfuhraunstindur (see Fig. 2) in the central part of the complex, and appears to be almost entirely encircled by granophyre (Blake, 1966).

Based on the structure of the intrusion and geochemistry of the mafic and silicic rocks at AIC, previous researchers have suggested that it developed within a short-lived immature transitional rift environment, analogous to the Eyjafjallajökull and Torfajökull central volcanoes in Iceland's modern Eastern Neovolcanic Zone (EVZ; Furman *et al.*, 1992a), which are constructed from both basaltic and silicic eruption products. The AIC is thus interpreted to represent the roots of an exhumed Neogene central volcano. Previous studies have constrained the depth of emplacement to ~2 km, primarily based on field relations and laumontite (zeolite) alteration in basaltic amygdales observed just outside the Austurhorn thermal aureole. The composition of these amygdales has been suggested to constrain the maximum depth to which basalt was buried at the time of alteration from AIC intrusions (Walker, 1960, 1964). The complex has been dated by K-Ar from biotite extracted from aplitic veins in the gabbroic intrusion at 6.6 ±0.4 Ma (Moorbath *et al.*, 1968), and by U-Pb isotope systematics in zircons from gabbro and granophyre at 6.6 ±0.4 and 6.5 ±0.2, respectively (Martin *et al.*, 2011; the only published zircon ages for Austurhorn).

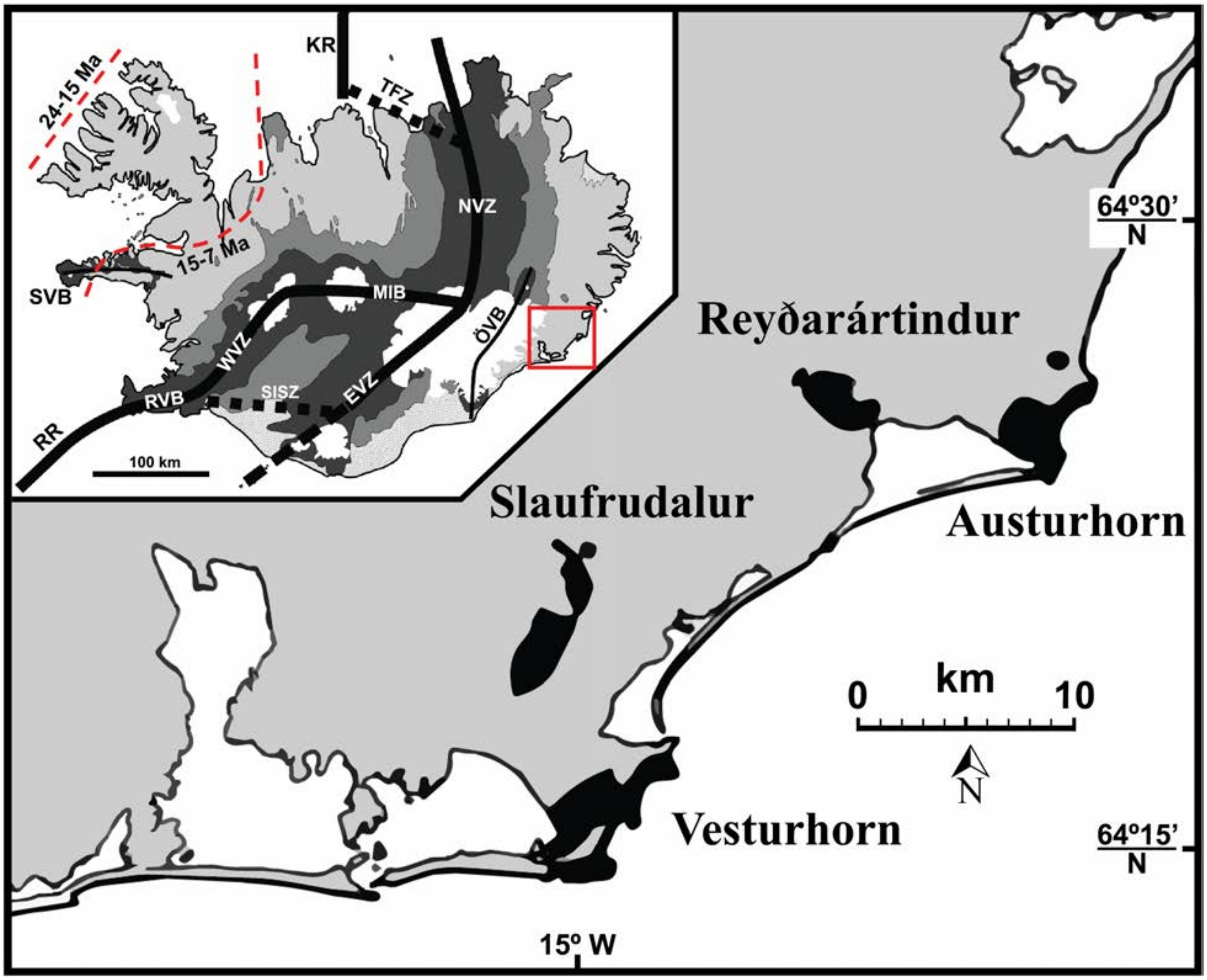

**Figure 1**

Regional map of Southeast Iceland outlining the four major composite silicic intrusions exposed in the area (black shaded areas; modified after Gale *et al.*, 1966). *Inset:* Overview map of Iceland and its major tectonovolcanic zones (modified after Carley *et al.*, 2011): Northern (NVZ), Eastern (EVZ), and Western Volcanic Zones (WVZ), Snæfellsness Volcanic Belt (SVB), Reykjanes Ridge (RR), Reykjanes Volcanic Belt (RVB), South Iceland Seismic Zone (SISZ), Öræfi Volcanic Belt (ÖVB), Tjornes Fracture Zone (TFZ), Kolbeinsey Ridge (KR), and the Mid-Iceland Belt (MIB). The red dashed lines represent extinct rifts (Martin *et al.*, 2011). The red box indicates the location of the intrusions. The shades of gray indicate age divisions: light gray = Neogene (17-3.3 Ma); medium gray = Plio-Pleistocene (3.3-0.7 Ma); dark gray = Upper Pleistocene to present (0.7-0 Ma); white = Ice caps.

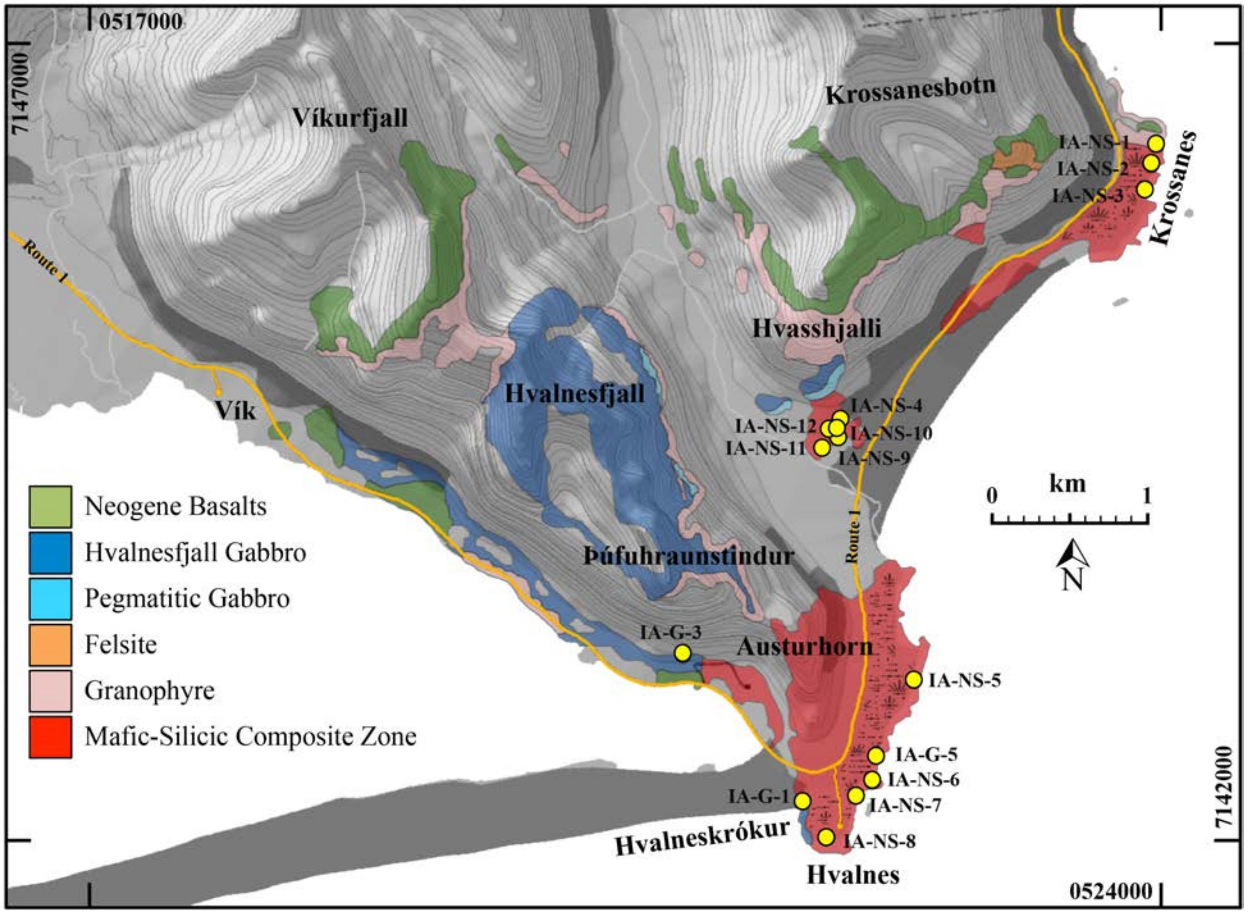

**Figure 2**

Geologic map of the Austurhorn Intrusive Complex (modified after Furman *et al.*, 1992b). Yellow labeled dots indicate sampling locations. Dark grey zones indicate thick alluvial cover. Light grey zones are talus cover and vegetated areas. Iceland national Route 1 is highlighted in yellow. Coordinates listed are in WGS84 UTM grid zone 28W. Patterned areas within the Mafic-Silicic Composite Zone denote marsh environment.

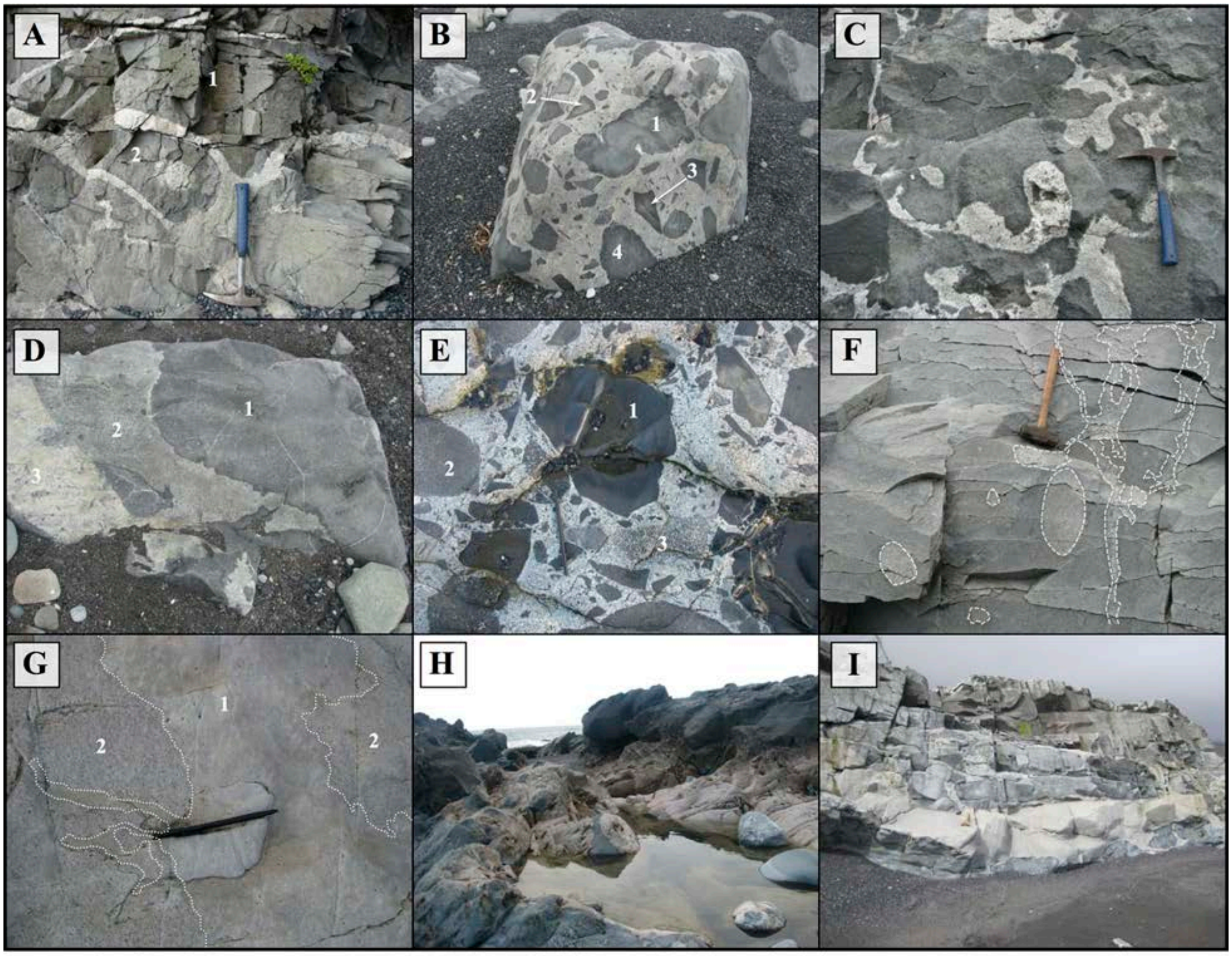

**Figure 3**

Diversity of magmatic interactions found within the MSCZ: A) mafic plume-like pillow structures (1, 2) in intermediate host, with a notable silicic core in pillow 2; B) mafic pillow-like enclaves with chilled and crenulate margins (1, 4), and mafic clasts with sharp and angular boundaries (2, 3), in silicic host; C) continuous and undulate dike-like silicic intrusions within a mafic host; D) skialithic pillow ("*pillow within a pillow*"), with dark mafic core (1) surrounded by lighter hybrid zone (2) all within a felsic host (3); E) diversity of mafic enclaves within a silicic host ranging from large clasts with angular boundaries (1) and less mafic enclaves with sharp boundaries (2), to smaller partially hybridized enclaves with diffuse boundaries (3) and abundant small mafic clasts (in matrix); F) silicic pipe-like networks within intermediate host rocks; G) felsic-felsic magmatic mingling; H/I) mafic sheet-like intrusions with margins disaggregating into large pillows and enclaves.

## 2.2. The Mafic-Silicic Composite Zone (MSCZ)

The Austurhorn composite zone, containing juxtaposed mafic and silicic rock units, occupies the lowest structural levels exposed, from the base of Þúfuhraunstindur south to the Hvalnes peninsula, and north to Krossanes point (Fig. 2) where it is bound by the surrounding homogeneous granophyre and intrudes Neogene volcanic rocks. It comprises approximately 30-40% of the AIC in three main areas at the eastern margins of the intrusion (Mattson *et al.*, 1986; Furman *et al.*, 1992). The MSCZ contains abundant mafic to intermediate enclaves (clasts, pillows, tabular bodies) with cuspate, crenulated, or angular boundaries and entirely surrounded by silicic rock, zones of intermediate rock, and sheets of diabasic and basaltic rock. The enclave density within a given outcrop is highly variable, ranging from a few volume percent up to 60 %.

The margins of the MSCZ have been defined by Furman *et al.* (1992) to be where a silicic host rock bearing mafic blocks > 5 cm in dimension is in contact with Hvalnesfjall gabbro or Miocene volcanics, or where mafic blocks disappear abruptly without apparent change in the silicic matrix itself.

## 2.3. Current Views on Silicic Magma Petrogenesis at Austurhorn

Previous research has addressed the question of magmatic sources for AIC silicic magmas using a range of petrologic and geochemical approaches. However, interpretations differ, with some researchers advocating for the generation of silicic melts at Austurhorn dominantly by fractional crystallization ± assimilation (FC or AFC) of tholeiitic magmas (e.g. Furman *et al.*, 1992b, Bindeman *et al.,* 2012), and others favoring partial melting of altered and hydrated basaltic crust as the central mechanism for generating silicic melts (e.g. Martin & Sigmarsson, 2010). Furman *et al.* (1992b) argue the major element composition of plagioclase and clinopyroxene (Cpx) from mafic units (Hvalnesfjall gabbro and MSCZ mafic pillows) support detailed field relationships between mafic and silicic units indicating fractionation of tholeiitic basalts. Bindeman *et al.* (2012) provide bulk and *in situ* zircon oxygen isotopes from an Austurhorn silicic sample that reflect a homogeneous mantle-like signature, providing further support for an interpretation involving dominantly AFC processes. In contrast, Martin & Sigmarsson (2010) present oxygen isotope evidence for extensive crustal recycling from intermediate silicic samples of the AIC. They advocate partial melting of low-$\delta^{18}$O hydrated metabasaltic crust as the dominant source of low whole-rock $\delta^{18}$O values (-2.1 ‰ for a 53.6 wt.% $SiO_2$ sample; +0.5 ‰ for a 64.8 wt.% $SiO_2$ sample), corroborated by the presence of low-$\delta^{18}$O rhyolitic glass and clinopyroxene phenocrysts in Austurhorn samples.

While elemental geochemistry and oxygen isotopes can provide valuable insight toward discerning between fractional crystallization and crustal melting processes (e.g. Bindeman *et al.*, 2012), most previous studies of Austurhorn have focused on few samples (1 or 2) from what is a very diverse and complex intrusion, where it is challenging to find a silicic rock that is representative of the broad range of silicic compositions at Austurhorn. With this study, we build on previous work by others and expand the geochemical dataset available for the Austurhorn system. We present zircon isotopic and elemental data on samples from a comprehensive range of compositions (from gabbros to granophyres), working towards building a more representative geochemical dataset that will, in turn, allow us to more critically assess the sources and mechanism that contributed to the generation of silicic magmas throughout the lifetime of the Austurhorn magmatic system.

# 3. **Methods**

## 3.1. Fieldwork

Our research team spent 15 days investigating the Austurhorn complex, characterizing the diversity of silicic rock units, the distribution and abundance of mafic bodies within the MSCZ, and the contact relationships and the nature of interaction between all units (see section 4.1). Our study built upon field descriptions of the Austurhorn intrusive complex and MSCZ by Furman *et al.* (1992a,b) and Mattson *et al.* (1986). We collected 13 representative samples from well-exposed outcrops of the MSCZ and surrounding gabbro and granophyre units within the AIC (see Fig. 2 and Table 1 for locations and sample descriptions). Silicic samples within the MSCZ were selected to represent the range of textures, grain size and/or mafic phenocryst content, as well as the abundance of mafic material (pillows, enclaves, and/or clasts).

## 3.2. Whole-Rock Analyses

### *3.2.a. Petrography and Elemental Geochemistry*

We used thin-sections, prepared by Idaho Petrographics (Grangeville, ID), and a Zeiss Axioskop petrographic microscope at Vanderbilt University to examine and characterize the mineral assemblage and textural relations for each sample (Table 1). All samples were analyzed for major and trace element abundances (Table 2) by a combination of wavelength dispersive X-ray fluorescence (WD-XRF) and laser ablation inductively-coupled plasma-mass spectrometry (LA-ICP-MS) at the Michigan State University Geological Analytical Services Laboratory (East Lansing, MI). One sample (IA-G-5) was analyzed at the Peter Hooper GeoAnalytical Laboratory at Washington State University (WSU; Pullman, WA), where major elements were determined by WD-XRF and trace element concentrations were determined by solution ICP-MS. International reference materials *RGM-1*, *W-2*, *JA-2*, and *BHVO-1* were used for calibration and quality control.

Based on whole-rock major element compositions and Zr concentrations, we calculated model zircon saturation temperatures (ZSTs) for all samples using the formulation of Watson and Harrison (1983) as revised by Boehnke *et al.* (2013). The saturation equation requires the composition of a melt that was saturated in zircon, and we acknowledge that large uncertainties are introduced because whole-rock compositions do not strictly equal melt compositions, particularly with intrusive rocks. ZSTs provide minima for the initial temperature of the magma represented by the sample, unless inherited and/or accumulated zircon is relatively abundant which would increase calculated model temperatures. For most silicic rocks, calculated ZSTs are likely to be low by a modest amount, whereas for mafic whole-rock compositions ZSTs tend to severely underestimate the temperatures at which zircon actually saturates (e.g. Miller *et al.*, 2003, Harrison *et al.*, 2007; Boehnke *et al.*, 2013; Moecher *et al.*, 2014; McDowell *et al.*, 2014). Given these uncertainties, we use ZSTs as estimates to generally compare model magmatic temperatures for the silicic units of the Austurhorn system, and do not discuss mafic ZSTs.

### *3.2.b. Solution MC-ICP-MS Hf Isotope Analyses*

We determined whole-rock Hf isotopic compositions of AIC samples at the Radiogenic Isotope and Geochronology Laboratory (RIGL) at WSU (Pullman, WA) by solution-multi-collector (S-MC) ICP-MS (Table 3). Approximately 0.25 g of each powdered sample were dissolved in Teflon vessels in ~7 mL 10:1 HF:$HNO_3$, then immediately dried at 120°C to reduce silica. Following dry down, ~7 mL 10:1 HF:$HNO_3$ was added to the vessels and placed in steel-jacketed Parr bombs at 150°C for 5-7 days. The solutions were dried and re-dissolved overnight in a mixture of 6M $HCl/H_3BO_3$ to convert to chlorides and minimize production of fluoride species. Lastly, samples were dried and re-dissolved in 6M HCl in Parr bombs at 150°C for 24 hours, until sample solutions became clear.

Samples were then dissolved in a mixture of 1M HCl and 0.05M HF. High-field-strength elements (including Hf) were initially separated on single cation exchange columns loaded with AG 50W-X12 resin (200-400 mesh). Following the method of Patchett & Tatsumoto (1981), we eluted Hf at the beginning of the procedure in 1M HCl/0.05M HF. We then removed Ti from the Hf fraction in a second stage chemistry (a crucial step, as excess Ti has been shown to alter the measured Hf isotopic composition; Blichert-Toft *et al.*, 1997). Any remaining Yb and Lu in the Hf aliquot were removed in a third stage of column chemistry using 0.18 mL of AG 50W-X12 resin.

We re-dissolved the purified Hf aliquots in 2% $HNO_3$ to determine their isotopic compositions on the RIGL ThermoFinnigan Neptune MC-ICP-MS using an Aridus desolvating nebulizer for sample introduction. Samples and standards were analyzed as 25 ppb solutions. Mass fractionation was corrected using $^{179}Hf/^{177}Hf = 0.7325$ and all sample analyses were normalized using the Hf isotope reference material JMC-475 (accepted $^{176}Hf/^{177}Hf = 0.282161$; Blichert-Toft *et al.*, 1997). Analyses of JMC-475 were conducted during the course of this study and yield a mean $^{176}Hf/^{177}Hf$ of 0.282135 ± 7 (2SD; n=15). Present day $\varepsilon_{Hf}$ values were calculated using the CHUR parameters reported by Bouvier *et al.* (2008).

**Table 1**. Locations, descriptions, and petrography for samples collected from the AIC

| Sample[5]: | Location (UTM)[6]: | | Mafic bodies?[7] | Silicic Rel. Abundance[8] | Major[9] Mineral Phases (relative abundance) | Accessory[10] Mineral Phases |
|---|---|---|---|---|---|---|
| | Northing | Easting | | | | |
| IA-NS-1 | 524180 | 7146224 | none | 100 % | Qz (~30%), Afs+Pl (~60%), Amph (5-7%), Cpx (~7%), Bt (<2%), Alt (<2%) | FeTi, Zrc, Sph, Ap |
| IA-NS-2 | 524147 | 7146097 | 10 cm - 1 m | ~75 % | Qz (30-35%), Afs+Pl (40-45%), Amph (~10%), Bt (<1%), Alt (8-10%) | FeTi, Zrc, Sph, Ap |
| IA-NS-3 | 524101 | 7145946 | > 1m | 60-70 % | Pl (~75%), Cpx (~10%), Amph (<5%), Qz (<5%), Alt (5-10%) | FeTi, Zrc, Sph |
| IA-NS-4a | 522153 | 7144490 | 1-10 cm | ~95 % | Qz (~30%), Afs+Pl (~60%), Amph (<2%), Bt (<1%), Alt (<5%) | FeTi, Zrc, Sph |
| IA-NS-4b* | 522153 | 7144490 | none | 100 % | Qz (~45%), Afs+Pl (~50%), Alt (<5%) | FeTi, Zrc, Ap, ±Sph |
| IA-NS-5 | 522643 | 7142846 | 1 cm - 10 m | ~30 % | Qz (~35%), Afs+Pl (~45%), Bt (~5%), Amph (~5%), Alt (~15%) | FeTi, Zrc, Sph, Ap |
| IA-NS-6 | 522378 | 7142211 | > 1 m | ~50 % | Pl±Afs (75-80%), Cpx (~10%), Qz (~5%), Alt (10-15%) | FeTi, Zrc, Sph, Ap |
| IA-NS-7 | 522275 | 7142118 | none | 100 % | Qz (~20%), Pl+Afs (~45%), Amph (10-15%), Bt (5-10%), Alt (5-10%) | FeTi, Zrc, Sph |
| IA-NS-8 | 522087 | 7141856 | 1-10 cm | ~95 % | Qz (~35%), Pl (~50%), Alt (~10%) | FeTi, Zrc, Sph, Ap |
| IA-NS-9* | 522130 | 7144385 | none | 100 % | Qz (~45%), Afs+Pl (~45%), Alt (<5%), Amph (<5%) | FeTi, Zrc, Ap, ±Sph |
| IA-NS-10* | 522083 | 7144427 | none | 100 % | Qz (~45%), Afs+Pl (~45%), Alt (<5%), FeTi (<5%) | Zrc, Ap, ±Sph |
| IA-NS-12* | 522115 | 7144432 | none | 100 % | Qz (~35%), Afs+Pl (~45%), Amph (~10%), FeTi (<10%) | Zrc, Ap, ±Sph |
| IA-G-1 | 521924 | 7142080 | n/a | 0 % | Pl (~40%), FeTi (~10%), Cpx (~35%), Amph (<5%), Qz (<5%), Alt (<5%) | Zrc, Sph, Ap |
| IA-G-3 | 521149 | 7142996 | n/a | 0 % | Pl (~45%), Cpx (~30%), FeTi (15-20%), Amph (<5%), Alt (<5%) | Zr, Ap |
| IA-G-5 | 522402 | 7142368 | n/a | 0 % | Pl (~45%), FeTi (5-10%), Cpx (~35%), Amph (<5%), Qz (<5%), Alt (<5%) | Zrc, Ap, ±Sph |

---

[5] Asterisks denote HSG zone samples: processed for zircon extraction and U-Pb geochronology, but not discussed in this manuscript (see section 4.1)
[6] All coordinates were obtained using the World Geodetic System 1984 (WGS 84), Grid 28W
[7] Refers to non-continuous bodies of mafic material surrounded by silicic host (e.g. mafic pillows, enclaves, and clasts; "n/a" = not applicable for mafic units)
[8] Relative abundance of silicic (vs. mafic) material within the outcrop where the sample was collected
[9] Major Minerals: Qz = quartz; Kfs = alkali feldspar; Pl = plagioclase feldspar; Amph = amphibole; Cpx = clinopyroxene; Bt = biotite; Alt = alteration phases
[10] Accessory Minerals: FeTi = Fe-Ti oxides (e.g. magnetite, ilmenite); Zrc = zircon; Ti = titanite; Sph = sphene

**Table 2**. Major oxide and trace element compositions of rocks from the AIC

| | Sample[11]: | **NS-1** | **NS-2** | **NS-3** | **NS-4a** | **NS-5** | **NS-6** | **NS-7** | **NS-8** | **G-1** | **G-3** | **G-5** |
|---|---|---|---|---|---|---|---|---|---|---|---|---|
| Major Element Oxides (wt.%)[12] | $SiO_2$ | 72.4 | 70.6 | 63.6 | 70.4 | 70.3 | 61.1 | 64.9 | 71.5 | 47.3 | 47.5 | 47.7 |
| | $TiO_2$ | 0.31 | 0.65 | 1.1 | 0.39 | 0.54 | 1.4 | 0.87 | 0.41 | 4.1 | 1.8 | 2.0 |
| | $Al_2O_3$ | 13.5 | 13.0 | 15.7 | 13.5 | 14.3 | 14.7 | 15.0 | 14.3 | 13.0 | 19.9 | 19.3 |
| | $Fe_2O_3$ | 3.6 | 4.5 | 6.4 | 5.0 | 3.9 | 7.8 | 7.1 | 3.6 | 16.4 | 10.0 | 9.5 |
| | MnO | 0.07 | 0.09 | 0.13 | 0.15 | 0.06 | 0.14 | 0.15 | 0.03 | 0.27 | 0.11 | 0.14 |
| | MgO | 0.11 | 0.91 | 1.3 | 0.12 | 0.53 | 2.4 | 0.92 | 0.21 | 4.3 | 4.4 | 6.2 |
| | CaO | 0.96 | 2.1 | 3.2 | 1.6 | 1.8 | 5.5 | 2.7 | 0.83 | 8.9 | 13.1 | 12.2 |
| | $Na_2O$ | 5.1 | 4.4 | 5.2 | 5.3 | 4.2 | 4.4 | 5.3 | 5.7 | 3.5 | 2.7 | 2.5 |
| | $K_2O$ | 3.9 | 3.7 | 3.2 | 3.4 | 4.3 | 2.5 | 2.8 | 3.3 | 0.89 | 0.37 | 0.31 |
| | $P_2O_5$ | 0.03 | 0.07 | 0.28 | 0.06 | 0.10 | 0.18 | 0.24 | 0.06 | 1.4 | 0.08 | 0.24 |
| | LOI (%) | 1.18 | 2.16 | 1.99 | 2.43 | 1.77 | 2.05 | 1.79 | 2.62 | 2.97 | 2.06 | -- |
| Trace Element Concentrations (ppm) | *Ni* | 1 | 8 | 3 | 1 | 2 | 17 | 1 | -- | 1 | 55 | 94 |
| | *Cu* | 10 | 14 | 23 | 4 | 5 | 26 | 10 | 7 | 33 | 147 | 64 |
| | *Zn* | 107 | 102 | 90 | 135 | 34 | 110 | 79 | 25 | 133 | 55 | 81 |
| | *Rb* | 74 | 77 | 51 | 63 | 76 | 40 | 51 | 45 | 16 | 5.0 | 4.7 |
| | *Sr* | 90 | 96 | 207 | 146 | 136 | 253 | 243 | 125 | 410 | 462 | 454 |
| | *Y* | 109 | 106 | 77 | 101 | 83 | 77 | 88 | 77 | 56 | 15 | 23 |
| | *Zr* | 874 | 586 | 1213 | 889 | 607 | 593 | 1037 | 816 | 214 | 69 | 124 |
| | *Nb* | 107 | 95 | 58 | 90 | 69 | 52 | 54 | 74 | 24 | 4.7 | 13 |
| | *Ba* | 886 | 481 | 763 | 631 | 669 | 440 | 552 | 662 | 158 | 82 | 84 |
| | *V* | 10 | 74 | 44 | 3.4 | 28 | 143 | 15 | 7.3 | 219 | 355 | 233 |
| | *Cr* | 2.1 | 18 | 3.2 | 0.54 | 1.2 | 31 | 0.53 | 1.7 | 1.8 | 44 | 108 |
| | **La** | 76 | 70 | 57 | 69 | 63 | 52 | 57 | 66 | 26 | 7.4 | 13 |
| | **Ce** | 205 | 172 | 127 | 174 | 154 | 116 | 128 | 168 | 60 | 16 | 29 |
| | **Pr** | 22 | 19 | 16 | 20 | 17 | 15 | 16 | 18 | 9.4 | 2.2 | 4.0 |
| | **Nd** | 87 | 77 | 65 | 79 | 66 | 61 | 69 | 69 | 48 | 10 | 18 |
| | **Sm** | 20 | 18 | 15 | 18 | 14 | 14 | 16 | 14 | 13 | 2.7 | 4.8 |
| | **Eu** | 3.9 | 2.7 | 4.1 | 3.9 | 2.4 | 3.5 | 4.9 | 3.0 | 4.6 | 1.3 | 1.8 |
| | **Gd** | 20 | 18 | 15 | 18 | 15 | 14 | 17 | 14 | 13 | 3.0 | 5.1 |
| | **Tb** | 3.4 | 3.2 | 2.5 | 3.2 | 2.4 | 2.4 | 2.8 | 2.3 | 2.0 | 0.47 | 0.83 |
| | **Dy** | 20 | 19 | 14 | 18 | 14 | 14 | 16 | 13 | 11 | 2.7 | 4.9 |
| | **Ho** | 4.0 | 3.9 | 2.8 | 3.7 | 2.9 | 2.8 | 3.2 | 2.7 | 2.0 | 0.53 | 0.95 |
| | **Er** | 11 | 11 | 7.8 | 10 | 8.2 | 7.6 | 8.9 | 7.5 | 5.1 | 1.4 | 2.3 |
| | **Yb** | 10 | 10 | 8.0 | 10.0 | 8.1 | 7.2 | 8.6 | 7.4 | 4.0 | 1.1 | 1.8 |
| | **Lu** | 1.6 | 1.5 | 1.2 | 1.5 | 1.2 | 1.1 | 1.3 | 1.1 | 0.57 | 0.16 | 0.28 |
| | *Hf* | 21 | 18 | 28 | 23 | 17 | 15 | 24 | 20 | 6.1 | 2.0 | 3.3 |
| | *Ta* | 6.2 | 6.4 | 3.5 | 5.4 | 4.6 | 3.4 | 3.5 | 4.6 | 1.8 | 0.33 | 0.86 |
| | *Pb* | 15 | 7.1 | 3.6 | 6.7 | 11 | 5.8 | 3.6 | 7.3 | 1.5 | 0.91 | 1.1 |
| | *Th* | 9.2 | 9.6 | 7.2 | 8.6 | 10 | 5.7 | 6.0 | 9.5 | 1.8 | 0.98 | 1.0 |
| | *U* | 6.4 | 4.7 | 3.0 | 3.9 | 4.7 | 1.9 | 2.2 | 4.6 | 0.56 | 0.31 | 0.33 |
| | Zr-Temp[13] (ºC) | 945 | 886 | 951 | 933 | 905 | 836 | 939 | 942 | 652 | 616 | 660 |

---

[11] All sample names preceded by the label "IA-" (e.g. "NS-1" = IA-NS-1)

[12] Anhydrous basis, normalized

[13] Zircon Saturation Temperature: calculated using the formula of Watson & Harrison (1983) (see Section 3.2.a)

## 3.3. Zircon and Imaging

### *3.3.a. Separation and Imaging*

We separated individual zircon grains from bulk-rock samples at Vanderbilt University, starting with 1-2 kg of each sample. To concentrate zircon grains, we followed standard separation techniques, including crushing, milling, sieving, density separation by water and heavy liquid (lithium heteropolytungstates in water; LST, $\rho \approx 2.8$ g/mL), separation by magnetic susceptibility (Frantz Isodynamic Magnetic Separator), and hand-picking individual zircon grains from the heavy separate fraction under a stereoscope.

The selected zircon grains were mounted in epoxy resin, polished to expose interiors, and imaged by reflected light, using a stereoscope, and cathodoluminescence (CL) using a Tescan Vega 3 LM variable pressure scanning electron microscope (SEM) at Vanderbilt University or a JEOL JSM 5600 SEM at the Stanford-USGS Micro Analytical Center (SUMAC). Zircon reflected light (RL) and CL images were our primary guides in selecting the location of spots on individual grains for ion microprobe analyses.

### *3.3.b. U-Pb Age and Trace Element Analyses*

We measured zircon trace element concentrations and U-Pb isotopes *in situ* using the SUMAC sensitive high-resolution ion microprobe reverse geometry (SHRIMP-RG), using a 1.5-2.5 nA $O_2^-$ ion primary beam with an analytical spot diameter of ~15 μm and sputter depth of ~1 μm for trace elements, and a 5.0-6.8 nA $O_2^-$ ion beam with a spot diameter of ~25 μm and sputter depth of ~2-3 μm for U-Pb analyses. Calculated model U-Pb ages are standardized relative to R33 zircon (419±1 Ma, Black *et al.*, 2004), which were analyzed repeatedly throughout the duration of the analytical session. All data were reduced using the Microsoft Excel add-in program Squid2.51 (Ludwig, 2009), and we report U-Pb ages with 2σ uncertainty, corrected for common lead ($^{207}$Pb, assuming concordance) and thorium ($^{230}$Th) disequilibrium using the Th/U ratio of each respective whole-rock sample as the assumed magma value (for full U-Pb isotope compositions, see Appendix B.1). We analyzed a large suite of trace elements, with particular emphasis on Ti for thermometry (see below), and U, Th, Hf, and the rare earth elements (REE) for evaluating magma evolution and characterizing zircon populations (Table 4; for full trace element compositions, see Appendix B.2-B.4). Trace element concentrations were standardized relative to well-characterized, homogeneous zircon standards MAD and MADDER (Barth & Wooden, 2010) following methods outlined by Grimes *et al.* (2007) and Claiborne *et al.* (2006, 2010b).

We apply the Ti-in-zircon thermometer of Ferry & Watson (2007) to estimate the range of crystallization temperatures for AIC zircons. Using this method, the accuracy of model crystallization temperatures relies on having accurate Ti measurements in zircon as well as good constraints for the activity of $TiO_2$ (rutile saturation: $a_{TiO_2} = 1$) and $SiO_2$ (quartz saturation: $a_{SiO_2} = 1$) in the magmas from which zircon grew.

The external errors (1σ SE) for Ti concentrations in AIC zircons measured by SHRIMP-RG range from ±2.1 to ±4.8 % (errors decrease with increasing Ti concentrations). Assuming uncertainties for $a_{SiO_2}$ and $a_{TiO_2}$ on the order of ±0.05 and ±0.1, these external errors introduce uncertainties on the order of ± 25-44 °C for a range of ~5-40 ppm Ti, the observed range of AIC zircons (see Table 4). Recent work by Ghiorso and Gualda (2013) suggests a likely range of $a_{TiO_2}$ for silicic magmas of 0.3-0.9. They infer that $a_{TiO_2}$ increases systematically with decreasing temperature during crystallization of magmas such that the difference between the maximum and minimum model Ti-in-zircon temperatures is likely to be an underestimate of the true range of crystallization temperatures. For melts saturated in Fe-Ti oxide phases, $a_{\mathrm{TiO_2}}$ is unlikely to vary substantially during crystallization (by more than a few tenths), thus allowing us to hold $a_{\mathrm{TiO_2}}$ constant in our calculations and make comparisons between model Ti-in-zircon crystallization temperatures, as well as identify any statistically significant temperature fluctuations in the lifetime of a magma or magmatic system as recorded by zircons (Ghiorso & Gualda 2013; see also McDowell *et al.*, 2014; Pamukcu *et al.,* 2013; Claiborne *et al.*, 2006).

In most silicic rocks from the AIC, Fe-Ti oxides (e.g. ilmenite and titanite) are coexisting accessory phases with zircon (see Table 1), and we can thus reasonably assume that $a_{\mathrm{TiO_2}}$ is relatively high (probably $\geq 0.5$) during zircon crystallization, and the absence of rutile in all Austurhorn rocks indicates that $a_{\mathrm{TiO_2}} < 1$. Furthermore, while some zircon crystallization may have occurred prior to quartz saturation, high silica concentrations in almost all samples and typical abundance of quartz suggests that zircon crystallization occurred at or near silica saturation ($a_{\mathrm{SiO_2}} = 1$). We infer that the zircon in the gabbro samples also crystallized in highly evolved melt pockets in which $a_{\mathrm{SiO_2}}$ was also high. Using these constraints, we assume uniform values of $a_{\mathrm{TiO_2}} = 0.5$ and $a_{\mathrm{SiO_2}} = 1.0$ in our estimates of model zircon crystallization temperatures (e.g. McDowell *et al.*, 2014).

**Table 3**. Whole-rock Hf isotope compositions, measured by Solution MC-ICP-MS

| **Sample** | **$^{176}$Hf/$^{177}$Hf** | **2SE** | **$^{178}$Hf/$^{177}$Hf** | **2SE** | **$^{180}$Hf/$^{177}$Hf** | **2SE** | **$\varepsilon_{Hf}$** | **2SE** |
|---|---|---|---|---|---|---|---|---|
| IA-NS-2 | 0.283140 | 7.0E+0 | 1.467182 | 1.1E+1 | 1.886801 | 2.6E+1 | **12.6** | **0.3** |
| IA-NS-6 | 0.283161 | 8.0E+0 | 1.467184 | 1.6E+1 | 1.886733 | 3.2E+1 | **13.3** | **0.3** |
| IA-NS-7 | 0.283182 | 5.8E+0 | 1.467189 | 9.9E+0 | 1.886814 | 1.6E+1 | **14.0** | **0.2** |
| IA-G-1 | 0.283138 | 6.3E+0 | 1.467179 | 9.7E+0 | 1.886861 | 2.1E+1 | **12.5** | **0.2** |
| IA-G-5 | 0.283128 | 7.3E+0 | 1.467163 | 1.5E+1 | 1.886663 | 2.2E+1 | **12.1** | **0.3** |

**Table 4**. Trace element compositions[14] of zircons from the AIC (summary)

| Sample Spot | P | Sc | Ti | Fe | Y | Nb | Hf | Th | U | Temp. (ºC) [15] |
|---|---|---|---|---|---|---|---|---|---|---|
| **IA-NS-2 (Granophyre)** | | | | | | | | | | |
| IA-NS-2_1.1 | 192 | 7.9 | 9.1 | 0.4 | 851 | 5.0 | 11074 | 17 | 50 | 772 |
| IA-NS-2_2.1 | 389 | 13 | 24 | 0.3 | 2260 | 5.9 | 8236 | 34 | 59 | 878 |
| IA-NS-2_3.1 | 1661 | 18 | 8.5 | 0.3 | 7733 | 108 | 10636 | 351 | 439 | 765 |
| IA-NS-2_4.1 | 272 | 1.7 | 9.1 | 0.9 | 1849 | 28 | 8384 | 53 | 107 | 771 |
| IA-NS-2_4.2 | 266 | 2.0 | 7.3 | 0.4 | 2888 | 15 | 8863 | 58 | 114 | 750 |
| IA-NS-2_4.3 | 482 | 2.3 | 6.2 | 0.5 | 2743 | 87 | 10129 | 158 | 290 | 734 |
| IA-NS-2_5.1 | 1276 | 62 | 14 | 0.4 | 12914 | 51 | 8339 | 1042 | 841 | 816 |
| IA-NS-2_5.2 | 333 | 2.7 | 6.4 | 0.3 | 2826 | 36 | 9633 | 62 | 147 | 738 |
| IA-NS-2_6.1 | 985 | 9.1 | 11 | 0.4 | 5963 | 224 | 10204 | 887 | 719 | 789 |
| IA-NS-2_7.1 | 290 | 9.2 | 15 | 0.4 | 945 | 10 | 9107 | 28 | 55 | 821 |
| IA-NS-2_8.1 | 1472 | 17 | 14 | 3.8 | 6280 | 206 | 11028 | 768 | 695 | 815 |
| IA-NS-2_9.1 | 1263 | 21 | 11 | 0.2 | 4419 | 95 | 11882 | 552 | 508 | 789 |
| IA-NS-2_10.1 | 889 | 18 | 10.0 | 4.2 | 4905 | 64 | 11984 | 862 | 1118 | 780 |
| IA-NS-2_10.2 | 918 | 9.5 | 6.3 | 0.3 | 6891 | 24 | 11551 | 656 | 878 | 736 |
| IA-NS-2_11.1 | 297 | 1.6 | 5.9 | 0.3 | 4072 | 27 | 8720 | 101 | 177 | 730 |
| IA-NS-2_11.2 | 988 | 15 | 10 | 16 | 5074 | 299 | 13044 | 625 | 819 | 785 |
| IA-NS-2_12.1 | 351 | 3.3 | 7.6 | 0.3 | 3277 | 24 | 8552 | 75 | 136 | 753 |
| IA-NS-2_12.2 | 387 | 1.9 | 7.2 | 2.6 | 4548 | 31 | 8809 | 119 | 200 | 748 |
| IA-NS-2_13.1 | 712 | 4.5 | 11 | 19 | 7074 | 106 | 9548 | 436 | 454 | 793 |
| IA-NS-2_14.1 | 646 | 4.0 | 9.0 | 8.7 | 3713 | 130 | 9749 | 406 | 529 | 770 |
| IA-NS-2_14.2 | 607 | 2.3 | 6.6 | 0.5 | 7361 | 78 | 8469 | 263 | 381 | 741 |
| IA-NS-2_15.1 | 441 | 2.5 | 9.6 | 0.4 | 4519 | 67 | 8069 | 156 | 263 | 777 |
| IA-NS-2_15.2 | 354 | 2.8 | 7.9 | 0.4 | 1652 | 40 | 9744 | 93 | 159 | 757 |
| IA-NS-2_16.1 | 240 | 2.1 | 7.1 | 0.6 | 1398 | 40 | 9307 | 31 | 99 | 747 |
| IA-NS-2_16.2 | 290 | 0.9 | 10 | 4.3 | 3570 | 29 | 8676 | 94 | 166 | 784 |
| IA-NS-2_17.1 | 363 | 2.0 | 6.7 | 0.3 | 1942 | 46 | 9409 | 68 | 145 | 742 |
| IA-NS-2_17.2 | 1293 | 14 | 7.8 | 0.4 | 13749 | 145 | 10055 | 740 | 774 | 756 |
| IA-NS-2_18.1 | 386 | 1.9 | 6.1 | 0.3 | 4383 | 32 | 9094 | 131 | 212 | 733 |
| IA-NS-2_18.2 | 489 | 2.7 | 7.1 | 0.3 | 2989 | 78 | 9713 | 113 | 221 | 747 |
| IA-NS-2_19.1 | 419 | 2.8 | 6.9 | 0.4 | 2701 | 63 | 9149 | 76 | 166 | 745 |
| IA-NS-2_19.2 | 491 | 1.7 | 6.3 | 0.9 | 5784 | 49 | 8995 | 185 | 308 | 736 |
| IA-NS-2_20.1 | 360 | 2.0 | 7.3 | 6.9 | 4165 | 27 | 8762 | 100 | 167 | 749 |
| IA-NS-2_21.1 | 628 | 3.4 | 6.1 | 2.1 | 3478 | 89 | 9680 | 184 | 299 | 733 |
| IA-NS-2_21.2 | 425 | 2.3 | 8.2 | 10 | 4490 | 36 | 8650 | 135 | 211 | 761 |
| IA-NS-2_22.1 | 151 | 1.9 | 8.9 | 0.2 | 1829 | 6.6 | 8245 | 32 | 69 | 769 |
| IA-NS-2_23.1 | 290 | 2.5 | 7.4 | 0.3 | 1729 | 28 | 8792 | 40 | 94 | 751 |
| IA-NS-2_23.2 | 1452 | 8.1 | 13 | 3.3 | 11495 | 312 | 8828 | 1290 | 987 | 809 |
| IA-NS-2_24.1 | 283 | 1.8 | 7.3 | 0.5 | 2990 | 16 | 8829 | 62 | 119 | 749 |
| IA-NS-2_24.2 | 1022 | 11 | 11 | 0.2 | 5570 | 151 | 10043 | 513 | 606 | 791 |
| IA-NS-2_25.1 | 2565 | 22 | 24 | 384 | 11923 | 275 | 10570 | 1119 | 841 | 877 |
| IA-NS-2_25.2 | 684 | 5.2 | 6.1 | 5.9 | 3045 | 146 | 12820 | 235 | 461 | 733 |
| **IA-NS-6 (Diorite)** | | | | | | | | | | |
| IA-NS-6_1.1 | 417 | 3.2 | 10 | 0.4 | 2098 | 35 | 8638 | 108 | 162 | 784 |
| IA-NS-6_2.1 | 2309 | 63 | 15 | 0.6 | 17041 | 83 | 7161 | 1072 | 956 | 824 |
| IA-NS-6_3.1 | 2498 | 61 | 13 | 0.5 | 17707 | 82 | 7708 | 1082 | 898 | 810 |
| IA-NS-6_4.1 | 1617 | 86 | 20 | 0.4 | 11322 | 40 | 7240 | 500 | 449 | 855 |

---

[14] All values reported in parts per million (ppm), unless otherwise stated

[15] Model zircon crystallization temperatures (for details see Chapter III, section 3.3.b)

**Table 4**. Continued

| **Sample Spot** | **La** | **Ce** | **Nd** | **Sm** | **Eu** | **Gd** | **Tb** | **Dy** | **Ho** | **Er** | **Tm** | **Yb** | **Lu** |
|---|---|---|---|---|---|---|---|---|---|---|---|---|---|
| **IA-NS-2 (Granophyre)** | | | | | | | | | | | | | |
| IA-NS-2_1.1 | 0.02 | 12 | 0.5 | 1.9 | 0.5 | 21 | 7.9 | 90 | 36 | 165 | 33 | 259 | 45 |
| IA-NS-2_2.1 | 0.06 | 9.0 | 4.0 | 10 | 4.0 | 87 | 28 | 282 | 98 | 392 | 73 | 566 | 95 |
| IA-NS-2_3.1 | 0.09 | 150 | 9.0 | 23 | 3.7 | 217 | 76 | 836 | 321 | 1334 | 256 | 1954 | 312 |
| IA-NS-2_4.1 | 0.04 | 31 | 2.3 | 5.9 | 2.0 | 59 | 20 | 220 | 80 | 318 | 61 | 433 | 68 |
| IA-NS-2_4.2 | 0.04 | 21 | 4.8 | 10 | 2.8 | 95 | 32 | 346 | 127 | 512 | 90 | 651 | 104 |
| IA-NS-2_4.3 | 0.02 | 56 | 1.9 | 7.1 | 1.4 | 72 | 28 | 309 | 115 | 482 | 91 | 649 | 98 |
| IA-NS-2_5.1 | 0.27 | 201 | 30.8 | 70 | 7.4 | 537 | 166 | 1613 | 540 | 2020 | 370 | 2602 | 393 |
| IA-NS-2_5.2 | 0.02 | 46 | 2.7 | 7.6 | 1.8 | 80 | 28 | 311 | 116 | 477 | 89 | 626 | 99 |
| IA-NS-2_6.1 | 0.04 | 290 | 6.7 | 19 | 3.8 | 194 | 65 | 693 | 262 | 1002 | 189 | 1347 | 211 |
| IA-NS-2_7.1 | 0.01 | 12 | 1.0 | 2.7 | 1.2 | 26 | 9.4 | 101 | 40 | 172 | 34 | 256 | 44 |
| IA-NS-2_8.1 | 0.32 | 280 | 7.9 | 21 | 3.9 | 203 | 68 | 737 | 274 | 1097 | 207 | 1521 | 238 |
| IA-NS-2_9.1 | 0.02 | 151 | 4.2 | 13 | 2.7 | 129 | 46 | 505 | 187 | 763 | 147 | 1083 | 175 |
| IA-NS-2_10.1 | 0.02 | 178 | 4.3 | 12 | 1.5 | 120 | 43 | 488 | 196 | 849 | 175 | 1372 | 224 |
| IA-NS-2_10.2 | 0.08 | 100 | 9.2 | 20 | 2.4 | 189 | 65 | 742 | 282 | 1224 | 246 | 1878 | 311 |
| IA-NS-2_11.1 | 0.06 | 36 | 5.8 | 14 | 3.5 | 137 | 46 | 495 | 182 | 715 | 126 | 885 | 139 |
| IA-NS-2_11.2 | 0.29 | 151 | 3.7 | 11 | 1.6 | 116 | 45 | 526 | 208 | 862 | 170 | 1283 | 200 |
| IA-NS-2_12.1 | 0.06 | 29 | 4.3 | 10 | 2.9 | 107 | 35 | 374 | 141 | 560 | 101 | 695 | 111 |
| IA-NS-2_12.2 | 0.07 | 39 | 6.3 | 16 | 4.3 | 161 | 52 | 557 | 203 | 792 | 141 | 1003 | 154 |
| IA-NS-2_13.1 | 0.86 | 141 | 11.7 | 29 | 8.4 | 267 | 83 | 859 | 305 | 1146 | 201 | 1423 | 215 |
| IA-NS-2_14.1 | 0.22 | 96 | 3.1 | 9.9 | 1.9 | 100 | 36 | 410 | 157 | 615 | 119 | 844 | 128 |
| IA-NS-2_14.2 | 0.08 | 117 | 10.2 | 28 | 5.8 | 268 | 90 | 960 | 349 | 1371 | 244 | 1698 | 253 |
| IA-NS-2_15.1 | 0.04 | 85 | 6.8 | 16 | 4.9 | 160 | 55 | 548 | 199 | 781 | 137 | 965 | 145 |
| IA-NS-2_15.2 | 0.03 | 36 | 1.7 | 4.6 | 1.1 | 47 | 17 | 186 | 71 | 287 | 56 | 408 | 66 |
| IA-NS-2_16.1 | 0.23 | 25 | 1.4 | 3.7 | 0.9 | 38 | 14 | 156 | 59 | 260 | 51 | 384 | 64 |
| IA-NS-2_16.2 | 0.57 | 34 | 5.5 | 12 | 3.4 | 123 | 41 | 436 | 159 | 632 | 113 | 786 | 120 |
| IA-NS-2_17.1 | 0.02 | 43 | 2.1 | 5.6 | 1.3 | 56 | 20 | 226 | 84 | 343 | 65 | 470 | 73 |
| IA-NS-2_17.2 | 0.18 | 301 | 25.5 | 60 | 9.2 | 533 | 170 | 1775 | 625 | 2362 | 421 | 2920 | 432 |
| IA-NS-2_18.1 | 0.03 | 45 | 6.6 | 14 | 3.7 | 151 | 50 | 533 | 198 | 769 | 138 | 955 | 151 |
| IA-NS-2_18.2 | 0.03 | 74 | 3.0 | 8.2 | 1.9 | 87 | 32 | 358 | 130 | 537 | 98 | 726 | 112 |
| IA-NS-2_19.1 | 0.03 | 62 | 2.9 | 7.5 | 1.8 | 74 | 27 | 305 | 115 | 463 | 88 | 627 | 96 |
| IA-NS-2_19.2 | 0.25 | 64 | 7.9 | 19 | 4.2 | 190 | 65 | 704 | 256 | 1009 | 180 | 1232 | 190 |
| IA-NS-2_20.1 | 0.10 | 33 | 6.2 | 15 | 3.9 | 142 | 49 | 518 | 184 | 727 | 131 | 920 | 144 |
| IA-NS-2_21.1 | 31 | 184 | 44.8 | 21 | 2.7 | 116 | 38 | 404 | 144 | 580 | 107 | 761 | 117 |
| IA-NS-2_21.2 | 0.08 | 50 | 6.6 | 16 | 4.2 | 159 | 51 | 556 | 199 | 765 | 138 | 972 | 151 |
| IA-NS-2_22.1 | 0.02 | 12 | 3.8 | 8.2 | 2.9 | 68 | 22 | 229 | 84 | 332 | 59 | 413 | 67 |
| IA-NS-2_23.1 | 0.04 | 32 | 2.0 | 5.1 | 1.5 | 51 | 18 | 198 | 77 | 307 | 57 | 414 | 68 |
| IA-NS-2_23.2 | 44 | 502 | 73.4 | 63 | 12 | 463 | 144 | 1449 | 508 | 1898 | 333 | 2308 | 341 |
| IA-NS-2_24.1 | 0.07 | 22 | 4.8 | 10 | 2.8 | 96 | 33 | 355 | 132 | 519 | 94 | 669 | 105 |
| IA-NS-2_24.2 | 0.04 | 171 | 5.9 | 16 | 2.5 | 171 | 63 | 684 | 242 | 998 | 184 | 1338 | 209 |
| IA-NS-2_25.1 | 27 | 554 | 57.0 | 56 | 10 | 433 | 140 | 1467 | 522 | 2042 | 374 | 2715 | 418 |
| IA-NS-2_25.2 | 1.00 | 68 | 2.6 | 5.8 | 0.9 | 68 | 28 | 335 | 129 | 567 | 109 | 826 | 130 |
| **IA-NS-6 (Diorite)** | | | | | | | | | | | | | |
| IA-NS-6_1.1 | 0.02 | 38 | 2.4 | 6.5 | 2.0 | 66 | 22 | 238 | 88 | 355 | 68 | 486 | 76 |
| IA-NS-6_2.1 | 0.37 | 528 | 45.6 | 92 | 14 | 697 | 214 | 2122 | 731 | 2741 | 493 | 3405 | 507 |
| IA-NS-6_3.1 | 0.37 | 495 | 39.1 | 83 | 12 | 670 | 209 | 2121 | 733 | 2796 | 520 | 3667 | 530 |
| IA-NS-6_4.1 | 0.30 | 184 | 40.9 | 78 | 21 | 549 | 160 | 1522 | 490 | 1761 | 309 | 2120 | 299 |

**Table 4**. Continued

| Sample Spot | P | Sc | Ti | Fe | Y | Nb | Hf | Th | U | Temp. (ºC) |
|---|---|---|---|---|---|---|---|---|---|---|
| **IA-NS-6 (continued)** | | | | | | | | | | |
| IA-NS-6_5.1 | 1423 | 41 | 13 | 0.7 | 11160 | 208 | 9165 | 1590 | 1306 | 803 |
| IA-NS-6_6.1 | 441 | 2.1 | 11 | 0.3 | 3628 | 89 | 8191 | 324 | 367 | 788 |
| IA-NS-6_7.1 | 211 | 2.2 | 8.0 | 0.3 | 1473 | 39 | 8431 | 24 | 95 | 759 |
| IA-NS-6_9.1 | 2150 | 53 | 15 | 0.4 | 15701 | 74 | 8501 | 1182 | 906 | 824 |
| IA-NS-6_10.1 | 813 | 30 | 16 | 0.3 | 4097 | 58 | 9056 | 497 | 554 | 826 |
| IA-NS-6_12.1 | 206 | 1.2 | 6.7 | 0.5 | 2326 | 12 | 8730 | 40 | 87 | 742 |
| IA-NS-6_13.1 | 2187 | 68 | 41 | 0.3 | 11708 | 207 | 7641 | 3199 | 1810 | 944 |
| IA-NS-6_15.1 | 1349 | 46 | 14 | 0.4 | 9679 | 42 | 7834 | 512 | 526 | 816 |
| IA-NS-6_16.1 | 902 | 48 | 23 | 0.3 | 6125 | 18 | 8466 | 294 | 302 | 870 |
| IA-NS-6_17.1 | 562 | 26 | 15 | 6.6 | 4265 | 15 | 8158 | 320 | 374 | 825 |
| IA-NS-6_17.2 | 1845 | 62 | 15 | 0.3 | 13992 | 60 | 7880 | 793 | 686 | 822 |
| IA-NS-6_18.1 | 578 | 33 | 16 | 5.6 | 1372 | 8.9 | 8772 | 34 | 72 | 832 |
| IA-NS-6_18.2 | 213 | 1.8 | 7.2 | 0.5 | 2156 | 9.9 | 8665 | 42 | 80 | 749 |
| IA-NS-6_19.1 | 1918 | 66 | 19 | 0.4 | 14369 | 60 | 7728 | 964 | 777 | 848 |
| IA-NS-6_20.2 | 1329 | 52 | 23 | 0.5 | 9805 | 38 | 8730 | 513 | 442 | 871 |
| IA-NS-6_21.1 | 219 | 2.4 | 10 | 0.3 | 1409 | 28 | 8218 | 50 | 107 | 782 |
| IA-NS-6_22.1 | 165 | 2.0 | 7.7 | 0.4 | 1430 | 12 | 8719 | 40 | 89 | 754 |
| IA-NS-6_22.2 | 454 | 35 | 21 | 0.4 | 1635 | 12 | 8476 | 49 | 93 | 861 |
| IA-NS-6_23.1 | 274 | 4.2 | 15 | 2.8 | 1693 | 18 | 7702 | 79 | 114 | 826 |
| IA-NS-6_24.1 | 305 | 19 | 18 | 0.2 | 1779 | 8.2 | 8668 | 43 | 80 | 846 |
| IA-NS-6_24.2 | 303 | 1.5 | 13 | 113 | 3904 | 40 | 8221 | 93 | 156 | 811 |
| IA-NS-6_24.3 | 259 | 2.5 | 10.0 | 1.2 | 1410 | 19 | 8627 | 35 | 81 | 780 |
| IA-NS-6_26.1 | 1693 | 48 | 13 | 0.4 | 14934 | 73 | 8056 | 1088 | 993 | 806 |
| **IA-NS-7 (Granodiorite)** | | | | | | | | | | |
| IA-NS-7_1.1 | 509 | 36 | 18 | 3.0 | 4901 | 12 | 7926 | 133 | 190 | 842 |
| IA-NS-7_2.1 | 2063 | 46 | 17 | 3.8 | 14503 | 453 | 10290 | 3769 | 2992 | 835 |
| IA-NS-7_3.1 | 1937 | 66 | 20 | 4.6 | 11321 | 279 | 6789 | 1098 | 1342 | 857 |
| IA-NS-7_4.1 | 267 | 35 | 14 | 3.0 | 1899 | 4.6 | 8196 | 35 | 73 | 815 |
| IA-NS-7_4.2 | 1302 | 40 | 14 | 3.0 | 6497 | 153 | 7180 | 1000 | 1093 | 819 |
| IA-NS-7_5.1 | 765 | 89 | 19 | 3.1 | 7789 | 22 | 7411 | 258 | 284 | 851 |
| IA-NS-7_6.1 | 741 | 15 | 6.5 | 25 | 12165 | 90 | 15425 | 3606 | 3230 | 739 |
| IA-NS-7_7.1 | 275 | 32 | 13 | 108 | 1870 | 8.0 | 8366 | 47 | 81 | 809 |
| IA-NS-7_8.1 | 476 | 43 | 16 | 3.0 | 4291 | 8.9 | 8146 | 108 | 163 | 831 |
| IA-NS-7_8.2 | 1472 | 86 | 18 | 3.1 | 8984 | 239 | 7162 | 1305 | 1270 | 840 |
| IA-NS-7_9.1 | 1587 | 56 | 9.4 | 3.5 | 13451 | 82 | 6353 | 523 | 704 | 774 |
| IA-NS-7_10.1 | 2350 | 84 | 29 | 3.6 | 15246 | 394 | 6127 | 2682 | 2243 | 899 |
| IA-NS-7_11.1 | 459 | 45 | 17 | 130 | 3752 | 12 | 8042 | 99 | 156 | 839 |
| IA-NS-7_11.2 | 2455 | 19 | 15 | 32 | 15666 | 718 | 13324 | 5164 | 5933 | 825 |
| IA-NS-7_12.1 | 1861 | 104 | 37 | 3.5 | 12385 | 299 | 6807 | 2247 | 1684 | 930 |
| IA-NS-7_12.2 | 1830 | 78 | 27 | 4.6 | 11714 | 254 | 6986 | 2430 | 1763 | 890 |
| IA-NS-7_13.1 | 1179 | 34 | 9.3 | 4.1 | 9942 | 58 | 7550 | 482 | 606 | 773 |
| IA-NS-7_13.2 | 954 | 42 | 20 | 2.9 | 8564 | 24 | 7323 | 306 | 316 | 856 |
| IA-NS-7_14.1 | 474 | 26 | 17 | 2.9 | 4247 | 9.4 | 7923 | 117 | 178 | 839 |
| IA-NS-7_15.1 | 2586 | 51 | 9.2 | 3.8 | 20787 | 107 | 8825 | 1444 | 1331 | 772 |
| IA-NS-7_16.1 | 423 | 42 | 17 | 3.4 | 3982 | 7.4 | 7969 | 116 | 175 | 838 |
| IA-NS-7_16.2 | 2255 | 70 | 20 | 3.7 | 15396 | 342 | 9135 | 3190 | 2057 | 854 |
| IA-NS-7_17.1 | 2313 | 100 | 29 | 3.6 | 15022 | 435 | 6355 | 2428 | 2117 | 901 |

**Table 4**. Continued

| Sample Spot | La | Ce | Nd | Sm | Eu | Gd | Tb | Dy | Ho | Er | Tm | Yb | Lu |
|---|---|---|---|---|---|---|---|---|---|---|---|---|---|
| **IA-NS-6 (continued)** | | | | | | | | | | | | | |
| IA-NS-6_5.1 | 0.13 | 300 | 16.6 | 43 | 3.0 | 384 | 125 | 1296 | 475 | 1801 | 333 | 2364 | 366 |
| IA-NS-6_6.1 | 0.03 | 96 | 4.4 | 12 | 3.5 | 122 | 42 | 444 | 161 | 611 | 111 | 751 | 114 |
| IA-NS-6_7.1 | 0.02 | 18 | 1.3 | 3.4 | 1.1 | 36 | 14 | 160 | 64 | 276 | 56 | 423 | 72 |
| IA-NS-6_9.1 | 0.37 | 451 | 38.8 | 80 | 11 | 625 | 194 | 1970 | 684 | 2606 | 476 | 3391 | 500 |
| IA-NS-6_10.1 | 0.04 | 87 | 4.6 | 13 | 1.9 | 131 | 43 | 463 | 167 | 693 | 135 | 970 | 159 |
| IA-NS-6_12.1 | 0.02 | 18 | 3.5 | 8.7 | 2.5 | 79 | 27 | 286 | 102 | 404 | 71 | 513 | 81 |
| IA-NS-6_13.1 | 0.13 | 594 | 29.4 | 69 | 11 | 509 | 153 | 1461 | 504 | 1881 | 341 | 2365 | 353 |
| IA-NS-6_15.1 | 0.17 | 222 | 25.0 | 47 | 8.2 | 372 | 117 | 1174 | 414 | 1568 | 288 | 2051 | 306 |
| IA-NS-6_16.1 | 0.12 | 75 | 14.8 | 32 | 8.8 | 247 | 78 | 787 | 276 | 1077 | 203 | 1491 | 241 |
| IA-NS-6_17.1 | 0.11 | 81 | 10.3 | 23 | 5.0 | 181 | 59 | 599 | 215 | 854 | 160 | 1178 | 183 |
| IA-NS-6_17.2 | 0.32 | 328 | 36.6 | 73 | 13 | 565 | 174 | 1723 | 604 | 2279 | 415 | 2922 | 440 |
| IA-NS-6_18.1 | 0.03 | 16 | 0.9 | 2.8 | 1.0 | 31 | 11 | 135 | 54 | 236 | 48 | 382 | 67 |
| IA-NS-6_18.2 | 0.02 | 17 | 3.4 | 8.6 | 2.6 | 77 | 26 | 277 | 98 | 382 | 71 | 501 | 79 |
| IA-NS-6_19.1 | 0.48 | 376 | 49.9 | 91 | 16 | 642 | 196 | 1888 | 649 | 2366 | 433 | 3006 | 442 |
| IA-NS-6_20.2 | 0.21 | 132 | 23.3 | 52 | 12 | 397 | 119 | 1206 | 425 | 1595 | 294 | 2086 | 325 |
| IA-NS-6_21.1 | 0.02 | 18 | 1.4 | 3.9 | 1.5 | 39 | 14 | 159 | 60 | 260 | 51 | 371 | 62 |
| IA-NS-6_22.1 | 0.03 | 16 | 1.7 | 4.7 | 1.6 | 50 | 16 | 187 | 68 | 269 | 51 | 377 | 62 |
| IA-NS-6_22.2 | 0.02 | 20 | 1.4 | 3.6 | 1.2 | 37 | 14 | 165 | 68 | 303 | 61 | 505 | 87 |
| IA-NS-6_23.1 | 12 | 50 | 13.5 | 7.6 | 2.7 | 53 | 18 | 198 | 74 | 280 | 57 | 415 | 65 |
| IA-NS-6_24.1 | 0.01 | 18 | 2.7 | 6.3 | 1.8 | 55 | 18 | 201 | 77 | 312 | 61 | 458 | 77 |
| IA-NS-6_24.2 | 0.56 | 41 | 5.8 | 15 | 4.5 | 139 | 46 | 472 | 179 | 667 | 123 | 841 | 134 |
| IA-NS-6_24.3 | 0.15 | 24 | 1.9 | 4.3 | 1.4 | 44 | 15 | 164 | 62 | 253 | 47 | 346 | 58 |
| IA-NS-6_26.1 | 0.33 | 293 | 37.3 | 74 | 6.2 | 586 | 186 | 1876 | 647 | 2454 | 450 | 3204 | 486 |
| **IA-NS-7 (Granodiorite)** | | | | | | | | | | | | | |
| IA-NS-7_1.1 | 0.08 | 24 | 9.0 | 23 | 8.0 | 187 | 59 | 592 | 213 | 810 | 150 | 1136 | 182 |
| IA-NS-7_2.1 | 0.08 | 559 | 14.3 | 46 | 3.1 | 440 | 157 | 1673 | 597 | 2352 | 433 | 3123 | 455 |
| IA-NS-7_3.1 | 0.14 | 451 | 18.5 | 47 | 4.0 | 403 | 135 | 1401 | 481 | 1901 | 348 | 2488 | 370 |
| IA-NS-7_4.1 | 0.02 | 12 | 3.4 | 7.7 | 2.4 | 60 | 20 | 217 | 79 | 313 | 62 | 455 | 78 |
| IA-NS-7_4.2 | 0.02 | 217 | 9.7 | 26 | 2.4 | 222 | 77 | 792 | 273 | 1082 | 203 | 1465 | 230 |
| IA-NS-7_5.1 | 0.22 | 58 | 25.7 | 48 | 15 | 346 | 107 | 1044 | 342 | 1275 | 226 | 1643 | 251 |
| IA-NS-7_6.1 | 0.98 | 220 | 7.2 | 18 | 1.6 | 174 | 71 | 911 | 400 | 1860 | 434 | 3657 | 558 |
| IA-NS-7_7.1 | 0.36 | 14 | 2.8 | 7.1 | 2.0 | 58 | 20 | 204 | 74 | 313 | 60 | 467 | 76 |
| IA-NS-7_8.1 | 0.07 | 21 | 8.8 | 20 | 6.6 | 161 | 51 | 510 | 174 | 669 | 125 | 942 | 151 |
| IA-NS-7_8.2 | 0.08 | 339 | 13.9 | 38 | 3.3 | 331 | 108 | 1110 | 388 | 1467 | 272 | 1954 | 295 |
| IA-NS-7_9.1 | 0.26 | 290 | 28.3 | 62 | 5.5 | 499 | 162 | 1662 | 569 | 2210 | 397 | 2847 | 428 |
| IA-NS-7_10.1 | 0.20 | 787 | 37.2 | 94 | 7.5 | 694 | 214 | 2028 | 658 | 2410 | 409 | 2952 | 421 |
| IA-NS-7_11.1 | 0.74 | 19 | 7.7 | 17 | 5.9 | 141 | 46 | 460 | 164 | 655 | 122 | 935 | 150 |
| IA-NS-7_11.2 | 0.13 | 361 | 6.5 | 22 | 1.7 | 262 | 114 | 1406 | 564 | 2506 | 520 | 3973 | 568 |
| IA-NS-7_12.1 | 0.15 | 539 | 30.1 | 78 | 7.6 | 588 | 175 | 1652 | 532 | 1978 | 338 | 2349 | 344 |
| IA-NS-7_12.2 | 0.14 | 525 | 22.9 | 61 | 5.7 | 501 | 155 | 1524 | 497 | 1888 | 332 | 2354 | 345 |
| IA-NS-7_13.1 | 0.89 | 150 | 13.5 | 36 | 3.5 | 341 | 113 | 1223 | 434 | 1694 | 319 | 2308 | 359 |
| IA-NS-7_13.2 | 0.13 | 48 | 18.9 | 46 | 16 | 372 | 116 | 1145 | 382 | 1464 | 266 | 1952 | 301 |
| IA-NS-7_14.1 | 0.08 | 15 | 6.5 | 18 | 6.5 | 155 | 51 | 525 | 185 | 746 | 138 | 1030 | 170 |
| IA-NS-7_15.1 | 0.42 | 462 | 40.2 | 89 | 8.6 | 732 | 244 | 2518 | 875 | 3300 | 590 | 4183 | 610 |
| IA-NS-7_16.1 | 0.10 | 22 | 9.6 | 20 | 6.3 | 160 | 51 | 508 | 177 | 688 | 125 | 928 | 150 |
| IA-NS-7_16.2 | 0.14 | 700 | 21.0 | 61 | 5.5 | 560 | 189 | 1949 | 681 | 2634 | 475 | 3410 | 503 |
| IA-NS-7_17.1 | 0.11 | 769 | 30.7 | 78 | 6.2 | 655 | 202 | 1941 | 638 | 2375 | 422 | 2953 | 426 |

**Table 4**. Continued

| Sample Spot | P | Sc | Ti | Fe | Y | Nb | Hf | Th | U | Temp. (ºC) |
|---|---|---|---|---|---|---|---|---|---|---|
| **IA-NS-7 (continued)** | | | | | | | | | | |
| IA-NS-7_17.2 | 1193 | 61 | 8.7 | 3.3 | 10735 | 64 | 6342 | 457 | 579 | 767 |
| IA-NS-7_18.1 | 977 | 98 | 38 | 3.4 | 6067 | 59 | 6523 | 697 | 650 | 935 |
| IA-NS-7_19.1 | 1058 | 32 | 9.7 | 96 | 8780 | 52 | 7008 | 385 | 545 | 778 |
| IA-NS-7_19.2 | 841 | 80 | 20 | 3.8 | 7941 | 23 | 7181 | 242 | 283 | 853 |
| **IA-G-1 (Gabbro)** | | | | | | | | | | |
| IA-G-1_1.1 | 298 | 23 | 15 | 4.3 | 2178 | 1.4 | 9519 | 97 | 144 | 823 |
| IA-G-1_2.1 | 303 | 18 | 13 | 4.0 | 2445 | 1.7 | 9767 | 108 | 158 | 811 |
| IA-G-1_3.1 | 321 | 37 | 17 | 3.8 | 1119 | 2.3 | 9393 | 33 | 100 | 834 |
| IA-G-1_4.1 | 514 | 18 | 21 | 3.8 | 4000 | 3.2 | 8629 | 220 | 237 | 862 |
| IA-G-1_5.1 | 270 | 24 | 21 | 3.8 | 1900 | 0.89 | 9059 | 59 | 92 | 861 |
| IA-G-1_6.1 | 250 | 23 | 9.1 | 3.6 | 1735 | 0.96 | 9917 | 85 | 137 | 771 |
| IA-G-1_6.2 | 209 | 19 | 11 | 4.0 | 1350 | 1.1 | 10347 | 44 | 77 | 794 |
| IA-G-1_7.1 | 301 | 20 | 15 | 3.6 | 2072 | 1.0 | 9728 | 76 | 119 | 823 |
| IA-G-1_8.1 | 315 | 21 | 17 | 4.0 | 2261 | 1.5 | 9155 | 73 | 106 | 839 |
| IA-G-1_9.1 | 298 | 29 | 20 | 3.7 | 1980 | 1.4 | 8733 | 48 | 74 | 855 |
| IA-G-1_10.1 | 328 | 19 | 14 | 3.6 | 2440 | 1.4 | 9781 | 93 | 139 | 817 |
| IA-G-1_11.1 | 390 | 21 | 19 | 4.1 | 2863 | 1.7 | 9269 | 108 | 144 | 850 |
| IA-G-1_12.1 | 693 | 28 | 21 | 3.9 | 5003 | 3.7 | 8823 | 197 | 216 | 862 |
| IA-G-1_13.1 | 229 | 20 | 17 | 3.7 | 1467 | 0.76 | 9640 | 36 | 61 | 835 |
| IA-G-1_14.1 | 602 | 44 | 33 | 3.7 | 2273 | 2.6 | 8418 | 222 | 187 | 916 |
| IA-G-1_15.1 | 250 | 19 | 12 | 2.9 | 2157 | 1.4 | 9573 | 94 | 143 | 802 |
| IA-G-1_16.1 | 217 | 25 | 18 | 3.6 | 1278 | 0.63 | 9026 | 31 | 51 | 843 |
| IA-G-1_17.1 | 747 | 31 | 25 | 3.6 | 5197 | 4.2 | 8536 | 198 | 204 | 882 |
| IA-G-1_18.1 | 680 | 19 | 23 | 2.3 | 5227 | 3.8 | 8592 | 234 | 242 | 874 |
| IA-G-1_19.1 | 350 | 20 | 19 | 3.6 | 2446 | 1.6 | 9078 | 82 | 115 | 848 |
| IA-G-1_20.1 | 243 | 20 | 14 | 3.0 | 1572 | 1.1 | 10002 | 41 | 72 | 816 |
| IA-G-1_21.1 | 284 | 21 | 18 | 2.9 | 1981 | 1.1 | 9301 | 59 | 93 | 843 |
| IA-G-1_22.1 | 891 | 78 | 16 | 3.3 | 5021 | 9.0 | 9973 | 1143 | 1123 | 831 |
| IA-G-1_22.2 | 919 | 58 | 10 | 3.4 | 7450 | 4.9 | 10149 | 798 | 755 | 784 |
| IA-G-1_23.1 | 608 | 21 | 24 | 3.5 | 3976 | 2.4 | 8656 | 131 | 160 | 876 |
| IA-G-1_24.1 | 285 | 19 | 12 | 3.5 | 2152 | 1.4 | 9797 | 100 | 150 | 795 |
| IA-G-1_24.2 | 897 | 56 | 9.2 | 3.6 | 4731 | 11 | 11878 | 846 | 1247 | 772 |
| IA-G-1_25.1 | 318 | 23 | 8.2 | 3.7 | 2061 | 1.0 | 10938 | 129 | 204 | 761 |
| IA-G-1_26.1 | 677 | 53 | 33 | 2.7 | 2455 | 3.2 | 8256 | 231 | 197 | 915 |
| IA-G-1_27.1 | 289 | 24 | 14 | 2.9 | 2288 | 1.3 | 9837 | 101 | 155 | 817 |
| **IA-G-5 (Gabbro)** | | | | | | | | | | |
| IA-G-5_2.1 | -- | 88 | 37 | 5.3 | 7919 | 36 | 6786 | 1768 | 1232 | 931 |
| IA-G-5_4.1 | -- | 91 | 31 | 2.7 | 8302 | 50 | 7813 | 1516 | 1072 | 907 |
| IA-G-5_6.1 | -- | 75 | 24 | 1.5 | 9149 | 26 | 7712 | 893 | 651 | 878 |
| IA-G-5_7.1 | -- | 45 | 19 | 0.1 | 6244 | 12 | 6860 | 276 | 316 | 850 |
| IA-G-5_8.1 | 1667 | 99 | 38 | 2.6 | 7440 | 53 | 8715 | 2857 | 1471 | 935 |
| IA-G-5_9.1 | 1652 | 86 | 12 | 2.9 | 13075 | 16 | 9060 | 3573 | 1423 | 798 |
| IA-G-5_10.1 | 861 | 33 | 5.4 | 4.0 | 4681 | 4.0 | 9127 | 906 | 1088 | 721 |
| IA-G-5_11.1 | 1376 | 60 | 23 | 3.8 | 7882 | 12 | 6518 | 471 | 415 | 872 |
| IA-G-5_12.1 | 1075 | 58 | 18 | 4.2 | 6527 | 8.9 | 7399 | 373 | 410 | 844 |
| IA-G-5_13.1 | 1743 | 88 | 20 | 3.9 | 9393 | 22 | 7182 | 1721 | 939 | 853 |
| IA-G-5_14.1 | 1663 | 78 | 36 | 4.2 | 6768 | 31 | 8011 | 871 | 783 | 926 |

**Table 4**. Continued

| Sample Spot | La | Ce | Nd | Sm | Eu | Gd | Tb | Dy | Ho | Er | Tm | Yb | Lu |
|---|---|---|---|---|---|---|---|---|---|---|---|---|---|
| **IA-NS-7 (continued)** | | | | | | | | | | | | | |
| IA-NS-7_17.2 | 0.20 | 204 | 22.5 | 49 | 3.8 | 397 | 129 | 1326 | 470 | 1772 | 320 | 2304 | 348 |
| IA-NS-7_18.1 | 0.09 | 105 | 12.3 | 38 | 11 | 298 | 90 | 846 | 265 | 954 | 162 | 1126 | 158 |
| IA-NS-7_19.1 | 1.0 | 136 | 13.5 | 32 | 3.0 | 278 | 94 | 1009 | 375 | 1437 | 275 | 1984 | 315 |
| IA-NS-7_19.2 | 0.20 | 57 | 23.7 | 51 | 16 | 364 | 111 | 1070 | 348 | 1252 | 218 | 1528 | 228 |
| **IA-G-1 (Gabbro)** | | | | | | | | | | | | | |
| IA-G-1_1.1 | 0.03 | 11 | 3.7 | 7.6 | 3.1 | 70 | 24 | 257 | 91 | 392 | 75 | 558 | 91 |
| IA-G-1_2.1 | 0.04 | 12 | 3.5 | 7.4 | 3.1 | 70 | 25 | 278 | 102 | 424 | 81 | 615 | 102 |
| IA-G-1_3.1 | 0.01 | 8.9 | 0.9 | 2.5 | 1.1 | 24 | 8.9 | 105 | 45 | 208 | 44 | 358 | 66 |
| IA-G-1_4.1 | 0.09 | 13 | 4.5 | 8.5 | 4.0 | 104 | 40 | 474 | 183 | 788 | 147 | 1097 | 177 |
| IA-G-1_5.1 | 0.04 | 5.6 | 2.7 | 6.1 | 3.4 | 61 | 22 | 229 | 82 | 348 | 65 | 512 | 84 |
| IA-G-1_6.1 | 0.01 | 13 | 2.7 | 6.6 | 1.7 | 56 | 20 | 209 | 75 | 319 | 59 | 446 | 70 |
| IA-G-1_6.2 | 0.01 | 8.4 | 1.6 | 5.0 | 1.7 | 36 | 13 | 139 | 52 | 211 | 42 | 321 | 54 |
| IA-G-1_7.1 | 0.02 | 11 | 3.2 | 6.4 | 2.5 | 61 | 22 | 239 | 85 | 365 | 69 | 527 | 85 |
| IA-G-1_8.1 | 0.05 | 10 | 3.7 | 7.7 | 3.5 | 77 | 25 | 263 | 94 | 393 | 72 | 531 | 87 |
| IA-G-1_9.1 | 0.02 | 9.5 | 3.8 | 8.3 | 3.7 | 69 | 23 | 229 | 82 | 326 | 63 | 470 | 77 |
| IA-G-1_10.1 | 0.03 | 12 | 3.5 | 7.0 | 2.7 | 70 | 24 | 262 | 100 | 414 | 79 | 591 | 94 |
| IA-G-1_11.1 | 0.08 | 11 | 4.0 | 9.0 | 4.2 | 88 | 31 | 334 | 123 | 508 | 96 | 726 | 118 |
| IA-G-1_12.1 | 0.13 | 20 | 6.5 | 18 | 7.9 | 175 | 58 | 606 | 215 | 862 | 159 | 1177 | 186 |
| IA-G-1_13.1 | 0.03 | 6.9 | 2.4 | 5.4 | 2.4 | 46 | 16 | 170 | 62 | 255 | 50 | 379 | 61 |
| IA-G-1_14.1 | 0.03 | 20 | 3.1 | 7.4 | 3.6 | 70 | 24 | 253 | 94 | 390 | 72 | 548 | 89 |
| IA-G-1_15.1 | 0.05 | 11 | 3.5 | 7.5 | 3.0 | 63 | 21 | 237 | 90 | 370 | 69 | 512 | 85 |
| IA-G-1_16.1 | 0.02 | 4.6 | 2.3 | 5.0 | 2.6 | 42 | 14 | 152 | 53 | 223 | 42 | 334 | 57 |
| IA-G-1_17.1 | 0.08 | 22 | 7.6 | 21 | 9.8 | 190 | 62 | 634 | 218 | 870 | 162 | 1184 | 190 |
| IA-G-1_18.1 | 0.09 | 17 | 5.3 | 12 | 6.0 | 152 | 55 | 602 | 222 | 914 | 167 | 1227 | 196 |
| IA-G-1_19.1 | 0.05 | 9.1 | 3.8 | 7.9 | 3.7 | 81 | 28 | 297 | 106 | 431 | 81 | 606 | 101 |
| IA-G-1_20.1 | 0.01 | 8.9 | 2.2 | 5.2 | 2.1 | 46 | 15 | 162 | 61 | 243 | 48 | 355 | 57 |
| IA-G-1_21.1 | 0.06 | 8.9 | 3.2 | 6.6 | 3.0 | 60 | 21 | 232 | 83 | 342 | 65 | 496 | 81 |
| IA-G-1_22.1 | 0.05 | 89 | 3.9 | 13 | 4.3 | 142 | 53 | 569 | 210 | 888 | 170 | 1297 | 205 |
| IA-G-1_22.2 | 0.14 | 56 | 11.0 | 28 | 9.2 | 252 | 86 | 903 | 316 | 1298 | 244 | 1815 | 276 |
| IA-G-1_23.1 | 0.08 | 13 | 4.4 | 12 | 5.9 | 126 | 42 | 432 | 155 | 643 | 116 | 880 | 139 |
| IA-G-1_24.1 | 0.05 | 12 | 3.1 | 6.3 | 2.5 | 63 | 22 | 233 | 89 | 371 | 70 | 527 | 86 |
| IA-G-1_24.2 | 0.04 | 116 | 3.9 | 12 | 1.8 | 121 | 45 | 514 | 192 | 836 | 166 | 1224 | 186 |
| IA-G-1_25.1 | 0.15 | 11 | 2.7 | 6.6 | 2.3 | 59 | 22 | 236 | 87 | 385 | 72 | 561 | 91 |
| IA-G-1_26.1 | 0.03 | 26 | 2.7 | 7.0 | 3.7 | 75 | 26 | 282 | 102 | 424 | 79 | 588 | 96 |
| IA-G-1_27.1 | 0.03 | 7.8 | 2.6 | 6.8 | 3.3 | 69 | 23 | 249 | 91 | 383 | 72 | 564 | 92 |
| **IA-G-5 (Gabbro)** | | | | | | | | | | | | | |
| IA-G-5_2.1 | 0.07 | 273 | 13.8 | 35 | 9.3 | 293 | -- | 868 | 312 | 1165 | -- | 1503 | 217 |
| IA-G-5_4.1 | 0.13 | 304 | 11.1 | 31 | 6.3 | 279 | -- | 921 | 337 | 1229 | -- | 1645 | 242 |
| IA-G-5_6.1 | 0.17 | 189 | 16.1 | 37 | 11 | 320 | -- | 1082 | 385 | 1370 | -- | 1769 | 270 |
| IA-G-5_7.1 | 0.15 | 84 | 12.4 | 27 | 7.7 | 206 | -- | 629 | 245 | 898 | -- | 1252 | 192 |
| IA-G-5_8.1 | 0.08 | 330 | 11.7 | 42 | 8.0 | 302 | 104 | 1020 | 327 | 1248 | 232 | 1613 | 232 |
| IA-G-5_9.1 | 0.47 | 428 | 29.7 | 82 | 13 | 496 | 173 | 1713 | 581 | 1982 | 359 | 2488 | 347 |
| IA-G-5_10.1 | 0.03 | 85 | 5.6 | 15 | 2.9 | 141 | 53 | 585 | 214 | 880 | 164 | 1166 | 166 |
| IA-G-5_11.1 | 0.21 | 150 | 23.9 | 49 | 14 | 359 | 116 | 1127 | 392 | 1394 | 251 | 1785 | 255 |
| IA-G-5_12.1 | 0.09 | 102 | 14.3 | 29 | 8.5 | 227 | 88 | 883 | 294 | 1186 | 222 | 1595 | 222 |
| IA-G-5_13.1 | 0.19 | 281 | 26.8 | 53 | 13 | 391 | 132 | 1284 | 442 | 1581 | 284 | 2293 | 307 |
| IA-G-5_14.1 | 0.08 | 217 | 12.1 | 30 | 8.5 | 244 | 91 | 940 | 339 | 1331 | 243 | 1746 | 267 |

### *3.3.c. Oxygen Isotope Analyses*

We measured oxygen isotopic ratios on individual spots in zircon by secondary ion mass spectrometry (SIMS) in dual Faraday cup multi-collection mode using the CAMECA ims1270 ion microprobe at the University of California-Los Angeles' (UCLA) W.M. Keck Foundation Center for Isotope Geochemistry (Los Angeles, CA), following the methods outlined by Trail *et al.* (2007). We used a ~5 nA $Cs^+$ beam with an analytical spot size of 15-20 μm and sputter depth of ~1 μm, generating secondary ions at 20 keV total impact energy. We used R33 ($\delta^{18}O = 5.55 \pm 0.08$ ‰, 2σ, Valley, 2003) as our calibrating reference to correct for instrumental mass fractionation. All SIMS oxygen isotope data are reported in the $\delta^{18}O$ notation relative to Vienna Standard Mean Ocean Water (VSMOW), with 2σ uncertainties (calculated in quadrature using both the analytical uncertainty of individual analyses and the external reproducibility of reference materials), in Table 5, and full oxygen isotope data are reported in Appendix B.5.

### *3.3.d. Lu-Hf Isotope Analyses*

The Lu-Hf isotopic compositions of AIC zircons were measured *in situ* at the Memorial University of Newfoundland (MUN) Micro Analysis Facility (St. John's, Canada) and the Radiogenic Isotope and Geochronology Laboratory (RIGL) at WSU by laser ablation-multi-collector (LA-MC) ICP-MS. Analyses conducted at MUN utilized a ThermoFinnigan Neptune mass spectrometer attached to a Geolas Pro 193 nm Ar-F excimer laser with a spot size of ~50 μm, a laser fluence of 5 J/cm$^2$, and repetition rate of 10 Hz. Methods followed those of Fisher *et al.* (2011), with the exception that $N_2$ gas was added for increased sensitivity. Each analysis consisted of 30 s of gas background followed by 60 s of ablation. Analyses done at WSU utilized a ThermoFinnigan Neptune MC-ICP-MS attached to a New Wave 213 nm Nd-YAG laser with a spot size of 40 μm. We follow the instrument configuration, operating parameters, and data reduction methods outlined by Fisher *et al.* (2014), with the exception that U-Pb ages were not simultaneously determined. We use Mud Tank zircons ($^{176}$Hf/$^{177}$Hf = 0.282507 ± 6, Woodhead & Hergt, 2005) as the quality control reference material and to normalize all samples at WSU. We use MUNZirc 2 and 4 (S-MC-ICPMS $^{176}$Hf/$^{177}$Hf = 0.282135 ± 17, Fisher *et al.*, 2011) as the reference material and to normalize all samples at MUN. Analyses conducted at MUN did not require correction to an external standard. Additional ("secondary") reference zircons were analyzed interspersed with unknowns at both MUN and WSU. Given the narrow range of Hf isotope compositions present in Icelandic rocks, and large range of (Lu+Yb)/Hf present in AIC zircon samples, combined with the importance of highly accurate correction for the isobaric interference of $^{176}$Yb and $^{176}$Lu on $^{176}$Hf, quality control zircons used in this study covered the range of (Lu+Yb)/Hf of the samples studied. Analyses of FC-1 (S-MC-ICPMS $^{176}$Hf/$^{177}$Hf = 0.282186 ± 16, Woodhead & Hergt, 2005) and MUNZirc 2 and 4 at MUN yield LA-MC-ICP-MS $^{176}$Hf/$^{177}$Hf of 0.282173 ± 36 (2SD; n=9) and 0.282144 ± 52 (2SD; n=16; $^{176}$Yb/$^{176}$Hf ~0.07 to 0.22), respectively. Analyses of GJ-1 (S-MC-ICPMS $^{176}$Hf/$^{177}$Hf = 0.282000 ± 23, Morel *et al.*, 2008) and MUNZirc 4 at WSU yield LA-MC-ICPMS $^{176}$Hf/$^{177}$Hf of 0.282002 ± 32 (2SD; n=15) and 0.282131 ± 18 (2SD; n=13; $^{176}$Yb/$^{176}$Hf ~0.08 to 0.26), respectively. Analyses of quality control zircons from both laboratories agree well with published S-MC-ICP-MS isotope compositions of purified Hf from these zircons. Present day $\varepsilon_{Hf}$ values were calculated using the CHUR parameters reported by Bouvier *et al.* (2008). Laser $\varepsilon_{Hf}$ values are reported with 2SE uncertainty in Table 5, and full Lu-Hf isotopic data are reported in Appendix B.6.

**Table 5**. *In-situ* zircon oxygen and Lu-Hf isotope compositions[16]

| Sample Name | Mount | $\delta^{18}O$ (‰) | $2\sigma$ SE Total | $\varepsilon_{Hf}$ | $2\sigma$ SE |
|---|---|---|---|---|---|
| **IA-NS-2 (Granophyre)** | | | | | |
| IA-NS-2_1.1 | JW498 | 4.1 | 0.7 | 13.6 | 1.1 |
| IA-NS-2_2.1 | JW498 | 4.0 | 0.7 | 12.5 | 0.8 |
| IA-NS-2_3.1 | JW498 | 4.1 | 0.7 | 12.8 | 1.0 |
| IA-NS-2_4.1 | JW498 | 3.3 | 0.7 | 12.3 | 0.7 |
| IA-NS-2_4.2 | JW498 | 3.8 | 0.7 | -- | |
| IA-NS-2_5.1 | JW498 | 4.2 | 0.7 | -- | |
| IA-NS-2_5.2 | JW498 | 4.5 | 0.7 | -- | |
| IA-NS-2_6.1 | JW498 | 4.3 | 0.7 | 11.7 | 1.3 |
| IA-NS-2_7.1 | JW498 | 4.0 | 0.7 | 12.9 | 0.8 |
| IA-NS-2_8.1 | JW498 | 3.9 | 0.7 | 13.1 | 1.1 |
| IA-NS-2_9.1 | JW498 | 3.0 | 0.7 | 12.9 | 2.3 |
| IA-NS-2_10.1 | JW498 | 3.5 | 0.7 | 12.7 | 1.0 |
| IA-NS-2_10.2 | JW498 | 3.8 | 0.7 | -- | |
| IA-NS-2_11.1 | JW498 | 3.5 | 0.7 | 13.2 | 0.7 |
| IA-NS-2_12.1 | JW498 | 3.7 | 0.7 | -- | |
| IA-NS-2_12.2 | JW498 | 3.8 | 0.7 | 12.1 | 1.2 |
| IA-NS-2_13.1 | JW498 | 3.7 | 0.7 | -- | |
| IA-NS-2_14.1 | JW498 | 3.2 | 0.7 | -- | |
| IA-NS-2_15.1 | JW498 | 3.6 | 0.7 | 11.6 | 1.4 |
| IA-NS-2_17.2 | JW498 | 3.7 | 0.7 | 14.3 | 1.4 |
| IA-NS-2_18.1 | JW498 | 4.4 | 0.7 | 11.8 | 1.4 |
| IA-NS-2_20.1 | JW498 | 4.2 | 0.7 | 13.1 | 0.8 |
| IA-NS-2_23.1 | JW498 | 3.5 | 0.7 | 13.5 | 0.7 |
| IA-NS-2_24.1 | JW498 | 3.7 | 0.7 | 12.9 | 1.5 |
| IA-NS-2_25.1 | JW498 | 3.4 | 0.7 | 14.7 | 1.7 |
| IA-NS-2_26.1 | JW498 | -- | | 13.8 | 0.7 |

| Sample Name | Mount | $\delta^{18}O$ (‰) | $2\sigma$ SE Total | $\varepsilon_{Hf}$ | $2\sigma$ SE |
|---|---|---|---|---|---|
| **IA-NS-6 (Diorite)** | | | | | |
| IA-NS-6_1.1 | JW498 | 3.5 | 0.7 | 13.9 | 1.0 |
| IA-NS-6_2.1 | JW498 | 3.3 | 0.7 | -- | |
| IA-NS-6_3.1 | JW498 | 4.0 | 0.7 | 13.5 | 1.4 |
| IA-NS-6_4.1 | JW498 | 3.8 | 0.7 | 12.6 | 1.9 |
| IA-NS-6_5.1 | JW498 | 3.7 | 0.7 | -- | |
| IA-NS-6_6.1 | JW498 | 3.5 | 0.7 | 13.1 | 0.7 |
| IA-NS-6_6.2 | JW498 | -- | | 12.4 | 1.0 |
| IA-NS-6_7.1 | JW498 | 3.4 | 0.7 | 13.4 | 1.2 |
| IA-NS-6_8.1 | JW498 | 3.5 | 0.7 | -- | |
| IA-NS-6_9.1 | JW498 | 3.7 | 0.7 | 14.1 | 2.0 |
| IA-NS-6_10.1 | JW498 | 3.6 | 0.7 | 12.8 | 1.5 |
| IA-NS-6_11.1 | JW498 | 4.5 | 0.7 | 14.6 | 1.0 |
| IA-NS-6_12.1 | JW498 | 3.3 | 0.7 | 13.8 | 0.9 |
| IA-NS-6_13.1 | JW498 | 4.1 | 0.7 | 12.5 | 1.9 |
| IA-NS-6_14.1 | JW498 | 3.2 | 0.7 | -- | |
| IA-NS-6_15.1 | JW498 | 4.2 | 0.7 | -- | |
| IA-NS-6_16.1 | JW498 | 2.7 | 0.7 | -- | |
| IA-NS-6_17.1 | JW498 | 3.4 | 0.7 | -- | |
| IA-NS-6_17.2 | JW498 | 4.2 | 0.7 | -- | |
| IA-NS-6_18.1 | JW498 | 3.9 | 0.7 | 12.3 | 0.8 |
| IA-NS-6_19.1 | JW498 | 4.2 | 0.7 | -- | |
| IA-NS-6_21.1 | JW498 | 3.6 | 0.7 | 13.3 | 1.4 |
| IA-NS-6_22.1 | JW498 | 3.7 | 0.7 | 13.3 | 1.0 |
| IA-NS-6_23.1 | JW498 | 3.4 | 0.7 | -- | |
| IA-NS-6_24.1 | JW498 | 3.8 | 0.7 | 12.4 | 1.2 |
| IA-NS-6_24.2 | JW498 | 3.3 | 0.7 | -- | |
| IA-NS-6_26.1 | JW498 | 3.8 | 0.7 | 12.9 | 2.4 |

---

[16] For full oxygen isotope compositions, see *Appendix B.5*. For full Lu-Hf isotopes, see *Appendix B.6*.

**Table 5**. Continued

| Sample Name | Mount | $\delta^{18}O$ (‰) | 2σ SE Total | $\varepsilon_{Hf}$ | 2σ SE |
|---|---|---|---|---|---|
| **IA-NS-7 (Granodiorite)** | | | | | |
| IA_NS-7_1.1 | JW510 | 3.8 | 0.5 | 13.1 | 1.1 |
| IA_NS-7_2.1 | JW510 | 3.9 | 0.4 | -- | |
| IA_NS-7_3.1 | JW510 | 2.9 | 0.5 | 13.5 | 1.5 |
| IA_NS-7_4.1 | JW510 | 4.3 | 0.5 | 12.5 | 1.1 |
| IA_NS-7_6.1 | JW510 | 3.6 | 0.5 | -- | |
| IA_NS-7_7.1 | JW510 | 4.1 | 0.5 | -- | |
| IA_NS-7_9.1 | JW510 | 3.6 | 0.5 | 12.6 | 1.3 |
| IA_NS-7_10.1 | JW510 | 4.4 | 0.5 | 10.9 | 1.7 |
| IA_NS-7_11.1 | JW510 | 4.0 | 0.4 | 13.7 | 1.3 |
| IA_NS-7_12.1 | JW510 | 3.7 | 0.5 | 12.4 | 1.5 |
| IA_NS-7_13.1 | JW510 | 3.8 | 0.5 | 13.1 | 1.1 |
| IA-NS-7_14.1 | JW510 | 3.7 | 0.5 | 13.1 | 1.2 |
| IA-NS-7_15.1 | JW510 | 4.1 | 0.5 | -- | |
| IA-NS-7_16.1 | JW510 | -- | | 15.1 | 1.0 |
| IA-NS-7_17.1 | JW510 | 4.1 | 0.5 | 12.7 | 1.2 |
| IA-NS-7_19.1 | JW510 | 4.2 | 0.5 | 13.1 | 1.7 |
| IA-NS-7_20.1 | JW510 | -- | | 12.3 | 1.7 |
| IA-NS-7_22.1 | JW510 | -- | | 12.6 | 1.2 |
| IA-NS-7_23.1 | JW510 | -- | | 12.2 | 1.5 |
| IA-NS-7_25.1 | JW510 | -- | | 13.0 | 1.1 |
| **IA-G-1 (Gabbro)** | | | | | |
| IA-G-1_1.1 | JW510 | 4.3 | 0.4 | 13.2 | 1.0 |
| IA-G-1_2.1 | JW510 | 4.5 | 0.5 | 12.2 | 0.9 |
| IA-G-1_3.1 | JW510 | -- | | 12.9 | 1.2 |
| IA-G-1_4.1 | JW510 | -- | | 13.0 | 1.0 |
| IA-G-1_6.1 | JW510 | 4.7 | 0.5 | 13.1 | 1.2 |
| IA-G-1_7.1 | JW510 | 4.5 | 0.5 | 12.1 | 1.4 |
| **IA-G-1 (continued)** | | | | | |
| IA-G-1_8.1 | JW510 | 4.3 | 0.5 | 12.7 | 0.9 |
| IA-G-1_10.1 | JW510 | -- | | 11.2 | 1.1 |
| IA-G-1_11.1 | JW510 | -- | | 15.9 | 1.6 |
| IA-G-1_12.1 | JW510 | 4.7 | 0.4 | 12.4 | 1.3 |
| IA-G-1_14.1 | JW510 | -- | | 13.1 | 1.1 |
| IA-G-1_15.1 | JW510 | 4.2 | 0.4 | 12.4 | 1.0 |
| IA-G-1_17.1 | JW510 | -- | | 13.0 | 1.1 |
| IA-G-1_18.1 | JW510 | 4.4 | 0.4 | 13.9 | 1.4 |
| IA-G-1_19.1 | JW510 | -- | | 13.8 | 1.0 |
| IA-G-1_22.1 | JW510 | 4.9 | 0.5 | -- | |
| IA-G-1_23.1 | JW510 | 4.9 | 0.5 | -- | |
| IA-G-1_24.1 | JW510 | 4.5 | 0.5 | 12.9 | 1.1 |
| IA-G-1_25.1 | JW510 | 4.8 | 0.5 | 12.5 | 0.8 |
| IA-G-1_26.1 | JW510 | 4.2 | 0.5 | 13.9 | 1.3 |
| IA-G-1_27.1 | JW510 | 4.6 | 0.5 | 12.1 | 1.1 |
| IA-G-1_28.1 | JW510 | 4.9 | 0.5 | 13.2 | 1.1 |
| **IA-G-5 (Gabbro)** | | | | | |
| IA-G-5_2.1 | AJP01 | 2.8 | 0.7 | -- | |
| IA-G-5_3.1 | AJP01 | 4.5 | 0.8 | -- | |
| IA-G-5_4.1 | AJP01 | 2.2 | 0.7 | -- | |
| IA-G-5_6.1 | AJP01 | 3.2 | 0.7 | -- | |
| IA-G-5_7.1 | AJP01 | 4.7 | 0.7 | 12.9 | 1.8 |
| IA-G-5_8.1 | AJP02 | 4.2 | 0.7 | -- | |
| IA-G-5_9.1 | AJP02 | 4.0 | 0.7 | -- | |
| IA-G-5_10.1 | AJP03 | 4.3 | 0.7 | -- | |
| IA-G-5_11.1 | AJP03 | 4.8 | 0.7 | 13.0 | 1.8 |
| IA-G-5_12.1 | AJP03 | -- | | 13.0 | 1.8 |

# 4. **Results**

## 4.1. Field Observations

The main focus of our study is to use zircon to quantify the complex magmatic processes suggested by exposures of the Mafic-Silicic Composite Zone. We recognize two types of mafic enclaves found throughout the MSCZ (Fig. 3) and distinguish these using the terms *pillows*, light to dark gray masses ranging in size from a few centimeters to meters in the long dimension that we interpret to represent melt-rich mafic magma enclosed by silicic magma, and *clasts*, which have the same range in size but which we interpret to represent fragments of solidified magma within silicic magma. Pillows commonly have cuspate or crenulated margins, sometimes chilled, or diffuse boundaries, whereas clasts typically have very sharp and angular edges (see Fig. 3a,b,d,e). Some enclaves are partially bounded by angular edges and partially by diffuse or crenulated margins. Double pillows or "pillows within other pillows" (see Mattson *et al.*, 1986), usually a chilled dark mafic pillow surrounded by a lighter intermediate gradational outer zone, which is commonly also chilled, all surrounded by the host silicic rock, are also present throughout the MSCZ (see Fig. 3d). Some large pillows are disaggregated into smaller enclaves at the margins.

In addition to mafic enclaves (both pillows and clasts), there are large uniform bodies of fine-grained, homogeneous mafic rock within the MSCZ that have a sill-like morphology (Fig. 3h,i), a feature also recognized by Furman *et al.* (1992a). The edges of these sill-like bodies are commonly found disaggregated into mafic clasts with veins of silicic material intruding as apophyses, and in some locations we find wide areas of clast- and pillow-free silicic rock between mafic sills. Groups of small mafic clasts are often concentrated along the edges of sills, and can be reconstructed in the manner of a jigsaw puzzle into the larger structures from which they disaggregated, indicating they were not transported very far by the host magma.

Silicic rocks in the MSCZ are typically fined-grained, and can be grouped into general “units” based on distinctive characteristics that extend over 10s of meters (or more) of outcrop. These units range in appearance from very large, homogeneous, and clast- and pillow-free bodies extending over 10s of meters, to extensively mingled composite bodies of silicic material with abundant mafic clasts and pillows of all types and sizes (see above for types; sizes range from cm to m-wide bodies). We refer to the latter as *heterogeneous* silicic units. These units commonly contain microenclaves (<1 cm across) with a thoroughly diffuse character (gradational contacts and generally becoming more mafic in composition than the host rock toward the center of the enclave), which are typically interpreted to represent magmatic hybridization (see Fig. 3e; e.g. Vernon, 1984; Wiebe *et al.*, 2002). Some of the less silicic rocks contain distinctive acicular amphibole crystals and are generally clast-free and pillow-free.

Near the structural top of the MSCZ there is a zone of nearly enclave-free granophyre that is widely intruded by small-volume dikes and pods of high-$SiO_2$ granophyre (HSG). These HSG units are volumetrically insignificant relative to the rest of the rocks in the MSCZ, making up far less than 1% of exposed silicic rocks. They display geochemical trends, both in their whole-rock and zircon composition, that differ significantly from those of other associated silicic rocks, and likely represent magmatic processes that may not be commonplace in the AIC (Padilla *et al.*, 2014). Because of their magmatic association with other units of the MSCZ, we include 4 samples from this HSG zone in our U-Pb zircon age determination for the entire Austurhorn complex (samples IA-NS-4b, IA-NS-9, IA-NS-10, and IA-NS-12; see section *4.4.f.*) in order to maximize age resolution, but these samples are not the focus of this study (see Padilla *et al.*, 2014), and are therefore not discussed in this paper.

A zone of homogeneous fine-grained granophyre, free of mafic enclaves and clasts, surrounds the MSCZ. This granophyre intrudes the country rock basalts marking the northern boundary of the AIC. In a few locations, the MSCZ is also in contact with the coarse-grained Hvalnesfjall gabbro (sample IA-G-3; see Fig. 2; Furman *et al.*, 1992a). A small body of gabbro that we refer to as the “coastal” MSCZ gabbro is exposed within the MSCZ at Hvalneskrókur Point, and unlike the mafic sheets elsewhere in the MSCZ it is coarse-grained and gradational with the surrounding silicic units (sample locality IA-G-1). Dikes, apophyses, and thin veins of silicic rock intruded into the coastal MSCZ gabbro. We refer to all other gabbroic units within the MSCZ as “sheet” gabbros (e.g. sample IA-G-5).

### 4.2. Petrography

All silicic and intermediate samples from the MSCZ display micrographic intergrowths of quartz and feldspar, with individual large (dominantly plagioclase) feldspar crystals and quartz ranging from ~500 to ~1000 μm across also present and common in the same matrix. In addition, minor amounts of prismatic clinopyroxene (Cpx) and amphibole are present in most silicic samples, and zircon and titanite are common accessory minerals in all units. One heterogeneous granophyre sample (IA-NS-2) contains abundant microenclaves with diffuse boundaries, and abundant large (>1cm in length) amphibole crystals.

Gabbro samples have the same mineral assemblage, composed mainly of very coarse plagioclase and Cpx (1-2 cm across), as well as Fe-Ti oxides, and minor amounts of biotite. Amphibole is also present, though typically as a secondary phase. Some Fe-Ti oxides from the coastal MSCZ gabbro (sample IA-G-1) display an acicular habit, a feature that is absent in the sheet gabbros of the MSCZ. The Hvalnesfjall gabbro (IA-G-3) is distinctively coarser than all MSCZ gabbros and displays the least alteration.

A small proportion of amphibole crystals, particularly in the intermediate and silicic samples, are fibrous and often occur as rims surrounding primary Cpx cores. We interpret these as secondary amphibole growth resulting from sub-solidus hydrothermal alteration of Cpx. Most samples (of all compositions) contain other secondary phases such as epidote, chlorite, and sericite, in minor amounts, also indicating that some sub-solidus alteration has occurred throughout the AIC.

## 4.3. Whole-Rock Geochemistry

We obtained whole-rock major oxide and trace element abundances from 11 representative samples in order to characterize the rock types found within the AIC (see Table 2). Of the 11 samples, three are most representative of gabbroic rocks present throughout the AIC (the coastal and sheet gabbros within the MSCZ, and the adjacent Hvalnesfjall gabbro), while the rest encompass the range of silicic compositions and textures that are most common within the MSCZ as well as the homogeneous granophyre zone that surrounds the MSCZ.

### *4.3.a. Major Oxides*

Major oxides in the silicic samples show a general increase in $K_2O$ and decrease in $TiO_2$, $Al_2O_3$, $Fe_2O_3$(Tot), MnO, MgO, CaO and $P_2O_5$ with increasing $SiO_2$ content (Fig. 4). $SiO_2$ concentrations range from 61 to 73 wt.% for the silicic samples, and the mafic samples are all near 47 wt.%. The mafic samples differ significantly from each other in their major oxide abundances. The coastal MSCZ gabbro (sample IA-G-1) has substantially higher $TiO_2$, $Fe_2O_3$(Tot), $K_2O$, and $P_2O_5$ abundances, as well as lower CaO concentrations and Mg#, than the

Hvalnesfjall gabbro (sample IA-G-3) or MSCZ sheet gabbro (IA-G-5). With the exception of MgO, the Hvalnesfjall and MSCZ sheet gabbro have nearly identical major element compositions. The sheet gabbro is enriched in Mg relative to the other gabbros. The chemical characteristics of the Hvalnesfjall and sheet gabbro are more cumulate-like in character, relative to the coastal gabbro.

### *4.3.b. Rare Earth Elements (REE)*

All intermediate to silicic AIC samples display LREE-enriched REE patterns with negative Eu anomalies (Fig. 5). The most silicic samples (e.g. granophyres) also have discernible positive Ce anomalies. All gabbro samples also have overall negative slopes, with LREE enrichment relative to HREE, but they have much lower REE concentrations than the intermediate to silicic samples. Both the coastal (IA-G-1) and sheet (IA-G-5) MSCZ gabbros display elevated MREE concentrations and slight positive Eu anomalies. The Hvalnesfjall gabbro (IA-G-3) has lower REE concentrations than MSCZ gabbros and a more noticeable positive Eu anomaly.

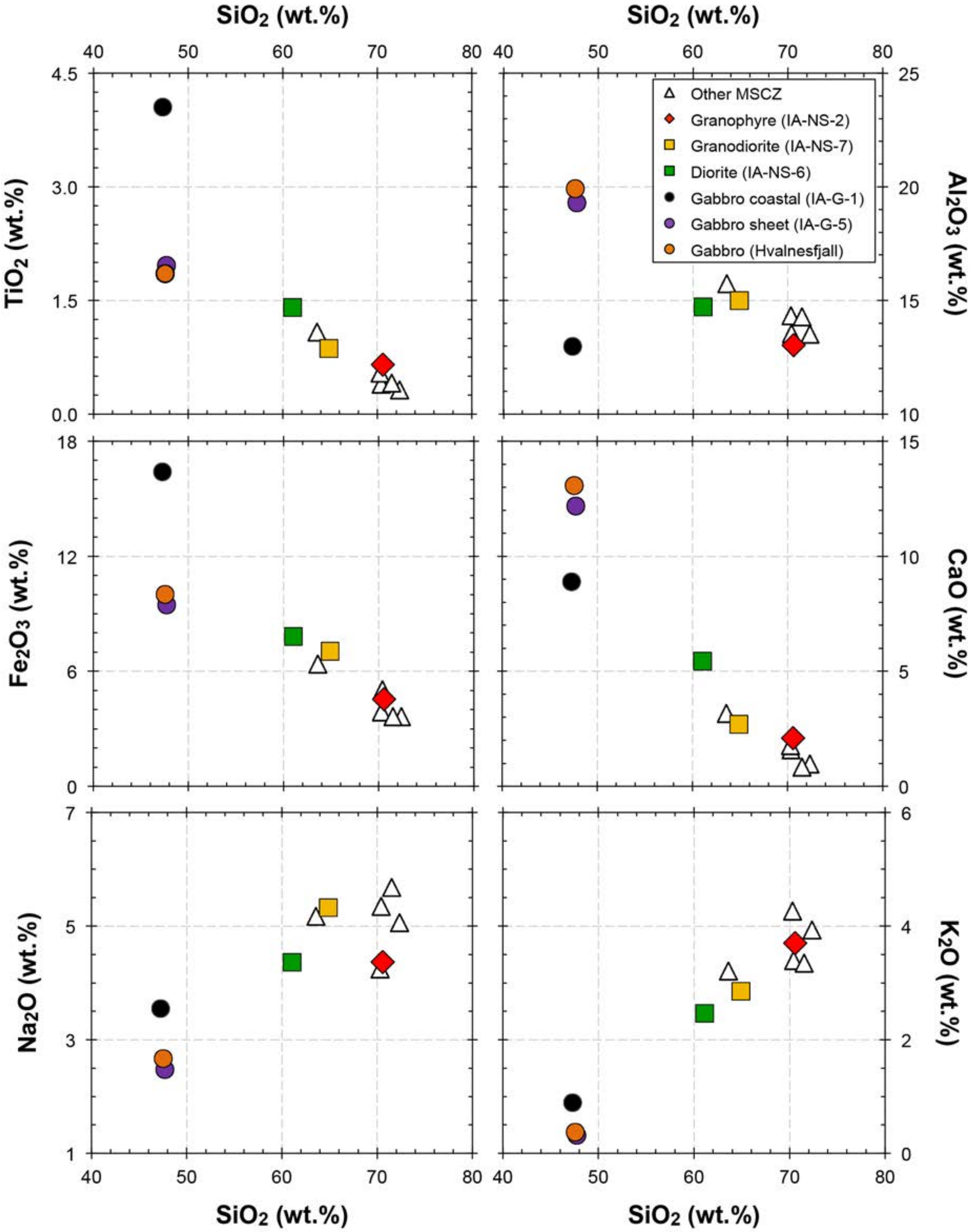

**Figure 4**

Whole-rock major oxide geochemistry for samples from the Austurhorn intrusive complex. Silicic samples not processed for zircon extraction are plotted as group "Other MSCZ."

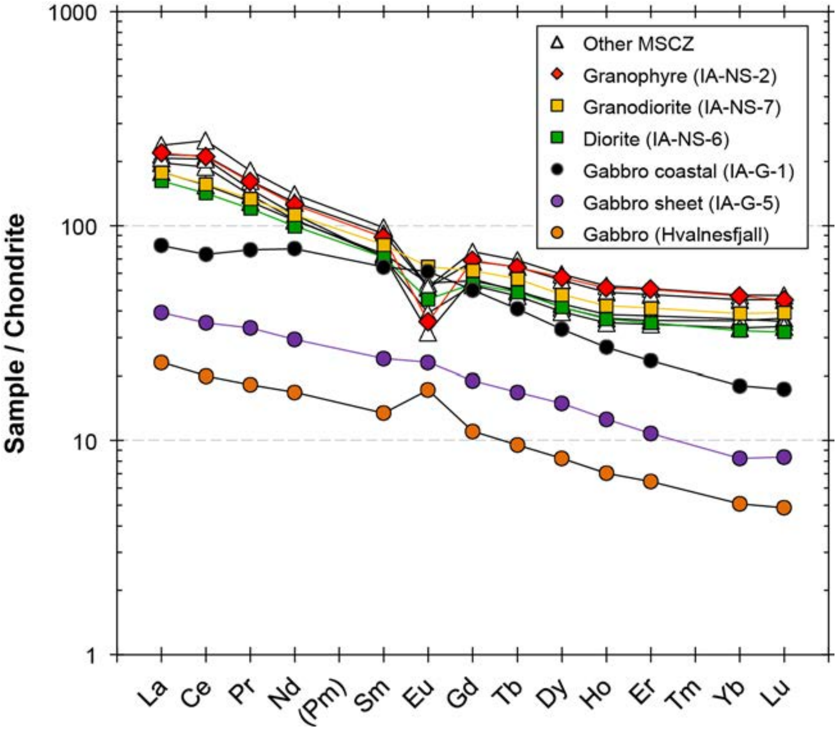

**Figure 5**

Whole-rock Rare Earth element (REE) geochemistry for samples from the Austurhorn Intrusive Complex. Silicic samples not processed for zircon extraction are plotted as group "Other MSCZ."

### *4.3.c. Other Trace Elements*

Whole-rock trace element abundances within the AIC generally display trends that are common for silicic rocks (Fig. 6). For example, Sr concentrations fall as rock compositions become more silicic (consistent with its compatibility in feldspars), Zr and Hf generally increase as $SiO_2$ and other indicators of magma evolution rise but fall in the most evolved samples (as a consequence of zircon saturation), Ba follows a similar trend (apparent response to late saturation in alkali feldspar), and U, Th, and Rb appear to behave incompatibly throughout the full range of silica concentrations. The coastal MSCZ gabbro (IA-G-1) is distinctly evolved compared to the other gabbros, with higher Zr, Hf, Ba, and Rb concentrations, as well as lower Sr. As with major oxide compositions for the coastal gabbro, these characteristics reflect a fractionated tholeiitic melt. In contrast, the lower concentrations of incompatible trace elements along with depleted REE in the Hvalnesfjall (IA-G-3) and sheet (IA-G-5) gabbros reflect more of a cumulate character.

### *4.3.d. Hf Isotopic Compositions*

Measured Hf isotopic compositions of AIC whole-rock samples range from +12 to +14 $\varepsilon_{Hf}$ (see Table 3). The gabbro samples and the granophyre make up the lower range of isotope compositions at +12.1 ± 0.3 (sheet gabbro IA-G-5), +12.5 ± 0.2 (coastal gabbro IA-G-1), and +12.6 ± 0.3 ε-units (granophyre IA-NS-2). The intermediate silicic units both have slightly higher $\varepsilon_{Hf}$ compositions at +13.3 ± 0.3 (diorite IA-NS-6) and +14.0 ± 0.2 (granodiorite IA-NS-7).

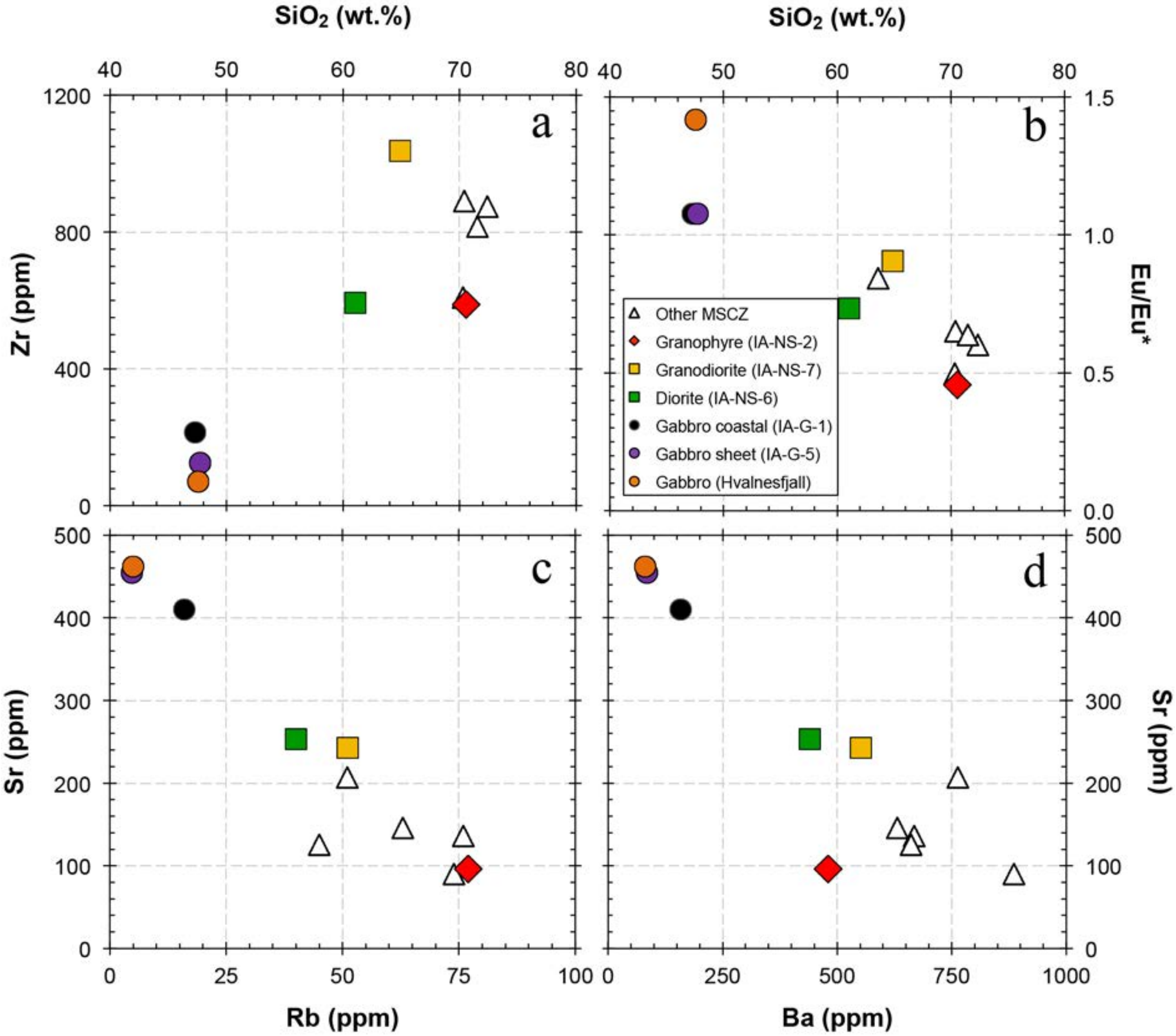

**Figure 6**

Whole-rock trace element geochemical comparison plots for samples from the Austurhorn intrusive complex. Silicic samples not processed for zircon extraction (i.e. excluding the Hvalnesfjall gabbro) are plotted as group "Other MSCZ." **a)** $SiO_2$ vs. Zr; **b)** $SiO_2$ vs. Eu/Eu* (Eu anomaly); **c)** Rb vs. Sr; and **d)** Ba vs. Sr.

## 4.4. Zircon Results

### *4.4.a.* *Samples Investigated*

We extracted zircon from 9 MSCZ samples for elemental geochemistry, U-Pb geochronology, and O and Hf isotopic analyses. As previously noted (section 4.1), we report ages for all 9 samples in this study (see section *4.4.f.*), but only discuss the 5 samples that are volumetrically significant and therefore representative of widespread magmatic processes in the MSCZ. The silicic samples encompass the range of textures and rock-types found within the MSCZ: a heterogeneous granophyre (IA-NS-2) that contains all mafic enclave types and displays extensive interactions between mafic input and silicic host; a homogeneous, fine-grained diorite (IA-NS-6) that hosts abundant mafic enclaves, both large, diffuse pillows, as well as smaller angular clasts; and a homogeneous, medium-grained and enclave-free micrographic granodiorite (IA-NS-7) characterized by abundant acicular amphibole crystals. We mechanically removed mafic enclaves and clasts from the silicic host matrix prior to processing all silicic samples for whole-rock geochemistry and zircon extraction. The selected mafic samples are from relatively homogeneous and voluminous exposures of gabbro within the MSCZ, and include a coarse-grained sample from the coastal gabbroic complex (IA-G-1) and a finer-grained sheet gabbro from the interior of the MSCZ (IA-G-5).

### *4.4.b.* *Abundance, Zoning, and Morphology*

A simple qualitative assessment of zircon yields from Icelandic silicic volcanic rocks (Carley *et al.*, 2011) and MSCZ rocks reveals that zircons are significantly more abundant in intrusive rocks than in volcanic products. Carley *et al.* (2011) report that zircon populations in 7 samples from different silicic volcanic systems were sparse (generally <10 grains/kg of starting whole-rock material), including one sample from Askja volcano that did not yield any zircons by the same standard separation techniques used in this study. In contrast, we find that every MSCZ rock, including gabbros and samples of intermediate compositions, yields abundant zircons (>>100 grains/kg, except for the sheet gabbro, IA-G-5, which yielded ~20 grains/kg).

Grain morphology and zoning patterns vary widely throughout all MSCZ samples, including complex oscillatory, patchy, sector, and simple zoning. Oscillatory-zoned euhedral and prismatic crystals, ranging from acicular to subequant, are common in all MSCZ rock types, though slightly rounded grains are also present in all samples (Fig. 7). A small number of grains preserve evidence of resorption and subsequent crystallization events in the form of irregular cores with truncated internal zoning surrounded by prismatic zircon overgrowth (Fig. 7).

The heterogeneous granophyre (IA-NS-2) has the highest proportion of oscillatory-zoned euhedral crystals, although there is a small proportion of grains that contain simple zoning (characterized by broad bands that appear homogeneous in CL intensity; see Fig. 7) and resemble zircon grains from Icelandic volcanic rocks. Crystals in the intermediate samples (IA-NS-6 and IA-NS-7) display the greatest amount of rounding and resorption, and a large proportion of grains from the diorite (IA-NS-6) are anhedral (Fig. 7).

Zircons from the coastal MSCZ gabbro (IA-G-1) are larger than those from silicic samples, and they display diverse internal patterns, including oscillatory, sector, and patchy zoning (characterized by irregular and discontinuous patches of high CL intensity) and largely un-zoned homogeneous interiors (Fig. 7). In contrast, zircons from the sheet MSCZ gabbro (IA-G-5) are typically small, generally exhibiting euhedral crystal shapes, bright in CL intensity, and commonly either sector-zoned or lacking visible zoning (see Fig. 7).

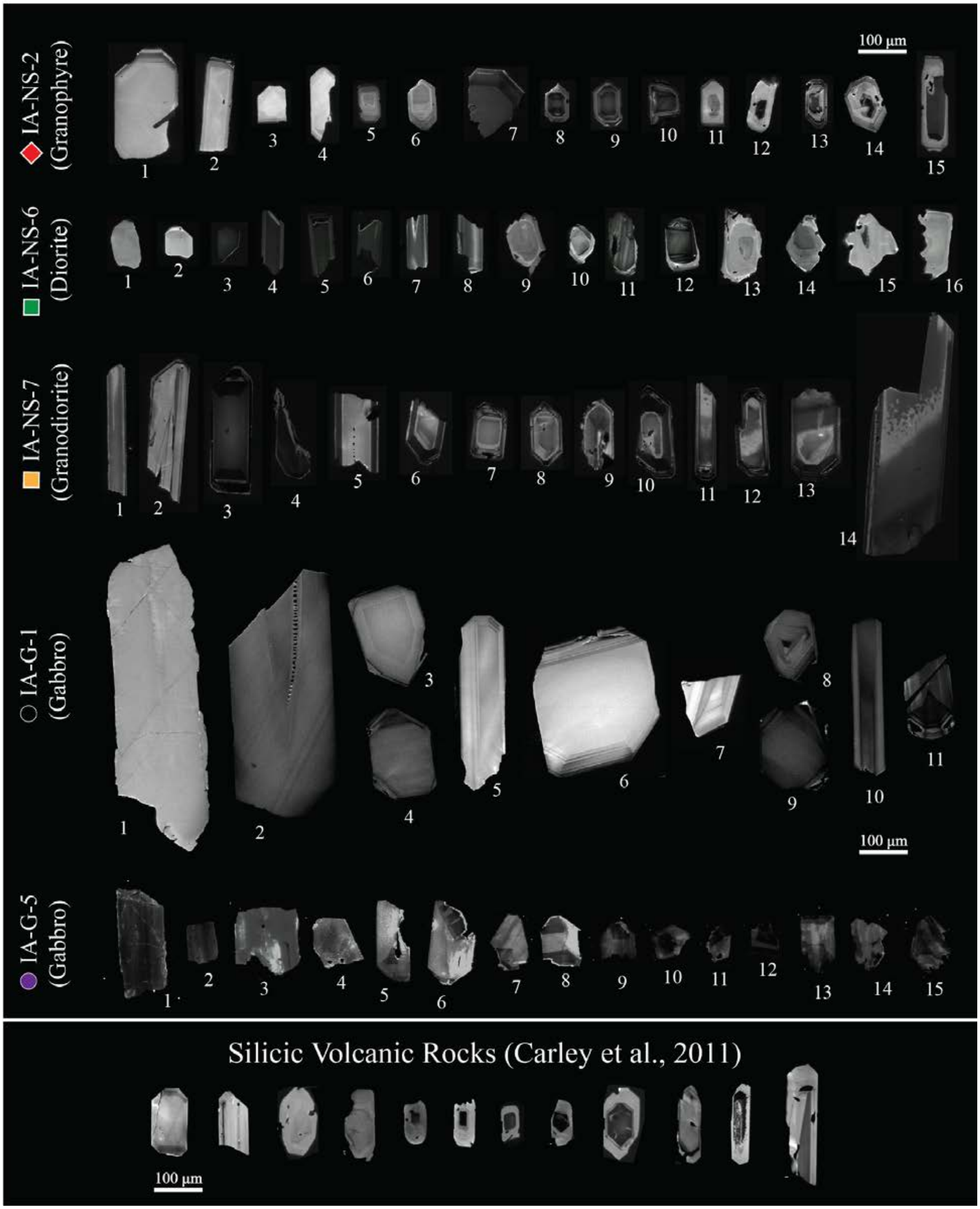

**Figure 7 (caption on next page)**

**Figure 7**

SEM cathodoluminescence images of representative zircons from Austurhorn rocks. *Granophyre*: morphologies include large (1,7) and small (6,8-11) euhedral, acicular (2,15), and slightly rounded (12,15) grains; zoning includes simple (1-7), oscillatory (8-10), and some anhedrally-shaped cores surrounded by zircon overgrowth (11-15). *Diorite*: morphologies include rounded (1-2, 9-12), acicular (4-8), and anhedral (13-16) grains; zoning includes simple/unzoned (1-3), sector (4-8,12), striped (3,5-6), and oscillatory (10,14), and anhedrally-shaped cores surrounded by zircon overgrowth are common (9-13), sometimes containing multiple anhedral zones (13). *Granodiorite*: morphologies include mainly acicular (1-5,11-14), and small euhedral (6-10) grains, some with slightly resorbed/rounded edges (2,4,7,9-10,13); zoning includes sector (3), simple (1-2,4,14), and oscillatory (5-13). *Coastal Gabbro*: grains are generally larger than those from silicic units; morphologies include acicular (1-2,5,10), euhedral (3-4,6-9,11), and occasionally resorbed (1) grains; zoning includes simple (1-3,9), sector (10-11), and oscillatory (5-8, 11). *Sheet Gabbro*: morphologies include acicular (1,5), small euhedral (6-9), and rounded/resorbed (2-4,11-15) grains; zoning includes CL-dark and simple (1-4,10-15), sector (6,8-9), and occasionally oscillatory (7).

For each sample, we targeted both rim and interior zones, including cores, during zircon trace element analyses so as to document any geochemical differences between earlier and later stages of zircon growth.

### *4.4.c.* *General Elemental Characteristics*

The elemental compositions of most AIC zircons are generally consistent with what has been observed for zircons from other Icelandic silicic rocks (Carley *et al.,* 2011, 2014). Uranium and thorium abundances range from ~50 to ~6000 ppm and ~15 to ~5000 ppm, respectively (Fig. 8b). Despite this wide range of concentrations, they form a well-defined array with a Th/U ratio that varies systematically from ~0.5 to ~2 with increasing U and Th. Hafnium concentrations mainly fall between ~6000 and ~12,000 ppm, and Ti abundances range from ~5 to ~40 ppm in all samples, similar to those in other Icelandic zircons (Fig. 8d). We also observe a general trend of decreasing Ti with increasing Hf concentrations, as is observed in most co-genetic zircon populations (e.g. Claiborne *et al.*, 2006). A majority of zircons from mafic samples, particularly the coastal gabbro (IA-G-1), have some elemental signatures that differ from the silicic array, most noticeably lower Nb concentrations and higher Eu/Eu* (Fig. 8a,c).

### *4.4.d.* *Rare Earth Elements (REE)*

With few exceptions, all zircons from the AIC have REE patterns that are broadly typical for zircon from silicic rocks (Carley *et al.*, 2011; Grimes *et al.*, 2007; Cavosie *et al.*, 2006; Hoskin & Schaltegger, 2003; Belousova *et al.*, 2002; Hoskin & Ireland, 2000), displaying chondrite-normalized trends of extreme enrichment in heavy rare earth elements (HREE) relative to light rare earth elements (LREE) and positive Ce and negative Eu anomalies (Fig. 9). A few zircon analyses from the heterogeneous granophyre (IA-NS-2) and the diorite (IA-NS-6) show distinct LREE enrichment. These are probably the result of encountering LREE-rich inclusions, such as glass or minerals that concentrate LREE (e.g. chevkinite, monazite), during analyses, and are omitted from our plots.

### *4.4.e. Oxygen and Hafnium Isotopic Compositions*

Oxygen isotopic values ($\delta^{18}O$) for AIC zircons range from +2.2 to +4.8 ‰ (see Table 5, Fig. 10a). All $\delta^{18}O$ values are depleted relative to zircon mantle values (+5.3 ± 0.6 ‰, 2σ; Valley *et al.*, 1998). Mean $\delta^{18}O$ for individual silicic samples are indistinguishable within error: +3.8 ±0.7 ‰ (all uncertainties are 2σ) for the granophyre (IA-NS-2), +3.7 ±0.8 ‰ for the diorite (IA-NS-6), and +3.9 ±0.7 ‰ for the granodiorite (IA-NS-7). The gabbros show oxygen values that are distinct from one another, with the coastal gabbro (IA-G-1) being the most reproducible and having the highest mean $\delta^{18}O$ (+4.5 ±0.5 ‰) and the sheet gabbro (IA-G-5) displaying the largest variability of any of the samples (from +2.2 to +4.8 ‰, with a mean of +3.8 ±1.8 ‰; Fig. 10a).

Measured hafnium isotope ratios (reported as $\varepsilon_{Hf}$) for zircon from analyzed samples range from +11 to +16 ε-units (see Table 5; Fig. 10b; average 2 SE for individual analyses is ~1.3 ε-units). When all units are pooled together, they yield a population weighted mean of +12.98 ± 0.18 ε-units (2σ, n = 74, MSWD = 2.0).

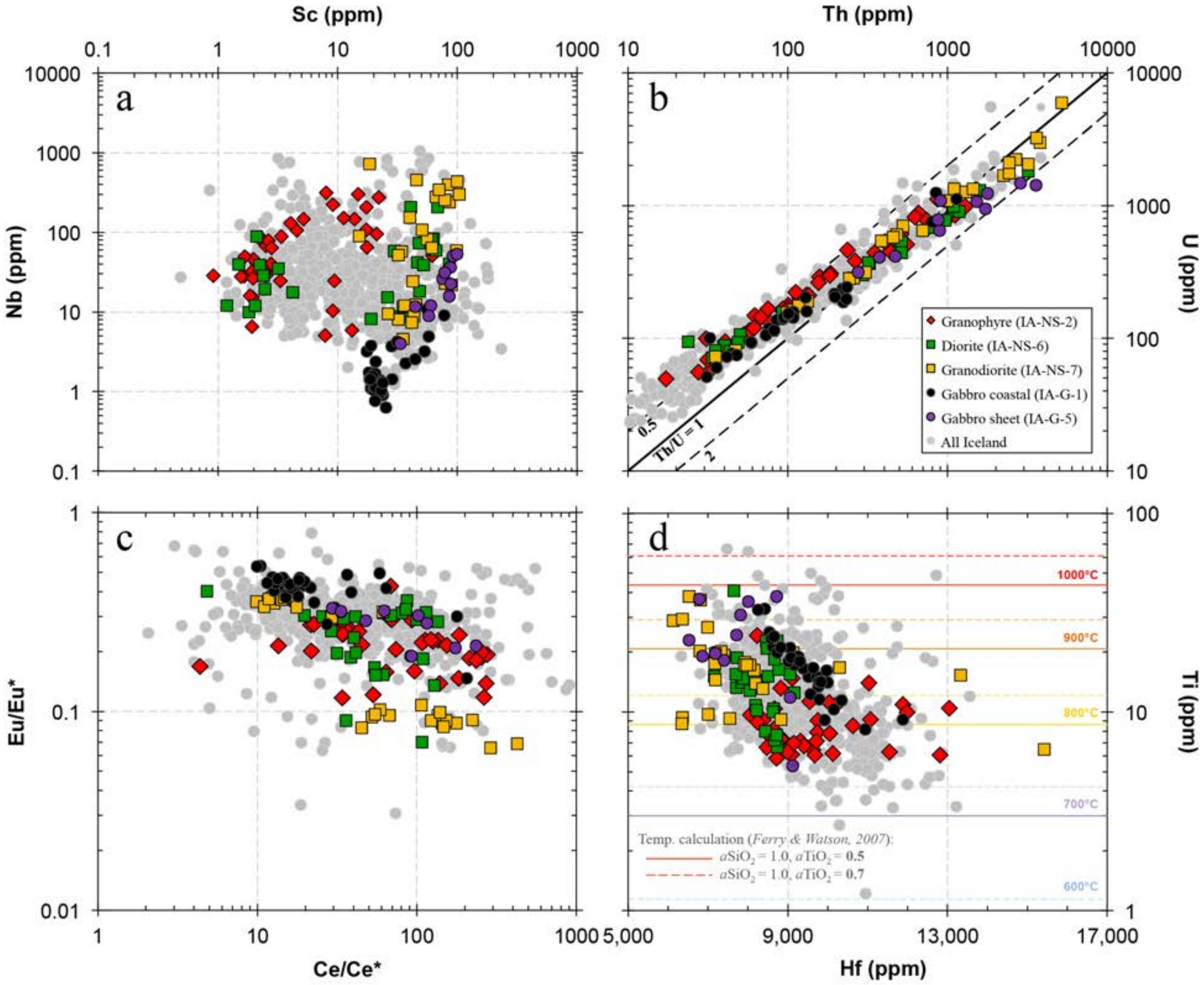

**Figure 8**

Trace element abundances and ratios for zircons from the Austurhorn Intrusive Complex. The "All Iceland" data group (gray symbols) refers to the Vanderbilt Iceland zircon database (includes volcanic, plutonic, and detrital Icelandic samples, for reference; see Carley *et al.*, 2014). **a)** Nb vs. Sc; **b)** Th vs. U; the solid line indicates a Th/U ratio of 1; the dashed lines indicate Th/U ratios of 0.5 (top) and 2 (bottom); **c)** Ce/Ce* (Ce anomaly) vs. Eu/Eu* (Eu anomaly); **d)** Hf vs. Ti; the colored lines indicate Ti-correlated zircon crystallization temperatures, calculated using the Ti-in-zircon thermometer of Ferry & Watson (2007).

**(Fig. 8 continued on next page)**

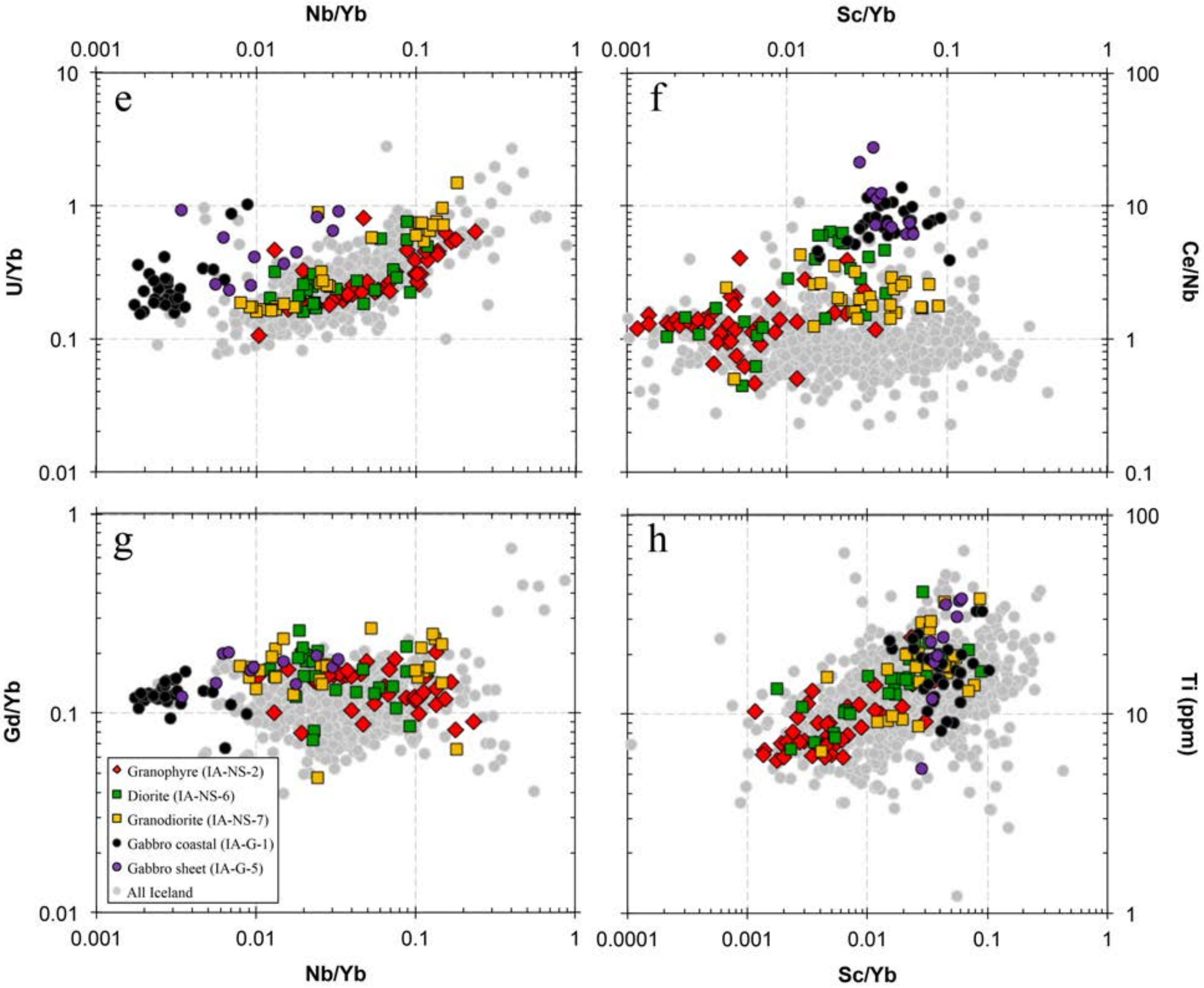

**Figure 8 (continued)**

Trace element abundances and ratios for zircons from the Austurhorn Intrusive Complex. The "All Iceland" data group (gray symbols) refers to the Vanderbilt Iceland zircon database (includes volcanic, plutonic, and detrital Icelandic samples, plotted for comparison; see Carley *et al.*, 2014). **e)** Nb/Yb vs. U/Yb; **f)** Sc/Yb vs. Ce/Nb; **g)** Nb/Yb vs. Gd/Yb; **h)** Sc/Yb vs. Ti.

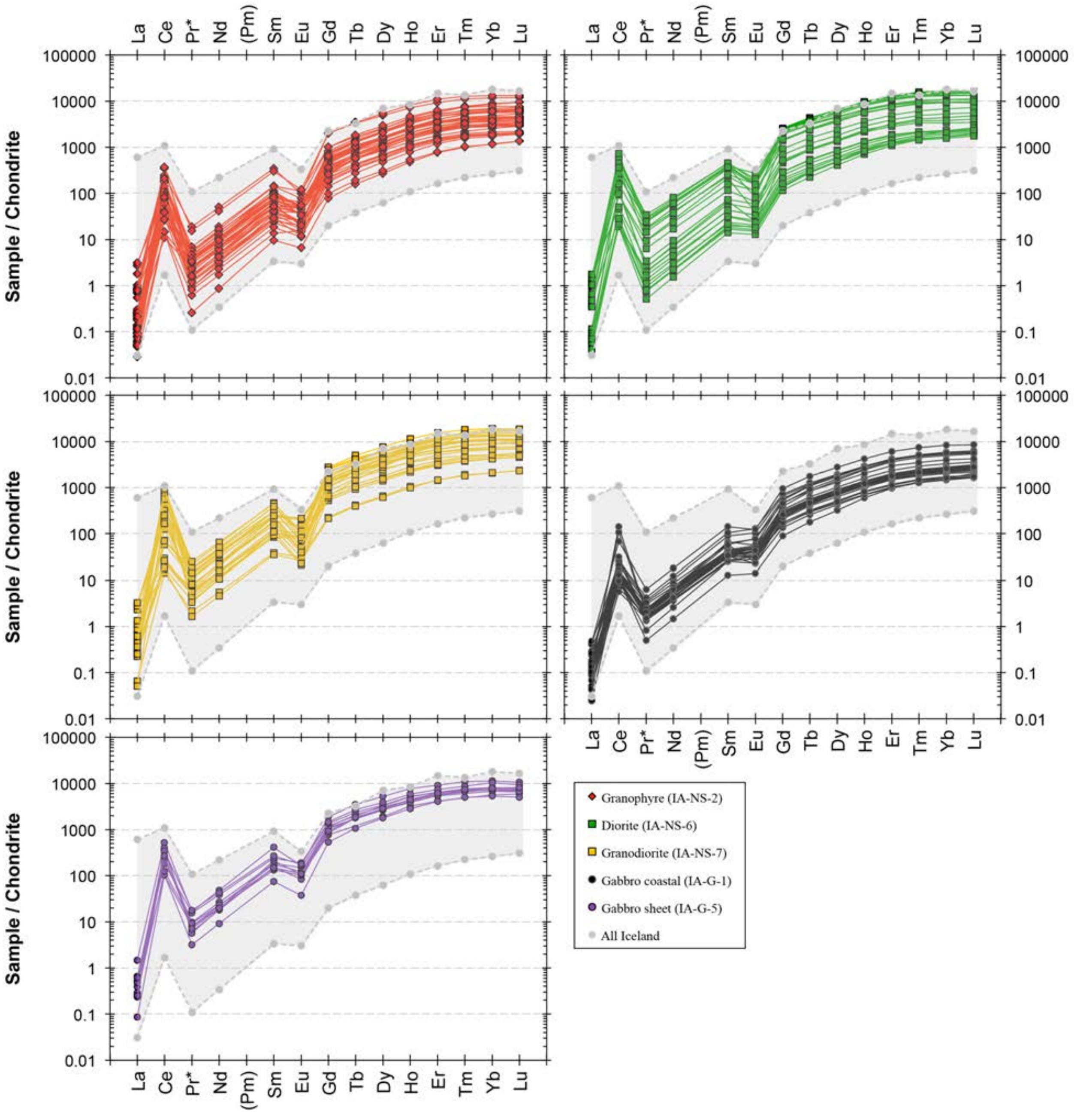

**Figure 9**

Chondrite-normalized zircon rare earth element (REE) abundances in samples from the Austurhorn Intrusive Complex. The grey shadow in each individual sample plot represents the range of REE abundances found in zircons from all other analyzed volcanic, plutonic, and detrital Icelandic samples (see Carley *et al.*, 2014), plotted for comparison to AIC zircons.

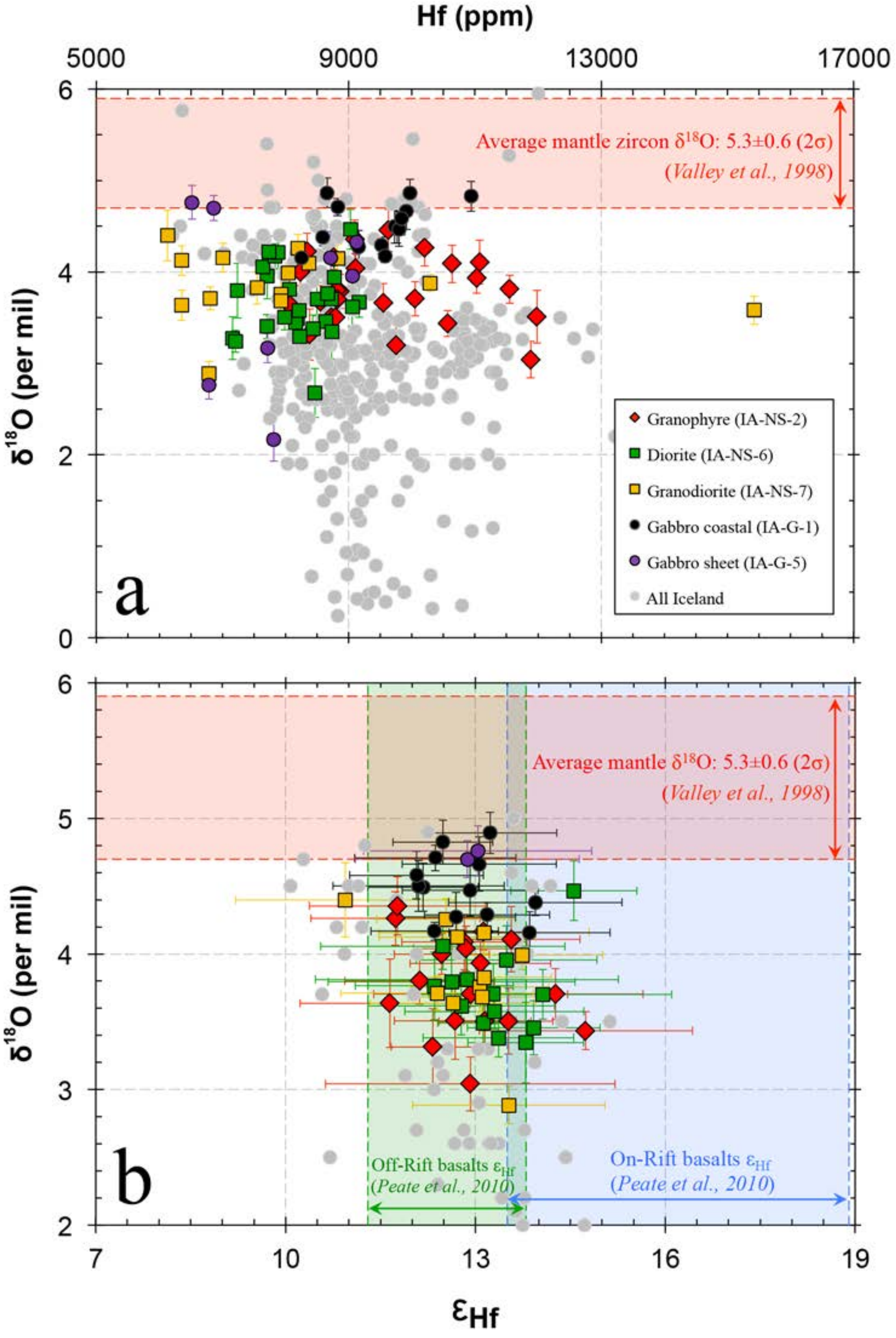

**Figure 10**

Isotopic compositions of zircons from the Austurhorn Intrusive Complex. All errors are plotted as 2σ. **a)** Hf (ppm) vs. $\delta^{18}O$; the red zone indicates the measured $\delta^{18}O$ range of mantle zircons (+5.3 ±0.6 ‰, Valley *et al.*, 1998). **b)** $\varepsilon_{Hf}$ vs. $\delta^{18}O$; the blue zone indicates the range of Hf isotopic compositions of Icelandic *on-rift* basalts (from the Northern and Western Volcanic Zones; Peate *et al.,* 2010); the green zone indicates the range of Hf isotopic compositions of Icelandic *off-rift* basalts (from the Eastern Volcanic Zone, Snæfellsnes Peninsula, Vestmannæyjar, andSnæfell volcano; Peate *et al.,* 2010).

### *4.4.f.* *U-Pb Geochronology*

Weighted mean zircon U-Pb ages span a range of approximately 300 k.y. (Fig. 11). The uncertainty for individual analyses is on average 9.8 %, but the precision generally decreases with increasing U concentration and/or common Pb. The gabbros and HSG-zone granophyres make up the older part of this range (granophyres & HSG: *IA-NS-4b*, 6.67 ± 0.06 Ma [all uncertainties are 2σ SE], MSWD = 2.3, n = 19; *IA-NS-9*, 6.53 ± 0.07 Ma, MSWD = 1.5, n = 17; *IA-NS-10*, 6.57 ± 0.24 Ma, MSWD = 1.3, n = 15; *IA-NS-12*, 6.61 ± 0.22 Ma, MSWD = 0.68, n = 17; sheet gabbro *IA-G-5*, 6.56 ± 0.05 Ma, MSWD = 2.2, n = 10; and coastal gabbro *IA-G-1*, 6.42 ± 0.09 Ma, MSWD = 0.81, n = 20). The younger ages are for granophyre IA-NS-2 (6.40 ± 0.12 Ma, MSWD = 1.3; n = 9), granodiorite IA-NS-7 (6.36 ± 0.08 Ma, MSWD = 1.4; n = 16), and diorite IA-NS-6 (6.35 ± 0.08 Ma, MSWD = 0.78; n = 14). All zircon data when pooled yield a mean age of 6.52 ± 0.03 Ma (MSWD = 1.8, n = 137, 25 rejected; see Fig. 11).

## 5. **Discussion**

### **5.1. Field Interpretations**

Evidence for open system processes, including repeated mafic magmatic replenishment, is ubiquitous within the MSCZ. The contacts between different silicic rock units within the MSCZ are typically gradational. They are primarily identified by an increase or decrease in the amount and type of mafic material present (e.g. abundant small clasts vs. large pillows or sheets) or observable changes in texture. In some instances, contacts between units are identified by changes in mineral assemblage (e.g. presence of acicular amphiboles or abundance of Fe-Ti oxides). Crenulated and chilled margins on some mafic enclaves indicate that they were a product of fluid-fluid magmatic interactions. Furthermore, enclaves with both angular and crenulated margins against what looks like the same silicic host rock suggest that quenched pillows can subsequently fracture within the same host magma after intrusion, an indication that the host silicic magma remained mobile after the mafic magma completely solidified. In some areas of the MSCZ large sheet-like mafic bodies are preserved, and their edges are commonly disaggregated into enclaves and clasts within the surrounding silicic rock (see Fig. 3h,i) suggesting that a common form of mafic recharge into the system may be through intrusion of mafic sheets that disaggregate into the host magma (e.g. Harper *et al.*, 2004; Wiebe *et al.,* 2004; Wiebe & Collins, 1998). Areas of what we interpret to be remobilized silicic material are often in intimate association with voluminous mafic rock, also indicative of magma replenishment events.

We interpret the field relationships to indicate a mush-like environment for the AIC in which the partially solidified silicic host material was continually reheated, revived, and remobilized within the MSCZ by the repeated intrusion of hotter mafic magmas, which provided new heat and energy and in turn prolonged the longevity of the Austurhorn magmatic system (e.g. Claiborne *et al.*, 2010a).

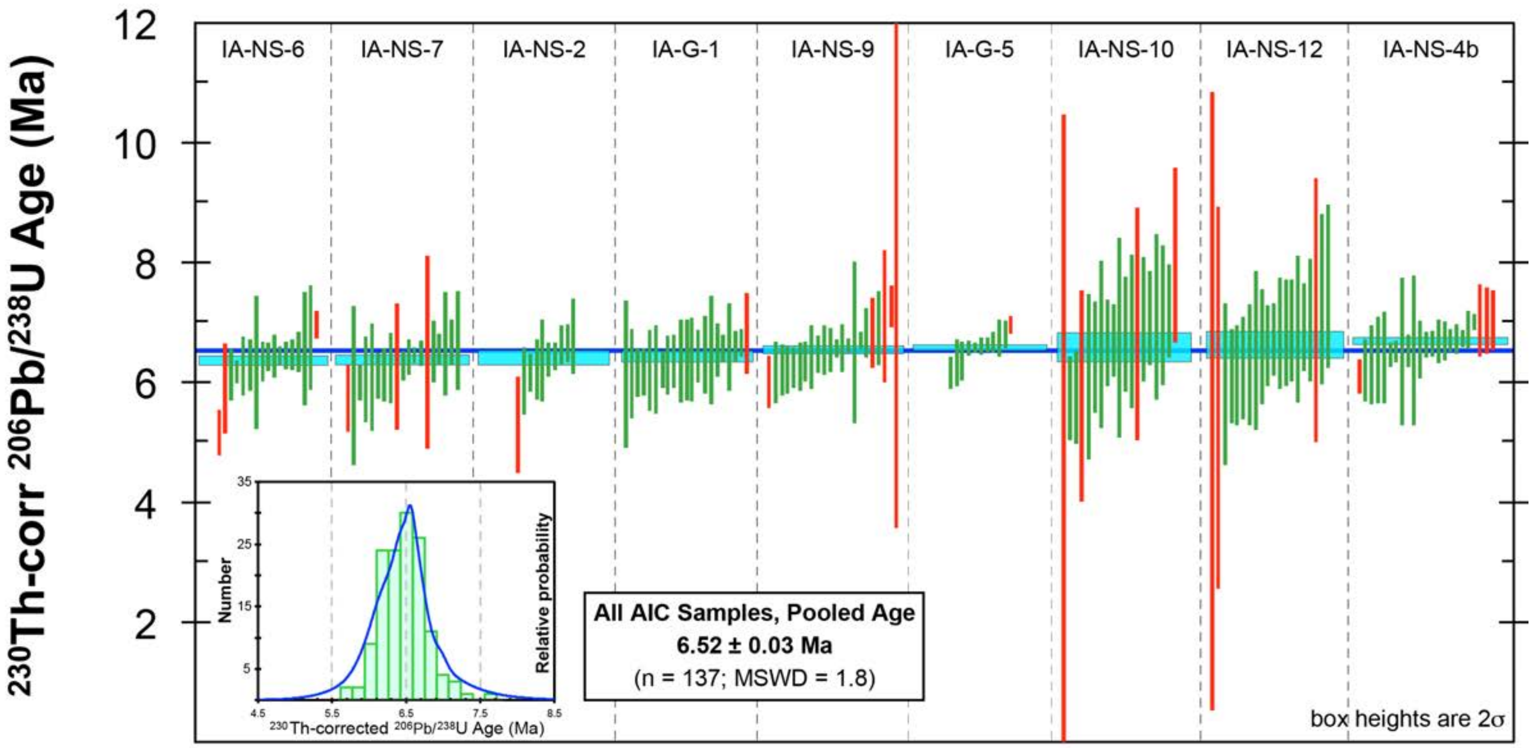

| | | | | | | | | | |
|---|---|---|---|---|---|---|---|---|---|
| **Wt. Mean Age (Ma):** | **6.35 ± 0.08** | **6.36 ± 0.08** | **6.40 ± 0.12** | **6.42 ± 0.09** | **6.53 ± 0.07** | **6.56 ± 0.05** | **6.57 ± 0.24** | **6.61 ± 0.22** | **6.67 ± 0.06** |
| n: | 14 | 16 | 9 | 20 | 17 | 10 | 15 | 17 | 19 |
| MSWD: | 0.78 | 1.4 | 1.3 | 0.81 | 1.5 | 2.2 | 1.3 | 0.68 | 2.3 |
| Rejected analyses: | 3 | 3 | 1 | 1 | 5 | 1 | 4 | 3 | 4 |

**Figure 11**

Zircon $^{206}Pb/^{238}Pb$ ages for MSCZ units from the AIC, corrected for initial $^{238}U$-$^{230}Th$ disequilibrium. Each green bar represents a single zircon age. Red bars represent outlier analyses (>2 standard deviations from sample mean), analyses with high common-$^{206}Pb$ (>20%), or analyses with high or low UO/U (>2 standard deviations from sample mean), and are therefore excluded. For each sample, the weighted mean age is plotted as a light blue horizontal box. The dark blue line represents the pooled population age for the entire AIC (6.52 ± 0.03 Ma). All errors are reported as 2σ standard errors (box heights for both individual and pooled ages are adjusted to represent error). The range in mean individual unit ages suggests a timescale of peak magmatic construction of the AIC of ~300 kyr. *Inset:* Probability density distribution and histogram for all AIC zircon ages in this study (n = 137).

## 5.2. Zircon Abundance, Size, and Morphology

Carley *et al.* (2011, 2014) demonstrated that zircons from silicic volcanic rocks from Holocene Icelandic eruptions record relatively brief, high-temperature histories that reflect magmatic conditions just prior to, and leading up to, eruptive events. These volcanic rocks are rich in Zr, mostly ranging from ~600 to ~800 ppm (Carley *et al.*, 2011), and yet zircon is extremely sparse. In contrast, we have found that both mafic and silicic rocks from the MSCZ at Austurhorn contain a vastly greater abundance of zircon, generally larger and with more complex zoning (see Fig. 7), likely reflecting slow and full crystallization of their parent magmas and suggesting that most zircon in Iceland may be stored and preserved within rocks from silicic intrusive complexes.

The complex morphology and zoning features observed in many AIC zircons have been interpreted by zircon studies on other volcanic systems to indicate thermal and chemical fluctuations of the melt within an open and dynamic system during the time of zircon crystallization (Hoskin & Schaltegger, 2003; Corfu *et al.*, 2003; Claiborne *et al.*, 2006, 2010b). Based on these observations, we suggest textures in the diorite (IA-NS-6) and granodiorite (IA-NS-7) samples likely reflect repeated stages of mafic magma replenishment into the silicic pluton throughout the history of the complex, consistent with the field interpretations described above.

## 5.3. Zircon Elemental & Isotopic Compositions

### *5.3.a. Trace Elements*

Following the work of Grimes *et al.* (2007), Carley *et al.* (2014) established compositional fields for zircon formed in silicic rocks from a range of tectonic settings, based on the abundance of Hf, U, REE, and Ti in zircon (Fig. 12). Though Hf concentrations in AIC zircons fall within the field for zircons from silicic rocks from continental-type environments, they are mostly restricted to the lower end of the range at <12,000 ppm (see Fig. 8d). Zircon incompatible element abundances and ratios show that AIC silicic magmas, and Icelandic silicic magmas in general, are less evolved relative to continental arc-type silicic environments, and most closely resemble silicic magmas from modern evolving continental rift and continental hotspot environments (e.g. higher Gd/Yb and U/Yb ratios, lower Hf abundances; see Fig. 12; e.g. Carley *et al.*, 2014; Claiborne *et al.*, 2010), with a few zircons (mostly from granodiorite IA-NS-7) falling outside of these fields.

The zircon population from the coastal gabbro (IA-G-1) generally forms the most coherent individual geochemical array. This zircon population likely reflects crystallization within internally fractionating parental melts that experienced little to no interactions with other magmas after zircon saturation. Zircons from the granophyre (IA-NS-2) display a large spread in composition, which may reflect sampling of different zone populations in the complex zircon. The geochemical variability in zircon zones may be a consequence of mixing and assimilation of magmas prior to zircon saturation and growth in the parental melt. In contrast, the granodiorite (IA-NS-7), and to a lesser extent also the diorite (IA-NS-6), has a geochemically bimodal zircon population best identified by their Eu/Eu* and Nb/Yb compositions (see Fig. 8c,g; for IA-NS-6, roughly identifiable by Th, Sc, Ce/Nb and Sc/Yb; see Fig. 8a,b,f). A substantial number of grains from the diorite, and some in the granodiorite, are anhedral, often with truncated CL-zoning surrounded by oscillatory overgrowth zones (Fig. 7), indicating resorption as a consequence of disequilibrium between zircon and melt. These features, along with the zircon geochemistry, support the open-system interactions suggested by field relationships between mafic and silicic rocks at the location where the samples were collected (see Table 1). We thus interpret these units to represent hybridized magmas, resulting from mixing of multiple compositionally different magma batches from which diverse zircon populations were incorporated.

### *5.3.b. Ti-in-Zircon Thermometry*

Our estimated zircon crystallization temperatures range from ~750 to ~990ºC (5-40 ppm; Fig. 8d). Maximum Ti-in-zircon temperatures in the most silicic sample for which zircons were analyzed (granophyre IA-NS-2) approximately equal zircon saturation temperatures (ZSTs) for their host rock (~850ºC; Fig. 13). The majority of zircon crystallization temperatures for the granodiorite (IA-NS-7) also fall near or below the ZST for their host rock (~900ºC). Minimum Ti-in-zircon temperatures are similar for all silicic samples (~760 to 770ºC). The diorite sample (IA-NS-6) has a lower ZST than the silicic samples (~760ºC), but its range of Ti-in-zircon temperatures is very similar (~760 to 990ºC), especially to the granodiorite. These data taken together suggest that zircon saturation occurred at roughly 900ºC and zircon crystallization continued to the solidus at <760ºC. As previously mentioned, the diorite sample likely represents a hybridized magma whose ZST of ~760ºC is therefore not meaningful (elemental composition is far from melt composition). Ti-in-zircon crystallization temperatures in MSCZ gabbros range from 750 to 980ºC. This likely represents the approximate temperature range from zircon saturation to the solidus for these internally fractionating mafic magmas.

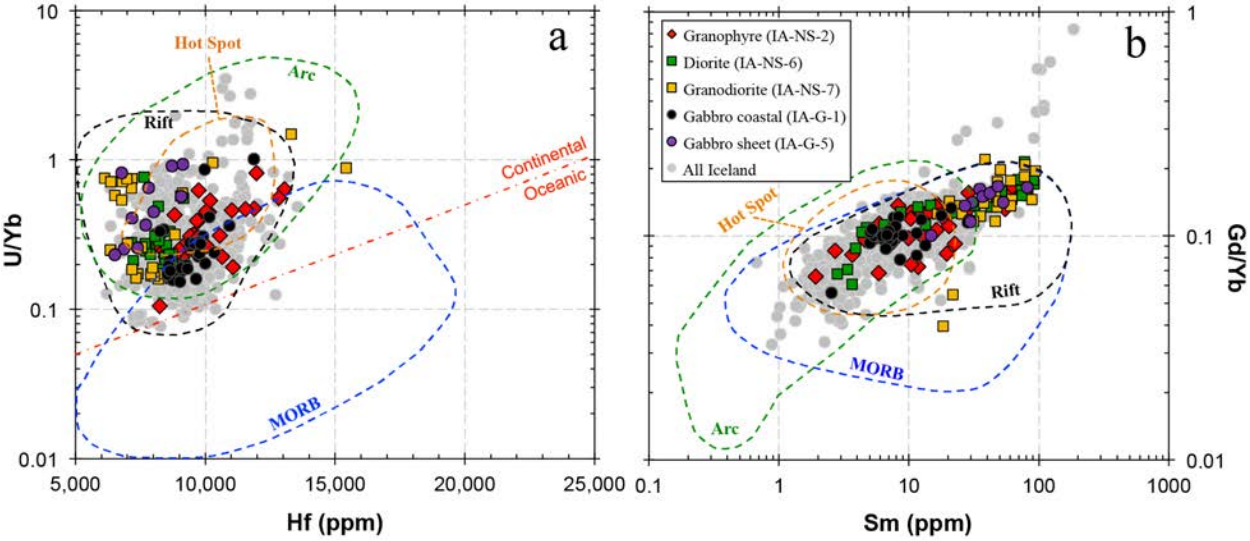

**Figure 12**

Discrimination plots for zircon from different tectonic settings (e.g. Grimes *et al.*, 2007) based on trace element geochemistry. The dashed regions represent the range of zircon geochemistry for different tectonic settings from around the world (modified after Carley *et al.*, 2014): blue = Mid-Ocean Ridge Basalt (MORB); black = evolving continental rift (Alid, E. Africa; Salton Sea, N. America); orange = continental hot spot (Yellowstone, N. America); green = continental arc (N. America: Mt. Saint Helens, Three Sisters, McCoy Mountain Complex). **a)** Hf vs. U/Yb. **b)** Sm vs. Gd/Yb.

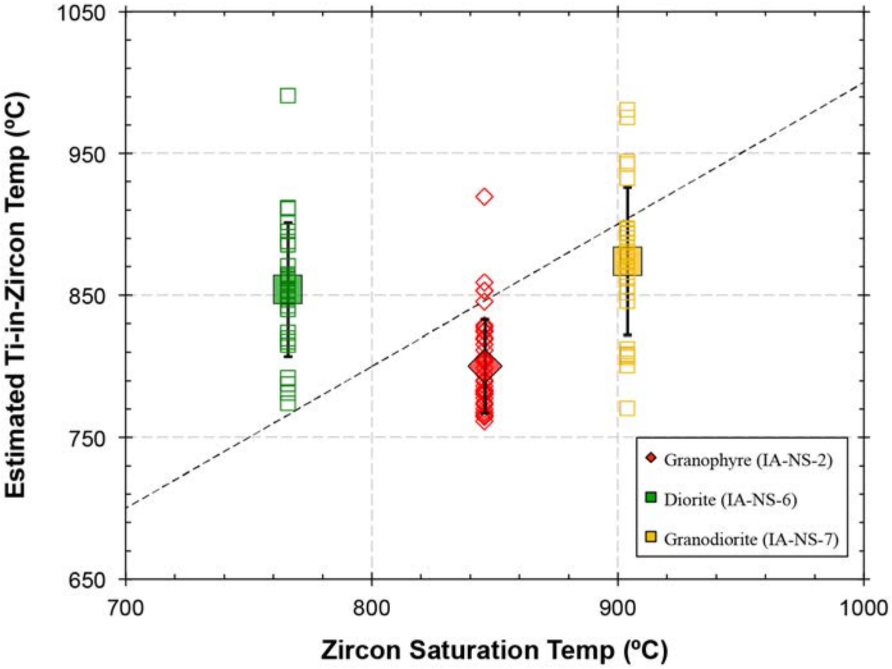

**Figure 13**

Estimated whole-rock zircon saturation temperatures (ZST), calculated using the formula derived by Watson & Harrison (1983) as revised by Boehnke *et al.* (2013), plotted against model zircon crystallization temperatures, calculated using the Ti-in-zircon thermometer of Ferry & Watson (2007), for silicic units of the Austurhorn Intrusive Complex. The large filled symbols represent the mean Ti-in-zircon crystallization temperature for each sample. Error bars are 1σ. The dashed line indicates a ratio of 1. The diorite sample likely represents a hybrid whose ZST is meaningless.

### 5.3.c. Oxygen and Hafnium Isotopes

Zircon populations in all but one of our samples (coastal gabbro IA-G-1) preserve a range in $\delta^{18}O$ that is beyond analytical uncertainty, which we interpret to reflect the open-system processes that affected the MSCZ. Generating such low and variable $\delta^{18}O$ in MSCZ zircons (+2.2 to +4.8 ‰; Fig. 10a and Table 5) appears to require substantial but variable contribution from pre-existing crust that had been hydrothermally altered in the presence of meteoric (isotopically-light) fluids, given that expected values for zircon equilibrated with mantle-derived magmas are generally accepted to be in the range of +5.3 ± 0.6 ‰ (e.g. Drew *et al.*, 2013, Bindeman *et al.*, 2008). For example, if we assume a zircon-equivalent $\delta^{18}O$ value of 0 ‰ for altered Icelandic crust and 5.3 ‰ for mantle-derived magma, it would require a nearly 60% crustal mass fraction in a hybrid magma to crystallize zircon with $\delta^{18}O$ of +2.2 ‰. If the altered crust were as low as -5 ‰, the crustal fraction would be 30%.

Recent oxygen isotopic studies suggest that the $\delta^{18}O$ signature of the Iceland mantle plume may be substantially lighter than that of typical mantle, and that $\delta^{18}O$ of primary olivines from uncontaminated basaltic magmas may extend to values as low as +3.2 to +4.0 ‰ (Maclennan *et al.*, 2003; Thirlwall *et al.*, 2006). Such a primary magma composition would require a smaller crustal fraction in low-$\delta^{18}O$ silicic magma; a magma crystallizing olivine with $\delta^{18}O$ of +3.2 to +4.0 ‰ would permit crystallization of zircon with values as low as ~3.5 ‰ to ~4.3 ‰ (based on $^{18}O$ magmatic fractionation differences $\Delta^{18}O_{Zrc\text{-}Ol} = +0.2$ to +0.3 ‰; Valley *et al.*, 1998). Even assuming such low primary values, there remains ~80% of our dataset (~95% when gabbros are excluded) that is below mantle zircon values if we extend the range down to +4.3 ‰, and ~20% (~25%, gabbros excluded) if extended down to +3.5 ‰, which would still require an interpretation that involves variable contributions from altered low-$\delta^{18}O$ crust for the observed range of $\delta^{18}O$ in AIC zircons.

Notably, zircons from the coastal gabbro (IA-G-1) have the least variability in oxygen values, with a range of +4.2 to +4.9 ‰ (see Fig. 10a). The facts that the coastal gabbro is, geochemically, the most consistent with closed-system fractionation and that it lacks field evidence for extensive interactions with silicic magmas suggest that its zircon $\delta^{18}O$ range represents the range for the parental mafic magmas of the AIC, and reflects a mantle plume signature of $\delta^{18}O$ > +4.2 ‰. Bindeman *et al.* (2012) present zircon $\delta^{18}O$ values for an intermediate silicic sample (~65 wt.% $SiO_2$) from Austurhorn that range from +4.4 to +5.6 ‰, which they interpret to reflect fractional crystallization of mantle plume magmas. This is consistent with our interpretation (above) for the $\delta^{18}O$ signature of the source magmas for the AIC. Furthermore, taking into consideration the fraction of zircons with lower than normal $\delta^{18}O$ in the silicic units (~85% if we assume the normal source magmas are > +4.2 ‰, per our gabbro data above), this would indicate that incorporation of hydrothermally altered low-$\delta^{18}O$ crust plays a major role in the petrogenesis of silicic melts with lower and more variable $\delta^{18}O$ (down to +2.2 ‰) throughout the MSCZ. The intruding mafic magmas likely encountered strongly hydrothermally altered country rock during ascent in the shallow crust, resulting in melting and variable assimilation of low-$\delta^{18}O$ crust, and subsequently facilitating the generation, accumulation, and emplacement of silicic melts in the MSCZ (e.g. Sigmarsson *et al.*, 1991; Bindeman *et al.*, 2008, 2012; Gurenko *et al.*, 2015). The elemental data of zircons from the granophyre suggest that contamination of altered crust occurred prior to zircon saturation in the initial magma(s), and was followed by fractionation and zircon crystallization from a compositionally variable melt. In contrast, the multiple populations of zircon in the diorite (IA-NS-6) and granodiorite (IA-NS-7) indicate that some zircon growth had taken place in a range of different melts prior to contamination and mechanical mixing of their host magmas, and continued down to the solidus. The wide range of $\delta^{18}O$ in zircons from the sheet gabbro (IA-G-5) suggests they are in part derived from the host silicic magma through mechanical interactions during intrusion.

In conjunction with oxygen isotopes, hafnium isotope ratios in zircon provide an additional constraint for identifying the mantle and/or crustal contributions to the Austurhorn magmatic system (e.g. Kemp *et al.*, 2007). The Hf isotopic compositions of MSCZ zircons cluster around a mean of +13 ε-units, with very minor and expected variability (Fig. 10b). These values fall within the lower, less-depleted portion of the Hf isotopic range of Icelandic basalts, including the off-rift and lowest end of the on-rift range (Peate *et al.*, 2010; see Fig. 10b and Table 5). The observed range in whole-rock Hf compositions for our samples also overlaps with that of zircons from all MSCZ units (Fig. 14). This suggests that MSCZ magmas were sourced from an off-rift or propagating rift environment, consistent with previous interpretations of a transitional rift, away from the main rift axis and significantly influenced by the Iceland plume, in southeast Iceland at the time of intrusion (*cf.* Martin *et al.*, 2011).

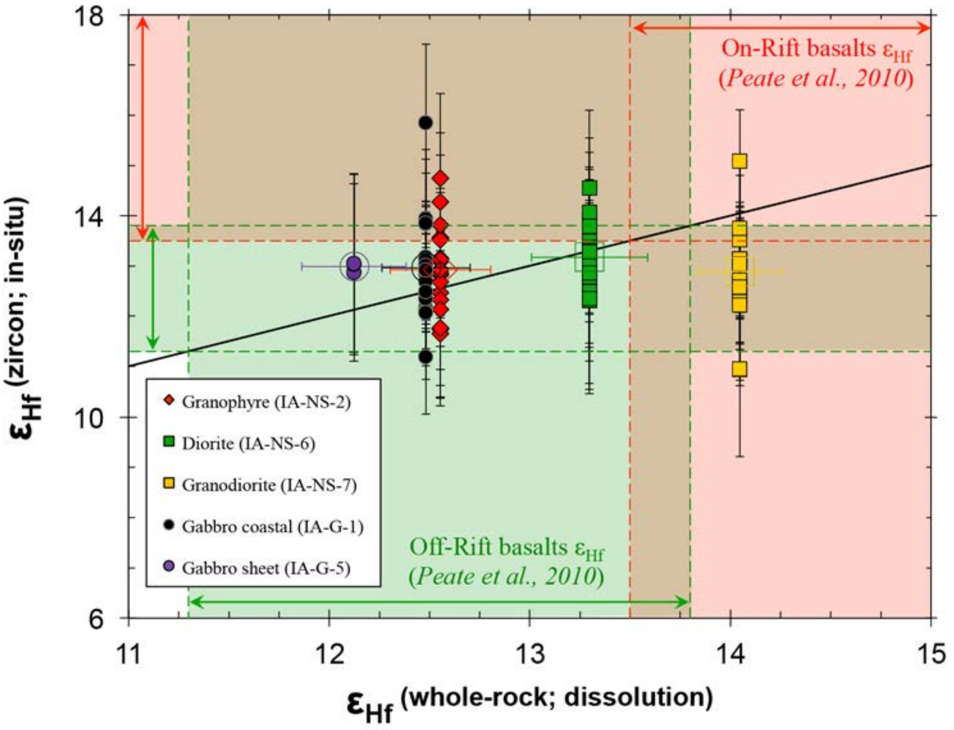

**Figure 14**

*In-situ* zircon vs. whole-rock $\varepsilon_{Hf}$ compositions for units of the Austurhorn Intrusive Complex. The larger open symbols for each sample represent the mean *in-situ* $\varepsilon_{Hf}$, plotted against WR values and their errors (2σ). The red and green zones and arrows indicate the $\varepsilon_{Hf}$ range of Icelandic *on-rift* basalts (from the Northern and Western Volcanic Zones: $\varepsilon_{Hf}$ = +13.5 to +18.9; Peate *et al.,* 2010) and *off-rift* basalts (from the Eastern Volcanic Zone, Snæfellsnes Peninsula, Vestmannæyjar, and Snæfell volcano: $\varepsilon_{Hf}$ = +11.3 to +13.8; Peate *et al.,* 2010), respectively. The dashed line indicates a ratio of 1.

## 5.4. U-Pb Geocrhonology

*In situ* U-Pb zircon geochronology data permit two interpretations regarding the construction and longevity of the Austurhorn magmatic system. When all samples are pooled together, they yield an age of 6.52 ± 0.03 Ma for the MSCZ (Fig. 11), which is consistent with the previously published K-Ar age of 6.6 ± 0.4 Ma (Moorbath *et al.*, 1968) for gabbro, as well as LA-ICP-MS U-Pb zircon ages of 6.6 ± 0.4 and 6.5 ± 0.2 Ma for granophyre and gabbro, respectively (Martin *et al.*, 2011). The pooled age data permit a single coherent population that represents one age for the entire complex. However, the MSWD for the number of individual zircon analyses (MSWD = 1.8; n = 137) exceeds the upper limit of the 95% confidence interval (Mahon, 1996), suggesting scatter beyond what would be expected for a single statistically coherent population. Alternatively, weighted mean ages for individual samples are statistically distinguishable at 2σ uncertainties, and suggest zircon crystallized in the AIC for up to ~300 k.y. from repeated magmatic intrusions (from approximately 6.67 to 6.35 Ma; Fig. 11), which may be interpreted to represent the approximate timescale of construction. We favor this interpretation, which is consistent with the composite field relationships that are preserved, indicating that the AIC system was periodically rejuvenated by repeated intrusions of hotter mafic magmas, thereby prolonging the window of zircon crystallization and longevity of the Austurhorn magmatic system.

# 6. **Conclusions**

With this study, we present the first detailed characterization of what is likely Iceland's dominant zircon population: plutonic zircon. In comparison to Iceland’s silicic volcanic rocks, both mafic and silicic rocks from the mafic-silicic composite zone at the Austurhorn intrusive complex contain a significantly greater abundance of zircon. These plutonic zircons are generally larger and display more distinct and complex zoning than volcanic zircon. Grain morphology is varied, and oscillatory-zoned euhedral grains are common in all samples. However, a large number of zircon grains retain evidence, as irregular cores and truncated internal zoning, for thermal and chemical fluctuations that mark repeated mafic-silicic magma interactions in the history of the complex.

The elemental composition of AIC zircons form a broad but coherent array that mostly overlaps with the well-constrained signature of zircons from Icelandic silicic volcanic rocks (Carley *et al.,* 2011, 2014). Titanium concentrations range from 6 to 40 ppm (Ti-in-zircon temperatures ~750-990ºC, assuming $a_{TiO_2} = 0.5$ and $a_{SiO_2} = 1.0$), and Hf concentrations are relatively low (below 12,000 ppm), typical of Iceland zircons. Oxygen isotope ($\delta^{18}O$) values extend from +2.2 to +4.8 ‰, consistent with the $\delta^{18}O$ range of other Icelandic magmatic zircon from silicic volcanic centers (Bindeman *et al.*, 2012; Carley *et al.*, 2014), and provide strong evidence for the influence of meteoric water, hydrothermal processes, and recycling of hydrothermally-altered crust as a major contributor to silicic magmas within the AIC system. Epsilon-Hf values, clustering around +13.0 ± 1.6 (2σ SD), are toward the lower end of previously measured values for Iceland basalts, similar to those from off-rift settings and the least depleted (lowest $\varepsilon_{Hf}$) on-rift basalts, suggesting that Austurhorn likely developed in a transitional rift environment.

*In situ* U-Pb zircon dating yields an age of 6.52 ± 0.03 Ma for the entire complex. However, the spread in average ages for each unit suggests that the construction and evolution of the Austurhorn intrusive complex extended over ~300 k.y., with multiple short-lived intrusion events occurring closely spaced in time from ~6.67 to ~6.35 Ma, allowing for periodic rejuvenation and a prolonged lifetime for the crystallizing mush.

The Austurhorn intrusive complex reveals extensive interaction between mafic and silicic magmas, as part of a very complex silicic magmatic system characterized by multiple episodes of mafic magmatic replenishment that is well preserved in the zircon record. It provides a useful example of the manifestation and consequences of mafic recharge in silicic systems at shallow depths, and an additional dimension in helping us better understand the accumulation of silicic magmas, and the subsequent evolution of silicic magmatic systems within the Earth's crust.

# CHAPTER IV

## Generating the world's lowest magmatic zircon $\delta^{18}O$: Melting of intensely hydrothermally altered crust beneath the Austurhorn magmatic system, SE Iceland

### Abstract

The 6.52 Ma Austurhorn intrusion, a shallowly emplaced (~2 km) complex exposed over ~15 $km^2$ in SE Iceland, comprises large bodies of granophyre, gabbro, and a mafic-silicic composite zone (MSCZ) that exemplifies magma interactions common in Icelandic silicic systems.

Oxygen isotopic analyses of zircon and primary quartz, feldspar, and pyroxene from samples representing the range of compositions in the MSCZ, from gabbros to high-silica granophyres (HSG), reveal extreme oxygen variability but small mineral-mineral fractionation, consistent with a hydrothermal-magmatic transition (>600°C). In most samples, individual zircon $\delta^{18}O$ falls between +2.2 and +4.9 ‰. These values suggest modest to major contributions from meteoric-hydrothermally altered crust in generating their parental magmas. A subset of *in situ* zircon analyses, all from HSG, preserve lower values (down to -11.3 ‰, the lowest $\delta^{18}O$ yet measured in Icelandic zircon). HSG whole rocks and major mineral separates also display low and variable $\delta^{18}O$ (e.g. +6.0 to -2.9 ‰ in quartz), consistent with a magmatic origin for the lower $\delta^{18}O$ zircons, making it also the lowest magmatic zircon $\delta^{18}O$ signature in the world.

We interpret zircon $\delta^{18}O$ diversity to indicate construction of the intrusion from multiple, isotopically diverse magma increments. The HSG with the lowest magmatic $\delta^{18}O$ zircon values comprise nearly pure granophyric quartz and feldspar (+ zircon). We interpret these to represent batches of small volume melts generated entirely by melting of intensely altered crust that

underwent nearly complete (large water/rock ratio) high-T exchange with ~ -10 to -14 ‰ hydrothermal meteoric fluids.

Heterogeneity in $\delta^{18}O$ in zircon and major minerals is consistent with field relationships at Austurhorn, suggesting that sustained melting activity, as a consequence of continuous mafic recharge, was a primary mechanism contributing to the generation and accumulation of silicic magmas throughout the lifetime of the Austurhorn system. Diverse $\delta^{18}O$ in zircons and other minerals provide important insights into magmatic-hydrothermal transition zones as well as physical mechanisms of shallow magma petrogenesis by amalgamation of diverse melts.

# 1. **Introduction**

Iceland has become a strong focus in studies of silicic magma petrogenesis because of the unusual abundance of silicic rocks (≥10% of exposed rocks) associated with Icelandic central volcanoes and composite intrusions (e.g. Bindeman *et al.*, 2012; Carley *et al.*, 2011, 2014; Charreteur *et al.*, 2013; Gunnarsson *et al.*, 1998; Gurenko, *et al.*, 2015; Jonasson, 2007; Marsh *et al.*, 1991; Martin and Sigmarsson, 2007, 2010; Thordarson and Larsen, 2007). The magmas feeding volcanic activity in Iceland are interpreted to be juvenile, derived either by direct partial melting of the mantle beneath Iceland, or by extensive recycling of altered juvenile Icelandic crust (Bindeman *et al.*, 2012; Gurenko, *et al.*, 2015; e.g. Marsh *et al.*, 1991; Sigmarsson *et al.*, 1991; Sigmarsson and Steinthorsson, 2007; Zellmer *et al.*, 2008).

Oxygen isotopic compositions of minerals and rocks can distinguish between magmatic and non-magmatic processes, such as sub-solidus hydrothermal alteration and metamorphism (e.g. Bindeman *et al.*, 2008; Bindeman *et al.*, 2010; Bindeman and Valley, 2001; Drew *et al.*, 2013; Elders *et al.*, 2011; Genske *et al.*, 2013; Hollis *et al.*, 2014; Wotzlaw *et al.*, 2012; Zheng *et al.*, 2004). Furthermore, in Iceland in particular, they can be especially useful in assessing the relative contributions to magmas from juvenile, mantle-derived melts and partial melts of altered crust (e.g. Bindeman *et al.*, 2012; Carley *et al.*, 2014; Gurenko, *et al.*, 2015; Marsh *et al.*, 1991; Martin and Sigmarsson, 2005; Reimink *et al.*, 2014; Sigmarsson *et al.*, 1991). Thus, much of the debate about the petrogenesis of silicic magmas in Iceland has focused on the $\delta^{18}O$ variation observed in volcanic products, either from bulk rock and bulk minerals (e.g. Bindeman *et al.*, 2012; Hattori and Muehlenbachs, 1982; Pope *et al.*, 2013; Schattel *et al.*, 2014; Thirlwall *et al.*, 2006) or from individual crystal separates (e.g. zircon: Bindeman *et al.*, 2012; Carley *et al.*, 2014; olivine: Eiler *et al.*, 2000; Maclennan *et al.*, 2003).

The occurrence of primitive lavas in active Icelandic rift systems with $\delta^{18}O$ below typical mantle values (mantle zircons: +5.3 ±0.6 ‰; Valley *et al.*, 1998) suggests incorporation of a hydrothermally altered crustal component into the magmas. Based on the extent of $^{18}O$ depletion in some of these lavas (down to ~ +1.8 ‰; e.g. Muehlenbachs *et al.*, 1974), some researchers advocate for partial melting of hydrothermally altered Icelandic crust as the dominant mechanism producing silicic melts in Iceland (e.g. Bindeman *et al.*, 2012; Gurenko, *et al.*, 2015; Martin and Sigmarsson, 2010; Pope *et al.*, 2013; Schattel *et al.*, 2014). However, others argue that some geochemical signatures in low-$\delta^{18}O$ lavas cannot be produced by assimilation of crustal material alone (e.g. high-Mg# primary olivines with $\delta^{18}O$ as low as +3.2 ‰), and therefore advocate for an alternative interpretation that involves fractional crystallization of mantle source that includes $^{18}O$-depleted material (e.g. Maclennan *et al.*, 2003; Thirlwall *et al.*, 2006). Combining isotopic data from multiple coexisting magmatic phases (e.g. pyroxene + olivine, or pyroxene + zircon) may allow us to more critically assess the origin of variable $\delta^{18}O$ lavas, especially for silicic magmatic systems, whether by partial melting alone or by assimilation processes.

In this study, we investigate the generation and accumulation of silicic magmas at the Austurhorn intrusive complex using an extensive oxygen isotopic dataset for zircon (*in-situ* analyses), whole-rocks, and major mineral separates. Zircons and major minerals in the most evolved rocks preserve a wide range of $\delta^{18}O$, including extremely low values that extend to -2.9 ‰ in quartz and -11.3 ‰ in zircon. We propose that these rocks represent the products of pure crustal melting of intensely and variably altered Icelandic crust, a unique end-member example of magmatic processes that can help us better understand the relative contributions of partial melting and fractional crystallization in the petrogenesis of silicic magmas.

## 2. **Geological Background: The Austurhorn Intrusive Complex**

The Austurhorn intrusive complex (AIC), in southeastern Iceland, is a small composite intrusion comprising granophyre, gabbro, and an extensive mafic-silicic composite zone (MSCZ) that preserves abundant evidence for extensive mingling and mixing of magmas (e.g. Padilla *et al.*, in review; Blake, 1966; Furman *et al.*, 1992; Mattson *et al.*, 1986). The structure of the shallowly emplaced AIC (~2 km; Walker, 1960, 1964), together with its geochemical characteristics, suggest that it developed in a transitional rift environment, similar to the Torfajökull central volcano in Iceland's modern Eastern Volcanic Zone (Padilla *et al.*, in review; Furman *et al.*, 1992b; Gunnarsson *et al.*, 1998; Martin *et al.*, 2011). The intrusion is well dated by U-Pb geochronology *in-situ* using zircon from 9 samples that span the compositional spectrum of exposed rocks in the AIC, from ~47% to ~79% $SiO_2$ (Padilla *et al.*, in review). Pooled together, zircons from the entire complex yield a mean age of 6.52 ±0.03 Ma. However, the spread in individual unit ages, from 6.35 to 6.67 Ma, suggests construction of the Austurhorn intrusive complex extended over ~300 k.y., with multiple short-lived intrusion events occurring closely spaced in time allowing for periodic rejuvenation and a prolonged lifetime for the crystallizing mush.

The MSCZ occupies the lowest structural levels exposed and comprises 30-40% of the AIC. The mafic enclave density is highly variable from outcrop to outcrop, ranging from a few volume percent up to 60%. Near the structural top of the MSCZ there is a zone of enclave-poor granophyre that is heavily intruded by small-volume dikes and pods of high-$SiO_2$ granophyre (HSG). These HSG units are leucocratic, very fine-grained, and most typically preserved as centimeters- to decimeters-wide dikes that are often folded, indicating that they were intruded into the MSCZ while the host granophyre was still hot, ductile (Fig. 1). The smaller dikes are only locally continuous within exposed outcrops in the HSG zone, often fragmented into individual pods, but some of the largest dikes can be traced for tens of meters across multiple outcrops. Furthermore, some dikes and pods of HSG are disaggregated and mingled with the coarser host granophyre into which they intruded, preserving evidence of silicic-silicic magmatic interactions, particularly in the form of diffuse boundaries (Fig. 1).

With the exception of the high-$SiO_2$ granophyres, the whole-rock and zircon geochemistry of MSCZ rocks and their significance are discussed by Padilla *et al.* (in review). Here we present a more focused discussion of the HSG samples, which, though volumetrically small, in our view represent important end-member magmatic processes that may be commonplace across the rest of the Austurhorn system, and likely many other silicic magmatic systems, yet not typically preserved in the rock record.

## 3. **Methods**

Prior to analytical work, all zircons were mounted on epoxy and imaged by cathodoluminescence (CL) using a Tescan Vega 3 LM variable pressure SEM, at the Vanderbilt University Department of Earth Sciences. We use CL images to characterize zoning patterns and internal structures, and to guide us in the placement of analytical spots on individual grains.

We used the SHRIMP-RG at the Stanford-USGS Microanalytical Center to measure trace element and U-Pb isotopic abundances of spots on individual zircon grains from 9 representative samples of the MSCZ. We follow the methods of Grimes *et al.* (2007) and Claiborne *et al.* (2010; 2006), using R33 zircons (419±1 Ma, Black *et al.*, 2004), and MAD and MADDER (Barth and Wooden, 2010), as our U-Pb geochronology and trace element reference materials, respectively, to correct for instrumental mass fractionation (IMF).

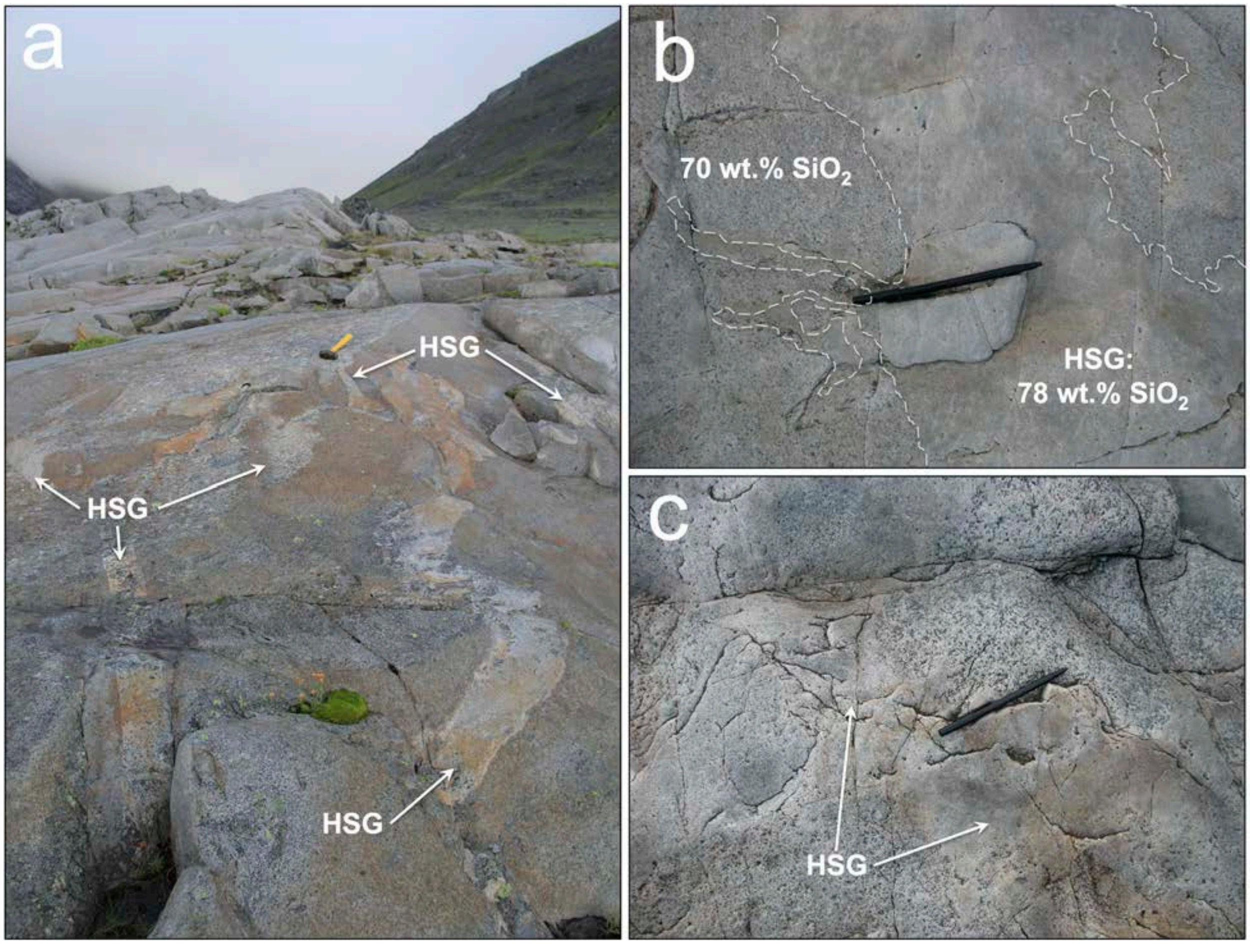

**Figure 1**

Exposures of high-$SiO_2$ granophyre (HSG) within the mafic-silicic composite zone (MSCZ) at the Austurhorn Intrusive Complex. They are found near the structural top of the MSCZ as fine-grained cm-wide to dm-wide dikes and pods intruded into enclave-poor granophyres. **(a)** Folded HSG dike section, continuous for only a few meters, surrounded by other fragments and pods of smaller disaggregated dikes. Sledge hammer (yellow handle) for scale. **(b)** Outcrop of fine-grained ~78 wt.% HSG mingled with coarser-grained ~70 wt.% granophyre. Bic pen for scale. **(c)** Mechanically mixed HSG (finer-grained, tan/reddish) and granophyre (coarser-grained, white/grayish), with diffuse boundaries between both units. Bic pen for scale.

We measured in-situ oxygen isotope ratios in the same zircons by SIMS at the UCLA W.M. Keck Foundation Center for Isotope Geochemistry, following the methods outlined by Trail *et al.* (2007) and using R33 ($\delta^{18}O$ = 5.55 ‰; Valley, 2003) as the reference material.

Lastly, we measured bulk oxygen isotopes in mineral separates (~1.2 mg aliquots, treated with HF to remove alteration) of major phases (quartz, feldspar, amphibole, pyroxene) and bulk granophyre (intergrown quartz and feldspars) using laser fluorination ICP-MS at the University of Oregon Stable Isotope laboratory, following the method of Bindeman (2008). We analyzed aliquots of Gore Mountain garnet (UOG, $\delta^{18}O$ = 6.52 ‰; Bindeman *et al.*, 2014) as the reference material along with the unknowns to correct for IMF.

## 4. **Results**

High-$SiO_2$ granophyres from the MSCZ preserve unique features that differ markedly from those observed in all other MSCZ samples (see Padilla *et al.*, in review, for a thorough discussion of non-HSG AIC samples). These HSGs and associated silicic units are among the oldest rocks in the MSCZ, with individual mean zircon ages clustering around 6.6 Ma (Padilla *et al.*, in review; for full U-Pb geochronology data see Appendix B.1). In contrast to other silicic rocks, which contain typical granitic mineral assemblages (quartz, feldspars, amphibole, accessory sphene, opaque oxides, and zircon, ±biotite), HSGs are composed of ~99% quartz and feldspar in very well developed micrographic intergrowths, with abundant accessory zircon (± minor sphene, apatite, and FeTi oxides). These rocks contain the lowest $TiO_2$ (<0.2 wt.%), $Al_2O_3$ (<13 wt.%), MgO (<0.05 wt.%), and CaO (<0.5 wt.%) concentrations of all rocks in the MSCZ, and also generally contain higher $K_2O$ (mostly >4 wt.%; Fig. 2; for full whole-rock geochemistry, see Appendix B.8). They are depleted in light and middle REE, Sr (~ 20-50 ppm), Ba (<420 and down to 20 ppm), and Zr (~ 350-450 ppm), relative to all other silicic rocks (for all others: Sr > 95 ppm; Ba > 440 ppm; Zr > 580; see Figs. 3, 4), and have larger negative Eu anomalies.

Zircons from the HSGs can be divided into two geochemical groups (Fig. 5). The elemental compositions of the first group (which make up ~60% of the HSG zircon population) are similar to those of zircons from all other MSCZ rocks as well as other Icelandic silicic rocks (Padilla *et al.*, in review; Carley *et al.*, 2011, 2014). Uranium and Th concentrations mostly range from ~50 to ~1000 ppm and ~15 to ~1000 ppm, respectively, Hf concentrations are characteristically low (<12,000 ppm), and Ti ranges from ~5 to ~40 ppm (Carley *et al.*, 2011; Cavosie *et al.*, 2006; Grimes *et al.*, 2007; Hoskin and Schaltegger, 2003).

The second group of HSG zircons is generally distinguished either by dark CL or convolute zoning, and commonly by abundant CL-bright inclusions (Fig. 6). These zircons are commonly enriched in U and Th (mostly >1000 ppm; up to ~5800 ppm U and ~9000 ppm Th), and contain much higher Hf than any other analyzed Icelandic zircon (>12,000 ppm, up to ~28,000 ppm). In addition, they have distinctly lower Ti abundances (~ 2-10 ppm), and are more strongly depleted in Eu than other MSCZ zircons (Eu/Eu* <0.06, down to 0.02, compared to >0.07 for all others; see Fig. 5; for full zircon trace element data, see Appendix B.2-B.4). Despite significant differences in concentrations, some elemental ratios (e.g. Th/U and Ce/Ce*) remain similar to those of more typical MSCZ zircons.

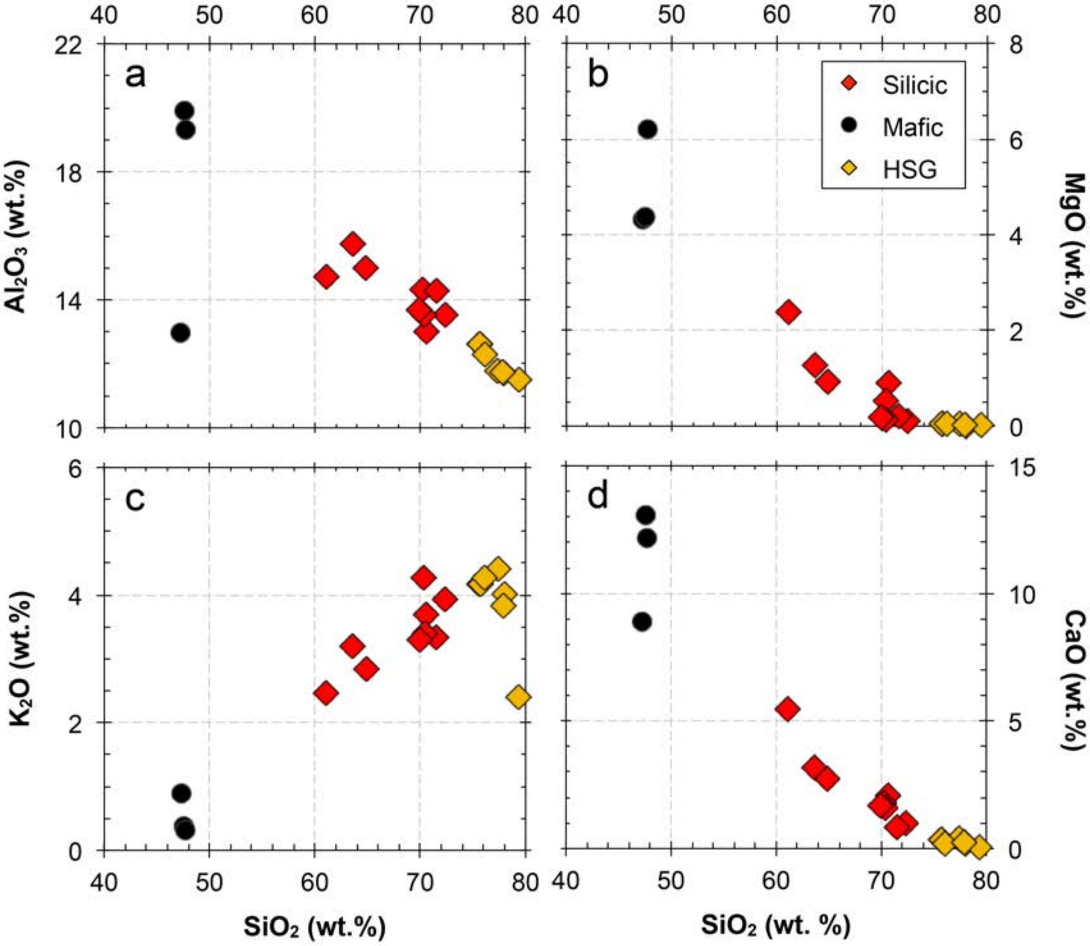

**Figure 2**

Whole-rock major element geochemical comparison plots for samples from the Austurhorn intrusive complex. **a)** $SiO_2$ vs. $Al_2O_3$; **b)** $SiO_2$ vs. MgO; **c)** $SiO_2$ vs. $K_2O$; and **d)** $SiO_2$ vs. CaO. For a list of the individual samples in each compositional group (e.g. "Silicic" group), see Appendix B.7.

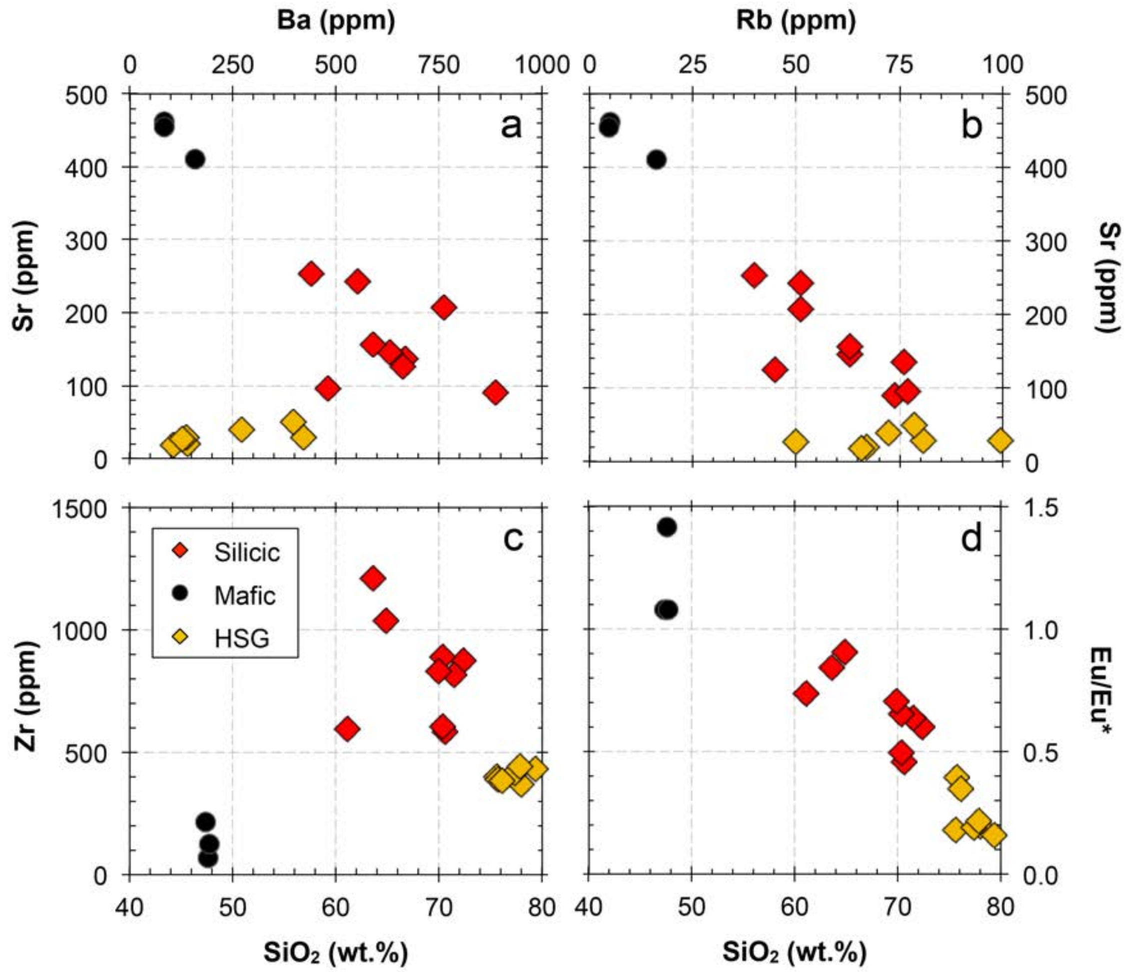

**Figure 3**

Whole-rock trace element geochemical comparison plots for samples from the Austurhorn intrusive complex. **a)** Ba vs. Sr; **b)** Rb vs. Sr; **c)** $SiO_2$ vs. Zr; and **d)** $SiO_2$ vs. Eu/Eu* (Eu anomaly).

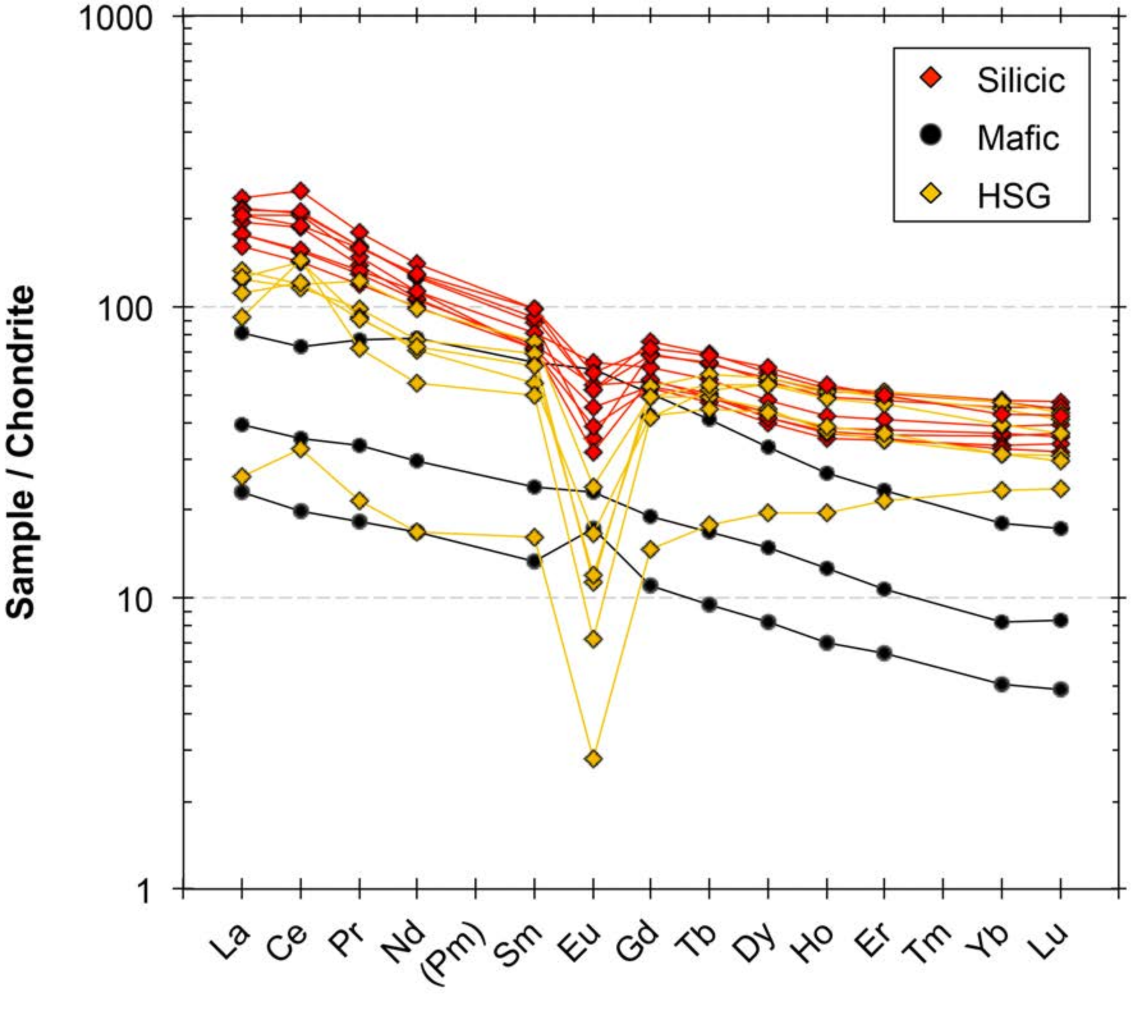

**Figure 4**

Whole-rock Rare Earth element (REE) geochemistry for samples from the Austurhorn Intrusive Complex.

The oxygen isotopic compositions ($\delta^{18}O$) of all HSG zircons are low relative to mantle zircons (+5.3 ± 0.6 ‰, 2σ; Valley *et al.*, 1998). The majority fall within the +2.2 to +4.9 ‰ range of zircons from the other MSCZ units, which we hereafter refer to as "normal-$\delta^{18}O$." This range is also consistent with Icelandic magmatic zircon compositions in general (Padilla *et al.*, in review; Bindeman *et al.*, 2012; Carley *et al.*, 2014). However, the full range of HSG zircons extends to far more depleted oxygen compositions, with ~30% of zircons depleted below 0 ‰ (Fig. 7; for full zircon oxygen isotopes data, see Appendix B.5). The most variable HSG sample contains zircons with oxygen compositions that span over ~16 ‰, from +4.5 to as low as -11.3 ‰. This is the largest known $\delta^{18}O$ range in zircons from any Icelandic sample, and to the best of our knowledge includes the lowest $\delta^{18}O$ value yet measured in any magmatic zircon in the world. Low-$\delta^{18}O$ zircons ($\delta^{18}O < 2.2$ ‰) can often be correlated with characteristics of the second geochemical zircon group described above, including higher Hf, U, and Th abundances, deeper Eu anomalies, and lower Ti concentrations (Fig. 5). Convolute zoning and abundant inclusions are also common features in low-$\delta^{18}O$ zircons, though the occurrence of low $\delta^{18}O$ values in normal-zoned crystals as well as normal $\delta^{18}O$ values in convolute-zoned crystals indicates that these are not mutually inclusive characteristics. Furthermore, pre- and post-analysis imaging of convolute-zoned zircons reveals variable and low $\delta^{18}O$ in HSG zircons regardless of the abundance (or absence) of inclusions in a grain (Fig. 6).

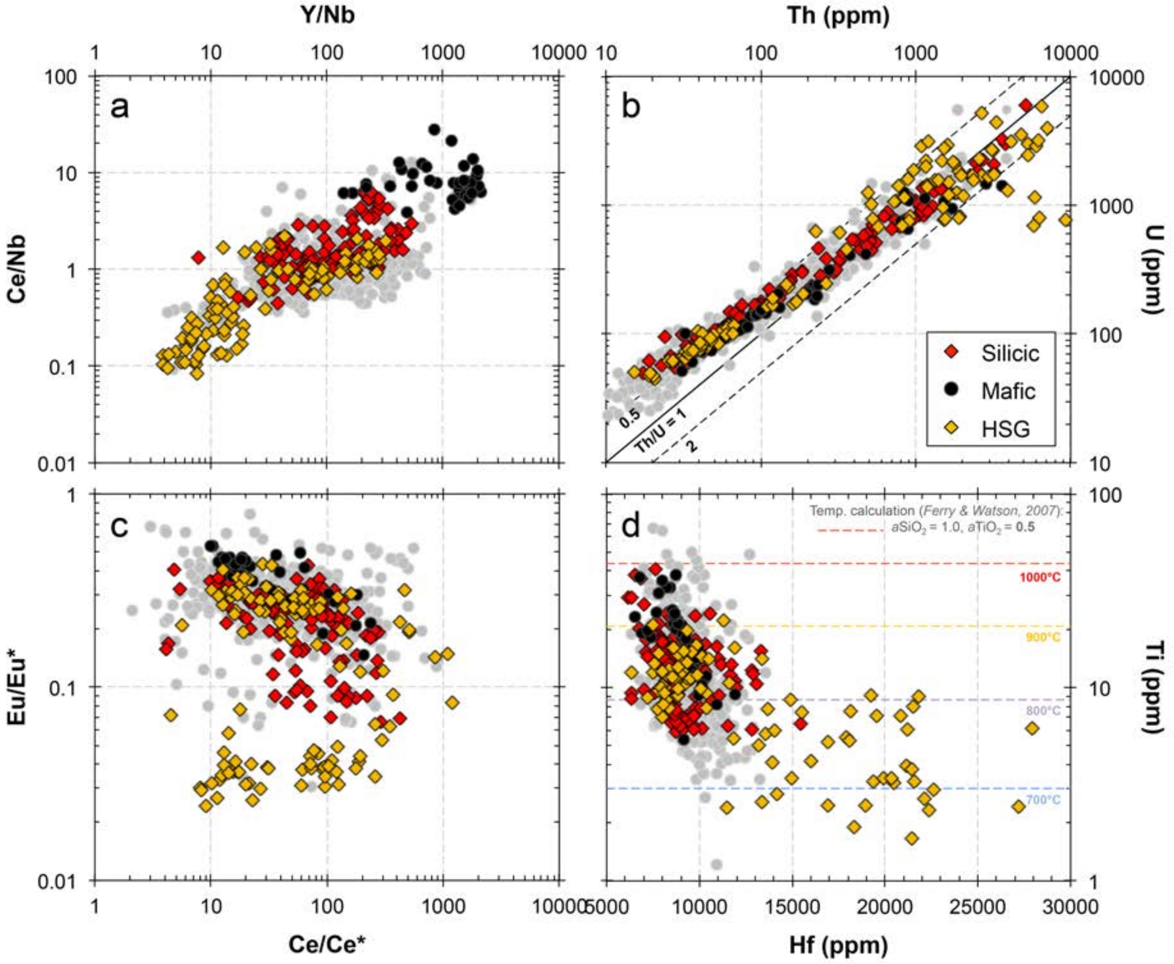

**Figure 5**

Trace element abundances and ratios for zircons from the Austurhorn Intrusive Complex. Gray symbols are data for the Vanderbilt Iceland zircon database (includes zircon data from volcanic, plutonic, and detrital samples; see Carley *et al*., 2014), plotted for comparison. **a)** Y/Nb vs. Ce/Nb; **b)** Th vs. U abundances; the solid line indicates a Th/U ratio of 1; the dashed lines indicate Th/U ratios of 0.5 (top) and 2 (bottom); **c)** Ce/Ce* (Ce anomaly) vs. Eu/Eu* (Eu anomaly); **d)** Hf vs. Ti abundances; the dashed lines indicate zircon model crystallization temperatures, calculated using the Ti-in-zircon thermometer of Ferry & Watson (2007).

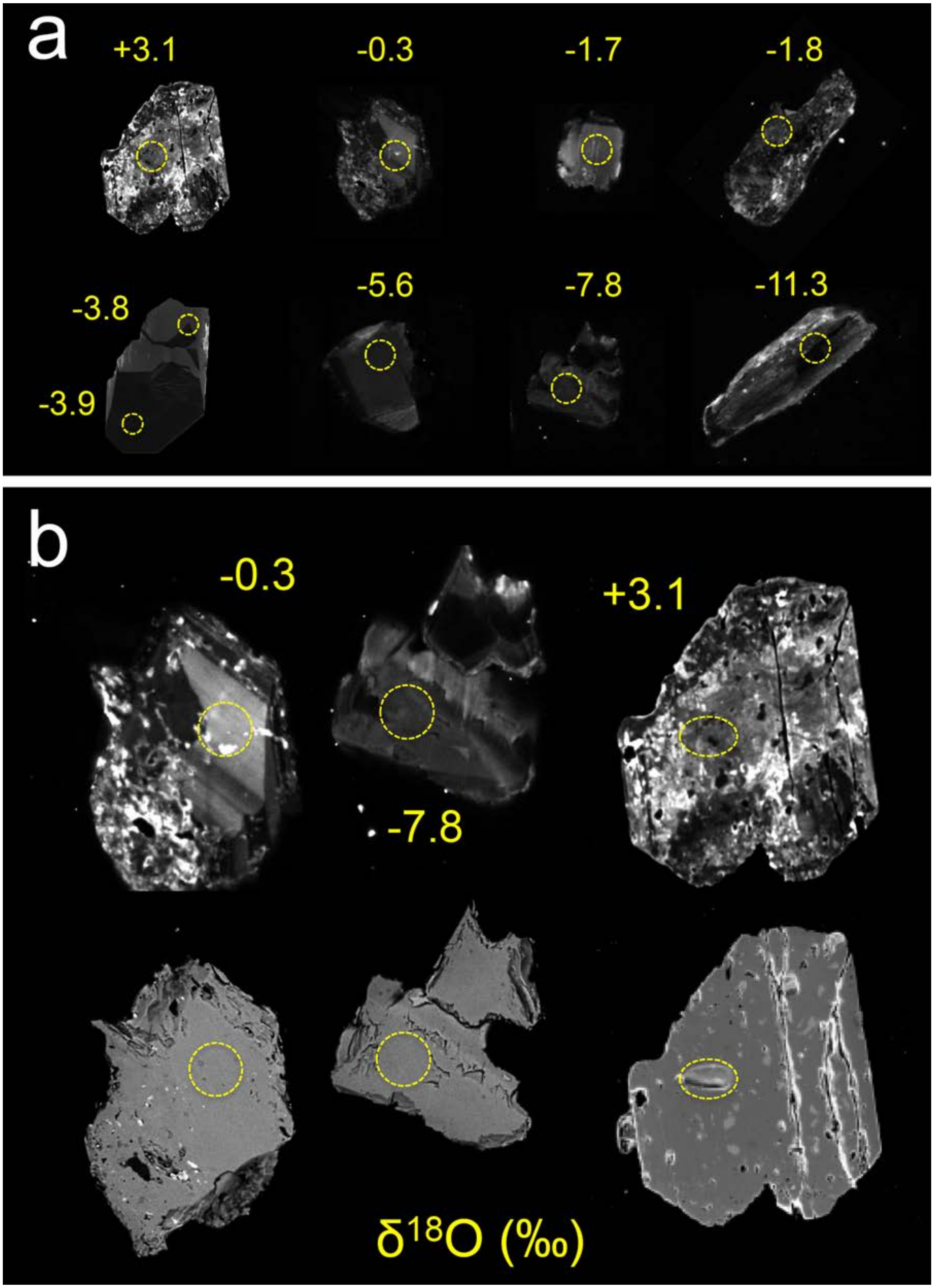

Figure 6 (caption on next page)

## Figure 6

Scanning electron microscope (SEM) images of representative zircons from high-$SiO_2$ granophyres (HSG) of the Austurhorn intrusive complex, and their corresponding oxygen isotope ($\delta^{18}O$) compositions. Dashed circles indicate the locations of *in-situ* analyses. **(a)** Observed cathodoluminescence (CL) zoning patterns for the range of $\delta^{18}O$ values in HSGs includes typical magmatic oscillatory growth zoning (bottom row, left 3 grains) as well as convolute zoning (top left grain, right-most grains in both rows), and grains with multiple zoning patterns (top row, middle 2 grains). **(b)** Comparison of analyzed spots in CL (top row) and secondary electron microscopy (bottom row). Low $\delta^{18}O$ values occur in grains with mixed as well as normal magmatic zoning (e.g. left and middle grains), and convolute-zoned grains can have normal $\delta^{18}O$ signatures (e.g. right grain), indicating that the observed variability in zircon $\delta^{18}O$ is magmatic in origin.

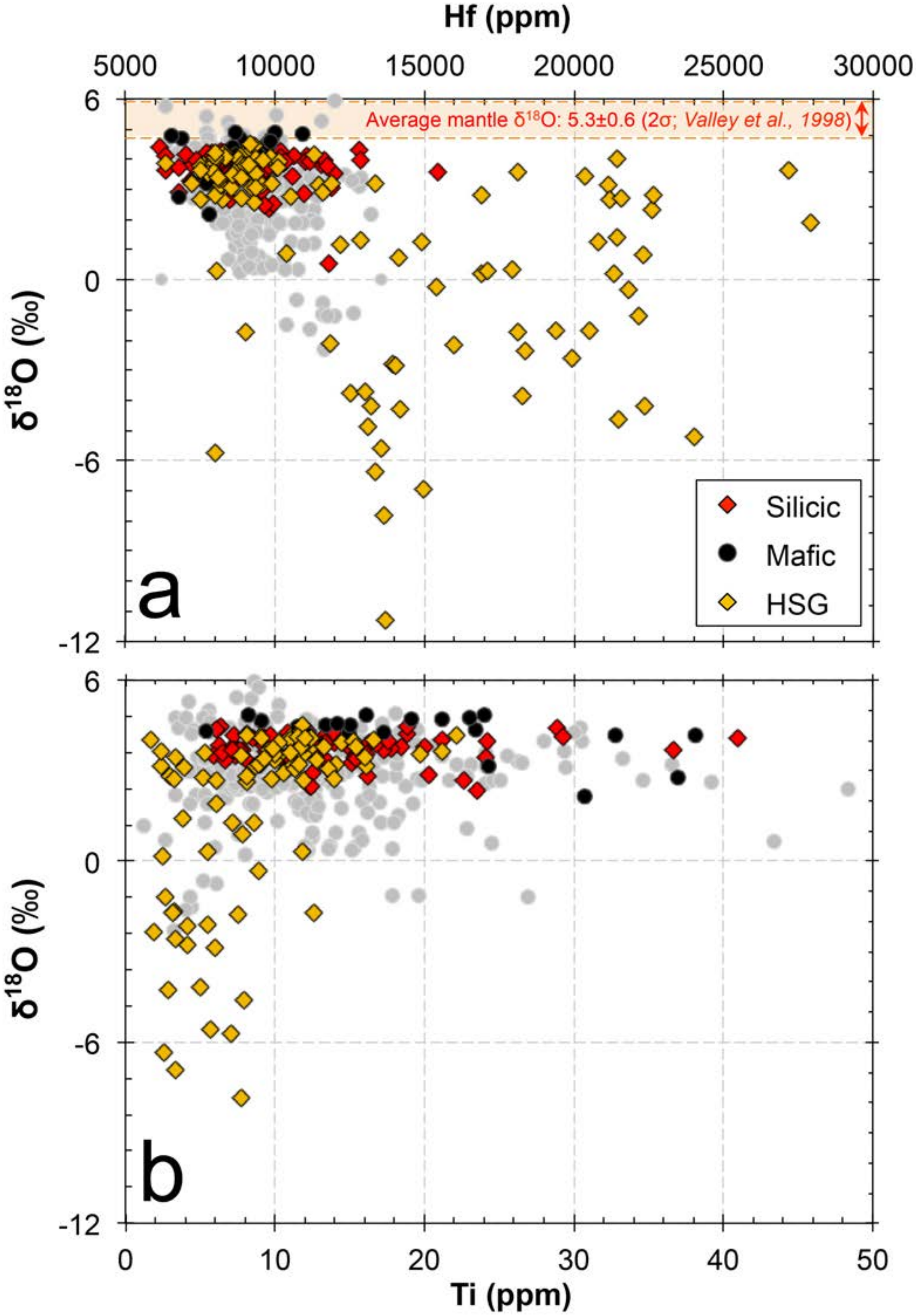

**Figure 7**

Isotopic compositions of zircons from the Austurhorn Intrusive Complex. **a)** Hf vs. $\delta^{18}O$; the orange zone indicates the measured $\delta^{18}O$ range of mantle zircons (+5.3 ±0.6 ‰, 2σ error; Valley et al., 1998). **b)** Ti vs. $\delta^{18}O$.

Major mineral phases from all samples, as well as bulk HSG, also preserve variable $\delta^{18}O$ values (Fig. 8; for full bulk oxygen isotopes data see Appendix B.9). The whole-rock, quartz, and feldspar $\delta^{18}O$ bulk compositions of HSGs are universally depleted relative to all other units, ranging from -2.9 to +0.02 ‰. In contrast, quartz compositions in other silicic units are in the range of +2.2 to +6.0 ‰. Feldspar compositions in the more intermediate rocks as well as one of the gabbros cluster around -0.5 ‰ (low-$\delta^{18}O$ feldspar in gabbro likely reflects secondary alteration), but are higher in granophyre (+2.6 ‰) and other gabbros (+3.2 ‰). Pyroxene and amphibole values mostly fall between +3.3 and +4.7 ‰, except for an intermediate sample with bulk amphibole $\delta^{18}O$ of +0.9 ‰, which may also reflect secondary alteration.

## 5. **Discussion & Conclusions**

Based on field relationships, whole-rock geochemistry, and zircon elemental and isotopic compositions, Padilla *et al.* (in review) determined that the Austhurhorn magmatic system was developed in a transitional rift environment, strongly influenced by the Iceland plume. They interpret the range of normal-$\delta^{18}O$ MSCZ zircons (+2.2 to +4.9 ‰) to indicate significant recycling and assimilation of hydrothermally-altered crust in the petrogenesis of silicic magmas at Austurhorn, followed by fractional crystallization of magmas (AFC), down to the solidus, in the shallow Icelandic crust (*cf.* Sigmarsson *et al.*, 1991).

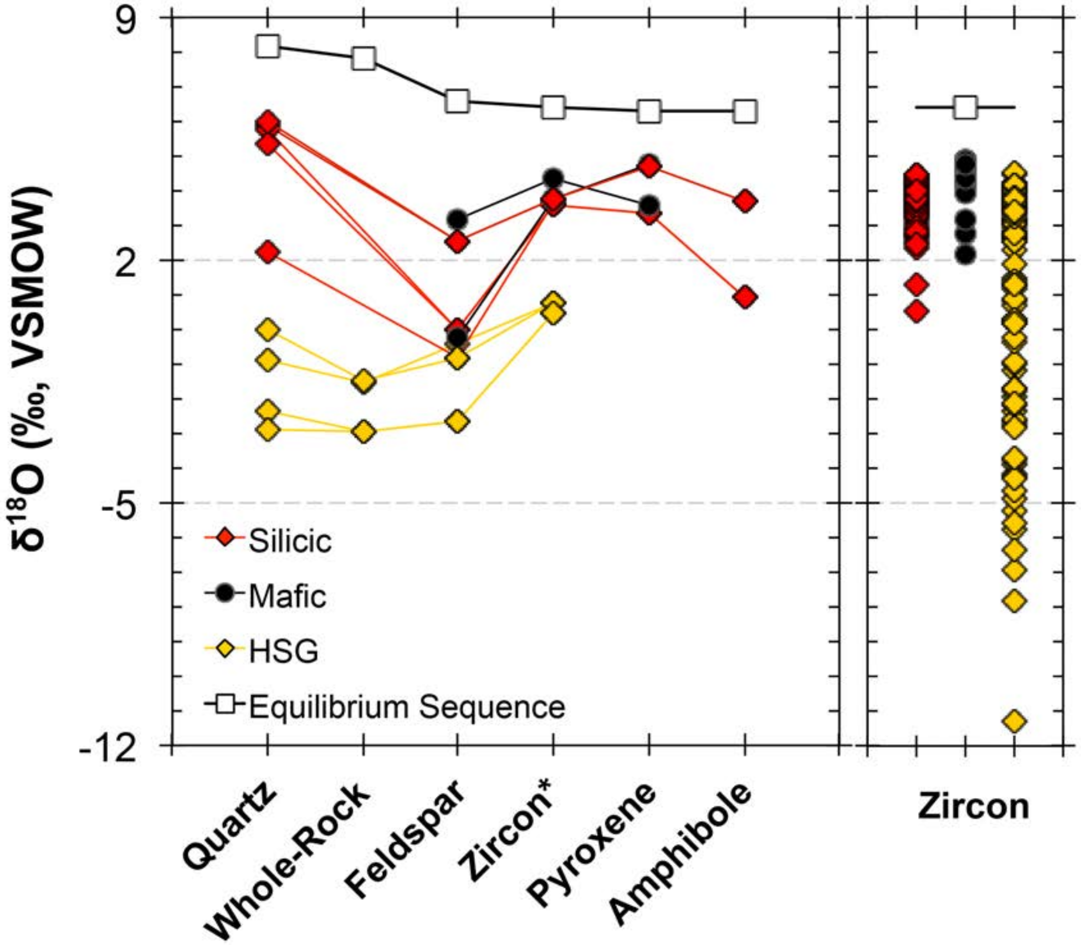

**Figure 8**

Bulk oxygen isotope compositions ($\delta^{18}O$) in major mineral phases from rocks of the Austurhorn intrusive complex. Right graph shows all measured in-situ zircon $\delta^{18}O$ compositions. “Zircon*” denotes the average $\delta^{18}O$ of all zircons in each group. The “equilibrium sequence” (white squares) shows the relative $^{18}O$ fractionation that would be expected, based on experimental and empirical data, for the listed minerals if they crystallized in equilibrium from the same silicate magma with a theoretical whole-rock $\delta^{18}O$ value of +7.8 ‰ at 850ºC (Bindeman, 2008).

The high-$SiO_2$ granophyres from the MSCZ, on the other hand, present a strongly contrasting geochemical record of magmatic processes to that observed in all other analyzed samples from Austurhorn. Given their relatively small abundance, they likely represent more extreme magmatic processes that may be taking place throughout the Austurhorn system. In order to relate their unique geochemical signatures to magmatic processes, it is important to establish that the distinctive compositional characteristics of these rocks are magmatic in origin, rather than products of sub-solidus/hydrothermal alteration. Their association with other silicic intrusive rocks of the MSCZ lends first order support to this interpretation, as there is abundant field evidence for ductile-magmatic behavior of the HSGs during intrusion into their granophyric host (e.g. mingling and disaggregation of dikes; evidence for mechanical mixing; diffuse and gradational boundaries between pods of intruding HSG and the host granophyre; see Fig. 1).

Because of its refractory nature, zircon provides an additional tool by which to distinguish between magmatic and hydrothermal origins. Well-developed growth (oscillatory) zoning is one of the more typical features of magmatic zircon (Corfu *et al.*, 2003; Hanchar and Miller, 1993; Hoskin and Schaltegger, 2003). All MSCZ rocks, including HSGs, contain zircons with this characteristic zoning (Padilla *et al.*, in review) as well as geochemical signatures that reflect magmatic crystallization (Bindeman *et al.*, 2012; Carley *et al.*, 2014; Hoskin and Schaltegger, 2003). In the case of the HSGs, a substantial fraction of zircons are convolute-zoned and contain abundant inclusions. It would be reasonable to conclude that these features may be the result of different, and perhaps non-magmatic, processes. However, some of the more distinct geochemical features of these grains, such as enrichment in Th, U, and Hf and extremely depleted $\delta^{18}O$ (see Fig. 6), are not unique to convolute-zoned grains. The occurrence of unaltered, growth-zoned, and inclusion-free zircons with the same geochemical characteristics indicates that these reflect magmatic processes rather than secondary alteration. Similarly, inclusions would not be able to account for many of these characteristics, especially high Hf abundances, given that no other magmatic phases concentrate > 1-2 % Hf, or $\delta^{18}O$, since few coexisting silicate phases, in equilibrium with zircon, fractionate oxygen with significantly lower $^{18}O/^{16}O$ ratios than zircon (e.g. $\Delta^{18}O_{zircon\text{-}sphene} \approx -1$ ‰; $\Delta^{18}O_{zircon\text{-}magnetite} \approx -3$ ‰; (Bindeman, 2008; Zheng, 1993). Even if low-$\delta^{18}O$ minerals were encountered as inclusions during oxygen analyses, these would be volumetrically insignificant relative to the analyzed in-situ zircon volumes, and their effect on the oxygen signature would be negligible. Furthermore, the full range of measured $\delta^{18}O$ in zircon (-11.3 to +4.9 ‰; Fig. 7) far exceeds any differences in fractionation between zircon and other coexisting minerals, such that we can dismiss inclusions as the source of the observed distinctive HSG zircon oxygen signatures.

Bulk major mineral oxygen compositions from MSCZ samples also reveal extreme oxygen variability but small mineral-mineral fractionation (Fig. 8), consistent with a hydrothermal-magmatic transition (>600°C), and disequilibrium in $\delta^{18}O$ among major minerals and zircon suggests that some of these magmas, especially the HSGs, are composed of multiple batches of isotopically diverse melts.

Individual *in situ* zircon $\delta^{18}O$ values in most samples suggest that there are significant contributions from altered crust in the genesis of their parental silicic magmas (*cf.* Bindeman *et al.*, 2012). In the HSGs, the extreme variation in zircon $\delta^{18}O$, which includes the largest known range of $\delta^{18}O$ (~ 16 ‰) and to the best of our knowledge also the lowest value yet measured in any magmatic zircon in the world (-11.3 ‰), requires considerable O-isotope heterogeneity in the magma and extreme levels of meteoric-hydrothermal alteration of the source. Modern hydrothermal fluids reported by Pope *et al.* (2013) for the Krafla central volcano in Iceland range between -10 and -14‰. They also report whole-rock $\delta^{18}O$ from altered basalts ranging from -3 to -11 ‰, and estimate that basalts that undergo heavy meteoric-hydrothermal alteration in Icelandic rift systems end up with approximately -10‰ $\delta^{18}O$. Using these values, both the large range and the lowest measured $\delta^{18}O$ values in HSG zircons can be explained by amalgamation of multiple batches of small volume magmas generated by pure melting of intensely but variably altered crust, some of which underwent nearly complete (large water/rock ratio), high-temperature exchange with ~ -10 to -14 ‰ meteorically-derived hydrothermal fluids. The observed heterogeneity in $\delta^{18}O$ in zircon and major minerals is also consistent with field relationships at Austurhorn, suggesting that sustained melting activity, as a consequence of continuous mafic recharge, was the primary mechanism in the generation and accumulation of the most evolved magmas (HSGs) throughout the lifetime of the Austurhorn system. These HSG magmas likely also represent the assimilant component in A/FC processes suggested by the rest of the silicic (non-HSG) rocks found in the MSCZ.

The HSGs found in the Austurhorn intrusive complex provide an excellent example of the pure partial melting end-member of magmatic processes related to the production of silicic magmas in the shallow crust. Understanding their origin can provide better insight into processes that may be significant and commonplace, both in the generation as well as the accumulation of silicic magmas, but are seldom preserved in the rock and geochemical records. The diverse $\delta^{18}O$ in zircons and other minerals from these rocks are useful for understanding the context of other geochemical markers, and provide important insights into the physical mechanisms of shallow magma petrogenesis by amalgamation of diverse melts.

# CHAPTER V

## The varied personalities of silicic intrusions in Iceland: a spatial and temporal comparison of shallow magmatic systems preserved in the zircon geochemical record

### 1. **Introduction**

In the preceding chapters of this dissertation, I have presented three case studies in which I investigated different geochemical characteristics of silicic magmatic systems in southeast Iceland and northern Arizona, largely based on the ability of mineral phases to influence and record the evolution the magmas from which they crystallize. In addition to these case studies, I conducted a larger-scale survey of zircon from Icelandic intrusions to assess the temporal and spatial evolution of shallow crustal magmatism in Iceland. Because of the significant volumes of silicic material, as well as their composite zones displaying intimate association (mixing and mingling) of mafic and silicic magmas that hold clues regarding the construction and evolution of their magmatic systems, Icelandic intrusions are ideal candidates for investigating systematic processes related to the generation of silicic magmas in the Icelandic crust.

In this chapter, I present preliminary results of this comparative study between shallow Icelandic intrusions. I investigated six intrusive complexes with varying amounts of composite relationships, silicic material, and ages spanning ~10 M.y. of Icelandic geologic history, from ~11.7 to ~1.1 Ma (Table 1, Figs. 1-3). Different intrusions are better suited to address different questions regarding evolution of silicic magmas. A subset of them are part of a group of closely related intrusions, all located in close proximity to each other along the coast of southeast Iceland (Fig. 1), which I collectively refer to as the Southeast Iceland Intrusives Suite (SIIS): Austurhorn, Reyðarártindur, Slaufrudalur, and Vesturhorn. These major intrusions are generally thought to be coeval (e.g. Furman *et al.*, 1992a,b; Moorbath *et al.*, 1968), which presents an exceptional opportunity to address the spatial variability of Icelandic intrusive magmatic systems. Furthermore, I explore the temporal differences in magmatism by comparing the SIIS to spatially unrelated intrusions elsewhere in Iceland: Lýsuskarð intrusion, a younger intrusion in Western Iceland, and Sandfell laccolith, an older intrusion in Eastern Iceland.

## 2. Geologic Background

### 2.1. Austurhorn Intrusive Complex

The Austurhorn Intrusive Complex (e.g. Padilla *et al.*, in review; Thorarinsson and Tegner, 2009; Furman *et al.*, 1992a,b; Mattson *et al.*, 1986; Blake, 1966), in southeast Iceland, presents a suite of rocks that best exemplifies the complex array of mafic-felsic magmatic interactions typical of silicic systems in Iceland (Fig. 2a, 3a). It has been previously dated using *in-situ* U-Pb zircon geochronology at 6.5-6.6 Ma (±0.4; Martin *et. al.*, 2011) and 6.52 ± 0.03 Ma (Padilla *et al.*, in review; see Chapter III). The intrusion comprises voluminous granophyre, gabbros, and a mafic-felsic composite zone (MFCZ) that makes up 30-40% of the exposed rocks. Because of its location along the coast, where constant wave-action helps expose and polish rock surfaces, and the abundance of mafic-felsic interactions it preserves, Austurhorn provides an ideal location to investigate the importance of magma recharge and mixing events in the evolution of silicic systems.

### 2.2. Reyðarártindur Intrusive Complex

The Reyðarártindur intrusion, located less than 10 km to the west of Austurhorn in southeast Iceland contains abundant silicic rocks, associated gabbros, and a MFCZ with extensive evidence for mixing and mingling preserved as hybrid rocks, though these interactions are largely confined to the lowest exposed sections of the intrusion in the Reyðará valley (Fig. 2b, 3b). Because of its proximity and similarity to other intrusions, Reyðarártindur is assumed to be coeval with the rest of the SIIS (e.g. Moorbath *et al.*, 1968), though it has not been previously dated, and no information about it has been published since it was first mapped by Cargill *et al.* (1928). Though smaller in size it contains similar characteristics, particularly in the MFCZ, and voluminous granophyres that make Reyðarártindur highly appropriate for geochemical comparison to the Austurhorn and other composite intrusions.

### 2.3. Slaufrudalur Intrusive Stock

With an area of roughly 20 km$^2$, the Slaufrudalur intrusive stock is perhaps the largest silicic intrusion exposed in Iceland (Fig. 2c, 3c; Burchardt *et al.*, 2011). Previous researchers have distinguished a textural spectrum of silicic rocks, with compositions ranging from granodiorite to granite making up the bulk of the intrusion in subhorizontal layers (e.g. Carmody, 1991; Beswick, 1965). Notably, there are MFCZ-type exposures confined to the lowest sections of the intrusion, but at the current level of exposure there are no significant gabbros associated with the Slaufrudalur intrusion. The only published ages for this complex are whole-rock K-Ar ages reported by Gale *et al.* (1966), which reflect two main stages of intrusion at 9.0-10.0 (±2.7) Ma and 6.5-6.6 (±0.8) Ma. Carmody (1991) distinguished two major groups of silicic units at Slaufrudalur, based on their mineralogy and whole-rock geochemistry, indicating the potential existence of two magma sources in the Slaufrudalur magmatic system, providing an opportunity to test the robustness of zircon as a reliable geochemical tracer of magmatic sources. Furthermore, the absence of gabbros in the Slaufrudalur system provides a contrasting geochemical comparison to the rest of the SIIS, helping further assess the effects of mafic magma replenishment on the evolution of silicic systems.

**Table 1**. Summary of Icelandic silicic composite intrusions

| Intrusion Name | Location | Age (Ma)[17] | Exposure ($km^2$) | Compositional Character |
|---|---|---|---|---|
| Austurhorn | SE Iceland (SIIS) | 6.5-6.6[A] | ~15 | Composite |
| Reyðarártindur | SE Iceland (SIIS) | n/a | 15-20 | Composite |
| Slaufrudalur | SE Iceland (SIIS) | 6.5-10.0[B] | ~20 | Composite<br>(silicic dominated) |
| Vesturhorn | SE Iceland (SIIS) | 3.7-6.6[A] | ~19 | Composite<br>(mafic dominated) |
| Lýsuskarð | Snæfellsness Peninsula | 1.1-2.1[B] | ~1 | Composite |
| Sandfell | E Iceland | 11.7[A] | <5 | Silicic Only |

---

[17] Previously published ages from literature:
[A]Martin *et al.*, 2011: zircon U-Pb geochronology
[B]Gale *et al.*, 1966: whole-rock K-Ar geochronology

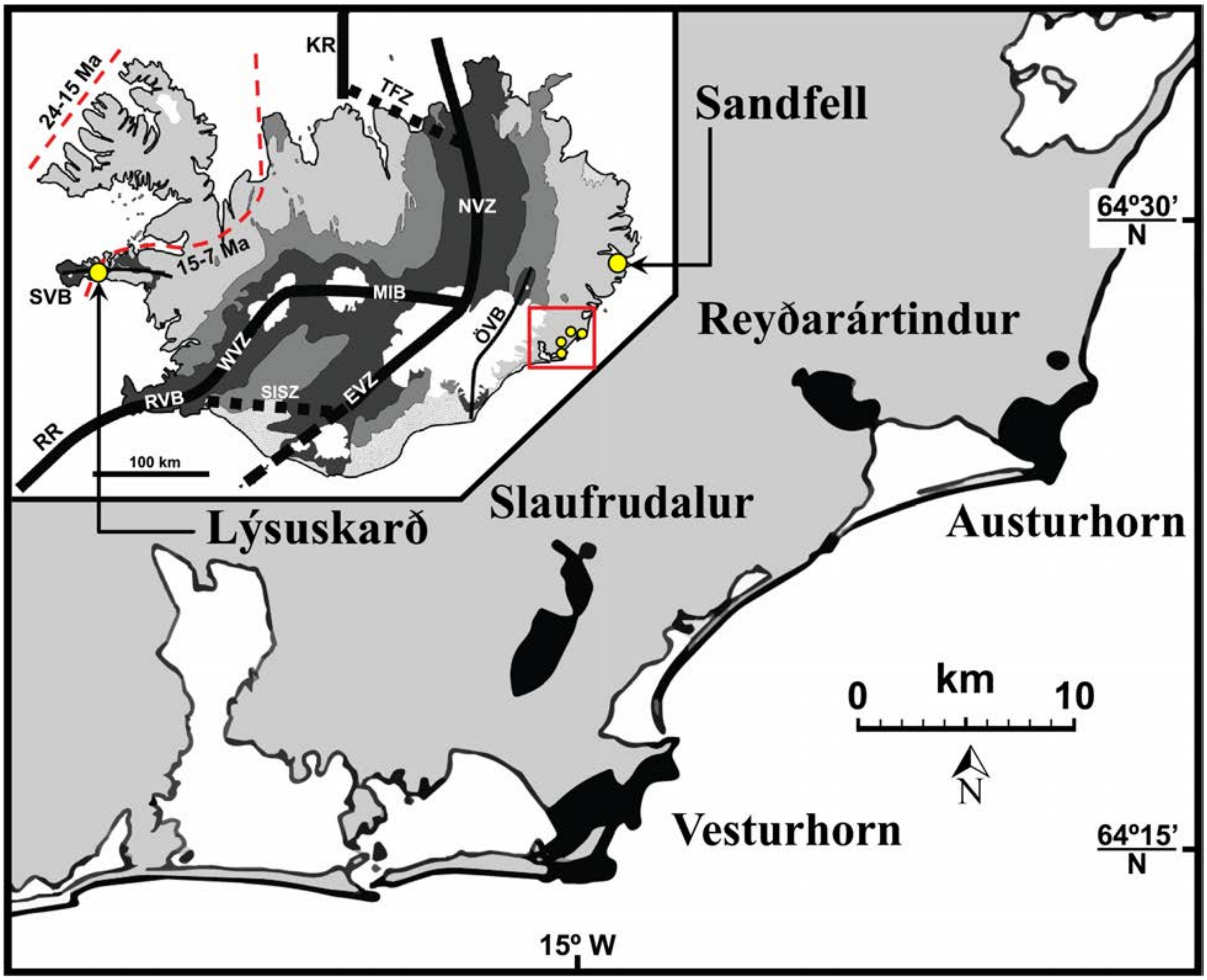

**Figure 1**

Regional map of southeast Iceland outlining the four major composite silicic intrusions exposed in the area (black shaded areas; modified after Gale *et al.*, 1966). *Inset:* Overview map indicating the location of two other silicic intrusions, as well as the major tectonovolcanic zones in Iceland (modified after Carley *et al.*, 2011): Northern (NVZ), Eastern (EVZ), and Western Volcanic Zones (WVZ), Snæfellsness Volcanic Belt (SVB), Reykjanes Ridge (RR), Reykjanes Volcanic Belt (RVB), South Iceland Seismic Zone (SISZ), Öræfi Volcanic Belt (ÖVB), Tjornes Fracture Zone (TFZ), Kolbeinsey Ridge (KR), and the Mid-Iceland Belt (MIB). The red dashed lines represent extinct rifts (Martin *et al.*, 2011). The red box indicates the location of the intrusions. The shades of gray indicate age divisions: light gray = Neogene (17-3.3 Ma); medium gray = Plio-Pleistocene (3.3-0.7 Ma); dark gray = Upper Pleistocene to present (0.7-0 Ma); white = Ice caps.

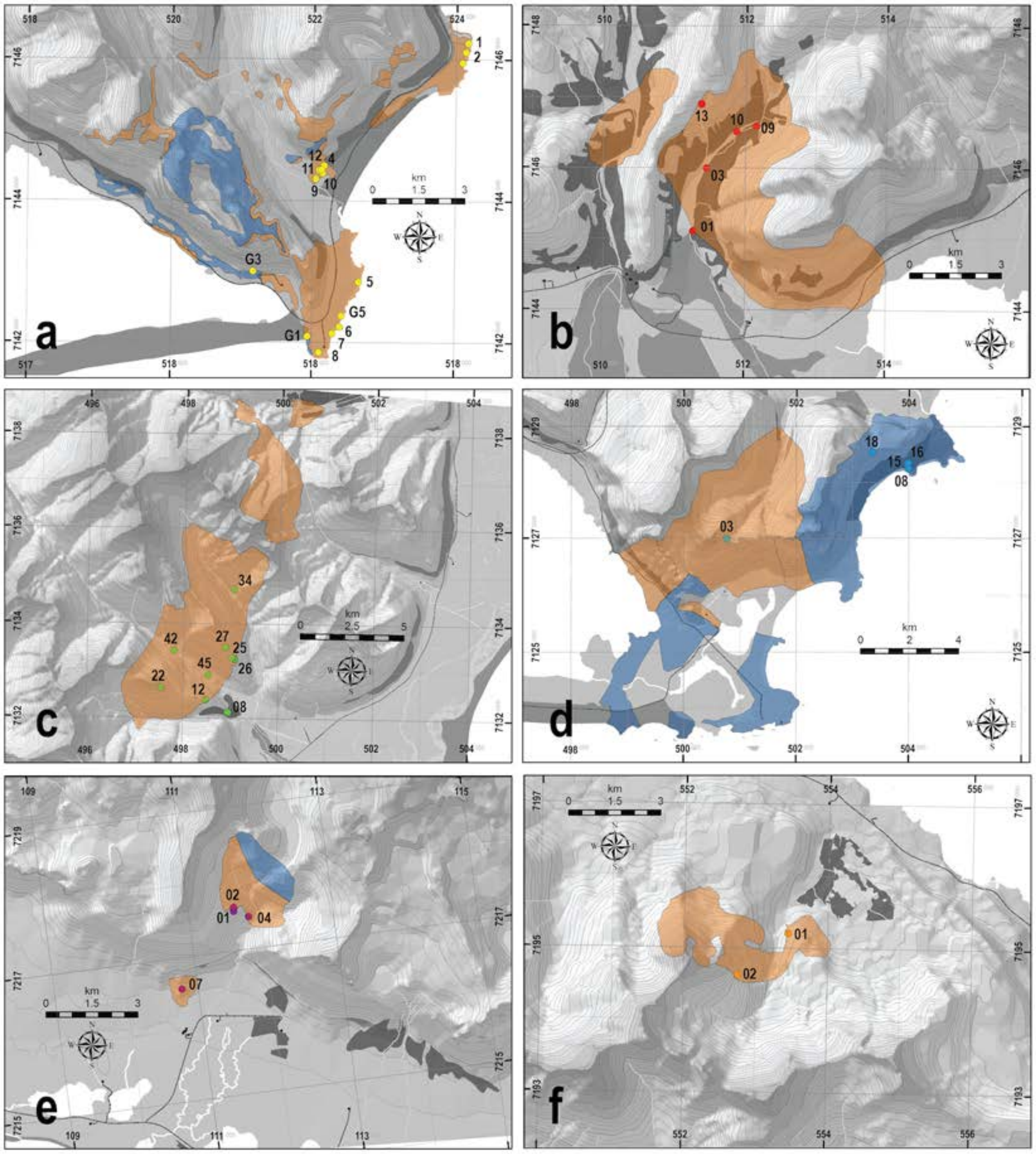

**Figure 2**

Simplified geologic maps of Icelandic silicic intrusions. All boundaries are inferred from previously published maps and fieldwork conducted in the course of this study. Orange zones indicate exposures that are dominantly silicic (e.g. silicic units, silicic-hosted composite zones); blue zones indicate exposures that are dominantly mafic. Labeled dots are sampling locations. The dark grey zones indicate thick alluvial cover. Light grey zones are talus cover and vegetated areas. White zones are water. Coordinates listed are all in WGS84 UTM grid. **a)** Austurhorn Intrusive Complex (modified after Furman *et al.*, 1992b); **b)** Reyðarártindur Intrusive Complex (modified after Gale *et al.*, 1966); **c)** Slaufrudalur Stock (modified after Burchardt *et al.*, 2011); **d)** Vesturhorn Intrusive Complex (modified after Roobol, 1974); **e)** Lýsuskarð Intrusive Complex (modified after Upton & Wright, 1961); **f)** Sandfell Laccolith (modified after Hawkes and Hawkes, 1932).

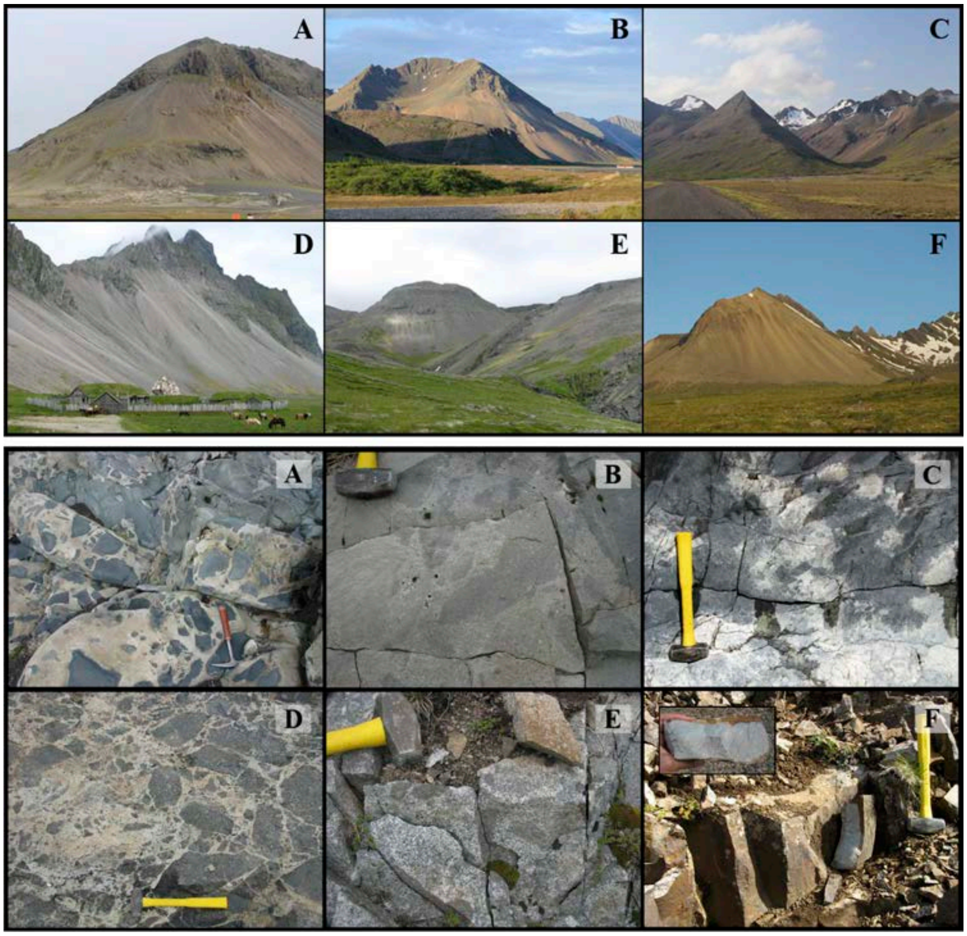

**Figure 3**

The exposed edifices (top) and sample magmatic interactions (bottom) preserved in some of Iceland's most well-known silicic and composite intrusions. The nature of interactions varies widely and differs greatly from intrusion to intrusion. **a)** Austurhorn Intrusive Complex (southeast Iceland); **b)** Reyðarártindur Intrusive Complex (southeast Iceland); **c)** Slaufrudalur Stock (southeast Iceland); **d)** Vesturhorn Intrusive Complex (southeast Iceland); **e)** Lýsuskarð Intrusive Complex (Snæfellsness Peninsula, western Iceland); **f)** Sandfell Laccolith (Fáskrúðsfjördur, eastern Iceland).

## 2.4. Vesturhorn Intrusive Complex

The Vesturhorn intrusion, at the southern end of Lón Bay in southeast Iceland, is exposed over an area of ~19 km$^2$, comprising two large gabbroic complexes and a central core of granophyric rocks (Fig. 2d, 3d; Roobol, 1974), with MFCZ-like exposures occurring along the margins of the intrusion, particularly where the central silicic complex is in contact with the gabbros. Notably, the gabbroic complexes are also composite, preserving evidence in the form of compositional layering and magmatic mingling for the input from and interaction of different batches of mafic magmas during construction of the intrusion. The complex has been dated at 3.7-3.9 (±0.1) Ma by U-Pb zircon geochronology (Martin *et. al.*, 2011). Field relationships suggest that the three main complexes of Vesturhorn were emplaced sequentially, with the voluminous granophyre core, which is exposed mainly at the highest stratigraphic levels, intruding first, closely followed by the sequence of gabbros that also generated the MFCZ upon contact with the earlier granophyre magma (Roobol, 1974). Unlike the MFCZ at Austurhorn, the composite zone in Vesturhorn comprises less than 10% of the exposed rocks (Mattson *et al.*, 1986), adding an important geochemical contrast to the rest of the SIIS in investigating the spatial variability of magmatic systems.

## 2.5. Lýsuskarð Intrusive Complex

Lýsuskarð, the youngest well-exposed silicic intrusion in Iceland, is located on the southern part of the Snæfellsness Peninsula, in western Iceland (Fig. 2e, 3e). It comprises gabbros, granophyres, and hybrid intermediates exposed over ~1 km$^2$. The granophyres and hybrids are intimately associated in what resembles a MFCZ. Dioritic rocks and gabbros contribute substantially to the contamination and hybridization of granophyres (Upton & Wright, 1961). The exposed units have been dated by whole-rock K-Ar at 1.2-2.1 ±0.7 Ma (Gale *et al.*, 1966). These rocks and their associations bear a close resemblance to those of the SIIS, in particular units of the Austurhorn and Vesturhorn intrusions. A careful study of the geochemical characteristics of Lýsuskarð permits the comparison between similar silicic magmatic systems from different tectonic regimes in Iceland, and provides a young perspective for addressing temporal variations in the dynamics of silicic magmatism.

### 2.6. Sandfell Laccolith

Located along the southern edge of Fáskrúðsfjördur, in eastern Iceland, the Sandfell laccolith is an aphanitic silicic porphyry that intrudes Tertiary lavas of the Icelandic plateau (Fig. 2f, 3f). Aside from small changes along the contact of the intrusion, there is no textural or compositional variation in the character of the exposures (Hawkes & Hawkes, 1932), suggesting it is an entirely-silicic and largely homogeneous intrusion. It has been dated at 11.7 ±0.1 Ma by Ar-Ar using single groundmass rock fragments (Martin *et. al.*, 2011), making it one of the oldest exposed shallow intrusions in Iceland. Composite interactions between mafic and silicic magmas, typical of silicic systems in Iceland, are completely absent at Sandfell. As such, it provides an excellent contrast to the composite intrusions of the SIIS, as well as a unique perspective on the evolution of silicic magmatic systems in the absence of mafic recharge and magma mixing, and insight into the character of early silicic magmatism in Iceland.

# 3. **Methods**

## 3.1. Whole-Rock Geochemistry

We analyzed 27 representative samples from all intrusions (see Table 2; data for Austurhorn samples are presented in Chapter III, Tables 1 and 2, and excluded from tables in this chapter) for major and trace element abundances at the Peter Hooper GeoAnalytical Laboratory at Washington State University (WSU; Pullman, WA), where major elements were determined by WD-XRF and trace element concentrations were determined by solution ICP-MS. International reference materials *RGM-1*, *W-2*, *JA-2*, and *BHVO-1* were used for calibration and quality control. Whole-rock geochemistry is presented in Table 3.

## 3.2. Zircon Geochemistry

I separated individual zircon grains from bulk-rock samples at Vanderbilt University, following standard separation techniques, including crushing, milling, sieving, density separation by water and heavy liquid (lithium heteropolytungstates in water; LST, $\rho \approx 2.8$ g/mL), separation by magnetic susceptibility, and lastly hand-picking individual zircon grains from the heavy separate fraction under a stereoscope. The selected zircon grains were mounted in epoxy, polished, and imaged by cathodoluminescence (CL) using a Tescan Vega 3 LM variable pressure scanning electron microscope (SEM) at Vanderbilt University.

Trace element and U-Pb isotopic abundances of spots on individual zircons were measured using the reverse geometry sensitive high-resolution ion microprobe (SHRIMP-RG) at the Stanford-USGS microanalytical center. I used R33 zircon (419±1 Ma, Black *et al.*, 2004) as the calibrating U-Pb geochronology standard, and in-house standards MAD and MADDER (Barth & Wooden, 2010) as trace element standards, and followed the basic operating parameters and technique employed for SHRIMP-RG elemental suite analyses as outlined by Grimes *et al.* (2007) and Claiborne *et al.* (2006, 2010b). A summary of all weighted mean U-Pb ages is presented in Fig. 4, and full U-Pb isotopic data are reported in Appendix C.1. Zircon trace element compositions are reported in Appendix C.2-C.4.

Oxygen isotope ratios on individual spots in zircon were measured by secondary ion mass spectrometry (SIMS) using the CAMECA ims1270 ion microprobe at the University of California-Los Angeles' (UCLA) W.M. Keck Foundation Center for Isotope Geochemistry (Los Angeles, CA), following the methods for zircon oxygen isotope determination outlined by Trail *et al.* (2007), using R33 ($\delta^{18}O$ = 5.55 ‰, Black *et al.*, 2004) as the calibrating standard to correct for instrumental mass fractionation. All zircon oxygen isotope data are reported in Appendix C.5.

*In situ* hafnium isotopic compositions of AIC zircons were obtained at the WSU Peter Hooper GeoAnalytical Laboratory (Pullman, WA) by laser ablation multi-collector inductively-coupled plasma mass spectrometry (LA-MC-ICP-MS), following the instrument configuration, operating parameters, and data reduction methods outlined by Fisher *et al.* (2011), and using Mud Tank (Woodhead & Hergt, 2005) as the primary calibrating standard, and R33 and 91500 as secondary standards. All zircon Lu-Hf isotopic compositions are reported in Appendix C.6.

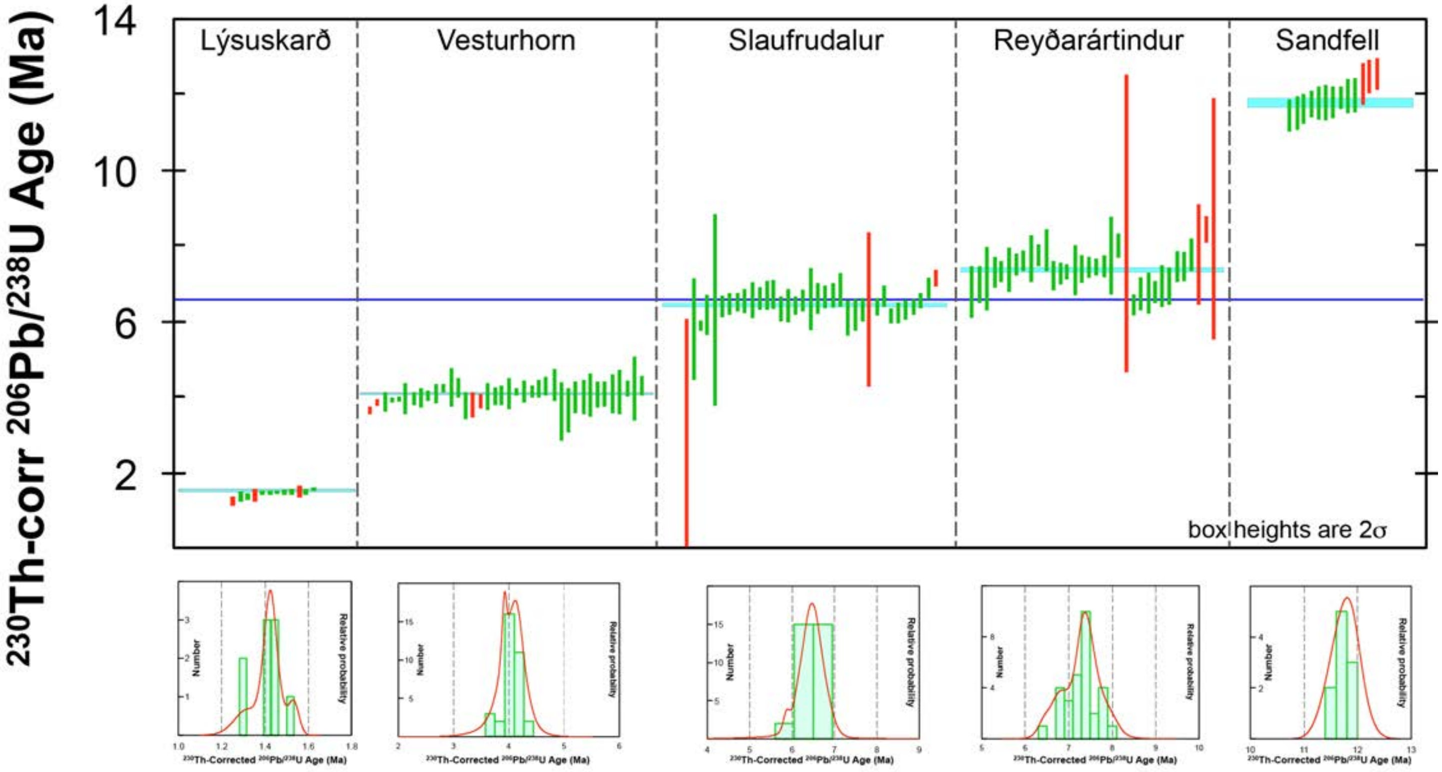

| | | | | | |
|---|---|---|---|---|---|
| **Wt. Mean Age (Ma):** | **1.44 ± 0.02** | **4.02 ± 0.03** | **6.38 ± 0.05** | **7.30 ± 0.06** | **11.77 ± 0.13** |
| n: | 9 | 34 | 32 | 30 | 10 |
| MSWD: | 3.3 | 1.9 | 3.4 | 4.3 | 0.77 |
| Rejected analyses: | 3 | 4 | 3 | 4 | 3 |

**Figure 4**

Zircon $^{206}Pb/^{238}Pb$ ages for Icelandic intrusions, corrected for initial $^{238}U$-$^{230}Th$ disequilibrium. Each green bar represents a single zircon age. Red bars represent outlier analyses (>2 standard deviations from sample mean), analyses with high common-$^{206}Pb$ (>20%), or analyses with high or low UO/U (>2 standard deviations from sample mean), and are therefore excluded. For each intrusion, the weighted mean age is plotted as a light blue horizontal box. The dark blue line is the age of the Austurhorn Intrusive Complex for comparison (Padilla *et al.*, in review; see also Chapter III). All errors are reported as 2σ standard errors (box heights for both individual and pooled ages are adjusted to represent error). *Lower figures:* zircon age probability density distribution and histogram for each Intrusion.

**Table 2**. Locations and descriptions for samples collected from Icelandic composite intrusions

| Sample[18] | Location (UTM)[19] |  | Mafic Bodies[20] | Silicic Rel. Abundance[21] | Nature of outcrop / Notes |
|---|---|---|---|---|---|
|  | Northing | Easting |  |  |  |
| IIV-03a | 500765 | 7126998 | none | 100 % | Fine-grained granophyre, continuous for 10s of meters, no visible mafic component |
| IIV-08c | 504000 | 7128345 | n/a | 0 % | Gabbro, gradational from Px-dominated to Plag-dominated, no visible silicic component |
| IIV-15 | 503977 | 7128334 | n/a | 5-10 % | Gabbro outcrop, cross-cut by abundant silicic dikes and veins |
| IIV-16 | 503995 | 7128238 | 10 cm - 1 m | 40 % | Edge of gabbro complex, extensively intruded by silicic units |
| IIV-18 | 503354 | 7128536 | n/a | 0 % | Coarse gabbro, no visible silicic component |
| IISlau-08a | 498954 | 7132107 | < 1 cm | 100 % | Poorly exposed small (< 1 m$^2$) outcrops, v.f.g. unit, no visible interactions with other units |
| IISlau-08b | 498954 | 7132107 | n/a | 0 % | Poorly exposed small (< 1 m$^2$) outcrops, v.f.g. unit, no visible interactions with other units |
| IISlau-12 | 498493 | 7132374 | none | 100 % | Homogeneous exposure on Mosfell (~230 m elevation), no visible mafic component |
| IISlau-22 | 497544 | 7132624 | none | 100 % | Homogeneous exposure on Mosfell (~550 m elevation), no visible mafic component |
| IISlau-25 | 499082 | 7133242 | none | 100 % | Homogeneous exposure on Bleikitindur (~245 m elevation), no visible mafic component |
| IISlau-26 | 499038 | 7133267 | none | 100 % | Silicic exposure on Bleikitindur (~265 m elev.), variable coarseness, no mafic component visible |
| IISlau-27 | 498893 | 7133487 | none | 100 % | Continuous exposure on Bleikitindur (~375 m elevation and upward), no visible mafic component |
| IISlau-34 | 499066 | 7134707 | none | 100 % | Homogeneous silicic exposure on Skeggtindar, no visible mafic component |
| IISlau-42 | 497815 | 7133416 | 1 cm - 1 m | 55 % | Silicic-hosted composite outcrop, abundant mafic enclaves, gradational mixing zones present |
| IISlau-45 | 498536 | 7132895 | < 1 cm | 100 % | Continuous and isolated exposure of coarse silicic rock |

---

[18] Sample prefixes refer to the Intrusive Complex where sample was collected: IIV = Vesturhorn; IISlau = Slaufrudalur

[19] All coordinates were obtained using the World Geodetic System 1984 (WGS 84)

[20] Refers to non-continuous bodies of mafic material surrounded by silicic host (e.g. mafic pillows, enclaves, and clasts; "n/a" = not applicable for mafic units)

[21] Relative abundance of silicic (vs. mafic) material within the outcrop where the sample was collected

**Table 2**. Continued

| Sample[22] | Location (UTM) | | Mafic Bodies | Silicic Rel. Abundance | Nature of outcrop / Notes |
|---|---|---|---|---|---|
| | Northing | Easting | | | |
| IIR-01 | 511265 | 7145105 | none | 100 % | Contact between granophyre and hornfels at edge of complex, no visible mafic interactions |
| IIR-03a | 511457 | 7145995 | 1 cm - 10 m | 40-50 % | Composite zone, extensive mafic-silicic interactions preserved, including mixing |
| IIR-03b | 511457 | 7145995 | 1 cm - 10 m | 40-50 % | Composite zone, extensive mafic-silicic interactions preserved, including mixing |
| IIR-09 | 512163 | 7146587 | none | 100 % | Isolated exposure of homogeneous silicic rock, no visible mafic component |
| IIR-10 | 511885 | 7146506 | 1 cm - 1 m | 60-70 % | Composite zone, extensive interactions, gradational and mixing zones common |
| IIR-13 | 511289 | 7146677 | none | 100 % | Silicic exposure along the roof contact, no mafic component or interactions with roof unit visible |
| IISand-01 | 553444 | 7195202 | none | 100 % | Homogenous exposure of aphanitic silicic rock, coarse Plag porphyries, no visible mafic component |
| IILys-01 | 395260 | 7194130 | n/a | < 10 % | Fine-grained silicic dike intruded into hornfels along edge of intrusion |
| IILys-02 | 395265 | 7194185 | none | 100 % | Fine-grained granophyre exposure continuous for a few meters, no mafic component visible |
| IILys-04 | 395469 | 7194053 | none | 100 % | Coarse diorite, variable texture and mineral assemblage, pockets of large amph phenocrysts present |
| IILys-07a | 394506 | 7193076 | none | 100 % | Isolated exposure, homog. silicic rock, strong hydrothermal alteration, no visible mafic component |
| IILys-07b | 394506 | 7193076 | none | 100 % | Isolated exposure of homog. silicic rock, strong hydrothermal alteration, no visible mafic component |

---

[22] Sample prefixes refer to the Intrusive Complex where sample was collected: IIR = Reyðarártindur; IISsand = Sandfell; IILys = Lýsuskarð

**Table 3**. Major oxide and trace element compositions of rocks from Icelandic silicic intrusions

| | Sample: | **REYÐARÁRTINDUR (IIR-)** | | | | | | **VESTURHORN (IIV-)** | | | | |
|---|---|---|---|---|---|---|---|---|---|---|---|---|
| | | **01** | **03a** | **03b** | **9** | **10** | **13** | **03a** | **08c** | **15** | **16** | **18** |
| Major Element Oxides (wt.%)[23] | $SiO_2$ | 73.9 | 67.0 | 69.6 | 73.2 | 72.5 | 73.7 | 75.8 | 49.1 | 45.5 | 65.6 | 46.2 |
| | $TiO_2$ | 0.21 | 0.70 | 0.38 | 0.25 | 0.28 | 0.24 | 0.17 | 2.1 | 4.6 | 0.98 | 3.2 |
| | $Al_2O_3$ | 13.7 | 15.6 | 15.2 | 14.1 | 14.4 | 13.6 | 13.1 | 23.2 | 16.9 | 15.6 | 18.5 |
| | $Fe_2O_3$ | 2.2 | 4.3 | 3.2 | 2.4 | 2.2 | 2.2 | 1.7 | 5.8 | 12.6 | 5.2 | 10.4 |
| | MnO | 0.06 | 0.10 | 0.07 | 0.04 | 0.05 | 0.06 | 0.05 | 0.10 | 0.16 | 0.11 | 0.12 |
| | MgO | 0.13 | 1.1 | 0.38 | 0.03 | 0.22 | 0.15 | 0.06 | 3.1 | 5.0 | 1.2 | 5.1 |
| | CaO | 0.82 | 2.2 | 1.4 | 0.43 | 0.76 | 1.2 | 0.26 | 12.9 | 12.5 | 3.5 | 13.7 |
| | $Na_2O$ | 4.0 | 5.2 | 5.2 | 4.8 | 4.8 | 3.7 | 4.4 | 3.0 | 2.4 | 4.8 | 2.2 |
| | $K_2O$ | 4.9 | 3.6 | 4.5 | 4.8 | 4.7 | 5.1 | 4.4 | 0.37 | 0.33 | 2.7 | 0.32 |
| | $P_2O_5$ | 0.02 | 0.19 | 0.07 | 0.03 | 0.04 | 0.03 | 0.02 | 0.31 | 0.10 | 0.25 | 0.13 |
| LOI (%) | | 3.02 | | | | | 2.07 | | | | | |
| Trace Element Concentrations (ppm) | *Sc* | 4.7 | 7.4 | 5.8 | 4.1 | 4.4 | 3.9 | 2 | 17 | 36 | 10 | 34 |
| | *Rb* | 112 | 86 | 97 | 110 | 101 | 119 | 93 | 5.7 | 5.8 | 60 | 7 |
| | *Sr* | 39 | 174 | 104 | 44 | 73 | 49 | 39 | 672 | 500 | 306 | 501 |
| | *Y* | 78 | 58 | 64 | 67 | 66 | 72 | 69 | 18 | 21 | 66 | 16 |
| | *Zr* | 375 | 706 | 566 | 434 | 415 | 446 | 318 | 104 | 117 | 608 | 74 |
| | *Nb* | 42 | 29 | 35 | 39 | 38 | 41 | 60 | 16 | 13 | 33 | 7.0 |
| | *Cs* | 0.67 | 0.81 | 0.60 | 0.87 | 0.40 | 0.55 | 0.39 | 0.05 | 0.08 | 0.37 | 0.14 |
| | *Ba* | 505 | 497 | 720 | 520 | 535 | 521 | 395 | 93 | 73 | 490 | 63 |
| | **La** | 67 | 50 | 58 | 58 | 68 | 60 | 51 | 9.2 | 7.4 | 46 | 6.5 |
| | **Ce** | 143 | 104 | 125 | 127 | 141 | 126 | 105 | 22 | 18 | 101 | 16 |
| | **Pr** | 17 | 13 | 15 | 15 | 17 | 15 | 13 | 3.2 | 2.8 | 13 | 2.3 |
| | **Nd** | 64 | 50 | 57 | 58 | 64 | 59 | 49 | 15 | 14 | 55 | 11 |
| | **Sm** | 14 | 12 | 13 | 13 | 14 | 14 | 12 | 4.2 | 4.3 | 13 | 3.4 |
| | **Eu** | 1.5 | 2.7 | 2.6 | 1.7 | 1.8 | 1.7 | 1.3 | 2.5 | 1.9 | 3.9 | 1.5 |
| | **Gd** | 14 | 11 | 12 | 13 | 13 | 13 | 12 | 4.6 | 4.8 | 13 | 3.8 |
| | **Tb** | 2.4 | 1.9 | 2.1 | 2.2 | 2.3 | 2.3 | 2.2 | 0.71 | 0.81 | 2.3 | 0.63 |
| | **Dy** | 15 | 11 | 13 | 13 | 13 | 14 | 13 | 4.0 | 4.8 | 13 | 3.7 |
| | **Ho** | 3.0 | 2.2 | 2.4 | 2.6 | 2.6 | 2.8 | 2.7 | 0.74 | 0.89 | 2.6 | 0.68 |
| | **Er** | 7.7 | 5.7 | 6.3 | 6.8 | 6.7 | 7.4 | 7.0 | 1.8 | 2.2 | 6.7 | 1.7 |
| | **Tm** | 1.2 | 0.81 | 0.90 | 0.99 | 0.99 | 1.1 | 0.99 | 0.22 | 0.29 | 0.96 | 0.22 |
| | **Yb** | 7.0 | 5.1 | 5.5 | 5.9 | 5.8 | 6.5 | 6.0 | 1.2 | 1.7 | 5.8 | 1.2 |
| | **Lu** | 1.0 | 0.77 | 0.83 | 0.89 | 0.87 | 0.99 | 0.85 | 0.18 | 0.24 | 0.88 | 0.17 |
| | *Hf* | 12 | 17 | 15 | 13 | 12 | 14 | 11 | 2.6 | 3.2 | 15 | 2.1 |
| | *Ta* | 3.0 | 2.2 | 2.4 | 2.8 | 2.7 | 3.0 | 4.4 | 1.1 | 0.94 | 2.2 | 0.54 |
| | *Pb* | 8.9 | 4.8 | 5.5 | 7.6 | 9.4 | 6.3 | 5.3 | 0.82 | 3.9 | 4.5 | 0.90 |
| | *Th* | 13 | 8.7 | 10.0 | 12 | 13 | 13 | 10 | 0.60 | 0.47 | 7.4 | 1.00 |
| | *U* | 4.2 | 2.6 | 2.7 | 3.5 | 3.2 | 3.7 | 2.8 | 0.19 | 0.19 | 2.3 | 0.26 |

---

[23] Anhydrous basis, normalized

**Table 3**. Continued

| Sample: | | **SLAUFRUDALUR (IISlau-)** | | | | | | | | | |
|---|---|---|---|---|---|---|---|---|---|---|---|
| | | **08a** | **08b** | **12** | **22** | **25** | **26** | **27** | **34** | **42** | **45** |
| Major Element Oxides (wt.%)[1] | $SiO_2$ | 71.1 | 49.8 | 73.6 | 74.0 | 73.9 | 73.7 | 77.2 | 76.3 | 74.6 | 73.6 |
| | $TiO_2$ | 0.51 | 4.0 | 0.36 | 0.25 | 0.33 | 0.36 | 0.12 | 0.14 | 0.28 | 0.34 |
| | $Al_2O_3$ | 13.6 | 13.1 | 13.7 | 12.7 | 13.7 | 13.8 | 12.1 | 12.4 | 13.3 | 13.6 |
| | $Fe_2O_3$ | 3.5 | 14.8 | 2.1 | 4.1 | 2.0 | 1.9 | 1.8 | 1.9 | 1.8 | 2.1 |
| | MnO | 0.07 | 0.28 | 0.04 | 0.03 | 0.03 | 0.03 | 0.02 | 0.06 | 0.03 | 0.04 |
| | MgO | 1.1 | 4.9 | 0.36 | 0.04 | 0.45 | 0.32 | 0.01 | 0.05 | 0.25 | 0.34 |
| | CaO | 2.2 | 8.9 | 0.92 | 0.59 | 0.94 | 1.1 | 0.27 | 1.1 | 0.98 | 1.1 |
| | $Na_2O$ | 4.1 | 3.0 | 4.3 | 4.6 | 4.1 | 4.1 | 4.4 | 4.2 | 4.2 | 4.4 |
| | $K_2O$ | 3.6 | 0.55 | 4.5 | 3.7 | 4.5 | 4.6 | 4.1 | 3.8 | 4.6 | 4.5 |
| | $P_2O_5$ | 0.07 | 0.66 | 0.05 | 0.02 | 0.03 | 0.05 | 0.01 | 0.01 | 0.03 | 0.05 |
| LOI (%) | | | | 0.20 | | | | | | | |
| Trace Element Concentrations (ppm) | *Sc* | 7 | 31 | 3 | 3 | 3 | 3 | 0.6 | 0.7 | 3 | 3.4 |
| | *Rb* | 72 | 16 | 99 | 73 | 94 | 103 | 102 | 76 | 97 | 96 |
| | *Sr* | 124 | 343 | 96 | 95 | 109 | 90 | 23 | 52 | 79 | 98 |
| | *Y* | 75 | 51 | 56 | 142 | 58 | 53 | 108 | 131 | 78 | 64 |
| | *Zr* | 374 | 272 | 350 | 639 | 264 | 336 | 504 | 477 | 302 | 369 |
| | *Nb* | 39 | 23 | 34 | 62 | 35 | 34 | 95 | 73 | 43 | 34 |
| | *Cs* | 0.35 | 0.18 | 0.73 | 0.51 | 0.38 | 0.88 | 0.57 | 0.31 | 0.60 | 0.51 |
| | *Ba* | 489 | 132 | 540 | 574 | 561 | 515 | 388 | 529 | 568 | 501 |
| | **La** | 57 | 23 | 55 | 121 | 57 | 43 | 75 | 74 | 67 | 54 |
| | **Ce** | 123 | 57 | 119 | 149 | 124 | 91 | 145 | 169 | 143 | 115 |
| | **Pr** | 16 | 8.2 | 14 | 33 | 14 | 10 | 22 | 22 | 17 | 14 |
| | **Nd** | 63 | 39 | 53 | 135 | 55 | 41 | 89 | 93 | 68 | 53 |
| | **Sm** | 15 | 11 | 11 | 32 | 12 | 9.7 | 22 | 24 | 16 | 12 |
| | **Eu** | 2.6 | 3.9 | 1.7 | 5.6 | 1.9 | 1.7 | 3.0 | 4.4 | 2.2 | 1.9 |
| | **Gd** | 15 | 12 | 11 | 32 | 11 | 9.3 | 20 | 25 | 15 | 12 |
| | **Tb** | 2.5 | 1.9 | 1.8 | 5.0 | 1.9 | 1.7 | 3.6 | 4.4 | 2.6 | 2.0 |
| | **Dy** | 15 | 11 | 11 | 28 | 12 | 10 | 22 | 27 | 15 | 13 |
| | **Ho** | 2.9 | 2.1 | 2.2 | 5.2 | 2.3 | 2.1 | 4.2 | 5.2 | 3.0 | 2.5 |
| | **Er** | 7.7 | 5.1 | 5.8 | 12 | 6.0 | 5.5 | 11 | 13 | 7.7 | 6.4 |
| | **Tm** | 1.1 | 0.68 | 0.82 | 1.6 | 0.85 | 0.82 | 1.6 | 1.9 | 1.1 | 0.93 |
| | **Yb** | 6.5 | 3.9 | 5.1 | 9.4 | 5.2 | 5.0 | 9.6 | 11 | 6.7 | 5.6 |
| | **Lu** | 0.95 | 0.56 | 0.73 | 1.4 | 0.75 | 0.75 | 1.4 | 1.6 | 0.98 | 0.81 |
| | *Hf* | 12 | 7.0 | 11 | 19 | 9.1 | 11 | 19 | 17 | 10 | 11 |
| | *Ta* | 2.8 | 1.6 | 2.6 | 4.3 | 2.6 | 2.6 | 6.4 | 5.1 | 3.2 | 2.6 |
| | *Pb* | 5.2 | 3.5 | 6.4 | 4.4 | 4.1 | 6.5 | 5.1 | 4.5 | 5.5 | 4.9 |
| | *Th* | 9.5 | 1.8 | 11 | 10 | 10 | 11 | 8.4 | 10 | 12 | 11 |
| | *U* | 2.8 | 0.58 | 2.9 | 3.2 | 2.8 | 3.3 | 4.0 | 3.1 | 3.0 | 3.1 |

**Table 3**. Continued

| Sample: | | Sandfell | LÝSUSKARÐ (IILys-) | | | | |
|---|---|---|---|---|---|---|---|
| | | **IISand-01** | **01** | **02** | **04** | **07a** | **07b** |
| Major Element Oxides (wt.%)$^1$ | $SiO_2$ | 74.2 | 72.6 | 67.3 | 57.5 | 72.2 | 71.6 |
| | $TiO_2$ | 0.13 | 0.32 | 0.69 | 2.6 | 0.31 | 0.32 |
| | $Al_2O_3$ | 13.8 | 13.5 | 14.5 | 15.4 | 13.5 | 13.6 |
| | $Fe_2O_3$ | 2.7 | 3.0 | 5.6 | 9.6 | 4.1 | 3.8 |
| | MnO | 0.10 | 0.04 | 0.22 | 0.25 | 0.14 | 0.10 |
| | MgO | 0.25 | 0.15 | 0.52 | 2.8 | 0.01 | 0.04 |
| | CaO | 0.91 | 0.99 | 2.0 | 4.1 | 0.03 | 0.49 |
| | $Na_2O$ | 4.0 | 3.2 | 5.0 | 4.3 | 4.7 | 4.8 |
| | $K_2O$ | 3.9 | 6.1 | 4.1 | 2.6 | 4.9 | 5.2 |
| | $P_2O_5$ | 0.02 | 0.03 | 0.12 | 0.87 | 0.02 | 0.02 |
| LOI (%) | | 2.45 | | 0.21 | | 1.04 | 0.89 |
| Trace Element Concentrations (ppm) | *Sc* | 3.6 | 4.6 | 8.3 | 18 | 1.4 | 1.3 |
| | *Rb* | 81 | 121 | 96 | 57 | 110 | 121 |
| | *Sr* | 91 | 184 | 200 | 398 | 17 | 31 |
| | *Y* | 125 | 81 | 70 | 49 | 78 | 94 |
| | *Zr* | 402 | 809 | 671 | 414 | 863 | 851 |
| | *Nb* | 83 | 176 | 145 | 116 | 182 | 180 |
| | *Cs* | 0.96 | 0.26 | 0.76 | 0.36 | 0.35 | 2.1 |
| | *Ba* | 828 | 738 | 1061 | 802 | 1322 | 1390 |
| | **La** | 97 | 114 | 98 | 66 | 64 | 121 |
| | **Ce** | 209 | 227 | 194 | 136 | 213 | 216 |
| | **Pr** | 26 | 26 | 22 | 17 | 15 | 28 |
| | **Nd** | 100 | 92 | 83 | 67 | 52 | 104 |
| | **Sm** | 23 | 17 | 16 | 13 | 11 | 20 |
| | **Eu** | 4.0 | 2.1 | 3.8 | 4.0 | 2.2 | 3.9 |
| | **Gd** | 22 | 15 | 13 | 11 | 9.6 | 18 |
| | **Tb** | 3.9 | 2.5 | 2.3 | 1.8 | 2.1 | 3.0 |
| | **Dy** | 24 | 16 | 14 | 10 | 14 | 18 |
| | **Ho** | 4.9 | 3.2 | 2.8 | 2.0 | 3.2 | 3.7 |
| | **Er** | 13 | 8.9 | 7.7 | 5.2 | 9.3 | 10 |
| | **Tm** | 1.9 | 1.4 | 1.2 | 0.73 | 1.5 | 1.5 |
| | **Yb** | 12 | 8.7 | 7.3 | 4.5 | 9.2 | 9.5 |
| | **Lu** | 1.8 | 1.4 | 1.2 | 0.70 | 1.4 | 1.5 |
| | *Hf* | 13 | 19 | 16 | 9.8 | 20 | 20 |
| | *Ta* | 5.5 | 11 | 9.0 | 6.9 | 11 | 11 |
| | *Pb* | 8.2 | 2.8 | 4.8 | 3.6 | 6.2 | 5.2 |
| | *Th* | 12 | 16 | 12 | 7.5 | 15 | 15 |
| | *U* | 2.8 | 4.6 | 3.5 | 2.1 | 4.4 | 4.3 |

## 4. **Preliminary results**

Based on the elemental and isotopic compositions of zircons from the Austurhorn Intrusive Complex, Padilla *et al.* (in review; see Chapter III) establish general compositional fields for intrusive zircons from Austurhorn. These fields are generally consistent with what is observed in zircons from other Icelandic silicic rocks (e.g. Carley *et al.,* 2011, 2014). Using a combination of field observations, whole-rock geochemistry, and zircon geochemistry, they demonstrate that the trends observed in Austurhorn zircons reflect assimilation of altered Icelandic crust into the magmatic system, followed by fractional crystallization processes (AFC) throughout the history of the intrusion, with some notable exceptions coming from zircons in high-$SiO_2$ granophyres (HSG). These HSG record more extreme processes, reflecting pure partial melting of variably altered crust (for detailed discussion on this, see Dissertation Chapter IV). Moreover, the extreme melts that these HSGs represent are likely the assimilant component in the AFC processes that are recorded by the rest of the silicic rocks at Austurhorn. With these results in mind, we compare other Icelandic intrusions to the extensive geochemical record presented for the Austurhorn intrusion (Padilla *et al.*, in review; see Chapters III and IV) in order to assess if and how magmatic systems in the shallow Icelandic crust have varied in space and time.

With few exceptions, the elemental geochemistry of zircons from other Icelandic intrusions is consistent with the geochemical array of Austurhorn and other silicic Icelandic rocks (Fig. 5). Notably, few grains in other intrusions share any of the extreme geochemical signatures observed in HSGs from Austurhorn. Abundances of U and Th range from ~20 to ~7000 ppm, and follow the same systematic increase in Th/U ratios, from ~0.5 to ~2, with increasing U and Th abundances that is observed in Austurhorn zircons (Fig. 5b). Hafnium concentrations are characteristically low, mostly falling between ~6000 and ~13,000 ppm, and Ti abundances range from ~3 to ~45 ppm in all samples, with some suspect grains (<5) extending up to ~95 ppm. Rare Earth element (REE) patterns are typical for zircon from silicic rocks (Fig. 5d; Carley *et al.*, 2014; Hoskin & Schaltegger, 2003; Hanchar & Miller, 1993), displaying chondrite-normalized trends of extreme enrichment in heavy rare earth elements (HREE) relative to light rare earth elements (LREE) and positive Ce and negative Eu anomalies (Fig. 6). Zircons from the Reyðarártindur intrusion have the lowest REE abundances, while those from Lýsuskarð have both the highest and the largest range of abundances. These elevated REE abundances in Lýsuskarð zircons are similar in magnitude to the elevated REE abundances in HSG zircons from Austurhorn.

Oxygen isotopic values ($\delta^{18}O$) for all zircons range from +0.5 to +5.7 ‰ (Fig. 7). Only zircons from the Vesturhorn intrusion extend into the accepted range for zircon mantle values (+5.3 ± 0.6 ‰, 2σ; Valley *et al.*, 1998), with a total range of +3.1 to +5.7 ‰. For all other intrusions, $\delta^{18}O$ falls below +4.8 ‰. The range of oxygen compositions from Reyðarártindur zircons best resembles what is observed for Austurhorn (excluding low-$\delta^{18}O$ zircons from HSG), with values extending continuously from +1.5 to +4.8 ‰ (compared to +2.2 to +4.8 ‰ for Austurhorn). Zircons from Lýsuskarð span the narrowest oxygen range, 2.7 to 3.2 ‰, with only a single value falling outside this range at 2.0 ‰.

*In situ* zircon hafnium isotope ratios ($\varepsilon_{Hf}$) for all intrusions span a significant range, extending from +7 to +16 ε-units (Fig. 7). Lýsuskarð falls on the lower end of this range, with all zircons having $\varepsilon_{Hf} < +12$, and zircons from Slaufrudalur preserve the largest range in $\varepsilon_{Hf}$.

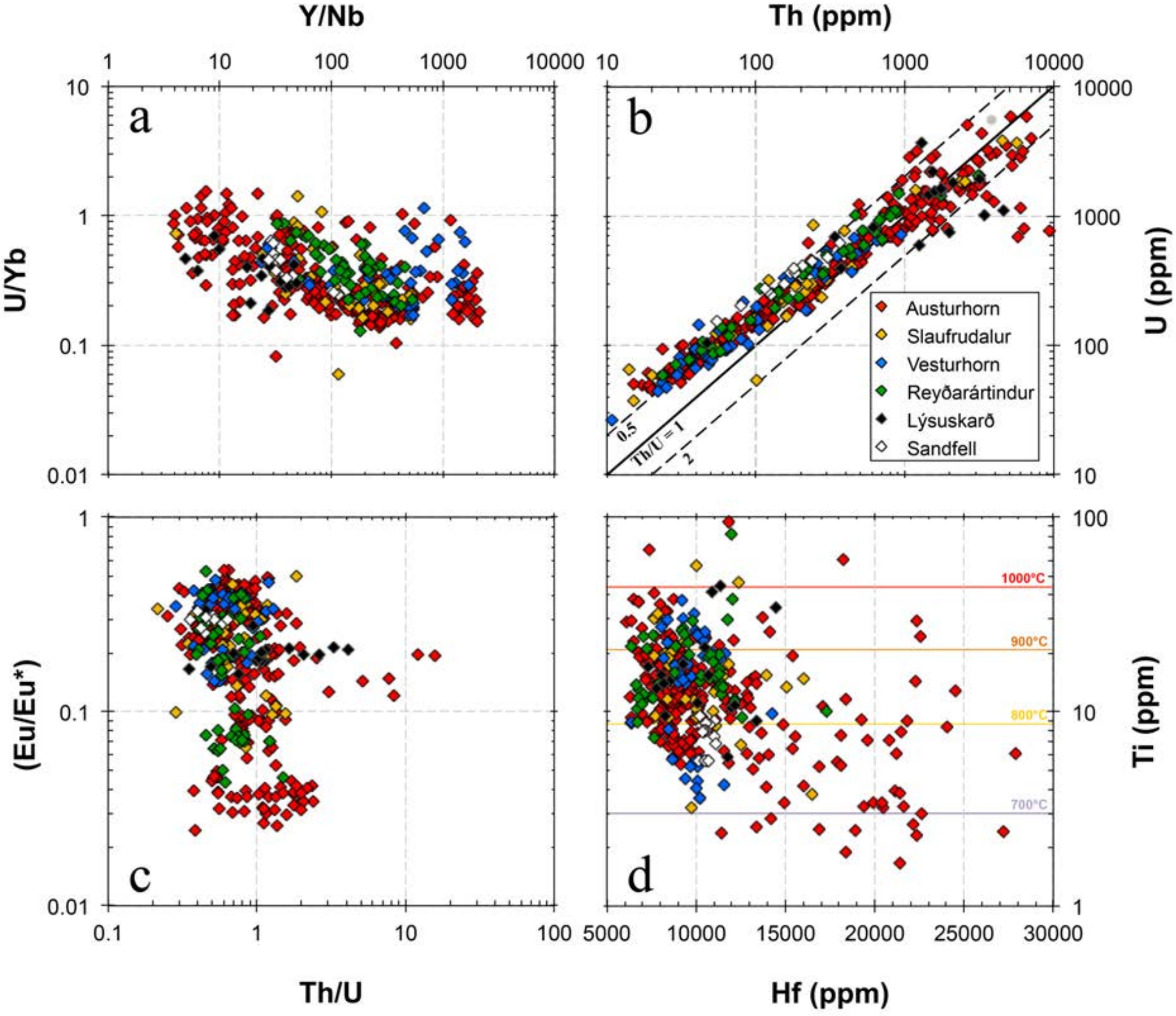

**Figure 5**

Trace element abundances and ratios for zircons from Icelandic silicic intrusions. **a)** Y/Nb vs. U/Yb; **b)** Th vs. U; the solid line indicates a Th/U ratio of 1; the dashed lines indicate Th/U ratios of 0.5 (top) and 2 (bottom); **c)** Th/U vs. Eu/Eu* (Eu anomaly). **d)** Hf vs. Ti; the colored lines indicate Ti-correlated model zircon crystallization temperatures, calculated using the Ti-in-zircon thermometer of Ferry & Watson (2007) using $a_{\mathrm{TiO_2}} = 0.5$ and $a_{\mathrm{SiO_2}} = 1.0$.

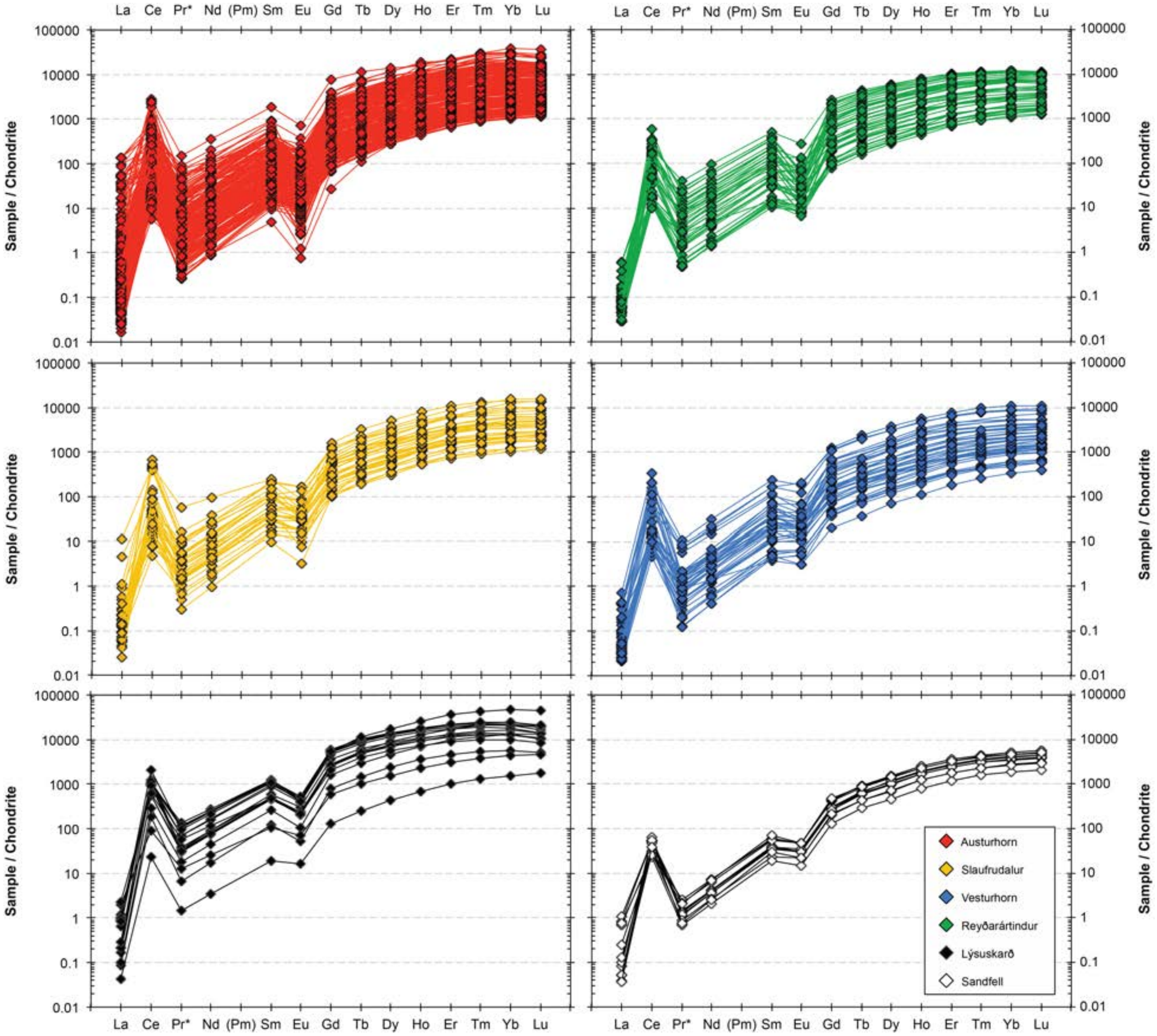

**Figure 6**

Chondrite-normalized zircon rare earth element (REE) abundances in samples from different Icelandic intrusions.

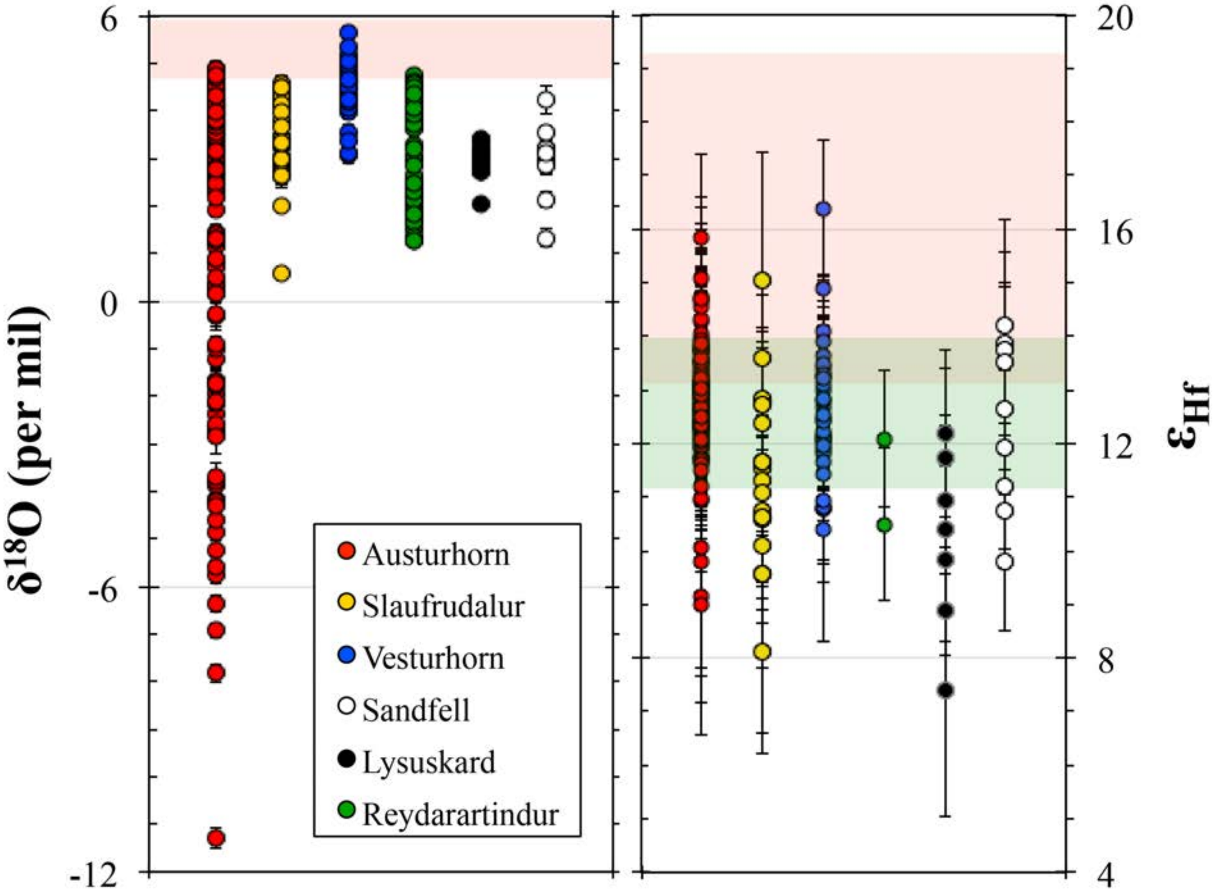

**Figure 7**

Isotopic compositions of zircons from silicic and composite Icelandic intrusions. **Left**: Oxygen isotope compositions ($\delta^{18}$O) plotted by sample. The light red zone indicates the $\delta^{18}$O range of mantle zircons (+5.3 ±0.6 ‰, Valley *et al.*, 1998). **Righ**t: Hafnium isotope compositions ($\varepsilon_{Hf}$) plotted by sample. The light red zone (upper) denotes the range of $\varepsilon_{Hf}$ values observed in lavas from active rift environments in Iceland. The light green zone (lower) denotes the range of $\varepsilon_{Hf}$ values in Icelandic lavas from off-rift and propagating-rift environments (Peate *et al.*, 2010).

High-precision zircon U-Pb geochronology yields an age of 6.38 ± 0.05 Ma (MSWD = 3.4, n = 32; all reported age uncertainties are 2σ SE) for the Slaufrudalur intrusion (see Fig. 4), consistent with the younger intrusion stage identified by Gale *et al.* (1966). The Vesturhorn intrusion, to the south, is the youngest in the SIIS, with a weighted mean age of 4.02 ± 0.03 Ma (MSWD = 1.9, n = 34), within error of the previously published zircon age of Martin *et al.* (2011). I obtained an age of 7.30 ± 0.06 Ma (MSWD = 4.3, n = 30) for the Reyðarártindur intrusion, the first reported age for this intrusion. Zircons from the Lýsuskarð intrusion yield an age of 1.43 ± 0.02 Ma (MSWD = 4.9, n = 10). Lastly, the mean age for the Sandfell laccolith is 11.90 ± 0.12 Ma (MSWD = 2.5, n = 13), indistinguishable from the most recent zircon age reported by Martin *et al.* (2011).

## 5. **Summary**

My preliminary results show that most Icelandic intrusions share the same general geochemical characteristics as other silicic rocks from Iceland, intrusive as well as extrusive (e.g. Padilla *et al.*, in review, see Dissertation Chapters III and IV; Carley *et al*, 2011, 2014). No correlations are observed between age of intrusion and the zircon elemental geochemical record, perhaps suggesting that magmatic processes in the shallow crust have not changed considerably throughout Iceland's geologic history. However, some differences in the isotopic compositions of zircons may be preserving shifts in the tectonic setting at the time of intrusion. Zircons from Sandfell as well as two of the intrusions from the SIIS, Slaufrudalur and Reyðarártindur, preserve $\delta^{18}$O variability that is similar to what is observed in non-HSG zircons from the Austurhorn intrusion (Fig. 7), perhaps suggesting considerable incorporation of hydrothermally altered crust into their parental magmas prior to zircon crystallization. In contrast, zircons from

Vesturhorn preserve, on average, the highest $\delta^{18}O$ values of all intrusions in this study, and many of these values overlap with the expected $\delta^{18}O$ range of mantle zircons. This is likely an indication that silicic magmas at Vesturhorn are generated dominantly by fractional crystallization (FC) of mantle melts, with little to no crustal contamination or assimilation. Similarly, the narrow range of $\delta^{18}O$ values in Lýsuskarð zircons may be indicative of the predominance of FC processes. However, the lower average values in those zircons requires a lower $\delta^{18}O$ source than that for Vesturhorn, which may be explained by either crustal assimilation followed by extensive hybridization and homogenization of magmas prior to zircon growth, or by a homogeneous low-$\delta^{18}O$ source beneath Lýsuskarð at the time of intrusion.

A more detailed and rigorous evaluation of the zircon geochemical dataset from Icelandic intrusions presented in this chapter, including sample-to-sample geochemical comparisons between whole-rock compositions (from which zircons were extracted) for each intrusion, may allow for a better assessment of individual magmatic histories. In conjunction with geochronology, the elemental and isotopic geochemistry of zircons from each intrusion may also provide insight about the regional tectonic environment during the lifetime of each magmatic system (*cf.* Martin *et al.*, 2011).

# CHAPTER VI

## Conclusions

Below, I provide a summary of the main conclusions and insights gained from the different studies that make up my doctorate dissertation research, which are presented in full in the preceding 3 chapters of this document.

In Chapter II, I present an extensive dataset of partition coefficients for 7 mineral phases from a single sample of Peach Spring Tuff high-silica rhyolite. The method employed, which involves measuring crystal rim compositions and unaltered glass by LA-ICP-MS, provides a high degree of internal consistency and yields a very reliable $K_d$ dataset reflecting equilibration conditions between crystals and melt in the volcanic system at or near the time of eruption. In addition, I demonstrate that, using the theoretical crystal lattice strain model of Blundy & Wood (1994, 2003), one can estimate the relative abundances of Eu and Ce in their multivalent states (2+, 3+, and 4+), with PST results indicating that >97% of total Ce exists as $Ce^{3+}$ whereas the relative proportions of Eu are less constrained, with ~50 to ~90% of Eu existing as $Eu^{3+}$. These results may have implications for estimating the oxidation state of magmas based on the occurrence Ce and Eu anomalies (*cf.* Trail *et al.*, 2012, 2015).

Chapter III presents the first detailed elemental and isotopic geochemical study of zircon from Icelandic intrusive rocks. The elemental compositions of AIC zircons form a broad but coherent array that mostly overlaps with the signature of zircons from Icelandic silicic volcanic rocks. I demonstrate that the diversity in oxygen isotopes ($\delta^{18}O$), from +2.2 to +4.8 ‰, provides strong evidence for the influence of meteoric-hydrothermal processes and recycling of hydrothermally-altered crust as a major contributor to silicic magmas within the AIC system.

Based on the geochemical evidence, I establish that that silicic magmas at Austurhorn were generated by assimilation and fractional crystallization (AFC) processes in which a significant portion of the crustal assimilant was generated by partial melting of variably hydrothermally-altered crust in a transitional rift environment (*cf.* Sigmarsson *et al.*, 1991). Zircons from the Austurhorn intrusive complex preserve a useful geochemical record of the manifestation and consequences of multiple episodes of mafic magmatic recharge into silicic systems at shallow depths, and an additional dimension in helping us better understand the accumulation of silicic magmas and subsequent evolution of silicic magmatic systems within the Earth's crust.

In Chapter IV, I present a case study of oxygen isotopes in zircon and bulk major minerals from rocks of the Austurhorn intrusion. This study builds on the work presented in Chapter III, and focuses on high-$SiO_2$ granophyres (HSG), the most evolved rocks at Austurhorn. Zircons in these HSG units preserve geochemical signatures that differ significantly from the general geochemical characteristics of zircons in other silicic rocks of Austurhorn as well as the rest of Iceland. I demonstrate that the extreme oxygen variability in HSG zircons, extending from +4.9 to as low as -11.3 ‰, reflect true $\delta^{18}O$ heterogeneity in the source magmas rather than post-magmatic alteration. As such, these samples preserve both the largest range (~ 16 ‰) and the lowest $\delta^{18}O$ value (-11.3 ‰) yet measured in any magmatic zircon. Based on the isotopic evidence, as well as evidence from modern Icelandic volcanic systems with low-$\delta^{18}O$ rocks, I interpret HSGs at Austurhorn to represent batches of small volume melts generated entirely by melting of variably altered crust, some of which underwent nearly complete (large water/rock ratio), high-T exchange with ~ -10 to -14 ‰ hydrothermal meteoric fluids. These are an excellent example of the pure partial melting end-member of magmatic processes seldom preserved in the geologic record, and an important geochemical marker for better understanding the production of silicic magmas in the shallow crust.

Lastly, Chapter V contains preliminary results from a large-scale assessment of zircon in six different Icelandic intrusive centers. I find that there are general zircon geochemical characteristics that are consistent across all studied Icelandic intrusive centers. However, in some intrusions (e.g. Austurhorn, Slaufrudalur, Reyðarártindur) zircons record oxygen variability that reflects assimilation of hydrothermally-altered crust into the magmas from which they crystallized, whereas in other intrusions (e.g. Vesturhorn and Lýsuskarð) the narrower range of $\delta^{18}$O compositions suggests dominant fractional crystallization processes in the petrogenesis of their parental magmas, but in some cases (e.g. Lýsuskarð) still require homogenization of the magma or incorporation of a lower-$\delta^{18}$O magma source prior to zircon crystallization. More detailed evaluation of other zircon isotopic data from these intrusions (e.g. $\varepsilon_{Hf}$ compositions) may provide additional insights into the tectonic setting and magmatic evolution of each individual Intrusion, and would permit more rigorous assessment of the magmatic processes that contributed to the generation of silicic magmas in their respective tectonic environments throughout Iceland's geologic history.

# APPENDIX A

# ELEMENTAL PARTITIONING IN SILICIC MAGMATIC SYSTEMS

**Appendix A.1**. Instrument reproducibility (relative accuracy and error)[24] for secondary geochemical glass standard NIST-612 (Pearce *et al.*, 1997), analyzed as unknown at **20 µm**

| **Element:** | $C_{Expected}$ **(ppm)** | $C_{Measured}$ **(ppm)** | **Rel. Accuracy** | **Rel. Error**[25] |
|---|---|---|---|---|
| **Li$^{1+}$** | 42 | 55 | **32%** | 26% |
| **B$^{3+}$** | 35 | 226 | **551%** | 34% |
| **Na$^{1+}$** | 103719 | 96113 | **7.3%** | 2.5% |
| **Mg$^{2+}$** | 77 | 60 | **22%** | 11% |
| **Al$^{3+}$** | 11165 | 10233 | **8.3%** | 3.4% |
| **K$^{1+}$** | 66 | 262 | **295%** | 15% |
| **Ca$^{2+}$** | 85263 | 84199 | **1.2%** | 4.4% |
| **Sc$^{3+}$** | 41 | 39 | **6.1%** | 24% |
| **Ti$^{4+}$** | 48 | 220 | **357%** | -- |
| **V$^{5+}$** | 39 | 37 | **6.1%** | 14% |
| **Cr$^{3+}$** | 40 | 92 | **130%** | 22% |
| **Mn$^{2+}$** | 38 | 38 | **0.758%** | 15% |
| **Co$^{2+}$** | 35 | 36 | **0.989%** | 14% |
| **Ni$^{2+}$** | 38 | 44 | **14%** | 26% |
| **Cu$^{2+}$** | 37 | 35 | **5.8%** | 34% |
| **Zn$^{2+}$** | 38 | 132 | **249%** | 23% |
| **Ga$^{3+}$** | 36 | 35 | **3.1%** | 24% |
| **Ge$^{4+}$** | 35 | 37 | **5.9%** | 27% |
| **Rb$^{1+}$** | 32 | 31 | **0.755%** | 7.3% |
| **Sr$^{2+}$** | 76 | 75 | **2.1%** | 6.1% |
| **Y$^{3+}$** | 38 | 37 | **2.9%** | 13% |
| **Zr$^{4+}$** | 36 | 36 | **0.124%** | 10% |
| **Nb$^{5+}$** | 38 | 34 | **10%** | 9.8% |
| **Cs$^{1+}$** | 42 | 40 | **3.6%** | 7.1% |
| **Ba$^{2+}$** | 38 | 36 | **3.5%** | 9.3% |
| **La$^{3+}$** | 36 | 36 | **1.3%** | 9.2% |
| **Ce$^{3+}$** | 38 | 37 | **2.8%** | 7.9% |
| **Pr$^{3+}$** | 37 | 34 | **7.2%** | 9.0% |
| **Nd$^{3+}$** | 35 | 35 | **0.192%** | 24% |
| **Sm$^{3+}$** | 37 | 37 | **0.441%** | 19% |
| **Eu$^{3+}$** | 34 | 35 | **2.4%** | 15% |
| **Gd$^{3+}$** | 37 | 34 | **7.4%** | 23% |
| **Tb$^{3+}$** | 36 | 37 | **2.1%** | 10% |
| **Dy$^{3+}$** | 36 | 34 | **5.2%** | 22% |
| **Ho$^{3+}$** | 38 | 38 | **0.693%** | 9.6% |
| **Er$^{3+}$** | 37 | 35 | **7.1%** | 16% |
| **Tm$^{3+}$** | 38 | 35 | **6.0%** | 9.9% |
| **Yb$^{3+}$** | 40 | 39 | **1.7%** | 24% |
| **Lu$^{3+}$** | 38 | 36 | **4.9%** | 11% |
| **Hf$^{4+}$** | 35 | 36 | **3.1%** | 23% |
| **Ta$^{5+}$** | 40 | 31 | **21%** | 9.3% |
| **Tl$^{3+}$** | 15 | 14 | **8.3%** | 19% |
| **Pb$^{2}$+** | 39 | 38 | **2.7%** | 16% |
| **Th$^{4+}$** | 37 | 37 | **0.098%** | 9% |
| **U$^{4+}$** | 37 | 38 | **1.6%** | 10% |

---

[24] Rel. accuracy = ($C_{measured\text{-}average}$ – $C_{expected}$) ÷ ($C_{expected}$); Rel. Error = ($\sigma_{measured}$) ÷ ($C_{measured\text{-}average}$)

[25] “--" denotes that we obtained only one analysis at the specified laser spot size and are unable to calculate rel. error

**Appendix A.2**. Instrument reproducibility (relative accuracy and error) for secondary geochemical glass standard NIST-612 (Pearce *et al.*, 1997), analyzed as unknown at **40 µm**

| **Element:** | $C_{Expected}$ **(ppm)** | $C_{Measured}$ **(ppm)** | **Rel. Accuracy** | **Rel. Error** |
|---|---|---|---|---|
| **Li**$^{1+}$ | 42 | 44 | 6.9% | 17% |
| **B**$^{3+}$ | 35 | 65 | 86% | 21% |
| **Na**$^{1+}$ | 103719 | 96515 | 6.9% | 2.1% |
| **Mg**$^{2+}$ | 77 | 61 | 22% | 7.9% |
| **Al**$^{3+}$ | 11165 | 10183 | 8.8% | 2.1% |
| **K**$^{1+}$ | 66 | 68 | 2.6% | 22% |
| **Ca**$^{2+}$ | 85263 | 84997 | 0.311% | 2.4% |
| **Sc**$^{3+}$ | 41 | 36 | 12% | 6.4% |
| **Ti**$^{4+}$ | 48 | 51 | 5.2% | 26% |
| **V**$^{5+}$ | 39 | 38 | 3.1% | 7.3% |
| **Cr**$^{3+}$ | 40 | 38 | 5.3% | 31% |
| **Mn**$^{2+}$ | 38 | 38 | 1.9% | 4.8% |
| **Co**$^{2+}$ | 35 | 34 | 2.7% | 7.4% |
| **Ni**$^{2+}$ | 38 | 38 | 1.0% | 14% |
| **Cu**$^{2+}$ | 37 | 37 | 1.4% | 6.8% |
| **Zn**$^{2+}$ | 38 | 39 | 2.7% | 30% |
| **Ga**$^{3+}$ | 36 | 38 | 6.1% | 7.1% |
| **Ge**$^{4+}$ | 35 | 37 | 6.5% | 13% |
| **Rb**$^{1+}$ | 32 | 32 | 1.6% | 3.5% |
| **Sr**$^{2+}$ | 76 | 75 | 1.1% | 3.0% |
| **Y**$^{3+}$ | 38 | 37 | 2.9% | 6.2% |
| **Zr**$^{4+}$ | 36 | 37 | 2.1% | 5.8% |
| **Nb**$^{5+}$ | 38 | 34 | 9.9% | 3.1% |
| **Cs**$^{1+}$ | 42 | 41 | 0.367% | 3.9% |
| **Ba**$^{2+}$ | 38 | 37 | 0.818% | 3.5% |
| **La**$^{3+}$ | 36 | 37 | 2.7% | 3.8% |
| **Ce**$^{3+}$ | 38 | 39 | 0.914% | 3.8% |
| **Pr**$^{3+}$ | 37 | 37 | 1.5% | 3.2% |
| **Nd**$^{3+}$ | 35 | 34 | 4.5% | 10% |
| **Sm**$^{3+}$ | 37 | 37 | 0.449% | 8.6% |
| **Eu**$^{3+}$ | 34 | 36 | 5.6% | 6.2% |
| **Gd**$^{3+}$ | 37 | 35 | 4.0% | 13% |
| **Tb**$^{3+}$ | 36 | 37 | 3.7% | 4.3% |
| **Dy**$^{3+}$ | 36 | 34 | 6.8% | 7.8% |
| **Ho**$^{3+}$ | 38 | 37 | 1.3% | 4.1% |
| **Er**$^{3+}$ | 37 | 36 | 4.3% | 5.8% |
| **Tm**$^{3+}$ | 38 | 35 | 7.1% | 3.3% |
| **Yb**$^{3+}$ | 40 | 40 | 0.006% | 7.5% |
| **Lu**$^{3+}$ | 38 | 36 | 3.9% | 4.7% |
| **Hf**$^{4+}$ | 35 | 36 | 2.6% | 7.3% |
| **Ta**$^{5+}$ | 40 | 30 | 24% | 3.3% |
| **Tl**$^{3+}$ | 15 | 15 | 0.382% | 8.1% |
| **Pb**$^{2}$**+** | 39 | 37 | 6.1% | 6.9% |
| **Th**$^{4+}$ | 37 | 37 | 0.715% | 4.4% |
| **U**$^{4+}$ | 37 | 38 | 2.2% | 4.4% |

**Appendix A.3**. Instrument reproducibility (relative accuracy and error) for secondary geochemical glass standard NIST-612 (Pearce *et al.*, 1997), analyzed as unknown at **80 µm**

| Element: | $C_{Expected}$ (ppm) | $C_{Measured}$ (ppm) | Rel. Accuracy | Rel. Error |
|---|---|---|---|---|
| **$Li^{1+}$** | 42 | 41 | 1% | 7% |
| **$B^{3+}$** | 35 | 35 | 1.28% | 36% |
| **$Na^{1+}$** | 103719 | 94285 | 9.1% | 1.5% |
| **$Mg^{2+}$** | 77 | 58 | 25% | 4% |
| **$Al^{3+}$** | 11165 | 9354 | 16.2% | 2.5% |
| **$K^{1+}$** | 66 | 61 | 8.31% | 27% |
| **$Ca^{2+}$** | 85263 | 78240 | 8.2% | 2.5% |
| **$Sc^{3+}$** | 41 | 33 | 19.6% | 4% |
| **$Ti^{4+}$** | 48 | 38 | 20.1% | 15% |
| **$V^{5+}$** | 39 | 37 | 6.1% | 4% |
| **$Cr^{3+}$** | 40 | 34 | 14.62% | 9% |
| **$Mn^{2+}$** | 38 | 36 | 6.335% | 2% |
| **$Co^{2+}$** | 35 | 34 | 4.661% | 4% |
| **$Ni^{2+}$** | 38 | 36 | 7% | 5% |
| **$Cu^{2+}$** | 37 | 37 | 1.7% | 7% |
| **$Zn^{2+}$** | 38 | 32 | 15.2% | 16% |
| **$Ga^{3+}$** | 36 | 36 | 1.2% | 5% |
| **$Ge^{4+}$** | 35 | 36 | 5.3% | 5% |
| **$Rb^{1+}$** | 32 | 32 | 0.276% | 2.6% |
| **$Sr^{2+}$** | 76 | 71 | 7.3% | 3.0% |
| **$Y^{3+}$** | 38 | 33 | 12.4% | 5% |
| **$Zr^{4+}$** | 36 | 34 | 5.855% | 5% |
| **$Nb^{5+}$** | 38 | 32 | 17% | 4.4% |
| **$Cs^{1+}$** | 42 | 40 | 5.0% | 2.6% |
| **$Ba^{2+}$** | 38 | 35 | 6.8% | 3.5% |
| **$La^{3+}$** | 36 | 34 | 5.7% | 2.8% |
| **$Ce^{3+}$** | 38 | 36 | 6.1% | 1.7% |
| **$Pr^{3+}$** | 37 | 33 | 10.1% | 3.0% |
| **$Nd^{3+}$** | 35 | 33 | 6.911% | 8% |
| **$Sm^{3+}$** | 37 | 34 | 8.187% | 6% |
| **$Eu^{3+}$** | 34 | 33 | 3.7% | 4% |
| **$Gd^{3+}$** | 37 | 32 | 13.6% | 9% |
| **$Tb^{3+}$** | 36 | 33 | 7.7% | 5% |
| **$Dy^{3+}$** | 36 | 31 | 15.1% | 5% |
| **$Ho^{3+}$** | 38 | 33 | 11.652% | 4.1% |
| **$Er^{3+}$** | 37 | 32 | 14.3% | 4% |
| **$Tm^{3+}$** | 38 | 32 | 15.1% | 2.7% |
| **$Yb^{3+}$** | 40 | 35 | 12.4% | 9% |
| **$Lu^{3+}$** | 38 | 33 | 13.7% | 4% |
| **$Hf^{4+}$** | 35 | 31 | 12.1% | 7% |
| **$Ta^{5+}$** | 40 | 28 | 30% | 4.1% |
| **$Tl^{3+}$** | 15 | 15 | 0.0% | 5% |
| **$Pb^{2}+$** | 39 | 35 | 9.7% | 5% |
| **$Th^{4+}$** | 37 | 33 | 10.485% | 5% |
| **$U^{4+}$** | 37 | 36 | 4.2% | 3% |

**Appendix A.4**. Instrument reproducibility (relative accuracy and error) for secondary geochemical glass standard NIST-614 (Kurosawa *et al.*, 2002), analyzed as unknown at **120 µm**

| **Element:** | **$C_{Expected}$ (ppm)**[26] | **$C_{Measured}$ (ppm)** | **Rel. Accuracy** | **Rel. Error** |
|---|---|---|---|---|
| **Li$^{1+}$** | 1.69 | 1.83 | 8% | 43% |
| **B$^{3+}$** | 4.83 | 6.86 | 41.93% | 4% |
| **Na$^{1+}$** | -- | 103430 | -- | 2.1% |
| **Mg$^{2+}$** | 35 | 35 | 1% | 24% |
| **Al$^{3+}$** | -- | 10913 | -- | 2.5% |
| **K$^{1+}$** | -- | 50 | -- | 79% |
| **Ca$^{2+}$** | -- | 84769 | -- | 2.2% |
| **Sc$^{3+}$** | 1.53 | 1.66 | 8.4% | 24% |
| **Ti$^{4+}$** | 3.37 | 14 | 307% | 41% |
| **V$^{5+}$** | 1.00 | 0.959 | 4.1% | 27% |
| **Cr$^{3+}$** | 1.23 | 2.71 | 120% | -- |
| **Mn$^{2+}$** | 1.35 | 1.40 | 3.981% | 19% |
| **Co$^{2+}$** | 0.680 | 0.718 | 5.588% | 25% |
| **Ni$^{2+}$** | 1.04 | 1.30 | 25% | 35% |
| **Cu$^{2+}$** | 1.19 | 1.67 | 40.7% | 26% |
| **Zn$^{2+}$** | 2.16 | 3.23 | 49.4% | 18% |
| **Ga$^{3+}$** | 1.19 | 1.36 | 14.4% | 17% |
| **Ge$^{4+}$** | 0.880 | 1.06 | 20.8% | 30% |
| **Rb$^{1+}$** | 0.870 | 1.04 | 19.310% | 20.1% |
| **Sr$^{2+}$** | 45 | 44 | 2.9% | 2.3% |
| **Y$^{3+}$** | 0.790 | 0.789 | 0.1% | 12% |
| **Zr$^{4+}$** | 0.770 | 0.791 | 2.727% | 12% |
| **Nb$^{5+}$** | 0.780 | 0.765 | 2% | 19.4% |
| **Cs$^{1+}$** | 0.590 | 0.702 | 18.9% | 13.2% |
| **Ba$^{2+}$** | 3.15 | 3.08 | 2.1% | 6.5% |
| **La$^{3+}$** | 0.750 | 0.687 | 8.3% | 6.1% |
| **Ce$^{3+}$** | 0.780 | 0.772 | 1.0% | 16.7% |
| **Pr$^{3+}$** | 0.760 | 0.725 | 4.6% | 8.4% |
| **Nd$^{3+}$** | 0.770 | 0.781 | 1.443% | 38% |
| **Sm$^{3+}$** | 0.790 | 0.694 | 12.152% | 32% |
| **Eu$^{3+}$** | 0.780 | 0.732 | 6.2% | 10% |
| **Gd$^{3+}$** | 0.800 | 0.807 | 0.9% | 29% |
| **Tb$^{3+}$** | 0.760 | 0.695 | 8.6% | 9% |
| **Dy$^{3+}$** | 0.830 | 0.636 | 23.4% | 23% |
| **Ho$^{3+}$** | 0.810 | 0.761 | 6.086% | 5.6% |
| **Er$^{3+}$** | 0.810 | 0.774 | 4.4% | 23% |
| **Tm$^{3+}$** | 0.800 | 0.672 | 16.0% | 8.0% |
| **Yb$^{3+}$** | 0.840 | 0.749 | 10.8% | 29% |
| **Lu$^{3+}$** | 0.800 | 0.724 | 9.6% | 11% |
| **Hf$^{4+}$** | 0.740 | 0.756 | 2.2% | 25% |
| **Ta$^{5+}$** | 0.830 | 0.768 | 7% | 9.5% |
| **Tl$^{3+}$** | 0.240 | 0.238 | 1.0% | 23% |
| **Pb$^{2}$+** | 2.07 | 2.36 | 13.9% | 15% |
| **Th$^{4+}$** | 0.830 | 0.736 | 11.289% | 13% |
| **U$^{4+}$** | 0.800 | 0.847 | 5.8% | 9% |

---

[26] “--" denotes elements for which there is no reference data available and we are unable to calculate rel. accuracy

**Appendix A.5**. Partition coefficient ($K_d$) references and rock types for literature data used in *GERM* comparison plots (see Figs. 3-10, Chapter II)

| Reference # | Published Study | Rock Type | Code | Symbol[27] | Analytical Method(s)[28] |
|---|---|---|---|---|---|
| [1] | Colombini *et al.* 2011 | High-Si Rhyolite | (A) | □ | SHRIMP (titanite, zircon), LA-ICP-MS |
| [2] | Bachmann *et al.* 2005 | High-Si Rhyolite | (A) | □ | LA-ICP-MS |
| [3] | Troll *et al.* 2003 | Peralkaline Rhyolite | (D) | ◇ | SYXRF-MP |
| [4] | Mahood & Hildreth 1983 | High-Si Rhyolite | (A) | □ | INAA |
| [5] | Nagasawa 1970 | Granite | (E) | △ | ID-MS |
| [6] | Bea *et al.* 1994 | Per-aluminous Ganite | (F) | △ | LA-ICP-MS |
| [7] | Sano *et al.* 2002 | Dacite | (G) | ○ | SHRIMP |
| [8] | Ewart & Griffin 1994 | High-Si Rhyolite,<br>Low-Si Rhyolite | (A),<br>(C) | □,◇ | PMP, EMP (glass/matrix) |
| [9] | Sisson 1994 | Rhyolite | (B) | ◇ | SIMS |
| [10] | Bacon & Druitt 1988 | Rhyolite | (B) | ◇ | ARL-SEMQ (Whole-Rock/glass), XRF (glass), INAA |
| [11] | Anderson *et al.* 2000 | High-Si Rhyolite | (A) | □ | SIMS |
| [12] | Nash & Crecraft 1985 | Rhyolite | (B) | ◇ | INAA, XRF |
| [13] | Schnetzler & Philpotts 1970 | Rhyolite | (B) | ◇ | ID-MS |
| [14] | Stix & Gorton 1990 | High-Si Rhyolite | (A) | □ | INAA, ICP-MS (glass) |
| [15] | Leeman & Phelps 1981 | Rhyolite | (A) | □ | INAA |
| [16] | Streck & Grunder 1997 | High-Si Rhyolite | (A) | □ | INAA |
| [17] | Severs *et al.* 2009 | Dacite | (G) | ○ | LA-ICP-MS |

---

[27] These symbols correspond to those used in Chapter II, Figs. 3-10

[28] Methods:

SHRIMP: sensitive high-resolution ion microprobe
LA-ICP-MS: laser ablation inductively-coupled plasma mass-spectrometry
SYXRF-MP: synchrotron radiation X-ray fluorescence microprobe
INAA: instrument neutron activation analysis
ID-MS: isotope dilution mass spectrometry
PMP: proton microprobe
EMP: electron microprobe
SIMS: secondary ion mass spectrometry
ARL-SEMQ MP: scanning electron microprobe quantometer
XRF: X-ray fluorescence

**Appendix A.6**. Partition coefficients ($K_d$) used in literature comparison (Figs. 3-10, Chapter II)

| **Mineral:** | **Titanite** | **Titanite** | **Titanite** | **Titanite** | **Chevkinite** | **Zircon** | **Zircon** |
|---|---|---|---|---|---|---|---|
| **Reference**[29]**:** | [1],(A) | [1],(A) | [2],(A) | [3],(D) | [3],(D) | [1],(A) | [1],(A) |
| **Notes**[30]**:** | KPST01 | HRL 21 | | | | KPST01 | HRL 21 |
| **Li** | | | 0.04 | | | | |
| **Mg** | 0.74 | 1.7 | | | | | |
| **Al** | 0.15 | 0.15 | | | | | |
| **Ca** | 63 | 53 | | | | | |
| **Sc** | 23 | 36 | 5.9 | | | 15 | 44 |
| **Ti** | 269 | 358 | | | | 0.01 | 0.01 |
| **V** | 39 | 89 | | | | | |
| **Mn** | 6.2 | 8.9 | | | | | |
| **Co** | | | | | | | |
| **Ni** | | | | | | | |
| **Cu** | | | | | | | |
| **Zn** | | | | | | | |
| **Ga** | | | | | | | |
| **Ge** | | | | | | | |
| **Rb** | | | <0.01 | | | | |
| **Sr** | 0.85 | 0.56 | 0.37 | 8.5 | 84 | | |
| **Y** | 315 | 601 | 633 | 99 | 74 | 42 | 121 |
| **Zr** | 7 | 11 | 9.64 | 3.1 | 3.55 | 3406 | 6160 |
| **Nb** | 73 | 109 | 129 | 46 | 15 | 0.34 | 1.4 |
| **Cs** | | | | | | | |
| **Ba** | 0.73 | 0.83 | | | | | |
| **La** | 79 | 123 | 113 | 28 | 988 | 0.0025 | 0.0024 |
| **Ce** | 161 | 267 | 223 | 86 | 806 | 0.84 | 2.5 |
| **Pr** | 280 | 419 | | 98 | 626 | | |
| **Nd** | 412 | 750 | 639 | 134 | 615 | 0.05 | 0.08 |
| **Sm** | 614 | 1208 | 930 | 240 | 392 | 0.64 | 1.1 |
| **Eu** | 553 | 647 | 661 | 50 | 225 | 2.5 | 2.5 |
| **Gd** | 648 | 1332 | 855 | 96 | 142 | 5.8 | 13 |
| **Tb** | 619 | 1231 | | | | 14 | 34 |
| **Dy** | 480 | 1048 | 935 | 82 | 72 | 24 | 68 |
| **Ho** | 404 | 884 | | | | 45 | 134 |
| **Er** | 352 | 678 | 636 | | | 77 | 219 |
| **Tm** | 256 | 456 | | | | 105 | 293 |
| **Yb** | 166 | 316 | 393 | | | 112 | 359 |
| **Lu** | 117 | 237 | | | | 131 | 475 |
| **Hf** | 10 | 19 | 18.7 | | | 1829 | 3850 |
| **Ta** | 112 | 145 | 153 | | | | |
| **Tl** | | | | | | | |
| **Pb** | 0.08 | 0.12 | 0.10 | | | | |
| **Th** | 8.3 | 13 | 18.7 | | | 8.1 | 50 |
| **U** | 3 | 4.8 | 7 | | | 29 | 148 |

---

[29] See **Table A.5** for references (numbers in brackets”[ ]”) and sample compositions (letters in parentheses “( )”)

[30] *KPST01 & HRL21*: Sample names (see reference [1] for sample descriptions)

**Appendix A.6**. Continued

| **Mineral:** | **Zircon** | **Zircon** | **Zircon** | **Zircon** | **Zircon** | **Zircon** | **Apatite** |
|---|---|---|---|---|---|---|---|
| **Reference:** | [1],(B) | [2],(A) | [4],(A) | [5],(E) | [6],(F) | [7],(G) | [5],(E) |
| **Notes**[31]**:** | HRL 27 | | AVG | AVG | | | |
| **Li** | | | | | | | |
| **Mg** | | | | | | | |
| **Al** | | | | | | | |
| **Ca** | | | | | | | |
| **Sc** | 24 | 161 | 68.65 | | | | |
| **Ti** | 0.02 | | | | | | |
| **V** | | | | | | | |
| **Mn** | | | | | | | |
| **Co** | | | | | | | |
| **Ni** | | | | | | | |
| **Cu** | | | | | | | |
| **Zn** | | | | | | | |
| **Ga** | | | | | | | |
| **Ge** | | | | | | | |
| **Rb** | | | | | | | |
| **Sr** | | | | | | | |
| **Y** | 46 | 181 | | | 71.4 | | |
| **Zr** | 1778 | 1043 | | 1230 | | | |
| **Nb** | 0.18 | 2.09 | | | | | |
| **Cs** | | | | | | | |
| **Ba** | | <0.01 | | | | | |
| **La** | 0.00052 | 0.1 | 16.9 | | 1.3 | 0.00046 | |
| **Ce** | 0.37 | 1.1 | 16.75 | | 2.04 | 0.36 | 29.6 |
| **Pr** | | | | | | | |
| **Nd** | 0.05 | 0.41 | 13.3 | 0.405 | 3.35 | 0.077 | 57.1 |
| **Sm** | 0.61 | 3.28 | 14.4 | 2.055 | 3.79 | 0.8 | 84.8 |
| **Eu** | 2.4 | 4.35 | 16 | 0.875 | 0.45 | 1.22 | 9.22 |
| **Gd** | 6.2 | 19.8 | | | 9.21 | 8 | |
| **Tb** | 14 | | 37 | | 24.8 | 20.7 | |
| **Dy** | 26 | 106 | 101.5 | 65.1 | 38.8 | 45.9 | 246 |
| **Ho** | 50 | | | | 74.5 | 80 | |
| **Er** | 81 | 274 | | 265.75 | 165 | 136 | 275 |
| **Tm** | 122 | | | | 282 | 197 | |
| **Yb** | 125 | 465 | 527 | 534 | 278 | 277 | 232 |
| **Lu** | 172 | | 641.5 | | 923 | 325 | 199 |
| **Hf** | 997 | 3580 | 3193.5 | | | | |
| **Ta** | | 1.29 | 47.5 | | | | |
| **Tl** | | | | | | | |
| **Pb** | | 0.05 | | | 7.5 | | |
| **Th** | 4.5 | 10.6 | | | 22.1 | | |
| **U** | 16 | 48.6 | | | 254 | | |

---

[31] *AVG* = average of reported values for studies that report multiple $K_d$ values or the max. and min. of their study

**Appendix A.6**. Continued

| **Mineral:**<br>**Reference:**<br>**Notes:** | **Apatite**<br>[6],(F) | **Apatite**<br>[7],(G) | **Amphibole**<br>[2],(A) | **Amphibole**<br>[8],(A)<br>AVG | **Amphibole**<br>[8],(C)<br>AVG | **Amphibole**<br>[9],(B)<br>AVG |
|---|---|---|---|---|---|---|
| **Li** | | | 0.3 | | | |
| **Mg** | | | | | | |
| **Al** | | | | | | |
| **Ca** | | | | | | |
| **Sc** | | | 45 | | | 117 |
| **Ti** | | | | | | 15.8 |
| **V** | | | | | | 19.5 |
| **Mn** | | | | 19.55 | 10.45 | |
| **Co** | | | | | | |
| **Ni** | | | | | | |
| **Cu** | | | | | | |
| **Zn** | | | | 9.6 | 4.8 | |
| **Ga** | | | | 1.46 | 1 | |
| **Ge** | | | | 2.95 | 1.9 | |
| **Rb** | | | | 0.0335 | 0.199 | |
| **Sr** | | | 0.4 | 7.735 | 0.69 | 1.275 |
| **Y** | 162 | | 13.5 | 13.55 | 24.6 | 9.64 |
| **Zr** | | | 0.5 | 0.725 | 0.72 | 0.43 |
| **Nb** | | | 2 | 2.59 | 4.1 | |
| **Cs** | | | | | | |
| **Ba** | | | 0.08 | 2.39 | 0.54 | |
| **La** | 456 | 36 | 1.4 | | | 1.39 |
| **Ce** | 569 | 48 | 3.2 | | | 3.18 |
| **Pr** | 764 | 64 | | | | |
| **Nd** | 855 | 77 | 9.7 | | | 6.945 |
| **Sm** | 1105 | 93 | 15.5 | | | 9.53 |
| **Eu** | 23.8 | 55 | 10.8 | | | |
| **Gd** | 2133 | 127 | 14.9 | | | |
| **Tb** | 3643 | 102 | | | | |
| **Dy** | 3257 | 76 | 17.6 | | | 11.25 |
| **Ho** | 3143 | 62 | | | | |
| **Er** | 4231 | 57 | 13.2 | | | 7.53 |
| **Tm** | 3769 | 53 | | | | |
| **Yb** | 2216 | 48 | 9.6 | | | 4.955 |
| **Lu** | 2981 | 33 | | | | |
| **Hf** | | | 0.9 | | | |
| **Ta** | | | 0.5 | | | |
| **Tl** | | | | | | |
| **Pb** | 0.03 | | 0.1 | 0.255 | 0.43 | |
| **Th** | 41 | | 0.01 | | | |
| **U** | 43.7 | | 0.01 | | | |

**Appendix A.6**. Continued

| **Mineral:** | **Amphibole** | **Biotite** | **Biotite** | **Biotite** | **Biotite** | **Biotite** | **Biotite** |
|---|---|---|---|---|---|---|---|
| **Reference:** | [10],(B) | [2],(A) | [4],(A) | [6],(F) | [8],(A) | [8],(C) | [11],(A) |
| **Notes:** | | | AVG | | | | |
| **Li** | | 1.2 | | 45.4 | | | |
| **Mg** | | | | | | | |
| **Al** | | | | | | | |
| **Ca** | | | | | | | |
| **Sc** | 14 | 3.4 | 15.6 | 42.4 | | | |
| **Ti** | | | | | | | |
| **V** | | | | 79.5 | | | |
| **Mn** | | | 10.65 | | 15.5 | 5.7 | |
| **Co** | 37 | | 90 | | | | |
| **Ni** | | 92 | | 9.66 | | 15.1 | |
| **Cu** | | | | | 20.3 | 72.4 | |
| **Zn** | 2.3 | | 16 | 2.8 | 31.6 | 11.4 | |
| **Ga** | | | | | 3.1 | 1.7 | |
| **Ge** | | | | | | 1.5 | |
| **Rb** | 0.4 | 2 | 4.15 | 6.98 | 9.6 | 2.46 | 1.43 |
| **Sr** | 0.01 | 0.1 | | 0.01 | 7.2 | 0.25 | 0.063 |
| **Y** | | 0.02 | | 0.1 | 2.4 | 2.3 | |
| **Zr** | 0.5 | 0.05 | | | 0.47 | 0.19 | |
| **Nb** | | 2.9 | | 24.5 | 9.1 | 4.6 | |
| **Cs** | | 0.5 | 2.15 | 26.8 | | | |
| **Ba** | 0.3 | 4.4 | 5.35 | 0.59 | | 6.4 | 7.1 |
| **La** | 0.36 | <0.01 | 3.07 | 0.06 | | | |
| **Ce** | 0.68 | 0.01 | 2.82 | 0.05 | | | |
| **Pr** | | | | 0.07 | | | |
| **Nd** | 1.6 | 0.01 | 2.25 | 0.08 | | | |
| **Sm** | 2.3 | | | | | | |
| **Eu** | 3.2 | | | | | | |
| **Gd** | | | | | | | |
| **Tb** | 2.4 | | | | | | |
| **Dy** | | 0.01 | 0.775 | 0.17 | | | |
| **Ho** | | | | | | | |
| **Er** | | | | | | | |
| **Tm** | | | | | | | |
| **Yb** | 1.8 | | | | | | |
| **Lu** | 1.8 | | | | | | |
| **Hf** | 0.52 | | | | | | |
| **Ta** | 0.43 | 1 | 1.335 | 29.1 | | | |
| **Tl** | | | | 8.6 | | | |
| **Pb** | | 0.1 | | 0.04 | 2.1 | 0.21 | |
| **Th** | 0.16 | <0.01 | 1.1255 | 0.01 | | | |
| **U** | | | | | | | |

**Appendix A.6**. Continued

| **Mineral:** | **Biotite** | **Biotite** | **Sanidine** | **Sanidine** | **Sanidine** | **Sanidine** | **Sanidine** |
|---|---|---|---|---|---|---|---|
| **Reference:** | [12],(B) | [13],(B) | [2],(A) | [4],(A) | [8],(A) | [8],(C) | [11],(A) |
| **Notes:** | AVG | | | AVG | AVG | AVG | |
| **Li** | | | 0.01 | | | | |
| **Mg** | | | | | | | |
| **Al** | | | | | | | |
| **Ca** | | | | | | | |
| **Sc** | 12.45 | | 0.5 | 0.0415 | | | |
| **Ti** | | | | | | | |
| **V** | | | | | | | |
| **Mn** | 109.3 | | | 0.023 | 0.177 | 0.114 | |
| **Co** | | | | | | | |
| **Ni** | | | | | | | |
| **Cu** | | | | | | | |
| **Zn** | 136 | | | | | | |
| **Ga** | | | | | 0.95 | 1.225 | |
| **Ge** | | | | | 1.02 | 1.45 | |
| **Rb** | 3.2 | | 0.7 | 0.525 | 0.415 | 0.415 | 0.593 |
| **Sr** | 0.41 | | 7.4 | | 12.105 | 4.94 | 11.3 |
| **Y** | 1.2 | | | | | | |
| **Zr** | 1.295 | | <0.01 | | 0.1075 | 0.0435 | |
| **Nb** | 6.75 | | | | | | |
| **Cs** | 2.8 | | 0.02 | 0.035 | | | |
| **Ba** | 20.8 | | 17.1 | 3.85 | 11.8 | 9.35 | 28.4 |
| **La** | 7.93 | | 0.06 | 0.074 | | | |
| **Ce** | 5.93 | 0.234 | 0.02 | 0.063 | | | |
| **Pr** | | | | | | | |
| **Nd** | 3.3 | 0.339 | <0.01 | 0.053 | | | |
| **Sm** | | | | | | | |
| **Eu** | | | 2.9 | 2.75 | | | |
| **Gd** | | | | | | | |
| **Tb** | | | | | | | |
| **Dy** | 2.08 | 0.2 | | | | | |
| **Ho** | | | | | | | |
| **Er** | | | | | | | |
| **Tm** | | | | | | | |
| **Yb** | | | | | | | |
| **Lu** | | | | | | | |
| **Hf** | | | | | | | |
| **Ta** | 1.55 | | | | | | |
| **Tl** | | | | | | | |
| **Pb** | 0.85 | | 1.1 | | 0.75 | 0.475 | |
| **Th** | 1.135 | | | | | | |
| **U** | | | | | | | |

**Appendix A.6**. Continued

| **Mineral:** | **Sanidine** | **Sanidine** | **Plagioclase** | **Plagioclase** | **Plagioclase** | **Plagioclase** |
|---|---|---|---|---|---|---|
| **Reference:** | [14],(A) | [15],(A) | [2],(A) | [6],(F) | [8],(A) | [8],(C) |
| **Notes:** | AVG | | | | AVG | AVG |
| **Li** | | | 0.2 | 0.72 | | |
| **Mg** | | | | | | |
| **Al** | | | | | | |
| **Ca** | 0.49 | | | | | |
| **Sc** | | 0.029 | 0.5 | 1.62 | | |
| **Ti** | | | | | | |
| **V** | | | | 0.13 | | |
| **Mn** | | | | | 0.295 | 0.15 |
| **Co** | | | | | | |
| **Ni** | | | | | | |
| **Cu** | | | | 0.14 | 0.95 | 0.805 |
| **Zn** | | | | 0.07 | 0.175 | 0.365 |
| **Ga** | | | | | 1.145 | 1.78 |
| **Ge** | | | | | | 0.975 |
| **Rb** | 0.49 | 0.4 | <0.01 | 0.06 | 0.02 | 0.0965 |
| **Sr** | 4 | | 12.5 | 1.25 | 8.12 | 6.815 |
| **Y** | | | 0.02 | 0.78 | 0.053 | 0.3165 |
| **Zr** | | 0.36 | <0.01 | | 0.098 | 0.14 |
| **Nb** | | | | | | |
| **Cs** | 0.0315 | 0.024 | <0.01 | 0.44 | | |
| **Ba** | 22.5 | 22 | 0.61 | 0.19 | 1.4 | 0.375 |
| **La** | 0.088 | 0.129 | 0.4 | 4.61 | | |
| **Ce** | 0.056 | 0.065 | 0.3 | 3.87 | | |
| **Pr** | 0.051 | | | 4.22 | | |
| **Nd** | | 0.054 | 0.2 | 2.56 | | |
| **Sm** | | | | | | |
| **Eu** | 5.6 | 9.06 | 3.1 | 2.99 | | |
| **Gd** | | | | | | |
| **Tb** | | | | | | |
| **Dy** | | | | | | |
| **Ho** | | | | | | |
| **Er** | | | | | | |
| **Tm** | | | | | | |
| **Yb** | | | | | | |
| **Lu** | | | | | | |
| **Hf** | | | | | | |
| **Ta** | | | | | | |
| **Tl** | | | | | | |
| **Pb** | | | 0.5 | 0.77 | 0.66 | 0.595 |
| **Th** | | | | | | |
| **U** | | | | | | |

**Appendix A.6**. Continued

| **Mineral:**<br>**Reference:**<br>**Notes:** | **Plagioclase**<br>[10],(B) | **Plagioclase**<br>[11],(A) | **Plagioclase**<br>[12],(B)<br>AVG | **Plagioclase**<br>[16],(A)<br>AVG | **Plagioclase**<br>[17],(G) |
|---|---|---|---|---|---|
| **Li** | | | | | |
| **Mg** | | | | | |
| **Al** | | | | | |
| **Ca** | | | | | |
| **Sc** | 0.01 | | 0.04 | | |
| **Ti** | | | | | 0.043 |
| **V** | | | | | |
| **Mn** | | | 0.44 | 0.0155 | 0.06 |
| **Co** | | | | | |
| **Ni** | | | | | |
| **Cu** | | | | | |
| **Zn** | 0.48 | | 3.55 | | |
| **Ga** | | | | | |
| **Ge** | | | | | |
| **Rb** | 0.3 | 0.084 | 0.125 | 0.235 | |
| **Sr** | 4.4 | 14.6 | 19.9 | 11.8 | |
| **Y** | 0.2 | | 0.125 | | 0.012 |
| **Zr** | | | 0.2 | | 0.005 |
| **Nb** | | | | | |
| **Cs** | 0.03 | | 0.1 | 0.0545 | |
| **Ba** | 0.48 | 1.69 | 1.93 | 13.25 | 0.186 |
| **La** | 0.3 | | 0.375 | 0.12 | 0.088 |
| **Ce** | 0.22 | | 0.275 | 0.068 | |
| **Pr** | | | | | |
| **Nd** | 0.19 | | 0.215 | | 0.054 |
| **Sm** | | | | | |
| **Eu** | 2 | | 5.85 | 4.685 | 0.397 |
| **Gd** | | | | | |
| **Tb** | | | | | |
| **Dy** | | | | | |
| **Ho** | | | | | |
| **Er** | | | | | |
| **Tm** | | | | | |
| **Yb** | | | | | |
| **Lu** | | | | | |
| **Hf** | | | | | |
| **Ta** | | | | | |
| **Tl** | | | | | |
| **Pb** | | | 1.31 | | 0.134 |
| **Th** | | | | | |
| **U** | | | | | |

**Appendix A.7**. Mathematical method for forcing the apex of an *Onuma* curve to occur at a specific ionic radius.

The *Onuma* function relates the $K_d$ of an element and its ionic radius ($r$) to those of its host crystallographic site with the following equation (from Blundy & Wood, 1994):

**(1.1)** $K_d = K_d{}^{*} \times \exp\left(\frac{-4\pi E_M\left(\frac{r^*(r-r^*)^2}{2}+\frac{(r-r^*)^3}{3}\right)}{kT}\right)$, which, in logarithmic space, simplifies to

**(1.2)** $Ln(K_d) = Ln(K_d{}^{*}) - \left(\left(\frac{2\pi E_M r^*}{kT}\right)(r-r^*)^2\right) - \left(\left(\frac{4\pi E_M}{3kT}\right)(r-r^*)^3\right).$

Thus, the *Onuma* function has the polynomial form of: $y = ax^3 + bx^2 + c$, where $y$ is the $K_d$ of a particular element of interest in logarithmic space ($Ln[K_d]$), $x$ is the difference in ionic radius between that element and the ideal radius of the crystallographic site it occupies ($r$-$r^*$), $c$ is the ideal partition coefficient in logarithmic space ($Ln[K_d{}^{*}]$) of that site, and $a$ and $b$ are negative constants reflecting the elastic response of the crystallographic site ($\left[\frac{4\pi E_M}{3kT}\right]$ and $\left[\frac{2\pi E_M r^*}{kT}\right]$, respectively), which take into account its ideal radius ($r^*$) and Young's modulus ($E_M$), as well as the temperature ($T$) and Boltzmann's constant ($k$). For each group of elements, the *Onuma* (or best-fit) curve represents how they conform to the ideal radius of the crystallographic site they occupy, which occurs at the apex of the curve. This value ($x_{max}$) can be calculated by setting the first derivative of the *Onuma* function to zero (equation 1.5) and solving for $x_{max}$ (equations 1.6-1.8). In simplified polynomial form:

**(1.3)** $y' = 3ax^2 + 2bx$

**(1.4)** $0 = 3a(x_{max})^2 + 2b(x_{max})$

**(1.5)** $\boldsymbol{x_{max}} = -\frac{2b}{3a}$ and $\boldsymbol{b} = \frac{-3a(x_{max})}{2}$

Thus, we can fit any parabola to a particular $r^*$, where $x_{max} = r^*$, using a least-squares fit and fixing the ***b*** constant using formula 1.5 above.

# APPENDIX B

# AUSTURHORN INTRUSIVE COMPLEX

**Appendix B.1**. Zircon U-Pb Geochronology[32], measured *in-situ* by SHRIMP-RG

| Spot Name | Mount | $^{204}$Pb/$^{206}$Pb | % error | $^{206}$Pb/$^{238}$U | % error | U (ppm) | Th (ppm) | $^{232}$Th/$^{238}$U | % error | Total $^{238}$U/$^{206}$Pb | % error | Total $^{207}$Pb/$^{206}$Pb | % error | $^{207}$Pb-corr $^{204}$Pb/$^{206}$Pb | $^{207}$Pb-corr % $^{206}$Pb$_C$ |
|---|---|---|---|---|---|---|---|---|---|---|---|---|---|---|---|
| **IA-NS-2 (Granophyre)** | | | | | | | | | | | | | | | |
| IA-NS-2_2.1 | JW498 | 3.0E-2 | 71 | 0.0016 | 8.6 | 44 | 22 | 0.51 | 0.64 | 1185 | 7.1 | 0.0843 | 28 | 2.6E-3 | 4.83 |
| IA-NS-2_1.1 | JW498 | --- | 100 | 0.0017 | 6.5 | 65 | 30 | 0.48 | 1.21 | 1079 | 4.5 | 0.0554 | 26 | 6.2E-4 | 1.17 |
| IA-NS-2_8.1 | JW498 | 4.1E-3 | 50 | 0.0018 | 5.4 | 597 | 624 | 1.08 | 0.68 | 1041 | 2.6 | 0.0600 | 9 | 9.4E-4 | 1.75 |
| IA-NS-2_7.1 | JW498 | -6.3E-3 | 100 | 0.0018 | 5.5 | 89 | 43 | 0.50 | 0.46 | 1055 | 3.9 | 0.0479 | 23 | 1.2E-4 | 0.22 |
| IA-NS-2_3.1 | JW498 | 2.3E-3 | 100 | 0.0019 | 8.2 | 232 | 140 | 0.62 | 0.94 | 1016 | 5.4 | 0.0562 | 14 | 6.8E-4 | 1.26 |
| IA-NS-2_6.1 | JW498 | 3.1E-3 | 58 | 0.0019 | 4.3 | 558 | 441 | 0.82 | 1.00 | 1012 | 2.1 | 0.0554 | 9 | 6.3E-4 | 1.17 |
| IA-NS-2_5.1 | JW498 | 2.8E-3 | 50 | 0.0020 | 4.6 | 781 | 847 | 1.12 | 0.20 | 1016 | 1.8 | 0.0445 | 9 | -1.2E-4 | -0.22 |
| IA-NS-2_9.1 | JW498 | --- | 100 | 0.0020 | 2.4 | 498 | 523 | 1.08 | 0.93 | 973 | 2.4 | 0.0547 | 10 | 5.8E-4 | 1.08 |
| IA-NS-2_10.1 | JW498 | 2.1E-3 | 41 | 0.0020 | 4.9 | 1480 | 1437 | 1.00 | 0.10 | 977 | 2.4 | 0.0488 | 6 | 1.8E-4 | 0.33 |
| IA-NS-2_4.1 | JW498 | -5.3E-3 | 71 | 0.0020 | 3.5 | 208 | 105 | 0.52 | 0.30 | 978 | 4.7 | 0.0373 | 20 | -6.0E-4 | -1.13 |
| **IA-NS-4b (High-SiO$_2$ Granophyre)** | | | | | | | | | | | | | | | |
| IA-NS-4b_15.1 | JW498 | 1.5E-2 | 24 | 0.0019 | 6.3 | 676 | 518 | 0.79 | 0.71 | 1014 | 1.9 | 0.0924 | 12 | 3.1E-3 | 5.85 |
| IA-NS-4b_10.1 | JW498 | 5.2E-3 | 100 | 0.0019 | 4.9 | 115 | 46 | 0.41 | 0.45 | 1022 | 3.8 | 0.0748 | 19 | 1.9E-3 | 3.63 |
| IA-NS-4b_8.1 | JW498 | 1.8E-3 | 100 | 0.0020 | 3.1 | 346 | 186 | 0.55 | 1.29 | 1023 | 5.3 | 0.0615 | 12 | 1.0E-3 | 1.94 |
| IA-NS-4b_16.1 | JW498 | 1.9E-2 | 58 | 0.0018 | 5.5 | 96 | 35 | 0.38 | 0.50 | 1040 | 5.7 | 0.0391 | 26 | -4.8E-4 | -0.90 |
| IA-NS-4b_5.1 | JW498 | 2.1E-2 | 50 | 0.0018 | 4.9 | 118 | 61 | 0.53 | 0.41 | 1004 | 5.9 | 0.0611 | 19 | 1.0E-3 | 1.89 |
| IA-NS-4b_53.1 | AJP05 | 1.8E-3 | 65 | 0.0021 | 2.9 | 3327 | 1316 | 0.41 | 0.94 | 988 | 1.5 | 0.0676 | 6 | 0.0014 | 2.71 |
| IA-NS-4b_18.1 | JW498 | 2.7E-3 | 45 | 0.0020 | 3.9 | 1126 | 1421 | 1.30 | 3.53 | 994 | 1.4 | 0.0538 | 7 | 5.2E-4 | 0.96 |
| IA-NS-4b_2.1 | JW498 | ---- | --- | 0.0018 | 8.6 | 123 | 65 | 0.55 | 0.39 | 992 | 9.6 | 0.0574 | 19 | 7.6E-4 | 1.42 |
| IA-NS-4b_14.1 | JW498 | 2.1E-3 | 45 | 0.0019 | 6.4 | 1595 | 1215 | 0.79 | 0.76 | 996 | 2.0 | 0.0533 | 6 | 4.8E-4 | 0.90 |
| IA-NS-4b_6.1 | JW498 | 2.0E-2 | 71 | 0.0019 | 6.9 | 62 | 25 | 0.42 | 1.20 | 929 | 9.3 | 0.1059 | 20 | 4.0E-3 | 7.56 |
| IA-NS-4b_4.1 | JW498 | 9.1E-3 | 20 | 0.0022 | 1.1 | 1581 | 1010 | 0.66 | 2.54 | 883 | 2.2 | 0.1398 | 16 | 6.3E-3 | 11.86 |
| IA-NS-4b_51.1 | AJP05 | -6.1E-3 | 62 | 0.0020 | 3.4 | 1149 | 1594 | 1.43 | 1.34 | 970 | 1.6 | 0.0580 | 7 | 8.0E-4 | 1.50 |
| IA-NS-4b_12.1 | JW498 | 3.1E-3 | 45 | 0.0020 | 5.5 | 985 | 2095 | 2.20 | 0.22 | 965 | 1.5 | 0.0558 | 7 | 6.5E-4 | 1.22 |
| IA-NS-4b_17.1 | JW498 | 3.9E-3 | 30 | 0.0021 | 1.4 | 1484 | 1496 | 1.04 | 4.54 | 939 | 1.4 | 0.0787 | 23 | 2.2E-3 | 4.11 |
| IA-NS-4b_1.1 | JW498 | 9.2E-4 | 71 | 0.0020 | 5.7 | 1271 | 777 | 0.63 | 0.78 | 978 | 2.5 | 0.0473 | 7 | 7.3E-5 | 0.14 |
| IA-NS-4b_9.1 | JW498 | 8.5E-4 | 58 | 0.0021 | 4.8 | 2055 | 4579 | 2.30 | 0.66 | 964 | 1.4 | 0.0498 | 5 | 2.4E-4 | 0.45 |
| IA-NS-4b_7.1 | JW498 | 2.5E-3 | 27 | 0.0021 | 6.3 | 3430 | 5242 | 1.58 | 0.41 | 967 | 1.8 | 0.0476 | 4 | 9.2E-5 | 0.17 |
| IA-NS-4b_11.1 | JW498 | --- | 100 | 0.0021 | 3.1 | 263 | 171 | 0.67 | 0.24 | 981 | 0.7 | 0.0399 | 17 | -4.2E-4 | -0.79 |
| IA-NS-4b_55.1 | AJP05 | -2.9E-3 | 71 | 0.0026 | 4.6 | 1261 | 693 | 0.57 | 1.06 | 917 | 2.3 | 0.0756 | 5 | 2.0E-3 | 3.73 |
| IA-NS-4b_57.1 | AJP05 | -7.3E-4 | 91 | 0.0024 | 2.8 | 3666 | 11224 | 3.16 | 5.54 | 879 | 0.9 | 0.0830 | 3 | 2.5E-3 | 4.66 |
| IA-NS-4b_3.1 | JW498 | 4.3E-3 | 22 | 0.0021 | 9.2 | 2045 | 2655 | 1.34 | 23.28 | 863 | 4.1 | 0.1011 | 10 | 3.7E-3 | 6.95 |
| IA-NS-4b_13.1 | JW498 | 7.9E-3 | 71 | 0.0020 | 4.2 | 144 | 85 | 0.61 | 0.35 | 939 | 3.9 | 0.0382 | 21 | -5.4E-4 | -1.01 |
| IA-NS-4b_49.1 | AJP05 | 9.4E-3 | 46 | 0.0026 | 7.9 | 1297 | 21800 | 17.36 | 0.95 | 849 | 3.0 | 0.0522 | 22 | 4.1E-4 | 0.76 |

---

[32] Errors (%) are all 1σ; *Pb*$_C$ denotes proportion of common Pb; *Pb-corr* indicates correction made using the corresponding (labeled) measured Pb values

**Appendix B.1**. Continued[33]

| Spot Name | Mount | $^{204}$Pb-corr $^{207}$Pb*/$^{235}$U | % error | $^{204}$Pb-corr $^{206}$Pb*/$^{238}$U | % error | Error Corr. | $^{207}$Pb-corr[34] $^{206}$Pb/$^{238}$U Age (Ma) | 1σ error | $^{230}$Th-corr[35] $^{206}$Pb/$^{238}$U Age (Ma) | 2σ error | Reason for excluding? |
|---|---|---|---|---|---|---|---|---|---|---|---|
| **IA-NS-2 (Granophyre)** | | | | | | | | | | | |
| IA-NS-2_2.1 | JW498 | 0.045 | 174 | 3.7E-4 | 92 | 0.53 | 5.2 | 0.40 | ~~**5.26**~~ | ~~**0.80**~~ | **High comm-Pb, low U, outlier (>2SD)** |
| IA-NS-2_1.1 | JW498 | 0.007 | 26 | 9.3E-4 | 4 | 0.17 | 5.9 | 0.28 | **5.99** | **0.57** | |
| IA-NS-2_8.1 | JW498 | 0.000 | 848 | 8.9E-4 | 5 | 0.01 | 6.1 | 0.16 | **6.13** | **0.33** | |
| IA-NS-2_7.1 | JW498 | 0.019 | 58 | 1.1E-3 | 11 | 0.19 | 6.1 | 0.25 | **6.18** | **0.50** | |
| IA-NS-2_3.1 | JW498 | 0.003 | 189 | 9.4E-4 | 7 | 0.04 | 6.3 | 0.34 | **6.34** | **0.68** | |
| IA-NS-2_6.1 | JW498 | 0.001 | 360 | 9.3E-4 | 4 | 0.01 | 6.3 | 0.14 | **6.36** | **0.28** | |
| IA-NS-2_5.1 | JW498 | 0.000 | 8083 | 9.3E-4 | 3 | 0.00 | 6.4 | 0.12 | **6.41** | **0.23** | |
| IA-NS-2_9.1 | JW498 | 0.008 | 10 | 1.0E-3 | 2 | 0.24 | 6.6 | 0.16 | **6.60** | **0.33** | |
| IA-NS-2_10.1 | JW498 | 0.002 | 88 | 9.8E-4 | 3 | 0.03 | 6.6 | 0.16 | **6.63** | **0.32** | |
| IA-NS-2_4.1 | JW498 | 0.017 | 44 | 1.1E-3 | 8 | 0.18 | 6.7 | 0.32 | **6.74** | **0.63** | |
| **IA-NS-4b (High-SiO2 Granophyre)** | | | | | | | | | | | |
| IA-NS-4b_15.1 | JW498 | 0.019 | 21 | 7.1E-4 | 9 | 0.44 | 6.0 | 0.15 | ~~**6.07**~~ | ~~**0.29**~~ | **Younger grain, Outlier (>2SD)** |
| IA-NS-4b_10.1 | JW498 | 0.001 | 980 | 8.8E-4 | 12 | 0.01 | 6.1 | 0.26 | **6.17** | **0.52** | |
| IA-NS-4b_8.1 | JW498 | 0.004 | 86 | 9.4E-4 | 6 | 0.07 | 6.2 | 0.33 | **6.26** | **0.67** | |
| IA-NS-4b_16.1 | JW498 | 0.034 | 87 | 6.2E-4 | 32 | 0.37 | 6.3 | 0.36 | **6.35** | **0.73** | |
| IA-NS-4b_5.1 | JW498 | 0.036 | 77 | 6.1E-4 | 32 | 0.42 | 6.3 | 0.38 | **6.39** | **0.76** | |
| IA-NS-4b_53.1 | AJP05 | 0.005 | 46 | 9.8E-4 | 3 | 0.06 | 6.3 | 0.10 | **6.44** | **0.21** | |
| IA-NS-4b_18.1 | JW498 | 0.002 | 164 | 9.6E-4 | 3 | 0.02 | 6.4 | 0.09 | **6.48** | **0.19** | |
| IA-NS-4b_2.1 | JW498 | 0.008 | 22 | 1.0E-3 | 10 | 0.44 | 6.4 | 0.62 | **6.49** | **1.24** | |
| IA-NS-4b_14.1 | JW498 | 0.003 | 68 | 9.7E-4 | 3 | 0.04 | 6.4 | 0.13 | **6.49** | **0.27** | |
| IA-NS-4b_6.1 | JW498 | 0.030 | 86 | 6.8E-4 | 42 | 0.49 | 6.4 | 0.63 | **6.50** | **1.25** | |
| IA-NS-4b_4.1 | JW498 | 0.000 | 1135 | 9.4E-4 | 5 | 0.00 | 6.4 | 0.24 | **6.52** | **0.49** | |
| IA-NS-4b_51.1 | AJP05 | 0.022 | 33 | 1.1E-3 | 7 | 0.20 | 6.5 | 0.11 | **6.60** | **0.22** | |
| IA-NS-4b_12.1 | JW498 | 0.001 | 273 | 9.8E-4 | 3 | 0.01 | 6.6 | 0.11 | **6.62** | **0.21** | |
| IA-NS-4b_17.1 | JW498 | 0.003 | 143 | 9.9E-4 | 3 | 0.02 | 6.6 | 0.18 | **6.66** | **0.37** | |
| IA-NS-4b_1.1 | JW498 | 0.005 | 31 | 1.0E-3 | 3 | 0.09 | 6.6 | 0.17 | **6.66** | **0.33** | |
| IA-NS-4b_9.1 | JW498 | 0.005 | 21 | 1.0E-3 | 2 | 0.08 | 6.7 | 0.10 | **6.68** | **0.19** | |
| IA-NS-4b_7.1 | JW498 | 0.001 | 125 | 9.9E-4 | 2 | 0.02 | 6.7 | 0.12 | **6.70** | **0.25** | |
| IA-NS-4b_11.1 | JW498 | 0.006 | 17 | 1.0E-3 | 1 | 0.04 | 6.6 | 0.07 | **6.71** | **0.15** | |
| IA-NS-4b_55.1 | AJP05 | 0.018 | 23 | 1.1E-3 | 4 | 0.18 | 6.8 | 0.16 | **6.85** | **0.32** | |
| IA-NS-4b_57.1 | AJP05 | 0.015 | 10 | 1.2E-3 | 2 | 0.15 | 7.0 | 0.07 | **6.98** | **0.14** | |
| IA-NS-4b_3.1 | JW498 | 0.005 | 52 | 1.1E-3 | 5 | 0.09 | 6.9 | 0.30 | ~~**7.01**~~ | ~~**0.60**~~ | **Older grain, outlier** |
| IA-NS-4b_13.1 | JW498 | 0.013 | 54 | 9.1E-4 | 13 | 0.24 | 6.9 | 0.28 | ~~**7.02**~~ | ~~**0.56**~~ | **Older grain, outlier** |
| IA-NS-4b_49.1 | AJP05 | 0.015 | 34 | 9.7E-4 | 10 | 0.30 | 7.5 | 0.25 | ~~**7.02**~~ | ~~**0.50**~~ | **Older grain, outlier** |

---

[33] *Pb** denotes proportion of radiogenic Pb; discarded ages are listed in red strikethrough font

[34] Corrected for common Pb assuming $^{206}$Pb/$^{238}$U-$^{207}$Pb/$^{235}$U age concordance

[35] Corrected for initial $^{238}$U-$^{230}$Th disequilibrium using whole-rock Th/U for each sample

**Appendix B.1**. Continued

| Spot Name | Mount | $^{204}$Pb/ $^{206}$Pb | % error | $^{206}$Pb/ $^{238}$U | % error | U (ppm) | Th (ppm) | $^{232}$Th/ $^{238}$U | % error | Total $^{238}$U/$^{206}$Pb | % error | Total $^{207}$Pb/$^{206}$Pb | % error | $^{207}$Pb-corr $^{204}$Pb/$^{206}$Pb | $^{207}$Pb-corr % $^{206}$Pb$_C$ |
|---|---|---|---|---|---|---|---|---|---|---|---|---|---|---|---|
| **IA-NS-6 (Diorite)** | | | | | | | | | | | | | | | |
| IA-NS-6_14.1 | JW498 | 6.2E-3 | 100 | 0.0015 | 5.2 | 108 | 56 | 0.54 | 0.40 | 1236 | 3.3 | 0.0744 | 21 | 1.9E-3 | 3.57 |
| IA-NS-6_1.1 | JW498 | 6.7E-3 | 100 | 0.0017 | 9.3 | 94 | 43 | 0.47 | 0.47 | 1071 | 6.3 | 0.0776 | 19 | 2.1E-3 | 3.98 |
| IA-NS-6_5.1 | JW498 | 4.3E-3 | 45 | 0.0018 | 7.4 | 697 | 565 | 0.84 | 1.28 | 1062 | 3.6 | 0.0521 | 10 | 4.0E-4 | 0.75 |
| IA-NS-6_3.1 | JW498 | 8.4E-4 | 100 | 0.0019 | 5.6 | 759 | 704 | 0.96 | 0.25 | 1040 | 1.4 | 0.0621 | 8 | 1.1E-3 | 2.02 |
| IA-NS-6_8.1 | JW498 | 3.8E-3 | 50 | 0.0019 | 2.1 | 681 | 660 | 1.00 | 0.14 | 1029 | 4.0 | 0.0582 | 9 | 8.1E-4 | 1.52 |
| IA-NS-6_4.1 | JW498 | 2.6E-3 | 71 | 0.0018 | 5.1 | 523 | 601 | 1.19 | 0.42 | 1035 | 3.4 | 0.0512 | 12 | 3.4E-4 | 0.64 |
| IA-NS-6_7.1 | JW498 | 3.1E-2 | 45 | 0.0018 | 11.4 | 93 | 43 | 0.47 | 0.46 | 1035 | 8.9 | 0.0471 | 23 | 6.3E-5 | 0.12 |
| IA-NS-6_9.1 | JW498 | 2.2E-3 | 58 | 0.0019 | 6.6 | 855 | 974 | 1.18 | 0.48 | 1016 | 2.6 | 0.0567 | 8 | 7.1E-4 | 1.33 |
| IA-NS-6_17.1 | JW498 | 3.4E-3 | 50 | 0.0019 | 6.5 | 709 | 730 | 1.06 | 0.75 | 1011 | 1.8 | 0.0508 | 9 | 3.1E-4 | 0.58 |
| IA-NS-6_13.1 | JW498 | 8.3E-3 | 30 | 0.0018 | 2.1 | 844 | 1043 | 1.28 | 0.24 | 1008 | 2.8 | 0.0514 | 8 | 3.5E-4 | 0.66 |
| IA-NS-6_10.1 | JW498 | 1.0E-2 | 33 | 0.0019 | 2.3 | 505 | 409 | 0.84 | 0.32 | 1014 | 1.1 | 0.0479 | 11 | 1.1E-4 | 0.21 |
| IA-NS-6_2.1 | JW498 | 2.7E-3 | 38 | 0.0017 | 6.0 | 1888 | 2502 | 1.37 | 0.79 | 1010 | 1.7 | 0.0476 | 11 | 9.5E-5 | 0.18 |
| IA-NS-6_16.1 | JW498 | 5.6E-3 | 50 | 0.0021 | 2.6 | 346 | 388 | 1.16 | 0.60 | 1005 | 1.8 | 0.0518 | 12 | 3.8E-4 | 0.71 |
| IA-NS-6_15.1 | JW498 | -2.2E-3 | 71 | 0.0019 | 2.2 | 556 | 538 | 1.00 | 0.60 | 1002 | 2.6 | 0.0476 | 10 | 9.8E-5 | 0.18 |
| IA-NS-6_11.1 | JW498 | 4.7E-3 | 100 | 0.0019 | 10.1 | 113 | 74 | 0.68 | 0.71 | 994 | 7.3 | 0.0499 | 20 | 2.5E-4 | 0.47 |
| IA-NS-6_12.1 | JW498 | --- | 100 | 0.0020 | 8.8 | 88 | 36 | 0.43 | 0.50 | 969 | 6.5 | 0.0485 | 23 | 1.5E-4 | 0.29 |
| IA-NS-6_6.1 | JW498 | -5.2E-3 | 71 | 0.0020 | 3.4 | 204 | 127 | 0.64 | 1.11 | 951 | 1.4 | 0.0377 | 19 | -5.8E-4 | -1.08 |
| **IA-NS-7 (Granodiorite)** | | | | | | | | | | | | | | | |
| IA-NS-7_17.1 | JW510 | 4.2E-3 | 100 | 0.0013 | 4.9 | 129 | 92 | 0.74 | 0.34 | 1140 | 4.8 | 0.0507 | 21 | 3.0E-4 | 0.57 |
| IA-NS-7_26.1 | JW510 | 4.9E-3 | 71 | 0.0021 | 13.3 | 91 | 90 | 1.03 | 4.16 | 977 | 10.7 | 0.1358 | 20 | 6.1E-3 | 11.34 |
| IA-NS-7_18.1 | JW510 | 3.7E-3 | 58 | 0.0016 | 2.6 | 354 | 173 | 0.50 | 1.30 | 1088 | 2.3 | 0.0531 | 12 | 4.7E-4 | 0.88 |
| IA-NS-7_25.1 | JW510 | 2.1E-3 | 100 | 0.0019 | 3.5 | 167 | 121 | 0.75 | 0.52 | 1088 | 6.0 | 0.0442 | 17 | -1.4E-4 | -0.25 |
| IA-NS-7_24.1 | JW510 | --- | 100 | 0.0018 | 4.8 | 102 | 61 | 0.62 | 1.54 | 1077 | 7.6 | 0.0474 | 19 | 8.4E-5 | 0.16 |
| IA-NS-7_1.1 | JW510 | 3.0E-3 | 71 | 0.0018 | 2.9 | 236 | 187 | 0.82 | 0.56 | 1077 | 3.1 | 0.0431 | 14 | -2.1E-4 | -0.39 |
| IA-NS-7_23.1 | JW510 | 1.1E-3 | 100 | 0.0019 | 2.5 | 289 | 306 | 1.09 | 0.74 | 1061 | 3.6 | 0.0512 | 11 | 3.4E-4 | 0.64 |
| IA-NS-7_21.1 | JW510 | --- | 100 | 0.0017 | 5.6 | 296 | 267 | 0.93 | 0.43 | 1053 | 4.8 | 0.0427 | 14 | -2.3E-4 | -0.44 |
| IA-NS-7_19.1 | JW510 | 2.4E-2 | 15 | 0.0038 | 4.9 | 382 | 375 | 1.01 | 0.34 | 513 | 3.4 | 0.4485 | 7 | 2.7E-2 | 50.93 |
| IA-NS-7_4.1 | JW510 | 4.2E-4 | 100 | 0.0022 | 5.0 | 1328 | 1395 | 1.08 | 0.38 | 1038 | 2.0 | 0.0491 | 6 | 2.0E-4 | 0.367 |
| IA-NS-7_27.1 | JW510 | 2.0E-3 | 71 | 0.0020 | 2.3 | 348 | 355 | 1.06 | 0.26 | 1025 | 2.2 | 0.0409 | 12 | -3.6E-4 | -0.66 |
| IA-NS-7_2.1 | JW510 | 5.7E-4 | 50 | 0.0020 | 1.8 | 2476 | 3088 | 1.29 | 0.11 | 1003 | 1.1 | 0.0526 | 4 | 4.4E-4 | 0.81 |
| IA-NS-7_9.1 | JW510 | 1.2E-3 | 41 | 0.0020 | 1.7 | 1891 | 2157 | 1.18 | 0.15 | 1001 | 1.7 | 0.0508 | 5 | 3.1E-4 | 0.58 |
| IA-NS-7_14.1 | JW510 | 2.1E-2 | 28 | 0.0024 | 10.1 | 173 | 115 | 0.68 | 0.26 | 792 | 9.8 | 0.2157 | 23 | 1.1E-2 | 21.46 |
| IA-NS-7_16.1 | JW510 | 9.2E-4 | 100 | 0.0019 | 4.2 | 381 | 433 | 1.18 | 4.31 | 990 | 4.0 | 0.0557 | 10 | 6.4E-4 | 1.20 |
| IA-NS-7_15.1 | JW510 | --- | 100 | 0.0025 | 3.6 | 1203 | 1177 | 1.01 | 0.51 | 998 | 1.9 | 0.0469 | 13 | 4.9E-5 | 0.092 |
| IA-NS-7_12.2 | JW510 | 6.7E-3 | 19 | 0.0021 | 3.4 | 1389 | 1054 | 0.78 | 1.35 | 882 | 5.0 | 0.1290 | 25 | 5.6E-3 | 10.48 |
| IA-NS-7_20.1 | JW510 | 5.0E-4 | 100 | 0.0021 | 3.1 | 683 | 560 | 0.85 | 0.24 | 984 | 2.9 | 0.0433 | 8 | -2.0E-4 | -0.37 |
| IA-NS-7_22.1 | JW510 | -6.6E-3 | 50 | 0.0019 | 6.0 | 207 | 156 | 0.78 | 1.92 | 994 | 6.3 | 0.0331 | 19 | -8.9E-4 | -1.66 |

**Appendix B.1**. Continued

| **Spot Name** | **Mount** | **$^{204}$Pb-corr $^{207}$Pb*/$^{235}$U** | **% error** | **$^{204}$Pb-corr $^{206}$Pb*/$^{238}$U** | **% error** | **Error Corr.** | **$^{207}$Pb-corr $^{206}$Pb/$^{238}$U Age (Ma)** | **1σ error** | **$^{230}$Th-corr $^{206}$Pb/$^{238}$U Age (Ma)** | **2σ error** | **Reason for excluding?** |
|---|---|---|---|---|---|---|---|---|---|---|---|
| **IA-NS-6 (Diorite)** | | | | | | | | | | | |
| IA-NS-6_14.1 | JW498 | 0.002 | 232 | 7.2E-4 | 13 | 0.06 | 5.0 | 0.19 | ~~**5.12**~~ | ~~**0.39**~~ | **Younger grain, outlier (>2SD)** |
| IA-NS-6_1.1 | JW498 | 0.003 | 183 | 8.2E-4 | 16 | 0.09 | 5.8 | 0.38 | ~~**5.87**~~ | ~~**0.76**~~ | **Younger grain, outlier (>2SD)** |
| IA-NS-6_5.1 | JW498 | 0.002 | 106 | 8.7E-4 | 5 | 0.05 | 6.0 | 0.22 | **6.10** | **0.44** | |
| IA-NS-6_3.1 | JW498 | 0.006 | 27 | 9.5E-4 | 2 | 0.08 | 6.1 | 0.09 | **6.14** | **0.19** | |
| IA-NS-6_8.1 | JW498 | 0.000 | 4077 | 9.0E-4 | 5 | 0.00 | 6.2 | 0.25 | **6.24** | **0.50** | |
| IA-NS-6_4.1 | JW498 | 0.002 | 253 | 9.2E-4 | 5 | 0.02 | 6.2 | 0.22 | **6.25** | **0.43** | |
| IA-NS-6_7.1 | JW498 | 0.058 | 120 | 4.1E-4 | 63 | 0.52 | 6.2 | 0.56 | **6.31** | **1.12** | |
| IA-NS-6_9.1 | JW498 | 0.003 | 89 | 9.4E-4 | 4 | 0.04 | 6.3 | 0.17 | **6.32** | **0.34** | |
| IA-NS-6_17.1 | JW498 | 0.000 | 1491 | 9.3E-4 | 4 | 0.00 | 6.3 | 0.12 | **6.40** | **0.24** | |
| IA-NS-6_13.1 | JW498 | 0.011 | 18 | 8.4E-4 | 6 | 0.35 | 6.3 | 0.18 | **6.41** | **0.36** | |
| IA-NS-6_10.1 | JW498 | 0.016 | 29 | 7.9E-4 | 8 | 0.28 | 6.3 | 0.08 | **6.42** | **0.16** | |
| IA-NS-6_2.1 | JW498 | 0.001 | 336 | 9.4E-4 | 3 | 0.01 | 6.4 | 0.11 | **6.42** | **0.23** | |
| IA-NS-6_16.1 | JW498 | 0.005 | 24 | 8.9E-4 | 6 | 0.25 | 6.4 | 0.13 | **6.43** | **0.25** | |
| IA-NS-6_15.1 | JW498 | 0.011 | 28 | 1.0E-3 | 4 | 0.14 | 6.4 | 0.17 | **6.49** | **0.34** | |
| IA-NS-6_11.1 | JW498 | 0.003 | 110 | 9.2E-4 | 12 | 0.11 | 6.5 | 0.48 | **6.53** | **0.95** | |
| IA-NS-6_12.1 | JW498 | 0.007 | 24 | 1.0E-3 | 7 | 0.27 | 6.6 | 0.44 | **6.72** | **0.88** | |
| IA-NS-6_6.1 | JW498 | 0.017 | 43 | 1.2E-3 | 6 | 0.15 | 6.9 | 0.12 | ~~**6.94**~~ | ~~**0.23**~~ | **Older grain, outlier (>2SD)** |
| **IA-NS-7 (Granodiorite)** | | | | | | | | | | | |
| IA-NS-7_17.1 | JW510 | 0.002 | 233 | 8.1E-4 | 10 | 0.04 | 5.62 | 0.28 | ~~**5.70**~~ | ~~**0.56**~~ | **Low UO/U, outlier (>2SD)** |
| IA-NS-7_26.1 | JW510 | 0.008 | 98 | 9.3E-4 | 13 | 0.13 | 5.85 | 0.67 | **5.92** | **1.34** | |
| IA-NS-7_18.1 | JW510 | 0.001 | 609 | 8.6E-4 | 5 | 0.01 | 5.87 | 0.15 | **5.96** | **0.29** | |
| IA-NS-7_25.1 | JW510 | 0.001 | 283 | 8.8E-4 | 7 | 0.03 | 5.94 | 0.36 | **6.01** | **0.72** | |
| IA-NS-7_24.1 | JW510 | 0.006 | 21 | 9.3E-4 | 8 | 0.36 | 5.97 | 0.46 | **6.06** | **0.91** | |
| IA-NS-7_1.1 | JW510 | 0.001 | 684 | 8.8E-4 | 5 | 0.01 | 6.01 | 0.19 | **6.08** | **0.38** | |
| IA-NS-7_23.1 | JW510 | 0.004 | 54 | 9.2E-4 | 4 | 0.08 | 6.03 | 0.22 | **6.10** | **0.45** | |
| IA-NS-7_21.1 | JW510 | 0.006 | 14 | 9.5E-4 | 5 | 0.33 | 6.15 | 0.30 | **6.22** | **0.59** | |
| IA-NS-7_19.1 | JW510 | 0.021 | 73 | 1.1E-3 | 12 | 0.17 | 6.16 | 0.53 | ~~**6.23**~~ | ~~**1.06**~~ | **High comm-Pb (>20%)** |
| IA-NS-7_4.1 | JW510 | 0.006 | 16 | 9.6E-4 | 2 | 0.13 | 6.2 | 0.13 | **6.25** | **0.25** | |
| IA-NS-7_27.1 | JW510 | 0.001 | 221 | 9.4E-4 | 4 | 0.02 | 6.33 | 0.15 | **6.39** | **0.29** | |
| IA-NS-7_2.1 | JW510 | 0.006 | 11 | 9.9E-4 | 1 | 0.11 | 6.37 | 0.07 | **6.43** | **0.14** | |
| IA-NS-7_9.1 | JW510 | 0.004 | 23 | 9.8E-4 | 2 | 0.08 | 6.40 | 0.11 | **6.46** | **0.22** | |
| IA-NS-7_14.1 | JW510 | 0.018 | 54 | 7.8E-4 | 20 | 0.37 | 6.39 | 0.81 | ~~**6.47**~~ | ~~**1.63**~~ | **High comm-Pb (>20%)** |
| IA-NS-7_16.1 | JW510 | 0.006 | 36 | 9.9E-4 | 4 | 0.12 | 6.43 | 0.26 | **6.49** | **0.52** | |
| IA-NS-7_15.1 | JW510 | 0.006 | 13 | 1.0E-3 | 2 | 0.15 | 6.4 | 0.13 | **6.52** | **0.26** | |
| IA-NS-7_12.2 | JW510 | 0.004 | 153 | 9.9E-4 | 6 | 0.04 | 6.54 | 0.44 | **6.62** | **0.87** | |
| IA-NS-7_20.1 | JW510 | 0.005 | 24 | 1.0E-3 | 3 | 0.13 | 6.57 | 0.19 | **6.65** | **0.39** | |
| IA-NS-7_22.1 | JW510 | 0.019 | 34 | 1.1E-3 | 8 | 0.25 | 6.59 | 0.42 | **6.67** | **0.83** | |

**Appendix B.1**. Continued

| **Spot Name** | **Mount** | **$^{204}$Pb/ $^{206}$Pb** | **% error** | **$^{206}$Pb/ $^{238}$U** | **% error** | **U (ppm)** | **Th (ppm)** | **$^{232}$Th/ $^{238}$U** | **% error** | **Total $^{238}$U/$^{206}$Pb** | **% error** | **Total $^{207}$Pb/$^{206}$Pb** | **% error** | **$^{207}$Pb-corr $^{204}$Pb/$^{206}$Pb** | **$^{207}$Pb-corr % $^{206}$Pb$_C$** |
|---|---|---|---|---|---|---|---|---|---|---|---|---|---|---|---|
| **IA-NS-9 (High-SiO$_2$ Granophyre)** | | | | | | | | | | | | | | | |
| IA-NS-9_12.1 | AJP03 | 1.7E-2 | 65 | 0.0017 | 6.2 | 147 | 120 | 0.84 | 5.05 | 1062 | 3.5 | 0.0675 | 16 | 1.4E-3 | 2.71 |
| IA-NS-9_20.1 | AJP03 | 8.4E-3 | 120 | 0.0019 | 3.0 | 69 | 27 | 0.40 | 0.40 | 1055 | 4.1 | 0.0539 | 21 | 5.2E-4 | 0.98 |
| IA-NS-9_11.1 | AJP03 | -2.5E-3 | 129 | 0.0019 | 3.6 | 222 | 121 | 0.56 | 0.71 | 1016 | 3.3 | 0.0780 | 11 | 2.2E-3 | 4.03 |
| IA-NS-9_9.1 | AJP03 | -2.1E-3 | 183 | 0.0021 | 3.8 | 113 | 54 | 0.49 | 0.29 | 999 | 2.8 | 0.0902 | 13 | 3.0E-3 | 5.58 |
| IA-NS-9_10.1 | AJP03 | 1.0E-2 | 77 | 0.0020 | 3.7 | 137 | 79 | 0.59 | 0.24 | 1043 | 2.6 | 0.0516 | 16 | 3.7E-4 | 0.69 |
| IA-NS-9_8.1 | AJP03 | 3.7E-3 | 158 | 0.0020 | 4.3 | 86 | 42 | 0.51 | 0.33 | 1020 | 2.8 | 0.0677 | 19 | 1.5E-3 | 2.73 |
| IA-NS-9_5.1 | AJP03 | 1.2E-2 | 85 | 0.0021 | 2.6 | 88 | 39 | 0.45 | 0.91 | 1028 | 2.4 | 0.0503 | 18 | 2.8E-4 | 0.52 |
| IA-NS-9_22.1 | AJP02 | 4.7E-3 | 120 | 0.0022 | 2.1 | 152 | 78 | 0.53 | 1.70 | 981 | 3.4 | 0.0774 | 25 | 2.1E-3 | 3.96 |
| IA-NS-9_4.1 | AJP03 | 9.2E-3 | 95 | 0.0022 | 2.5 | 87 | 45 | 0.54 | 0.31 | 1000 | 2.0 | 0.0572 | 20 | 7.4E-4 | 1.39 |
| IA-NS-9_7.1 | AJP03 | -4.5E-3 | 129 | 0.0021 | 2.3 | 95 | 50 | 0.55 | 0.45 | 991 | 3.0 | 0.0551 | 18 | 6.0E-4 | 1.13 |
| IA-NS-9_16.1 | AJP03 | 7.2E-3 | 100 | 0.0020 | 2.3 | 121 | 69 | 0.58 | 0.49 | 997 | 2.6 | 0.0491 | 19 | 2.0E-4 | 0.37 |
| IA-NS-9_21.1 | AJP03 | 1.9E-4 | 141 | 0.0023 | 2.8 | 2088 | 718 | 0.36 | 0.66 | 1000 | 1.2 | 0.0463 | 4 | 9.8E-6 | 0.02 |
| IA-NS-9_15.1 | AJP03 | 8.3E-3 | 120 | 0.0022 | 2.9 | 63 | 30 | 0.49 | 0.38 | 995 | 2.8 | 0.0485 | 22 | 1.6E-4 | 0.29 |
| IA-NS-9_18.1 | AJP03 | 1.1E-3 | 58 | 0.0020 | 5.5 | 2017 | 2028 | 1.04 | 0.73 | 982 | 0.9 | 0.0509 | 6 | 3.2E-4 | 0.60 |
| IA-NS-9_6.1 | AJP03 | 2.2E-2 | 61 | 0.0025 | 11.5 | 73 | 39 | 0.55 | 0.33 | 886 | 8.5 | 0.1250 | 34 | 5.3E-3 | 9.98 |
| IA-NS-9_2.1 | AJP03 | -2.7E-4 | 183 | 0.0022 | 2.0 | 848 | 291 | 0.35 | 0.20 | 977 | 1.1 | 0.0475 | 6 | 8.7E-5 | 0.16 |
| IA-NS-9_1.1 | AJP03 | -2.1E-3 | 183 | 0.0023 | 3.8 | 100 | 61 | 0.63 | 0.58 | 954 | 2.9 | 0.0502 | 19 | 2.7E-4 | 0.50 |
| IA-NS-9_19.1 | AJP03 | 1.6E-2 | 21 | 0.0029 | 3.0 | 763 | 7339 | 9.94 | 1.09 | 672 | 2.2 | 0.2488 | 8 | 1.4E-2 | 25.65 |
| IA-NS-9_13.1 | AJP03 | --- | 100 | 0.0023 | 5.9 | 87 | 53 | 0.63 | 0.30 | 930 | 4.4 | 0.0614 | 18 | 1.0E-3 | 1.92 |
| IA-NS-9_17.1 | AJP03 | 2.1E-2 | 20 | 0.0038 | 1.2 | 2174 | 1793 | 0.85 | 1.86 | 523 | 4.2 | 0.3871 | 8 | 2.3E-2 | 43.15 |
| IA-NS-9_14.1 | AJP03 | 3.6E-3 | 37 | 0.0028 | 4.9 | 3322 | 4159 | 1.29 | 0.90 | 861 | 2.5 | 0.0761 | 3 | 2.0E-3 | 3.79 |
| IA-NS-9_3.1 | AJP03 | 1.6E-2 | 37 | 0.0037 | 22.9 | 872 | 1587 | 1.88 | 0.11 | 557 | 25.5 | 0.2965 | 21 | 1.7E-2 | 31.68 |
| **IA-NS-10 (High-SiO$_2$ Granophyre)** | | | | | | | | | | | | | | | |
| IA-NS-10_25.1 | AJP05 | 2.6E-2 | 62 | 0.0052 | 17.6 | 91 | 63 | 0.706 | 2.83 | 413 | 19.4 | 0.5882 | 22 | 3.7E-2 | 68.63 |
| IA-NS-10_17.1 | AJP05 | --- | --- | 0.0021 | 8.2 | 86 | 39 | 0.470 | 0.50 | 1019 | 5.2 | 0.1351 | 18 | 6.0E-3 | 11.26 |
| IA-NS-10_19.1 | AJP05 | 3.0E-2 | 75 | 0.0020 | 9.5 | 141 | 93 | 0.677 | 0.62 | 988 | 6.4 | 0.1538 | 12 | 7.3E-3 | 13.63 |
| IA-NS-10_8.1 | AJP05 | 1.1E-1 | 51 | 0.0026 | 3.9 | 67 | 20 | 0.301 | 0.67 | 858 | 6.4 | 0.2429 | 35 | 1.3E-2 | 24.90 |
| IA-NS-10_16.1 | AJP05 | --- | --- | 0.0023 | 13.3 | 82 | 34 | 0.425 | 0.62 | 923 | 8.8 | 0.1605 | 32 | 7.7E-3 | 14.48 |
| IA-NS-10_23.1 | AJP05 | 1.4E-1 | 46 | 0.0024 | 6.5 | 71 | 28 | 0.408 | 0.65 | 987 | 7.2 | 0.0737 | 19 | 1.9E-3 | 3.48 |
| IA-NS-10_22.1 | AJP05 | -5.1E-2 | 71 | 0.0021 | 9.0 | 96 | 44 | 0.471 | 0.48 | 946 | 10.4 | 0.0802 | 27 | 2.3E-3 | 4.30 |
| IA-NS-10_5.1 | AJP05 | -2.6E-2 | 75 | 0.0025 | 2.3 | 130 | 78 | 0.617 | 0.84 | 970 | 5.3 | 0.0578 | 20 | 7.8E-4 | 1.47 |
| IA-NS-10_24.1 | AJP05 | 1.9E-2 | 44 | 0.0036 | 2.3 | 345 | 328 | 0.981 | 1.88 | 816 | 3.3 | 0.1752 | 12 | 8.7E-3 | 16.34 |
| IA-NS-10_27.1 | AJP05 | -4.2E-2 | 79 | 0.0022 | 15.6 | 74 | 32 | 0.441 | 0.54 | 828 | 12.0 | 0.1637 | 18 | 8.0E-3 | 14.87 |
| IA-NS-10_14.1 | AJP05 | 4.6E-2 | 65 | 0.0025 | 2.7 | 116 | 70 | 0.630 | 1.02 | 945 | 7.0 | 0.0602 | 21 | 9.5E-4 | 1.77 |
| IA-NS-10_10.1 | AJP05 | 6.7E-2 | 54 | 0.0022 | 7.8 | 114 | 58 | 0.527 | 1.11 | 905 | 9.4 | 0.0881 | 18 | 2.8E-3 | 5.31 |
| IA-NS-10_9.1 | AJP05 | -3.6E-3 | 224 | 0.0029 | 6.2 | 95 | 48 | 0.524 | 0.75 | 699 | 6.4 | 0.2478 | 30 | 1.4E-2 | 25.52 |
| IA-NS-10_21.1 | AJP05 | -8.5E-2 | 60 | 0.0026 | 3.6 | 65 | 28 | 0.445 | 0.67 | 800 | 5.9 | 0.1550 | 21 | 7.4E-3 | 13.78 |

**Appendix B.1**. Continued

| Spot Name | Mount | $^{204}$Pb-corr $^{207}$Pb*/$^{235}$U | % error | $^{204}$Pb-corr $^{206}$Pb*/$^{238}$U | % error | Error Corr. | $^{207}$Pb-corr $^{206}$Pb/$^{238}$U Age (Ma) | 1σ error | $^{230}$Th-corr $^{206}$Pb/$^{238}$U Age (Ma) | 2σ error | Reason for excluding? |
|---|---|---|---|---|---|---|---|---|---|---|---|
| **IA-NS-9 (High-SiO2 Granophyre)** | | | | | | | | | | | |
| IA-NS-9_12.1 | AJP03 | 0.025 | 77 | 6.5E-4 | 29 | 0.38 | 5.9 | 0.22 | ~~**5.98**~~ | ~~**0.44**~~ | **Low UO/U, outlier** |
| IA-NS-9_20.1 | AJP03 | 0.010 | 64 | 8.0E-4 | 23 | 0.35 | 6.0 | 0.26 | **6.14** | **0.52** | |
| IA-NS-9_11.1 | AJP03 | 0.016 | 39 | 1.0E-3 | 7 | 0.17 | 6.1 | 0.22 | **6.17** | **0.43** | |
| IA-NS-9_9.1 | AJP03 | 0.017 | 44 | 1.0E-3 | 7 | 0.17 | 6.1 | 0.20 | **6.18** | **0.40** | |
| IA-NS-9_10.1 | AJP03 | 0.014 | 61 | 7.8E-4 | 18 | 0.30 | 6.1 | 0.17 | **6.22** | **0.35** | |
| IA-NS-9_8.1 | AJP03 | 0.001 | 882 | 9.1E-4 | 12 | 0.01 | 6.1 | 0.20 | **6.23** | **0.40** | |
| IA-NS-9_5.1 | AJP03 | 0.018 | 80 | 7.6E-4 | 24 | 0.30 | 6.2 | 0.17 | **6.32** | **0.34** | |
| IA-NS-9_22.1 | AJP02 | 0.000 | 2749 | 9.3E-4 | 12 | 0.00 | 6.3 | 0.27 | **6.39** | **0.54** | |
| IA-NS-9_4.1 | AJP03 | 0.012 | 57 | 8.3E-4 | 20 | 0.35 | 6.4 | 0.16 | **6.44** | **0.31** | |
| IA-NS-9_7.1 | AJP03 | 0.017 | 64 | 1.1E-3 | 10 | 0.16 | 6.4 | 0.21 | **6.51** | **0.42** | |
| IA-NS-9_16.1 | AJP03 | 0.009 | 44 | 8.7E-4 | 16 | 0.36 | 6.4 | 0.18 | **6.52** | **0.37** | |
| IA-NS-9_21.1 | AJP03 | 0.006 | 10 | 1.0E-3 | 1 | 0.12 | 6.4 | 0.08 | **6.54** | **0.15** | |
| IA-NS-9_15.1 | AJP03 | 0.011 | 74 | 8.5E-4 | 22 | 0.30 | 6.5 | 0.20 | **6.54** | **0.40** | |
| IA-NS-9_18.1 | AJP03 | 0.005 | 31 | 1.0E-3 | 2 | 0.05 | 6.5 | 0.06 | **6.58** | **0.12** | |
| IA-NS-9_6.1 | AJP03 | 0.035 | 86 | 6.6E-4 | 45 | 0.52 | 6.5 | 0.68 | **6.64** | **1.36** | |
| IA-NS-9_2.1 | AJP03 | 0.007 | 15 | 1.0E-3 | 1 | 0.09 | 6.6 | 0.07 | **6.68** | **0.15** | |
| IA-NS-9_1.1 | AJP03 | 0.012 | 67 | 1.1E-3 | 8 | 0.11 | 6.7 | 0.21 | **6.80** | **0.43** | |
| IA-NS-9_19.1 | AJP03 | 0.001 | 1036 | 1.0E-3 | 9 | 0.01 | 7.1 | 0.30 | ~~**6.81**~~ | ~~**0.59**~~ | **High comm-Pb (>20%)** |
| IA-NS-9_13.1 | AJP03 | 0.009 | 19 | 1.1E-3 | 4 | 0.24 | 6.8 | 0.31 | **6.88** | **0.63** | |
| IA-NS-9_17.1 | AJP03 | 0.018 | 97 | 1.2E-3 | 13 | 0.14 | 7.0 | 0.56 | ~~**7.08**~~ | ~~**1.11**~~ | **High comm-Pb (>20%)** |
| IA-NS-9_14.1 | AJP03 | 0.003 | 104 | 1.1E-3 | 4 | 0.04 | 7.2 | 0.18 | ~~**7.25**~~ | ~~**0.36**~~ | **High UO/U, outlier (>2SD)** |
| IA-NS-9_3.1 | AJP03 | 0.010 | 282 | 1.2E-3 | 30 | 0.11 | 7.9 | 2.21 | ~~**7.93**~~ | ~~**4.42**~~ | **High comm-Pb (>20%)** |
| **IA-NS-10 (High-SiO2 Granophyre)** | | | | | | | | | | | |
| IA-NS-10_25.1 | AJP05 | 0.060 | 126 | 1.2E-3 | 62 | 0.50 | 4.9 | 2.75 | ~~**4.98**~~ | ~~**5.50**~~ | **High comm-Pb (>20%), outlier (>2SD)** |
| IA-NS-10_17.1 | AJP05 | 0.018 | 19 | 9.8E-4 | 5 | 0.27 | 5.6 | 0.35 | **5.70** | **0.71** | |
| IA-NS-10_19.1 | AJP05 | 0.044 | 163 | 4.5E-4 | 95 | 0.58 | 5.6 | 0.39 | **5.72** | **0.79** | |
| IA-NS-10_8.1 | AJP05 | -0.227 | 113 | -1.1E-3 | 104 | 0.92 | 5.6 | 0.89 | ~~**5.74**~~ | ~~**1.78**~~ | **High comm-Pb (>20%)** |
| IA-NS-10_16.1 | AJP05 | 0.024 | 33 | 1.1E-3 | 9 | 0.26 | 6.0 | 0.70 | **6.07** | **1.39** | |
| IA-NS-10_23.1 | AJP05 | -0.287 | 81 | -1.6E-3 | 76 | 0.94 | 6.3 | 0.47 | **6.39** | **0.93** | |
| IA-NS-10_22.1 | AJP05 | 0.128 | 47 | 2.1E-3 | 36 | 0.77 | 6.5 | 0.71 | **6.61** | **1.41** | |
| IA-NS-10_5.1 | AJP05 | 0.067 | 48 | 1.5E-3 | 25 | 0.53 | 6.5 | 0.36 | **6.64** | **0.73** | |
| IA-NS-10_24.1 | AJP05 | 0.022 | 32 | 7.8E-4 | 25 | 0.80 | 6.6 | 0.31 | **6.68** | **0.61** | |
| IA-NS-10_27.1 | AJP05 | 0.137 | 47 | 2.2E-3 | 37 | 0.79 | 6.6 | 0.84 | **6.72** | **1.69** | |
| IA-NS-10_14.1 | AJP05 | 0.097 | 648 | 1.4E-4 | 428 | 0.66 | 6.7 | 0.48 | **6.78** | **0.97** | |
| IA-NS-10_10.1 | AJP05 | -0.146 | 346 | -2.7E-4 | 273 | 0.79 | 6.7 | 0.65 | **6.83** | **1.30** | |
| IA-NS-10_9.1 | AJP05 | 0.060 | 40 | 1.5E-3 | 16 | 0.39 | 6.9 | 0.98 | ~~**6.96**~~ | ~~**1.96**~~ | **High comm-Pb (>20%)** |
| IA-NS-10_21.1 | AJP05 | 0.255 | 41 | 3.2E-3 | 37 | 0.91 | 6.9 | 0.53 | **7.03** | **1.05** | |

**Appendix B.1**. Continued

| Spot Name | Mount | $^{204}$Pb/ $^{206}$Pb | % error | $^{206}$Pb/ $^{238}$U | % error | U (ppm) | Th (ppm) | $^{232}$Th/ $^{238}$U | % error | Total $^{238}$U/$^{206}$Pb | % error | Total $^{207}$Pb/$^{206}$Pb | % error | $^{207}$Pb-corr $^{204}$Pb/$^{206}$Pb | $^{207}$Pb-corr % $^{206}$Pb$_C$ |
|---|---|---|---|---|---|---|---|---|---|---|---|---|---|---|---|
| **IA-NS-10 (continued)** | | | | | | | | | | | | | | | |
| IA-NS-10_26.1 | AJP05 | 4.4E-2 | 62 | 0.0020 | 4.2 | 159 | 93 | 0.603 | 0.36 | 852 | 5.3 | 0.1084 | 14 | 4.2E-3 | 7.88 |
| IA-NS-10_18.1 | AJP05 | -1.3E-2 | 129 | 0.0025 | 8.9 | 91 | 45 | 0.510 | 0.47 | 840 | 9.7 | 0.1161 | 15 | 4.7E-3 | 8.84 |
| IA-NS-10_13.1 | AJP05 | 2.9E-2 | 75 | 0.0024 | 8.6 | 139 | 84 | 0.621 | 1.10 | 840 | 8.1 | 0.1141 | 15 | 4.6E-3 | 8.59 |
| IA-NS-10_28.1 | AJP05 | 1.2E-2 | 112 | 0.0024 | 3.9 | 143 | 71 | 0.516 | 1.95 | 882 | 5.3 | 0.0706 | 17 | 1.6E-3 | 3.08 |
| IA-NS-10_11.1 | AJP05 | 2.6E-2 | 100 | 0.0028 | 10.8 | 70 | 29 | 0.436 | 0.57 | 769 | 9.0 | 0.0800 | 18 | 2.3E-3 | 4.27 |
| **IA-NS-12 (High-SiO$_2$ Granophyre)** | | | | | | | | | | | | | | | |
| IA-NS-12_14.1 | AJP05 | 1.1E-1 | 38 | 0.0036 | 12.9 | 81 | 39 | 0.49 | 1.09 | 601 | 15.4 | 0.4256 | 43 | 2.6E-2 | 48.04 |
| IA-NS-12_15.1 | AJP05 | -1.5E-2 | 79 | 0.0025 | 18.1 | 187 | 169 | 0.93 | 0.42 | 888 | 12.3 | 0.2220 | 71 | 1.2E-2 | 22.26 |
| IA-NS-12_9.1 | AJP05 | -8.9E-3 | 158 | 0.0021 | 6.5 | 116 | 57 | 0.51 | 2.12 | 992 | 9.1 | 0.1254 | 42 | 5.4E-3 | 10.03 |
| IA-NS-12_17.1 | AJP05 | -1.3E-2 | 100 | 0.0021 | 5.0 | 182 | 107 | 0.61 | 0.89 | 1021 | 5.9 | 0.0871 | 27 | 2.8E-3 | 5.18 |
| IA-NS-12_26.1 | AJP05 | 2.1E-2 | 112 | 0.0022 | 3.7 | 81 | 37 | 0.47 | 2.10 | 937 | 2.5 | 0.1461 | 31 | 6.8E-3 | 12.64 |
| IA-NS-12_20.1 | AJP05 | 1.4E-2 | 75 | 0.0031 | 1.7 | 218 | 144 | 0.68 | 1.26 | 846 | 5.4 | 0.2004 | 14 | 1.0E-2 | 19.52 |
| IA-NS-12_28.1 | AJP05 | -5.6E-3 | 224 | 0.0024 | 8.6 | 76 | 34 | 0.46 | 1.96 | 929 | 7.7 | 0.1325 | 16 | 5.8E-3 | 10.92 |
| IA-NS-12_16.1 | AJP05 | 8.3E-2 | 60 | 0.0028 | 12.2 | 64 | 27 | 0.44 | 0.98 | 877 | 9.7 | 0.1473 | 18 | 6.8E-3 | 12.80 |
| IA-NS-12_13.1 | AJP05 | 4.3E-2 | 75 | 0.0025 | 5.9 | 82 | 41 | 0.51 | 1.35 | 851 | 6.8 | 0.1599 | 13 | 7.7E-3 | 14.40 |
| IA-NS-12_21.1 | AJP05 | -3.1E-2 | 112 | 0.0027 | 3.8 | 49 | 13 | 0.28 | 1.86 | 815 | 1.1 | 0.1876 | 18 | 9.6E-3 | 17.91 |
| IA-NS-12_11.1 | AJP05 | -2.3E-2 | 91 | 0.0023 | 5.3 | 117 | 64 | 0.57 | 0.95 | 943 | 4.1 | 0.0718 | 22 | 1.7E-3 | 3.24 |
| IA-NS-12_22.1 | AJP05 | --- | --- | 0.0024 | 5.9 | 151 | 73 | 0.50 | 0.37 | 903 | 6.8 | 0.0941 | 14 | 3.2E-3 | 6.06 |
| IA-NS-12_6.1 | AJP05 | -4.6E-2 | 85 | 0.0021 | 7.0 | 74 | 32 | 0.45 | 0.56 | 909 | 6.3 | 0.0880 | 19 | 2.8E-3 | 5.30 |
| IA-NS-12_18.1 | AJP05 | -2.1E-2 | 91 | 0.0027 | 2.8 | 111 | 57 | 0.53 | 0.42 | 817 | 5.7 | 0.1591 | 12 | 7.6E-3 | 14.29 |
| IA-NS-12_3.1 | AJP05 | -4.8E-3 | 224 | 0.0028 | 10.5 | 82 | 43 | 0.54 | 1.05 | 785 | 8.4 | 0.1834 | 12 | 9.3E-3 | 17.37 |
| IA-NS-12_24.1 | AJP05 | 1.8E-2 | 112 | 0.0027 | 2.9 | 80 | 39 | 0.50 | 1.31 | 884 | 4.6 | 0.0986 | 21 | 3.5E-3 | 6.63 |
| IA-NS-12_10.1 | AJP05 | 1.8E-2 | 100 | 0.0025 | 5.4 | 104 | 58 | 0.57 | 0.40 | 858 | 6.1 | 0.1070 | 29 | 4.1E-3 | 7.70 |
| IA-NS-12_23.1 | AJP05 | 7.2E-2 | 33 | 0.0060 | 15.4 | 111 | 46 | 0.43 | 1.21 | 368 | 13.9 | 0.5156 | 5 | 3.2E-2 | 59.42 |
| IA-NS-12_27.1 | AJP05 | -3.6E-2 | 91 | 0.0025 | 9.1 | 67 | 32 | 0.50 | 1.30 | 846 | 9.6 | 0.0816 | 19 | 2.4E-3 | 4.48 |
| IA-NS-12_19.1 | AJP05 | -2.0E-2 | 85 | 0.0024 | 7.8 | 139 | 70 | 0.52 | 0.67 | 857 | 9.1 | 0.0493 | 22 | 2.1E-4 | 0.39 |
| **IA-G-1 (Gabbro)** | | | | | | | | | | | | | | | |
| IA-G-1_14.1 | JW510 | 1.4E-2 | 58 | 0.0020 | 10.6 | 65 | 39 | 0.62 | 0.43 | 1040 | 10.1 | 0.0685 | 19 | 1.5E-3 | 2.83 |
| IA-G-1_3.1 | JW510 | 6.7E-3 | 58 | 0.0017 | 5.8 | 161 | 122 | 0.79 | 1.25 | 1043 | 6.1 | 0.0647 | 14 | 1.3E-3 | 2.35 |
| IA-G-1_19.1 | JW510 | 9.6E-3 | 50 | 0.0017 | 3.6 | 149 | 78 | 0.54 | 0.30 | 1066 | 3.2 | 0.0476 | 17 | 9.3E-5 | 0.17 |
| IA-G-1_1.1 | JW510 | 1.0E-2 | 41 | 0.0019 | 3.1 | 197 | 152 | 0.80 | 0.23 | 1046 | 3.2 | 0.0583 | 14 | 8.2E-4 | 1.54 |
| IA-G-1_2.1 | JW510 | --- | 100 | 0.0017 | 4.1 | 128 | 85 | 0.69 | 0.30 | 1060 | 5.5 | 0.0459 | 18 | -1.8E-5 | -0.03 |
| IA-G-1_23.1 | JW510 | 2.7E-3 | 100 | 0.0017 | 3.9 | 143 | 102 | 0.73 | 1.87 | 1052 | 6.0 | 0.0495 | 19 | 2.3E-4 | 0.43 |
| IA-G-1_22.1 | JW510 | 3.3E-3 | 38 | 0.0019 | 3.5 | 695 | 785 | 1.17 | 0.31 | 1034 | 2.5 | 0.0605 | 7 | 9.7E-4 | 1.82 |
| IA-G-1_17.1 | JW510 | 2.4E-3 | 100 | 0.0022 | 3.4 | 212 | 206 | 1.00 | 2.13 | 1046 | 3.8 | 0.0432 | 18 | -2.0E-4 | -0.373 |
| IA-G-1_15.1 | JW510 | -5.1E-3 | 58 | 0.0018 | 3.1 | 210 | 172 | 0.85 | 0.62 | 1053 | 3.5 | 0.0305 | 20 | -1.1E-3 | -1.99 |

**Appendix B.1**. Continued

| Spot Name | Mount | $^{204}$Pb-corr $^{207}$Pb*/$^{235}$U | % error | $^{204}$Pb-corr $^{206}$Pb*/$^{238}$U | % error | Error Corr. | $^{207}$Pb-corr $^{206}$Pb/$^{238}$U Age (Ma) | 1σ error | $^{230}$Th-corr $^{206}$Pb/$^{238}$U Age (Ma) | 2σ error | Reason for excluding? |
|---|---|---|---|---|---|---|---|---|---|---|---|
| **IA-NS-10** | | | | | | | | | | | |
| IA-NS-10_26.1 | AJP05 | 0.094 | 443 | 2.1E-4 | 287 | 0.65 | 7.0 | 0.39 | **7.05** | **0.79** | |
| IA-NS-10_18.1 | AJP05 | 0.053 | 63 | 1.5E-3 | 27 | 0.43 | 7.0 | 0.70 | **7.08** | **1.40** | |
| IA-NS-10_13.1 | AJP05 | 0.056 | 166 | 5.4E-4 | 90 | 0.54 | 7.0 | 0.59 | **7.10** | **1.18** | |
| IA-NS-10_28.1 | AJP05 | 0.019 | 88 | 8.7E-4 | 34 | 0.38 | 7.1 | 0.39 | **7.17** | **0.79** | |
| IA-NS-10_11.1 | AJP05 | 0.058 | 192 | 6.8E-4 | 93 | 0.48 | 8.0 | 0.74 | ~~8.11~~ | ~~1.47~~ | **Outlier (>2SD)** |
| **IA-NS-12 (High-SiO2 Granophyre)** | | | | | | | | | | | |
| IA-NS-12_14.1 | AJP05 | -0.291 | 81 | -1.7E-3 | 76 | 0.94 | 5.6 | 2.61 | ~~5.66~~ | ~~5.21~~ | **High comm-Pb (>20%)** |
| IA-NS-12_15.1 | AJP05 | 0.071 | 47 | 1.4E-3 | 21 | 0.45 | 5.6 | 1.61 | ~~5.72~~ | ~~3.22~~ | **High comm-Pb (>20%)** |
| IA-NS-12_9.1 | AJP05 | 0.037 | 68 | 1.2E-3 | 24 | 0.36 | 5.8 | 0.68 | **5.93** | **1.36** | |
| IA-NS-12_17.1 | AJP05 | 0.040 | 55 | 1.2E-3 | 21 | 0.38 | 6.0 | 0.40 | **6.07** | **0.80** | |
| IA-NS-12_26.1 | AJP05 | 0.027 | 123 | 6.5E-4 | 73 | 0.59 | 6.0 | 0.42 | **6.10** | **0.84** | |
| IA-NS-12_20.1 | AJP05 | 0.004 | 523 | 8.6E-4 | 28 | 0.05 | 6.1 | 0.43 | **6.21** | **0.86** | |
| IA-NS-12_28.1 | AJP05 | 0.033 | 72 | 1.2E-3 | 22 | 0.31 | 6.2 | 0.51 | **6.27** | **1.01** | |
| IA-NS-12_16.1 | AJP05 | -0.181 | 196 | -6.3E-4 | 168 | 0.86 | 6.4 | 0.67 | **6.50** | **1.34** | |
| IA-NS-12_13.1 | AJP05 | 0.084 | 496 | 2.2E-4 | 324 | 0.65 | 6.5 | 0.48 | **6.57** | **0.97** | |
| IA-NS-12_21.1 | AJP05 | 0.115 | 57 | 1.9E-3 | 41 | 0.72 | 6.5 | 0.34 | **6.59** | **0.68** | |
| IA-NS-12_11.1 | AJP05 | 0.063 | 56 | 1.5E-3 | 28 | 0.49 | 6.6 | 0.30 | **6.70** | **0.61** | |
| IA-NS-12_22.1 | AJP05 | 0.014 | 15 | 1.1E-3 | 7 | 0.45 | 6.7 | 0.47 | **6.79** | **0.93** | |
| IA-NS-12_6.1 | AJP05 | 0.122 | 54 | 2.0E-3 | 39 | 0.73 | 6.7 | 0.45 | **6.81** | **0.90** | |
| IA-NS-12_18.1 | AJP05 | 0.081 | 44 | 1.7E-3 | 26 | 0.59 | 6.8 | 0.43 | **6.85** | **0.86** | |
| IA-NS-12_3.1 | AJP05 | 0.045 | 52 | 1.4E-3 | 20 | 0.39 | 6.8 | 0.61 | **6.87** | **1.23** | |
| IA-NS-12_24.1 | AJP05 | 0.029 | 124 | 7.5E-4 | 57 | 0.46 | 6.8 | 0.37 | **6.90** | **0.73** | |
| IA-NS-12_10.1 | AJP05 | 0.028 | 103 | 7.8E-4 | 51 | 0.49 | 6.9 | 0.51 | **7.02** | **1.03** | |
| IA-NS-12_23.1 | AJP05 | -0.229 | 146 | -9.5E-4 | 130 | 0.89 | 7.1 | 1.11 | ~~7.19~~ | ~~2.23~~ | **High comm-Pb (>20%)** |
| IA-NS-12_27.1 | AJP05 | 0.106 | 58 | 2.0E-3 | 38 | 0.66 | 7.3 | 0.71 | **7.37** | **1.43** | |
| IA-NS-12_19.1 | AJP05 | 0.059 | 56 | 1.6E-3 | 25 | 0.45 | 7.5 | 0.69 | **7.58** | **1.38** | |
| **IA-G-1 (Gabbro)** | | | | | | | | | | | |
| IA-G-1_14.1 | JW510 | 0.020 | 58 | 7.1E-4 | 23 | 0.40 | 6.0 | 0.62 | **6.11** | **1.24** | |
| IA-G-1_3.1 | JW510 | 0.005 | 38 | 8.4E-4 | 10 | 0.27 | 6.0 | 0.38 | **6.12** | **0.75** | |
| IA-G-1_19.1 | JW510 | 0.013 | 40 | 7.7E-4 | 11 | 0.28 | 6.0 | 0.20 | **6.12** | **0.40** | |
| IA-G-1_1.1 | JW510 | 0.013 | 30 | 7.7E-4 | 10 | 0.34 | 6.1 | 0.20 | **6.15** | **0.41** | |
| IA-G-1_2.1 | JW510 | 0.006 | 19 | 9.4E-4 | 6 | 0.29 | 6.1 | 0.34 | **6.16** | **0.68** | |
| IA-G-1_23.1 | JW510 | 0.001 | 525 | 9.0E-4 | 8 | 0.02 | 6.1 | 0.37 | **6.18** | **0.75** | |
| IA-G-1_22.1 | JW510 | 0.001 | 222 | 9.1E-4 | 4 | 0.02 | 6.1 | 0.16 | **6.18** | **0.31** | |
| IA-G-1_17.1 | JW510 | 0.001 | 777 | 9.1E-4 | 6 | 0.01 | 6.2 | 0.25 | **6.26** | **0.49** | |
| IA-G-1_15.1 | JW510 | 0.015 | 38 | 1.0E-3 | 6 | 0.16 | 6.2 | 0.22 | **6.32** | **0.44** | |

**Appendix B.1**. Continued

| Spot Name | Mount | $^{204}$Pb/ $^{206}$Pb | % error | $^{206}$Pb/ $^{238}$U | % error | U (ppm) | Th (ppm) | $^{232}$Th/ $^{238}$U | % error | Total $^{238}$U/$^{206}$Pb | % error | Total $^{207}$Pb/$^{206}$Pb | % error | $^{207}$Pb-corr $^{204}$Pb/$^{206}$Pb | $^{207}$Pb-corr % $^{206}$Pb$_C$ |
|---|---|---|---|---|---|---|---|---|---|---|---|---|---|---|---|
| **IA-G-1 (continued)** | | | | | | | | | | | | | | | |
| IA-G-1_18.1 | JW510 | 3.6E-3 | 71 | 0.0019 | 5.3 | 194 | 177 | 0.94 | 0.68 | 1018 | 5.5 | 0.0546 | 14 | 5.7E-4 | 1.07 |
| IA-G-1_8.1 | JW510 | -2.5E-3 | 100 | 0.0019 | 3.8 | 129 | 93 | 0.75 | 0.29 | 1032 | 5.4 | 0.0442 | 19 | -1.3E-4 | -0.25 |
| IA-G-1_27.1 | JW510 | 4.1E-3 | 71 | 0.0019 | 5.5 | 157 | 108 | 0.71 | 1.26 | 1032 | 5.5 | 0.0426 | 17 | -2.4E-4 | -0.45 |
| IA-G-1_6.1 | JW510 | 6.1E-3 | 71 | 0.0019 | 4.2 | 107 | 67 | 0.65 | 1.36 | 1017 | 3.3 | 0.0479 | 19 | 1.2E-4 | 0.22 |
| IA-G-1_11.1 | JW510 | --- | 100 | 0.0022 | 7.1 | 151 | 109 | 0.74 | 0.30 | 1006 | 5.1 | 0.0532 | 17 | 4.7E-4 | 0.885 |
| IA-G-1_25.1 | JW510 | -3.2E-3 | 100 | 0.0019 | 4.3 | 108 | 62 | 0.60 | 0.78 | 1007 | 7.0 | 0.0434 | 20 | -1.9E-4 | -0.36 |
| IA-G-1_4.1 | JW510 | 1.9E-3 | 100 | 0.0019 | 3.3 | 173 | 143 | 0.86 | 0.24 | 1002 | 3.3 | 0.0449 | 16 | -8.5E-5 | -0.16 |
| IA-G-1_24.1 | JW510 | 1.6E-4 | 100 | 0.0021 | 2.0 | 1940 | 2665 | 1.42 | 0.11 | 992 | 1.8 | 0.0484 | 4 | 1.5E-4 | 0.28 |
| IA-G-1_7.1 | JW510 | -3.3E-3 | 100 | 0.0019 | 4.3 | 103 | 64 | 0.64 | 0.35 | 1006 | 5.6 | 0.0376 | 21 | -5.8E-4 | -1.09 |
| IA-G-1_10.1 | JW510 | -2.8E-3 | 100 | 0.0023 | 3.6 | 160 | 106 | 0.68 | 0.29 | 998 | 1.8 | 0.0411 | 18 | -3.4E-4 | -0.643 |
| IA-G-1_12.1 | JW510 | 4.8E-3 | 58 | 0.0020 | 3.0 | 210 | 197 | 0.97 | 0.21 | 992 | 1.6 | 0.0383 | 16 | -5.4E-4 | -1.00 |
| IA-G-1_26.1 | JW510 | --- | 100 | 0.0024 | 3.7 | 148 | 146 | 1.02 | 0.27 | 963 | 5.0 | 0.0420 | 18 | -2.8E-4 | -0.526 |
| **IA-G-5 (Gabbro)** | | | | | | | | | | | | | | | |
| IA-G-5_6.1 | AJP01 | 3.1E-3 | 41 | 0.0022 | 3.4 | 638 | 874 | 1.41 | 0.30 | 1062 | 2.2 | 0.0456 | 7 | -3.8E-5 | -0.07 |
| IA-G-5_7.1 | AJP01 | 1.4E-3 | 100 | 0.0019 | 4.4 | 309 | 270 | 0.90 | 0.76 | 1039 | 3.1 | 0.0439 | 12 | -1.6E-4 | -0.29 |
| IA-G-5_4.1 | AJP01 | 3.4E-4 | 100 | 0.0021 | 4.9 | 1051 | 1484 | 1.46 | 0.25 | 1025 | 2.6 | 0.0482 | 5 | 1.4E-4 | 0.26 |
| IA-G-5_13.1 | AJP03 | -1.4E-3 | 75 | 0.0023 | 2.1 | 1050 | 1451 | 1.43 | 0.32 | 988 | 0.9 | 0.0500 | 6 | 2.6E-4 | 0.49 |
| IA-G-5_2.1 | AJP01 | -3.0E-4 | 100 | 0.0022 | 1.2 | 1209 | 1730 | 1.48 | 0.14 | 991 | 0.5 | 0.0468 | 5 | 4.2E-5 | 0.08 |
| IA-G-5_8.1 | AJP02 | 2.0E-3 | 71 | 0.0020 | 2.1 | 1124 | 1575 | 1.45 | 0.24 | 985 | 1.0 | 0.0492 | 7 | 2.0E-4 | 0.38 |
| IA-G-5_14.1 | AJP03 | -2.0E-4 | 183 | 0.0022 | 2.1 | 1216 | 2240 | 1.90 | 0.24 | 982 | 0.8 | 0.0464 | 6 | 1.3E-5 | 0.02 |
| IA-G-5_10.1 | AJP03 | 4.0E-4 | 158 | 0.0023 | 3.0 | 806 | 1253 | 1.61 | 0.31 | 977 | 1.3 | 0.0461 | 7 | -7.9E-6 | -0.01 |
| IA-G-5_12.1 | AJP03 | 3.7E-3 | 71 | 0.0025 | 2.4 | 365 | 319 | 0.90 | 0.34 | 928 | 1.8 | 0.0803 | 14 | 2.3E-3 | 4.32 |
| IA-G-5_11.1 | AJP03 | -7.7E-4 | 183 | 0.0023 | 2.5 | 301 | 259 | 0.89 | 0.80 | 968 | 1.6 | 0.0408 | 12 | -3.6E-4 | -0.68 |
| IA-G-5_9.1 | AJP02 | -3.0E-4 | 105 | 0.0023 | 1.1 | 2889 | 2150 | 0.77 | 0.06 | 937 | 1.1 | 0.0473 | 4 | 7.7E-5 | 0.14 |

**Appendix B.1**. Continued

| Spot Name | Mount | $^{204}$Pb-corr $^{207}$Pb*/$^{235}$U | % error | $^{204}$Pb-corr $^{206}$Pb*/$^{238}$U | % error | Error Corr. | $^{207}$Pb-corr $^{206}$Pb/$^{238}$U Age (Ma) | 1σ error | $^{230}$Th-corr $^{206}$Pb/$^{238}$U Age (Ma) | 2σ error | Reason for excluding? |
|---|---|---|---|---|---|---|---|---|---|---|---|
| | | | | | | **IA-G-1 (Continued)** | | | | | |
| IA-G-1_18.1 | JW510 | 0.000 | 2420 | 9.2E-4 | 7 | 0.00 | 6.3 | 0.35 | **6.34** | **0.69** | |
| IA-G-1_8.1 | JW510 | 0.011 | 44 | 1.0E-3 | 7 | 0.16 | 6.3 | 0.34 | **6.35** | **0.69** | |
| IA-G-1_27.1 | JW510 | 0.003 | 72 | 8.9E-4 | 8 | 0.11 | 6.3 | 0.35 | **6.36** | **0.70** | |
| IA-G-1_6.1 | JW510 | 0.006 | 23 | 8.7E-4 | 10 | 0.42 | 6.3 | 0.22 | **6.41** | **0.44** | |
| IA-G-1_11.1 | JW510 | 0.007 | 18 | 9.9E-4 | 5 | 0.29 | 6.4 | 0.33 | **6.43** | **0.66** | |
| IA-G-1_25.1 | JW510 | 0.013 | 50 | 1.1E-3 | 9 | 0.18 | 6.4 | 0.46 | **6.51** | **0.92** | |
| IA-G-1_4.1 | JW510 | 0.002 | 204 | 9.6E-4 | 5 | 0.02 | 6.4 | 0.22 | **6.52** | **0.45** | |
| IA-G-1_24.1 | JW510 | 0.006 | 7 | 1.0E-3 | 2 | 0.25 | 6.5 | 0.12 | **6.54** | **0.23** | |
| IA-G-1_7.1 | JW510 | 0.012 | 54 | 1.1E-3 | 8 | 0.15 | 6.5 | 0.37 | **6.56** | **0.73** | |
| IA-G-1_10.1 | JW510 | 0.012 | 47 | 1.1E-3 | 5 | 0.11 | 6.5 | 0.13 | **6.58** | **0.26** | |
| IA-G-1_12.1 | JW510 | 0.005 | 18 | 9.2E-4 | 6 | 0.32 | 6.6 | 0.12 | **6.64** | **0.23** | |
| IA-G-1_26.1 | JW510 | 0.006 | 19 | 1.0E-3 | 5 | 0.27 | 6.7 | 0.34 | **~~6.80~~** | **~~0.68~~** | **Older grain, outlier (>2SD)** |
| | | | | | | **IA-G-5 (Gabbro)** | | | | | |
| IA-G-5_6.1 | AJP01 | 0.000 | 483 | 8.9E-4 | 3 | 0.01 | 6.1 | 0.14 | **6.13** | **0.28** | |
| IA-G-5_7.1 | AJP01 | 0.003 | 97 | 9.4E-4 | 4 | 0.04 | 6.2 | 0.20 | **6.30** | **0.39** | |
| IA-G-5_4.1 | AJP01 | 0.006 | 13 | 9.7E-4 | 3 | 0.20 | 6.3 | 0.17 | **6.33** | **0.33** | |
| IA-G-5_13.1 | AJP03 | 0.010 | 21 | 1.0E-3 | 2 | 0.10 | 6.5 | 0.06 | **6.55** | **0.12** | |
| IA-G-5_2.1 | AJP01 | 0.007 | 10 | 1.0E-3 | 1 | 0.08 | 6.5 | 0.04 | **6.55** | **0.08** | |
| IA-G-5_8.1 | AJP02 | 0.002 | 123 | 9.8E-4 | 3 | 0.02 | 6.5 | 0.07 | **6.58** | **0.14** | |
| IA-G-5_14.1 | AJP03 | 0.007 | 12 | 1.0E-3 | 1 | 0.09 | 6.6 | 0.06 | **6.60** | **0.11** | |
| IA-G-5_10.1 | AJP03 | 0.006 | 25 | 1.0E-3 | 2 | 0.07 | 6.6 | 0.09 | **6.65** | **0.18** | |
| IA-G-5_12.1 | AJP03 | 0.003 | 185 | 1.0E-3 | 6 | 0.03 | 6.6 | 0.15 | **6.72** | **0.31** | |
| IA-G-5_11.1 | AJP03 | 0.008 | 40 | 1.0E-3 | 3 | 0.08 | 6.7 | 0.12 | **6.78** | **0.23** | |
| IA-G-5_9.1 | AJP02 | 0.008 | 10 | 1.1E-3 | 1 | 0.13 | 6.9 | 0.08 | **~~6.95~~** | **~~0.15~~** | **Older grain, outlier (>2SD)** |

**Appendix B.2**. Zircon Trace Element Compositions (ppm), measured *in situ* by SHRIMP-RG (Atomic Number < 22)

| Sample | Rock Type | Grain # | Mount[1] | Date | Li | Be | B | F | Na | Al | P | K | Ca | Sc |
|---|---|---|---|---|---|---|---|---|---|---|---|---|---|---|
| IA-NS-2 | Granophyre | IA-NS-2-1.1 | JW498 | Dec. '10 | 0.0024 | 0.022 | 0.035 | 15 | 2 | 15 | 192 | 0.66 | 3.05 | 8 |
| IA-NS-2 | Granophyre | IA-NS-2-2.1 | JW498 | Dec. '10 | 0.0041 | 0.2 | 0.080 | 18 | 2 | 15 | 389 | 0.75 | 4.57 | 13 |
| IA-NS-2 | Granophyre | IA-NS-2-3.1 | JW498 | Dec. '10 | 0.02 | 4 | 0.1 | 38 | 2 | 14 | 1661 | 0.85 | 4.00 | 18 |
| IA-NS-2 | Granophyre | IA-NS-2-4.1 | JW498 | Dec. '10 | 0.0039 | 0.067 | 0.060 | 24 | 2 | 12 | 272 | 0.76 | 2.92 | 1.67 |
| IA-NS-2 | Granophyre | IA-NS-2-4.2 | JW498 | Dec. '10 | 0.0033 | 0.1 | 0.079 | 48 | 2 | 14 | 266 | 0.88 | 3.56 | 1.95 |
| IA-NS-2 | Granophyre | IA-NS-2-4.3 | JW498 | Dec. '10 | 0.02 | 0.043 | 0.080 | 31 | 3 | 18 | 482 | 0.93 | 3.72 | 2.26 |
| IA-NS-2 | Granophyre | IA-NS-2-5.1 | JW498 | Dec. '10 | 0.06 | 26 | 0.1 | 87 | 2 | 18 | 1276 | 0.76 | 4.46 | 62 |
| IA-NS-2 | Granophyre | IA-NS-2-5.2 | JW498 | Dec. '10 | 0.01 | 0.7 | 0.062 | 32 | 3 | 17 | 333 | 1.00 | 4.72 | 2.68 |
| IA-NS-2 | Granophyre | IA-NS-2-6.1 | JW498 | Dec. '10 | 0.05 | 0.7 | 0.081 | 54 | 2 | 15 | 985 | 0.74 | 2.95 | 9 |
| IA-NS-2 | Granophyre | IA-NS-2-7.1 | JW498 | Dec. '10 | 0.0040 | 0.025 | 0.035 | 16 | 2 | 15 | 290 | 0.68 | 2.40 | 9 |
| IA-NS-2 | Granophyre | IA-NS-2-8.1 | JW498 | Dec. '10 | 0.07 | 0.6 | 0.3 | 49 | 6 | 25 | 1472 | 46 | 7 | 17 |
| IA-NS-2 | Granophyre | IA-NS-2-9.1 | JW498 | Dec. '10 | 0.01 | 0.2 | 0.1 | 21 | 2 | 11 | 1263 | 0.85 | 3.92 | 21 |
| IA-NS-2 | Granophyre | IA-NS-2-10.1 | JW498 | Dec. '10 | 0.09 | 0.7 | 0.1 | 23 | 3 | 15 | 889 | 1.38 | 3.76 | 18 |
| IA-NS-2 | Granophyre | IA-NS-2-10.2 | JW498 | Dec. '10 | 0.06 | 2 | 0.1 | 28 | 2 | 16 | 918 | 1.13 | 2.69 | 9 |
| IA-NS-2 | Granophyre | IA-NS-2-11.1 | JW498 | Dec. '10 | 0.0090 | 0.4 | 0.044 | 52 | 0.9 | 9 | 297 | 0.51 | 1.95 | 1.57 |
| IA-NS-2 | Granophyre | IA-NS-2-11.2 | JW498 | Dec. '10 | 0.07 | 0.2 | 0.095 | 39 | 41 | 313 | 988 | 449 | 11 | 15 |
| IA-NS-2 | Granophyre | IA-NS-2-12.1 | JW498 | Dec. '10 | 0.02 | 0.3 | 0.1 | 45 | 3 | 14 | 351 | 1.08 | 4.83 | 3.32 |
| IA-NS-2 | Granophyre | IA-NS-2-12.2 | JW498 | Dec. '10 | 0.0067 | 0.5 | 0.064 | 67 | 2 | 15 | 387 | 0.99 | 3.97 | 1.91 |
| IA-NS-2 | Granophyre | IA-NS-2-13.1 | JW498 | Dec. '10 | 0.0008 | 3 | 0.2 | 127 | 6 | 27 | 712 | 3.78 | 4.43 | 4.53 |
| IA-NS-2 | Granophyre | IA-NS-2-14.1 | JW498 | Dec. '10 | 0.07 | 0.2 | 0.4 | 49 | 4 | 60 | 646 | 3.56 | 13 | 4.05 |
| IA-NS-2 | Granophyre | IA-NS-2-14.2 | JW498 | Dec. '10 | 0.04 | 0.7 | 0.2 | 102 | 3 | 21 | 607 | 1.12 | 6 | 2.33 |
| IA-NS-2 | Granophyre | IA-NS-2-15.1 | JW498 | Dec. '10 | 0.01 | 2 | 0.061 | 44 | 2 | 18 | 441 | 0.81 | 2.95 | 2.52 |
| IA-NS-2 | Granophyre | IA-NS-2-15.2 | JW498 | Dec. '10 | 0.0072 | 0.071 | 0.2 | 23 | 3 | 18 | 354 | 0.97 | 3.81 | 2.77 |
| IA-NS-2 | Granophyre | IA-NS-2-16.1 | JW498 | Dec. '10 | 0.0059 | 0.032 | 0.045 | 16 | 3 | 14 | 240 | 0.90 | 4.92 | 2.10 |
| IA-NS-2 | Granophyre | IA-NS-2-16.2 | JW498 | Dec. '10 | 0.01 | 0.5 | 0.1 | 67 | 17 | 53 | 290 | 28 | 8 | 0.91 |
| IA-NS-2 | Granophyre | IA-NS-2-17.1 | JW498 | Dec. '10 | 0.0032 | 0.1 | 0.1 | 19 | 2 | 15 | 363 | 0.76 | 3.07 | 1.99 |
| IA-NS-2 | Granophyre | IA-NS-2-17.2 | JW498 | Dec. '10 | 0.03 | 40 | 0.5 | 189 | 2 | 16 | 1293 | 0.87 | 4.13 | 14 |
| IA-NS-2 | Granophyre | IA-NS-2-18.1 | JW498 | Dec. '10 | 0.0089 | 1 | 0.087 | 56 | 2 | 13 | 386 | 0.72 | 2.58 | 1.93 |
| IA-NS-2 | Granophyre | IA-NS-2-18.2 | JW498 | Dec. '10 | 0.0084 | 0.1 | 0.055 | 35 | 2 | 15 | 489 | 0.73 | 3.09 | 2.67 |
| IA-NS-2 | Granophyre | IA-NS-2-19.1 | JW498 | Dec. '10 | 0.02 | 0.039 | 0.1 | 39 | 2 | 17 | 419 | 0.72 | 2.77 | 2.80 |
| IA-NS-2 | Granophyre | IA-NS-2-19.2 | JW498 | Dec. '10 | 0.02 | 3 | 0.089 | 103 | 4 | 21 | 491 | 3.99 | 3.89 | 1.68 |

**Appendix B.2**. Continued

| Sample | Rock Type[36] | Grain # | Mount | Date | Li | Be | B | F | Na | Al | P | K | Ca | Sc |
|---|---|---|---|---|---|---|---|---|---|---|---|---|---|---|
| IA-NS-2 | Granophyre | IA-NS-2-20.1 | JW498 | Dec. '10 | 0.02 | 0.2 | 0.045 | 50 | 4 | 27 | 360 | 15 | 3.64 | 1.97 |
| IA-NS-2 | Granophyre | IA-NS-2-21.2 | JW498 | Dec. '10 | 0.0049 | 2 | 0.044 | 50 | 2 | 16 | 425 | 18 | 4.32 | 2.32 |
| IA-NS-2 | Granophyre | IA-NS-2-22.1 | JW498 | Dec. '10 | 0.0008 | 0.033 | 0.043 | 30 | 2 | 16 | 151 | 0.99 | 4.30 | 1.92 |
| IA-NS-2 | Granophyre | IA-NS-2-23.1 | JW498 | Dec. '10 | 0.0008 | 0.1 | 0.052 | 18 | 2 | 14 | 290 | 0.71 | 3.05 | 2.52 |
| IA-NS-2 | Granophyre | IA-NS-2-24.1 | JW498 | Dec. '10 | 0.0082 | 0.7 | 0.1 | 54 | 5 | 27 | 283 | 10 | 3.60 | 1.84 |
| IA-NS-2 | Granophyre | IA-NS-2-24.2 | JW498 | Dec. '10 | 0.04 | 1 | 0.083 | 49 | 2 | 17 | 1022 | 0.85 | 3.47 | 11 |
| IA-NS-2 | Granophyre | IA-NS-2-25.2 | JW498 | Dec. '10 | 0.02 | 0.2 | 0.065 | 81 | 7 | 31 | 684 | 172 | 184 | 5 |
| IA-NS-2 | Granophyre | IA-NS-2-21.1 | JW498 | Dec. '10 | 0.03 | 0.045 | 0.018 | 52 | 8 | 17 | 628 | 0.97 | 277 | 3.38 |
| IA-NS-2 | Granophyre | IA-NS-2-23.2 | JW498 | Dec. '10 | 0.09 | 32 | 0.073 | 407 | 4 | 15 | 1452 | 1.43 | 414 | 8 |
| IA-NS-2 | Granophyre | IA-NS-2-25.1 | JW498 | Dec. '10 | 0.22 | 6 | 2 | 337 | 943 | 2809 | 2565 | 5274 | 1109 | 22 |
| IA-NS-4b | HSG | IA-NS-4b-1.1 | JW498 | Dec. '10 | 0.35 | 2 | 0.2 | 155 | 5 | 19 | 819 | 2.75 | 9 | 23 |
| IA-NS-4b | HSG | IA-NS-4b-1.2 | JW498 | Dec. '10 | 1 | 13 | 1 | 367 | 5 | 19 | 814 | 0.71 | 2.85 | 26 |
| IA-NS-4b | HSG | IA-NS-4b-2.1 | JW498 | Dec. '10 | 0.02 | 0.082 | 0.083 | 25 | 2 | 13 | 214 | 0.90 | 2.72 | 1.76 |
| IA-NS-4b | HSG | IA-NS-4b-4.1 | JW498 | Dec. '10 | 2 | 2 | 0.1 | 247 | 460 | 15 | 728 | 426 | 16 | 30 |
| IA-NS-4b | HSG | IA-NS-4b-6.1 | JW498 | Dec. '10 | 0.01 | 0.020 | 0.1 | 15 | 2 | 14 | 154 | 0.90 | 3.40 | 4.08 |
| IA-NS-4b | HSG | IA-NS-4b-7.1 | JW498 | Dec. '10 | 0.68 | 32 | 0.5 | 449 | 2 | 13 | 1249 | 4.03 | 2.29 | 78 |
| IA-NS-4b | HSG | IA-NS-4b-9.1 | JW498 | Dec. '10 | 0.36 | 0.2 | 0.088 | 53 | 2 | 14 | 661 | 1.32 | 3.79 | 40 |
| IA-NS-4b | HSG | IA-NS-4b-9.2 | JW498 | Dec. '10 | 0.47 | 1 | 0.3 | 312 | 13 | 47 | 705 | 37 | 6 | 27 |
| IA-NS-4b | HSG | IA-NS-4b-10.1 | JW498 | Dec. '10 | 0.12 | 0.042 | 0.025 | 23 | 1 | 12 | 615 | 0.63 | 2.08 | 10 |
| IA-NS-4b | HSG | IA-NS-4b-11.1 | JW498 | Dec. '10 | 0.07 | 0.5 | 0.044 | 83 | 2 | 15 | 403 | 0.69 | 2.25 | 1.49 |
| IA-NS-4b | HSG | IA-NS-4b-12.1 | JW498 | Dec. '10 | 0.14 | 8 | 0.3 | 86 | 2 | 16 | 1020 | 0.81 | 2.56 | 49 |
| IA-NS-4b | HSG | IA-NS-4b-14.1 | JW498 | Dec. '10 | 0.39 | 2 | 0.2 | 161 | 1 | 11 | 788 | 0.52 | 1.21 | 24 |
| IA-NS-4b | HSG | IA-NS-4b-15.1 | JW498 | Dec. '10 | 0.46 | 7 | 0.1 | 900 | 10 | 32 | 612 | 28 | 1.85 | 3.39 |
| IA-NS-4b | HSG | IA-NS-4b-18.1 | JW498 | Dec. '10 | 0.26 | 0.5 | 0.074 | 185 | 20 | 17 | 707 | 25 | 2.66 | 44 |
| IA-NS-4b | HSG | IA-NS-4b-19.1 | JW498 | Dec. '10 | 0.0059 | 0.063 | 0.036 | 24 | 1 | 12 | 147 | 0.85 | 2.79 | 1.75 |
| IA-NS-4b | HSG | IA-NS-4b-20.1 | JW498 | Dec. '10 | 0.02 | 0.088 | 0.045 | 40 | 2 | 15 | 207 | 1.21 | 3.68 | 1.60 |
| IA-NS-4b | HSG | IA-NS-4b-22.1 | JW498 | Dec. '10 | 0.20 | 0.3 | 0.080 | 77 | 5 | 21 | 293 | 16 | 4.80 | 13 |
| IA-NS-4b | HSG | IA-NS-4b-23.1 | JW498 | Dec. '10 | 0.15 | 0.4 | 0.090 | 183 | 1 | 11 | 658 | 11 | 1.74 | 43 |
| IA-NS-4b | HSG | IA-NS-4b-23.2 | JW498 | Dec. '10 | 0.46 | 2 | 0.2 | 110 | 1 | 13 | 1124 | 0.76 | 1.70 | 54 |

---

[36] HSG = High-SiO$_2$ Granophyre (> 75 wt.% SiO$_2$)

**Appendix B.2**. Continued

| Sample | Rock Type | Grain # | Mount | Date | Li | Be | B | F | Na | Al | P | K | Ca | Sc |
|---|---|---|---|---|---|---|---|---|---|---|---|---|---|---|
| IA-NS-4b | HSG | IA-NS-4b-24.1 | JW498 | Dec. '10 | 0.02 | 0.043 | 0.045 | 61 | 2 | 15 | 215 | 10 | 1.94 | 8 |
| IA-NS-4b | HSG | IA-NS-4b-25.1 | JW498 | Dec. '10 | 0.42 | 27 | 0.2 | 78 | 3 | 17 | 1028 | 0.79 | 2.64 | 53 |
| IA-NS-4b | HSG | IA-NS-4b-25.2 | JW498 | Dec. '10 | 0.39 | 11 | 0.1 | 73 | 3 | 17 | 1284 | 1.14 | 2.74 | 50 |
| IA-NS-4b | HSG | IA-NS-4b-26.1 | JW498 | Dec. '10 | 0.02 | 0.011 | 0.075 | 24 | 2 | 13 | 296 | 0.85 | 1.75 | 13 |
| IA-NS-4b | HSG | IA-NS-4b-27.1 | JW498 | Dec. '10 | 0.01 | 0.050 | 0.059 | 35 | 1 | 12 | 230 | 0.83 | 1.53 | 1.69 |
| IA-NS-4b | HSG | IA-NS-4b-28.1 | JW498 | Dec. '10 | 0.02 | 0.008 | 0.035 | 23 | 2 | 16 | 205 | 0.89 | 2.01 | 6 |
| IA-NS-4b | HSG | IA-NS-4b-29.1 | JW498 | Dec. '10 | 0.92 | 5 | 0.7 | 452 | 2 | 18 | 350 | 2.92 | 1.89 | 2.63 |
| IA-NS-4b | HSG | IA-NS-4b-40 | AJP05 | Feb. '15 | 3 | 1 | 0.5 | 400 | 514 | 23 | 325 | 2018 | 14 | 9 |
| IA-NS-4b | HSG | IA-NS-4b-43 | AJP05 | Feb. '15 | 0.96 | 4 | 0.3 | 916 | 21 | 5 | 1054 | 43 | 74 | 21 |
| IA-NS-4b | HSG | IA-NS-4b-44 | AJP05 | Feb. '15 | 0.26 | 0.4 | 0.1 | 100 | 2 | 4 | 332 | 3.69 | 1.69 | 19 |
| IA-NS-4b | HSG | IA-NS-4b-45 | AJP05 | Feb. '15 | 0.46 | 7 | 0.8 | 548 | 18 | 10 | 783 | 55 | 5 | 17 |
| IA-NS-4b | HSG | IA-NS-4b-49 | AJP05 | Feb. '15 | 4 | 10 | 6 | 1194 | 3 | 4 | 1436 | 1.61 | 2.71 | 0.39 |
| IA-NS-4b | HSG | IA-NS-4b-50 | AJP05 | Feb. '15 | 4 | 6 | 0.8 | 565 | 1 | 3 | 617 | 0.89 | 2.16 | 1.30 |
| IA-NS-4b | HSG | IA-NS-4b-51 | AJP05 | Feb. '15 | 0.17 | 0.050 | 0.058 | 91 | 4 | 5 | 469 | 5 | 3.24 | 31 |
| IA-NS-4b | HSG | IA-NS-4b-52 | AJP05 | Feb. '15 | 0.67 | 3 | 0.4 | 258 | 6 | 6 | 702 | 53 | 3.17 | 42 |
| IA-NS-4b | HSG | IA-NS-4b-53 | AJP05 | Feb. '15 | 0.64 | 1 | 0.2 | 269 | 29 | 10 | 692 | 80 | 4.04 | 50 |
| IA-NS-4b | HSG | IA-NS-4b-55 | AJP05 | Feb. '15 | 0.34 | 0.2 | 0.100 | 95 | 27 | 4 | 115 | 61 | 3.94 | 2.17 |
| IA-NS-4b | HSG | IA-NS-4b-56 | AJP05 | Feb. '15 | 0.30 | 0.6 | 0.1 | 145 | 50 | 7 | 253 | 113 | 4.70 | 5 |
| IA-NS-4b | HSG | IA-NS-4b-57 | AJP05 | Feb. '15 | 0.89 | 24 | 2 | 1139 | 38 | 28 | 968 | 335 | 14 | 56 |
| IA-NS-4b | HSG | IA-NS-4b-58 | AJP05 | Feb. '15 | 0.41 | 7 | 0.3 | 295 | 5 | 3 | 654 | 3.32 | 2.71 | 22 |
| IA-NS-4b | HSG | IA-NS-4b-59 | AJP05 | Feb. '15 | 0.41 | 0.5 | 0.1 | 104 | 4 | 4 | 682 | 2.36 | 3.51 | 39 |
| IA-NS-4b | HSG | IA-NS-4b-3.1 | JW498 | Dec. '10 | 0.37 | 2 | 0.1 | 178 | 27 | 20 | 500 | 2752 | 42 | 19 |
| IA-NS-4b | HSG | IA-NS-4b-14.2 | JW498 | Dec. '10 | 3 | 0.3 | 0.2 | 232 | 667 | 24 | 301 | 642 | 24 | 8 |
| IA-NS-4b | HSG | IA-NS-4b-21.1 | JW498 | Dec. '10 | 1 | 3 | 0.4 | 1063 | 254 | 616 | 138 | 744 | 3.73 | 0.52 |
| IA-NS-4b | HSG | IA-NS-4b-21.2 | JW498 | Dec. '10 | 11 | 4 | 5 | 411 | 1276 | 389 | 142 | 1660 | 123 | 1.01 |
| IA-NS-4b | HSG | IA-NS-4b-27.2 | JW498 | Dec. '10 | 0.39 | 3 | 0.1 | 655 | 40 | 110 | 802 | 93 | 464 | 8 |
| IA-NS-4b | HSG | IA-NS-4b-41 | AJP05 | Feb. '15 | 2 | 2 | 0.9 | 970 | 59 | 11 | 1096 | 132 | 203 | 18 |
| IA-NS-4b | HSG | IA-NS-4b-42 | AJP05 | Feb. '15 | 0.66 | 3 | 0.4 | 1673 | 38 | 14 | 738 | 135 | 488 | 31 |
| IA-NS-4b | HSG | IA-NS-4b-46 | AJP05 | Feb. '15 | 3 | 1 | 0.6 | 466 | 251 | 10 | 915 | 924 | 16 | 11 |
| IA-NS-4b | HSG | IA-NS-4b-47 | AJP05 | Feb. '15 | 2 | 0.6 | 0.4 | 456 | 19 | 9 | 804 | 269 | 53 | 27 |
| IA-NS-4b | HSG | IA-NS-4b-48 | AJP05 | Feb. '15 | 5 | 9 | 9 | 3825 | 463 | 37 | 1469 | 580 | 227 | 29 |

**Appendix B.2**. Continued

| Sample | Rock Type | Grain # | Mount | Date | Li | Be | B | F | Na | Al | P | K | Ca | Sc |
|---|---|---|---|---|---|---|---|---|---|---|---|---|---|---|
| IA-NS-4b | HSG | IA-NS-4b-54 | AJP05 | Feb. '15 | 7 | 4 | 2 | 1570 | 616 | 35 | 2311 | 845 | 211 | 19 |
| IA-NS-4b | HSG | IA-NS-4b-60 | AJP05 | Feb. '15 | 3 | 3 | 1.0 | 881 | 233 | 25 | 558 | 551 | 130 | 13 |
| IA-NS-6 | Diorite | IA-NS-6-1.1 | JW498 | Dec. '10 | 0.0079 | 0.052 | 0.077 | 29 | 2 | 16 | 417 | 0.70 | 3.27 | 3.18 |
| IA-NS-6 | Diorite | IA-NS-6-2.1 | JW498 | Dec. '10 | 0.04 | 0.5 | 0.7 | 43 | 2 | 15 | 2309 | 0.87 | 4.02 | 63 |
| IA-NS-6 | Diorite | IA-NS-6-3.1 | JW498 | Dec. '10 | 0.05 | 0.4 | 0.3 | 73 | 2 | 15 | 2498 | 1.09 | 4.31 | 61 |
| IA-NS-6 | Diorite | IA-NS-6-4.1 | JW498 | Dec. '10 | 0.01 | 0.3 | 0.084 | 26 | 2 | 14 | 1617 | 0.99 | 4.60 | 86 |
| IA-NS-6 | Diorite | IA-NS-6-5.1 | JW498 | Dec. '10 | 0.04 | 4 | 0.037 | 116 | 3 | 12 | 1423 | 1.08 | 5 | 41 |
| IA-NS-6 | Diorite | IA-NS-6-6.1 | JW498 | Dec. '10 | 0.0092 | 0.1 | 0.075 | 37 | 2 | 10 | 441 | 0.78 | 3.62 | 2.12 |
| IA-NS-6 | Diorite | IA-NS-6-7.1 | JW498 | Dec. '10 | 0.0016 | 0.019 | 0.043 | 17 | 2 | 14 | 211 | 1.05 | 4.00 | 2.23 |
| IA-NS-6 | Diorite | IA-NS-6-9.1 | JW498 | Dec. '10 | 0.05 | 0.8 | 0.3 | 41 | 2 | 14 | 2150 | 1.01 | 5 | 53 |
| IA-NS-6 | Diorite | IA-NS-6-10.1 | JW498 | Dec. '10 | 0.03 | 0.2 | 0.052 | 17 | 2 | 12 | 813 | 0.93 | 3.33 | 30 |
| IA-NS-6 | Diorite | IA-NS-6-12.1 | JW498 | Dec. '10 | 0.0017 | 0.023 | 0.045 | 33 | 2 | 15 | 206 | 1.11 | 6 | 1.18 |
| IA-NS-6 | Diorite | IA-NS-6-13.1 | JW498 | Dec. '10 | 0.07 | 0.3 | 0.2 | 29 | 2 | 14 | 2187 | 0.65 | 2.92 | 68 |
| IA-NS-6 | Diorite | IA-NS-6-15.1 | JW498 | Dec. '10 | 0.03 | 0.2 | 0.072 | 19 | 2 | 11 | 1349 | 0.69 | 2.04 | 46 |
| IA-NS-6 | Diorite | IA-NS-6-16.1 | JW498 | Dec. '10 | 0.02 | 0.1 | 0.052 | 19 | 2 | 12 | 902 | 0.95 | 2.86 | 48 |
| IA-NS-6 | Diorite | IA-NS-6-17.1 | JW498 | Dec. '10 | 0.01 | 0.009 | 0.063 | 12 | 2 | 13 | 562 | 1.53 | 3.06 | 26 |
| IA-NS-6 | Diorite | IA-NS-6-17.2 | JW498 | Dec. '10 | 0.02 | 0.2 | 0.048 | 27 | 2 | 15 | 1845 | 0.86 | 3.08 | 62 |
| IA-NS-6 | Diorite | IA-NS-6-18.1 | JW498 | Dec. '10 | 0.02 | 0.018 | 0.075 | 11 | 3 | 27 | 578 | 17 | 8 | 33 |
| IA-NS-6 | Diorite | IA-NS-6-18.2 | JW498 | Dec. '10 | 0.0041 | 0.031 | 0.062 | 28 | 2 | 17 | 213 | 0.96 | 3.77 | 1.82 |
| IA-NS-6 | Diorite | IA-NS-6-19.1 | JW498 | Dec. '10 | 0.02 | 0.4 | 0.1 | 26 | 2 | 14 | 1918 | 0.95 | 4.22 | 66 |
| IA-NS-6 | Diorite | IA-NS-6-20.2 | JW498 | Dec. '10 | 0.06 | 0.014 | 0.036 | 25 | 54 | 163 | 1329 | 3.59 | 7 | 52 |
| IA-NS-6 | Diorite | IA-NS-6-21.1 | JW498 | Dec. '10 | 0.0017 | -- | 0.027 | 9 | 3 | 15 | 219 | 1.18 | 4.37 | 2.39 |
| IA-NS-6 | Diorite | IA-NS-6-22.1 | JW498 | Dec. '10 | 0.0040 | 0.047 | 0.069 | 22 | 4 | 19 | 165 | 3.22 | 3.54 | 2.05 |
| IA-NS-6 | Diorite | IA-NS-6-22.2 | JW498 | Dec. '10 | 0.0066 | 0.020 | 0.098 | 15 | 3 | 16 | 454 | 1.23 | 4.02 | 35 |
| IA-NS-6 | Diorite | IA-NS-6-24.1 | JW498 | Dec. '10 | 0.0016 | -- | 0.009 | 7 | 0.7 | 11 | 305 | 0.84 | 0.82 | 19 |
| IA-NS-6 | Diorite | IA-NS-6-24.2 | JW498 | Dec. '10 | 0.0008 | 0.4 | 0.1 | 86 | 28 | 94 | 303 | 63 | 8 | 1.49 |
| IA-NS-6 | Diorite | IA-NS-6-24.3 | JW498 | Dec. '10 | 0.0008 | 0.016 | 0.009 | 14 | 2 | 14 | 259 | 0.74 | 2.96 | 2.46 |
| IA-NS-6 | Diorite | IA-NS-6-26.1 | JW498 | Dec. '10 | 0.03 | 1 | 0.010 | 62 | 2 | 13 | 1693 | 0.97 | 4.00 | 48 |
| IA-NS-6 | Diorite | IA-NS-6-23.1 | JW498 | Dec. '10 | 0.0050 | 0.006 | 0.045 | 22 | 2 | 16 | 274 | 0.99 | 149 | 4.21 |
| IA-NS-7 | Granodiorite | IA-NS-7-1.1 | JW510 | Feb. '11 | 0.01 | 0.1 | 0.2 | 13 | 5 | 1 | 509 | 1.29 | 2.64 | 36 |
| IA-NS-7 | Granodiorite | IA-NS-7-2.1 | JW510 | Feb. '11 | 0.23 | 6 | 0.2 | 126 | 6 | 4 | 2063 | 1.54 | 4.38 | 46 |

**Appendix B.2**. Continued

| Sample | Rock Type | Grain # | Mount | Date | Li | Be | B | F | Na | Al | P | K | Ca | Sc |
|---|---|---|---|---|---|---|---|---|---|---|---|---|---|---|
| IA-NS-7 | Granodiorite | IA-NS-7-3.1 | JW510 | Feb. '11 | 0.83 | 0.6 | 0.6 | 56 | 9 | 31 | 1937 | 2.48 | 6 | 66 |
| IA-NS-7 | Granodiorite | IA-NS-7-4.1 | JW510 | Feb. '11 | 0.02 | 0.033 | 0.1 | 7 | 7 | 2 | 267 | 1.59 | 3.16 | 35 |
| IA-NS-7 | Granodiorite | IA-NS-7-4.2 | JW510 | Feb. '11 | 0.15 | 0.3 | 0.1 | 25 | 9 | 2 | 1302 | 3.09 | 2.89 | 40 |
| IA-NS-7 | Granodiorite | IA-NS-7-5.1 | JW510 | Feb. '11 | 0.04 | 5 | 0.4 | 64 | 7 | 2 | 765 | 1.72 | 3.33 | 89 |
| IA-NS-7 | Granodiorite | IA-NS-7-6.1 | JW510 | Feb. '11 | 2 | 1 | 1 | 351 | 87 | 42 | 741 | 337 | 17 | 15 |
| IA-NS-7 | Granodiorite | IA-NS-7-7.1 | JW510 | Feb. '11 | 0.77 | 0.026 | 0.2 | 19 | 58 | 238 | 275 | 22 | 9 | 32 |
| IA-NS-7 | Granodiorite | IA-NS-7-8.1 | JW510 | Feb. '11 | 0.02 | 0.3 | 0.7 | 12 | 8 | 2 | 476 | 1.99 | 3.18 | 43 |
| IA-NS-7 | Granodiorite | IA-NS-7-8.2 | JW510 | Feb. '11 | 0.12 | 2 | 0.5 | 33 | 9 | 2 | 1472 | 2.04 | 6 | 86 |
| IA-NS-7 | Granodiorite | IA-NS-7-9.1 | JW510 | Feb. '11 | 0.11 | 2 | 0.3 | 221 | 33 | 58 | 1587 | 7 | 3.35 | 56 |
| IA-NS-7 | Granodiorite | IA-NS-7-10.1 | JW510 | Feb. '11 | 0.60 | 6 | 3 | 111 | 10 | 3 | 2350 | 2.38 | 3.51 | 84 |
| IA-NS-7 | Granodiorite | IA-NS-7-11.1 | JW510 | Feb. '11 | 0.44 | 0.2 | 0.8 | 75 | 19 | 975 | 459 | 680 | 8 | 45 |
| IA-NS-7 | Granodiorite | IA-NS-7-11.2 | JW510 | Feb. '11 | 0.93 | 2 | 0.7 | 236 | 45 | 281 | 2455 | 129 | 33 | 19 |
| IA-NS-7 | Granodiorite | IA-NS-7-12.1 | JW510 | Feb. '11 | 0.40 | 2 | 0.3 | 82 | 11 | 2 | 1861 | 2.53 | 6 | 104 |
| IA-NS-7 | Granodiorite | IA-NS-7-12.2 | JW510 | Feb. '11 | 0.45 | 0.7 | 0.9 | 71 | 11 | 15 | 1830 | 6 | 4.69 | 78 |
| IA-NS-7 | Granodiorite | IA-NS-7-13.1 | JW510 | Feb. '11 | 0.16 | 0.4 | 0.5 | 131 | 23 | 19 | 1179 | 17 | 7 | 34 |
| IA-NS-7 | Granodiorite | IA-NS-7-13.2 | JW510 | Feb. '11 | 0.05 | 0.3 | 0.4 | 48 | 8 | 2 | 954 | 1.46 | 4.15 | 42 |
| IA-NS-7 | Granodiorite | IA-NS-7-14.1 | JW510 | Feb. '11 | 0.02 | 0.075 | 0.5 | 15 | 8 | 2 | 474 | 1.50 | 3.49 | 26 |
| IA-NS-7 | Granodiorite | IA-NS-7-15.1 | JW510 | Feb. '11 | 0.56 | 5 | 0.8 | 244 | 16 | 3 | 2586 | 3.35 | 13 | 51 |
| IA-NS-7 | Granodiorite | IA-NS-7-16.1 | JW510 | Feb. '11 | 0.0057 | 0.1 | 0.1 | 10 | 9 | 5 | 423 | 2.16 | 4.00 | 42 |
| IA-NS-7 | Granodiorite | IA-NS-7-16.2 | JW510 | Feb. '11 | 0.22 | 0.7 | 0.3 | 180 | 9 | 4 | 2255 | 1.63 | 4.27 | 70 |
| IA-NS-7 | Granodiorite | IA-NS-7-17.1 | JW510 | Feb. '11 | 0.17 | 29 | 0.3 | 109 | 8 | 2 | 2313 | 2.76 | 8 | 100 |
| IA-NS-7 | Granodiorite | IA-NS-7-17.2 | JW510 | Feb. '11 | 0.06 | 3 | 0.3 | 31 | 4 | 2 | 1193 | 1.18 | 2.26 | 61 |
| IA-NS-7 | Granodiorite | IA-NS-7-18.1 | JW510 | Feb. '11 | 0.06 | 0.4 | 0.4 | 18 | 10 | 9 | 977 | 4.31 | 4.65 | 98 |
| IA-NS-7 | Granodiorite | IA-NS-7-19.2 | JW510 | Feb. '11 | 0.03 | 0.4 | 0.086 | 53 | 10 | 3 | 841 | 2.30 | 5.00 | 80 |
| IA-NS-7 | Granodiorite | IA-NS-7-19.1 | JW510 | Feb. '11 | 4 | 0.6 | 0.7 | 146 | 137 | 571 | 1058 | 97 | 10 | 32 |
| IA-NS-9 | HSG | IA-NS-9_01.1 | AJP03 | Jan. '14 | 0.03 | 0.023 | 0.088 | 12 | 8 | 10 | 319 | 1.36 | 3.85 | 10 |
| IA-NS-9 | HSG | IA-NS-9_02.1 | AJP03 | Jan. '14 | 0.13 | 0.6 | 0.1 | 250 | 11 | 14 | 114 | 1.25 | 3.77 | 0.46 |
| IA-NS-9 | HSG | IA-NS-9_04.1 | AJP03 | Jan. '14 | 0.03 | 0.057 | 0.074 | 46 | 7 | 9 | 276 | 0.97 | 2.31 | 8 |
| IA-NS-9 | HSG | IA-NS-9_05.1 | AJP03 | Jan. '14 | 0.03 | 0.043 | 0.053 | 47 | 10 | 10 | 328 | 1.28 | 2.61 | 8 |
| IA-NS-9 | HSG | IA-NS-9_06.1 | AJP03 | Jan. '14 | 0.02 | 0.048 | 0.092 | 46 | 15 | 17 | 240 | 1.63 | 4.35 | 12 |
| IA-NS-9 | HSG | IA-NS-9_07.1 | AJP03 | Jan. '14 | 0.05 | 0.081 | 0.089 | 134 | 20 | 13 | 421 | 1.83 | 3.89 | 9 |

**Appendix B.2**. Continued

| Sample | Rock Type | Grain # | Mount | Date | Li | Be | B | F | Na | Al | P | K | Ca | Sc |
|---|---|---|---|---|---|---|---|---|---|---|---|---|---|---|
| IA-NS-9 | HSG | IA-NS-9_08.1 | AJP03 | Jan. '14 | 0.01 | 0.006 | 0.069 | 16 | 10 | 10 | 161 | 1.10 | 3.46 | 11 |
| IA-NS-9 | HSG | IA-NS-9_09.2 | AJP03 | Jan. '14 | 0.02 | 0.023 | 0.012 | 25 | 9 | 10 | 287 | 4.73 | 2.81 | 8 |
| IA-NS-9 | HSG | IA-NS-9_10.2 | AJP03 | Jan. '14 | 0.08 | 0.028 | 0.078 | 8 | 31 | 17 | 276 | 1.31 | 22 | 10 |
| IA-NS-9 | HSG | IA-NS-9_11.1 | AJP03 | Jan. '14 | 0.05 | 0.2 | 0.067 | 92 | 15 | 12 | 290 | 1.45 | 4.18 | 10 |
| IA-NS-9 | HSG | IA-NS-9_12.2 | AJP03 | Jan. '14 | 0.06 | 0.2 | 0.2 | 32 | 5 | 8 | 387 | 0.70 | 2.15 | 15 |
| IA-NS-9 | HSG | IA-NS-9_13.1 | AJP03 | Jan. '14 | 0.03 | 0.1 | 0.068 | 113 | 9 | 11 | 229 | 2.41 | 3.42 | 7 |
| IA-NS-9 | HSG | IA-NS-9_14.2 | AJP03 | Jan. '14 | 1 | 7 | 0.2 | 570 | 20 | 23 | 645 | 35 | 2.76 | 33 |
| IA-NS-9 | HSG | IA-NS-9_15.1 | AJP03 | Jan. '14 | 0.03 | 0.011 | 0.045 | 23 | 8 | 9 | 230 | 1.21 | 3.84 | 10 |
| IA-NS-9 | HSG | IA-NS-9_16.1 | AJP03 | Jan. '14 | 0.03 | 0.068 | 0.051 | 29 | 12 | 12 | 301 | 1.38 | 3.71 | 11 |
| IA-NS-9 | HSG | IA-NS-9_17.2 | AJP03 | Jan. '14 | 0.37 | 1.0 | 0.1 | 285 | 10 | 20 | 330 | 28 | 4.79 | 1.70 |
| IA-NS-9 | HSG | IA-NS-9_18.1 | AJP03 | Jan. '14 | 0.30 | 1 | 0.2 | 246 | 9 | 11 | 862 | 1.37 | 2.56 | 7 |
| IA-NS-9 | HSG | IA-NS-9_18.2 | AJP03 | Jan. '14 | 0.46 | 2 | 0.2 | 675 | 20 | 33 | 1191 | 20 | 17 | 7 |
| IA-NS-9 | HSG | IA-NS-9_20.1 | AJP03 | Jan. '14 | 0.03 | 0.1 | 0.088 | 94 | 22 | 29 | 271 | 10 | 5 | 12 |
| IA-NS-9 | HSG | IA-NS-9_21.1 | AJP03 | Jan. '14 | 0.38 | 0.4 | 0.2 | 277 | 24 | 14 | 175 | 67 | 5 | 0.48 |
| IA-NS-9 | HSG | IA-NS-9_22.1 | AJP02 | Jan. '14 | 0.0076 | 0.006 | 0.1 | 43 | 4 | 5 | 178 | 2.36 | 2.29 | 9 |
| IA-NS-9 | HSG | IA-NS-9_27 | AJP05 | Feb. '15 | 1.00 | 2 | 1 | 648 | 21 | 24 | 432 | 131 | 11 | 14 |
| IA-NS-9 | HSG | IA-NS-9_29 | AJP05 | Feb. '15 | 1 | 7 | 8 | 1237 | 150 | 136 | 1101 | 2589 | 3.04 | 53 |
| IA-NS-9 | HSG | IA-NS-9_30 | AJP05 | Feb. '15 | 3 | 2 | 4 | 1112 | 299 | 17 | 636 | 1520 | 50 | 16 |
| IA-NS-9 | HSG | IA-NS-9_31 | AJP05 | Feb. '15 | 2 | 13 | 5 | 1868 | 21 | 4 | 1590 | 1.43 | 2.11 | 40 |
| IA-NS-9 | HSG | IA-NS-9_32 | AJP05 | Feb. '15 | 0.46 | 0.2 | 0.2 | 201 | 7 | 7 | 205 | 463 | 7 | 11 |
| IA-NS-9 | HSG | IA-NS-9_33 | AJP05 | Feb. '15 | 0.03 | 0.003 | 0.2 | 18 | 3 | 3 | 238 | 2.09 | 3.30 | 12 |
| IA-NS-9 | HSG | IA-NS-9_34 | AJP05 | Feb. '15 | 0.29 | 0.028 | 0.1 | 43 | 4 | 4 | 296 | 7 | 2.36 | 7 |
| IA-NS-9 | HSG | IA-NS-9_35 | AJP05 | Feb. '15 | 0.07 | 0.3 | 0.1 | 43 | 3 | 3 | 384 | 1.63 | 2.76 | 21 |
| IA-NS-9 | HSG | IA-NS-9_36 | AJP05 | Feb. '15 | 0.0023 | -- | 0.069 | 24 | 3 | 2 | 236 | 1.18 | 2.34 | 13 |
| IA-NS-9 | HSG | IA-NS-9_37 | AJP05 | Feb. '15 | 0.03 | 0.2 | 0.2 | 62 | 10 | 5 | 188 | 3.38 | 2.80 | 9 |
| IA-NS-9 | HSG | IA-NS-9_38 | AJP05 | Feb. '15 | 0.02 | 0.1 | 0.1 | 36 | 2 | 2 | 230 | 1.17 | 1.81 | 10 |
| IA-NS-9 | HSG | IA-NS-9_03.1 | AJP03 | Jan. '14 | 0.34 | 7 | 0.7 | 1096 | 21 | 14 | 1478 | 22 | 4.51 | 39 |
| IA-NS-9 | HSG | IA-NS-9_03.2 | AJP03 | Jan. '14 | 1 | 6 | 2 | 826 | 2924 | 12 | 881 | 638 | 89 | 34 |
| IA-NS-9 | HSG | IA-NS-9_14.1 | AJP03 | Jan. '14 | 96 | 4 | 2 | 2882 | 179 | 477 | 1109 | 1390 | 1180 | 30 |
| IA-NS-9 | HSG | IA-NS-9_17.1 | AJP03 | Jan. '14 | 2 | 1 | 1 | 2293 | 84 | 516 | 1028 | 108 | 146 | 7 |
| IA-NS-9 | HSG | IA-NS-9_19.1 | AJP03 | Jan. '14 | 3 | 64 | 1 | 3671 | 1079 | 207 | 628 | 379 | 414 | 0.05 |

**Appendix B.2**. Continued

| Sample | Rock Type | Grain # | Mount | Date | Li | Be | B | F | Na | Al | P | K | Ca | Sc |
|---|---|---|---|---|---|---|---|---|---|---|---|---|---|---|
| IA-NS-9 | HSG | IA-NS-9_19.2 | AJP03 | Jan. '14 | 5 | 20 | 18 | 3132 | 1083 | 229 | 1024 | 663 | 463 | 0.05 |
| IA-NS-9 | HSG | IA-NS-9_21.2 | AJP03 | Jan. '14 | 7 | 0.3 | 0.2 | 1075 | 2070 | 111 | 704 | 1352 | 149 | 10 |
| IA-NS-9 | HSG | IA-NS-9_25 | AJP05 | Feb. '15 | 5 | 5 | 2 | 1921 | 42 | 11 | 545 | 143 | 333 | 33 |
| IA-NS-9 | HSG | IA-NS-9_26 | AJP05 | Feb. '15 | 5 | 5 | 2 | 7914 | 71 | 82 | 741 | 1288 | 1283 | 29 |
| IA-NS-9 | HSG | IA-NS-9_28 | AJP05 | Feb. '15 | 3 | 3 | 3 | 4143 | 278 | 9 | 963 | 789 | 892 | 4.98 |
| IA-NS-10 | HSG | IA-NS-10_1.1 | AJP05 | Feb. '15 | 0.13 | 8 | 0.2 | 122 | 4 | 3 | 1151 | 1.84 | 3.11 | 39 |
| IA-NS-10 | HSG | IA-NS-10_3.1 | AJP05 | Feb. '15 | 0.02 | 0.062 | 0.4 | 36 | 28 | 17 | 294 | 87 | 5 | 10 |
| IA-NS-10 | HSG | IA-NS-10_4.1 | AJP05 | Feb. '15 | 0.0098 | -- | 0.1 | 24 | 3 | 4 | 217 | 1.31 | 3.04 | 10 |
| IA-NS-10 | HSG | IA-NS-10_5.1 | AJP05 | Feb. '15 | 0.01 | 0.025 | 0.2 | 19 | 4 | 4 | 310 | 2.52 | 4.03 | 12 |
| IA-NS-10 | HSG | IA-NS-10_6.1 | AJP05 | Feb. '15 | 0.01 | 0.040 | 0.3 | 25 | 4 | 3 | 434 | 1.82 | 4.15 | 28 |
| IA-NS-10 | HSG | IA-NS-10_7.1 | AJP05 | Feb. '15 | 0.17 | 4 | 0.6 | 539 | 38 | 147 | 619 | 27 | 16 | 13 |
| IA-NS-10 | HSG | IA-NS-10_8.1 | AJP05 | Feb. '15 | 0.0092 | 0.4 | 0.3 | 38 | 3 | 5 | 162 | 6 | 3.77 | 15 |
| IA-NS-10 | HSG | IA-NS-10_9.1 | AJP05 | Feb. '15 | 0.03 | 0.2 | 0.2 | 33 | 3 | 3 | 216 | 3.11 | 3.22 | 9 |
| IA-NS-10 | HSG | IA-NS-10_10.1 | AJP05 | Feb. '15 | 0.02 | 0.3 | 0.2 | 45 | 5 | 4 | 203 | 17 | 3.54 | 7 |
| IA-NS-10 | HSG | IA-NS-10_11.1 | AJP05 | Feb. '15 | 0.01 | -- | 0.085 | 18 | 3 | 3 | 250 | 1.86 | 2.90 | 12 |
| IA-NS-10 | HSG | IA-NS-10_12.1 | AJP05 | Feb. '15 | 0.0086 | 0.017 | 0.099 | 17 | 2 | 2 | 218 | 1.84 | 2.57 | 11 |
| IA-NS-10 | HSG | IA-NS-10_13.1 | AJP05 | Feb. '15 | 0.02 | 0.060 | 0.3 | 543 | 32 | 12 | 349 | 24 | 13 | 11 |
| IA-NS-10 | HSG | IA-NS-10_14.1 | AJP05 | Feb. '15 | 0.02 | 0.015 | 0.1 | 21 | 3 | 4 | 402 | 1.92 | 3.14 | 37 |
| IA-NS-10 | HSG | IA-NS-10_16.1 | AJP05 | Feb. '15 | 0.0083 | 0.006 | 0.069 | 31 | 3 | 3 | 207 | 1.94 | 2.49 | 9 |
| IA-NS-10 | HSG | IA-NS-10_17.1 | AJP05 | Feb. '15 | 0.0081 | 0.006 | 0.1 | 11 | 2 | 3 | 271 | 1.10 | 1.95 | 10 |
| IA-NS-10 | HSG | IA-NS-10_18.1 | AJP05 | Feb. '15 | 0.02 | 0.2 | 0.048 | 27 | 2 | 3 | 331 | 1.53 | 2.57 | 27 |
| IA-NS-10 | HSG | IA-NS-10_19.1 | AJP05 | Feb. '15 | 0.04 | 0.083 | 0.2 | 16 | 4 | 4 | 358 | 1.91 | 3.61 | 18 |
| IA-NS-10 | HSG | IA-NS-10_20.1 | AJP05 | Feb. '15 | 0.0097 | 0.007 | 0.2 | 86 | 18 | 24 | 240 | 17 | 12 | 16 |
| IA-NS-10 | HSG | IA-NS-10_21.1 | AJP05 | Feb. '15 | 0.0057 | -- | 0.2 | 120 | 9 | 15 | 290 | 13 | 8 | 13 |
| IA-NS-10 | HSG | IA-NS-10_22.1 | AJP05 | Feb. '15 | 0.01 | 0.024 | 0.2 | 121 | 5 | 4 | 292 | 5 | 3.13 | 11 |
| IA-NS-10 | HSG | IA-NS-10_23.1 | AJP05 | Feb. '15 | 0.0025 | 0.013 | 0.092 | 44 | 2 | 4 | 178 | 1.73 | 2.47 | 12 |
| IA-NS-10 | HSG | IA-NS-10_24.1 | AJP05 | Feb. '15 | 0.02 | -- | 0.2 | 36 | 6 | 4 | 223 | 7 | 3.83 | 11 |
| IA-NS-12 | Granophyre | IA-NS-12_4.1 | AJP05 | Feb. '15 | 0.18 | 0.1 | 0.5 | 36 | 3 | 4 | 645 | 2.44 | 3.28 | 40 |
| IA-NS-12 | Granophyre | IA-NS-12_6.1 | AJP05 | Feb. '15 | 0.02 | 0.005 | 0.1 | 18 | 3 | 4 | 200 | 2.03 | 3.58 | 11 |
| IA-NS-12 | Granophyre | IA-NS-12_8.1 | AJP05 | Feb. '15 | 0.01 | 0.009 | 0.1 | 28 | 3 | 3 | 222 | 1.80 | 3.06 | 10 |
| IA-NS-12 | Granophyre | IA-NS-12_10.1 | AJP05 | Feb. '15 | 0.02 | 0.018 | 0.3 | 163 | 23 | 12 | 210 | 7 | 8 | 13 |

**Appendix B.2**. Continued

| Sample | Rock Type | Grain # | Mount | Date | Li | Be | B | F | Na | Al | P | K | Ca | Sc |
|---|---|---|---|---|---|---|---|---|---|---|---|---|---|---|
| IA-NS-12 | Granophyre | IA-NS-12_11.1 | AJP05 | Feb. '15 | 0.03 | 0.003 | 0.2 | 23 | 3 | 4 | 263 | 1.53 | 2.77 | 26 |
| IA-NS-12 | Granophyre | IA-NS-12_12.1 | AJP05 | Feb. '15 | 0.26 | 5 | 3 | 92 | 6 | 12 | 786 | 4.66 | 3.59 | 47 |
| IA-NS-12 | Granophyre | IA-NS-12_13.1 | AJP05 | Feb. '15 | 0.02 | 0.037 | 0.2 | 43 | 3 | 4 | 239 | 1.42 | 3.52 | 26 |
| IA-NS-12 | Granophyre | IA-NS-12_14.1 | AJP05 | Feb. '15 | 0.04 | 0.007 | 0.2 | 42 | 4 | 6 | 263 | 2.39 | 3.07 | 12 |
| IA-NS-12 | Granophyre | IA-NS-12_15.1 | AJP05 | Feb. '15 | 0.07 | 0.041 | 0.4 | 41 | 14 | 9 | 419 | 3.88 | 3.03 | 20 |
| IA-NS-12 | Granophyre | IA-NS-12_16.1 | AJP05 | Feb. '15 | 0.03 | 0.034 | 0.4 | 232 | 19 | 12 | 267 | 65 | 13 | 13 |
| IA-NS-12 | Granophyre | IA-NS-12_17.1 | AJP05 | Feb. '15 | 0.01 | 0.003 | 0.1 | 16 | 4 | 4 | 233 | 1.85 | 3.04 | 14 |
| IA-NS-12 | Granophyre | IA-NS-12_18.1 | AJP05 | Feb. '15 | 0.02 | 0.019 | 0.2 | 43 | 4 | 5 | 262 | 2.68 | 4.10 | 16 |
| IA-NS-12 | Granophyre | IA-NS-12_19.1 | AJP05 | Feb. '15 | 0.01 | 0.018 | 0.2 | 24 | 6 | 5 | 216 | 1.98 | 4.44 | 14 |
| IA-NS-12 | Granophyre | IA-NS-12_20.1 | AJP05 | Feb. '15 | 0.05 | 0.1 | 0.1 | 78 | 4 | 3 | 427 | 1.98 | 2.81 | 10 |
| IA-NS-12 | Granophyre | IA-NS-12_21.1 | AJP05 | Feb. '15 | 0.02 | 0.014 | 0.2 | 21 | 7 | 5 | 274 | 3.16 | 3.45 | 17 |
| IA-NS-12 | Granophyre | IA-NS-12_22.1 | AJP05 | Feb. '15 | 0.0069 | -- | 0.069 | 15 | 7 | 4 | 258 | 2.71 | 4.15 | 12 |
| IA-NS-12 | Granophyre | IA-NS-12_23.1 | AJP05 | Feb. '15 | 0.24 | 0.007 | 0.2 | 13 | 6 | 4 | 273 | 3.96 | 4.02 | 13 |
| IA-NS-12 | Granophyre | IA-NS-12_24.1 | AJP05 | Feb. '15 | 0.02 | 0.013 | 0.2 | 21 | 3 | 3 | 270 | 2.19 | 2.60 | 12 |
| IA-NS-12 | Granophyre | IA-NS-12_25.1 | AJP05 | Feb. '15 | 0.02 | 0.009 | 0.6 | 241 | 15 | 9 | 330 | 40 | 8 | 18 |
| IA-NS-12 | Granophyre | IA-NS-12_26.1 | AJP05 | Feb. '15 | 0.02 | 0.033 | 0.5 | 758 | 24 | 8 | 426 | 14 | 10 | 12 |
| IA-NS-12 | Granophyre | IA-NS-12_27.1 | AJP05 | Feb. '15 | 0.02 | 0.054 | 0.064 | 32 | 4 | 3 | 284 | 2.02 | 2.36 | 30 |
| IA-NS-12 | Granophyre | IA-NS-12_1.1 | AJP05 | Feb. '15 | 9 | 3 | 2 | 3855 | 333 | 134 | 789 | 2129 | 637 | 11 |
| IA-NS-12 | Granophyre | IA-NS-12_3.1 | AJP05 | Feb. '15 | 0.03 | 0.031 | 0.098 | 424 | 7 | 4 | 469 | 2.11 | 259 | 19 |
| IA-NS-12 | Granophyre | IA-NS-12_9.1 | AJP05 | Feb. '15 | 0.65 | 37 | 1 | 2687 | 41 | 52 | 1023 | 856 | 170 | 9 |
| IA-G-1 | Gabbro | IA-G-1-1.1 | JW510 | Feb. '11 | 0.0096 | -- | 0.035 | 7 | 8 | 5 | 298 | 1.72 | 3.77 | 23 |
| IA-G-1 | Gabbro | IA-G-1-2.1 | JW510 | Feb. '11 | 0.0014 | -- | 0.047 | 8 | 7 | 4 | 303 | 1.85 | 6 | 18 |
| IA-G-1 | Gabbro | IA-G-1-3.1 | JW510 | Feb. '11 | -- | -- | 0.1 | 11 | 8 | 3 | 321 | 1.79 | 2.50 | 37 |
| IA-G-1 | Gabbro | IA-G-1-4.1 | JW510 | Feb. '11 | 0.04 | 0.008 | 0.1 | 26 | 7 | 2 | 514 | 2.11 | 3.80 | 18 |
| IA-G-1 | Gabbro | IA-G-1-5.1 | JW510 | Feb. '11 | 0.02 | 0.004 | 0.080 | 9 | 8 | 4 | 270 | 1.94 | 3.69 | 24 |
| IA-G-1 | Gabbro | IA-G-1-6.1 | JW510 | Feb. '11 | 0.0040 | -- | 0.045 | 7 | 7 | 10 | 250 | 1.60 | 5 | 23 |
| IA-G-1 | Gabbro | IA-G-1-6.2 | JW510 | Feb. '11 | 0.0054 | -- | 0.080 | 8 | 7 | 3 | 209 | 1.81 | 3.05 | 19 |
| IA-G-1 | Gabbro | IA-G-1-7.1 | JW510 | Feb. '11 | 0.01 | -- | 0.1 | 11 | 6 | 2 | 301 | 1.90 | 4.28 | 20 |
| IA-G-1 | Gabbro | IA-G-1-8.1 | JW510 | Feb. '11 | 0.01 | 0.012 | 0.092 | 10 | 9 | 4 | 315 | 2.17 | 12 | 21 |
| IA-G-1 | Gabbro | IA-G-1-9.1 | JW510 | Feb. '11 | 0.0014 | 0.004 | 0.058 | 10 | 6 | 2 | 298 | 1.45 | 2.78 | 29 |
| IA-G-1 | Gabbro | IA-G-1-10.1 | JW510 | Feb. '11 | 0.03 | 0.004 | 0.068 | 12 | 7 | 2 | 328 | 2.13 | 3.89 | 19 |

**Appendix B.2**. Continued

| Sample | Rock Type | Grain # | Mount | Date | Li | Be | B | F | Na | Al | P | K | Ca | Sc |
|---|---|---|---|---|---|---|---|---|---|---|---|---|---|---|
| IA-G-1 | Gabbro | IA-G-1-11.1 | JW510 | Feb. '11 | 0.0027 | 0.051 | 0.070 | 10 | 6 | 5 | 390 | 1.66 | 3.55 | 21 |
| IA-G-1 | Gabbro | IA-G-1-12.1 | JW510 | Feb. '11 | 0.0028 | -- | 0.048 | 12 | 7 | 3 | 693 | 1.93 | 4.91 | 28 |
| IA-G-1 | Gabbro | IA-G-1-13.1 | JW510 | Feb. '11 | 0.0014 | 0.012 | 0.1 | 8 | 6 | 2 | 229 | 1.77 | 3.73 | 20 |
| IA-G-1 | Gabbro | IA-G-1-14.1 | JW510 | Feb. '11 | 0.0066 | 0.008 | 0.078 | 9 | 7 | 6 | 602 | 2.16 | 3.69 | 44 |
| IA-G-1 | Gabbro | IA-G-1-15.1 | JW510 | Feb. '11 | 0.0041 | -- | 0.035 | 4 | 1 | 0.9 | 250 | 0.47 | 0.74 | 19 |
| IA-G-1 | Gabbro | IA-G-1-16.1 | JW510 | Feb. '11 | -- | 0.011 | -- | 8 | 7 | 22 | 217 | 1.75 | 2.66 | 25 |
| IA-G-1 | Gabbro | IA-G-1-17.1 | JW510 | Feb. '11 | 0.01 | 0.004 | 0.1 | 12 | 9 | 2 | 747 | 1.63 | 3.03 | 31 |
| IA-G-1 | Gabbro | IA-G-1-18.1 | JW510 | Feb. '11 | 0.0024 | 0.003 | 0.020 | 21 | 3 | 1 | 680 | 0.71 | 1.32 | 19 |
| IA-G-1 | Gabbro | IA-G-1-19.1 | JW510 | Feb. '11 | -- | 0.003 | 0.072 | 9 | 11 | 7 | 350 | 4.00 | 2.93 | 20 |
| IA-G-1 | Gabbro | IA-G-1-20.1 | JW510 | Feb. '11 | 0.0023 | 0.003 | 0.1 | 8 | 8 | 3 | 243 | 1.84 | 2.69 | 20 |
| IA-G-1 | Gabbro | IA-G-1-21.1 | JW510 | Feb. '11 | 0.02 | -- | 0.1 | 10 | 10 | 4 | 284 | 2.45 | 2.37 | 21 |
| IA-G-1 | Gabbro | IA-G-1-22.1 | JW510 | Feb. '11 | 0.16 | 0.038 | 0.091 | 8 | 6 | 7 | 891 | 1.31 | 1.80 | 78 |
| IA-G-1 | Gabbro | IA-G-1-22.2 | JW510 | Feb. '11 | 0.14 | 0.2 | 0.1 | 23 | 8 | 3 | 919 | 1.81 | 3.60 | 58 |
| IA-G-1 | Gabbro | IA-G-1-23.1 | JW510 | Feb. '11 | 0.06 | 0.021 | 0.2 | 16 | 6 | 3 | 608 | 1.57 | 3.06 | 21 |
| IA-G-1 | Gabbro | IA-G-1-24.1 | JW510 | Feb. '11 | 0.0095 | 0.014 | 0.091 | 10 | 8 | 3 | 285 | 1.55 | 2.51 | 19 |
| IA-G-1 | Gabbro | IA-G-1-24.2 | JW510 | Feb. '11 | 0.11 | 0.059 | 0.1 | 12 | 7 | 2 | 897 | 1.52 | 2.73 | 56 |
| IA-G-1 | Gabbro | IA-G-1-25.1 | JW510 | Feb. '11 | 0.03 | 0.031 | 0.1 | 13 | 13 | 8 | 318 | 3.49 | 6 | 23 |
| IA-G-1 | Gabbro | IA-G-1-26.1 | JW510 | Feb. '11 | 0.03 | 0.003 | 0.2 | 10 | 10 | 2 | 677 | 2.23 | 3.46 | 53 |
| IA-G-1 | Gabbro | IA-G-1-27.1 | JW510 | Feb. '11 | 0.02 | 0.044 | 0.1 | 13 | 12 | 6 | 289 | 2.10 | 3.97 | 24 |
| IA-G-5 | Gabbro | IA-G-5-2.1 | AJP01 | May '13 | | | | | | | | | | 88 |
| IA-G-5 | Gabbro | IA-G-5-4.1 | AJP01 | May '13 | | | | | | | | | | 91 |
| IA-G-5 | Gabbro | IA-G-5-6.1 | AJP01 | May '13 | | | | | | | | | | 75 |
| IA-G-5 | Gabbro | IA-G-5-7.1 | AJP01 | May '13 | | | | | | | | | | 45 |
| IA-G-5 | Gabbro | IA-G-5_8.1 | AJP02 | Jan. '14 | 0.05 | 0.015 | 0.6 | 11 | 3 | 5 | 1667 | 1.31 | 1.15 | 99 |
| IA-G-5 | Gabbro | IA-G-5_9.1 | AJP02 | Jan. '14 | 0.06 | 0.016 | 0.8 | 83 | 10 | 41 | 1652 | 15 | 5 | 86 |
| IA-G-5 | Gabbro | IA-G-5_10.1 | AJP03 | Jan. '14 | 0.02 | 0.012 | 0.2 | 4 | 12 | 9 | 861 | 1.72 | 4.92 | 33 |
| IA-G-5 | Gabbro | IA-G-5_11.1 | AJP03 | Jan. '14 | 0.0096 | 0.019 | 0.2 | 10 | 9 | 9 | 1376 | 1.86 | 4.31 | 60 |
| IA-G-5 | Gabbro | IA-G-5_12.1 | AJP03 | Jan. '14 | 0.0099 | 0.017 | 0.2 | 8 | 7 | 9 | 1075 | 1.00 | 2.32 | 58 |
| IA-G-5 | Gabbro | IA-G-5_13.1 | AJP03 | Jan. '14 | 0.01 | 0.019 | 0.8 | 11 | 7 | 8 | 1743 | 0.76 | 2.38 | 88 |
| IA-G-5 | Gabbro | IA-G-5_14.1 | AJP03 | Jan. '14 | 0.02 | 0.009 | 0.2 | 10 | 10 | 11 | 1663 | 1.90 | 2.81 | 78 |

**Appendix B.3**. Zircon Trace Element Compositions (ppm), measured *in situ* by SHRIMP-RG (Atomic Numbers 22-71)

| **Sample**[37] | **Grain #** | **Ti** | **Fe** | **Y** | **Nb** | **La** | **Ce** | **Nd** | **Sm** | **Eu** | **Gd** | **Tb** | **Dy** | **Ho** | **Er** | **Tm** | **Yb** | **Lu** |
|---|---|---|---|---|---|---|---|---|---|---|---|---|---|---|---|---|---|---|
| IA-NS-2 | IA-NS-2-1.1 | 9 | 0.36 | 851 | 5 | 0.02 | 12 | 0.5 | 1.92 | 0.50 | 21 | 8 | 90 | 36 | 165 | 33 | 259 | 45 |
| IA-NS-2 | IA-NS-2-2.1 | 24 | 0.27 | 2260 | 6 | 0.06 | 9 | 4.0 | 10 | 3.97 | 87 | 28 | 282 | 98 | 392 | 73 | 566 | 95 |
| IA-NS-2 | IA-NS-2-3.1 | 9 | 0.34 | 7733 | 108 | 0.09 | 150 | 9 | 23 | 3.66 | 217 | 76 | 836 | 321 | 1334 | 256 | 1954 | 312 |
| IA-NS-2 | IA-NS-2-4.1 | 9 | 0.86 | 1849 | 28 | 0.04 | 31 | 2.3 | 6 | 1.98 | 59 | 20 | 220 | 80 | 318 | 61 | 433 | 68 |
| IA-NS-2 | IA-NS-2-4.2 | 7 | 0.43 | 2888 | 15 | 0.04 | 21 | 4.8 | 10 | 2.78 | 95 | 32 | 346 | 127 | 512 | 90 | 651 | 104 |
| IA-NS-2 | IA-NS-2-4.3 | 6 | 0.48 | 2743 | 87 | 0.02 | 56 | 1.9 | 7 | 1.38 | 72 | 28 | 309 | 115 | 482 | 91 | 649 | 98 |
| IA-NS-2 | IA-NS-2-5.1 | 14 | 0.41 | 12914 | 51 | 0.27 | 201 | 31 | 70 | 7 | 537 | 166 | 1613 | 540 | 2020 | 370 | 2602 | 393 |
| IA-NS-2 | IA-NS-2-5.2 | 6 | 0.33 | 2826 | 36 | 0.02 | 46 | 2.7 | 8 | 1.84 | 80 | 28 | 311 | 116 | 477 | 89 | 626 | 99 |
| IA-NS-2 | IA-NS-2-6.1 | 11 | 0.37 | 5963 | 224 | 0.04 | 290 | 7 | 19 | 3.82 | 194 | 65 | 693 | 262 | 1002 | 189 | 1347 | 211 |
| IA-NS-2 | IA-NS-2-7.1 | 15 | 0.37 | 945 | 10 | 0.01 | 12 | 1.0 | 2.70 | 1.18 | 26 | 9 | 101 | 40 | 172 | 34 | 256 | 44 |
| IA-NS-2 | IA-NS-2-8.1 | 14 | 3.76 | 6280 | 206 | 0.32 | 280 | 8 | 21 | 3.92 | 203 | 68 | 737 | 274 | 1097 | 207 | 1521 | 238 |
| IA-NS-2 | IA-NS-2-9.1 | 11 | 0.21 | 4419 | 95 | 0.02 | 151 | 4.2 | 13 | 2.66 | 129 | 46 | 505 | 187 | 763 | 147 | 1083 | 175 |
| IA-NS-2 | IA-NS-2-10.1 | 10 | 4.19 | 4905 | 64 | 0.02 | 178 | 4.3 | 12 | 1.46 | 120 | 43 | 488 | 196 | 849 | 175 | 1372 | 224 |
| IA-NS-2 | IA-NS-2-10.2 | 6 | 0.30 | 6891 | 24 | 0.08 | 100 | 9 | 20 | 2.43 | 189 | 65 | 742 | 282 | 1224 | 246 | 1878 | 311 |
| IA-NS-2 | IA-NS-2-11.1 | 6 | 0.28 | 4072 | 27 | 0.06 | 36 | 6 | 14 | 3.47 | 137 | 46 | 495 | 182 | 715 | 126 | 885 | 139 |
| IA-NS-2 | IA-NS-2-11.2 | 10 | 16 | 5074 | 299 | 0.29 | 151 | 3.7 | 11 | 1.58 | 116 | 45 | 526 | 208 | 862 | 170 | 1283 | 200 |
| IA-NS-2 | IA-NS-2-12.1 | 8 | 0.35 | 3277 | 24 | 0.06 | 29 | 4.3 | 10 | 2.92 | 107 | 35 | 374 | 141 | 560 | 101 | 695 | 111 |
| IA-NS-2 | IA-NS-2-12.2 | 7 | 2.62 | 4548 | 31 | 0.07 | 39 | 6 | 16 | 4.28 | 161 | 52 | 557 | 203 | 792 | 141 | 1003 | 154 |
| IA-NS-2 | IA-NS-2-13.1 | 11 | 19 | 7074 | 106 | 0.86 | 141 | 12 | 29 | 8 | 267 | 83 | 859 | 305 | 1146 | 201 | 1423 | 215 |
| IA-NS-2 | IA-NS-2-14.1 | 9 | 9 | 3713 | 130 | 0.22 | 96 | 3.1 | 10 | 1.86 | 100 | 36 | 410 | 157 | 615 | 119 | 844 | 128 |
| IA-NS-2 | IA-NS-2-14.2 | 7 | 0.50 | 7361 | 78 | 0.08 | 117 | 10 | 28 | 6 | 268 | 90 | 960 | 349 | 1371 | 244 | 1698 | 253 |
| IA-NS-2 | IA-NS-2-15.1 | 10 | 0.41 | 4519 | 67 | 0.04 | 85 | 7 | 16 | 4.88 | 160 | 55 | 548 | 199 | 781 | 137 | 965 | 145 |
| IA-NS-2 | IA-NS-2-15.2 | 8 | 0.39 | 1652 | 40 | 0.03 | 36 | 1.7 | 4.58 | 1.11 | 47 | 17 | 186 | 71 | 287 | 56 | 408 | 66 |
| IA-NS-2 | IA-NS-2-16.1 | 7 | 0.58 | 1398 | 40 | 0.23 | 25 | 1.4 | 3.68 | 0.86 | 38 | 14 | 156 | 59 | 260 | 51 | 384 | 64 |
| IA-NS-2 | IA-NS-2-16.2 | 10 | 4.30 | 3570 | 29 | 0.57 | 34 | 5 | 12 | 3.42 | 123 | 41 | 436 | 159 | 632 | 113 | 786 | 120 |
| IA-NS-2 | IA-NS-2-17.1 | 7 | 0.33 | 1942 | 46 | 0.02 | 43 | 2.1 | 6 | 1.31 | 56 | 20 | 226 | 84 | 343 | 65 | 470 | 73 |
| IA-NS-2 | IA-NS-2-17.2 | 8 | 0.44 | 13749 | 145 | 0.18 | 301 | 26 | 60 | 9 | 533 | 170 | 1775 | 625 | 2362 | 421 | 2920 | 432 |
| IA-NS-2 | IA-NS-2-18.1 | 6 | 0.27 | 4383 | 32 | 0.03 | 45 | 7 | 14 | 3.73 | 151 | 50 | 533 | 198 | 769 | 138 | 955 | 151 |
| IA-NS-2 | IA-NS-2-18.2 | 7 | 0.31 | 2989 | 78 | 0.03 | 74 | 3.0 | 8 | 1.88 | 87 | 32 | 358 | 130 | 537 | 98 | 726 | 112 |

---

[37] See **Appendix B.2** for mount names and analysis dates

**Appendix B.3**. Continued

| Sample | Grain # | Ti | Fe | Y | Nb | La | Ce | Nd | Sm | Eu | Gd | Tb | Dy | Ho | Er | Tm | Yb | Lu |
|---|---|---|---|---|---|---|---|---|---|---|---|---|---|---|---|---|---|---|
| IA-NS-2 | IA-NS-2-19.1 | 7 | 0.45 | 2701 | 63 | 0.03 | 62 | 2.9 | 7 | 1.78 | 74 | 27 | 305 | 115 | 463 | 88 | 627 | 96 |
| IA-NS-2 | IA-NS-2-19.2 | 6 | 0.86 | 5784 | 49 | 0.25 | 64 | 8 | 19 | 4.24 | 190 | 65 | 704 | 256 | 1009 | 180 | 1232 | 190 |
| IA-NS-2 | IA-NS-2-20.1 | 7 | 7 | 4165 | 27 | 0.10 | 33 | 6 | 15 | 3.90 | 142 | 49 | 518 | 184 | 727 | 131 | 920 | 144 |
| IA-NS-2 | IA-NS-2-21.2 | 8 | 10 | 4490 | 36 | 0.08 | 50 | 7 | 16 | 4.19 | 159 | 51 | 556 | 199 | 765 | 138 | 972 | 151 |
| IA-NS-2 | IA-NS-2-22.1 | 9 | 0.25 | 1829 | 7 | 0.02 | 12 | 3.8 | 8 | 2.88 | 68 | 22 | 229 | 84 | 332 | 59 | 413 | 67 |
| IA-NS-2 | IA-NS-2-23.1 | 7 | 0.26 | 1729 | 28 | 0.04 | 32 | 2.0 | 5 | 1.53 | 51 | 18 | 198 | 77 | 307 | 57 | 414 | 68 |
| IA-NS-2 | IA-NS-2-24.1 | 7 | 0.46 | 2990 | 16 | 0.07 | 22 | 4.8 | 10 | 2.83 | 96 | 33 | 355 | 132 | 519 | 94 | 669 | 105 |
| IA-NS-2 | IA-NS-2-24.2 | 11 | 0.23 | 5570 | 151 | 0.04 | 171 | 6 | 16 | 2.54 | 171 | 63 | 684 | 242 | 998 | 184 | 1338 | 209 |
| IA-NS-2 | IA-NS-2-25.2 | 6 | 6 | 3045 | 146 | 1.00 | 68 | 2.6 | 6 | 0.90 | 68 | 28 | 335 | 129 | 567 | 109 | 826 | 130 |
| IA-NS-2 | IA-NS-2-21.1 | 6 | 2.13 | 3478 | 89 | 31 | 184 | 45 | 21 | 2.71 | 116 | 38 | 404 | 144 | 580 | 107 | 761 | 117 |
| IA-NS-2 | IA-NS-2-23.2 | 13 | 3.35 | 11495 | 312 | 44 | 502 | 73 | 63 | 12 | 463 | 144 | 1449 | 508 | 1898 | 333 | 2308 | 341 |
| IA-NS-2 | IA-NS-2-25.1 | -- | 384 | 11923 | 275 | 27 | 554 | 57 | 56 | 10 | 433 | 140 | 1467 | 522 | 2042 | 374 | 2715 | 418 |
| IA-NS-4b | IA-NS-4b-1.1 | 5 | 3.22 | 5457 | 300 | 1.2 | 50 | 26 | 49 | 1.15 | 274 | 119 | 1241 | 401 | 1593 | 325 | 2353 | 308 |
| IA-NS-4b | IA-NS-4b-1.2 | -- | 9 | 12779 | 3272 | 2.2 | 418 | 123 | 183 | 4.36 | 880 | 317 | 3056 | 921 | 3218 | 601 | 3947 | 492 |
| IA-NS-4b | IA-NS-4b-2.1 | 8 | 0.36 | 3046 | 15 | 0.04 | 20 | 5 | 12 | 4.48 | 117 | 37 | 383 | 137 | 536 | 95 | 670 | 107 |
| IA-NS-4b | IA-NS-4b-4.1 | 2.6 | 5 | 4156 | 643 | 1.8 | 111 | 4.8 | 17 | 0.70 | 159 | 80 | 988 | 355 | 1545 | 339 | 2665 | 368 |
| IA-NS-4b | IA-NS-4b-6.1 | 12 | 0.27 | 1132 | 11 | 0.02 | 7 | 1.4 | 3.61 | 1.59 | 34 | 11 | 122 | 47 | 199 | 39 | 302 | 51 |
| IA-NS-4b | IA-NS-4b-7.1 | 3.0 | 1.22 | 15985 | 1087 | 0.29 | 385 | 41 | 116 | 3.70 | 777 | 370 | 4015 | 1274 | 4840 | 977 | 7140 | 924 |
| IA-NS-4b | IA-NS-4b-9.1 | 3.9 | 0.55 | 3008 | 497 | 0.03 | 82 | 2.8 | 12 | 0.66 | 114 | 62 | 771 | 283 | 1322 | 310 | 2554 | 376 |
| IA-NS-4b | IA-NS-4b-9.2 | 6 | 2.10 | 5422 | 634 | 0.25 | 96 | 8 | 25 | 0.86 | 198 | 102 | 1245 | 467 | 2052 | 469 | 3720 | 535 |
| IA-NS-4b | IA-NS-4b-10.1 | 10 | 0.25 | 3731 | 97 | 0.02 | 94 | 4.2 | 12 | 2.15 | 123 | 44 | 462 | 166 | 664 | 128 | 926 | 146 |
| IA-NS-4b | IA-NS-4b-11.1 | 8 | 0.28 | 5777 | 40 | 0.07 | 58 | 9 | 22 | 7 | 219 | 70 | 734 | 255 | 990 | 176 | 1191 | 185 |
| IA-NS-4b | IA-NS-4b-12.1 | 6 | 2.15 | 9637 | 329 | 0.51 | 129 | 51 | 107 | 2.85 | 575 | 228 | 2283 | 705 | 2616 | 524 | 3769 | 488 |
| IA-NS-4b | IA-NS-4b-14.1 | 7 | 1.30 | 7907 | 905 | 0.22 | 145 | 31 | 75 | 1.79 | 443 | 176 | 1750 | 532 | 1978 | 376 | 2619 | 333 |
| IA-NS-4b | IA-NS-4b-15.1 | 12 | 2.30 | 14492 | 1373 | 0.18 | 951 | 15 | 46 | 15 | 452 | 163 | 1777 | 625 | 2297 | 407 | 2675 | 354 |
| IA-NS-4b | IA-NS-4b-18.1 | 3.2 | 1.08 | 5826 | 449 | 0.20 | 94 | 9 | 28 | 1.13 | 224 | 115 | 1417 | 510 | 2243 | 504 | 3955 | 566 |
| IA-NS-4b | IA-NS-4b-19.1 | 8 | 0.24 | 1991 | 7 | 0.03 | 12 | 3.6 | 8 | 2.80 | 67 | 22 | 239 | 89 | 343 | 62 | 435 | 70 |
| IA-NS-4b | IA-NS-4b-20.1 | 8 | 0.37 | 2595 | 11 | 0.04 | 14 | 4.0 | 9 | 3.00 | 84 | 29 | 297 | 108 | 436 | 79 | 544 | 87 |
| IA-NS-4b | IA-NS-4b-22.1 | 1.9 | 15 | 1291 | 191 | 0.21 | 35 | 0.9 | 3.31 | 0.22 | 33 | 18 | 250 | 111 | 516 | 125 | 1044 | 169 |
| IA-NS-4b | IA-NS-4b-23.1 | 2.5 | 0.85 | 4753 | 316 | 0.10 | 90 | 6 | 22 | 0.88 | 187 | 94 | 1179 | 450 | 2005 | 465 | 3736 | 556 |
| IA-NS-4b | IA-NS-4b-23.2 | 2.3 | 0.51 | 9885 | 651 | 0.08 | 213 | 17 | 54 | 1.91 | 419 | 203 | 2405 | 834 | 3473 | 738 | 5624 | 771 |

**Appendix B.3**. Continued

| Sample | Grain # | Ti | Fe | Y | Nb | La | Ce | Nd | Sm | Eu | Gd | Tb | Dy | Ho | Er | Tm | Yb | Lu |
|---|---|---|---|---|---|---|---|---|---|---|---|---|---|---|---|---|---|---|
| IA-NS-4b | IA-NS-4b-24.1 | 11 | 0.30 | 2532 | 10 | 0.07 | 13 | 4.3 | 10 | 2.81 | 89 | 31 | 324 | 117 | 472 | 86 | 626 | 103 |
| IA-NS-4b | IA-NS-4b-25.1 | 5 | 4.09 | 9612 | 505 | 0.93 | 132 | 60 | 119 | 2.79 | 596 | 233 | 2249 | 627 | 2287 | 441 | 3109 | 393 |
| IA-NS-4b | IA-NS-4b-25.2 | 7 | 2.08 | 9209 | 491 | 0.35 | 107 | 33 | 76 | 2.24 | 461 | 197 | 2059 | 673 | 2572 | 528 | 3783 | 505 |
| IA-NS-4b | IA-NS-4b-26.1 | 12 | 0.20 | 1602 | 25 | 0.01 | 16 | 1.7 | 4.12 | 1.04 | 42 | 15 | 166 | 65 | 288 | 57 | 432 | 71 |
| IA-NS-4b | IA-NS-4b-27.1 | 9 | 0.26 | 2736 | 20 | 0.04 | 22 | 3.9 | 9 | 3.15 | 91 | 31 | 320 | 120 | 476 | 86 | 603 | 95 |
| IA-NS-4b | IA-NS-4b-28.1 | 15 | 0.26 | 1129 | 11 | 0.02 | 9 | 1.5 | 3.38 | 1.49 | 34 | 12 | 128 | 50 | 200 | 40 | 292 | 48 |
| IA-NS-4b | IA-NS-4b-29.1 | 8 | 2.93 | 31162 | 973 | 0.74 | 1763 | 26 | 52 | 6 | 435 | 185 | 2337 | 927 | 4129 | 969 | 8453 | 1225 |
| IA-NS-4b | IA-NS-4b-40 | 3.4 | 46 | 2309 | 339 | 1.4 | 65 | 9 | 12 | 0.27 | 56 | 27 | 307 | 123 | 553 | 134 | 1126 | 160 |
| IA-NS-4b | IA-NS-4b-43 | 1.7 | 12 | 6527 | 505 | 0.21 | 204 | 12 | 41 | 1.07 | 258 | 126 | 1451 | 485 | 1922 | 387 | 2842 | 344 |
| IA-NS-4b | IA-NS-4b-44 | 3.2 | 0.82 | 3222 | 751 | 0.02 | 99 | 3.6 | 15 | 0.46 | 110 | 50 | 640 | 214 | 859 | 181 | 1393 | 188 |
| IA-NS-4b | IA-NS-4b-45 | 2.4 | 52 | 4245 | 310 | 0.32 | 112 | 8 | 21 | 0.55 | 139 | 70 | 991 | 354 | 1629 | 370 | 3221 | 468 |
| IA-NS-4b | IA-NS-4b-49 | -- | 1.66 | 39007 | 2947 | 3.0 | 2291 | 216 | 376 | 55 | 2017 | 555 | 4671 | 1202 | 3637 | 627 | 3916 | 436 |
| IA-NS-4b | IA-NS-4b-50 | -- | 1.27 | 31020 | 1264 | 0.99 | 2106 | 81 | 177 | 28 | 1048 | 335 | 2925 | 916 | 3152 | 641 | 4654 | 597 |
| IA-NS-4b | IA-NS-4b-51 | 3.4 | 1.12 | 1956 | 261 | 0.09 | 27 | 1.3 | 6 | 0.25 | 56 | 30 | 455 | 189 | 962 | 221 | 2057 | 300 |
| IA-NS-4b | IA-NS-4b-52 | 6 | 10 | 7740 | 2020 | 0.09 | 212 | 16 | 51 | 1.45 | 326 | 154 | 1749 | 551 | 2239 | 460 | 3342 | 443 |
| IA-NS-4b | IA-NS-4b-53 | -- | 19 | 2809 | 309 | 1.9 | 66 | 3.0 | 6 | 0.20 | 40 | 25 | 401 | 193 | 1068 | 302 | 2837 | 466 |
| IA-NS-4b | IA-NS-4b-55 | 2.6 | 6 | 788 | 115 | 0.51 | 36 | 0.6 | 0.97 | 0.06 | 7 | 6 | 91 | 40 | 232 | 63 | 540 | 86 |
| IA-NS-4b | IA-NS-4b-56 | 2.8 | 4.98 | 1649 | 218 | 0.80 | 59 | 2.5 | 3.25 | 0.10 | 18 | 10 | 159 | 74 | 412 | 106 | 924 | 144 |
| IA-NS-4b | IA-NS-4b-57 | 3.8 | 38 | 9681 | 1312 | 0.66 | 293 | 28 | 82 | 2.70 | 508 | 221 | 2450 | 753 | 2816 | 534 | 3784 | 476 |
| IA-NS-4b | IA-NS-4b-58 | 2.5 | 0.79 | 4900 | 377 | 0.05 | 87 | 6 | 24 | 0.76 | 168 | 92 | 1224 | 444 | 2004 | 447 | 3634 | 537 |
| IA-NS-4b | IA-NS-4b-59 | 2.4 | 0.73 | 3517 | 822 | 0.01 | 80 | 3.8 | 14 | 0.47 | 103 | 52 | 670 | 255 | 1112 | 251 | 2199 | 340 |
| IA-NS-4b | IA-NS-4b-3.1 | -- | 106 | 2983 | 594 | 15 | 83 | 3.5 | 6 | 0.24 | 48 | 28 | 371 | 165 | 815 | 197 | 1631 | 235 |
| IA-NS-4b | IA-NS-4b-14.2 | 3.3 | 33 | 3156 | 496 | 4.3 | 124 | 25 | 35 | 0.85 | 144 | 46 | 440 | 149 | 546 | 110 | 803 | 106 |
| IA-NS-4b | IA-NS-4b-21.1 | 7 | 34 | 12095 | 369 | 0.45 | 591 | 7 | 17 | 3.38 | 169 | 77 | 1007 | 436 | 2062 | 448 | 3373 | 467 |
| IA-NS-4b | IA-NS-4b-21.2 | -- | 829 | 8153 | 1423 | 17 | 272 | 4.9 | 4.99 | 0.62 | 44 | 26 | 404 | 235 | 1355 | 381 | 3569 | 595 |
| IA-NS-4b | IA-NS-4b-27.2 | 15 | 2.62 | 8783 | 445 | 42 | 669 | 57 | 40 | 7 | 280 | 94 | 1033 | 384 | 1528 | 285 | 2014 | 294 |
| IA-NS-4b | IA-NS-4b-41 | 4.1 | 32 | 3574 | 345 | 8.9 | 80 | 10 | 7 | 0.30 | 54 | 38 | 701 | 355 | 1853 | 476 | 4093 | 626 |
| IA-NS-4b | IA-NS-4b-42 | -- | 92 | 7438 | 1215 | 16 | 180 | 24 | 42 | 1.30 | 250 | 102 | 1238 | 508 | 1877 | 456 | 3737 | 544 |
| IA-NS-4b | IA-NS-4b-46 | 5 | 101 | 2807 | 178 | 8.0 | 74 | 9 | 6 | 0.19 | 35 | 21 | 382 | 181 | 1001 | 265 | 2166 | 347 |
| IA-NS-4b | IA-NS-4b-47 | 3.4 | 67 | 3785 | 390 | 17 | 130 | 16 | 14 | 0.41 | 83 | 50 | 731 | 293 | 1452 | 345 | 2805 | 408 |
| IA-NS-4b | IA-NS-4b-48 | -- | 346 | 22774 | 822 | 9.8 | 842 | 75 | 173 | 4.39 | 1062 | 374 | 3793 | 1434 | 4403 | 883 | 6573 | 832 |

**Appendix B.3**. Continued

| Sample | Grain # | Ti | Fe | Y | Nb | La | Ce | Nd | Sm | Eu | Gd | Tb | Dy | Ho | Er | Tm | Yb | Lu |
|---|---|---|---|---|---|---|---|---|---|---|---|---|---|---|---|---|---|---|
| IA-NS-4b | IA-NS-4b-54 | -- | 293 | 7369 | 651 | 12 | 86 | 12 | 11 | 0.39 | 98 | 64 | 1063 | 496 | 2178 | 516 | 4217 | 589 |
| IA-NS-4b | IA-NS-4b-60 | -- | 328 | 2982 | 297 | 18 | 154 | 25 | 25 | 1.02 | 115 | 48 | 590 | 242 | 1068 | 260 | 2194 | 316 |
| IA-NS-6 | IA-NS-6-1.1 | 10 | 0.37 | 2098 | 35 | 0.02 | 38 | 2.4 | 6 | 1.96 | 66 | 22 | 238 | 88 | 355 | 68 | 486 | 76 |
| IA-NS-6 | IA-NS-6-2.1 | 15 | 0.56 | 17041 | 83 | 0.37 | 528 | 46 | 92 | 14 | 697 | 214 | 2122 | 731 | 2741 | 493 | 3405 | 507 |
| IA-NS-6 | IA-NS-6-3.1 | 13 | 0.50 | 17707 | 82 | 0.37 | 495 | 39 | 83 | 12 | 670 | 209 | 2121 | 733 | 2796 | 520 | 3667 | 530 |
| IA-NS-6 | IA-NS-6-4.1 | 20 | 0.38 | 11322 | 40 | 0.30 | 184 | 41 | 78 | 21 | 549 | 160 | 1522 | 490 | 1761 | 309 | 2120 | 299 |
| IA-NS-6 | IA-NS-6-5.1 | 13 | 0.74 | 11160 | 208 | 0.13 | 300 | 17 | 43 | 2.96 | 384 | 125 | 1296 | 475 | 1801 | 333 | 2364 | 366 |
| IA-NS-6 | IA-NS-6-6.1 | 11 | 0.35 | 3628 | 89 | 0.03 | 96 | 4.4 | 12 | 3.52 | 122 | 42 | 444 | 161 | 611 | 111 | 751 | 114 |
| IA-NS-6 | IA-NS-6-7.1 | 8 | 0.34 | 1473 | 39 | 0.02 | 18 | 1.3 | 3.40 | 1.14 | 36 | 14 | 160 | 64 | 276 | 56 | 423 | 72 |
| IA-NS-6 | IA-NS-6-9.1 | 15 | 0.42 | 15701 | 74 | 0.37 | 451 | 39 | 80 | 11 | 625 | 194 | 1970 | 684 | 2606 | 476 | 3391 | 500 |
| IA-NS-6 | IA-NS-6-10.1 | 16 | 0.28 | 4097 | 58 | 0.04 | 87 | 4.6 | 13 | 1.86 | 131 | 43 | 463 | 167 | 693 | 135 | 970 | 159 |
| IA-NS-6 | IA-NS-6-12.1 | 7 | 0.55 | 2326 | 12 | 0.02 | 18 | 3.5 | 9 | 2.55 | 79 | 27 | 286 | 102 | 404 | 71 | 513 | 81 |
| IA-NS-6 | IA-NS-6-13.1 | 41 | 0.32 | 11708 | 207 | 0.13 | 594 | 29 | 69 | 11 | 509 | 153 | 1461 | 504 | 1881 | 341 | 2365 | 353 |
| IA-NS-6 | IA-NS-6-15.1 | 14 | 0.45 | 9679 | 42 | 0.17 | 222 | 25 | 47 | 8 | 372 | 117 | 1174 | 414 | 1568 | 288 | 2051 | 306 |
| IA-NS-6 | IA-NS-6-16.1 | 23 | 0.31 | 6125 | 18 | 0.12 | 75 | 15 | 32 | 9 | 247 | 78 | 787 | 276 | 1077 | 203 | 1491 | 241 |
| IA-NS-6 | IA-NS-6-17.1 | 15 | 7 | 4265 | 15 | 0.11 | 81 | 10 | 23 | 4.99 | 181 | 59 | 599 | 215 | 854 | 160 | 1178 | 183 |
| IA-NS-6 | IA-NS-6-17.2 | 15 | 0.27 | 13992 | 60 | 0.32 | 328 | 37 | 73 | 13 | 565 | 174 | 1723 | 604 | 2279 | 415 | 2922 | 440 |
| IA-NS-6 | IA-NS-6-18.1 | 16 | 6 | 1372 | 9 | 0.03 | 16 | 0.9 | 2.82 | 0.97 | 31 | 11 | 135 | 54 | 236 | 48 | 382 | 67 |
| IA-NS-6 | IA-NS-6-18.2 | 7 | 0.45 | 2156 | 10 | 0.02 | 17 | 3.4 | 9 | 2.56 | 77 | 26 | 277 | 98 | 382 | 71 | 501 | 79 |
| IA-NS-6 | IA-NS-6-19.1 | 19 | 0.38 | 14369 | 60 | 0.48 | 376 | 50 | 91 | 16 | 642 | 196 | 1888 | 649 | 2366 | 433 | 3006 | 442 |
| IA-NS-6 | IA-NS-6-20.2 | 23 | 0.45 | 9805 | 38 | 0.21 | 132 | 23 | 52 | 12 | 397 | 119 | 1206 | 425 | 1595 | 294 | 2086 | 325 |
| IA-NS-6 | IA-NS-6-21.1 | 10 | 0.35 | 1409 | 28 | 0.02 | 18 | 1.4 | 3.91 | 1.48 | 39 | 14 | 159 | 60 | 260 | 51 | 371 | 62 |
| IA-NS-6 | IA-NS-6-22.1 | 8 | 0.37 | 1430 | 12 | 0.03 | 16 | 1.7 | 4.71 | 1.57 | 50 | 16 | 187 | 68 | 269 | 51 | 377 | 62 |
| IA-NS-6 | IA-NS-6-22.2 | 21 | 0.35 | 1635 | 12 | 0.02 | 20 | 1.4 | 3.64 | 1.25 | 37 | 14 | 165 | 68 | 303 | 61 | 505 | 87 |
| IA-NS-6 | IA-NS-6-24.1 | 18 | 0.20 | 1779 | 8 | 0.01 | 18 | 2.7 | 6 | 1.79 | 55 | 18 | 201 | 77 | 312 | 61 | 458 | 77 |
| IA-NS-6 | IA-NS-6-24.2 | 13 | 113 | 3904 | 40 | 0.56 | 41 | 6 | 15 | 4.47 | 139 | 46 | 472 | 179 | 667 | 123 | 841 | 134 |
| IA-NS-6 | IA-NS-6-24.3 | 10 | 1.24 | 1410 | 19 | 0.15 | 24 | 1.9 | 4.34 | 1.37 | 44 | 15 | 164 | 62 | 253 | 47 | 346 | 58 |
| IA-NS-6 | IA-NS-6-26.1 | 13 | 0.37 | 14934 | 73 | 0.33 | 293 | 37 | 74 | 6 | 586 | 186 | 1876 | 647 | 2454 | 450 | 3204 | 486 |
| IA-NS-6 | IA-NS-6-23.1 | 15 | 2.79 | 1693 | 18 | 12 | 50 | 13 | 8 | 2.65 | 53 | 18 | 198 | 74 | 280 | 57 | 415 | 65 |
| IA-NS-7 | IA-NS-7-1.1 | 18 | 3.00 | 4901 | 12 | 0.08 | 24 | 9 | 23 | 8 | 187 | 59 | 592 | 213 | 810 | 150 | 1136 | 182 |
| IA-NS-7 | IA-NS-7-2.1 | 17 | 3.80 | 14503 | 453 | 0.08 | 559 | 14 | 46 | 3.08 | 440 | 157 | 1673 | 597 | 2352 | 433 | 3123 | 455 |

**Appendix B.3**. Continued

| Sample | Grain # | Ti | Fe | Y | Nb | La | Ce | Nd | Sm | Eu | Gd | Tb | Dy | Ho | Er | Tm | Yb | Lu |
|---|---|---|---|---|---|---|---|---|---|---|---|---|---|---|---|---|---|---|
| IA-NS-7 | IA-NS-7-3.1 | 20 | 4.58 | 11321 | 279 | 0.14 | 451 | 19 | 47 | 3.96 | 403 | 135 | 1401 | 481 | 1901 | 348 | 2488 | 370 |
| IA-NS-7 | IA-NS-7-4.1 | 14 | 2.97 | 1899 | 4.6 | 0.02 | 12 | 3.4 | 8 | 2.37 | 60 | 20 | 217 | 79 | 313 | 62 | 455 | 78 |
| IA-NS-7 | IA-NS-7-4.2 | 14 | 3.04 | 6497 | 153 | 0.02 | 217 | 10 | 26 | 2.38 | 222 | 77 | 792 | 273 | 1082 | 203 | 1465 | 230 |
| IA-NS-7 | IA-NS-7-5.1 | 19 | 3.13 | 7789 | 22 | 0.22 | 58 | 26 | 48 | 15 | 346 | 107 | 1044 | 342 | 1275 | 226 | 1643 | 251 |
| IA-NS-7 | IA-NS-7-6.1 | 6 | 25 | 12165 | 90 | 0.98 | 220 | 7 | 18 | 1.62 | 174 | 71 | 911 | 400 | 1860 | 434 | 3657 | 558 |
| IA-NS-7 | IA-NS-7-7.1 | 13 | 108 | 1870 | 8 | 0.36 | 14 | 2.8 | 7 | 1.97 | 58 | 20 | 204 | 74 | 313 | 60 | 467 | 76 |
| IA-NS-7 | IA-NS-7-8.1 | 16 | 3.00 | 4291 | 9 | 0.07 | 21 | 9 | 20 | 7 | 161 | 51 | 510 | 174 | 669 | 125 | 942 | 151 |
| IA-NS-7 | IA-NS-7-8.2 | 18 | 3.07 | 8984 | 239 | 0.08 | 339 | 14 | 38 | 3.30 | 331 | 108 | 1110 | 388 | 1467 | 272 | 1954 | 295 |
| IA-NS-7 | IA-NS-7-9.1 | 9 | 3.50 | 13451 | 82 | 0.26 | 290 | 28 | 62 | 5 | 499 | 162 | 1662 | 569 | 2210 | 397 | 2847 | 428 |
| IA-NS-7 | IA-NS-7-10.1 | 29 | 3.63 | 15246 | 394 | 0.20 | 787 | 37 | 94 | 8 | 694 | 214 | 2028 | 658 | 2410 | 409 | 2952 | 421 |
| IA-NS-7 | IA-NS-7-11.1 | 17 | 130 | 3752 | 12 | 0.74 | 19 | 8 | 17 | 6 | 141 | 46 | 460 | 164 | 655 | 122 | 935 | 150 |
| IA-NS-7 | IA-NS-7-11.2 | 15 | 32 | 15666 | 718 | 0.13 | 361 | 7 | 22 | 1.72 | 262 | 114 | 1406 | 564 | 2506 | 520 | 3973 | 568 |
| IA-NS-7 | IA-NS-7-12.1 | 37 | 3.48 | 12385 | 299 | 0.15 | 539 | 30 | 78 | 8 | 588 | 175 | 1652 | 532 | 1978 | 338 | 2349 | 344 |
| IA-NS-7 | IA-NS-7-12.2 | 27 | 4.63 | 11714 | 254 | 0.14 | 525 | 23 | 61 | 6 | 501 | 155 | 1524 | 497 | 1888 | 332 | 2354 | 345 |
| IA-NS-7 | IA-NS-7-13.1 | 9 | 4.06 | 9942 | 58 | 0.89 | 150 | 14 | 36 | 3.46 | 341 | 113 | 1223 | 434 | 1694 | 319 | 2308 | 359 |
| IA-NS-7 | IA-NS-7-13.2 | 20 | 2.91 | 8564 | 24 | 0.13 | 48 | 19 | 46 | 16 | 372 | 116 | 1145 | 382 | 1464 | 266 | 1952 | 301 |
| IA-NS-7 | IA-NS-7-14.1 | 17 | 2.95 | 4247 | 9 | 0.08 | 15 | 6 | 18 | 6 | 155 | 51 | 525 | 185 | 746 | 138 | 1030 | 170 |
| IA-NS-7 | IA-NS-7-15.1 | 9 | 3.76 | 20787 | 107 | 0.42 | 462 | 40 | 89 | 9 | 732 | 244 | 2518 | 875 | 3300 | 590 | 4183 | 610 |
| IA-NS-7 | IA-NS-7-16.1 | 17 | 3.37 | 3982 | 7 | 0.10 | 22 | 10 | 20 | 6 | 160 | 51 | 508 | 177 | 688 | 125 | 928 | 150 |
| IA-NS-7 | IA-NS-7-16.2 | 20 | 3.65 | 15396 | 342 | 0.14 | 700 | 21 | 61 | 6 | 560 | 189 | 1949 | 681 | 2634 | 475 | 3410 | 503 |
| IA-NS-7 | IA-NS-7-17.1 | 29 | 3.64 | 15022 | 435 | 0.11 | 769 | 31 | 78 | 6 | 655 | 202 | 1941 | 638 | 2375 | 422 | 2953 | 426 |
| IA-NS-7 | IA-NS-7-17.2 | 9 | 3.27 | 10735 | 64 | 0.20 | 204 | 23 | 49 | 3.79 | 397 | 129 | 1326 | 470 | 1772 | 320 | 2304 | 348 |
| IA-NS-7 | IA-NS-7-18.1 | 38 | 3.36 | 6067 | 59 | 0.09 | 105 | 12 | 38 | 11 | 298 | 90 | 846 | 265 | 954 | 162 | 1126 | 158 |
| IA-NS-7 | IA-NS-7-19.2 | 20 | 3.78 | 7941 | 23 | 0.20 | 57 | 24 | 51 | 16 | 364 | 111 | 1070 | 348 | 1252 | 218 | 1528 | 228 |
| IA-NS-7 | IA-NS-7-19.1 | 10 | 96 | 8780 | 52 | 1.0 | 136 | 13 | 32 | 2.96 | 278 | 94 | 1009 | 375 | 1437 | 275 | 1984 | 315 |
| IA-NS-9 | IA-NS-9_01.1 | 12 | 4.45 | 1436 | 19 | 0.05 | 19 | 1.6 | 4.46 | 1.18 | 39 | 15 | 162 | 64 | 261 | 50 | 379 | 62 |
| IA-NS-9 | IA-NS-9_02.1 | 6 | 4.24 | 5200 | 193 | 0.07 | 194 | 2.5 | 7 | 1.51 | 75 | 35 | 460 | 201 | 923 | 192 | 1458 | 202 |
| IA-NS-9 | IA-NS-9_04.1 | 9 | 4.26 | 2717 | 11 | 0.03 | 14 | 4.5 | 8 | 2.23 | 77 | 28 | 311 | 113 | 465 | 84 | 624 | 100 |
| IA-NS-9 | IA-NS-9_05.1 | 9 | 4.27 | 2695 | 12 | 0.02 | 14 | 4.2 | 9 | 2.17 | 78 | 26 | 272 | 111 | 423 | 77 | 577 | 89 |
| IA-NS-9 | IA-NS-9_06.1 | 12 | 3.91 | 1948 | 6 | 0.05 | 12 | 4.7 | 8 | 2.36 | 65 | 23 | 242 | 83 | 348 | 67 | 498 | 78 |
| IA-NS-9 | IA-NS-9_07.1 | 11 | 4.27 | 2819 | 16 | 0.11 | 32 | 4.3 | 12 | 2.38 | 137 | 49 | 528 | 194 | 746 | 141 | 1023 | 155 |

**Appendix B.3**. Continued

| Sample | Grain # | Ti | Fe | Y | Nb | La | Ce | Nd | Sm | Eu | Gd | Tb | Dy | Ho | Er | Tm | Yb | Lu |
|---|---|---|---|---|---|---|---|---|---|---|---|---|---|---|---|---|---|---|
| IA-NS-9 | IA-NS-9_08.1 | 11 | 4.20 | 1034 | 6 | 0.01 | 7 | 1.3 | 3.66 | 1.12 | 33 | 12 | 133 | 49 | 209 | 40 | 310 | 50 |
| IA-NS-9 | IA-NS-9_09.2 | 12 | 4.35 | 1301 | 18 | 0.10 | 17 | 1.6 | 3.94 | 0.99 | 34 | 13 | 153 | 59 | 247 | 48 | 381 | 60 |
| IA-NS-9 | IA-NS-9_10.2 | 12 | 4.37 | 1103 | 13 | 0.01 | 12 | 1.3 | 3.11 | 0.78 | 28 | 12 | 123 | 48 | 202 | 40 | 294 | 51 |
| IA-NS-9 | IA-NS-9_11.1 | 12 | 4.77 | 2630 | 10 | 0.05 | 13 | 3.6 | 6 | 1.76 | 49 | 20 | 202 | 71 | 284 | 49 | 404 | 63 |
| IA-NS-9 | IA-NS-9_12.2 | 13 | 4.26 | 4739 | 33 | 0.06 | 40 | 9 | 18 | 6 | 150 | 57 | 580 | 196 | 783 | 139 | 1035 | 151 |
| IA-NS-9 | IA-NS-9_13.1 | 10 | 3.85 | 2078 | 11 | 0.13 | 14 | 3.9 | 9 | 2.34 | 66 | 24 | 256 | 94 | 396 | 69 | 508 | 83 |
| IA-NS-9 | IA-NS-9_14.2 | 7 | 4.28 | 9853 | 1785 | 0.40 | 193 | 42 | 90 | 1.57 | 380 | 193 | 1992 | 614 | 2360 | 498 | 3882 | 486 |
| IA-NS-9 | IA-NS-9_15.1 | 12 | 3.89 | 1816 | 8 | 0.03 | 10 | 3.2 | 7 | 2.04 | 60 | 21 | 222 | 80 | 320 | 61 | 461 | 76 |
| IA-NS-9 | IA-NS-9_16.1 | 12 | 4.10 | 2418 | 9 | 0.04 | 12 | 4.3 | 8 | 2.50 | 79 | 29 | 316 | 111 | 476 | 90 | 673 | 109 |
| IA-NS-9 | IA-NS-9_17.2 | 9 | 4.70 | 5623 | 954 | 0.46 | 103 | 1.1 | 6 | 0.48 | 54 | 29 | 394 | 176 | 834 | 191 | 1633 | 240 |
| IA-NS-9 | IA-NS-9_18.1 | 8 | 4.65 | 7668 | 244 | 0.03 | 147 | 5 | 17 | 2.23 | 185 | 72 | 806 | 313 | 1231 | 228 | 1630 | 239 |
| IA-NS-9 | IA-NS-9_18.2 | 9 | 4.49 | 10260 | 467 | 0.32 | 250 | 6 | 24 | 2.29 | 242 | 101 | 1109 | 434 | 1705 | 327 | 2304 | 315 |
| IA-NS-9 | IA-NS-9_20.1 | 13 | 3.93 | 2490 | 9 | 0.15 | 11 | 4.3 | 8 | 2.48 | 77 | 27 | 289 | 107 | 411 | 77 | 561 | 92 |
| IA-NS-9 | IA-NS-9_21.1 | 8 | 4.41 | 6925 | 469 | 0.37 | 271 | 3.5 | 8 | 1.87 | 82 | 43 | 561 | 248 | 1171 | 247 | 1913 | 251 |
| IA-NS-9 | IA-NS-9_22.1 | 12 | 2.52 | 1408 | 6 | 0.06 | 11 | 2.5 | 7 | 1.60 | 56 | 17 | 188 | 67 | 266 | 52 | 382 | 60 |
| IA-NS-9 | IA-NS-9_27 | 4.2 | 189 | 2548 | 331 | 1.7 | 43 | 3.0 | 12 | 0.51 | 87 | 49 | 688 | 245 | 1164 | 272 | 2282 | 327 |
| IA-NS-9 | IA-NS-9_29 | 9 | 9 | 8076 | 1071 | 0.78 | 88 | 44 | 78 | 1.57 | 343 | 154 | 1728 | 544 | 2167 | 443 | 3296 | 423 |
| IA-NS-9 | IA-NS-9_30 | 5 | 166 | 4007 | 350 | 5.4 | 138 | 8 | 16 | 0.55 | 79 | 44 | 654 | 282 | 1428 | 376 | 3460 | 509 |
| IA-NS-9 | IA-NS-9_31 | 11 | 9 | 9629 | 579 | 0.69 | 87 | 46 | 93 | 1.64 | 450 | 217 | 2569 | 844 | 3490 | 819 | 6422 | 845 |
| IA-NS-9 | IA-NS-9_32 | 12 | 2.45 | 2039 | 28 | 1.2 | 23 | 4.2 | 8 | 1.95 | 55 | 20 | 230 | 86 | 336 | 62 | 485 | 76 |
| IA-NS-9 | IA-NS-9_33 | 10 | 0.55 | 909 | 11 | 0.01 | 10 | 1.2 | 2.50 | 0.74 | 23 | 9 | 100 | 40 | 162 | 33 | 259 | 42 |
| IA-NS-9 | IA-NS-9_34 | 10 | 0.54 | 1509 | 28 | 0.05 | 22 | 1.5 | 3.93 | 1.10 | 37 | 15 | 196 | 64 | 267 | 50 | 377 | 59 |
| IA-NS-9 | IA-NS-9_35 | 12 | 0.48 | 4760 | 26 | 0.04 | 22 | 6 | 20 | 5 | 165 | 54 | 617 | 209 | 800 | 144 | 1078 | 167 |
| IA-NS-9 | IA-NS-9_36 | 11 | 0.43 | 1086 | 14 | 0.01 | 12 | 1.2 | 3.57 | 0.81 | 25 | 10 | 123 | 46 | 201 | 40 | 307 | 51 |
| IA-NS-9 | IA-NS-9_37 | 8 | 0.64 | 3847 | 40 | 0.04 | 39 | 5 | 14 | 2.63 | 123 | 46 | 518 | 181 | 722 | 132 | 921 | 151 |
| IA-NS-9 | IA-NS-9_38 | 10 | 0.36 | 1898 | 15 | 0.02 | 14 | 2.2 | 6 | 1.33 | 52 | 20 | 214 | 79 | 316 | 63 | 469 | 76 |
| IA-NS-9 | IA-NS-9_03.1 | 9 | 4.08 | 8114 | 598 | 0.17 | 76 | 17 | 50 | 1.59 | 331 | 173 | 2004 | 710 | 2887 | 614 | 4630 | 613 |
| IA-NS-9 | IA-NS-9_03.2 | -- | 7 | 6498 | 891 | 2.4 | 101 | 29 | 58 | 1.80 | 298 | 130 | 1391 | 500 | 1940 | 424 | 3413 | 462 |
| IA-NS-9 | IA-NS-9_14.1 | -- | 33 | 13388 | 410 | 13 | 320 | 95 | 136 | 2.45 | 571 | 219 | 2254 | 810 | 2911 | 681 | 5798 | 800 |
| IA-NS-9 | IA-NS-9_17.1 | 8 | 11 | 6507 | 533 | 5.3 | 72 | 25 | 21 | 2.84 | 82 | 38 | 469 | 192 | 960 | 242 | 2141 | 317 |
| IA-NS-9 | IA-NS-9_19.1 | -- | 21 | 29171 | 2215 | 2.2 | 1509 | 9 | 26 | 4.06 | 264 | 117 | 1612 | 873 | 3275 | 680 | 4739 | 550 |

**Appendix B.3**. Continued

| Sample | Grain # | Ti | Fe | Y | Nb | La | Ce | Nd | Sm | Eu | Gd | Tb | Dy | Ho | Er | Tm | Yb | Lu |
|---|---|---|---|---|---|---|---|---|---|---|---|---|---|---|---|---|---|---|
| IA-NS-9 | IA-NS-9_19.2 | -- | 16 | 38389 | 896 | 3.8 | 1961 | 14 | 38 | 6 | 390 | 157 | 2175 | 1224 | 4522 | 941 | 6666 | 754 |
| IA-NS-9 | IA-NS-9_21.2 | -- | 4.67 | 2738 | 250 | 11 | 78 | 8 | 6 | 0.43 | 45 | 36 | 537 | 232 | 1236 | 283 | 2407 | 332 |
| IA-NS-9 | IA-NS-9_25 | -- | 156 | 8397 | 742 | 17 | 350 | 68 | 115 | 2.36 | 462 | 189 | 1935 | 616 | 2247 | 511 | 4185 | 539 |
| IA-NS-9 | IA-NS-9_26 | -- | 126 | 9924 | 940 | 44 | 368 | 59 | 90 | 2.65 | 449 | 188 | 2056 | 782 | 2501 | 544 | 4121 | 559 |
| IA-NS-9 | IA-NS-9_28 | 6 | 60 | 5055 | 395 | 152 | 669 | 111 | 35 | 1.23 | 78 | 32 | 407 | 199 | 908 | 216 | 1762 | 255 |
| IA-NS-10 | IA-NS-10_1.1 | 17 | 0.71 | 8993 | 195 | 0.04 | 195 | 13 | 32 | 5 | 272 | 98 | 1074 | 386 | 1479 | 278 | 2052 | 321 |
| IA-NS-10 | IA-NS-10_3.1 | 14 | 1.83 | 1282 | 19 | 0.07 | 15 | 1.7 | 3.61 | 0.97 | 35 | 12 | 138 | 51 | 221 | 44 | 346 | 55 |
| IA-NS-10 | IA-NS-10_4.1 | 14 | 0.55 | 1220 | 16 | 0.02 | 14 | 1.3 | 3.41 | 1.08 | 33 | 12 | 133 | 50 | 202 | 41 | 306 | 50 |
| IA-NS-10 | IA-NS-10_5.1 | 15 | 0.71 | 1053 | 11 | 0.01 | 12 | 1.1 | 3.32 | 0.78 | 27 | 9 | 118 | 44 | 186 | 37 | 302 | 50 |
| IA-NS-10 | IA-NS-10_6.1 | 20 | 0.53 | 2224 | 29 | 0.03 | 28 | 2.8 | 7 | 1.99 | 63 | 22 | 257 | 92 | 388 | 78 | 607 | 99 |
| IA-NS-10 | IA-NS-10_7.1 | 16 | 3.85 | 4709 | 51 | 0.07 | 41 | 6 | 15 | 3.04 | 121 | 41 | 477 | 181 | 687 | 128 | 927 | 145 |
| IA-NS-10 | IA-NS-10_8.1 | 14 | 1.04 | 2388 | 11 | 0.41 | 15 | 4.5 | 9 | 2.14 | 79 | 25 | 280 | 105 | 408 | 74 | 558 | 93 |
| IA-NS-10 | IA-NS-10_9.1 | 10 | 0.78 | 2849 | 16 | 0.04 | 15 | 3.7 | 10 | 2.54 | 95 | 31 | 347 | 119 | 469 | 92 | 650 | 106 |
| IA-NS-10 | IA-NS-10_10.1 | 9 | 0.98 | 2139 | 12 | 0.25 | 12 | 3.5 | 8 | 2.33 | 64 | 23 | 264 | 93 | 366 | 69 | 476 | 79 |
| IA-NS-10 | IA-NS-10_11.1 | 8 | 0.49 | 834 | 11 | 0.01 | 10 | 0.6 | 2.44 | 0.66 | 18 | 8 | 95 | 35 | 149 | 31 | 236 | 39 |
| IA-NS-10 | IA-NS-10_12.1 | 11 | 0.51 | 798 | 11 | 0.01 | 9 | 0.6 | 2.17 | 0.57 | 21 | 7 | 90 | 34 | 148 | 29 | 227 | 37 |
| IA-NS-10 | IA-NS-10_13.1 | 11 | 1.72 | 1238 | 17 | 0.61 | 19 | 2.5 | 4.57 | 1.18 | 35 | 12 | 136 | 53 | 222 | 42 | 318 | 51 |
| IA-NS-10 | IA-NS-10_14.1 | 22 | 0.53 | 1768 | 23 | 0.03 | 13 | 1.7 | 4.96 | 1.37 | 42 | 15 | 181 | 68 | 311 | 62 | 517 | 87 |
| IA-NS-10 | IA-NS-10_16.1 | 15 | 0.73 | 1016 | 12 | 0.02 | 11 | 1.0 | 3.33 | 0.83 | 29 | 10 | 114 | 43 | 173 | 35 | 265 | 44 |
| IA-NS-10 | IA-NS-10_17.1 | 14 | 0.70 | 1100 | 13 | 0.01 | 12 | 1.4 | 3.40 | 0.87 | 31 | 10 | 120 | 45 | 198 | 39 | 305 | 49 |
| IA-NS-10 | IA-NS-10_18.1 | 21 | 0.44 | 3073 | 11 | 0.03 | 10 | 5 | 15 | 5 | 106 | 36 | 389 | 136 | 536 | 98 | 733 | 124 |
| IA-NS-10 | IA-NS-10_19.1 | 16 | 0.51 | 2070 | 29 | 0.04 | 24 | 2.3 | 6 | 1.93 | 59 | 20 | 228 | 85 | 325 | 65 | 449 | 75 |
| IA-NS-10 | IA-NS-10_20.1 | 14 | 1.57 | 1160 | 13 | 0.03 | 13 | 1.4 | 4.13 | 1.12 | 34 | 12 | 128 | 52 | 207 | 40 | 317 | 55 |
| IA-NS-10 | IA-NS-10_21.1 | 12 | 1.31 | 1038 | 14 | 0.12 | 14 | 1.3 | 3.09 | 0.72 | 26 | 10 | 116 | 44 | 185 | 37 | 285 | 48 |
| IA-NS-10 | IA-NS-10_22.1 | 13 | 0.75 | 1326 | 19 | 0.02 | 15 | 1.6 | 4.45 | 1.02 | 35 | 12 | 147 | 57 | 226 | 45 | 345 | 57 |
| IA-NS-10 | IA-NS-10_23.1 | 10 | 1.70 | 2063 | 7 | 0.02 | 10 | 3.4 | 8 | 2.29 | 65 | 23 | 253 | 91 | 349 | 67 | 496 | 78 |
| IA-NS-10 | IA-NS-10_24.1 | 9 | 0.65 | 759 | 11 | 0.17 | 10 | 0.7 | 2.54 | 0.66 | 18 | 7 | 90 | 33 | 137 | 28 | 225 | 40 |
| IA-NS-12 | IA-NS-12_4.1 | 18 | 0.71 | 5161 | 121 | 0.02 | 101 | 6 | 20 | 3.95 | 177 | 62 | 688 | 248 | 907 | 184 | 1238 | 195 |
| IA-NS-12 | IA-NS-12_6.1 | 12 | 0.60 | 1019 | 13 | 0.02 | 11 | 0.9 | 2.85 | 0.75 | 26 | 9 | 113 | 42 | 178 | 36 | 276 | 49 |
| IA-NS-12 | IA-NS-12_8.1 | 11 | 1.96 | 957 | 13 | 0.03 | 12 | 0.9 | 2.68 | 0.83 | 23 | 9 | 111 | 43 | 168 | 35 | 259 | 46 |
| IA-NS-12 | IA-NS-12_10.1 | 12 | 1.31 | 926 | 12 | 0.01 | 11 | 1.0 | 3.02 | 0.74 | 24 | 9 | 105 | 41 | 160 | 33 | 254 | 44 |

**Appendix B.3**. Continued

| Sample | Grain # | Ti | Fe | Y | Nb | La | Ce | Nd | Sm | Eu | Gd | Tb | Dy | Ho | Er | Tm | Yb | Lu |
|---|---|---|---|---|---|---|---|---|---|---|---|---|---|---|---|---|---|---|
| IA-NS-12 | IA-NS-12_11.1 | 12 | 0.68 | 1432 | 14 | 0.01 | 14 | 1.5 | 5 | 1.58 | 39 | 14 | 157 | 60 | 242 | 50 | 371 | 65 |
| IA-NS-12 | IA-NS-12_12.1 | -- | 0.99 | 8627 | 131 | 0.07 | 143 | 15 | 43 | 10 | 349 | 107 | 1123 | 399 | 1398 | 251 | 1743 | 273 |
| IA-NS-12 | IA-NS-12_13.1 | 16 | 0.76 | 2505 | 9 | 0.04 | 10 | 4.1 | 11 | 3.50 | 84 | 27 | 315 | 112 | 417 | 81 | 588 | 109 |
| IA-NS-12 | IA-NS-12_14.1 | 12 | 0.63 | 2783 | 16 | 0.04 | 15 | 4.2 | 10 | 2.20 | 86 | 28 | 338 | 128 | 489 | 92 | 660 | 108 |
| IA-NS-12 | IA-NS-12_15.1 | 16 | 0.69 | 3131 | 43 | 0.03 | 34 | 3.3 | 12 | 3.18 | 100 | 34 | 385 | 140 | 531 | 98 | 703 | 116 |
| IA-NS-12 | IA-NS-12_16.1 | 12 | 1.80 | 1342 | 18 | 0.04 | 16 | 1.7 | 4.64 | 1.09 | 33 | 12 | 146 | 56 | 226 | 45 | 337 | 56 |
| IA-NS-12 | IA-NS-12_17.1 | 12 | 0.84 | 1065 | 15 | 0.04 | 9 | 0.9 | 2.84 | 0.74 | 25 | 9 | 115 | 45 | 185 | 40 | 292 | 49 |
| IA-NS-12 | IA-NS-12_18.1 | 12 | 0.57 | 2865 | 12 | 0.01 | 14 | 5.0 | 11 | 2.63 | 86 | 30 | 346 | 125 | 508 | 92 | 693 | 108 |
| IA-NS-12 | IA-NS-12_19.1 | 13 | 0.77 | 1241 | 15 | 0.01 | 12 | 1.0 | 3.53 | 0.81 | 30 | 11 | 127 | 51 | 207 | 40 | 316 | 52 |
| IA-NS-12 | IA-NS-12_20.1 | 7 | 0.75 | 4591 | 42 | 0.01 | 47 | 7 | 16 | 2.22 | 133 | 46 | 520 | 195 | 743 | 137 | 980 | 157 |
| IA-NS-12 | IA-NS-12_21.1 | 13 | 0.48 | 1054 | 14 | 0.03 | 11 | 1.0 | 3.38 | 0.90 | 29 | 10 | 123 | 44 | 188 | 36 | 299 | 50 |
| IA-NS-12 | IA-NS-12_22.1 | 12 | 0.67 | 1870 | 30 | 0.02 | 23 | 2.1 | 6 | 1.31 | 53 | 19 | 226 | 85 | 341 | 65 | 503 | 83 |
| IA-NS-12 | IA-NS-12_23.1 | 13 | 0.76 | 1351 | 19 | 0.04 | 16 | 1.2 | 3.80 | 0.91 | 37 | 13 | 153 | 56 | 240 | 47 | 364 | 58 |
| IA-NS-12 | IA-NS-12_24.1 | 12 | 0.70 | 1613 | 27 | 0.03 | 21 | 1.5 | 4.52 | 0.99 | 37 | 15 | 174 | 65 | 283 | 55 | 416 | 68 |
| IA-NS-12 | IA-NS-12_25.1 | 19 | 0.97 | 939 | 8 | 0.01 | 9 | 1.0 | 2.81 | 1.01 | 25 | 9 | 104 | 38 | 167 | 33 | 266 | 45 |
| IA-NS-12 | IA-NS-12_26.1 | 13 | 1.06 | 1572 | 24 | 0.94 | 25 | 3.8 | 5 | 1.07 | 40 | 14 | 170 | 66 | 268 | 51 | 402 | 68 |
| IA-NS-12 | IA-NS-12_27.1 | 21 | 0.45 | 2169 | 8 | 0.01 | 8 | 3.9 | 9 | 3.10 | 70 | 22 | 251 | 86 | 339 | 67 | 491 | 79 |
| IA-NS-12 | IA-NS-12_1.1 | -- | 912 | 8243 | 1058 | 179 | 1393 | 379 | 184 | 16 | 520 | 143 | 1287 | 444 | 1414 | 274 | 2044 | 293 |
| IA-NS-12 | IA-NS-12_3.1 | 15 | 5 | 2182 | 10 | 3.3 | 32 | 12 | 10 | 2.98 | 75 | 25 | 260 | 95 | 374 | 72 | 517 | 89 |
| IA-NS-12 | IA-NS-12_9.1 | 24 | 15 | 14024 | 276 | 3.6 | 294 | 21 | 48 | 3.63 | 400 | 141 | 1580 | 608 | 2225 | 432 | 2964 | 447 |
| IA-G-1 | IA-G-1-1.1 | 15 | 4.28 | 2178 | 1.4 | 0.03 | 11 | 3.7 | 8 | 3.14 | 70 | 24 | 257 | 91 | 392 | 75 | 558 | 91 |
| IA-G-1 | IA-G-1-2.1 | 13 | 3.98 | 2445 | 1.7 | 0.04 | 12 | 3.5 | 7 | 3.11 | 70 | 25 | 278 | 102 | 424 | 81 | 615 | 102 |
| IA-G-1 | IA-G-1-3.1 | 17 | 3.76 | 1119 | 2.3 | 0.01 | 9 | 0.9 | 2.53 | 1.07 | 24 | 9 | 105 | 45 | 208 | 44 | 358 | 66 |
| IA-G-1 | IA-G-1-4.1 | 21 | 3.78 | 4000 | 3.2 | 0.09 | 13 | 4.5 | 9 | 3.97 | 104 | 40 | 474 | 183 | 788 | 147 | 1097 | 177 |
| IA-G-1 | IA-G-1-5.1 | 21 | 3.82 | 1900 | 0.9 | 0.04 | 6 | 2.7 | 6 | 3.41 | 61 | 22 | 229 | 82 | 348 | 65 | 512 | 84 |
| IA-G-1 | IA-G-1-6.1 | 9 | 3.56 | 1735 | 1.0 | 0.01 | 13 | 2.7 | 7 | 1.73 | 56 | 20 | 209 | 75 | 319 | 59 | 446 | 70 |
| IA-G-1 | IA-G-1-6.2 | 11 | 3.98 | 1350 | 1.1 | 0.01 | 8 | 1.6 | 4.99 | 1.75 | 36 | 13 | 139 | 52 | 211 | 42 | 321 | 54 |
| IA-G-1 | IA-G-1-7.1 | 15 | 3.64 | 2072 | 1.0 | 0.02 | 11 | 3.2 | 6 | 2.52 | 61 | 22 | 239 | 85 | 365 | 69 | 527 | 85 |
| IA-G-1 | IA-G-1-8.1 | 17 | 3.98 | 2261 | 1.5 | 0.05 | 10 | 3.7 | 8 | 3.53 | 77 | 25 | 263 | 94 | 393 | 72 | 531 | 87 |
| IA-G-1 | IA-G-1-9.1 | 20 | 3.72 | 1980 | 1.4 | 0.02 | 9 | 3.8 | 8 | 3.71 | 69 | 23 | 229 | 82 | 326 | 63 | 470 | 77 |
| IA-G-1 | IA-G-1-10.1 | 14 | 3.57 | 2440 | 1.4 | 0.03 | 12 | 3.5 | 7 | 2.71 | 70 | 24 | 262 | 100 | 414 | 79 | 591 | 94 |

**Appendix B.3**. Continued

| Sample | Grain # | Ti | Fe | Y | Nb | La | Ce | Nd | Sm | Eu | Gd | Tb | Dy | Ho | Er | Tm | Yb | Lu |
|---|---|---|---|---|---|---|---|---|---|---|---|---|---|---|---|---|---|---|
| IA-G-1 | IA-G-1-11.1 | 19 | 4.06 | 2863 | 1.7 | 0.08 | 11 | 4.0 | 9 | 4.20 | 88 | 31 | 334 | 123 | 508 | 96 | 726 | 118 |
| IA-G-1 | IA-G-1-12.1 | 21 | 3.93 | 5003 | 3.7 | 0.13 | 20 | 6 | 18 | 8 | 175 | 58 | 606 | 215 | 862 | 159 | 1177 | 186 |
| IA-G-1 | IA-G-1-13.1 | 17 | 3.71 | 1467 | 0.8 | 0.03 | 7 | 2.4 | 5 | 2.43 | 46 | 16 | 170 | 62 | 255 | 50 | 379 | 61 |
| IA-G-1 | IA-G-1-14.1 | 33 | 3.68 | 2273 | 2.6 | 0.03 | 20 | 3.1 | 7 | 3.63 | 70 | 24 | 253 | 94 | 390 | 72 | 548 | 89 |
| IA-G-1 | IA-G-1-15.1 | 12 | 2.85 | 2157 | 1.4 | 0.05 | 11 | 3.5 | 7 | 2.95 | 63 | 21 | 237 | 90 | 370 | 69 | 512 | 85 |
| IA-G-1 | IA-G-1-16.1 | 18 | 3.60 | 1278 | 0.6 | 0.02 | 5 | 2.3 | 5 | 2.57 | 42 | 14 | 152 | 53 | 223 | 42 | 334 | 57 |
| IA-G-1 | IA-G-1-17.1 | 25 | 3.63 | 5197 | 4.2 | 0.08 | 22 | 8 | 21 | 10 | 190 | 62 | 634 | 218 | 870 | 162 | 1184 | 190 |
| IA-G-1 | IA-G-1-18.1 | 23 | 2.33 | 5227 | 3.8 | 0.09 | 17 | 5 | 12 | 6 | 152 | 55 | 602 | 222 | 914 | 167 | 1227 | 196 |
| IA-G-1 | IA-G-1-19.1 | 19 | 3.60 | 2446 | 1.6 | 0.05 | 9 | 3.8 | 8 | 3.69 | 81 | 28 | 297 | 106 | 431 | 81 | 606 | 101 |
| IA-G-1 | IA-G-1-20.1 | 14 | 2.98 | 1572 | 1.1 | 0.01 | 9 | 2.2 | 5 | 2.14 | 46 | 15 | 162 | 61 | 243 | 48 | 355 | 57 |
| IA-G-1 | IA-G-1-21.1 | 18 | 2.93 | 1981 | 1.1 | 0.06 | 9 | 3.2 | 7 | 3.04 | 60 | 21 | 232 | 83 | 342 | 65 | 496 | 81 |
| IA-G-1 | IA-G-1-22.1 | 16 | 3.26 | 5021 | 9 | 0.05 | 89 | 3.9 | 13 | 4.30 | 142 | 53 | 569 | 210 | 888 | 170 | 1297 | 205 |
| IA-G-1 | IA-G-1-22.2 | 10 | 3.36 | 7450 | 4.9 | 0.14 | 56 | 11 | 28 | 9 | 252 | 86 | 903 | 316 | 1298 | 244 | 1815 | 276 |
| IA-G-1 | IA-G-1-23.1 | 24 | 3.48 | 3976 | 2.4 | 0.08 | 13 | 4.4 | 12 | 6 | 126 | 42 | 432 | 155 | 643 | 116 | 880 | 139 |
| IA-G-1 | IA-G-1-24.1 | 12 | 3.47 | 2152 | 1.4 | 0.05 | 12 | 3.1 | 6 | 2.48 | 63 | 22 | 233 | 89 | 371 | 70 | 527 | 86 |
| IA-G-1 | IA-G-1-24.2 | 9 | 3.56 | 4731 | 11 | 0.04 | 116 | 3.9 | 12 | 1.80 | 121 | 45 | 514 | 192 | 836 | 166 | 1224 | 186 |
| IA-G-1 | IA-G-1-25.1 | 8 | 3.73 | 2061 | 1.0 | 0.15 | 11 | 2.7 | 7 | 2.29 | 59 | 22 | 236 | 87 | 385 | 72 | 561 | 91 |
| IA-G-1 | IA-G-1-26.1 | 33 | 2.71 | 2455 | 3.2 | 0.03 | 26 | 2.7 | 7 | 3.72 | 75 | 26 | 282 | 102 | 424 | 79 | 588 | 96 |
| IA-G-1 | IA-G-1-27.1 | 14 | 2.88 | 2288 | 1.3 | 0.03 | 8 | 2.6 | 7 | 3.27 | 69 | 23 | 249 | 91 | 383 | 72 | 564 | 92 |
| IA-G-5 | IA-G-5-2.1 | 37 | 5 | 7919 | 36 | 0.07 | 273 | 14 | 35 | 9 | 293 |  | 868 | 312 | 1165 |  | 1503 | 217 |
| IA-G-5 | IA-G-5-4.1 | 31 | 2.75 | 8302 | 50 | 0.13 | 304 | 11 | 31 | 6 | 279 |  | 921 | 337 | 1229 |  | 1645 | 242 |
| IA-G-5 | IA-G-5-6.1 | 24 | 1.53 | 9149 | 26 | 0.17 | 189 | 16 | 37 | 11 | 320 |  | 1082 | 385 | 1370 |  | 1769 | 270 |
| IA-G-5 | IA-G-5-7.1 | 19 | 0.07 | 6244 | 12 | 0.15 | 84 | 12 | 27 | 8 | 206 |  | 629 | 245 | 898 |  | 1252 | 192 |
| IA-G-5 | IA-G-5_8.1 | 38 | 2.57 | 7440 | 53 | 0.08 | 330 | 12 | 42 | 8 | 302 | 104 | 1020 | 327 | 1248 | 232 | 1613 | 232 |
| IA-G-5 | IA-G-5_9.1 | 12 | 2.87 | 13075 | 16 | 0.47 | 428 | 30 | 82 | 13 | 496 | 173 | 1713 | 581 | 1982 | 359 | 2488 | 347 |
| IA-G-5 | IA-G-5_10.1 | 5 | 3.95 | 4681 | 4.0 | 0.03 | 85 | 6 | 15 | 2.85 | 141 | 53 | 585 | 214 | 880 | 164 | 1166 | 166 |
| IA-G-5 | IA-G-5_11.1 | 23 | 3.83 | 7882 | 12 | 0.21 | 150 | 24 | 49 | 14 | 359 | 116 | 1127 | 392 | 1394 | 251 | 1785 | 255 |
| IA-G-5 | IA-G-5_12.1 | 18 | 4.16 | 6527 | 9 | 0.09 | 102 | 14 | 29 | 9 | 227 | 88 | 883 | 294 | 1186 | 222 | 1595 | 222 |
| IA-G-5 | IA-G-5_13.1 | 20 | 3.91 | 9393 | 22 | 0.19 | 281 | 27 | 53 | 13 | 391 | 132 | 1284 | 442 | 1581 | 284 | 2293 | 307 |
| IA-G-5 | IA-G-5_14.1 | 36 | 4.22 | 6768 | 31 | 0.08 | 217 | 12 | 30 | 8 | 244 | 91 | 940 | 339 | 1331 | 243 | 1746 | 267 |

**Appendix B.4**. Zircon Trace Element Compositions (ppm), measured *in situ* by SHRIMP-RG (Atomic Number > 71), REE anomalies[38], and estimated model crystallization temperatures[39]

| Sample | Grain # | Hf | Th | U | Eu* | Ce* | Ce/Ce* | Eu/Eu* | Crystallization Temp (ºC) |
|---|---|---|---|---|---|---|---|---|---|
| IA-NS-2 | IA-NS-2-1.1 | 11074 | 17 | 50 | 27 | 0.08 | 185 | 0.24 | 806 |
| IA-NS-2 | IA-NS-2-2.1 | 8236 | 34 | 59 | 129 | 0.84 | 13 | 0.40 | 919 |
| IA-NS-2 | IA-NS-2-3.1 | 10636 | 351 | 439 | 303 | 1.9 | 96 | 0.16 | 799 |
| IA-NS-2 | IA-NS-2-4.1 | 8384 | 53 | 107 | 81 | 0.46 | 83 | 0.32 | 805 |
| IA-NS-2 | IA-NS-2-4.2 | 8863 | 58 | 114 | 135 | 1.2 | 22 | 0.27 | 782 |
| IA-NS-2 | IA-NS-2-4.3 | 10129 | 158 | 290 | 97 | 0.27 | 257 | 0.19 | 766 |
| IA-NS-2 | IA-NS-2-5.1 | 8339 | 1042 | 841 | 837 | 7.2 | 34 | 0.12 | 853 |
| IA-NS-2 | IA-NS-2-5.2 | 9633 | 62 | 147 | 106 | 0.50 | 112 | 0.23 | 770 |
| IA-NS-2 | IA-NS-2-6.1 | 10204 | 887 | 719 | 260 | 1.3 | 276 | 0.19 | 824 |
| IA-NS-2 | IA-NS-2-7.1 | 9107 | 28 | 55 | 37 | 0.22 | 68 | 0.43 | 859 |
| IA-NS-2 | IA-NS-2-8.1 | 11028 | 768 | 695 | 279 | 1.6 | 214 | 0.19 | 853 |
| IA-NS-2 | IA-NS-2-9.1 | 11882 | 552 | 508 | 176 | 0.72 | 255 | 0.20 | 825 |
| IA-NS-2 | IA-NS-2-10.1 | 11984 | 862 | 1118 | 163 | 0.83 | 263 | 0.12 | 815 |
| IA-NS-2 | IA-NS-2-10.2 | 11551 | 656 | 878 | 263 | 2.3 | 53 | 0.12 | 768 |
| IA-NS-2 | IA-NS-2-11.1 | 8720 | 101 | 177 | 188 | 1.3 | 34 | 0.24 | 761 |
| IA-NS-2 | IA-NS-2-11.2 | 13044 | 625 | 819 | 151 | 0.68 | 271 | 0.14 | 820 |
| IA-NS-2 | IA-NS-2-12.1 | 8552 | 75 | 136 | 145 | 0.95 | 37 | 0.27 | 786 |
| IA-NS-2 | IA-NS-2-12.2 | 8809 | 119 | 200 | 219 | 1.3 | 36 | 0.26 | 781 |
| IA-NS-2 | IA-NS-2-13.1 | 9548 | 436 | 454 | 379 | 2.5 | 69 | 0.29 | 829 |
| IA-NS-2 | IA-NS-2-14.1 | 9749 | 406 | 529 | 136 | 0.50 | 235 | 0.18 | 804 |
| IA-NS-2 | IA-NS-2-14.2 | 8469 | 263 | 381 | 377 | 1.9 | 74 | 0.20 | 773 |
| IA-NS-2 | IA-NS-2-15.1 | 8069 | 156 | 263 | 222 | 1.5 | 69 | 0.29 | 811 |
| IA-NS-2 | IA-NS-2-15.2 | 9744 | 93 | 159 | 64 | 0.32 | 136 | 0.23 | 790 |
| IA-NS-2 | IA-NS-2-16.1 | 9307 | 31 | 99 | 51 | 0.28 | 108 | 0.22 | 780 |
| IA-NS-2 | IA-NS-2-16.2 | 8676 | 94 | 166 | 167 | 1.3 | 32 | 0.27 | 819 |
| IA-NS-2 | IA-NS-2-17.1 | 9409 | 68 | 145 | 77 | 0.42 | 126 | 0.22 | 774 |
| IA-NS-2 | IA-NS-2-17.2 | 10055 | 740 | 774 | 773 | 5.7 | 64 | 0.16 | 789 |
| IA-NS-2 | IA-NS-2-18.1 | 9094 | 131 | 212 | 201 | 1.6 | 34 | 0.24 | 765 |
| IA-NS-2 | IA-NS-2-18.2 | 9713 | 113 | 221 | 116 | 0.59 | 154 | 0.21 | 780 |
| IA-NS-2 | IA-NS-2-19.1 | 9149 | 76 | 166 | 102 | 0.61 | 122 | 0.23 | 778 |
| IA-NS-2 | IA-NS-2-19.2 | 8995 | 185 | 308 | 258 | 1.7 | 45 | 0.22 | 768 |
| IA-NS-2 | IA-NS-2-20.1 | 8762 | 100 | 167 | 197 | 1.4 | 29 | 0.26 | 782 |
| IA-NS-2 | IA-NS-2-21.2 | 8650 | 135 | 211 | 219 | 1.4 | 43 | 0.25 | 794 |
| IA-NS-2 | IA-NS-2-22.1 | 8245 | 32 | 69 | 103 | 0.91 | 16 | 0.37 | 803 |
| IA-NS-2 | IA-NS-2-23.1 | 8792 | 40 | 94 | 70 | 0.42 | 93 | 0.29 | 784 |
| IA-NS-2 | IA-NS-2-24.1 | 8829 | 62 | 119 | 136 | 1.2 | 23 | 0.27 | 782 |
| IA-NS-2 | IA-NS-2-24.2 | 10043 | 513 | 606 | 229 | 1.1 | 182 | 0.15 | 827 |
| IA-NS-2 | IA-NS-2-25.2 | 12820 | 235 | 461 | 86 | 0.60 | 139 | 0.14 | 765 |

---

[38] REE anomalies: Ce* and Eu* calculated by logarithmic extrapolation of Sm and Nd, and Nd and Gd, respectively

[39] Model temperatures estimated using the Ti-in-zircon thermometer of Ferry & Watson (2007), see Chapter III, 3.3.b

**Appendix B.4**. Continued

| Sample | Grain # | Hf | Th | U | Eu* | Ce* | Ce/Ce* | Eu/Eu* | Crystallization Temp ($^{o}$C) |
|---|---|---|---|---|---|---|---|---|---|
| IA-NS-2 | IA-NS-2-21.1 | 9680 | 184 | 299 | 212 | 51 | 4 | 0.17 | 764 |
| IA-NS-2 | IA-NS-2-23.2 | 8828 | 1290 | 987 | 738 | 45 | 14 | 0.21 | 845 |
| IA-NS-2 | IA-NS-2-25.1 | 10570 | 1119 | 841 | 671 | 31 | 22 | 0.20 | -- |
| IA-NS-4b | IA-NS-4b-1.1 | 16898 | 725 | 1065 | 501 | 7.5 | 8 | 0.03 | 750 |
| IA-NS-4b | IA-NS-4b-1.2 | 22578 | 7063 | 3985 | 1738 | 43 | 12 | 0.03 | -- |
| IA-NS-4b | IA-NS-4b-2.1 | 8226 | 58 | 110 | 163 | 1.1 | 21 | 0.36 | 793 |
| IA-NS-4b | IA-NS-4b-4.1 | 22139 | 1828 | 1262 | 225 | 0.72 | 188 | 0.04 | 689 |
| IA-NS-4b | IA-NS-4b-6.1 | 7514 | 15 | 51 | 48 | 0.30 | 28 | 0.43 | 835 |
| IA-NS-4b | IA-NS-4b-7.1 | 22628 | 5273 | 2984 | 1297 | 7.7 | 61 | 0.04 | 699 |
| IA-NS-4b | IA-NS-4b-9.1 | 21137 | 2303 | 1710 | 162 | 0.34 | 294 | 0.05 | 724 |
| IA-NS-4b | IA-NS-4b-9.2 | 17930 | 1887 | 1827 | 301 | 1.3 | 90 | 0.04 | 755 |
| IA-NS-4b | IA-NS-4b-10.1 | 9170 | 354 | 454 | 168 | 0.77 | 149 | 0.17 | 818 |
| IA-NS-4b | IA-NS-4b-11.1 | 7999 | 151 | 232 | 301 | 1.8 | 39 | 0.29 | 793 |
| IA-NS-4b | IA-NS-4b-12.1 | 21201 | 1529 | 763 | 1074 | 13 | 12 | 0.03 | 764 |
| IA-NS-4b | IA-NS-4b-14.1 | 20815 | 1969 | 1709 | 789 | 6.6 | 27 | 0.03 | 780 |
| IA-NS-4b | IA-NS-4b-15.1 | 8055 | 2674 | 1695 | 623 | 2.5 | 462 | 0.32 | 834 |
| IA-NS-4b | IA-NS-4b-18.1 | 21589 | 2020 | 1184 | 341 | 1.6 | 71 | 0.04 | 707 |
| IA-NS-4b | IA-NS-4b-19.1 | 8293 | 31 | 67 | 100 | 0.84 | 17 | 0.37 | 794 |
| IA-NS-4b | IA-NS-4b-20.1 | 8345 | 43 | 90 | 117 | 0.96 | 18 | 0.34 | 790 |
| IA-NS-4b | IA-NS-4b-22.1 | 18342 | 821 | 690 | 45 | 0.12 | 350 | 0.06 | 662 |
| IA-NS-4b | IA-NS-4b-23.1 | 18920 | 1919 | 812 | 278 | 1.00 | 110 | 0.04 | 683 |
| IA-NS-4b | IA-NS-4b-23.2 | 22353 | 2928 | 1651 | 651 | 2.7 | 94 | 0.04 | 679 |
| IA-NS-4b | IA-NS-4b-24.1 | 8926 | 65 | 112 | 127 | 1.0 | 15 | 0.29 | 826 |
| IA-NS-4b | IA-NS-4b-25.1 | 18104 | 1632 | 1486 | 1151 | 16 | 10 | 0.03 | 751 |
| IA-NS-4b | IA-NS-4b-25.2 | 19579 | 1619 | 1209 | 808 | 7.6 | 17 | 0.04 | 781 |
| IA-NS-4b | IA-NS-4b-26.1 | 9144 | 39 | 104 | 57 | 0.36 | 53 | 0.24 | 832 |
| IA-NS-4b | IA-NS-4b-27.1 | 8213 | 64 | 116 | 125 | 0.88 | 30 | 0.33 | 800 |
| IA-NS-4b | IA-NS-4b-28.1 | 7824 | 45 | 78 | 46 | 0.35 | 33 | 0.42 | 861 |
| IA-NS-4b | IA-NS-4b-29.1 | 21483 | 5758 | 693 | 652 | 7.0 | 305 | 0.12 | 791 |
| IA-NS-4b | IA-NS-4b-40 | 14936 | 891 | 1600 | 113 | 3.7 | 21 | 0.03 | 711 |
| IA-NS-4b | IA-NS-4b-43 | 21419 | 2550 | 2287 | 447 | 2.0 | 125 | 0.03 | 652 |
| IA-NS-4b | IA-NS-4b-44 | 20493 | 1899 | 796 | 176 | 0.47 | 258 | 0.03 | 706 |
| IA-NS-4b | IA-NS-4b-45 | 11447 | 1182 | 1429 | 235 | 1.4 | 97 | 0.03 | 681 |
| IA-NS-4b | IA-NS-4b-49 | 18265 | 12612 | 803 | 3766 | 66 | 43 | 0.19 | -- |
| IA-NS-4b | IA-NS-4b-50 | 12530 | 9330 | 763 | 1866 | 19 | 132 | 0.20 | -- |
| IA-NS-4b | IA-NS-4b-51 | 20367 | 515 | 1030 | 76 | 0.17 | 194 | 0.04 | 711 |
| IA-NS-4b | IA-NS-4b-52 | 27915 | 5967 | 2874 | 558 | 2.7 | 96 | 0.03 | 765 |
| IA-NS-4b | IA-NS-4b-53 | 22358 | 1081 | 2850 | 68 | 0.79 | 103 | 0.04 | -- |
| IA-NS-4b | IA-NS-4b-55 | 13360 | 320 | 613 | 11 | 0.17 | 258 | 0.06 | 687 |
| IA-NS-4b | IA-NS-4b-56 | 14189 | 771 | 1419 | 33 | 0.98 | 74 | 0.04 | 695 |
| IA-NS-4b | IA-NS-4b-57 | 21430 | 5276 | 2433 | 881 | 5.0 | 71 | 0.04 | 721 |
| IA-NS-4b | IA-NS-4b-58 | 16893 | 1186 | 1384 | 275 | 0.88 | 121 | 0.04 | 684 |

## **Appendix B.4**. Continued

| Sample | Grain # | Hf | Th | U | Eu* | Ce* | Ce/Ce* | Eu/Eu* | Crystallization Temp (ºC) |
|---|---|---|---|---|---|---|---|---|---|
| IA-NS-4b | IA-NS-4b-59 | 27190 | 2345 | 1560 | 163 | 0.55 | 175 | 0.04 | 682 |
| IA-NS-4b | IA-NS-4b-3.1 | 24018 | 962 | 1878 | 71 | 1.2 | 85 | 0.05 | -- |
| IA-NS-4b | IA-NS-4b-14.2 | 19398 | 901 | 758 | 307 | 9.7 | 15 | 0.04 | 707 |
| IA-NS-4b | IA-NS-4b-21.1 | 8007 | 745 | 1074 | 231 | 1.4 | 503 | 0.19 | 779 |
| IA-NS-4b | IA-NS-4b-21.2 | 13113 | 3933 | 1298 | 64 | 2.6 | 128 | 0.13 | -- |
| IA-NS-4b | IA-NS-4b-27.2 | 8916 | 918 | 819 | 458 | 43 | 19 | 0.19 | 857 |
| IA-NS-4b | IA-NS-4b-41 | 13913 | 1596 | 2945 | 86 | 7.5 | 13 | 0.05 | 728 |
| IA-NS-4b | IA-NS-4b-42 | 22319 | 1512 | 2761 | 441 | 7.2 | 30 | 0.04 | -- |
| IA-NS-4b | IA-NS-4b-46 | 13197 | 1777 | 2113 | 63 | 6.9 | 13 | 0.04 | 747 |
| IA-NS-4b | IA-NS-4b-47 | 19930 | 1472 | 2210 | 148 | 9.1 | 18 | 0.04 | 711 |
| IA-NS-4b | IA-NS-4b-48 | 12172 | 4129 | 3125 | 1856 | 17 | 60 | 0.03 | -- |
| IA-NS-4b | IA-NS-4b-54 | 14113 | 3285 | 4421 | 140 | 7.4 | 14 | 0.04 | -- |
| IA-NS-4b | IA-NS-4b-60 | 12991 | 1338 | 1576 | 232 | 13 | 14 | 0.06 | -- |
| IA-NS-6 | IA-NS-6-1.1 | 8638 | 108 | 162 | 89 | 0.46 | 100 | 0.29 | 820 |
| IA-NS-6 | IA-NS-6-2.1 | 7161 | 1072 | 956 | 1099 | 12 | 54 | 0.17 | 862 |
| IA-NS-6 | IA-NS-6-3.1 | 7708 | 1082 | 898 | 1017 | 9.8 | 62 | 0.15 | 847 |
| IA-NS-6 | IA-NS-6-4.1 | 7240 | 500 | 449 | 894 | 11 | 20 | 0.30 | 895 |
| IA-NS-6 | IA-NS-6-5.1 | 9165 | 1590 | 1306 | 555 | 3.4 | 108 | 0.07 | 840 |
| IA-NS-6 | IA-NS-6-6.1 | 8191 | 324 | 367 | 164 | 0.86 | 135 | 0.28 | 824 |
| IA-NS-6 | IA-NS-6-7.1 | 8431 | 24 | 95 | 48 | 0.27 | 80 | 0.31 | 792 |
| IA-NS-6 | IA-NS-6-9.1 | 8501 | 1182 | 906 | 966 | 10.0 | 55 | 0.15 | 862 |
| IA-NS-6 | IA-NS-6-10.1 | 9056 | 497 | 554 | 182 | 0.82 | 129 | 0.13 | 865 |
| IA-NS-6 | IA-NS-6-12.1 | 8730 | 40 | 87 | 113 | 0.74 | 29 | 0.30 | 774 |
| IA-NS-6 | IA-NS-6-13.1 | 7641 | 3199 | 1810 | 813 | 6.6 | 110 | 0.18 | 991 |
| IA-NS-6 | IA-NS-6-15.1 | 7834 | 512 | 526 | 574 | 7.0 | 39 | 0.19 | 854 |
| IA-NS-6 | IA-NS-6-16.1 | 8466 | 294 | 302 | 385 | 3.6 | 26 | 0.30 | 911 |
| IA-NS-6 | IA-NS-6-17.1 | 8158 | 320 | 374 | 278 | 2.5 | 40 | 0.24 | 863 |
| IA-NS-6 | IA-NS-6-17.2 | 7880 | 793 | 686 | 880 | 9.7 | 41 | 0.20 | 859 |
| IA-NS-6 | IA-NS-6-18.1 | 8772 | 34 | 72 | 41 | 0.17 | 114 | 0.32 | 871 |
| IA-NS-6 | IA-NS-6-18.2 | 8665 | 42 | 80 | 112 | 0.71 | 29 | 0.30 | 782 |
| IA-NS-6 | IA-NS-6-19.1 | 7728 | 964 | 777 | 1046 | 15 | 32 | 0.20 | 888 |
| IA-NS-6 | IA-NS-6-20.2 | 8730 | 513 | 442 | 620 | 5.5 | 29 | 0.25 | 912 |
| IA-NS-6 | IA-NS-6-21.1 | 8218 | 50 | 107 | 54 | 0.25 | 86 | 0.36 | 817 |
| IA-NS-6 | IA-NS-6-22.1 | 8719 | 40 | 89 | 66 | 0.32 | 62 | 0.31 | 788 |
| IA-NS-6 | IA-NS-6-22.2 | 8476 | 49 | 93 | 50 | 0.28 | 85 | 0.33 | 901 |
| IA-NS-6 | IA-NS-6-24.1 | 8668 | 43 | 80 | 80 | 0.63 | 35 | 0.29 | 886 |
| IA-NS-6 | IA-NS-6-24.2 | 8221 | 93 | 156 | 196 | 1.2 | 41 | 0.30 | 848 |
| IA-NS-6 | IA-NS-6-24.3 | 8627 | 35 | 81 | 60 | 0.42 | 69 | 0.30 | 815 |
| IA-NS-6 | IA-NS-6-26.1 | 8056 | 1088 | 993 | 902 | 9.9 | 36 | 0.09 | 842 |
| IA-NS-6 | IA-NS-6-23.1 | 7702 | 79 | 114 | 87 | 13 | 5 | 0.40 | 864 |
| IA-NS-7 | IA-NS-7-1.1 | 7926 | 133 | 190 | 283 | 1.9 | 16 | 0.37 | 881 |
| IA-NS-7 | IA-NS-7-2.1 | 10290 | 3769 | 2992 | 617 | 2.3 | 291 | 0.07 | 874 |

**Appendix B.4**. Continued

| Sample | Grain # | Hf | Th | U | Eu* | Ce* | Ce/Ce* | Eu/Eu* | Crystallization Temp ($^{o}$C) |
|---|---|---|---|---|---|---|---|---|---|
| IA-NS-7 | IA-NS-7-3.1 | 6789 | 1098 | 1342 | 598 | 3.8 | 143 | 0.09 | 897 |
| IA-NS-7 | IA-NS-7-4.2 | 7180 | 1000 | 1093 | 327 | 2.0 | 136 | 0.10 | 857 |
| IA-NS-7 | IA-NS-7-5.1 | 7411 | 258 | 284 | 560 | 7.2 | 10 | 0.36 | 891 |
| IA-NS-7 | IA-NS-7-6.1 | 15425 | 3606 | 3230 | 244 | 1.5 | 177 | 0.09 | 771 |
| IA-NS-7 | IA-NS-7-4.1 | 8196 | 35 | 73 | 93 | 0.81 | 18 | 0.34 | 852 |
| IA-NS-7 | IA-NS-7-7.1 | 8366 | 47 | 81 | 88 | 0.58 | 29 | 0.30 | 846 |
| IA-NS-7 | IA-NS-7-8.1 | 8146 | 108 | 163 | 248 | 2.0 | 13 | 0.35 | 870 |
| IA-NS-7 | IA-NS-7-8.2 | 7162 | 1305 | 1270 | 483 | 2.7 | 152 | 0.09 | 879 |
| IA-NS-7 | IA-NS-7-9.1 | 6353 | 523 | 704 | 763 | 6.8 | 52 | 0.09 | 809 |
| IA-NS-7 | IA-NS-7-10.1 | 6127 | 2682 | 2243 | 1103 | 7.8 | 123 | 0.09 | 943 |
| IA-NS-7 | IA-NS-7-11.1 | 8042 | 99 | 156 | 210 | 1.9 | 12 | 0.37 | 878 |
| IA-NS-7 | IA-NS-7-11.2 | 13324 | 5164 | 5933 | 327 | 1.0 | 424 | 0.07 | 863 |
| IA-NS-7 | IA-NS-7-12.1 | 6807 | 2247 | 1684 | 926 | 6.2 | 107 | 0.11 | 975 |
| IA-NS-7 | IA-NS-7-12.2 | 6986 | 2430 | 1763 | 755 | 4.6 | 140 | 0.10 | 932 |
| IA-NS-7 | IA-NS-7-13.1 | 7550 | 482 | 606 | 477 | 2.7 | 67 | 0.10 | 808 |
| IA-NS-7 | IA-NS-7-13.2 | 7323 | 306 | 316 | 566 | 4.1 | 14 | 0.37 | 896 |
| IA-NS-7 | IA-NS-7-14.1 | 7923 | 117 | 178 | 228 | 1.2 | 15 | 0.37 | 878 |
| IA-NS-7 | IA-NS-7-15.1 | 8825 | 1444 | 1331 | 1104 | 9.6 | 59 | 0.10 | 806 |
| IA-NS-7 | IA-NS-7-16.1 | 7969 | 116 | 175 | 247 | 2.4 | 11 | 0.34 | 877 |
| IA-NS-7 | IA-NS-7-16.2 | 9135 | 3190 | 2057 | 800 | 3.8 | 223 | 0.09 | 894 |
| IA-NS-7 | IA-NS-7-17.1 | 6355 | 2428 | 2117 | 975 | 6.4 | 146 | 0.08 | 944 |
| IA-NS-7 | IA-NS-7-17.2 | 6342 | 457 | 579 | 602 | 5.5 | 45 | 0.08 | 801 |
| IA-NS-7 | IA-NS-7-18.1 | 6523 | 697 | 650 | 462 | 2.1 | 61 | 0.32 | 981 |
| IA-NS-7 | IA-NS-7-19.2 | 7181 | 242 | 283 | 587 | 5.9 | 12 | 0.37 | 893 |
| IA-NS-7 | IA-NS-7-19.1 | 7008 | 385 | 545 | 405 | 3.0 | 54 | 0.10 | 812 |
| IA-NS-9 | IA-NS-9_01.1 | 9160 | 49 | 90 | 57 | 0.31 | 73 | 0.27 | 834 |
| IA-NS-9 | IA-NS-9_02.1 | 13542 | 224 | 625 | 101 | 0.46 | 512 | 0.20 | 759 |
| IA-NS-9 | IA-NS-9_04.1 | 8797 | 62 | 115 | 110 | 1.3 | 13 | 0.27 | 805 |
| IA-NS-9 | IA-NS-9_05.1 | 8841 | 46 | 89 | 115 | 1.1 | 16 | 0.25 | 806 |
| IA-NS-9 | IA-NS-9_06.1 | 8748 | 41 | 75 | 98 | 1.5 | 10 | 0.32 | 839 |
| IA-NS-9 | IA-NS-9_07.1 | 9351 | 263 | 244 | 176 | 0.80 | 49 | 0.18 | 827 |
| IA-NS-9 | IA-NS-9_08.1 | 8784 | 20 | 45 | 47 | 0.23 | 38 | 0.31 | 826 |
| IA-NS-9 | IA-NS-9_09.2 | 9147 | 61 | 105 | 50 | 0.34 | 60 | 0.26 | 835 |
| IA-NS-9 | IA-NS-9_10.2 | 8871 | 37 | 79 | 40 | 0.27 | 53 | 0.25 | 833 |
| IA-NS-9 | IA-NS-9_11.1 | 6330 | 25 | 62 | 74 | 1.2 | 13 | 0.31 | 835 |
| IA-NS-9 | IA-NS-9_12.2 | 7536 | 187 | 207 | 226 | 2.6 | 19 | 0.37 | 847 |
| IA-NS-9 | IA-NS-9_13.1 | 8164 | 53 | 85 | 102 | 0.93 | 19 | 0.30 | 815 |
| IA-NS-9 | IA-NS-9_14.2 | 15534 | 4806 | 3516 | 800 | 10 | 23 | 0.03 | 785 |
| IA-NS-9 | IA-NS-9_15.1 | 8258 | 41 | 76 | 86 | 0.82 | 15 | 0.31 | 831 |
| IA-NS-9 | IA-NS-9_16.1 | 8350 | 63 | 105 | 110 | 1.2 | 12 | 0.30 | 839 |
| IA-NS-9 | IA-NS-9_17.2 | 19222 | 848 | 1155 | 76 | 0.11 | 1197 | 0.08 | 805 |
| IA-NS-9 | IA-NS-9_18.1 | 10391 | 523 | 777 | 244 | 0.92 | 193 | 0.12 | 790 |

**Appendix B.4**. Continued

| Sample | Grain # | Hf | Th | U | Eu* | Ce* | Ce/Ce* | Eu/Eu* | Crystallization Temp (ºC) |
|---|---|---|---|---|---|---|---|---|---|
| IA-NS-9 | IA-NS-9_18.2 | 10360 | 1394 | 1572 | 328 | 0.83 | 368 | 0.09 | 808 |
| IA-NS-9 | IA-NS-9_20.1 | 8998 | 48 | 89 | 110 | 1.2 | 11 | 0.30 | 841 |
| IA-NS-9 | IA-NS-9_21.1 | 13666 | 494 | 1239 | 113 | 0.78 | 421 | 0.22 | 789 |
| IA-NS-9 | IA-NS-9_22.1 | 9103 | 33 | 64 | 85 | 0.46 | 29 | 0.25 | 836 |
| IA-NS-9 | IA-NS-9_27 | 15998 | 1170 | 2197 | 137 | 0.42 | 124 | 0.05 | 729 |
| IA-NS-9 | IA-NS-9_29 | 14895 | 1507 | 957 | 706 | 13 | 8 | 0.03 | 800 |
| IA-NS-9 | IA-NS-9_30 | 11857 | 2639 | 5138 | 154 | 2.2 | 76 | 0.05 | 754 |
| IA-NS-9 | IA-NS-9_31 | 11621 | 1203 | 3139 | 886 | 12 | 9 | 0.02 | 821 |
| IA-NS-9 | IA-NS-9_32 | 8966 | 56 | 105 | 89 | 1.3 | 22 | 0.29 | 833 |
| IA-NS-9 | IA-NS-9_33 | 7987 | 27 | 61 | 33 | 0.31 | 39 | 0.29 | 818 |
| IA-NS-9 | IA-NS-9_34 | 7789 | 110 | 163 | 53 | 0.31 | 88 | 0.28 | 811 |
| IA-NS-9 | IA-NS-9_35 | 8013 | 119 | 169 | 247 | 1.0 | 27 | 0.28 | 836 |
| IA-NS-9 | IA-NS-9_36 | 9541 | 32 | 72 | 41 | 0.22 | 65 | 0.26 | 828 |
| IA-NS-9 | IA-NS-9_37 | 7742 | 119 | 188 | 181 | 0.98 | 49 | 0.19 | 789 |
| IA-NS-9 | IA-NS-9_38 | 8865 | 49 | 98 | 77 | 0.41 | 40 | 0.23 | 814 |
| IA-NS-9 | IA-NS-9_03.1 | 21798 | 1540 | 782 | 555 | 2.9 | 32 | 0.04 | 804 |
| IA-NS-9 | IA-NS-9_03.2 | 24528 | 3187 | 1747 | 571 | 7.5 | 16 | 0.04 | -- |
| IA-NS-9 | IA-NS-9_14.1 | 12856 | 6536 | 5859 | 1207 | 35 | 11 | 0.03 | -- |
| IA-NS-9 | IA-NS-9_17.1 | 18140 | 3141 | 2623 | 178 | 16 | 6 | 0.21 | 787 |
| IA-NS-9 | IA-NS-9_19.1 | 13693 | 6295 | 805 | 358 | 1.7 | 1086 | 0.15 | -- |
| IA-NS-9 | IA-NS-9_19.2 | 12077 | 5921 | 1159 | 528 | 2.8 | 856 | 0.14 | -- |
| IA-NS-9 | IA-NS-9_21.2 | 18365 | 1740 | 2175 | 74 | 5.4 | 18 | 0.08 | -- |
| IA-NS-9 | IA-NS-9_25 | 15383 | 6232 | 3155 | 996 | 21 | 20 | 0.03 | -- |
| IA-NS-9 | IA-NS-9_26 | 17079 | 3080 | 2723 | 871 | 20 | 22 | 0.04 | -- |
| IA-NS-9 | IA-NS-9_28 | 14042 | 1164 | 2010 | 228 | 183 | 4 | 0.07 | 763 |
| IA-NS-10 | IA-NS-10_1.1 | 9829 | 570 | 681 | 402 | 2.9 | 82 | 0.16 | 872 |
| IA-NS-10 | IA-NS-10_3.1 | 9211 | 60 | 112 | 48 | 0.43 | 43 | 0.26 | 849 |
| IA-NS-10 | IA-NS-10_4.1 | 10153 | 45 | 92 | 46 | 0.27 | 63 | 0.31 | 856 |
| IA-NS-10 | IA-NS-10_5.1 | 9602 | 40 | 81 | 41 | 0.19 | 77 | 0.25 | 862 |
| IA-NS-10 | IA-NS-10_6.1 | 9351 | 160 | 172 | 93 | 0.57 | 61 | 0.28 | 893 |
| IA-NS-10 | IA-NS-10_7.1 | 11888 | 146 | 241 | 183 | 1.3 | 39 | 0.22 | 869 |
| IA-NS-10 | IA-NS-10_8.1 | 13364 | 42 | 83 | 118 | 1.1 | 16 | 0.24 | 853 |
| IA-NS-10 | IA-NS-10_9.1 | 7929 | 67 | 117 | 135 | 0.73 | 26 | 0.25 | 816 |
| IA-NS-10 | IA-NS-10_10.1 | 7213 | 45 | 92 | 99 | 0.78 | 19 | 0.31 | 803 |
| IA-NS-10 | IA-NS-10_11.1 | 8023 | 19 | 47 | 29 | 0.08 | 161 | 0.30 | 794 |
| IA-NS-10 | IA-NS-10_12.1 | 8636 | 20 | 47 | 29 | 0.08 | 138 | 0.26 | 827 |
| IA-NS-10 | IA-NS-10_13.1 | 8541 | 59 | 100 | 55 | 0.70 | 32 | 0.28 | 829 |
| IA-NS-10 | IA-NS-10_14.1 | 11323 | 42 | 101 | 62 | 0.30 | 52 | 0.29 | 908 |
| IA-NS-10 | IA-NS-10_16.1 | 9125 | 34 | 70 | 43 | 0.16 | 86 | 0.26 | 864 |
| IA-NS-10 | IA-NS-10_17.1 | 9360 | 41 | 86 | 44 | 0.28 | 52 | 0.26 | 849 |
| IA-NS-10 | IA-NS-10_18.1 | 7525 | 66 | 101 | 170 | 1.0 | 13 | 0.40 | 902 |
| IA-NS-10 | IA-NS-10_19.1 | 8586 | 168 | 178 | 80 | 0.48 | 60 | 0.32 | 868 |

**Appendix B.4**. Continued

| Sample | Grain # | Hf | Th | U | Eu* | Ce* | Ce/Ce* | Eu/Eu* | Crystallization Temp (ºC) |
|---|---|---|---|---|---|---|---|---|---|
| IA-NS-10 | IA-NS-10_20.1 | 10515 | 34 | 76 | 51 | 0.25 | 62 | 0.29 | 852 |
| IA-NS-10 | IA-NS-10_21.1 | 9888 | 27 | 62 | 39 | 0.27 | 63 | 0.24 | 832 |
| IA-NS-10 | IA-NS-10_22.1 | 8853 | 47 | 92 | 54 | 0.29 | 61 | 0.25 | 842 |
| IA-NS-10 | IA-NS-10_23.1 | 10098 | 36 | 75 | 100 | 0.75 | 17 | 0.30 | 814 |
| IA-NS-10 | IA-NS-10_24.1 | 8119 | 19 | 50 | 30 | 0.10 | 124 | 0.29 | 808 |
| IA-NS-12 | IA-NS-12_4.1 | 9784 | 337 | 426 | 256 | 1.0 | 123 | 0.20 | 879 |
| IA-NS-12 | IA-NS-12_6.1 | 8793 | 26 | 67 | 38 | 0.15 | 92 | 0.26 | 831 |
| IA-NS-12 | IA-NS-12_8.1 | 9522 | 32 | 69 | 34 | 0.15 | 94 | 0.32 | 825 |
| IA-NS-12 | IA-NS-12_10.1 | 9533 | 28 | 64 | 37 | 0.16 | 85 | 0.26 | 840 |
| IA-NS-12 | IA-NS-12_11.1 | 9950 | 58 | 97 | 61 | 0.23 | 72 | 0.34 | 838 |
| IA-NS-12 | IA-NS-12_12.1 | 7358 | 487 | 483 | 530 | 2.9 | 61 | 0.24 | -- |
| IA-NS-12 | IA-NS-12_13.1 | 10945 | 43 | 84 | 132 | 0.82 | 14 | 0.35 | 870 |
| IA-NS-12 | IA-NS-12_14.1 | 11640 | 61 | 122 | 124 | 0.95 | 19 | 0.23 | 832 |
| IA-NS-12 | IA-NS-12_15.1 | 8507 | 210 | 237 | 147 | 0.51 | 82 | 0.29 | 869 |
| IA-NS-12 | IA-NS-12_16.1 | 9657 | 46 | 91 | 54 | 0.32 | 60 | 0.27 | 839 |
| IA-NS-12 | IA-NS-12_17.1 | 10208 | 19 | 62 | 36 | 0.16 | 65 | 0.27 | 839 |
| IA-NS-12 | IA-NS-12_18.1 | 12837 | 62 | 116 | 132 | 1.2 | 14 | 0.26 | 837 |
| IA-NS-12 | IA-NS-12_19.1 | 11186 | 33 | 81 | 45 | 0.15 | 102 | 0.24 | 845 |
| IA-NS-12 | IA-NS-12_20.1 | 9691 | 153 | 249 | 199 | 1.5 | 38 | 0.15 | 780 |
| IA-NS-12 | IA-NS-12_21.1 | 9095 | 23 | 57 | 43 | 0.15 | 92 | 0.28 | 847 |
| IA-NS-12 | IA-NS-12_22.1 | 12889 | 91 | 168 | 77 | 0.39 | 74 | 0.22 | 832 |
| IA-NS-12 | IA-NS-12_23.1 | 11749 | 38 | 94 | 52 | 0.19 | 104 | 0.23 | 846 |
| IA-NS-12 | IA-NS-12_24.1 | 10337 | 60 | 114 | 56 | 0.28 | 91 | 0.23 | 836 |
| IA-NS-12 | IA-NS-12_25.1 | 9000 | 20 | 46 | 37 | 0.19 | 55 | 0.36 | 888 |
| IA-NS-12 | IA-NS-12_26.1 | 9818 | 74 | 135 | 62 | 1.5 | 20 | 0.23 | 842 |
| IA-NS-12 | IA-NS-12_27.1 | 7816 | 42 | 73 | 111 | 0.85 | 11 | 0.37 | 902 |
| IA-NS-12 | IA-NS-12_1.1 | 11812 | 2524 | 1830 | 1338 | 414 | 4 | 0.16 | -- |
| IA-NS-12 | IA-NS-12_3.1 | 10025 | 39 | 74 | 121 | 7.2 | 5 | 0.32 | 863 |
| IA-NS-12 | IA-NS-12_9.1 | 9789 | 913 | 1130 | 601 | 5.0 | 71 | 0.08 | 916 |
| IA-G-1 | IA-G-1-1.1 | 9519 | 97 | 144 | 100 | 0.95 | 14 | 0.41 | 861 |
| IA-G-1 | IA-G-1-2.1 | 9767 | 108 | 158 | 99 | 0.87 | 17 | 0.41 | 848 |
| IA-G-1 | IA-G-1-3.1 | 9393 | 33 | 100 | 34 | 0.17 | 64 | 0.42 | 873 |
| IA-G-1 | IA-G-1-4.1 | 8629 | 220 | 237 | 129 | 1.3 | 13 | 0.41 | 903 |
| IA-G-1 | IA-G-1-5.1 | 9059 | 59 | 92 | 83 | 0.65 | 10 | 0.54 | 901 |
| IA-G-1 | IA-G-1-6.1 | 9917 | 85 | 137 | 83 | 0.59 | 27 | 0.27 | 805 |
| IA-G-1 | IA-G-1-6.2 | 10347 | 44 | 77 | 58 | 0.26 | 39 | 0.40 | 830 |
| IA-G-1 | IA-G-1-7.1 | 9728 | 76 | 119 | 86 | 0.86 | 15 | 0.39 | 861 |
| IA-G-1 | IA-G-1-8.1 | 9155 | 73 | 106 | 105 | 0.94 | 13 | 0.44 | 878 |
| IA-G-1 | IA-G-1-9.1 | 8733 | 48 | 74 | 104 | 0.93 | 12 | 0.47 | 895 |
| IA-G-1 | IA-G-1-10.1 | 9781 | 93 | 139 | 95 | 0.94 | 15 | 0.37 | 855 |
| IA-G-1 | IA-G-1-11.1 | 9269 | 108 | 144 | 122 | 0.93 | 15 | 0.45 | 889 |
| IA-G-1 | IA-G-1-12.1 | 8823 | 197 | 216 | 241 | 1.2 | 20 | 0.43 | 902 |

**Appendix B.4**. Continued

| Sample | Grain # | Hf | Th | U | Eu* | Ce* | Ce/Ce* | Eu/Eu* | Crystallization Temp (ºC) |
|---|---|---|---|---|---|---|---|---|---|
| IA-G-1 | IA-G-1-13.1 | 9640 | 36 | 61 | 68 | 0.58 | 14 | 0.47 | 873 |
| IA-G-1 | IA-G-1-14.1 | 8418 | 222 | 187 | 99 | 0.67 | 37 | 0.48 | 961 |
| IA-G-1 | IA-G-1-15.1 | 9573 | 94 | 143 | 94 | 0.85 | 16 | 0.42 | 838 |
| IA-G-1 | IA-G-1-16.1 | 9026 | 31 | 51 | 63 | 0.56 | 10 | 0.54 | 882 |
| IA-G-1 | IA-G-1-17.1 | 8536 | 198 | 204 | 274 | 1.5 | 18 | 0.47 | 924 |
| IA-G-1 | IA-G-1-18.1 | 8592 | 234 | 242 | 181 | 1.3 | 16 | 0.43 | 915 |
| IA-G-1 | IA-G-1-19.1 | 9078 | 82 | 115 | 109 | 0.97 | 12 | 0.44 | 888 |
| IA-G-1 | IA-G-1-20.1 | 10002 | 41 | 72 | 67 | 0.50 | 22 | 0.42 | 854 |
| IA-G-1 | IA-G-1-21.1 | 9301 | 59 | 93 | 86 | 0.81 | 13 | 0.46 | 882 |
| IA-G-1 | IA-G-1-22.1 | 9973 | 1143 | 1123 | 188 | 0.60 | 179 | 0.30 | 869 |
| IA-G-1 | IA-G-1-22.2 | 10149 | 798 | 755 | 366 | 2.2 | 31 | 0.33 | 819 |
| IA-G-1 | IA-G-1-23.1 | 8656 | 131 | 160 | 171 | 0.81 | 20 | 0.45 | 918 |
| IA-G-1 | IA-G-1-24.1 | 9797 | 100 | 150 | 86 | 0.80 | 18 | 0.38 | 831 |
| IA-G-1 | IA-G-1-24.2 | 11878 | 846 | 1247 | 162 | 0.69 | 206 | 0.15 | 806 |
| IA-G-1 | IA-G-1-25.1 | 10938 | 129 | 204 | 86 | 0.58 | 23 | 0.35 | 795 |
| IA-G-1 | IA-G-1-26.1 | 8256 | 231 | 197 | 99 | 0.54 | 59 | 0.50 | 960 |
| IA-G-1 | IA-G-1-27.1 | 9837 | 101 | 155 | 94 | 0.53 | 18 | 0.46 | 854 |
| IA-G-5 | IA-G-5-2.1 | 6786 | 1768 | 1232 | 438 | 2.9 | 116 | 0.28 | 976 |
| IA-G-5 | IA-G-5-4.1 | 7813 | 1516 | 1072 | 401 | 2.1 | 175 | 0.21 | 951 |
| IA-G-5 | IA-G-5-6.1 | 7712 | 893 | 651 | 470 | 3.7 | 62 | 0.32 | 920 |
| IA-G-5 | IA-G-5-7.1 | 6860 | 276 | 316 | 321 | 3.0 | 34 | 0.32 | 890 |
| IA-G-5 | IA-G-5_8.1 | 8715 | 2857 | 1471 | 489 | 1.7 | 235 | 0.21 | 981 |
| IA-G-5 | IA-G-5_9.1 | 9060 | 3573 | 1423 | 870 | 5.7 | 92 | 0.19 | 834 |
| IA-G-5 | IA-G-5_10.1 | 9127 | 906 | 1088 | 198 | 1.1 | 93 | 0.19 | 752 |
| IA-G-5 | IA-G-5_11.1 | 6518 | 471 | 415 | 571 | 6.2 | 29 | 0.33 | 913 |
| IA-G-5 | IA-G-5_12.1 | 7399 | 373 | 410 | 351 | 3.7 | 33 | 0.32 | 884 |
| IA-G-5 | IA-G-5_13.1 | 7182 | 1721 | 939 | 622 | 7.2 | 48 | 0.29 | 893 |
| IA-G-5 | IA-G-5_14.1 | 8011 | 871 | 783 | 369 | 2.6 | 102 | 0.30 | 972 |

**Appendix B.5**. Zircon oxygen isotope compositions, measured *in-situ* by SIMS[40]

| Spot Name | Mount | Date | $^{16}$O Measured | $^{16}$O Error | $^{18}$O Measured | $^{18}$O Error | $^{18}$O/$^{16}$O Measured | $^{18}$O/$^{16}$O Error | $^{18}$O/$^{16}$O Corrected | $\delta^{18}$O Corrected | Error (1σ) | Total Error (2σ)[41] |
|---|---|---|---|---|---|---|---|---|---|---|---|---|
| **IA-NS-2 (Granophyre)** | | | | | | | | | | | | |
| IA-NS-2_1.1 | JW498 | Oct. '11 | 1.939E+9 | | 3.880E+6 | | 0.0020012 | 2.4E-7 | 0.0020134 | 4.1 | 0.12 | 0.71 |
| IA-NS-2_2.1 | JW498 | Oct. '11 | 1.923E+9 | | 3.848E+6 | | 0.0020010 | 1.5E-7 | 0.0020132 | 4.0 | 0.07 | 0.68 |
| IA-NS-2_3.1 | JW498 | Oct. '11 | 1.934E+9 | | 3.870E+6 | | 0.0020012 | 2.0E-7 | 0.0020134 | 4.1 | 0.10 | 0.70 |
| IA-NS-2_4.1 | JW498 | Oct. '11 | 1.950E+9 | | 3.900E+6 | | 0.0019997 | 2.8E-7 | 0.0020118 | 3.3 | 0.14 | 0.72 |
| IA-NS-2_4.2 | JW498 | Oct. '11 | 1.954E+9 | | 3.909E+6 | | 0.0020006 | 1.9E-7 | 0.0020128 | 3.8 | 0.09 | 0.69 |
| IA-NS-2_5.1 | JW498 | Oct. '11 | 1.945E+9 | | 3.893E+6 | | 0.0020015 | 2.0E-7 | 0.0020137 | 4.2 | 0.10 | 0.69 |
| IA-NS-2_5.2 | JW498 | Oct. '11 | 1.926E+9 | | 3.855E+6 | | 0.0020019 | 2.3E-7 | 0.0020141 | 4.5 | 0.11 | 0.70 |
| IA-NS-2_6.1 | JW498 | Oct. '11 | 1.955E+9 | | 3.912E+6 | | 0.0020016 | 2.0E-7 | 0.0020137 | 4.3 | 0.10 | 0.69 |
| IA-NS-2_7.1 | JW498 | Oct. '11 | 1.960E+9 | | 3.922E+6 | | 0.0020011 | 1.7E-7 | 0.0020133 | 4.0 | 0.08 | 0.69 |
| IA-NS-2_8.1 | JW498 | Oct. '11 | 1.944E+9 | | 3.890E+6 | | 0.0020009 | 1.6E-7 | 0.0020131 | 3.9 | 0.08 | 0.68 |
| IA-NS-2_9.1 | JW498 | Oct. '11 | 1.860E+9 | | 3.719E+6 | | 0.0019991 | 2.0E-7 | 0.0020113 | 3.0 | 0.10 | 0.69 |
| IA-NS-2_10.1 | JW498 | Oct. '11 | 1.922E+9 | | 3.845E+6 | | 0.0020000 | 2.9E-7 | 0.0020122 | 3.5 | 0.14 | 0.72 |
| IA-NS-2_10.2 | JW498 | Oct. '11 | 1.898E+9 | | 3.798E+6 | | 0.0020007 | 1.5E-7 | 0.0020128 | 3.8 | 0.08 | 0.68 |
| IA-NS-2_11.1 | JW498 | Oct. '11 | 1.928E+9 | | 3.856E+6 | | 0.0020000 | 1.8E-7 | 0.0020122 | 3.5 | 0.09 | 0.69 |
| IA-NS-2_12.1 | JW498 | Oct. '11 | 1.892E+9 | | 3.784E+6 | | 0.0020004 | 1.8E-7 | 0.0020126 | 3.7 | 0.09 | 0.69 |
| IA-NS-2_12.2 | JW498 | Oct. '11 | 1.915E+9 | | 3.832E+6 | | 0.0020006 | 1.7E-7 | 0.0020128 | 3.8 | 0.08 | 0.69 |
| IA-NS-2_13.1 | JW498 | Oct. '11 | 1.924E+9 | | 3.849E+6 | | 0.0020003 | 2.2E-7 | 0.0020125 | 3.7 | 0.11 | 0.70 |
| IA-NS-2_14.1 | JW498 | Oct. '11 | 1.926E+9 | | 3.851E+6 | | 0.0019994 | 2.3E-7 | 0.0020116 | 3.2 | 0.12 | 0.70 |
| IA-NS-2_15.1 | JW498 | Oct. '11 | 1.941E+9 | | 3.882E+6 | | 0.0020003 | 3.3E-7 | 0.0020125 | 3.6 | 0.16 | 0.74 |
| IA-NS-2_17.2 | JW498 | Oct. '11 | 1.950E+9 | | 3.900E+6 | | 0.0020004 | 1.9E-7 | 0.0020126 | 3.7 | 0.09 | 0.69 |
| IA-NS-2_18.1 | JW498 | Oct. '11 | 1.913E+9 | | 3.830E+6 | | 0.0020017 | 2.1E-7 | 0.0020139 | 4.4 | 0.11 | 0.70 |
| IA-NS-2_20.1 | JW498 | Oct. '11 | 1.875E+9 | | 3.753E+6 | | 0.0020014 | 1.4E-7 | 0.0020135 | 4.2 | 0.07 | 0.68 |
| IA-NS-2_23.1 | JW498 | Oct. '11 | 1.932E+9 | | 3.865E+6 | | 0.0020000 | 2.4E-7 | 0.0020122 | 3.5 | 0.12 | 0.71 |
| IA-NS-2_24.1 | JW498 | Oct. '11 | 1.903E+9 | | 3.806E+6 | | 0.0020004 | 8.9E-8 | 0.0020126 | 3.7 | 0.04 | 0.67 |
| IA-NS-2_25.1 | JW498 | Oct. '11 | 1.936E+9 | | 3.871E+6 | | 0.0019999 | 1.4E-7 | 0.0020121 | 3.4 | 0.07 | 0.68 |

---

[40] Errors are 1σ unless otherwise noted

[41] Total errors, calculated in quadrature, include propagated analytical and external errors

**Appendix B.5**. Continued

| Spot Name | Mount | Date | $^{16}$O Measured | $^{16}$O Error | $^{18}$O Measured | $^{18}$O Error | $^{18}$O/$^{16}$O Measured | $^{18}$O/$^{16}$O Error | $^{18}$O/$^{16}$O Corrected | δ$^{18}$O Corrected | Error (1σ) | Total Error (2σ) |
|---|---|---|---|---|---|---|---|---|---|---|---|---|
| **IA-NS-4b (High-SiO$_2$ Granophyre)** | | | | | | | | | | | | |
| IA-NS-4b_1.1 | JW498 | Oct. '11 | 1.963E+9 | | 3.924E+6 | | 0.0019986 | 1.9E-7 | 0.0020108 | 2.8 | 0.10 | 0.69 |
| IA-NS-4b_1.2 | JW498 | Oct. '11 | 1.988E+9 | | 3.971E+6 | | 0.0019976 | 2.6E-7 | 0.0020098 | 2.3 | 0.13 | 0.71 |
| IA-NS-4b_2.1 | JW498 | Oct. '11 | 1.952E+9 | | 3.902E+6 | | 0.0019983 | 2.0E-7 | 0.0020105 | 2.7 | 0.10 | 0.69 |
| IA-NS-4b_3.1 | JW498 | Oct. '11 | 1.948E+9 | | 3.862E+6 | | 0.0019826 | 2.1E-7 | 0.0019947 | -5.2 | 0.11 | 0.70 |
| IA-NS-4b_4.1 | JW498 | Oct. '11 | 1.902E+9 | | 3.787E+6 | | 0.0019907 | 2.8E-7 | 0.0020028 | -1.2 | 0.14 | 0.72 |
| IA-NS-4b_5.1 | JW498 | Oct. '11 | 1.881E+9 | | 3.767E+6 | | 0.0020020 | 2.2E-7 | 0.0020141 | 4.5 | 0.11 | 0.70 |
| IA-NS-4b_6.1 | JW498 | Oct. '11 | 1.961E+9 | | 3.919E+6 | | 0.0019984 | 1.3E-7 | 0.0020106 | 2.7 | 0.07 | 0.68 |
| IA-NS-4b_7.1 | JW498 | Oct. '11 | 1.951E+9 | | 3.899E+6 | | 0.0019986 | 1.9E-7 | 0.0020108 | 2.8 | 0.09 | 0.69 |
| IA-NS-4b_8.1 | JW498 | Oct. '11 | 1.960E+9 | | 3.916E+6 | | 0.0019981 | 2.7E-7 | 0.0020103 | 2.5 | 0.13 | 0.72 |
| IA-NS-4b_9.1 | JW498 | Oct. '11 | 1.959E+9 | | 3.916E+6 | | 0.0019993 | 1.9E-7 | 0.0020115 | 3.1 | 0.09 | 0.69 |
| IA-NS-4b_9.2 | JW498 | Oct. '11 | 1.953E+9 | | 3.893E+6 | | 0.0019937 | 2.6E-7 | 0.0020058 | 0.3 | 0.13 | 0.71 |
| IA-NS-4b_10.1 | JW498 | Oct. '11 | 1.967E+9 | | 3.933E+6 | | 0.0020000 | 1.9E-7 | 0.0020122 | 3.5 | 0.09 | 0.69 |
| IA-NS-4b_11.1 | JW498 | Oct. '11 | 1.957E+9 | | 3.911E+6 | | 0.0019986 | 1.5E-7 | 0.0020108 | 2.8 | 0.08 | 0.68 |
| IA-NS-4b_12.1 | JW498 | Oct. '11 | 1.959E+9 | | 3.914E+6 | | 0.0019984 | 2.0E-7 | 0.0020106 | 2.7 | 0.10 | 0.70 |
| IA-NS-4b_13.1 | JW498 | Oct. '11 | 1.865E+9 | | 3.731E+6 | | 0.0020007 | 2.2E-7 | 0.0020129 | 3.8 | 0.11 | 0.70 |
| IA-NS-4b_14.1 | JW498 | Oct. '11 | 1.895E+9 | | 3.782E+6 | | 0.0019956 | 1.7E-7 | 0.0020077 | 1.3 | 0.08 | 0.69 |
| IA-NS-4b_14.2 | JW498 | Oct. '11 | 1.908E+9 | | 3.795E+6 | | 0.0019897 | 2.5E-7 | 0.0020018 | -1.7 | 0.12 | 0.71 |
| IA-NS-4b_15.1 | JW498 | Oct. '11 | 1.955E+9 | | 3.898E+6 | | 0.0019937 | 1.4E-7 | 0.0020058 | 0.3 | 0.07 | 0.68 |
| IA-NS-4b_17.1 | JW498 | Oct. '11 | 1.842E+9 | | 3.671E+6 | | 0.0019934 | 1.9E-7 | 0.0020056 | 0.2 | 0.10 | 0.69 |
| IA-NS-4b_18.1 | JW498 | Oct. '11 | 1.943E+9 | | 3.882E+6 | | 0.0019985 | 2.7E-7 | 0.0020107 | 2.7 | 0.13 | 0.72 |
| IA-NS-4b_19.1 | JW498 | Oct. '11 | 1.884E+9 | | 3.770E+6 | | 0.0020015 | 1.7E-7 | 0.0020137 | 4.2 | 0.08 | 0.68 |
| IA-NS-4b_21.1 | JW498 | Oct. '11 | 1.881E+9 | | 3.728E+6 | | 0.0019816 | 1.9E-7 | 0.0019937 | -5.7 | 0.10 | 0.69 |
| IA-NS-4b_21.2 | JW498 | Oct. '11 | 1.867E+9 | | 3.703E+6 | | 0.0019834 | 1.8E-7 | 0.0019955 | -4.9 | 0.09 | 0.69 |
| IA-NS-4b_22.1 | JW498 | Oct. '11 | 1.937E+9 | | 3.851E+6 | | 0.0019884 | 2.6E-7 | 0.0020005 | -2.4 | 0.13 | 0.72 |
| IA-NS-4b_24.1 | JW498 | Oct. '11 | 1.925E+9 | | 3.852E+6 | | 0.0020013 | 2.4E-7 | 0.0020135 | 4.1 | 0.12 | 0.71 |
| IA-NS-4b_25.1 | JW498 | Oct. '11 | 1.864E+9 | | 3.729E+6 | | 0.0020002 | 2.0E-7 | 0.0020124 | 3.6 | 0.10 | 0.69 |
| IA-NS-4b_26.1 | JW498 | Oct. '11 | 1.869E+9 | | 3.741E+6 | | 0.0020015 | 1.3E-7 | 0.0020137 | 4.3 | 0.07 | 0.68 |
| IA-NS-4b_27.1 | JW498 | Oct. '11 | 1.857E+9 | | 3.713E+6 | | 0.0019993 | 1.3E-7 | 0.0020115 | 3.1 | 0.07 | 0.68 |
| IA-NS-4b_29.1 | JW498 | Oct. '11 | 1.923E+9 | | 3.815E+6 | | 0.0019839 | 2.2E-7 | 0.0019959 | -4.6 | 0.11 | 0.70 |
| IA-NS-4b_30.1 | JW498 | Oct. '11 | 1.830E+9 | | 3.637E+6 | | 0.0019878 | 1.9E-7 | 0.0019999 | -2.7 | 0.10 | 0.69 |
| IA-NS-4b_31.1 | JW498 | Oct. '11 | 1.825E+9 | | 3.631E+6 | | 0.0019892 | 2.2E-7 | 0.0020013 | -1.9 | 0.11 | 0.70 |
| IA-NS-4b_32.1 | JW498 | Oct. '11 | 1.870E+9 | | 3.732E+6 | | 0.0019959 | 1.6E-7 | 0.0020081 | 1.4 | 0.08 | 0.68 |

**Appendix B.5**. Continued

| Spot Name | Mount | Date | $^{16}$O Measured | $^{16}$O Error | $^{18}$O Measured | $^{18}$O Error | $^{18}$O/$^{16}$O Measured | $^{18}$O/$^{16}$O Error | $^{18}$O/$^{16}$O Corrected | $\delta^{18}$O Corrected | Error (1σ) | Total Error (2σ) |
|---|---|---|---|---|---|---|---|---|---|---|---|---|
| **IA-NS-4b (continued)** | | | | | | | | | | | | |
| IA-NS-4b_33.1 | JW498 | Oct. '11 | 1.872E+9 | | 3.727E+6 | | 0.0019911 | 1.3E-7 | 0.0020032 | -1.0 | 0.07 | 0.68 |
| IA-NS-4b_34.1 | JW498 | Oct. '11 | 1.843E+9 | | 3.670E+6 | | 0.0019912 | 1.9E-7 | 0.0020033 | -0.9 | 0.10 | 0.69 |
| IA-NS-4b_40.1 | AJP05 | Dec. '14 | 4.142E+9 | 1.8E+7 | 8.223E+6 | 3.5E+4 | 0.0019854 | 1.4E-7 | 0.0019913 | -6.9 | 0.07 | 0.58 |
| IA-NS-4b_41.1 | AJP05 | Dec. '14 | 4.092E+9 | 1.2E+7 | 8.159E+6 | 2.5E+4 | 0.0019937 | 1.2E-7 | 0.0019996 | -2.8 | 0.06 | 0.57 |
| IA-NS-4b_42.1 | AJP05 | Dec. '14 | 3.987E+9 | 1.2E+7 | 7.978E+6 | 2.3E+4 | 0.0020009 | 1.3E-7 | 0.0020069 | 0.8 | 0.07 | 0.57 |
| IA-NS-4b_43.1 | AJP05 | Dec. '14 | 3.992E+9 | 1.4E+7 | 8.013E+6 | 2.8E+4 | 0.0020073 | 1.2E-7 | 0.0020133 | 4.0 | 0.06 | 0.57 |
| IA-NS-4b_44.1 | AJP05 | Dec. '14 | 3.854E+9 | 9.1E+6 | 7.691E+6 | 1.9E+4 | 0.0019958 | 3.2E-7 | 0.0020018 | -1.7 | 0.16 | 0.64 |
| IA-NS-4b_45.1 | AJP05 | Dec. '14 | 3.984E+9 | 2.0E+7 | 7.990E+6 | 3.9E+4 | 0.0020055 | 1.8E-7 | 0.0020115 | 3.1 | 0.09 | 0.59 |
| IA-NS-4b_46.1 | AJP05 | Dec. '14 | 3.941E+9 | 6.3E+6 | 7.846E+6 | 1.2E+4 | 0.0019908 | 2.5E-7 | 0.0019968 | -4.2 | 0.13 | 0.61 |
| IA-NS-4b_47.1 | AJP05 | Dec. '14 | 3.895E+9 | 1.0E+7 | 7.767E+6 | 1.9E+4 | 0.0019940 | 2.5E-7 | 0.0020000 | -2.6 | 0.13 | 0.61 |
| IA-NS-4b_48.1 | AJP05 | Dec. '14 | 4.008E+9 | 2.7E+7 | 8.022E+6 | 5.2E+4 | 0.0020015 | 3.3E-7 | 0.0020075 | 1.2 | 0.16 | 0.65 |
| IA-NS-4b_49.1 | AJP05 | Dec. '14 | 4.005E+9 | 1.7E+7 | 7.975E+6 | 3.3E+4 | 0.0019915 | 2.2E-7 | 0.0019974 | -3.9 | 0.11 | 0.60 |
| IA-NS-4b_50.1 | AJP05 | Dec. '14 | 4.079E+9 | 1.8E+7 | 8.123E+6 | 3.5E+4 | 0.0019917 | 1.8E-7 | 0.0019976 | -3.8 | 0.09 | 0.59 |
| IA-NS-4b_51.1 | AJP05 | Dec. '14 | 4.002E+9 | 1.4E+7 | 8.027E+6 | 2.8E+4 | 0.0020061 | 1.6E-7 | 0.0020121 | 3.4 | 0.08 | 0.58 |
| IA-NS-4b_52.1 | AJP05 | Dec. '14 | 3.982E+9 | 1.3E+7 | 7.975E+6 | 2.7E+4 | 0.0020030 | 1.1E-7 | 0.0020090 | 1.9 | 0.05 | 0.57 |
| IA-NS-4b_53.1 | AJP05 | Dec. '14 | 3.957E+9 | 2.0E+7 | 7.878E+6 | 3.9E+4 | 0.0019908 | 1.7E-7 | 0.0019968 | -4.2 | 0.08 | 0.58 |
| IA-NS-4b_54.1 | AJP05 | Dec. '14 | 4.079E+9 | 2.2E+7 | 8.161E+6 | 4.3E+4 | 0.0020006 | 3.4E-7 | 0.0020066 | 0.7 | 0.17 | 0.66 |
| IA-NS-4b_55.1 | AJP05 | Dec. '14 | 3.953E+9 | 1.1E+7 | 7.852E+6 | 2.2E+4 | 0.0019865 | 1.8E-7 | 0.0019925 | -6.3 | 0.09 | 0.59 |
| IA-NS-4b_56.1 | AJP05 | Dec. '14 | 3.936E+9 | 7.6E+6 | 7.836E+6 | 1.5E+4 | 0.0019907 | 1.4E-7 | 0.0019966 | -4.3 | 0.07 | 0.58 |
| IA-NS-4b_57.1 | AJP05 | Dec. '14 | 4.027E+9 | 1.9E+7 | 8.063E+6 | 3.6E+4 | 0.0020020 | 2.0E-7 | 0.0020080 | 1.4 | 0.10 | 0.59 |
| IA-NS-4b_58.1 | AJP05 | Dec. '14 | 3.963E+9 | 1.8E+7 | 7.924E+6 | 3.5E+4 | 0.0019996 | 2.1E-7 | 0.0020056 | 0.2 | 0.11 | 0.60 |
| IA-NS-4b_59.1 | AJP05 | Dec. '14 | 3.887E+9 | 1.3E+7 | 7.800E+6 | 2.6E+4 | 0.0020065 | 1.6E-7 | 0.0020125 | 3.6 | 0.08 | 0.58 |
| IA-NS-4b_60.1 | AJP05 | Dec. '14 | 3.938E+9 | 1.6E+7 | 7.844E+6 | 3.0E+4 | 0.0019918 | 2.9E-7 | 0.0019978 | -3.7 | 0.15 | 0.63 |
| **IA-NS-6 (Diorite)** | | | | | | | | | | | | |
| IA-NS-6_1.1 | JW498 | Oct. '11 | 1.921E+9 | | 3.842E+6 | | 0.0019999 | 2.0E-7 | 0.0020121 | 3.5 | 0.10 | 0.69 |
| IA-NS-6_2.1 | JW498 | Oct. '11 | 1.895E+9 | | 3.789E+6 | | 0.0019996 | 2.3E-7 | 0.0020118 | 3.3 | 0.12 | 0.70 |
| IA-NS-6_3.1 | JW498 | Oct. '11 | 1.907E+9 | | 3.817E+6 | | 0.0020009 | 2.5E-7 | 0.0020131 | 4.0 | 0.13 | 0.71 |
| IA-NS-6_4.1 | JW498 | Oct. '11 | 1.927E+9 | | 3.856E+6 | | 0.0020006 | 3.0E-7 | 0.0020128 | 3.8 | 0.15 | 0.73 |
| IA-NS-6_5.1 | JW498 | Oct. '11 | 1.936E+9 | | 3.874E+6 | | 0.0020004 | 1.6E-7 | 0.0020126 | 3.7 | 0.08 | 0.68 |
| IA-NS-6_6.1 | JW498 | Oct. '11 | 1.915E+9 | | 3.830E+6 | | 0.0020000 | 1.9E-7 | 0.0020122 | 3.5 | 0.10 | 0.69 |
| IA-NS-6_7.1 | JW498 | Oct. '11 | 1.930E+9 | | 3.859E+6 | | 0.0019998 | 1.4E-7 | 0.0020120 | 3.4 | 0.07 | 0.68 |

**Appendix B.5**. Continued

| Spot Name | Mount | Date | $^{16}$O Measured | $^{16}$O Error | $^{18}$O Measured | $^{18}$O Error | $^{18}$O/$^{16}$O Measured | $^{18}$O/$^{16}$O Error | $^{18}$O/$^{16}$O Corrected | $\delta^{18}$O Corrected | Error (1σ) | Total Error (2σ) |
|---|---|---|---|---|---|---|---|---|---|---|---|---|
| **IA-NS-6 (continued)** | | | | | | | | | | | | |
| IA-NS-6_8.1 | JW498 | Oct. '11 | 1.822E+9 | | 3.644E+6 | | 0.0020000 | 1.4E-7 | 0.0020122 | 3.5 | 0.07 | 0.68 |
| IA-NS-6_9.1 | JW498 | Oct. '11 | 1.915E+9 | | 3.831E+6 | | 0.0020004 | 1.8E-7 | 0.0020126 | 3.7 | 0.09 | 0.69 |
| IA-NS-6_10.1 | JW498 | Oct. '11 | 1.932E+9 | | 3.864E+6 | | 0.0020003 | 2.2E-7 | 0.0020125 | 3.6 | 0.11 | 0.70 |
| IA-NS-6_11.1 | JW498 | Oct. '11 | 1.894E+9 | | 3.792E+6 | | 0.0020020 | 2.2E-7 | 0.0020142 | 4.5 | 0.11 | 0.70 |
| IA-NS-6_12.1 | JW498 | Oct. '11 | 1.908E+9 | | 3.815E+6 | | 0.0019997 | 3.0E-7 | 0.0020119 | 3.3 | 0.15 | 0.73 |
| IA-NS-6_13.1 | JW498 | Oct. '11 | 1.938E+9 | | 3.877E+6 | | 0.0020011 | 1.7E-7 | 0.0020133 | 4.1 | 0.08 | 0.69 |
| IA-NS-6_14.1 | JW498 | Oct. '11 | 1.893E+9 | | 3.784E+6 | | 0.0019995 | 1.2E-7 | 0.0020117 | 3.2 | 0.06 | 0.68 |
| IA-NS-6_15.1 | JW498 | Oct. '11 | 1.935E+9 | | 3.873E+6 | | 0.0020014 | 1.4E-7 | 0.0020136 | 4.2 | 0.07 | 0.68 |
| IA-NS-6_16.1 | JW498 | Oct. '11 | 1.874E+9 | | 3.745E+6 | | 0.0019984 | 2.7E-7 | 0.0020106 | 2.7 | 0.13 | 0.72 |
| IA-NS-6_17.1 | JW498 | Oct. '11 | 1.926E+9 | | 3.852E+6 | | 0.0019999 | 1.8E-7 | 0.0020121 | 3.4 | 0.09 | 0.69 |
| IA-NS-6_17.2 | JW498 | Oct. '11 | 1.903E+9 | | 3.809E+6 | | 0.0020015 | 1.8E-7 | 0.0020136 | 4.2 | 0.09 | 0.69 |
| IA-NS-6_18.1 | JW498 | Oct. '11 | 1.899E+9 | | 3.801E+6 | | 0.0020009 | 1.3E-7 | 0.0020131 | 3.9 | 0.06 | 0.68 |
| IA-NS-6_19.1 | JW498 | Oct. '11 | 1.921E+9 | | 3.844E+6 | | 0.0020015 | 1.8E-7 | 0.0020137 | 4.2 | 0.09 | 0.69 |
| IA-NS-6_21.1 | JW498 | Oct. '11 | 1.888E+9 | | 3.775E+6 | | 0.0020002 | 1.3E-7 | 0.0020124 | 3.6 | 0.07 | 0.68 |
| IA-NS-6_22.1 | JW498 | Oct. '11 | 1.880E+9 | | 3.760E+6 | | 0.0020004 | 2.2E-7 | 0.0020126 | 3.7 | 0.11 | 0.70 |
| IA-NS-6_23.1 | JW498 | Oct. '11 | 1.866E+9 | | 3.732E+6 | | 0.0019998 | 1.3E-7 | 0.0020120 | 3.4 | 0.07 | 0.68 |
| IA-NS-6_24.1 | JW498 | Oct. '11 | 1.928E+9 | | 3.857E+6 | | 0.0020006 | 2.5E-7 | 0.0020127 | 3.8 | 0.13 | 0.71 |
| IA-NS-6_24.2 | JW498 | Oct. '11 | 1.930E+9 | | 3.858E+6 | | 0.0019996 | 1.6E-7 | 0.0020118 | 3.3 | 0.08 | 0.68 |
| IA-NS-6_26.1 | JW498 | Oct. '11 | 1.936E+9 | | 3.873E+6 | | 0.0020007 | 2.1E-7 | 0.0020128 | 3.8 | 0.10 | 0.70 |
| **IA-NS-7 (Granodiorite)** | | | | | | | | | | | | |
| IA-NS-7_1.1 | JW510 | Apr. '12 | 2.112E+9 | 1.6E+6 | 4.245E+6 | 3.3E+3 | 0.0020104 | 1.8E-7 | 0.0020127 | 3.8 | 0.09 | 0.47 |
| IA-NS-7_2.1 | JW510 | Apr. '12 | 2.103E+9 | 8.2E+5 | 4.229E+6 | 1.6E+3 | 0.0020106 | 9.2E-8 | 0.0020130 | 3.9 | 0.05 | 0.44 |
| IA-NS-7_3.1 | JW510 | Apr. '12 | 2.128E+9 | 2.2E+6 | 4.275E+6 | 4.4E+3 | 0.0020086 | 1.4E-7 | 0.0020110 | 2.9 | 0.07 | 0.45 |
| IA-NS-7_4.1 | JW510 | Apr. '12 | 2.100E+9 | 1.3E+6 | 4.225E+6 | 2.7E+3 | 0.0020114 | 1.5E-7 | 0.0020137 | 4.3 | 0.08 | 0.46 |
| IA-NS-7_6.1 | JW510 | Apr. '12 | 2.104E+9 | 1.9E+6 | 4.229E+6 | 3.9E+3 | 0.0020100 | 1.5E-7 | 0.0020124 | 3.6 | 0.08 | 0.46 |
| IA-NS-7_7.1 | JW510 | Apr. '12 | 2.107E+9 | 1.6E+6 | 4.238E+6 | 3.3E+3 | 0.0020111 | 1.4E-7 | 0.0020134 | 4.1 | 0.07 | 0.46 |
| IA-NS-7_9.1 | JW510 | Apr. '12 | 2.109E+9 | 1.0E+6 | 4.239E+6 | 2.0E+3 | 0.0020101 | 1.7E-7 | 0.0020125 | 3.6 | 0.08 | 0.46 |
| IA-NS-7_10.1 | JW510 | Apr. '12 | 2.054E+9 | 1.9E+6 | 4.132E+6 | 4.1E+3 | 0.0020117 | 2.8E-7 | 0.0020140 | 4.4 | 0.14 | 0.51 |
| IA-NS-7_11.1 | JW510 | Apr. '12 | 2.106E+9 | 9.5E+5 | 4.235E+6 | 1.9E+3 | 0.0020108 | 1.1E-7 | 0.0020132 | 4.0 | 0.05 | 0.45 |
| IA-NS-7_12.1 | JW510 | Apr. '12 | 2.140E+9 | 2.1E+6 | 4.303E+6 | 4.2E+3 | 0.0020103 | 1.3E-7 | 0.0020126 | 3.7 | 0.06 | 0.45 |
| IA-NS-7_13.1 | JW510 | Apr. '12 | 2.119E+9 | 7.2E+5 | 4.259E+6 | 1.3E+3 | 0.0020105 | 1.8E-7 | 0.0020129 | 3.8 | 0.09 | 0.47 |

**Appendix B.5**. Continued

| Spot Name | Mount | Date | $^{16}$O Measured | $^{16}$O Error | $^{18}$O Measured | $^{18}$O Error | $^{18}$O/$^{16}$O Measured | $^{18}$O/$^{16}$O Error | $^{18}$O/$^{16}$O Corrected | δ$^{18}$O Corrected | Error (1σ) | Total Error (2σ) |
|---|---|---|---|---|---|---|---|---|---|---|---|---|
| **IA-NS-7 (continued)** | | | | | | | | | | | | |
| IA-NS-7_14.1 | JW510 | Apr. '12 | 2.120E+9 | 1.3E+6 | 4.261E+6 | 2.7E+3 | 0.0020102 | 1.3E-7 | 0.0020126 | 3.7 | 0.06 | 0.45 |
| IA-NS-7_15.1 | JW510 | Apr. '12 | 2.098E+9 | 9.7E+5 | 4.220E+6 | 2.0E+3 | 0.0020112 | 1.6E-7 | 0.0020135 | 4.1 | 0.08 | 0.46 |
| IA-NS-7_17.1 | JW510 | Apr. '12 | 2.113E+9 | 1.4E+6 | 4.250E+6 | 2.8E+3 | 0.0020111 | 1.6E-7 | 0.0020135 | 4.1 | 0.08 | 0.46 |
| IA-NS-7_19.1 | JW510 | Apr. '12 | 2.119E+9 | 1.3E+6 | 4.262E+6 | 2.7E+3 | 0.0020112 | 1.6E-7 | 0.0020135 | 4.2 | 0.08 | 0.46 |
| **IA-NS-9 (High-SiO$_2$ Granophyre)** | | | | | | | | | | | | |
| IA-NS-9_1.1 | AJP03 | Nov. '13 | 1.673E+9 | 3.3E+6 | 3.367E+6 | 6.6E+3 | 0.0020126 | 1.5E-7 | 0.0020142 | 4.5 | 0.07 | 0.68 |
| IA-NS-9_2.1 | AJP03 | Nov. '13 | 1.634E+9 | 8.7E+5 | 3.255E+6 | 1.7E+3 | 0.0019924 | 2.3E-7 | 0.0019940 | -5.6 | 0.11 | 0.70 |
| IA-NS-9_3.1 | AJP03 | Nov. '13 | 1.594E+9 | 2.8E+5 | 3.192E+6 | 6.4E+2 | 0.0020029 | 2.0E-7 | 0.0020045 | -0.3 | 0.10 | 0.70 |
| IA-NS-9_4.1 | AJP03 | Nov. '13 | 1.588E+9 | 4.5E+5 | 3.195E+6 | 9.4E+2 | 0.0020119 | 2.4E-7 | 0.0020135 | 4.1 | 0.12 | 0.71 |
| IA-NS-9_5.1 | AJP03 | Nov. '13 | 1.601E+9 | 1.2E+6 | 3.221E+6 | 2.4E+3 | 0.0020118 | 1.9E-7 | 0.0020134 | 4.1 | 0.09 | 0.69 |
| IA-NS-9_6.1 | AJP03 | Nov. '13 | 1.593E+9 | 2.2E+6 | 3.204E+6 | 4.4E+3 | 0.0020111 | 1.0E-7 | 0.0020127 | 3.7 | 0.05 | 0.67 |
| IA-NS-9_7.1 | AJP03 | Nov. '13 | 1.617E+9 | 1.7E+6 | 3.253E+6 | 3.5E+3 | 0.0020116 | 2.2E-7 | 0.0020132 | 4.0 | 0.11 | 0.70 |
| IA-NS-9_8.1 | AJP03 | Nov. '13 | 1.632E+9 | 3.1E+6 | 3.283E+6 | 6.2E+3 | 0.0020117 | 2.5E-7 | 0.0020133 | 4.0 | 0.13 | 0.71 |
| IA-NS-9_9.2 | AJP03 | Nov. '13 | 1.670E+9 | 4.5E+6 | 3.357E+6 | 9.1E+3 | 0.0020107 | 1.9E-7 | 0.0020123 | 3.6 | 0.10 | 0.69 |
| IA-NS-9_10.2 | AJP03 | Nov. '13 | 1.672E+9 | 1.6E+6 | 3.363E+6 | 3.4E+3 | 0.0020113 | 2.6E-7 | 0.0020129 | 3.8 | 0.13 | 0.71 |
| IA-NS-9_11.1 | AJP03 | Nov. '13 | 1.713E+9 | 2.5E+6 | 3.445E+6 | 4.9E+3 | 0.0020114 | 1.7E-7 | 0.0020130 | 3.9 | 0.08 | 0.69 |
| IA-NS-9_12.2 | AJP03 | Nov. '13 | 1.704E+9 | 9.3E+5 | 3.427E+6 | 2.0E+3 | 0.0020111 | 3.3E-7 | 0.0020128 | 3.8 | 0.16 | 0.74 |
| IA-NS-9_13.1 | AJP03 | Nov. '13 | 1.710E+9 | 1.1E+6 | 3.437E+6 | 2.6E+3 | 0.0020103 | 2.4E-7 | 0.0020119 | 3.4 | 0.12 | 0.71 |
| IA-NS-9_14.1 | AJP03 | Nov. '13 | 1.695E+9 | 3.8E+6 | 3.401E+6 | 7.7E+3 | 0.0020062 | 1.7E-7 | 0.0020078 | 1.3 | 0.08 | 0.69 |
| IA-NS-9_15.1 | AJP03 | Nov. '13 | 1.734E+9 | 2.5E+6 | 3.489E+6 | 5.0E+3 | 0.0020119 | 1.8E-7 | 0.0020135 | 4.1 | 0.09 | 0.69 |
| IA-NS-9_16.1 | AJP03 | Nov. '13 | 1.763E+9 | 8.5E+5 | 3.547E+6 | 1.9E+3 | 0.0020117 | 2.7E-7 | 0.0020133 | 4.1 | 0.13 | 0.72 |
| IA-NS-9_17.1 | AJP03 | Nov. '13 | 1.797E+9 | 1.6E+6 | 3.593E+6 | 3.2E+3 | 0.0020001 | 2.0E-7 | 0.0020017 | -1.8 | 0.10 | 0.70 |
| IA-NS-9_18.1 | AJP03 | Nov. '13 | 1.767E+9 | 9.4E+5 | 3.543E+6 | 2.0E+3 | 0.0020053 | 2.4E-7 | 0.0020069 | 0.9 | 0.12 | 0.71 |
| IA-NS-9_19.1 | AJP03 | Nov. '13 | 1.686E+9 | 2.6E+6 | 3.341E+6 | 5.4E+3 | 0.0019809 | 2.1E-7 | 0.0019825 | -11.3 | 0.11 | 0.70 |
| IA-NS-9_20.1 | AJP03 | Nov. '13 | 1.768E+9 | 4.6E+6 | 3.537E+6 | 9.6E+3 | 0.0020001 | 3.4E-7 | 0.0020017 | -1.7 | 0.17 | 0.75 |
| IA-NS-9_21.1 | AJP03 | Nov. '13 | 1.793E+9 | 2.6E+6 | 3.565E+6 | 5.2E+3 | 0.0019879 | 1.7E-7 | 0.0019895 | -7.8 | 0.09 | 0.69 |
| IA-NS-9_25.1 | AJP05 | Dec. '14 | 3.868E+9 | 2.1E+7 | 7.732E+6 | 4.0E+4 | 0.0019987 | 3.5E-7 | 0.0020047 | -0.3 | 0.17 | 0.66 |
| IA-NS-9_26.1 | AJP05 | Dec. '14 | 3.948E+9 | 1.0E+7 | 7.896E+6 | 2.0E+4 | 0.0019998 | 1.6E-7 | 0.0020058 | 0.3 | 0.08 | 0.58 |
| IA-NS-9_27.1 | AJP05 | Dec. '14 | 3.885E+9 | 1.8E+7 | 7.751E+6 | 3.4E+4 | 0.0019949 | 2.8E-7 | 0.0020009 | -2.2 | 0.14 | 0.63 |
| IA-NS-9_28.1 | AJP05 | Dec. '14 | 3.906E+9 | 3.2E+7 | 7.787E+6 | 6.2E+4 | 0.0019935 | 3.6E-7 | 0.0019995 | -2.8 | 0.18 | 0.66 |
| IA-NS-9_29.1 | AJP05 | Dec. '14 | 3.934E+9 | 1.2E+7 | 7.875E+6 | 2.4E+4 | 0.0020018 | 1.2E-7 | 0.0020078 | 1.3 | 0.06 | 0.57 |

**Appendix B.5**. Continued

| Spot Name | Mount | Date | $^{16}$O Measured | $^{16}$O Error | $^{18}$O Measured | $^{18}$O Error | $^{18}$O/$^{16}$O Measured | $^{18}$O/$^{16}$O Error | $^{18}$O/$^{16}$O Corrected | $\delta^{18}$O Corrected | Error (1σ) | Total Error (2σ) |
|---|---|---|---|---|---|---|---|---|---|---|---|---|
| **IA-NS-9 (continued)** | | | | | | | | | | | | |
| IA-NS-9_30.1 | AJP05 | Dec. '14 | 3.928E+9 | 1.2E+7 | 7.837E+6 | 2.4E+4 | 0.0019950 | 2.6E-7 | 0.0020010 | -2.1 | 0.13 | 0.61 |
| IA-NS-9_31.1 | AJP05 | Dec. '14 | 3.896E+9 | 1.4E+7 | 7.811E+6 | 2.7E+4 | 0.0020050 | 1.6E-7 | 0.0020110 | 2.9 | 0.08 | 0.58 |
| IA-NS-9_32.1 | AJP05 | Dec. '14 | 3.942E+9 | 1.3E+7 | 7.910E+6 | 2.6E+4 | 0.0020068 | 1.3E-7 | 0.0020128 | 3.8 | 0.06 | 0.57 |
| IA-NS-9_33.1 | AJP05 | Dec. '14 | 3.973E+9 | 1.4E+7 | 7.974E+6 | 2.8E+4 | 0.0020071 | 1.8E-7 | 0.0020131 | 3.9 | 0.09 | 0.59 |
| IA-NS-9_34.1 | AJP05 | Dec. '14 | 4.022E+9 | 1.7E+7 | 8.071E+6 | 3.3E+4 | 0.0020066 | 1.7E-7 | 0.0020126 | 3.7 | 0.09 | 0.59 |
| IA-NS-9_35.1 | AJP05 | Dec. '14 | 3.963E+9 | 1.4E+7 | 7.955E+6 | 2.8E+4 | 0.0020074 | 1.3E-7 | 0.0020134 | 4.1 | 0.06 | 0.57 |
| IA-NS-9_36.1 | AJP05 | Dec. '14 | 3.855E+9 | 1.3E+7 | 7.731E+6 | 2.6E+4 | 0.0020055 | 1.3E-7 | 0.0020115 | 3.1 | 0.07 | 0.57 |
| IA-NS-9_37.1 | AJP05 | Dec. '14 | 3.753E+9 | 1.6E+7 | 7.529E+6 | 3.3E+4 | 0.0020063 | 1.5E-7 | 0.0020123 | 3.5 | 0.07 | 0.58 |
| IA-NS-9_38.1 | AJP05 | Dec. '14 | 3.895E+9 | 1.1E+7 | 7.809E+6 | 2.2E+4 | 0.0020046 | 1.6E-7 | 0.0020106 | 2.7 | 0.08 | 0.58 |
| **IA-NS-10 (High-SiO$_2$ Granophyre)** | | | | | | | | | | | | |
| IA-NS-10_1.1 | AJP05 | Dec. '14 | 3.787E+9 | 1.7E+7 | 7.602E+6 | 3.3E+4 | 0.0020073 | 1.9E-7 | 0.0020133 | 4.0 | 0.09 | 0.59 |
| IA-NS-10_2.1 | AJP05 | Dec. '14 | 3.940E+9 | 2.3E+7 | 7.897E+6 | 4.5E+4 | 0.0020043 | 2.0E-7 | 0.0020103 | 2.6 | 0.10 | 0.59 |
| IA-NS-10_3.1 | AJP05 | Dec. '14 | 4.025E+9 | 1.8E+7 | 8.072E+6 | 3.6E+4 | 0.0020053 | 1.3E-7 | 0.0020113 | 3.0 | 0.07 | 0.57 |
| IA-NS-10_4.1 | AJP05 | Dec. '14 | 3.931E+9 | 1.8E+7 | 7.891E+6 | 3.5E+4 | 0.0020070 | 1.3E-7 | 0.0020131 | 3.9 | 0.07 | 0.57 |
| IA-NS-10_5.1 | AJP05 | Dec. '14 | 3.972E+9 | 1.5E+7 | 7.973E+6 | 2.9E+4 | 0.0020072 | 2.1E-7 | 0.0020132 | 4.0 | 0.11 | 0.60 |
| IA-NS-10_6.1 | AJP05 | Dec. '14 | 3.933E+9 | 1.5E+7 | 7.891E+6 | 3.0E+4 | 0.0020063 | 1.1E-7 | 0.0020123 | 3.5 | 0.05 | 0.57 |
| IA-NS-10_7.1 | AJP05 | Dec. '14 | 3.924E+9 | 1.5E+7 | 7.869E+6 | 2.9E+4 | 0.0020056 | 1.1E-7 | 0.0020116 | 3.2 | 0.06 | 0.57 |
| IA-NS-10_8.1 | AJP05 | Dec. '14 | 4.016E+9 | 9.6E+6 | 8.054E+6 | 1.9E+4 | 0.0020056 | 1.3E-7 | 0.0020116 | 3.2 | 0.06 | 0.57 |
| IA-NS-10_9.1 | AJP05 | Dec. '14 | 3.964E+9 | 1.5E+7 | 7.954E+6 | 3.0E+4 | 0.0020063 | 1.6E-7 | 0.0020123 | 3.6 | 0.08 | 0.58 |
| IA-NS-10_10.1 | AJP05 | Dec. '14 | 3.994E+9 | 1.5E+7 | 8.010E+6 | 3.0E+4 | 0.0020056 | 1.7E-7 | 0.0020116 | 3.2 | 0.09 | 0.59 |
| IA-NS-10_11.1 | AJP05 | Dec. '14 | 3.900E+9 | 1.4E+7 | 7.830E+6 | 2.8E+4 | 0.0020076 | 1.4E-7 | 0.0020136 | 4.2 | 0.07 | 0.58 |
| IA-NS-10_12.1 | AJP05 | Dec. '14 | 3.928E+9 | 1.8E+7 | 7.881E+6 | 3.5E+4 | 0.0020064 | 2.5E-7 | 0.0020124 | 3.6 | 0.12 | 0.61 |
| IA-NS-10_13.1 | AJP05 | Dec. '14 | 3.916E+9 | 1.9E+7 | 7.853E+6 | 3.8E+4 | 0.0020053 | 1.7E-7 | 0.0020113 | 3.0 | 0.08 | 0.58 |
| IA-NS-10_14.1 | AJP05 | Dec. '14 | 3.954E+9 | 1.4E+7 | 7.937E+6 | 2.9E+4 | 0.0020075 | 9.3E-8 | 0.0020135 | 4.2 | 0.05 | 0.57 |
| IA-NS-10_15.1 | AJP05 | Dec. '14 | 3.807E+9 | 1.4E+7 | 7.612E+6 | 2.8E+4 | 0.0019996 | 1.9E-7 | 0.0020056 | 0.2 | 0.10 | 0.59 |
| IA-NS-10_16.1 | AJP05 | Dec. '14 | 3.961E+9 | 1.4E+7 | 7.949E+6 | 2.8E+4 | 0.0020068 | 2.3E-7 | 0.0020128 | 3.8 | 0.12 | 0.60 |
| IA-NS-10_17.1 | AJP05 | Dec. '14 | 3.922E+9 | 1.5E+7 | 7.865E+6 | 3.1E+4 | 0.0020053 | 1.5E-7 | 0.0020113 | 3.0 | 0.07 | 0.58 |
| IA-NS-10_18.1 | AJP05 | Dec. '14 | 3.973E+9 | 1.5E+7 | 7.971E+6 | 3.0E+4 | 0.0020065 | 1.1E-7 | 0.0020125 | 3.6 | 0.06 | 0.57 |
| IA-NS-10_19.1 | AJP05 | Dec. '14 | 3.946E+9 | 1.3E+7 | 7.916E+6 | 2.5E+4 | 0.0020062 | 1.7E-7 | 0.0020122 | 3.5 | 0.08 | 0.58 |
| IA-NS-10_20.1 | AJP05 | Dec. '14 | 3.906E+9 | 1.7E+7 | 7.831E+6 | 3.4E+4 | 0.0020047 | 1.9E-7 | 0.0020107 | 2.7 | 0.09 | 0.59 |
| IA-NS-10_21.1 | AJP05 | Dec. '14 | 3.925E+9 | 1.4E+7 | 7.871E+6 | 2.8E+4 | 0.0020056 | 1.8E-7 | 0.0020116 | 3.2 | 0.09 | 0.59 |

**Appendix B.5**. Continued

| Spot Name | Mount | Date | $^{16}$O Measured | $^{16}$O Error | $^{18}$O Measured | $^{18}$O Error | $^{18}$O/$^{16}$O Measured | $^{18}$O/$^{16}$O Error | $^{18}$O/$^{16}$O Corrected | δ$^{18}$O Corrected | Error (1σ) | Total Error (2σ) |
|---|---|---|---|---|---|---|---|---|---|---|---|---|
| **IA-NS-10 (continued)** | | | | | | | | | | | | |
| IA-NS-10_22.1 | AJP05 | Dec. '14 | 3.925E+9 | 1.9E+7 | 7.873E+6 | 3.7E+4 | 0.0020059 | 2.5E-7 | 0.0020119 | 3.4 | 0.13 | 0.61 |
| IA-NS-10_23.1 | AJP05 | Dec. '14 | 3.920E+9 | 1.3E+7 | 7.867E+6 | 2.5E+4 | 0.0020067 | 1.5E-7 | 0.0020127 | 3.7 | 0.07 | 0.58 |
| IA-NS-10_24.1 | AJP05 | Dec. '14 | 3.936E+9 | 1.1E+7 | 7.896E+6 | 2.1E+4 | 0.0020060 | 2.0E-7 | 0.0020120 | 3.4 | 0.10 | 0.59 |
| **IA-NS-12 (Granophyre)** | | | | | | | | | | | | |
| IA-NS-12_1.1 | AJP05 | Dec. '14 | 3.903E+9 | 2.2E+7 | 7.807E+6 | 4.4E+4 | 0.0020002 | 1.4E-7 | 0.0020062 | 0.5 | 0.07 | 0.58 |
| IA-NS-12_2.1 | AJP05 | Dec. '14 | 3.815E+9 | 2.1E+7 | 7.647E+6 | 4.1E+4 | 0.0020045 | 1.7E-7 | 0.0020105 | 2.6 | 0.08 | 0.58 |
| IA-NS-12_3.1 | AJP05 | Dec. '14 | 3.883E+9 | 1.5E+7 | 7.793E+6 | 3.0E+4 | 0.0020070 | 1.6E-7 | 0.0020130 | 3.9 | 0.08 | 0.58 |
| IA-NS-12_4.1 | AJP05 | Dec. '14 | 3.877E+9 | 1.5E+7 | 7.782E+6 | 2.9E+4 | 0.0020072 | 2.3E-7 | 0.0020132 | 4.0 | 0.12 | 0.60 |
| IA-NS-12_5.1 | AJP05 | Dec. '14 | 3.859E+9 | 1.8E+7 | 7.725E+6 | 3.5E+4 | 0.0020018 | 1.0E-7 | 0.0020078 | 1.3 | 0.05 | 0.57 |
| IA-NS-12_6.1 | AJP05 | Dec. '14 | 3.785E+9 | 1.3E+7 | 7.599E+6 | 2.6E+4 | 0.0020077 | 2.0E-7 | 0.0020137 | 4.2 | 0.10 | 0.59 |
| IA-NS-12_7.1 | AJP05 | Dec. '14 | 3.832E+9 | 2.1E+7 | 7.681E+6 | 4.2E+4 | 0.0020047 | 1.6E-7 | 0.0020107 | 2.7 | 0.08 | 0.58 |
| IA-NS-12_8.1 | AJP05 | Dec. '14 | 3.820E+9 | 1.9E+7 | 7.663E+6 | 3.7E+4 | 0.0020061 | 1.1E-7 | 0.0020121 | 3.5 | 0.06 | 0.57 |
| IA-NS-12_9.1 | AJP05 | Dec. '14 | 3.867E+9 | 1.5E+7 | 7.749E+6 | 2.9E+4 | 0.0020039 | 1.3E-7 | 0.0020099 | 2.4 | 0.06 | 0.57 |
| IA-NS-12_10.1 | AJP05 | Dec. '14 | 3.849E+9 | 1.6E+7 | 7.717E+6 | 3.2E+4 | 0.0020051 | 1.6E-7 | 0.0020111 | 2.9 | 0.08 | 0.58 |
| IA-NS-12_11.1 | AJP05 | Dec. '14 | 3.927E+9 | 1.5E+7 | 7.870E+6 | 2.9E+4 | 0.0020042 | 2.2E-7 | 0.0020102 | 2.5 | 0.11 | 0.60 |
| IA-NS-12_12.1 | AJP05 | Dec. '14 | 3.695E+9 | 1.6E+7 | 7.417E+6 | 3.1E+4 | 0.0020071 | 1.3E-7 | 0.0020131 | 3.9 | 0.06 | 0.57 |
| IA-NS-12_13.1 | AJP05 | Dec. '14 | 3.700E+9 | 1.8E+7 | 7.418E+6 | 3.6E+4 | 0.0020049 | 1.5E-7 | 0.0020109 | 2.8 | 0.07 | 0.58 |
| IA-NS-12_14.1 | AJP05 | Dec. '14 | 3.605E+9 | 7.0E+6 | 7.236E+6 | 1.4E+4 | 0.0020071 | 1.8E-7 | 0.0020131 | 3.9 | 0.09 | 0.59 |
| IA-NS-12_15.1 | AJP05 | Dec. '14 | 2.986E+9 | 9.5E+6 | 5.991E+6 | 1.9E+4 | 0.0020063 | 1.9E-7 | 0.0020123 | 3.6 | 0.10 | 0.59 |
| IA-NS-12_16.1 | AJP05 | Dec. '14 | 3.799E+9 | 2.0E+7 | 7.613E+6 | 3.9E+4 | 0.0020042 | 1.9E-7 | 0.0020102 | 2.5 | 0.09 | 0.59 |
| IA-NS-12_17.1 | AJP05 | Dec. '14 | 3.883E+9 | 1.2E+7 | 7.794E+6 | 2.3E+4 | 0.0020073 | 1.6E-7 | 0.0020133 | 4.0 | 0.08 | 0.58 |
| IA-NS-12_18.1 | AJP05 | Dec. '14 | 3.832E+9 | 1.2E+7 | 7.694E+6 | 2.4E+4 | 0.0020079 | 1.5E-7 | 0.0020139 | 4.3 | 0.08 | 0.58 |
| IA-NS-12_19.1 | AJP05 | Dec. '14 | 3.731E+9 | 7.5E+6 | 7.487E+6 | 1.5E+4 | 0.0020070 | 1.2E-7 | 0.0020130 | 3.9 | 0.06 | 0.57 |
| IA-NS-12_20.1 | AJP05 | Dec. '14 | 3.807E+9 | 1.1E+7 | 7.638E+6 | 2.2E+4 | 0.0020066 | 1.4E-7 | 0.0020126 | 3.7 | 0.07 | 0.58 |
| IA-NS-12_21.1 | AJP05 | Dec. '14 | 3.873E+9 | 1.2E+7 | 7.772E+6 | 2.4E+4 | 0.0020070 | 2.1E-7 | 0.0020130 | 3.9 | 0.11 | 0.60 |
| IA-NS-12_22.1 | AJP05 | Dec. '14 | 3.850E+9 | 1.3E+7 | 7.728E+6 | 2.6E+4 | 0.0020072 | 1.7E-7 | 0.0020132 | 4.0 | 0.09 | 0.58 |
| IA-NS-12_23.1 | AJP05 | Dec. '14 | 3.819E+9 | 1.3E+7 | 7.664E+6 | 2.6E+4 | 0.0020068 | 9.9E-8 | 0.0020128 | 3.8 | 0.05 | 0.57 |
| IA-NS-12_24.1 | AJP05 | Dec. '14 | 3.809E+9 | 1.3E+7 | 7.644E+6 | 2.6E+4 | 0.0020070 | 1.2E-7 | 0.0020130 | 3.9 | 0.06 | 0.57 |
| IA-NS-12_25.1 | AJP05 | Dec. '14 | 3.686E+9 | 1.2E+7 | 7.402E+6 | 2.4E+4 | 0.0020081 | 1.8E-7 | 0.0020141 | 4.4 | 0.09 | 0.59 |
| IA-NS-12_26.1 | AJP05 | Dec. '14 | 3.738E+9 | 1.3E+7 | 7.502E+6 | 2.7E+4 | 0.0020068 | 1.4E-7 | 0.0020128 | 3.8 | 0.07 | 0.58 |
| IA-NS-12_27.1 | AJP05 | Dec. '14 | 3.779E+9 | 1.2E+7 | 7.584E+6 | 2.4E+4 | 0.0020072 | 1.7E-7 | 0.0020132 | 4.0 | 0.08 | 0.58 |

**Appendix B.5**. Continued

| Spot Name | Mount | Date | $^{16}$O Measured | $^{16}$O Error | $^{18}$O Measured | $^{18}$O Error | $^{18}$O/$^{16}$O Measured | $^{18}$O/$^{16}$O Error | $^{18}$O/$^{16}$O Corrected | $\delta^{18}$O Corrected | Error (1σ) | Total Error (2σ) |
|---|---|---|---|---|---|---|---|---|---|---|---|---|
| **IA-G-1 (Gabbro)** | | | | | | | | | | | | |
| IA-G-1_1.1 | JW510 | Apr. '12 | 2.111E+9 | 2.1E+6 | 4.247E+6 | 4.3E+3 | 0.0020114 | 9.1E-8 | 0.0020138 | 4.3 | 0.05 | 0.44 |
| IA-G-1_2.1 | JW510 | Apr. '12 | 2.116E+9 | 1.2E+6 | 4.257E+6 | 2.6E+3 | 0.0020119 | 1.8E-7 | 0.0020142 | 4.5 | 0.09 | 0.47 |
| IA-G-1_6.1 | JW510 | Apr. '12 | 2.120E+9 | 1.3E+6 | 4.266E+6 | 2.5E+3 | 0.0020122 | 2.0E-7 | 0.0020146 | 4.7 | 0.10 | 0.48 |
| IA-G-1_7.1 | JW510 | Apr. '12 | 2.106E+9 | 1.7E+6 | 4.238E+6 | 3.5E+3 | 0.0020119 | 1.9E-7 | 0.0020142 | 4.5 | 0.09 | 0.47 |
| IA-G-1_8.1 | JW510 | Apr. '12 | 2.128E+9 | 1.0E+6 | 4.280E+6 | 2.1E+3 | 0.0020114 | 1.8E-7 | 0.0020138 | 4.3 | 0.09 | 0.47 |
| IA-G-1_12.1 | JW510 | Apr. '12 | 2.116E+9 | 9.8E+5 | 4.259E+6 | 2.0E+3 | 0.0020123 | 9.5E-8 | 0.0020146 | 4.7 | 0.05 | 0.44 |
| IA-G-1_15.1 | JW510 | Apr. '12 | 2.117E+9 | 1.3E+6 | 4.258E+6 | 2.7E+3 | 0.0020112 | 6.7E-8 | 0.0020136 | 4.2 | 0.03 | 0.44 |
| IA-G-1_18.1 | JW510 | Apr. '12 | 2.117E+9 | 8.2E+5 | 4.258E+6 | 1.7E+3 | 0.0020116 | 9.8E-8 | 0.0020140 | 4.4 | 0.05 | 0.44 |
| IA-G-1_22.1 | JW510 | Apr. '12 | 2.113E+9 | 1.1E+6 | 4.253E+6 | 2.3E+3 | 0.0020126 | 1.6E-7 | 0.0020149 | 4.9 | 0.08 | 0.46 |
| IA-G-1_23.1 | JW510 | Apr. '12 | 2.119E+9 | 5.5E+5 | 4.266E+6 | 1.3E+3 | 0.0020126 | 1.6E-7 | 0.0020150 | 4.9 | 0.08 | 0.46 |
| IA-G-1_29.1 | JW510 | Apr. '12 | 2.108E+9 | 1.0E+6 | 4.241E+6 | 2.2E+3 | 0.0020118 | 1.9E-7 | 0.0020142 | 4.5 | 0.10 | 0.47 |
| IA-G-1_25.1 | JW510 | Apr. '12 | 2.127E+9 | 1.6E+6 | 4.280E+6 | 3.3E+3 | 0.0020125 | 1.6E-7 | 0.0020149 | 4.8 | 0.08 | 0.46 |
| IA-G-1_26.1 | JW510 | Apr. '12 | 2.106E+9 | 1.4E+6 | 4.236E+6 | 2.9E+3 | 0.0020112 | 1.5E-7 | 0.0020135 | 4.2 | 0.08 | 0.46 |
| IA-G-1_27.1 | JW510 | Apr. '12 | 2.128E+9 | 1.0E+6 | 4.281E+6 | 2.1E+3 | 0.0020120 | 1.8E-7 | 0.0020144 | 4.6 | 0.09 | 0.47 |
| IA-G-1_28.1 | JW510 | Apr. '12 | 2.128E+9 | 2.0E+6 | 4.282E+6 | 4.0E+3 | 0.0020127 | 1.5E-7 | 0.0020150 | 4.9 | 0.08 | 0.46 |
| **IA-G-5 (Gabbro)** | | | | | | | | | | | | |
| IA-G-5_2.1 | AJP01 | May. '13 | 2.468E+9 | 7.4E+5 | 4.930E+6 | 1.6E+3 | 0.0019978 | 1.6E-7 | 0.0020107 | 2.8 | 0.08 | 0.66 |
| IA-G-5_3.1 | AJP01 | May. '13 | 1.166E+9 | 1.1E+7 | 2.334E+6 | 2.2E+4 | 0.0020013 | 5.1E-7 | 0.0020142 | 4.5 | 0.26 | 0.82 |
| IA-G-5_4.1 | AJP01 | May. '13 | 2.475E+9 | 4.2E+6 | 4.943E+6 | 8.6E+3 | 0.0019966 | 2.4E-7 | 0.0020095 | 2.2 | 0.12 | 0.69 |
| IA-G-5_6.1 | AJP01 | May. '13 | 2.512E+9 | 1.5E+6 | 5.021E+6 | 3.2E+3 | 0.0019986 | 1.6E-7 | 0.0020116 | 3.2 | 0.08 | 0.66 |
| IA-G-5_7.1 | AJP01 | May. '13 | 2.529E+9 | 6.3E+6 | 5.063E+6 | 1.3E+4 | 0.0020016 | 1.4E-7 | 0.0020146 | 4.7 | 0.07 | 0.66 |
| IA-G-5_8.1 | AJP02 | Nov. '13 | 1.446E+9 | 6.5E+5 | 2.909E+6 | 1.4E+3 | 0.0020118 | 3.0E-7 | 0.0020135 | 4.2 | 0.15 | 0.74 |
| IA-G-5_9.1 | AJP02 | Nov. '13 | 1.448E+9 | 9.6E+5 | 2.913E+6 | 1.9E+3 | 0.0020114 | 1.8E-7 | 0.0020131 | 4.0 | 0.09 | 0.70 |
| IA-G-5_10.1 | AJP03 | Nov. '13 | 1.754E+9 | 9.1E+5 | 3.529E+6 | 2.0E+3 | 0.0020123 | 1.3E-7 | 0.0020139 | 4.3 | 0.07 | 0.68 |
| IA-G-5_11.1 | AJP03 | Nov. '13 | 1.797E+9 | 2.4E+6 | 3.618E+6 | 4.7E+3 | 0.0020131 | 1.9E-7 | 0.0020147 | 4.8 | 0.09 | 0.69 |

**Appendix B.6**. Zircon Lu-Hf isotope compositions, measured *in-situ* by LA-MC-ICP-MS

| **Spot Name** | **Mount** | **Total Hf Beam (V)** | **$^{176}$Hf/$^{177}$Hf** | **2SE** | **$^{176}$Lu/$^{177}$Hf** | **2SE** | **$^{176}$Yb/$^{177}$Hf** | **2SE** | **$^{178}$Hf/$^{177}$Hf** | **2SE** | **$\varepsilon_{Hf}$** | **2SE** |
|---|---|---|---|---|---|---|---|---|---|---|---|---|
| **IA-NS-2 (Granophyre)** | | | | | | | | | | | | |
| IA-NS-2_1.1 | JW498 | 10.4 | 0.283169 | 3.1E-5 | 0.00251 | 2.7E-4 | 0.0703 | 7.6E-3 | 1.467264 | 5.0E-5 | **13.6** | **1.1** |
| IA-NS-2_2.1 | JW498 | 11.0 | 0.283138 | 2.1E-5 | 0.00150 | 6.4E-5 | 0.0417 | 1.7E-3 | 1.467268 | 3.4E-5 | **12.5** | **0.8** |
| IA-NS-2_3.1 | JW498 | 12.8 | 0.283148 | 2.8E-5 | 0.00156 | 8.6E-5 | 0.0444 | 2.5E-3 | 1.467223 | 4.2E-5 | **12.8** | **1.0** |
| IA-NS-2_4.1 | JW498 | 11.9 | 0.283134 | 1.9E-5 | 0.00103 | 1.5E-5 | 0.0294 | 4.0E-4 | 1.467268 | 2.8E-5 | **12.3** | **0.7** |
| IA-NS-2_6.1 | JW498 | 14.4 | 0.283117 | 3.8E-5 | 0.00438 | 1.7E-4 | 0.1272 | 4.9E-3 | 1.467220 | 3.9E-5 | **11.7** | **1.3** |
| IA-NS-2_7.1 | JW498 | 12.0 | 0.283149 | 2.3E-5 | 0.00131 | 1.3E-4 | 0.0366 | 3.7E-3 | 1.467232 | 3.5E-5 | **12.9** | **0.8** |
| IA-NS-2_8.1 | JW498 | 14.7 | 0.283155 | 3.1E-5 | 0.00443 | 1.9E-4 | 0.1270 | 5.6E-3 | 1.467253 | 4.5E-5 | **13.1** | **1.1** |
| IA-NS-2_10.1 | JW498 | 16.6 | 0.283144 | 2.7E-5 | 0.00417 | 1.8E-5 | 0.1182 | 8.9E-4 | 1.467225 | 3.3E-5 | **12.7** | **1.0** |
| IA-NS-2_11.1 | JW498 | 12.6 | 0.283157 | 2.1E-5 | 0.00186 | 1.0E-4 | 0.0546 | 2.9E-3 | 1.467257 | 3.3E-5 | **13.2** | **0.7** |
| IA-NS-2_12.2 | JW498 | 14.3 | 0.283128 | 3.3E-5 | 0.00191 | 9.4E-5 | 0.0568 | 2.6E-3 | 1.467204 | 4.2E-5 | **12.1** | **1.2** |
| IA-NS-2_15.1 | JW498 | 15.7 | 0.283114 | 4.0E-5 | 0.00220 | 3.4E-5 | 0.0652 | 1.1E-3 | 1.467191 | 3.8E-5 | **11.6** | **1.4** |
| IA-NS-2_17.1 | JW498 | 15.5 | 0.283188 | 3.9E-5 | 0.00364 | 5.3E-4 | 0.1101 | 1.6E-2 | 1.467211 | 3.6E-5 | **14.3** | **1.4** |
| IA-NS-2_18.1 | JW498 | 17.6 | 0.283118 | 3.9E-5 | 0.00278 | 1.2E-4 | 0.0834 | 3.9E-3 | 1.467234 | 3.5E-5 | **11.8** | **1.4** |
| IA-NS-2_20.1 | JW498 | 14.1 | 0.283156 | 2.2E-5 | 0.00245 | 8.2E-5 | 0.0733 | 3.2E-3 | 1.467215 | 5.5E-5 | **13.1** | **0.8** |
| IA-NS-2_23.1 | JW498 | 15.9 | 0.283167 | 2.0E-5 | 0.00182 | 1.0E-4 | 0.0528 | 3.1E-3 | 1.467215 | 4.7E-5 | **13.5** | **0.7** |
| IA-NS-2_24.1 | JW498 | 17.6 | 0.283151 | 4.3E-5 | 0.00335 | 2.1E-4 | 0.1004 | 6.6E-3 | 1.467222 | 4.4E-5 | **12.9** | **1.5** |
| IA-NS-2_25.1 | JW498 | 16.7 | 0.283202 | 4.8E-5 | 0.00484 | 2.7E-4 | 0.1429 | 8.1E-3 | 1.467186 | 4.4E-5 | **14.7** | **1.7** |
| IA-NS-2_26.1 | JW498 | 14.2 | 0.283176 | 2.1E-5 | 0.00165 | 3.4E-5 | 0.0482 | 9.6E-4 | 1.467225 | 4.1E-5 | **13.8** | **0.7** |
| **IA-NS-4b (High-SiO$_2$ Granophyre)** | | | | | | | | | | | | |
| IA-NS-4b_2.1 | JW498 | 12.5 | 0.283122 | 2.4E-5 | 0.00126 | 4.2E-5 | 0.0372 | 1.1E-3 | 1.467272 | 3.5E-5 | **11.9** | **0.9** |
| IA-NS-4b_3.1 | JW498 | 27.8 | 0.283145 | 3.1E-5 | 0.00325 | 2.1E-4 | 0.1156 | 7.6E-3 | 1.467267 | 2.4E-5 | **12.7** | **1.1** |
| IA-NS-4b_4.1 | JW498 | 18.5 | 0.283142 | 2.3E-5 | 0.00318 | 1.4E-4 | 0.1022 | 4.6E-3 | 1.467251 | 2.9E-5 | **12.6** | **0.8** |
| IA-NS-4b_5.1 | JW498 | 13.5 | 0.283132 | 2.5E-5 | 0.00114 | 3.1E-5 | 0.0314 | 9.1E-4 | 1.467230 | 3.8E-5 | **12.3** | **0.9** |
| IA-NS-4b_8.1 | JW498 | 13.6 | 0.283174 | 4.2E-5 | 0.00302 | 1.6E-4 | 0.0926 | 6.2E-3 | 1.467224 | 2.8E-5 | **13.8** | **1.5** |
| IA-NS-4b_9.1 | JW498 | 16.8 | 0.283172 | 2.6E-5 | 0.00349 | 1.5E-4 | 0.1099 | 4.6E-3 | 1.467242 | 4.0E-5 | **13.7** | **0.9** |
| IA-NS-4b_9.2 | JW498 | 15.7 | 0.283124 | 2.4E-5 | 0.00372 | 2.6E-4 | 0.1198 | 9.4E-3 | 1.467260 | 3.1E-5 | **12.0** | **0.9** |
| IA-NS-4b_10.1 | JW498 | 8.1 | 0.283133 | 3.2E-5 | 0.00171 | 6.4E-5 | 0.0513 | 1.8E-3 | 1.467288 | 4.2E-5 | **12.3** | **1.1** |
| IA-NS-4b_11.1 | JW498 | 9.1 | 0.283159 | 5.3E-5 | 0.00278 | 2.0E-4 | 0.0895 | 7.2E-3 | 1.467202 | 6.9E-5 | **13.2** | **1.9** |

**Appendix B.6**. Continued

| Spot Name | Mount | Total Hf Beam (V) | $^{176}$Hf/$^{177}$Hf | 2SE | $^{176}$Lu/$^{177}$Hf | 2SE | $^{176}$Yb/$^{177}$Hf | 2SE | $^{178}$Hf/$^{177}$Hf | 2SE | $\varepsilon_{Hf}$ | 2SE |
|---|---|---|---|---|---|---|---|---|---|---|---|---|
| **IA-NS-4b (High-SiO$_2$ Granophyre)** | | | | | | | | | | | | |
| IA-NS-4b_12.1 | JW498 | 30.0 | 0.283171 | 3.1E-5 | 0.00639 | 5.0E-4 | 0.2240 | 1.7E-2 | 1.467253 | 3.2E-5 | **13.7** | **1.1** |
| IA-NS-4b_13.1 | JW498 | 12.7 | 0.283136 | 4.1E-5 | 0.00274 | 1.0E-4 | 0.0817 | 2.9E-3 | 1.467242 | 5.1E-5 | **12.4** | **1.4** |
| IA-NS-4b_14.1 | JW498 | 33.0 | 0.283143 | 1.7E-5 | 0.00110 | 4.5E-5 | 0.0399 | 1.9E-3 | 1.467232 | 3.3E-5 | **12.7** | **0.6** |
| IA-NS-4b_17.1 | JW498 | 28.9 | 0.283137 | 2.9E-5 | 0.00437 | 7.6E-5 | 0.1400 | 3.0E-3 | 1.467218 | 2.8E-5 | **12.4** | **1.0** |
| IA-NS-4b_19.1 | JW498 | 11.4 | 0.283117 | 2.6E-5 | 0.00130 | 4.3E-5 | 0.0368 | 1.3E-3 | 1.467239 | 4.2E-5 | **11.7** | **0.9** |
| IA-NS-4b_22.1 | JW498 | 26.3 | 0.283131 | 1.9E-5 | 0.00270 | 1.3E-4 | 0.0814 | 4.0E-3 | 1.467241 | 3.0E-5 | **12.2** | **0.7** |
| IA-NS-4b_23.1 | JW498 | 10.0 | 0.283121 | 3.7E-5 | 0.00571 | 5.6E-4 | 0.2014 | 2.1E-2 | 1.467223 | 2.5E-5 | **11.9** | **1.3** |
| IA-NS-4b_25.1 | JW498 | 27.9 | 0.283168 | 4.0E-5 | 0.00605 | 6.4E-4 | 0.2169 | 2.2E-2 | 1.467213 | 1.1E-4 | **13.6** | **1.4** |
| IA-NS-4b_27.1 | JW498 | 16.1 | 0.283165 | 3.9E-5 | 0.00405 | 4.6E-4 | 0.1256 | 1.4E-2 | 1.467211 | 5.7E-5 | **13.4** | **1.4** |
| IA-NS-4b_30.1 | JW498 | 21.0 | 0.283174 | 3.0E-5 | 0.00335 | 1.6E-4 | 0.1036 | 5.5E-3 | 1.467215 | 2.5E-5 | **13.8** | **1.1** |
| IA-NS-4b_32.1 | JW498 | 26.7 | 0.283140 | 2.8E-5 | 0.00482 | 1.7E-4 | 0.1583 | 6.1E-3 | 1.467234 | 2.2E-5 | **12.6** | **1.0** |
| IA-NS-4b_33.1 | JW498 | 31.9 | 0.283190 | 3.7E-5 | 0.00091 | 4.5E-5 | 0.0313 | 1.9E-3 | 1.467187 | 4.5E-5 | **14.3** | **1.3** |
| IA-NS-4b_34.1 | JW498 | 26.4 | 0.283139 | 3.1E-5 | 0.00286 | 5.0E-5 | 0.0915 | 1.7E-3 | 1.467226 | 2.9E-5 | **12.5** | **1.1** |
| IA-NS-4b_31.1 | JW498 | 29.7 | 0.283123 | 2.2E-5 | 0.00154 | 1.1E-4 | 0.0521 | 3.6E-3 | 1.467242 | 2.5E-5 | **12.0** | **0.8** |
| IA-NS-4b_35.1 | JW498 | 27.3 | 0.283151 | 3.9E-5 | 0.00582 | 7.3E-4 | 0.2019 | 2.5E-2 | 1.467224 | 3.3E-5 | **12.9** | **1.4** |
| **IA-NS-6 (Diorite)** | | | | | | | | | | | | |
| IA-NS-6_1.1 | JW498 | 12.7 | 0.283179 | 3.0E-5 | 0.00174 | 5.5E-5 | 0.0504 | 1.6E-3 | 1.467268 | 4.1E-5 | **13.9** | **1.0** |
| IA-NS-6_3.1 | JW498 | 9.6 | 0.283167 | 4.0E-5 | 0.00824 | 1.2E-4 | 0.2564 | 3.3E-3 | 1.467229 | 4.4E-5 | **13.5** | **1.4** |
| IA-NS-6_4.1 | JW498 | 14.6 | 0.283142 | 5.5E-5 | 0.00797 | 2.2E-4 | 0.2519 | 6.8E-3 | 1.467217 | 5.8E-5 | **12.6** | **1.9** |
| IA-NS-6_6.1 | JW498 | 11.3 | 0.283156 | 2.0E-5 | 0.00262 | 4.1E-5 | 0.0789 | 1.1E-3 | 1.467212 | 3.4E-5 | **13.1** | **0.7** |
| IA-NS-6_6.2 | JW498 | 15.1 | 0.283136 | 2.9E-5 | 0.00205 | 1.1E-4 | 0.0604 | 3.6E-3 | 1.467205 | 4.6E-5 | **12.4** | **1.0** |
| IA-NS-6_7.1 | JW498 | 13.0 | 0.283163 | 3.4E-5 | 0.00355 | 2.0E-4 | 0.1029 | 5.6E-3 | 1.467209 | 5.0E-5 | **13.4** | **1.2** |
| IA-NS-6_10.1 | JW498 | 15.1 | 0.283146 | 4.2E-5 | 0.00529 | 1.5E-4 | 0.1510 | 4.5E-3 | 1.467212 | 4.4E-5 | **12.8** | **1.5** |
| IA-NS-6_11.1 | JW498 | 12.3 | 0.283197 | 2.8E-5 | 0.00092 | 4.8E-5 | 0.0255 | 1.3E-3 | 1.467246 | 3.7E-5 | **14.6** | **1.0** |
| IA-NS-6_12.1 | JW498 | 11.6 | 0.283175 | 2.6E-5 | 0.00137 | 4.5E-5 | 0.0401 | 1.4E-3 | 1.467240 | 3.5E-5 | **13.8** | **0.9** |
| IA-NS-6_18.2 | JW498 | 11.8 | 0.283133 | 2.4E-5 | 0.00172 | 3.1E-5 | 0.0485 | 9.3E-4 | 1.467235 | 4.1E-5 | **12.3** | **0.8** |
| IA-NS-6_21.1 | JW498 | 12.2 | 0.283161 | 4.0E-5 | 0.00118 | 2.9E-5 | 0.0323 | 6.5E-4 | 1.467215 | 5.0E-5 | **13.3** | **1.4** |
| IA-NS-6_22.1 | JW498 | 16.4 | 0.283161 | 2.9E-5 | 0.00187 | 4.3E-5 | 0.0542 | 1.1E-3 | 1.467228 | 4.5E-5 | **13.3** | **1.0** |
| IA-NS-6_24.1 | JW498 | 10.8 | 0.283134 | 3.5E-5 | 0.00245 | 3.2E-5 | 0.0721 | 9.7E-4 | 1.467268 | 5.4E-5 | **12.4** | **1.2** |

**Appendix B.6**. Continued

| **Spot Name** | **Mount** | **Total Hf Beam (V)** | **$^{176}$Hf/$^{177}$Hf** | **2SE** | **$^{176}$Lu/$^{177}$Hf** | **2SE** | **$^{176}$Yb/$^{177}$Hf** | **2SE** | **$^{178}$Hf/$^{177}$Hf** | **2SE** | **$\varepsilon_{Hf}$** | **2SE** |
|---|---|---|---|---|---|---|---|---|---|---|---|---|
| **IA-NS-7 (Granodiorite)** | | | | | | | | | | | | |
| IA-NS-7_1.1 | JW510 | 12.0 | 0.283155 | 3.1E-5 | 0.00390 | 3.9E-5 | 0.1083 | 1.2E-3 | 1.467137 | 4.1E-5 | **13.1** | **1.1** |
| IA-NS-7_4.1 | JW510 | 11.0 | 0.283140 | 3.1E-5 | 0.00383 | 2.2E-4 | 0.1078 | 6.5E-3 | 1.467159 | 3.9E-5 | **12.5** | **1.1** |
| IA-NS-7_9.1 | JW510 | 10.7 | 0.283143 | 3.7E-5 | 0.00807 | 5.4E-4 | 0.2410 | 1.6E-2 | 1.467142 | 4.1E-5 | **12.6** | **1.3** |
| IA-NS-7_10.1 | JW510 | 10.8 | 0.283095 | 4.9E-5 | 0.00698 | 7.1E-4 | 0.2060 | 2.2E-2 | 1.467117 | 4.7E-5 | **10.9** | **1.7** |
| IA-NS-7_11.1 | JW510 | 15.9 | 0.283174 | 3.6E-5 | 0.00532 | 5.3E-4 | 0.1560 | 1.6E-2 | 1.467200 | 4.6E-5 | **13.7** | **1.3** |
| IA-NS-7_12.1 | JW510 | 13.0 | 0.283136 | 4.3E-5 | 0.00545 | 7.3E-4 | 0.1600 | 2.2E-2 | 1.467133 | 3.6E-5 | **12.4** | **1.5** |
| IA-NS-7_13.1 | JW510 | 14.2 | 0.283157 | 3.0E-5 | 0.00383 | 4.0E-4 | 0.1100 | 1.2E-2 | 1.467186 | 4.7E-5 | **13.1** | **1.1** |
| IA-NS-7_14.1 | JW510 | 11.1 | 0.283156 | 3.3E-5 | 0.00331 | 1.1E-4 | 0.0916 | 2.8E-3 | 1.467150 | 4.4E-5 | **13.1** | **1.2** |
| IA-NS-7_16.1 | JW510 | 14.9 | 0.283212 | 2.9E-5 | 0.00441 | 5.9E-4 | 0.1240 | 1.7E-2 | 1.467176 | 5.2E-5 | **15.1** | **1.0** |
| IA-NS-7_17.1 | JW510 | 12.4 | 0.283145 | 3.5E-5 | 0.00621 | 1.7E-4 | 0.1843 | 5.3E-3 | 1.467113 | 4.0E-5 | **12.7** | **1.2** |
| IA-NS-7_19.1 | JW510 | 7.6 | 0.283157 | 4.7E-5 | 0.00299 | 2.3E-4 | 0.0962 | 6.5E-3 | 1.467163 | 5.5E-5 | **13.1** | **1.7** |
| IA-NS-7_20.1 | JW510 | 16.1 | 0.283133 | 4.7E-5 | 0.00358 | 1.4E-4 | 0.1024 | 4.0E-3 | 1.467173 | 5.6E-5 | **12.3** | **1.7** |
| IA-NS-7_22.1 | JW510 | 11.6 | 0.283141 | 3.5E-5 | 0.00507 | 4.0E-4 | 0.1490 | 1.3E-2 | 1.467173 | 3.8E-5 | **12.6** | **1.2** |
| IA-NS-7_23.1 | JW510 | 11.1 | 0.283131 | 4.2E-5 | 0.00185 | 1.3E-4 | 0.0513 | 3.8E-3 | 1.467142 | 4.4E-5 | **12.2** | **1.5** |
| IA-NS-7_25.1 | JW510 | 11.5 | 0.283154 | 3.0E-5 | 0.00373 | 4.6E-4 | 0.1070 | 1.4E-2 | 1.467137 | 3.9E-5 | **13.0** | **1.1** |
| **IA-NS-9 (High-SiO$_2$ Granophyre)** | | | | | | | | | | | | |
| IA-NS-9_1.1 | AJP03 | 12.8 | 0.283044 | 5.6E-5 | 0.00152 | 1.2E-4 | 0.0469 | 3.3E-3 | 1.467127 | 7.1E-5 | **9.1** | **2.0** |
| IA-NS-9_2.1 | AJP03 | 22.0 | 0.283151 | 2.0E-5 | 0.00193 | 7.9E-5 | 0.0731 | 3.0E-3 | 1.467150 | 2.5E-5 | **12.9** | **0.7** |
| IA-NS-9_5.1 | AJP03 | 13.7 | 0.283126 | 3.4E-5 | 0.00159 | 7.0E-5 | 0.0521 | 1.9E-3 | 1.467171 | 3.5E-5 | **12.0** | **1.2** |
| IA-NS-9_8.1 | AJP03 | 13.3 | 0.283116 | 5.6E-5 | 0.00181 | 5.0E-5 | 0.0601 | 2.6E-3 | 1.467093 | 6.7E-5 | **11.7** | **2.0** |
| IA-NS-9_11.1 | AJP03 | 13.6 | 0.283096 | 3.9E-5 | 0.00162 | 1.4E-4 | 0.0527 | 4.0E-3 | 1.467131 | 4.0E-5 | **11.0** | **1.4** |
| IA-NS-9_12.1 | AJP03 | 13.1 | 0.283146 | 2.5E-5 | 0.00149 | 1.0E-5 | 0.0501 | 6.9E-4 | 1.467189 | 3.2E-5 | **12.8** | **0.9** |
| IA-NS-9_15.1 | AJP03 | 13.0 | 0.283136 | 2.4E-5 | 0.00097 | 3.2E-5 | 0.0306 | 8.9E-4 | 1.467149 | 3.8E-5 | **12.4** | **0.8** |
| IA-NS-9_17.1 | AJP03 | 31.8 | 0.283114 | 4.3E-5 | 0.00355 | 5.3E-5 | 0.1317 | 3.8E-3 | 1.467138 | 4.9E-5 | **11.6** | **1.5** |
| IA-NS-9_21.1 | AJP03 | 24.2 | 0.283170 | 2.4E-5 | 0.00207 | 4.9E-5 | 0.0765 | 3.1E-3 | 1.467173 | 2.9E-5 | **13.6** | **0.8** |

**Appendix B.6**. Continued

| **Spot Name** | **Mount** | **Total Hf Beam (V)** | **$^{176}$Hf/$^{177}$Hf** | **2SE** | **$^{176}$Lu/$^{177}$Hf** | **2SE** | **$^{176}$Yb/$^{177}$Hf** | **2SE** | **$^{178}$Hf/$^{177}$Hf** | **2SE** | **$\varepsilon_{Hf}$** | **2SE** |
|---|---|---|---|---|---|---|---|---|---|---|---|---|
| **IA-G-1 (Gabbro)** | | | | | | | | | | | | |
| IA-G-1_1.1 | JW510 | 9.6 | 0.283158 | 2.8E-5 | 0.00220 | 7.9E-5 | 0.0626 | 2.3E-3 | 1.467211 | 4.6E-5 | **13.2** | **1.0** |
| IA-G-1_2.1 | JW510 | 9.6 | 0.283129 | 2.5E-5 | 0.00161 | 2.3E-5 | 0.0454 | 6.5E-4 | 1.467179 | 4.3E-5 | **12.2** | **0.9** |
| IA-G-1_3.1 | JW510 | 9.2 | 0.283148 | 3.3E-5 | 0.00239 | 9.0E-5 | 0.0662 | 2.6E-3 | 1.467228 | 4.2E-5 | **12.9** | **1.2** |
| IA-G-1_4.1 | JW510 | 9.3 | 0.283151 | 2.9E-5 | 0.00200 | 1.5E-4 | 0.0559 | 4.3E-3 | 1.467199 | 4.3E-5 | **13.0** | **1.0** |
| IA-G-1_6.1 | JW510 | 11.3 | 0.283154 | 3.4E-5 | 0.00193 | 2.6E-4 | 0.0539 | 7.4E-3 | 1.467210 | 6.4E-5 | **13.1** | **1.2** |
| IA-G-1_7.1 | JW510 | 9.9 | 0.283127 | 3.8E-5 | 0.00207 | 1.5E-4 | 0.0575 | 4.2E-3 | 1.467226 | 4.5E-5 | **12.1** | **1.4** |
| IA-G-1_8.1 | JW510 | 9.5 | 0.283144 | 2.7E-5 | 0.00213 | 6.2E-5 | 0.0594 | 1.8E-3 | 1.467217 | 4.2E-5 | **12.7** | **0.9** |
| IA-G-1_10.1 | JW510 | 10.8 | 0.283102 | 3.2E-5 | 0.00249 | 1.6E-4 | 0.0701 | 4.6E-3 | 1.467193 | 4.0E-5 | **11.2** | **1.1** |
| IA-G-1_11.1 | JW510 | 8.6 | 0.283233 | 4.4E-5 | 0.00124 | 2.1E-4 | 0.0334 | 6.0E-3 | 1.467244 | 5.2E-5 | **15.9** | **1.6** |
| IA-G-1_12.1 | JW510 | 9.4 | 0.283135 | 3.6E-5 | 0.00116 | 3.0E-5 | 0.0305 | 8.8E-4 | 1.467243 | 4.1E-5 | **12.4** | **1.3** |
| IA-G-1_14.1 | JW510 | 9.7 | 0.283156 | 3.1E-5 | 0.00170 | 4.4E-5 | 0.0471 | 1.2E-3 | 1.467241 | 4.7E-5 | **13.1** | **1.1** |
| IA-G-1_15.1 | JW510 | 10.1 | 0.283134 | 2.8E-5 | 0.00159 | 2.4E-5 | 0.0433 | 4.3E-4 | 1.467246 | 5.3E-5 | **12.4** | **1.0** |
| IA-G-1_17.1 | JW510 | 9.2 | 0.283153 | 3.0E-5 | 0.00230 | 1.1E-4 | 0.0647 | 3.2E-3 | 1.467225 | 4.4E-5 | **13.0** | **1.1** |
| IA-G-1_18.1 | JW510 | 12.0 | 0.283179 | 3.9E-5 | 0.00287 | 3.4E-4 | 0.0810 | 9.7E-3 | 1.467236 | 5.0E-5 | **13.9** | **1.4** |
| IA-G-1_19.1 | JW510 | 9.7 | 0.283176 | 2.9E-5 | 0.00205 | 1.0E-4 | 0.0573 | 2.9E-3 | 1.467234 | 4.4E-5 | **13.8** | **1.0** |
| IA-G-1_24.1 | JW510 | 10.5 | 0.283150 | 3.0E-5 | 0.00267 | 3.7E-5 | 0.0776 | 1.2E-3 | 1.467188 | 3.9E-5 | **12.9** | **1.1** |
| IA-G-1_25.1 | JW510 | 10.3 | 0.283138 | 2.2E-5 | 0.00141 | 7.8E-5 | 0.0390 | 2.1E-3 | 1.467219 | 4.5E-5 | **12.5** | **0.8** |
| IA-G-1_26.1 | JW510 | 11.9 | 0.283177 | 3.6E-5 | 0.00226 | 7.3E-5 | 0.0635 | 2.1E-3 | 1.467259 | 5.9E-5 | **13.9** | **1.3** |
| IA-G-1_27.1 | JW510 | 10.0 | 0.283126 | 3.0E-5 | 0.00137 | 4.1E-5 | 0.0374 | 1.1E-3 | 1.467219 | 3.7E-5 | **12.1** | **1.1** |
| IA-G-1_28.1 | JW510 | 9.2 | 0.283159 | 3.0E-5 | 0.00279 | 2.0E-4 | 0.0772 | 5.7E-3 | 1.467199 | 4.0E-5 | **13.2** | **1.1** |
| **IA-G-5 (Gabbro)** | | | | | | | | | | | | |
| IA-G-5_7.1 | AJP01 | 9.1 | 0.283149 | 5.0E-5 | 0.00379 | 7.0E-5 | 0.1168 | 2.6E-3 | 1.467163 | 5.8E-5 | **12.9** | **1.8** |
| IA-G-5_11.1 | AJP03 | 10.6 | 0.283154 | 5.1E-5 | 0.00275 | 2.9E-4 | 0.1000 | 1.3E-2 | 1.467140 | 5.2E-5 | **13.0** | **1.8** |
| IA-G-5_12.1 | AJP03 | 9.7 | 0.283154 | 5.0E-5 | 0.00486 | 7.0E-5 | 0.1810 | 3.2E-3 | 1.467187 | 4.2E-5 | **13.0** | **1.8** |

**Appendix B.7**. Compositional groups for data comparison and data references for Chapter IV

| Group: | Sample | Rock Type | Whole-Rock Data | Zircon Data | | Bulk Oxygen Isotopes |
|---|---|---|---|---|---|---|
| | | | | Elemental Geochemistry | Oxygen Isotopes | |
| Silicic | IA-NS-1 | Granophyre | Chapter III, Table 2 (p. 75) | -- | -- | -- |
| | IA-NS-2 | Granophyre | Chapter III, Table 2 (p. 75) | Appendix B.2 (p. 186-187)<br>Appendix B.3 (p. 195-196)<br>Appendix B.4 (p. 204-205) | Appendix B.5 (p. 211) | Appendix B.9 (p. 225) |
| | IA-NS-3 | Granodiorite | Chapter III, Table 2 (p. 75) | -- | -- | -- |
| | IA-NS-4a | Granophyre | Chapter III, Table 2 (p. 75) | -- | -- | -- |
| | IA-NS-5 | Granophyre | Chapter III, Table 2 (p. 75) | -- | -- | -- |
| | IA-NS-6 | Diorite | Chapter III, Table 2 (p. 75) | Appendix B.2 (p. 189)<br>Appendix B.3 (p. 198)<br>Appendix B.4 (p. 206) | Appendix B.5 (p. 213-214) | Appendix B.9 (p. 225) |
| | IA-NS-7 | Granodiorite | Chapter III, Table 2 (p. 75) | Appendix B.2 (p. 189-190)<br>Appendix B.3 (p. 198-199)<br>Appendix B.4 (p. 206-207) | Appendix B.5 (p. 214-215) | Appendix B.9 (p. 225) |
| | IA-NS-8 | Granophyre | Chapter III, Table 2 (p. 75) | -- | -- | -- |
| | IA-NS-12 | Granophyre | Appendix B.5 (p. 224) | Appendix B.2 (p. 192-193)<br>Appendix B.3 (p. 201-202)<br>Appendix B.4 (p. 209) | Appendix B.5 (p. 217) | -- |
| Mafic | IA-G-1 | Gabbro | Chapter III, Table 2 (p. 75) | Appendix B.2 (p. 193-194)<br>Appendix B.3 (p. 202-203)<br>Appendix B.4 (p. 209-210) | Appendix B.5 (p. 218) | Appendix B.9 (p. 225) |
| | IA-G-3 | Gabbro | Chapter III, Table 2 (p. 75) | -- | -- | -- |
| | IA-G-5 | Gabbro | Chapter III, Table 2 (p. 75) | Appendix B.2 (p. 194)<br>Appendix B.3 (p. 203)<br>Appendix B.4 (p. 210) | Appendix B.5 (p. 218) | Appendix B.9 (p. 225) |
| HSG | IA-NS-4b | High-SiO$_2$ Granophyre | Appendix B.5 (p. 224) | Appendix B.2 (p. 187-189)<br>Appendix B.3 (p. 196-198)<br>Appendix B.4 (p. 205-206) | Appendix B.5 (p. 212-213) | Appendix B.9 (p. 225) |
| | IA-NS-9 | High-SiO$_2$ Granophyre | Appendix B.5 (p. 224) | Appendix B.2 (p. 190-192)<br>Appendix B.3 (p. 199-201)<br>Appendix B.4 (p. 207-208) | Appendix B.5 (p. 215-216) | Appendix B.9 (p. 225) |
| | IA-NS-10 | High-SiO$_2$ Granophyre | Appendix B.5 (p. 224) | Appendix B.2 (p. 192)<br>Appendix B.3 (p. 201)<br>Appendix B.4 (p. 208-209) | Appendix B.5 (p. 216-217) | -- |
| | IA-NS-11 | High-SiO$_2$ Granophyre | Appendix B.5 (p. 224) | -- | -- | -- |

**Appendix B.8**. Major oxide and trace element compositions of rocks from the high-$SiO_2$ granophyre zone at the Austurhorn Intrusive Complex.

| | Sample[42]: | **IA-NS-4b** | **IA-NS-4b_R** | **IA-NS-9** | **IA-NS-10a** | **IA-NS-10b** | **IA-NS-11** | **IA-NS-12** |
|---|---|---|---|---|---|---|---|---|
| Major Element Oxides (wt.%)[43] | $SiO_2$ | 75.6 | 75.7 | 77.4 | 76.1 | 79.4 | 77.8 | 69.9 |
| | $TiO_2$ | 0.16 | 0.16 | 0.08 | 0.17 | 0.09 | 0.14 | 0.43 |
| | $Al_2O_3$ | 12.6 | 12.6 | 11.8 | 12.3 | 11.5 | 11.8 | 13.7 |
| | $Fe_2O_3$ | 2.0 | 2.0 | 1.5 | 2.4 | 1.2 | 1.7 | 4.9 |
| | MnO | 0.05 | 0.05 | 0.04 | 0.04 | 0.02 | 0.02 | 0.15 |
| | MgO | 0.04 | 0.04 | 0.05 | 0.04 | 0.01 | 0.03 | 0.19 |
| | CaO | 0.34 | 0.34 | 0.39 | 0.17 | 0.05 | 0.22 | 1.7 |
| | $Na_2O$ | 5.0 | 4.9 | 4.4 | 4.4 | 5.3 | 4.5 | 5.7 |
| | $K_2O$ | 4.2 | 4.2 | 4.4 | 4.3 | 2.4 | 3.8 | 3.3 |
| | $P_2O_5$ | 0.01 | 0.01 | 0.00 | 0.01 | 0.01 | 0.01 | 0.06 |
| | LOI (%) | | | | | | | |
| Trace Element Concentrations (ppm) | *Ni* | 1 | 1 | 2 | 2 | 0.6 | 2 | 3 |
| | *Cu* | 1.4 | 1.6 | 3 | 5 | 5.3 | 5.0 | 2 |
| | *Zn* | 68 | 69 | 137 | 76 | 43 | 33 | 127 |
| | *Rb* | 66 | 81 | 100 | 79 | 50 | 72 | 63 |
| | *Sr* | 17 | 29 | 29 | 49 | 26 | 39 | 156 |
| | *Y* | 38 | 65 | 92 | 71 | 97 | 91 | 99 |
| | *Zr* | 402 | 391 | 413 | 384 | 430 | 444 | 831 |
| | *Nb* | 58 | 69 | 71 | 56 | 87 | 67 | 66 |
| | *Ba* | 106 | 420 | 135 | 396 | 127 | 272 | 591 |
| | *V* | 1.8 | 2.6 | 1.1 | 3.4 | 1.7 | 1.1 | 4.3 |
| | *Cr* | 3.7 | 4.0 | 5.6 | 1.9 | 3.9 | 2.9 | 2.8 |
| | **La** | 4.8 | 5.6 | 6.9 | 4.5 | 7.6 | 5.5 | 4.2 |
| | **Ce** | 8.3 | 43 | 39 | 40 | 29 | 36 | 66 |
| | **Pr** | 27 | 98 | 95 | 117 | 119 | 99 | 156 |
| | **Nd** | 2.6 | 15 | 12 | 11 | 8.7 | 11 | 19 |
| | **Sm** | 10 | 60 | 48 | 44 | 34 | 45 | 80 |
| | **Eu** | 3.2 | 15 | 14 | 11 | 10 | 12 | 20 |
| | **Gd** | 0.21 | 1.8 | 0.86 | 1.3 | 0.55 | 0.91 | 4.5 |
| | **Tb** | 3.9 | 13 | 14 | 11 | 11 | 13 | 19 |
| | **Dy** | 0.88 | 2.4 | 2.9 | 2.2 | 2.6 | 2.7 | 3.3 |
| | **Ho** | 6.4 | 15 | 19 | 14 | 18 | 18 | 21 |
| | **Er** | 1.5 | 2.8 | 3.9 | 2.9 | 3.9 | 3.7 | 4.1 |
| | **Yb** | 4.6 | 7.5 | 11 | 8.0 | 11 | 10 | 11 |
| | **Lu** | 5.2 | 6.9 | 9.9 | 6.9 | 10 | 8.7 | 9.5 |
| | *Hf* | 0.79 | 1.0 | 1.4 | 0.97 | 1.4 | 1.2 | 1.4 |
| | *Ta* | 15 | 13 | 18 | 13 | 18 | 15 | 21 |
| | *Pb* | 7.9 | 5.9 | 4.4 | 5.2 | 9.2 | 5.2 | 4.1 |
| | *Th* | 9.7 | 8.4 | 11 | 8.4 | 12 | 9.1 | 7.6 |
| | *U* | 3.2 | 2.9 | 4.2 | 2.4 | 3.9 | 3.0 | 2.3 |
| | Temp[44] (ºC) | 869 | 866 | 872 | 873 | 889 | 888 | 919 |

---

[42] All sample names preceded by the label "IA-" (e.g. "NS-4b" = IA-NS-4b)

[43] Anhydrous basis, normalized

[44] Zircon Saturation Temperature: calculated using the formula of Watson & Harrison (1983) (see Section 3.2.a)

**Appendix B.9**. Bulk oxygen isotope compositions, measured *in-situ* by laser fluorination Mass Spectrometry

| Sample | Phase | Date | Initial Mass (mg) | Yield (µmol/mg) | $\delta^{13}C/^{12}C$ | $\delta^{18}O$ Measured | $\delta^{18}O$ Corrected | 2σ | Notes |
|---|---|---|---|---|---|---|---|---|---|
| **IA-NS-2 (Granophyre)** | | | | | | | | | |
| IA-NS-2 | Quartz | May '14 | 1.236 | 18.52 | -23.97 | 6.1 | 5.9 | 0.1 | |
| IA-NS-2 | Pyroxene | May '14 | 1.454 | 14.48 | -23.94 | 5.0 | 4.7 | 0.1 | |
| IA-NS-2 | Feldspar | May '14 | 2.540 | 13.25 | -23.99 | 2.7 | 2.6 | 0.8 | Airlock; small part jumped |
| IA-NS-2 | Quartz | Nov. '11 | 1.450 | 15.03 | -23.97 | 6.1 | 6.0 | 0.1 | |
| IA-NS-2 | Amphibole | Nov. '11 | 1.290 | 12.07 | -23.95 | 3.7 | 3.7 | 0.1 | |
| **IA-NS-4b (High-$SiO_2$ Granophyre)** | | | | | | | | | |
| IA-NS-4b | Quartz | May '14 | 1.213 | 16.98 | -23.97 | -0.6 | -0.9 | 0.1 | |
| IA-NS-4b | Quartz | May '14 | 1.204 | 16.36 | -23.96 | 0.3 | 0.0 | 0.1 | |
| IA-NS-4b | Feldspar | May '14 | 1.691 | 6.81 | -24.00 | -0.2 | -0.4 | 0.1 | |
| IA-NS-4b | Feldspar | May '14 | 2.490 | 18.21 | -24.01 | -0.7 | -0.8 | 0.8 | Airlock |
| IA-NS-4b | Granophyre | May '14 | 2.523 | 16.29 | -24.02 | -1.4 | -1.5 | 0.8 | Airlock |
| IA-NS-4b | Whole-rock | May '14 | 2.400 | 15.39 | -24.01 | -1.4 | -1.5 | 0.8 | Airlock |
| **IA-NS-6 (Diorite)** | | | | | | | | | |
| IA-NS-6 | Quartz | May '14 | 1.101 | 18.96 | -23.95 | 2.5 | 2.2 | 0.1 | |
| IA-NS-6 | Feldspar | May '14 | 2.480 | 13.97 | -24.01 | -0.7 | -0.8 | 0.8 | Airlock |
| **IA-NS-7 (Granodiorite)** | | | | | | | | | |
| IA-NS-7 | Quartz | May '14 | 1.252 | 16.49 | -23.93 | 5.6 | 5.4 | 0.1 | |
| IA-NS-7 | Pyroxene | May '14 | 1.413 | 12.48 | -23.97 | 1.2 | 0.9 | 0.1 | |
| IA-NS-7 | Feldspar | May '14 | 2.538 | 8.07 | -24.01 | 0.1 | 0.0 | 0.8 | Airlock; part jumped |
| IA-NS-7 | Quartz | Nov. '11 | 1.970 | 16.29 | -23.98 | 5.8 | 5.8 | 0.1 | |
| IA-NS-7 | Pyroxene | Nov. '11 | 1.820 | 12.59 | -23.93 | 3.4 | 3.3 | 0.1 | |
| **IA-NS-9 (High-$SiO_2$ Granophyre)** | | | | | | | | | |
| IA-NS-9 | Quartz | May '14 | 1.252 | 17.61 | -23.97 | -2.1 | -2.4 | 0.1 | |
| IA-NS-9 | Quartz | May '14 | 1.343 | 16.50 | -23.99 | -2.6 | -2.9 | 0.1 | |
| IA-NS-9 | Feldspar | May '14 | 2.515 | 10.76 | -24.02 | -2.5 | -2.6 | 0.8 | Airlock; part jumped |
| IA-NS-9 | Granophyre | May '14 | 2.495 | 16.26 | -24.02 | -2.8 | -3.0 | 0.8 | Airlock |
| IA-NS-9 | Whole-rock | May '14 | 2.537 | 15.33 | -24.02 | -2.8 | -3.0 | 0.8 | Airlock |
| **IA-G-1 (Gabbro)** | | | | | | | | | |
| IA-G-1 | Feldspar | May '14 | 1.620 | 6.77 | -23.96 | 3.4 | 3.2 | 0.1 | |
| IA-G-1 | Pyroxene | May '14 | 1.169 | 13.90 | -23.96 | 3.8 | 3.6 | 0.1 | |
| **IA-G-5 (Gabbro)** | | | | | | | | | |
| IA-G-5 | Feldspar | May '14 | 1.776 | 12.08 | -23.97 | 0.0 | -0.3 | 0.1 | |
| IA-G-5 | Pyroxene | May '14 | 1.261 | 14.66 | -23.96 | 5.0 | 4.7 | 0.1 | |

# APPENDIX C

# ICELANDIC SILICIC INTRUSIVE COMPLEXES

**Appendix C.1**. Zircon U-Pb Geochronology[45], measured *in-situ* by SHRIMP-RG

| Spot Name | Mount | $^{204}$Pb/ $^{206}$Pb | % error | $^{206}$Pb/ $^{238}$U | % error | U (ppm) | Th (ppm) | $^{232}$Th/ $^{238}$U | % error | Total $^{238}$U/$^{206}$Pb | % error | Total $^{207}$Pb/$^{206}$Pb | % error | $^{207}$Pb-corr $^{204}$Pb/$^{206}$Pb | $^{207}$Pb-corr % $^{206}$Pb$_C$ |
|---|---|---|---|---|---|---|---|---|---|---|---|---|---|---|---|
| **SLAUFRUDALUR** | | | | | | | | | | | | | | | |
| IISlau-12_11.1 | AJP03 | 6.0E-2 | 10 | 0.03966 | 7.9 | 190 | 158 | 0.86 | 0.30 | 41 | 15.1 | 0.828 | 1 | 5.3E-2 | 99.0 |
| IISlau-12_4.1 | AJP01 | --- | 100 | 0.00191 | 9.2 | 36 | 15 | 0.42 | 3.10 | 1042 | 11.2 | 0.109 | 26 | 4.3E-3 | 8.0 |
| IISlau-12_9.1 | AJP01 | 2.5E-3 | 71 | 0.00226 | 3.6 | 262 | 215 | 0.85 | 3.56 | 1097 | 1.0 | 0.058 | 10 | 8.3E-4 | 1.5 |
| IISlau-12_2.1 | AJP01 | 2.5E-3 | 100 | 0.00223 | 3.0 | 138 | 116 | 0.87 | 0.97 | 1038 | 4.3 | 0.063 | 13 | 1.1E-3 | 2.1 |
| IISlau-12_5.1 | AJP01 | 8.1E-3 | 27 | 0.00260 | 29.7 | 383 | 430 | 1.16 | 0.78 | 1032 | 20.5 | 0.048 | 9 | 1.5E-4 | 0.3 |
| IISlau-12_14.1 | AJP03 | -2.6E-3 | 105 | 0.00198 | 1.4 | 275 | 256 | 0.96 | 0.31 | 1023 | 2.2 | 0.044 | 12 | -1.4E-4 | -0.3 |
| IISlau-12_17.1 | AJP03 | -2.0E-3 | 129 | 0.00214 | 4.0 | 218 | 153 | 0.73 | 0.17 | 1019 | 2.1 | 0.040 | 14 | -4.0E-4 | -0.8 |
| IISlau-12_12.1 | AJP03 | 2.5E-3 | 100 | 0.00223 | 1.5 | 290 | 253 | 0.90 | 1.47 | 1005 | 1.7 | 0.045 | 11 | -7.6E-5 | -0.1 |
| IISlau-12_16.1 | AJP03 | -5.1E-4 | 183 | 0.00210 | 3.5 | 442 | 525 | 1.23 | 0.30 | 995 | 2.4 | 0.048 | 9 | 1.2E-4 | 0.2 |
| IISlau-12_7.1 | AJP01 | 6.6E-3 | 50 | 0.00218 | 2.5 | 231 | 271 | 1.21 | 0.49 | 993 | 3.6 | 0.047 | 12 | 3.0E-5 | 0.1 |
| IISlau-12_15.1 | AJP03 | -1.2E-3 | 183 | 0.00198 | 3.4 | 204 | 180 | 0.91 | 0.16 | 993 | 2.1 | 0.041 | 14 | -3.3E-4 | -0.6 |
| IISlau-12_1.1 | AJP01 | 3.1E-3 | 100 | 0.00221 | 3.4 | 116 | 68 | 0.61 | 0.33 | 971 | 2.7 | 0.052 | 16 | 4.0E-4 | 0.7 |
| IISlau-12_13.1 | AJP03 | 5.3E-3 | 100 | 0.00205 | 2.0 | 141 | 95 | 0.69 | 0.22 | 985 | 2.8 | 0.037 | 19 | -6.5E-4 | -1.2 |
| IISlau-22_3.1 | AJP03 | 7.2E-3 | 61 | 0.00200 | 2.6 | 294 | 214 | 0.75 | 0.44 | 1025 | 2.6 | 0.052 | 11 | 4.0E-4 | 0.7 |
| IISlau-22_7.1 | AJP03 | -2.1E-3 | 183 | 0.00200 | 4.3 | 111 | 59 | 0.54 | 0.43 | 1032 | 3.4 | 0.036 | 20 | -6.6E-4 | -1.2 |
| IISlau-22_4.1 | AJP03 | 8.3E-4 | 158 | 0.00215 | 2.5 | 342 | 333 | 1.01 | 1.57 | 1011 | 1.8 | 0.049 | 10 | 2.2E-4 | 0.4 |
| IISlau-22_5.1 | AJP03 | --- | 100 | 0.00201 | 3.6 | 222 | 131 | 0.61 | 0.33 | 1013 | 2.1 | 0.034 | 15 | -8.0E-4 | -1.5 |
| IISlau-22_12.1 | AJP02 | 3.6E-3 | 100 | 0.00222 | 3.1 | 251 | 162 | 0.67 | 2.10 | 897 | 4.4 | 0.123 | 27 | 5.2E-3 | 9.7 |
| IISlau-22_1.1 | AJP03 | -6.5E-3 | 129 | 0.00217 | 2.9 | 69 | 34 | 0.51 | 0.36 | 996 | 2.9 | 0.041 | 23 | -3.3E-4 | -0.6 |
| IISlau-22_6.1 | AJP03 | -1.9E-3 | 183 | 0.00204 | 3.9 | 122 | 65 | 0.55 | 0.26 | 991 | 2.1 | 0.040 | 19 | -3.9E-4 | -0.7 |
| IISlau-22_13.1 | AJP02 | 3.8E-3 | 120 | 0.00207 | 3.5 | 196 | 96 | 0.51 | 0.25 | 995 | 2.3 | 0.032 | 20 | -9.6E-4 | -1.8 |
| IISlau-22_11.1 | AJP02 | --- | 100 | 0.00197 | 3.0 | 84 | 31 | 0.38 | 0.44 | 949 | 2.9 | 0.053 | 23 | 4.4E-4 | 0.8 |
| IISlau-25_1.1 | AJP04 | -2.2E-3 | 129 | 0.00180 | 5.2 | 523 | 652 | 1.29 | 0.88 | 1080 | 3.9 | 0.040 | 15 | -4.3E-4 | -0.8 |
| IISlau-25_3.1 | AJP04 | 1.8E-3 | 224 | 0.00185 | 6.0 | 179 | 88 | 0.51 | 0.63 | 1021 | 3.0 | 0.077 | 17 | 2.1E-3 | 3.9 |
| IISlau-25_5.1 | AJP04 | -1.4E-3 | 158 | 0.00189 | 4.6 | 458 | 263 | 0.59 | 0.51 | 1027 | 2.3 | 0.055 | 12 | 5.7E-4 | 1.1 |
| IISlau-25_4.1 | AJP04 | 1.3E-2 | 46 | 0.00243 | 7.7 | 469 | 344 | 0.76 | 1.82 | 797 | 10.1 | 0.227 | 35 | 1.2E-2 | 22.9 |
| IISlau-25_2.1 | AJP04 | 2.8E-3 | 158 | 0.00193 | 2.2 | 207 | 109 | 0.55 | 0.26 | 1011 | 1.2 | 0.058 | 17 | 7.9E-4 | 1.5 |
| IISlau-25_6.1 | AJP04 | 4.7E-3 | 49 | 0.00213 | 4.3 | 1348 | 640 | 0.49 | 2.82 | 975 | 2.0 | 0.050 | 7 | 2.7E-4 | 0.5 |
| IISlau-26_1.1 | AJP04 | 8.4E-4 | 129 | 0.00172 | 4.7 | 1547 | 1309 | 0.87 | 0.43 | 1030 | 1.5 | 0.070 | 7 | 1.6E-3 | 3.1 |
| IISlau-26_3.1 | AJP04 | 3.1E-3 | 48 | 0.00190 | 5.9 | 2294 | 3298 | 1.49 | 1.13 | 1014 | 2.1 | 0.070 | 9 | 1.6E-3 | 3.1 |
| IISlau-26_2.1 | AJP04 | 6.8E-4 | 62 | 0.00196 | 5.8 | 5638 | 10497 | 1.92 | 0.51 | 1023 | 2.1 | 0.053 | 3 | 4.7E-4 | 0.9 |
| IISlau-26_5.1 | AJP04 | 2.3E-3 | 79 | 0.00215 | 2.4 | 1120 | 136 | 0.13 | 5.37 | 976 | 1.5 | 0.086 | 6 | 2.7E-3 | 5.0 |
| IISlau-26_7.1 | AJP04 | -3.8E-4 | 129 | 0.00198 | 5.0 | 3042 | 3110 | 1.06 | 1.36 | 974 | 1.4 | 0.063 | 5 | 1.1E-3 | 2.1 |
| IISlau-26_6.1 | AJP04 | 4.7E-3 | 30 | 0.00242 | 4.2 | 3788 | 6255 | 1.71 | 1.28 | 876 | 2.1 | 0.103 | 3 | 3.9E-3 | 7.2 |
| IISlau-26_4.1 | AJP04 | -7.2E-4 | 100 | 0.00263 | 1.9 | 1607 | 2364 | 1.52 | 0.10 | 911 | 1.5 | 0.045 | 6 | -9.5E-5 | -0.2 |

---

[45] Errors (%) are all 1σ; *Pb$_C$* denotes proportion of common Pb; *Pb-corr* indicates correction made using the corresponding (labeled) measured Pb values

**Appendix C.1**. Continued[46]

| **Spot Name** | **Mount** | **$^{204}$Pb-corr $^{207}$Pb*/$^{235}$U** | **% error** | **$^{204}$Pb-corr $^{206}$Pb*/$^{238}$U** | **% error** | **Error Corr.** | **$^{207}$Pb-corr[47] $^{206}$Pb/$^{238}$U Age (Ma)** | **1σ error** | **$^{230}$Th-corr[48] $^{206}$Pb/$^{238}$U Age (Ma)** | **2σ error** | **Reason for excluding?** |
|---|---|---|---|---|---|---|---|---|---|---|---|
| | | | | | | **SLAUFRUDALUR** | | | | | |
| IISlau-12_11.1 | AJP03 | -0.3784 | 94 | -3.0E-3 | 93.2 | 0.99 | 1.62 | 2.17 | ~~**1.71**~~ | ~~**4.34**~~ | **High comm-Pb (>20%), outlier (>2SD)** |
| IISlau-12_4.1 | AJP01 | 0.0144 | 28 | 9.6E-4 | 11.2 | 0.40 | 5.69 | 0.67 | **5.79** | **1.35** | |
| IISlau-12_9.1 | AJP01 | 0.0025 | 135 | 8.7E-4 | 3.5 | 0.03 | 5.78 | 0.07 | **5.87** | **0.15** | |
| IISlau-12_2.1 | AJP01 | 0.0032 | 160 | 9.2E-4 | 6.5 | 0.04 | 6.07 | 0.27 | **6.16** | **0.54** | |
| IISlau-12_5.1 | AJP01 | 0.0104 | 27 | 8.2E-4 | 21.0 | 0.79 | 6.23 | 1.27 | **6.30** | **2.55** | |
| IISlau-12_14.1 | AJP03 | 0.0113 | 46 | 1.0E-3 | 5.3 | 0.11 | 6.31 | 0.15 | **6.40** | **0.29** | |
| IISlau-12_17.1 | AJP03 | 0.0097 | 53 | 1.0E-3 | 5.2 | 0.10 | 6.37 | 0.14 | **6.46** | **0.28** | |
| IISlau-12_12.1 | AJP03 | 0.0008 | 632 | 9.5E-4 | 5.2 | 0.01 | 6.42 | 0.12 | **6.50** | **0.23** | |
| IISlau-12_16.1 | AJP03 | 0.0078 | 26 | 1.0E-3 | 3.0 | 0.12 | 6.46 | 0.16 | **6.54** | **0.32** | |
| IISlau-12_7.1 | AJP01 | 0.0077 | 20 | 8.8E-4 | 7.8 | 0.40 | 6.49 | 0.24 | **6.56** | **0.47** | |
| IISlau-12_15.1 | AJP03 | 0.0082 | 53 | 1.0E-3 | 4.4 | 0.08 | 6.53 | 0.15 | **6.61** | **0.30** | |
| IISlau-12_1.1 | AJP01 | 0.0005 | 1351 | 9.7E-4 | 6.7 | 0.00 | 6.59 | 0.19 | **6.68** | **0.38** | |
| IISlau-12_13.1 | AJP03 | 0.0064 | 36 | 9.2E-4 | 11.2 | 0.31 | 6.62 | 0.19 | **6.71** | **0.39** | |
| IISlau-22_3.1 | AJP03 | 0.0082 | 23 | 8.4E-4 | 9.8 | 0.43 | 6.24 | 0.17 | **6.32** | **0.33** | |
| IISlau-22_7.1 | AJP03 | 0.0093 | 81 | 1.0E-3 | 7.8 | 0.10 | 6.32 | 0.22 | **6.41** | **0.44** | |
| IISlau-22_4.1 | AJP03 | 0.0050 | 56 | 9.7E-4 | 3.1 | 0.06 | 6.35 | 0.12 | **6.42** | **0.25** | |
| IISlau-22_5.1 | AJP03 | 0.0047 | 15 | 9.9E-4 | 2.1 | 0.14 | 6.45 | 0.14 | **6.54** | **0.28** | |
| IISlau-22_12.1 | AJP02 | 0.0103 | 92 | 1.0E-3 | 8.4 | 0.09 | 6.49 | 0.42 | **6.57** | **0.83** | |
| IISlau-22_1.1 | AJP03 | 0.0199 | 79 | 1.1E-3 | 14.3 | 0.18 | 6.51 | 0.20 | **6.60** | **0.41** | |
| IISlau-22_6.1 | AJP03 | 0.0097 | 72 | 1.0E-3 | 6.5 | 0.09 | 6.55 | 0.15 | **6.64** | **0.30** | |
| IISlau-22_13.1 | AJP02 | 0.0037 | 29 | 9.3E-4 | 9.3 | 0.32 | 6.59 | 0.16 | **6.69** | **0.33** | |
| IISlau-22_11.1 | AJP02 | 0.0077 | 23 | 1.1E-3 | 2.9 | 0.13 | 6.73 | 0.22 | **6.83** | **0.44** | |
| IISlau-25_1.1 | AJP04 | 0.0094 | 55 | 9.6E-4 | 6.4 | 0.12 | 6.01 | 0.24 | **6.08** | **0.48** | |
| IISlau-25_3.1 | AJP04 | 0.0066 | 125 | 9.5E-4 | 8.4 | 0.07 | 6.07 | 0.21 | **6.16** | **0.43** | |
| IISlau-25_5.1 | AJP04 | 0.0104 | 43 | 1.0E-3 | 4.8 | 0.11 | 6.21 | 0.15 | **6.30** | **0.31** | |
| IISlau-25_4.1 | AJP04 | 0.0049 | 417 | 9.6E-4 | 17.5 | 0.04 | 6.23 | 1.03 | ~~**6.32**~~ | ~~**2.06**~~ | **High comm-Pb (>20%)** |
| IISlau-25_2.1 | AJP04 | 0.0019 | 502 | 9.4E-4 | 8.9 | 0.02 | 6.28 | 0.11 | **6.38** | **0.22** | |
| IISlau-25_6.1 | AJP04 | 0.0032 | 56 | 9.4E-4 | 5.1 | 0.09 | 6.58 | 0.14 | **6.67** | **0.27** | |
| IISlau-26_1.1 | AJP04 | 0.0077 | 29 | 9.6E-4 | 2.5 | 0.09 | 6.06 | 0.10 | **6.14** | **0.20** | |
| IISlau-26_3.1 | AJP04 | 0.0029 | 110 | 9.3E-4 | 3.6 | 0.03 | 6.16 | 0.14 | **6.22** | **0.28** | |
| IISlau-26_2.1 | AJP04 | 0.0057 | 15 | 9.7E-4 | 2.3 | 0.15 | 6.24 | 0.13 | **6.29** | **0.26** | |
| IISlau-26_5.1 | AJP04 | 0.0071 | 54 | 9.8E-4 | 3.9 | 0.07 | 6.27 | 0.10 | **6.38** | **0.21** | |
| IISlau-26_7.1 | AJP04 | 0.0098 | 11 | 1.0E-3 | 1.7 | 0.15 | 6.47 | 0.10 | **6.55** | **0.19** | |
| IISlau-26_6.1 | AJP04 | 0.0047 | 72 | 1.0E-3 | 3.5 | 0.05 | 6.82 | 0.14 | **6.88** | **0.29** | |
| IISlau-26_4.1 | AJP04 | 0.0085 | 20 | 1.1E-3 | 2.0 | 0.10 | 7.08 | 0.11 | ~~**7.14**~~ | ~~**0.22**~~ | **Low UO/U** |

---

[46] *Pb** denotes proportion of radiogenic Pb; discarded ages are listed in red strikethrough font

[47] Corrected for common Pb assuming $^{206}$Pb/$^{238}$U-$^{207}$Pb/$^{235}$U age concordance

[48] Corrected for initial $^{238}$U-$^{230}$Th disequilibrium using whole-rock Th/U for each sample

**Appendix C.1**. Continued

| Spot Name | Mount | $^{204}$Pb/ $^{206}$Pb | % error | $^{206}$Pb/ $^{238}$U | % error | U (ppm) | Th (ppm) | $^{232}$Th/ $^{238}$U | % error | Total $^{238}$U/$^{206}$Pb | % error | Total $^{207}$Pb/$^{206}$Pb | % error | $^{207}$Pb-corr $^{204}$Pb/$^{206}$Pb | $^{207}$Pb-corr % $^{206}$Pb$_C$ |
|---|---|---|---|---|---|---|---|---|---|---|---|---|---|---|---|
| **VESTURHORN** | | | | | | | | | | | | | | | |
| IIV-03a_2.1 | AJP01 | 7.3E-3 | 58 | 0.00112 | 3.0 | 249 | 125 | 0.52 | 0.23 | 1768 | 0.6 | 0.071 | 12 | 1.7E-3 | 3.1 |
| IIV-03a_14.1 | AJP01 | --- | --- | 0.00155 | 2.2 | 354 | 247 | 0.72 | 0.16 | 1712 | 1.1 | 0.050 | 11 | 2.6E-4 | 0.5 |
| IIV-03a_17.1 | AJP01 | ---- | --- | 0.00120 | 2.8 | 325 | 279 | 0.89 | 1.80 | 1698 | 3.2 | 0.055 | 13 | 6.0E-4 | 1.1 |
| IIV-03a_13.1 | AJP01 | 1.9E-3 | 71 | 0.00127 | 1.9 | 668 | 448 | 0.69 | 1.94 | 1668 | 0.8 | 0.057 | 8 | 7.2E-4 | 1.4 |
| IIV-03a_16.1 | AJP01 | --- | --- | 0.00144 | 1.9 | 499 | 461 | 0.96 | 0.40 | 1680 | 0.6 | 0.044 | 10 | -1.7E-4 | -0.3 |
| IIV-03a_11.1 | AJP01 | -1.5E-3 | 100 | 0.00132 | 5.9 | 426 | 250 | 0.61 | 0.38 | 1675 | 5.0 | 0.047 | 19 | 4.4E-5 | 0.1 |
| IIV-03a_6.1 | AJP01 | --- | --- | 0.00124 | 5.2 | 326 | 152 | 0.48 | 0.24 | 1632 | 2.0 | 0.068 | 11 | 1.5E-3 | 2.7 |
| IIV-03a_5.1 | AJP01 | 1.6E-3 | 100 | 0.00116 | 6.7 | 359 | 210 | 0.60 | 1.45 | 1632 | 3.2 | 0.063 | 10 | 1.1E-3 | 2.1 |
| IIV-03a_12.1 | AJP01 | -2.1E-3 | 100 | 0.00128 | 2.8 | 319 | 165 | 0.53 | 0.78 | 1583 | 1.2 | 0.076 | 11 | 2.0E-3 | 3.8 |
| IIV-03a_9.1 | AJP01 | --- | 100 | 0.00144 | 1.9 | 522 | 291 | 0.58 | 0.18 | 1610 | 3.0 | 0.053 | 16 | 4.7E-4 | 0.9 |
| IIV-03a_10.1 | AJP01 | 9.5E-4 | 100 | 0.00141 | 1.9 | 561 | 531 | 0.98 | 0.76 | 1563 | 1.2 | 0.046 | 9 | -3.7E-6 | 0.0 |
| IIV-03a_15.1 | AJP01 | 2.7E-3 | 100 | 0.00148 | 3.2 | 194 | 100 | 0.53 | 0.30 | 1503 | 5.5 | 0.074 | 27 | 1.9E-3 | 3.6 |
| IIV-03a_8.1 | AJP01 | 1.2E-2 | 58 | 0.00133 | 3.9 | 126 | 56 | 0.46 | 3.34 | 1529 | 2.8 | 0.062 | 16 | 1.0E-3 | 2.0 |
| IIV-16_4.1 | AJP03 | 2.0E-2 | 100 | 0.00146 | 3.9 | 51 | 22 | 0.44 | 1.09 | 1444 | 1.2 | 0.189 | 16 | 9.7E-3 | 18.1 |
| IIV-16_3.1 | AJP03 | 4.1E-2 | 32 | 0.00179 | 2.5 | 161 | 116 | 0.75 | 0.18 | 1135 | 3.5 | 0.322 | 4 | 1.9E-2 | 35.0 |
| IIV-16_8.1 | AJP03 | 1.7E-2 | 41 | 0.00114 | 3.4 | 467 | 293 | 0.65 | 2.23 | 1641 | 2.3 | 0.074 | 9 | 1.9E-3 | 3.5 |
| IIV-16_2.1 | AJP03 | -3.5E-3 | 129 | 0.00126 | 5.2 | 175 | 130 | 0.77 | 1.21 | 1658 | 4.3 | 0.043 | 27 | -1.9E-4 | -0.4 |
| IIV-16_7.1 | AJP03 | 7.4E-3 | 120 | 0.00132 | 2.8 | 112 | 52 | 0.48 | 0.62 | 1555 | 2.2 | 0.092 | 16 | 3.1E-3 | 5.7 |
| IIV-16_5.1 | AJP03 | -1.0E-3 | 183 | 0.00133 | 4.2 | 352 | 395 | 1.16 | 0.80 | 1617 | 3.1 | 0.054 | 12 | 5.1E-4 | 1.0 |
| IIV-16_14.1 | AJP02 | -3.3E-3 | 183 | 0.00135 | 6.1 | 133 | 87 | 0.68 | 0.89 | 1581 | 4.8 | 0.064 | 19 | 1.2E-3 | 2.3 |
| IIV-16_1.1 | AJP03 | 1.3E-3 | 100 | 0.00138 | 3.8 | 747 | 886 | 1.22 | 0.22 | 1587 | 1.2 | 0.049 | 6 | 1.7E-4 | 0.3 |
| IIV-16_15.1 | AJP02 | 9.4E-3 | 100 | 0.00136 | 2.5 | 151 | 62 | 0.43 | 0.29 | 1586 | 3.3 | 0.054 | 19 | 5.5E-4 | 1.0 |
| IIV-16_12.1 | AJP02 | -1.3E-3 | 183 | 0.00145 | 2.8 | 325 | 289 | 0.92 | 0.49 | 1597 | 1.7 | 0.045 | 15 | -1.1E-4 | -0.2 |
| IIV-16_13.1 | AJP02 | 6.3E-3 | 120 | 0.00132 | 2.4 | 165 | 122 | 0.77 | 0.22 | 1558 | 2.6 | 0.049 | 19 | 1.6E-4 | 0.3 |
| IIV-16_11.1 | AJP02 | 1.5E-2 | 61 | 0.00147 | 2.2 | 230 | 182 | 0.82 | 0.79 | 1518 | 2.8 | 0.056 | 15 | 6.9E-4 | 1.3 |
| IIV-16_6.1 | AJP03 | --- | 100 | 0.00146 | 4.7 | 143 | 91 | 0.66 | 1.02 | 1465 | 4.5 | 0.079 | 19 | 2.2E-3 | 4.1 |
| IIV-15_7.1 | AJP04 | --- | 100 | 0.00122 | 12.2 | 74 | 49 | 0.69 | 1.75 | 1773 | 10.6 | 0.075 | 34 | 2.0E-3 | 3.7 |
| IIV-15_13.1 | AJP04 | -1.5E-2 | 158 | 0.00110 | 10.4 | 69 | 53 | 0.79 | 3.10 | 1688 | 7.6 | 0.104 | 27 | 3.9E-3 | 7.3 |
| IIV-15_3.1 | AJP04 | 2.2E-2 | 112 | 0.00122 | 4.3 | 112 | 86 | 0.79 | 0.34 | 1593 | 4.5 | 0.077 | 27 | 2.1E-3 | 3.9 |
| IIV-15_1.1 | AJP04 | -5.9E-3 | 158 | 0.00120 | 7.0 | 199 | 234 | 1.21 | 1.20 | 1660 | 5.7 | 0.038 | 28 | -5.2E-4 | -1.0 |
| IIV-15_17.1 | AJP04 | -1.9E-2 | 158 | 0.00130 | 5.7 | 63 | 32 | 0.52 | 0.56 | 1571 | 6.4 | 0.077 | 36 | 2.1E-3 | 3.9 |
| IIV-15_15.1 | AJP04 | -7.0E-3 | 224 | 0.00128 | 4.9 | 82 | 46 | 0.58 | 0.45 | 1624 | 3.7 | 0.049 | 38 | 1.9E-4 | 0.3 |
| IIV-15_19.1 | AJP04 | --- | 100 | 0.00129 | 4.7 | 97 | 69 | 0.73 | 0.40 | 1544 | 2.9 | 0.084 | 28 | 2.5E-3 | 4.7 |
| IIV-15_16.1 | AJP04 | -7.8E-3 | 224 | 0.00133 | 5.1 | 71 | 49 | 0.71 | 1.89 | 1552 | 5.6 | 0.078 | 32 | 2.1E-3 | 4.0 |
| IIV-15_6.1 | AJP04 | 2.2E-2 | 129 | 0.00126 | 5.2 | 81 | 59 | 0.75 | 0.41 | 1558 | 6.6 | 0.066 | 34 | 1.3E-3 | 2.5 |
| IIV-15_2.1 | AJP04 | --- | 100 | 0.00129 | 4.8 | 453 | 302 | 0.69 | 1.03 | 1547 | 2.3 | 0.055 | 16 | 6.1E-4 | 1.1 |
| IIV-15_11.1 | AJP04 | 1.3E-2 | 158 | 0.00131 | 4.8 | 83 | 60 | 0.75 | 0.39 | 1575 | 10.0 | 0.040 | 41 | -4.1E-4 | -0.8 |
| IIV-15_18.1 | AJP04 | -2.5E-3 | 224 | 0.00127 | 2.9 | 257 | 84 | 0.34 | 0.35 | 1547 | 3.0 | 0.043 | 24 | -2.1E-4 | -0.4 |

**Appendix C.1**. Continued

| Spot Name | Mount | $^{204}$Pb-corr $^{207}$Pb*/$^{235}$U | % error | $^{204}$Pb-corr $^{206}$Pb*/$^{238}$U | % error | Error Corr. | $^{207}$Pb-corr $^{206}$Pb/$^{238}$U Age (Ma) | 1σ error | $^{230}$Th-corr $^{206}$Pb/$^{238}$U Age (Ma) | 2σ error | Reason for excluding? |
|---|---|---|---|---|---|---|---|---|---|---|---|
| **VESTURHORN** | | | | | | | | | | | |
| IIV-03a_2.1 | AJP01 | 0.0033 | 36 | 4.9E-4 | 9.1 | 0.25 | 3.53 | 0.05 | ~~**3.62**~~ | ~~**0.09**~~ | **Younger Age, outlier (>2SD)** |
| IIV-03a_14.1 | AJP01 | 0.0040 | 11 | 5.8E-4 | 1.1 | 0.10 | 3.75 | 0.05 | ~~**3.83**~~ | ~~**0.10**~~ | **High UO/U** |
| IIV-03a_17.1 | AJP01 | 0.0045 | 14 | 5.9E-4 | 3.2 | 0.23 | 3.75 | 0.13 | **3.84** | **0.25** | |
| IIV-03a_13.1 | AJP01 | 0.0022 | 78 | 5.8E-4 | 2.8 | 0.04 | 3.81 | 0.04 | **3.90** | **0.08** | |
| IIV-03a_16.1 | AJP01 | 0.0036 | 10 | 6.0E-4 | 0.6 | 0.06 | 3.85 | 0.03 | **3.93** | **0.06** | |
| IIV-03a_11.1 | AJP01 | 0.0057 | 33 | 6.1E-4 | 5.7 | 0.17 | 3.84 | 0.20 | **3.93** | **0.40** | |
| IIV-03a_6.1 | AJP01 | 0.0057 | 11 | 6.1E-4 | 2.0 | 0.18 | 3.84 | 0.08 | **3.94** | **0.17** | |
| IIV-03a_5.1 | AJP01 | 0.0032 | 64 | 5.9E-4 | 4.4 | 0.07 | 3.86 | 0.13 | **3.96** | **0.26** | |
| IIV-03a_12.1 | AJP01 | 0.0095 | 28 | 6.6E-4 | 4.0 | 0.14 | 3.92 | 0.06 | **4.01** | **0.13** | |
| IIV-03a_9.1 | AJP01 | 0.0045 | 16 | 6.2E-4 | 3.0 | 0.18 | 3.97 | 0.13 | **4.06** | **0.25** | |
| IIV-03a_10.1 | AJP01 | 0.0028 | 48 | 6.3E-4 | 2.2 | 0.05 | 4.12 | 0.05 | **4.20** | **0.11** | |
| IIV-03a_15.1 | AJP01 | 0.0029 | 146 | 6.3E-4 | 7.7 | 0.05 | 4.13 | 0.25 | **4.23** | **0.50** | |
| IIV-03a_8.1 | AJP01 | 0.0113 | 50 | 5.1E-4 | 16.9 | 0.34 | 4.13 | 0.13 | **4.23** | **0.26** | |
| IIV-16_4.1 | AJP03 | 0.0123 | 67 | 4.3E-4 | 61.4 | 0.91 | 3.65 | 0.18 | **3.75** | **0.35** | |
| IIV-16_3.1 | AJP03 | 0.0381 | 144 | 2.1E-4 | 102.1 | 0.71 | 3.69 | 0.17 | ~~**3.78**~~ | ~~**0.33**~~ | **High comm-Pb (>20%)** |
| IIV-16_8.1 | AJP03 | 0.0165 | 49 | 4.1E-4 | 19.7 | 0.40 | 3.79 | 0.09 | ~~**3.88**~~ | ~~**0.19**~~ | **Low UO/U, outlier (>2SD)** |
| IIV-16_2.1 | AJP03 | 0.0082 | 66 | 6.4E-4 | 9.0 | 0.14 | 3.90 | 0.18 | **3.98** | **0.35** | |
| IIV-16_7.1 | AJP03 | 0.0021 | 334 | 5.5E-4 | 19.2 | 0.06 | 3.91 | 0.12 | **4.00** | **0.23** | |
| IIV-16_5.1 | AJP03 | 0.0059 | 40 | 6.3E-4 | 4.7 | 0.12 | 3.95 | 0.13 | **4.02** | **0.26** | |
| IIV-16_14.1 | AJP02 | 0.0100 | 72 | 6.7E-4 | 11.5 | 0.16 | 3.98 | 0.20 | **4.07** | **0.40** | |
| IIV-16_1.1 | AJP03 | 0.0024 | 74 | 6.1E-4 | 2.8 | 0.04 | 4.05 | 0.05 | **4.12** | **0.10** | |
| IIV-16_15.1 | AJP02 | 0.0080 | 67 | 5.2E-4 | 21.5 | 0.3 | 4.02 | 0.14 | **4.12** | **0.29** | |
| IIV-16_12.1 | AJP02 | 0.0056 | 54 | 6.4E-4 | 4.6 | 0.1 | 4.04 | 0.08 | **4.12** | **0.15** | |
| IIV-16_13.1 | AJP02 | 0.0044 | 31 | 5.7E-4 | 16.1 | 0.5 | 4.12 | 0.12 | **4.21** | **0.23** | |
| IIV-16_11.1 | AJP02 | 0.0158 | 69 | 4.8E-4 | 23.4 | 0.3 | 4.19 | 0.13 | **4.27** | **0.25** | |
| IIV-16_6.1 | AJP03 | 0.0074 | 20 | 6.8E-4 | 4.5 | 0.23 | 4.22 | 0.21 | **4.30** | **0.42** | |
| IIV-15_7.1 | AJP04 | 0.0059 | 35 | 5.6E-4 | 10.6 | 0.30 | 3.50 | 0.39 | **3.58** | **0.78** | |
| IIV-15_13.1 | AJP04 | 0.0274 | 83 | 7.6E-4 | 35.1 | 0.42 | 3.54 | 0.30 | **3.61** | **0.60** | |
| IIV-15_3.1 | AJP04 | 0.0230 | 176 | 3.7E-4 | 77.9 | 0.44 | 3.89 | 0.20 | **3.96** | **0.41** | |
| IIV-15_1.1 | AJP04 | 0.0109 | 98 | 6.7E-4 | 16.7 | 0.17 | 3.92 | 0.23 | **3.98** | **0.46** | |
| IIV-15_17.1 | AJP04 | 0.0332 | 94 | 8.7E-4 | 42.4 | 0.45 | 3.94 | 0.29 | **4.03** | **0.58** | |
| IIV-15_15.1 | AJP04 | 0.0134 | 132 | 7.0E-4 | 26.1 | 0.20 | 3.95 | 0.17 | **4.04** | **0.35** | |
| IIV-15_19.1 | AJP04 | 0.0075 | 28 | 6.5E-4 | 2.9 | 0.10 | 3.98 | 0.17 | **4.05** | **0.34** | |
| IIV-15_16.1 | AJP04 | 0.0177 | 113 | 7.4E-4 | 28.9 | 0.26 | 3.99 | 0.26 | **4.06** | **0.51** | |
| IIV-15_6.1 | AJP04 | 0.0245 | 209 | 3.8E-4 | 90.1 | 0.43 | 4.03 | 0.29 | **4.11** | **0.58** | |
| IIV-15_2.1 | AJP04 | 0.0049 | 16 | 6.5E-4 | 2.3 | 0.14 | 4.12 | 0.11 | **4.20** | **0.21** | |
| IIV-15_11.1 | AJP04 | 0.0148 | 182 | 4.8E-4 | 53.6 | 0.30 | 4.12 | 0.42 | **4.20** | **0.84** | |
| IIV-15_18.1 | AJP04 | 0.0074 | 98 | 6.8E-4 | 10.5 | 0.11 | 4.18 | 0.14 | **4.28** | **0.27** | |

**Appendix C.1**. Continued

| Spot Name | Mount | $^{204}$Pb/ $^{206}$Pb | % error | $^{206}$Pb/ $^{238}$U | % error | U (ppm) | Th (ppm) | $^{232}$Th/ $^{238}$U | % error | Total $^{238}$U/$^{206}$Pb | % error | Total $^{207}$Pb/$^{206}$Pb | % error | $^{207}$Pb-corr $^{204}$Pb/$^{206}$Pb | $^{207}$Pb-corr % $^{206}$Pb$_C$ |
|---|---|---|---|---|---|---|---|---|---|---|---|---|---|---|---|
| **REYÐARÁRTINDUR** | | | | | | | | | | | | | | | |
| IIR-01_5.1 | AJP04 | -8.4E-3 | 129 | 0.00205 | 7.6 | 94 | 54 | 0.60 | 0.38 | 886 | 4.3 | 0.111 | 18 | 4.4E-3 | 8.2 |
| IIR-01_3.1 | AJP04 | --- | 100 | 0.00176 | 5.7 | 195 | 109 | 0.58 | 0.93 | 894 | 3.0 | 0.083 | 16 | 2.5E-3 | 4.7 |
| IIR-01_14.1 | AJP04 | -1.5E-3 | 224 | 0.00202 | 9.9 | 203 | 121 | 0.62 | 0.62 | 911 | 5.9 | 0.049 | 19 | 2.2E-4 | 0.4 |
| IIR-01_7.1 | AJP04 | 1.6E-2 | 75 | 0.00227 | 3.8 | 169 | 122 | 0.75 | 0.49 | 871 | 2.3 | 0.067 | 19 | 1.4E-3 | 2.6 |
| IIR-01_4.1 | AJP04 | -1.7E-3 | 158 | 0.00170 | 9.0 | 479 | 474 | 1.02 | 0.35 | 905 | 1.7 | 0.033 | 19 | -9.2E-4 | -1.7 |
| IIR-01_8.1 | AJP04 | -3.5E-3 | 158 | 0.00236 | 5.7 | 167 | 109 | 0.67 | 0.29 | 858 | 3.7 | 0.070 | 17 | 1.6E-3 | 3.1 |
| IIR-01_11.1 | AJP04 | -6.9E-4 | 129 | 0.00215 | 5.4 | 1485 | 1750 | 1.22 | 0.26 | 868 | 1.9 | 0.045 | 8 | -5.7E-5 | -0.1 |
| IIR-01_9.1 | AJP04 | -7.0E-4 | 224 | 0.00243 | 4.5 | 442 | 371 | 0.87 | 0.31 | 871 | 1.7 | 0.035 | 15 | -7.7E-4 | -1.4 |
| IIR-01_1.1 | AJP04 | -2.5E-3 | 112 | 0.00171 | 7.5 | 464 | 296 | 0.66 | 1.59 | 856 | 4.1 | 0.043 | 13 | -2.4E-4 | -0.5 |
| IIR-01_12.1 | AJP04 | 2.2E-3 | 75 | 0.00247 | 4.3 | 1242 | 1503 | 1.25 | 0.45 | 839 | 1.8 | 0.046 | 14 | -9.4E-6 | 0.0 |
| IIR-01_6.1 | AJP04 | -2.1E-3 | 224 | 0.00209 | 6.0 | 170 | 89 | 0.54 | 1.20 | 803 | 3.2 | 0.070 | 19 | 1.6E-3 | 3.0 |
| IIR-03a_17.1 | AJP04 | -6.6E-4 | 129 | 0.00209 | 7.1 | 1125 | 973 | 0.89 | 0.78 | 909 | 2.7 | 0.043 | 8 | -1.9E-4 | -0.4 |
| IIR-03a_11.1 | AJP04 | 2.2E-3 | 62 | 0.00223 | 4.6 | 1199 | 929 | 0.80 | 0.25 | 901 | 1.9 | 0.044 | 11 | -1.7E-4 | -0.3 |
| IIR-03a_8.1 | AJP04 | 4.2E-3 | 48 | 0.00231 | 4.4 | 1091 | 1102 | 1.04 | 0.58 | 896 | 1.3 | 0.044 | 7 | -1.2E-4 | -0.2 |
| IIR-03a_7.1 | AJP04 | 1.0E-3 | 158 | 0.00202 | 5.6 | 391 | 244 | 0.64 | 0.67 | 831 | 4.5 | 0.096 | 9 | 3.4E-3 | 6.4 |
| IIR-03a_15.1 | AJP04 | 3.7E-4 | 158 | 0.00213 | 5.7 | 1261 | 1307 | 1.07 | 0.45 | 881 | 2.5 | 0.049 | 6 | 1.8E-4 | 0.3 |
| IIR-03a_10.1 | AJP04 | 8.2E-4 | 112 | 0.00199 | 5.8 | 1179 | 1258 | 1.10 | 0.58 | 875 | 1.7 | 0.049 | 12 | 1.6E-4 | 0.3 |
| IIR-03a_18.1 | AJP04 | 1.8E-3 | 58 | 0.00197 | 6.0 | 2204 | 1700 | 0.80 | 0.96 | 871 | 1.5 | 0.052 | 5 | 4.1E-4 | 0.8 |
| IIR-03a_14.1 | AJP04 | 7.3E-4 | 112 | 0.00219 | 5.0 | 1170 | 1138 | 1.00 | 1.30 | 873 | 1.8 | 0.047 | 12 | 5.3E-5 | 0.1 |
| IIR-03a_5.1 | AJP04 | 5.3E-3 | 54 | 0.00237 | 6.0 | 1543 | 1331 | 0.89 | 0.73 | 851 | 6.7 | 0.038 | 23 | -5.8E-4 | -1.1 |
| IIR-03a_4.1 | AJP04 | 1.6E-3 | 112 | 0.00191 | 7.1 | 836 | 660 | 0.82 | 2.37 | 810 | 1.9 | 0.050 | 10 | 2.6E-4 | 0.5 |
| IIR-03a_9.1 | AJP04 | 4.7E-2 | 11 | 0.00658 | 10.5 | 660 | 546 | 0.86 | 0.62 | 225 | 10.4 | 0.601 | 8 | 3.8E-2 | 70.3 |
| IIR-13_16.1 | AJP04 | -9.2E-4 | 158 | 0.00185 | 3.5 | 493 | 345 | 0.72 | 0.49 | 994 | 2.0 | 0.063 | 9 | 1.1E-3 | 2.1 |
| IIR-13_17.1 | AJP04 | 5.2E-3 | 112 | 0.00170 | 6.4 | 180 | 144 | 0.83 | 0.98 | 956 | 3.1 | 0.057 | 16 | 7.5E-4 | 1.4 |
| IIR-13_15.1 | AJP04 | -1.9E-3 | 224 | 0.00211 | 6.3 | 147 | 71 | 0.50 | 0.33 | 937 | 3.6 | 0.073 | 18 | 1.8E-3 | 3.4 |
| IIR-13_2.1 | AJP04 | 2.7E-2 | 67 | 0.00191 | 6.2 | 100 | 60 | 0.61 | 0.32 | 969 | 1.6 | 0.044 | 24 | -1.8E-4 | -0.3 |
| IIR-13_3.1 | AJP04 | --- | 100 | 0.00194 | 6.9 | 81 | 38 | 0.48 | 0.40 | 901 | 3.5 | 0.083 | 19 | 2.5E-3 | 4.6 |
| IIR-13_7.1 | AJP04 | 1.2E-3 | 100 | 0.00193 | 5.9 | 902 | 843 | 0.97 | 0.51 | 924 | 3.6 | 0.061 | 7 | 1.0E-3 | 1.9 |
| IIR-13_13.1 | AJP04 | 1.0E-3 | 224 | 0.00225 | 4.5 | 336 | 360 | 1.11 | 3.11 | 892 | 2.6 | 0.031 | 18 | -1.0E-3 | -1.9 |
| IIR-13_10.1 | AJP04 | 2.2E-3 | 54 | 0.00198 | 8.7 | 1895 | 3088 | 1.68 | 1.73 | 862 | 2.6 | 0.056 | 5 | 6.5E-4 | 1.2 |
| IIR-13_18.1 | AJP04 | 1.7E-3 | 129 | 0.00224 | 5.8 | 373 | 298 | 0.82 | 0.50 | 837 | 2.7 | 0.049 | 12 | 2.1E-4 | 0.4 |
| IIR-13_20.1 | AJP04 | 1.6E-3 | 224 | 0.00303 | 10.5 | 104 | 59 | 0.58 | 0.63 | 600 | 7.6 | 0.272 | 9 | 1.5E-2 | 28.6 |
| IIR-13_8.1 | AJP04 | 1.1E-3 | 100 | 0.00240 | 5.5 | 972 | 219 | 0.23 | 3.05 | 778 | 2.1 | 0.041 | 8 | -3.5E-4 | -0.6 |
| IIR-13_4.1 | AJP04 | 2.8E-2 | 31 | 0.00405 | 16.5 | 232 | 191 | 0.85 | 0.22 | 501 | 15.9 | 0.307 | 17 | 1.8E-2 | 33.0 |

**Appendix C.1**. Continued

| Spot Name | Mount | $^{204}$Pb-corr $^{207}$Pb*/$^{235}$U | % error | $^{204}$Pb-corr $^{206}$Pb*/$^{238}$U | % error | Error Corr. | $^{207}$Pb-corr $^{206}$Pb/$^{238}$U Age (Ma) | 1σ error | $^{230}$Th-corr $^{206}$Pb/$^{238}$U Age (Ma) | 2σ error | Reason for excluding? |
|---|---|---|---|---|---|---|---|---|---|---|---|
| **REYÐARÁRTINDUR** | | | | | | | | | | | |
| IIR-01_5.1 | AJP04 | 0.0378 | 56 | 1.3E-3 | 18.1 | 0.32 | 6.68 | 0.34 | **6.76** | **0.69** | |
| IIR-01_3.1 | AJP04 | 0.0128 | 16 | 1.1E-3 | 3.0 | 0.19 | 6.87 | 0.24 | **6.96** | **0.48** | |
| IIR-01_14.1 | AJP04 | 0.0111 | 69 | 1.1E-3 | 8.6 | 0.13 | 7.04 | 0.42 | **7.13** | **0.85** | |
| IIR-01_7.1 | AJP04 | 0.0285 | 84 | 8.1E-4 | 31.2 | 0.37 | 7.20 | 0.20 | **7.29** | **0.40** | |
| IIR-01_4.1 | AJP04 | 0.0091 | 67 | 1.1E-3 | 5.2 | 0.08 | 7.24 | 0.14 | **7.31** | **0.28** | |
| IIR-01_8.1 | AJP04 | 0.0202 | 61 | 1.2E-3 | 10.5 | 0.17 | 7.28 | 0.29 | **7.36** | **0.59** | |
| IIR-01_11.1 | AJP04 | 0.0089 | 24 | 1.2E-3 | 2.5 | 0.10 | 7.43 | 0.15 | **7.50** | **0.29** | |
| IIR-01_9.1 | AJP04 | 0.0073 | 52 | 1.2E-3 | 3.4 | 0.06 | 7.51 | 0.14 | **7.59** | **0.27** | |
| IIR-01_1.1 | AJP04 | 0.0131 | 49 | 1.2E-3 | 6.4 | 0.13 | 7.56 | 0.31 | **7.65** | **0.62** | |
| IIR-01_12.1 | AJP04 | 0.0019 | 225 | 1.1E-3 | 3.7 | 0.02 | 7.68 | 0.15 | **7.74** | **0.30** | |
| IIR-01_6.1 | AJP04 | 0.0177 | 65 | 1.3E-3 | 9.0 | 0.14 | 7.78 | 0.28 | **7.87** | **0.56** | |
| IIR-03a_17.1 | AJP04 | 0.0081 | 24 | 1.1E-3 | 3.1 | 0.13 | 7.11 | 0.19 | **7.19** | **0.39** | |
| IIR-03a_11.1 | AJP04 | 0.0013 | 254 | 1.1E-3 | 3.3 | 0.01 | 7.17 | 0.14 | **7.25** | **0.28** | |
| IIR-03a_8.1 | AJP04 | 0.0032 | 53 | 1.0E-3 | 4.2 | 0.08 | 7.21 | 0.10 | **7.28** | **0.20** | |
| IIR-03a_7.1 | AJP04 | 0.0133 | 31 | 1.2E-3 | 5.5 | 0.17 | 7.26 | 0.33 | **7.35** | **0.67** | |
| IIR-03a_15.1 | AJP04 | 0.0067 | 22 | 1.1E-3 | 2.7 | 0.13 | 7.28 | 0.18 | **7.36** | **0.36** | |
| IIR-03a_10.1 | AJP04 | 0.0057 | 41 | 1.1E-3 | 2.4 | 0.06 | 7.34 | 0.14 | **7.41** | **0.27** | |
| IIR-03a_18.1 | AJP04 | 0.0038 | 67 | 1.1E-3 | 2.5 | 0.04 | 7.34 | 0.11 | **7.42** | **0.22** | |
| IIR-03a_14.1 | AJP04 | 0.0056 | 38 | 1.1E-3 | 2.4 | 0.06 | 7.37 | 0.14 | **7.45** | **0.28** | |
| IIR-03a_5.1 | AJP04 | 0.0074 | 26 | 1.1E-3 | 9.0 | 0.34 | 7.65 | 0.52 | **7.73** | **1.04** | |
| IIR-03a_4.1 | AJP04 | 0.0043 | 109 | 1.2E-3 | 3.9 | 0.04 | 7.91 | 0.16 | **7.99** | **0.32** | |
| IIR-03a_9.1 | AJP04 | 0.0841 | 100 | 5.2E-4 | 82.3 | 0.82 | 8.50 | 1.98 | ~~**8.59**~~ | ~~**3.96**~~ | **High comm-Pb (>20%)** |
| IIR-13_16.1 | AJP04 | 0.0108 | 28 | 1.0E-3 | 3.4 | 0.12 | 6.35 | 0.14 | **6.43** | **0.27** | |
| IIR-13_17.1 | AJP04 | 0.0035 | 145 | 9.4E-4 | 12.5 | 0.09 | 6.64 | 0.22 | **6.73** | **0.44** | |
| IIR-13_15.1 | AJP04 | 0.0151 | 59 | 1.1E-3 | 8.5 | 0.14 | 6.64 | 0.27 | **6.74** | **0.54** | |
| IIR-13_2.1 | AJP04 | 0.0530 | 143 | 5.2E-4 | 66.8 | 0.47 | 6.67 | 0.14 | **6.76** | **0.28** | |
| IIR-13_3.1 | AJP04 | 0.0126 | 19 | 1.1E-3 | 3.5 | 0.18 | 6.82 | 0.27 | **6.91** | **0.55** | |
| IIR-13_7.1 | AJP04 | 0.0064 | 42 | 1.1E-3 | 4.2 | 0.10 | 6.84 | 0.25 | **6.92** | **0.49** | |
| IIR-13_13.1 | AJP04 | 0.0023 | 242 | 1.1E-3 | 5.1 | 0.02 | 7.36 | 0.20 | **7.44** | **0.40** | |
| IIR-13_10.1 | AJP04 | 0.0034 | 87 | 1.1E-3 | 3.5 | 0.04 | 7.39 | 0.19 | **7.44** | **0.39** | |
| IIR-13_18.1 | AJP04 | 0.0037 | 152 | 1.2E-3 | 5.1 | 0.03 | 7.67 | 0.22 | **7.75** | **0.44** | |
| IIR-13_20.1 | AJP04 | 0.0566 | 21 | 1.6E-3 | 10.3 | 0.48 | 7.67 | 0.67 | ~~**7.76**~~ | ~~**1.33**~~ | **High comm-Pb (>20%)** |
| IIR-13_8.1 | AJP04 | 0.0043 | 67 | 1.3E-3 | 2.9 | 0.04 | 8.33 | 0.17 | ~~**8.43**~~ | ~~**0.35**~~ | **Outlier (>2SD)** |
| IIR-13_4.1 | AJP04 | 0.0347 | 56 | 9.6E-4 | 36.6 | 0.65 | 8.62 | 1.61 | ~~**8.70**~~ | ~~**3.22**~~ | **High comm-Pb (>20%)** |

**Appendix C.1**. Continued

| Spot Name | Mount | $^{204}$Pb/ $^{206}$Pb | % error | $^{206}$Pb/ $^{238}$U | % error | U (ppm) | Th (ppm) | $^{232}$Th/ $^{238}$U | % error | Total $^{238}$U/$^{206}$Pb | % error | Total $^{207}$Pb/$^{206}$Pb | % error | $^{207}$Pb-corr $^{204}$Pb/$^{206}$Pb | $^{207}$Pb-corr % $^{206}$Pb$_C$ |
|---|---|---|---|---|---|---|---|---|---|---|---|---|---|---|---|
| **SANDFELL** | | | | | | | | | | | | | | | |
| IISand-01_12.1 | AJP02 | --- | 100 | 0.00349 | 2.7 | 181 | 57 | 0.33 | 0.83 | 562 | 1.7 | 0.054 | 12 | 5.3E-4 | 1.0 |
| IISand-01_2.1 | AJP03 | 2.8E-3 | 71 | 0.00366 | 4.6 | 288 | 141 | 0.50 | 0.57 | 543 | 1.8 | 0.076 | 6 | 2.0E-3 | 3.8 |
| IISand-01_8.1 | AJP03 | 9.2E-4 | 120 | 0.00370 | 4.6 | 309 | 139 | 0.46 | 0.60 | 552 | 1.6 | 0.056 | 7 | 6.3E-4 | 1.2 |
| IISand-01_4.1 | AJP03 | --- | 100 | 0.00395 | 2.1 | 426 | 239 | 0.58 | 0.44 | 551 | 1.4 | 0.048 | 6 | 1.1E-4 | 0.2 |
| IISand-01_1.1 | AJP03 | -2.8E-4 | 183 | 0.00395 | 3.2 | 441 | 168 | 0.39 | 0.26 | 550 | 1.8 | 0.047 | 7 | 4.6E-5 | 0.1 |
| IISand-01_13.1 | AJP02 | 1.6E-3 | 100 | 0.00387 | 2.8 | 317 | 135 | 0.44 | 0.34 | 556 | 2.0 | 0.039 | 10 | -5.2E-4 | -1.0 |
| IISand-01_3.1 | AJP03 | 1.7E-3 | 71 | 0.00367 | 3.3 | 483 | 219 | 0.47 | 0.14 | 549 | 1.7 | 0.048 | 6 | 9.1E-5 | 0.2 |
| IISand-01_7.1 | AJP03 | 1.4E-3 | 85 | 0.00388 | 3.1 | 402 | 193 | 0.50 | 1.03 | 548 | 1.2 | 0.042 | 7 | -3.0E-4 | -0.6 |
| IISand-01_5.1 | AJP03 | -5.6E-4 | 129 | 0.00384 | 2.9 | 431 | 236 | 0.57 | 0.14 | 541 | 1.9 | 0.049 | 6 | 1.6E-4 | 0.3 |
| IISand-01_6.1 | AJP03 | 4.3E-4 | 158 | 0.00374 | 2.8 | 405 | 189 | 0.48 | 0.16 | 544 | 1.9 | 0.043 | 7 | -2.5E-4 | -0.5 |
| IISand-01_11.1 | AJP02 | 9.9E-3 | 38 | 0.00442 | 1.9 | 326 | 148 | 0.47 | 0.40 | 469 | 2.1 | 0.134 | 5 | 5.9E-3 | 11.1 |
| IISand-01_10.1 | AJP03 | -8.7E-4 | 129 | 0.00417 | 2.0 | 250 | 108 | 0.45 | 0.19 | 525 | 1.7 | 0.038 | 16 | -5.9E-4 | -1.1 |
| IISand-01_9.1 | AJP03 | 5.6E-3 | 45 | 0.00452 | 0.9 | 320 | 130 | 0.42 | 0.18 | 479 | 0.8 | 0.103 | 11 | 3.9E-3 | 7.2 |
| **LÝSUSKARÐ** | | | | | | | | | | | | | | | |
| IILys-07a_8.1 | AJP04 | -6.1E-3 | 158 | 0.00032 | 7.5 | 702 | 1367 | 2.01 | 1.13 | 5396 | 4.8 | 0.085 | 19 | 2.6E-3 | 5.0 |
| IILys-07a_12.1 | AJP04 | 2.5E-2 | 100 | 0.00037 | 8.8 | 435 | 492 | 1.17 | 1.58 | 5173 | 5.3 | 0.050 | 32 | 2.5E-4 | 0.5 |
| IILys-07a_9.1 | AJP04 | 2.1E-2 | 75 | 0.00044 | 3.0 | 739 | 699 | 0.98 | 0.38 | 5046 | 3.8 | 0.069 | 19 | 1.5E-3 | 2.9 |
| IILys-07a_7.1 | AJP04 | 1.6E-2 | 62 | 0.00054 | 4.3 | 1058 | 4705 | 4.59 | 0.79 | 3217 | 4.7 | 0.290 | 7 | 1.7E-2 | 30.9 |
| IILys-07a_1.1 | AJP04 | -6.7E-4 | 224 | 0.00050 | 6.5 | 2850 | 4995 | 1.81 | 1.27 | 4717 | 2.0 | 0.052 | 13 | 3.8E-4 | 0.7 |
| IILys-07a_3.1 | AJP04 | --- | 100 | 0.00045 | 4.5 | 1430 | 1118 | 0.81 | 1.20 | 4781 | 2.0 | 0.052 | 17 | 4.2E-4 | 0.8 |
| IILys-07a_5.1 | AJP04 | 2.7E-3 | 129 | 0.00045 | 4.5 | 2182 | 2810 | 1.33 | 0.51 | 4793 | 1.3 | 0.037 | 17 | -6.1E-4 | -1.1 |
| IILys-07a_2.1 | AJP04 | 1.7E-3 | 100 | 0.00048 | 7.6 | 4560 | 7921 | 1.79 | 2.41 | 4623 | 2.3 | 0.053 | 9 | 4.9E-4 | 0.9 |
| IILys-07a_11.1 | AJP04 | 3.0E-3 | 158 | 0.00044 | 6.3 | 1329 | 2795 | 2.17 | 1.33 | 4616 | 2.7 | 0.045 | 18 | -9.8E-5 | -0.2 |
| IILys-07a_13.1 | AJP04 | 8.9E-3 | 62 | 0.00058 | 4.4 | 2271 | 3299 | 1.50 | 0.46 | 3725 | 2.6 | 0.205 | 17 | 1.1E-2 | 20.1 |
| IILys-07a_16.1 | AJP04 | -1.8E-3 | 224 | 0.00045 | 5.3 | 698 | 987 | 1.46 | 0.64 | 4632 | 2.6 | 0.052 | 19 | 3.8E-4 | 0.7 |
| IILys-07a_14.1 | AJP04 | 1.7E-3 | 100 | 0.00050 | 4.7 | 3607 | 6689 | 1.92 | 0.52 | 4278 | 1.5 | 0.057 | 8 | 7.6E-4 | 1.4 |

**Appendix C.1**. Continued

| **Spot Name** | **Mount** | **$^{204}$Pb-corr $^{207}$Pb*/$^{235}$U** | **% error** | **$^{204}$Pb-corr $^{206}$Pb*/$^{238}$U** | **% error** | **Error Corr.** | **$^{207}$Pb-corr $^{206}$Pb/$^{238}$U Age (Ma)** | **1σ error** | **$^{230}$Th-corr $^{206}$Pb/$^{238}$U Age (Ma)** | **2σ error** | **Reason for excluding?** |
|---|---|---|---|---|---|---|---|---|---|---|---|
| **SANDFELL** | | | | | | | | | | | |
| IISand-01_12.1 | AJP02 | 0.0133 | 12 | 1.8E-3 | 1.7 | 0.14 | 11.35 | 0.21 | **11.45** | **0.42** | |
| IISand-01_2.1 | AJP03 | 0.0084 | 90 | 1.7E-3 | 4.2 | 0.05 | 11.42 | 0.22 | **11.52** | **0.44** | |
| IISand-01_8.1 | AJP03 | 0.0103 | 41 | 1.8E-3 | 2.7 | 0.06 | 11.53 | 0.20 | **11.62** | **0.40** | |
| IISand-01_4.1 | AJP03 | 0.0120 | 6 | 1.8E-3 | 1.4 | 0.22 | 11.67 | 0.17 | **11.76** | **0.35** | |
| IISand-01_1.1 | AJP03 | 0.0129 | 16 | 1.8E-3 | 2.1 | 0.13 | 11.69 | 0.22 | **11.79** | **0.44** | |
| IISand-01_13.1 | AJP02 | 0.0033 | 191 | 1.7E-3 | 3.7 | 0.02 | 11.69 | 0.24 | **11.79** | **0.48** | |
| IISand-01_3.1 | AJP03 | 0.0052 | 92 | 1.8E-3 | 2.9 | 0.03 | 11.70 | 0.21 | **11.80** | **0.42** | |
| IISand-01_7.1 | AJP03 | 0.0050 | 93 | 1.8E-3 | 2.6 | 0.03 | 11.82 | 0.15 | **11.92** | **0.30** | |
| IISand-01_5.1 | AJP03 | 0.0147 | 19 | 1.9E-3 | 2.3 | 0.12 | 11.87 | 0.23 | **11.96** | **0.45** | |
| IISand-01_6.1 | AJP03 | 0.0091 | 30 | 1.8E-3 | 2.3 | 0.08 | 11.90 | 0.23 | **11.99** | **0.46** | |
| IISand-01_11.1 | AJP02 | 0.0061 | 199 | 1.7E-3 | 8.8 | 0.04 | 12.21 | 0.28 | **~~12.30~~** | **~~0.55~~** | **Outlier (>2SD)** |
| IISand-01_10.1 | AJP03 | 0.0135 | 34 | 1.9E-3 | 2.7 | 0.08 | 12.41 | 0.23 | **~~12.51~~** | **~~0.45~~** | **Outlier (>2SD)** |
| IISand-01_9.1 | AJP03 | 0.0043 | 268 | 1.9E-3 | 5.3 | 0.02 | 12.47 | 0.22 | **~~12.56~~** | **~~0.44~~** | **Outlier (>2SD)** |
| **LÝSUSKARÐ** | | | | | | | | | | | |
| IILys-07a_8.1 | AJP04 | 0.0046 | 70 | 2.1E-4 | 16.9 | 0.24 | 1.14 | 0.06 | **1.18** | **0.12** | |
| IILys-07a_12.1 | AJP04 | 0.0090 | 193 | 1.0E-4 | 87.3 | 0.45 | 1.24 | 0.07 | **1.31** | **0.14** | |
| IILys-07a_9.1 | AJP04 | 0.0072 | 116 | 1.2E-4 | 49.6 | 0.43 | 1.24 | 0.05 | **1.32** | **0.10** | |
| IILys-07a_7.1 | AJP04 | 0.0015 | 438 | 2.2E-4 | 27.8 | 0.06 | 1.38 | 0.08 | **~~1.34~~** | **~~0.17~~** | **High comm-Pb (>20%)** |
| IILys-07a_1.1 | AJP04 | 0.0018 | 37 | 2.1E-4 | 3.4 | 0.09 | 1.36 | 0.03 | **1.41** | **0.06** | |
| IILys-07a_3.1 | AJP04 | 0.0015 | 17 | 2.1E-4 | 2.0 | 0.12 | 1.34 | 0.03 | **1.42** | **0.06** | |
| IILys-07a_5.1 | AJP04 | 0.0001 | 888 | 2.0E-4 | 6.9 | 0.01 | 1.36 | 0.02 | **1.43** | **0.04** | |
| IILys-07a_2.1 | AJP04 | 0.0008 | 93 | 2.1E-4 | 4.0 | 0.04 | 1.38 | 0.03 | **1.43** | **0.07** | |
| IILys-07a_11.1 | AJP04 | 0.0001 | 3032 | 2.0E-4 | 9.8 | 0.00 | 1.40 | 0.04 | **1.44** | **0.08** | |
| IILys-07a_13.1 | AJP04 | 0.0024 | 132 | 2.2E-4 | 12.7 | 0.10 | 1.38 | 0.08 | **~~1.44~~** | **~~0.17~~** | **High comm-Pb (>20%)** |
| IILys-07a_16.1 | AJP04 | 0.0024 | 73 | 2.2E-4 | 7.7 | 0.11 | 1.38 | 0.04 | **1.44** | **0.08** | |
| IILys-07a_14.1 | AJP04 | 0.0010 | 88 | 2.3E-4 | 3.7 | 0.04 | 1.49 | 0.02 | **1.53** | **0.05** | |

**Appendix C.2**. Zircon Trace Element Compositions (ppm), measured *in situ* by SHRIMP-RG (Atomic Number < 22)

| Intrusion[49] | Rock Type | Grain # | Mount | Date | Li | Be | B | F | Na | Al | P | K | Ca | Sc |
|---|---|---|---|---|---|---|---|---|---|---|---|---|---|---|
| Slaufrudalur | Granophyre | IISlau-12-1.1 | AJP01 | May '13 | | | | | | | | | | 52 |
| Slaufrudalur | Granophyre | IISlau-12-2.1 | AJP01 | May '13 | | | | | | | | | | 58 |
| Slaufrudalur | Granophyre | IISlau-12-4.1 | AJP01 | May '13 | | | | | | | | | | 33 |
| Slaufrudalur | Granophyre | IISlau-12-5.1 | AJP01 | May '13 | | | | | | | | | | 27 |
| Slaufrudalur | Granophyre | IISlau-12-7.1 | AJP01 | May '13 | | | | | | | | | | 51 |
| Slaufrudalur | Granophyre | IISlau-12-9.1 | AJP01 | May '13 | | | | | | | | | | 44 |
| Slaufrudalur | Granophyre | IISlau-12_12.1 | AJP03 | Jan. '14 | 0.04 | 0.3 | 0.044 | 15 | 9 | 12 | 620 | 1.11 | 3.51 | 62 |
| Slaufrudalur | Granophyre | IISlau-12_13.1 | AJP03 | Jan. '14 | 0.02 | 0.1 | 0.048 | 8 | 10 | 13 | 392 | 1.17 | 2.73 | 41 |
| Slaufrudalur | Granophyre | IISlau-12_14.1 | AJP03 | Jan. '14 | 0.02 | 0.4 | 0.030 | 10 | 8 | 12 | 574 | 1.13 | 2.80 | 57 |
| Slaufrudalur | Granophyre | IISlau-12_15.1 | AJP03 | Jan. '14 | 0.01 | 0.027 | 0.053 | 7 | 9 | 13 | 426 | 1.02 | 3.41 | 47 |
| Slaufrudalur | Granophyre | IISlau-12_16.1 | AJP03 | Jan. '14 | 0.08 | 0.2 | 0.051 | 40 | 10 | 11 | 1032 | 1.55 | 3.34 | 64 |
| Slaufrudalur | Granophyre | IISlau-12_17.1 | AJP03 | Jan. '14 | 0.0086 | 0.3 | 0.092 | 19 | 10 | 13 | 633 | 1.38 | 4.07 | 48 |
| Slaufrudalur | Granophyre | IISlau-12_11.1 | AJP03 | Jan. '14 | 0.07 | 2 | 0.1 | 6 | 10440 | 13796 | 284 | 2886 | 238 | 28 |
| Slaufrudalur | Granophyre | IISlau-22_1.1 | AJP03 | Jan. '14 | 0.0011 | 0.1 | 0.046 | 42 | 7 | 9 | 385 | 1.11 | 1.79 | 21 |
| Slaufrudalur | Granophyre | IISlau-22_3.1 | AJP03 | Jan. '14 | 0.01 | 0.8 | 0.047 | 29 | 7 | 10 | 554 | 0.82 | 2.93 | 16 |
| Slaufrudalur | Granophyre | IISlau-22_4.1 | AJP03 | Jan. '14 | 0.0006 | 0.012 | 0.067 | 9 | 9 | 10 | 370 | 1.05 | 2.51 | 15 |
| Slaufrudalur | Granophyre | IISlau-22_5.1 | AJP03 | Jan. '14 | 0.0017 | 0.007 | 0.019 | 26 | 9 | 11 | 462 | 1.21 | 3.42 | 13 |
| Slaufrudalur | Granophyre | IISlau-22_6.1 | AJP03 | Jan. '14 | 0.0011 | 0.020 | 0.018 | 36 | 11 | 10 | 450 | 1.10 | 3.69 | 16 |
| Slaufrudalur | Granophyre | IISlau-22_7.1 | AJP03 | Jan. '14 | 0.0011 | 0.038 | 0.029 | 37 | 24 | 8 | 317 | 2.08 | 14 | 18 |
| Slaufrudalur | Granophyre | IISlau-22_11.1 | AJP02 | Jan. '14 | 0.0005 | 0.055 | 0.054 | 31 | 11 | 6 | 171 | 10 | 2.21 | 11 |
| Slaufrudalur | Granophyre | IISlau-22_12.1 | AJP02 | Jan. '14 | 0.0013 | 0.1 | 0.2 | 163 | 61 | 26 | 383 | 75 | 14 | 7 |
| Slaufrudalur | Granophyre | IISlau-22_13.1 | AJP02 | Jan. '14 | 0.0005 | 0.3 | 0.052 | 91 | 4 | 5 | 518 | 2.17 | 3.33 | 12 |
| Slaufrudalur | Granophyre | IISlau-25-1.1 | AJP04 | May '14 | 0.0042 | 2 | 0.023 | 106 | 55 | 43 | 525 | 68 | 10 | 3.66 |
| Slaufrudalur | Granophyre | IISlau-25-2.1 | AJP04 | May '14 | 0.0027 | 0.084 | 0.032 | 192 | 6 | 10 | 307 | 4.23 | 77 | 6 |
| Slaufrudalur | Granophyre | IISlau-25-3.1 | AJP04 | May '14 | 0.0024 | 0.018 | 0.051 | 162 | 5 | 8 | 284 | 4.10 | 10 | 3.96 |
| Slaufrudalur | Granophyre | IISlau-25-5.1 | AJP04 | May '14 | 0.05 | 2 | 1 | 229 | 55 | 38 | 593 | 158 | 65 | 4.92 |
| Slaufrudalur | Granophyre | IISlau-25-6.1 | AJP04 | May '14 | 0.01 | 0.2 | 0.1 | 120 | 52 | 12 | 190 | 635 | 37 | 6 |
| Slaufrudalur | Granophyre | IISlau-26-3.1 | AJP04 | May '14 | 0.02 | 0.1 | 0.035 | 454 | 23 | 34 | 380 | 69 | 174 | 17 |
| Slaufrudalur | Granophyre | IISlau-26-4.1 | AJP04 | May '14 | 0.02 | 2 | 0.2 | 43 | 9 | 15 | 565 | 15 | 38 | 57 |
| Slaufrudalur | Granophyre | IISlau-26-5.1 | AJP04 | May '14 | 0.0045 | 2 | 0.2 | 323 | 11 | 8 | 978 | 16 | 10 | 40 |

---

[49] For intrusion locations, see **Table #** and **Fig. #** in Chapter V

**Appendix C.2**. Continued

| **Intrusion** | **Rock Type**[50] | **Grain #** | **Mount** | **Date** | **Li** | **Be** | **B** | **F** | **Na** | **Al** | **P** | **K** | **Ca** | **Sc** |
|---|---|---|---|---|---|---|---|---|---|---|---|---|---|---|
| Slaufrudalur | Granophyre | IISlau-26-6.1 | AJP04 | May '14 | 0.13 | 8 | 1 | 113 | 42 | 23 | 639 | 72 | 25 | 56 |
| Slaufrudalur | Granophyre | IISlau-26-7.1 | AJP04 | May '14 | 0.04 | 4 | 0.3 | 91 | 6 | 6 | 646 | 6 | 3.61 | 64 |
| Slaufrudalur | Granophyre | IISlau-26_8.1 | AJP02 | May '14 | 0.07 | 0.063 | 0.2 | 5 | 69 | 13 | 293 | 63 | 17 | 122 |
| Slaufrudalur | Granophyre | IISlau-26-1.1 | AJP04 | May '14 | 0.0011 | 15 | 0.2 | 596 | 202 | 27 | 1789 | 83 | 2053 | 22 |
| Slaufrudalur | Granophyre | IISlau-26-2.1 | AJP04 | May '14 | 0.53 | 6 | 2 | 408 | 1476 | 591 | 464 | 14240 | 106 | 75 |
| Vesturhorn | HSG | IIV-03a-2.1 | AJP01 | May '13 | | | | | | | | | | 5 |
| Vesturhorn | HSG | IIV-03a-6.1 | AJP01 | May '13 | | | | | | | | | | 9 |
| Vesturhorn | HSG | IIV-03a-8.1 | AJP01 | May '13 | | | | | | | | | | 7 |
| Vesturhorn | HSG | IIV-03a-9.1 | AJP01 | May '13 | | | | | | | | | | 13 |
| Vesturhorn | HSG | IIV-03a-10.1 | AJP01 | May '13 | | | | | | | | | | 20 |
| Vesturhorn | HSG | IIV-03a-11.1 | AJP01 | May '13 | | | | | | | | | | 6 |
| Vesturhorn | HSG | IIV-03a-12.1 | AJP01 | May '13 | | | | | | | | | | 7 |
| Vesturhorn | HSG | IIV-03a-13.1 | AJP01 | May '13 | | | | | | | | | | 8 |
| Vesturhorn | HSG | IIV-03a-14.1 | AJP01 | May '13 | | | | | | | | | | 11 |
| Vesturhorn | HSG | IIV-03a-16.1 | AJP01 | May '13 | | | | | | | | | | 10 |
| Vesturhorn | HSG | IIV-03a-17.1 | AJP01 | May '13 | | | | | | | | | | 22 |
| Vesturhorn | HSG | IIV-03a-5.1 | AJP01 | May '13 | | | | | | | | | | 6 |
| Vesturhorn | HSG | IIV-03a-15.1 | AJP01 | May '13 | | | | | | | | | | 9 |
| Vesturhorn | Gabbro | IIV-15-1.1 | AJP04 | May '14 | 0.0091 | -- | 0.1 | 76 | 4 | 6 | 236 | 3.13 | 2.22 | 38 |
| Vesturhorn | Gabbro | IIV-15-2.1 | AJP04 | May '14 | 0.03 | 0.014 | 1 | 44 | 4 | 5 | 387 | 3.05 | 1.15 | 36 |
| Vesturhorn | Gabbro | IIV-15-3.1 | AJP04 | May '14 | 0.0035 | 0.001 | 0.096 | -- | 4 | 5 | 225 | 3.16 | 2.64 | 40 |
| Vesturhorn | Gabbro | IIV-15-6.2 | AJP04 | May '14 | 0.0026 | -- | 0.064 | 19 | 3 | 6 | 217 | 2.19 | 1.53 | 38 |
| Vesturhorn | Gabbro | IIV-15-6.1 | AJP04 | May '14 | 0.0066 | -- | 0.040 | -- | 3 | 4 | 189 | 2.67 | 4.45 | 38 |
| Vesturhorn | Gabbro | IIV-15-7.1 | AJP04 | May '14 | 0.0040 | -- | 0.068 | -- | 3 | 5 | 188 | 2.72 | 0.99 | 32 |
| Vesturhorn | Gabbro | IIV-15-10.1 | AJP04 | May '14 | 0.0013 | 0.001 | 0.064 | -- | 9 | 9 | 129 | 6 | 8 | 23 |
| Vesturhorn | Gabbro | IIV-15-11.1 | AJP04 | May '14 | 0.0027 | 0.001 | 0.091 | -- | 8 | 5 | 196 | 6 | 7 | 39 |
| Vesturhorn | Gabbro | IIV-15-13.1 | AJP04 | May '14 | 0.02 | -- | 0.1 | 155 | 47 | 31 | 239 | 88 | 198 | 22 |
| Vesturhorn | Gabbro | IIV-15-15.1 | AJP04 | May '14 | 0.0062 | -- | 0.073 | -- | 5 | 6 | 223 | 7 | 6 | 32 |
| Vesturhorn | Gabbro | IIV-15-16.2 | AJP04 | May '14 | 0.0048 | -- | 0.1 | 70 | 8 | 6 | 206 | 7 | 4.44 | 29 |
| Vesturhorn | Gabbro | IIV-15-16.1 | AJP04 | May '14 | 0.0041 | -- | 0.025 | 23 | 11 | 6 | 195 | 12 | 7 | 37 |

---

[50] HSG = High-$SiO_2$ Granophyre (> 75 wt.% $SiO_2$)

**Appendix C.2**. Continued

| Intrusion | Rock Type | Grain # | Mount | Date | Li | Be | B | F | Na | Al | P | K | Ca | Sc |
|---|---|---|---|---|---|---|---|---|---|---|---|---|---|---|
| Vesturhorn | Gabbro | IIV-15-17.1 | AJP04 | May '14 | 0.0052 | -- | 0.051 | 23 | 11 | 8 | 299 | 11 | 7 | 53 |
| Vesturhorn | Gabbro | IIV-15-18.1 | AJP04 | May '14 | 0.0099 | -- | 0.052 | 47 | 10 | 8 | 364 | 9 | 7 | 57 |
| Vesturhorn | Gabbro | IIV-15-19.2 | AJP04 | May '14 | 0.0022 | -- | 0.052 | -- | 8 | 8 | 199 | 9 | 9 | 27 |
| Vesturhorn | Gabbro | IIV-15-19.1 | AJP04 | May '14 | 0.0047 | -- | 0.052 | 47 | 7 | 6 | 202 | 7 | 6 | 40 |
| Vesturhorn | Gabbro | IIV-15-19.3 | AJP04 | May '14 | 0.02 | 0.002 | 0.054 | 49 | 8 | 10 | 398 | 8 | 5 | 34 |
| Vesturhorn | Granophyre | IIV-16_1.1 | AJP03 | Jan. '14 | 0.04 | 3 | 0.3 | 31 | 10 | 8 | 1253 | 0.96 | 3.91 | 74 |
| Vesturhorn | Granophyre | IIV-16_2.1 | AJP03 | Jan. '14 | -- | 0.011 | 0.043 | 3 | 8 | 8 | 265 | 0.94 | 2.80 | 31 |
| Vesturhorn | Granophyre | IIV-16_3.1 | AJP03 | Jan. '14 | 0.0003 | 0.021 | 0.012 | 13 | 11 | 9 | 320 | 3.80 | 3.59 | 38 |
| Vesturhorn | Granophyre | IIV-16_4.1 | AJP03 | Jan. '14 | 0.0050 | 0.010 | 0.054 | 8 | 10 | 20 | 340 | 2.02 | 4.35 | 42 |
| Vesturhorn | Granophyre | IIV-16_5.1 | AJP03 | Jan. '14 | 0.02 | 1 | 0.1 | 32 | 12 | 9 | 1235 | 1.52 | 3.62 | 61 |
| Vesturhorn | Granophyre | IIV-16_6.1 | AJP03 | Jan. '14 | 0.0059 | 0.024 | 0.1 | 12 | 14 | 15 | 266 | 1.91 | 5 | 36 |
| Vesturhorn | Granophyre | IIV-16_7.1 | AJP03 | Jan. '14 | 0.0049 | 0.012 | 0.025 | 11 | 6 | 9 | 356 | 0.83 | 1.93 | 44 |
| Vesturhorn | Granophyre | IIV-16_8.1 | AJP03 | Jan. '14 | 0.01 | 0.020 | 0.047 | 7 | 6 | 8 | 463 | 0.63 | 1.94 | 45 |
| Vesturhorn | Granophyre | IIV-16_11.1 | AJP02 | Jan. '14 | 0.03 | 5 | 1 | 82 | 3 | 5 | 1142 | 1.93 | 1.55 | 63 |
| Vesturhorn | Granophyre | IIV-16_12.1 | AJP02 | Jan. '14 | 0.0039 | 0.013 | 0.2 | 12 | 2 | 5 | 286 | 1.42 | 1.19 | 36 |
| Vesturhorn | Granophyre | IIV-16_13.1 | AJP02 | Jan. '14 | 0.0058 | 0.1 | 0.074 | 13 | 3 | 5 | 420 | 1.37 | 1.69 | 52 |
| Vesturhorn | Granophyre | IIV-16_14.1 | AJP02 | Jan. '14 | 0.0058 | 0.4 | 0.1 | 12 | 3 | 4 | 302 | 1.62 | 1.33 | 27 |
| Vesturhorn | Granophyre | IIV-16_15.1 | AJP02 | Jan. '14 | 0.0037 | 0.009 | 1 | 11 | 3 | 5 | 283 | 2.20 | 1.41 | 35 |
| Reyðarártindur | Granophyre | IIR-01-1.1 | AJP04 | May '14 | 0.05 | 0.2 | 0.6 | 649 | 121 | 76 | 861 | 349 | 98 | 47 |
| Reyðarártindur | Granophyre | IIR-01-4.1 | AJP04 | May '14 | 0.0026 | 0.012 | 0.039 | 53 | 6 | 6 | 326 | 6 | 39 | 28 |
| Reyðarártindur | Granophyre | IIR-01-5.1 | AJP04 | May '14 | 0.0020 | 0.011 | 0.2 | 51 | 19 | 9 | 429 | 32 | 55 | 33 |
| Reyðarártindur | Granophyre | IIR-01-6.1 | AJP04 | May '14 | 0.0004 | 0.015 | 0.089 | 64 | 3 | 5 | 467 | 5 | 2.33 | 36 |
| Reyðarártindur | Granophyre | IIR-01-7.1 | AJP04 | May '14 | 0.0022 | 0.008 | 0.092 | 83 | 4 | 3 | 500 | 3.96 | 2.40 | 33 |
| Reyðarártindur | Granophyre | IIR-01-8.1 | AJP04 | May '14 | 0.02 | 0.034 | 0.3 | 565 | 131 | 103 | 422 | 307 | 74 | 53 |
| Reyðarártindur | Granophyre | IIR-01-9.1 | AJP04 | May '14 | 0.0016 | 0.2 | -- | 121 | 6 | 15 | 610 | 9 | 3.96 | 46 |
| Reyðarártindur | Granophyre | IIR-01-11.1 | AJP04 | May '14 | 0.01 | 10 | 1 | 147 | 5 | 6 | 1900 | 5 | 16 | 141 |
| Reyðarártindur | Granophyre | IIR-01-12.1 | AJP04 | May '14 | 0.04 | 15 | 4 | 188 | 9 | 6 | 1939 | 9 | 10 | 92 |
| Reyðarártindur | Granophyre | IIR-01-13.1 | AJP04 | May '14 | 0.03 | 4 | 1 | 401 | 381 | 185 | 1908 | 556 | 481 | 82 |
| Reyðarártindur | Granophyre | IIR-01-14.1 | AJP04 | May '14 | 0.0031 | 0.011 | 0.094 | 106 | 20 | 10 | 415 | 24 | 171 | 31 |
| Reyðarártindur | Granophyre | IIR-01-2.1 | AJP04 | May '14 | 2 | 3 | 7 | 3352 | 263 | 13633 | 805 | 163909 | 1220 | 29 |
| Reyðarártindur | Granophyre | IIR-01-3.1 | AJP04 | May '14 | 0.67 | 0.2 | 0.6 | 2008 | 207 | 149 | 527 | 3373 | 89 | 29 |
| Reyðarártindur | Granophyre | IIR-03a-1.1 | AJP04 | May '14 | 0.19 | 0.6 | 5 | 133 | 108 | 30 | 1504 | 382 | 58 | 133 |

**Appendix C.2**. Continued

| Intrusion | Rock Type | Grain # | Mount | Date | Li | Be | B | F | Na | Al | P | K | Ca | Sc |
|---|---|---|---|---|---|---|---|---|---|---|---|---|---|---|
| Reyðarártindur | Granophyre | IIR-03a-2.1 | AJP04 | May '14 | 0.08 | 0.2 | 3 | 56 | 9 | 5 | 1108 | 13 | 5 | 99 |
| Reyðarártindur | Granophyre | IIR-03a-3.1 | AJP04 | May '14 | 0.02 | 0.1 | 0.2 | -- | 4 | 4 | 563 | 2.86 | 160 | 48 |
| Reyðarártindur | Granophyre | IIR-03a-4.1 | AJP04 | May '14 | 0.0068 | 0.046 | 0.3 | 77 | 44 | 48 | 652 | 89 | 56 | 62 |
| Reyðarártindur | Granophyre | IIR-03a-5.1 | AJP04 | May '14 | 0.02 | 0.053 | 0.042 | -- | 5 | 4 | 589 | 2.62 | 2.04 | 53 |
| Reyðarártindur | Granophyre | IIR-03a-6.1 | AJP04 | May '14 | 0.07 | 2 | 3 | 181 | 213 | 177 | 1647 | 434 | 121 | 139 |
| Reyðarártindur | Granophyre | IIR-03a-7.1 | AJP04 | May '14 | 0.05 | 0.2 | 0.2 | -- | 46 | 7 | 638 | 16 | 17 | 61 |
| Reyðarártindur | Granophyre | IIR-03a-8.1 | AJP04 | May '14 | 0.08 | 1 | 0.5 | 101 | 6 | 3 | 1370 | 3.88 | 5 | 110 |
| Reyðarártindur | Granophyre | IIR-03a-9.1 | AJP04 | May '14 | 0.01 | 0.076 | 0.2 | 59 | 9 | 4 | 737 | 19 | 3.90 | 64 |
| Reyðarártindur | Granophyre | IIR-03a-10.1 | AJP04 | May '14 | 0.07 | 0.3 | 1 | 140 | 8 | 5 | 846 | 9 | 6 | 90 |
| Reyðarártindur | Granophyre | IIR-03a-11.1 | AJP04 | May '14 | 0.08 | 0.5 | 0.5 | 101 | 4 | 5 | 1304 | 2.62 | 2.47 | 132 |
| Reyðarártindur | Granophyre | IIR-03a-14.1 | AJP04 | May '14 | 0.07 | 0.2 | 0.7 | 48 | 8 | 10 | 1088 | 11 | 66 | 84 |
| Reyðarártindur | Granophyre | IIR-03a-15.1 | AJP04 | May '14 | 0.05 | 0.8 | 0.7 | 287 | 26 | 11 | 1424 | 54 | 38 | 155 |
| Reyðarártindur | Granophyre | IIR-03a-16.1 | AJP04 | May '14 | 0.05 | 0.2 | 0.8 | 142 | 7 | 3 | 1294 | 16 | 4.90 | 136 |
| Reyðarártindur | Granophyre | IIR-03a-17.1 | AJP04 | May '14 | 0.07 | 2 | 0.4 | 51 | 4 | 4 | 1551 | 2.04 | 3.95 | 149 |
| Reyðarártindur | Granophyre | IIR-03a-18.1 | AJP04 | May '14 | 0.13 | 0.2 | 2 | 170 | 34 | 8 | 1738 | 42 | 18 | 111 |
| Reyðarártindur | Granophyre | IIR-13-1.1 | AJP04 | May '14 | 0.0023 | 0.052 | 0.019 | 68 | 12 | 5 | 209 | 12 | 3.98 | 6 |
| Reyðarártindur | Granophyre | IIR-13-2.1 | AJP04 | May '14 | 0.12 | 0.008 | 0.8 | 310 | 261 | 48 | 532 | 547 | 212 | 44 |
| Reyðarártindur | Granophyre | IIR-13-3.1 | AJP04 | May '14 | 0.06 | 0.078 | 0.019 | 154 | 23 | 143 | 376 | 512 | 95 | 31 |
| Reyðarártindur | Granophyre | IIR-13-4.1 | AJP04 | May '14 | 0.04 | 0.053 | 0.038 | 17 | 23 | 3 | 321 | 2.50 | 2.25 | 34 |
| Reyðarártindur | Granophyre | IIR-13-5.1 | AJP04 | May '14 | 0.0049 | 0.008 | 0.8 | 227 | 75 | 26 | 365 | 103 | 73 | 32 |
| Reyðarártindur | Granophyre | IIR-13-6.1 | AJP04 | May '14 | 0.0019 | 0.1 | 0.3 | 175 | 4 | 3 | 760 | 2.25 | 2.58 | 45 |
| Reyðarártindur | Granophyre | IIR-13-7.1 | AJP04 | May '14 | 0.0038 | 5 | 0.7 | 478 | 11 | 7 | 1397 | 9 | 47 | 97 |
| Reyðarártindur | Granophyre | IIR-13-8.1 | AJP04 | May '14 | 0.0002 | 0.031 | 0.2 | 220 | 4 | 3 | 356 | 3.28 | 3.33 | 28 |
| Reyðarártindur | Granophyre | IIR-13-9.1 | AJP04 | May '14 | 0.0005 | 0.063 | 0.6 | 214 | 5 | 4 | 352 | 3.88 | 14 | 29 |
| Reyðarártindur | Granophyre | IIR-13-10.1 | AJP04 | May '14 | 0.0019 | 0.3 | 0.020 | 144 | 5 | 3 | 782 | 3.02 | 2.29 | 44 |
| Reyðarártindur | Granophyre | IIR-13-12.1 | AJP04 | May '14 | 0.0007 | 8 | 0.4 | 1386 | 29 | 17 | 1301 | 35 | 19 | 20 |
| Reyðarártindur | Granophyre | IIR-13-13.1 | AJP04 | May '14 | 0.0002 | 0.4 | 0.4 | 278 | 6 | 4 | 657 | 4.03 | 13 | 43 |
| Reyðarártindur | Granophyre | IIR-13-14.1 | AJP04 | May '14 | 0.0051 | 1 | 0.3 | 241 | 373 | 47 | 537 | 300 | 3077 | 57 |
| Reyðarártindur | Granophyre | IIR-13-15.1 | AJP04 | May '14 | 0.0003 | 0.084 | -- | 38 | 5 | 4 | 536 | 4.57 | 3.16 | 80 |
| Reyðarártindur | Granophyre | IIR-13-16.1 | AJP04 | May '14 | 0.0014 | 0.051 | 0.1 | 95 | 7 | 5 | 359 | 5 | 21 | 28 |
| Reyðarártindur | Granophyre | IIR-13-17.1 | AJP04 | May '14 | 0.06 | 0.047 | 0.7 | 318 | 121 | 22 | 477 | 299 | 63 | 32 |
| Reyðarártindur | Granophyre | IIR-13-18.1 | AJP04 | May '14 | 0.0005 | 27 | 2 | 77 | 5 | 4 | 987 | 3.85 | 4.24 | 97 |

**Appendix C.2**. Continued

| **Intrusion** | **Rock Type** | **Grain #** | **Mount** | **Date** | **Li** | **Be** | **B** | **F** | **Na** | **Al** | **P** | **K** | **Ca** | **Sc** |
|---|---|---|---|---|---|---|---|---|---|---|---|---|---|---|
| Reyðarártindur | Granophyre | IIR-13-19.1 | AJP04 | May '14 | -- | 0.1 | 0.021 | 57 | 5 | 4 | 302 | 3.92 | 3.82 | 46 |
| Sandfell | Rhyolite | IISan-01_1.1 | AJP03 | Jan. '14 | 0.0053 | 9 | 0.2 | 41 | 9 | 12 | 423 | 1.23 | 8 | 29 |
| Sandfell | Rhyolite | IISan-01_2.1 | AJP03 | Jan. '14 | 0.0038 | 17 | 0.1 | 77 | 28 | 37 | 319 | 18 | 7 | 19 |
| Sandfell | Rhyolite | IISan-01_3.1 | AJP03 | Jan. '14 | 0.0087 | 17 | 0.1 | 292 | 38 | 44 | 756 | 36 | 504 | 30 |
| Sandfell | Rhyolite | IISan-01_4.1 | AJP03 | Jan. '14 | 0.0074 | 7 | 0.067 | 21 | 6 | 9 | 425 | 0.75 | 2.41 | 28 |
| Sandfell | Rhyolite | IISan-01_5.1 | AJP03 | Jan. '14 | 0.0042 | 7 | 0.1 | 80 | 46 | 87 | 395 | 9 | 12 | 29 |
| Sandfell | Rhyolite | IISan-01_6.1 | AJP03 | Jan. '14 | 0.0075 | 26 | 0.1 | 24 | 8 | 10 | 456 | 1.03 | 3.44 | 32 |
| Sandfell | Rhyolite | IISan-01_7.1 | AJP03 | Jan. '14 | 0.0058 | 5 | 0.081 | 14 | 7 | 10 | 387 | 0.96 | 2.86 | 30 |
| Sandfell | Rhyolite | IISan-01_8.1 | AJP03 | Jan. '14 | 0.0073 | 39 | 0.2 | 51 | 9 | 8 | 373 | 1.20 | 3.45 | 15 |
| Sandfell | Rhyolite | IISan-01_9.1 | AJP03 | Jan. '14 | 0.0048 | 19 | 0.086 | 26 | 5 | 8 | 449 | 0.75 | 2.52 | 34 |
| Sandfell | Rhyolite | IISan-01_10.1 | AJP03 | Jan. '14 | 0.0032 | 11 | 0.042 | 12 | 7 | 9 | 288 | 1.75 | 2.50 | 17 |
| Sandfell | Rhyolite | IISan-01_11.1 | AJP02 | Jan. '14 | 0.0022 | 0.7 | 0.2 | 30 | 14 | 9 | 219 | 33 | 3.69 | 17 |
| Sandfell | Rhyolite | IISan-01_12.1 | AJP02 | Jan. '14 | 0.0071 | 14 | 0.1 | 40 | 3 | 5 | 328 | 1.80 | 1.54 | 23 |
| Sandfell | Rhyolite | IISan-01_13.1 | AJP02 | Jan. '14 | 0.0056 | 3 | 0.2 | 15 | 3 | 5 | 332 | 1.79 | 1.69 | 26 |
| Lýsuskarð | Granophyre | IILYS-07a-1.1 | AJP04 | May '14 | 0.0003 | 8 | 3 | 1142 | 4 | 5 | 839 | 2.51 | 3.36 | 6 |
| Lýsuskarð | Granophyre | IILYS-07a-2.1 | AJP04 | May '14 | 0.01 | 10 | 1 | 567 | 3 | 5 | 910 | 2.12 | 3.60 | 4.19 |
| Lýsuskarð | Granophyre | IILYS-07a-3.1 | AJP04 | May '14 | 0.0036 | 2 | 2 | 299 | 3 | 3 | 723 | 1.47 | 1.71 | 1.15 |
| Lýsuskarð | Granophyre | IILYS-07a-4.1 | AJP04 | May '14 | 0.0049 | 2 | 2 | 337 | 3 | 4 | 695 | 2.79 | 1.89 | 4.42 |
| Lýsuskarð | Granophyre | IILYS-07a-5.1 | AJP04 | May '14 | 0.01 | 7 | 0.9 | 906 | 3 | 6 | 1194 | 2.24 | 25 | 1.37 |
| Lýsuskarð | Granophyre | IILYS-07a-6.1 | AJP04 | May '14 | 0.0018 | 0.4 | 0.5 | 198 | 4 | 5 | 416 | 2.31 | 3.10 | 0.49 |
| Lýsuskarð | Granophyre | IILYS-07a-7.1 | AJP04 | May '14 | 0.02 | 3 | 3 | 795 | 12 | 19 | 1349 | 15 | 8 | 0.45 |
| Lýsuskarð | Granophyre | IILYS-07a-8.1 | AJP04 | May '14 | 0.0025 | 6 | 3 | 761 | 11 | 7 | 1126 | 12 | 18 | 1.32 |
| Lýsuskarð | Granophyre | IILYS-07a-9.1 | AJP04 | May '14 | 0.0089 | 20 | 0.1 | 662 | 11 | 7 | 837 | 11 | 6 | 4.70 |
| Lýsuskarð | Granophyre | IILYS-07a-10.1 | AJP04 | May '14 | 0.01 | 3 | 7 | 976 | 8 | 7 | 1213 | 4.90 | 7 | 1.83 |
| Lýsuskarð | Granophyre | IILYS-07a-11.1 | AJP04 | May '14 | 0.0090 | 10 | 6 | 755 | 4 | 6 | 888 | 2.41 | 3.87 | 4.32 |
| Lýsuskarð | Granophyre | IILYS-07a-12.1 | AJP04 | May '14 | 0.0016 | 0.015 | -- | 23 | 5 | 5 | 159 | 2.20 | 2.05 | 2.27 |
| Lýsuskarð | Granophyre | IILYS-07a-13.1 | AJP04 | May '14 | 0.0032 | 10 | 6 | 1439 | 5 | 6 | 787 | 2.77 | 6 | 2.81 |
| Lýsuskarð | Granophyre | IILYS-07a-14.1 | AJP04 | May '14 | 0.02 | 2 | 3 | 341 | 43 | 5 | 1019 | 17 | 20 | 1.19 |
| Lýsuskarð | Granophyre | IILYS-07a-19.1 | AJP04 | May '14 | 0.08 | 0.3 | 0.4 | 1167 | 308 | 24 | 387 | 534 | 1242 | 3.47 |
| Lýsuskarð | Granophyre | IILYS-07a-17.1 | AJP04 | May '14 | 0.84 | 41 | 12 | 4200 | 25390 | 3066 | 896 | 22587 | 79 | 4.78 |
| Lýsuskarð | Granophyre | IILYS-07a-20.1 | AJP04 | May '14 | 0.30 | 6 | 1 | 215 | 4142 | 356 | 553 | 19642 | 266 | 8 |

**Appendix C.3**. Zircon Trace Element Compositions (ppm), measured *in situ* by SHRIMP-RG (Atomic Numbers 22-71)

| **Intrusion**[51] | **Grain #** | **Ti** | **Fe** | **Y** | **Nb** | **La** | **Ce** | **Nd** | **Sm** | **Eu** | **Gd** | **Tb** | **Dy** | **Ho** | **Er** | **Tm** | **Yb** | **Lu** |
|---|---|---|---|---|---|---|---|---|---|---|---|---|---|---|---|---|---|---|
| Slaufrudalur | IISlau-12-1.1 | 19 | 0.37 | 2086 | 9 | 0.16 | 8 | 2.8 | 8 | 2.14 | 65 |  | 190 | 80 | 322 |  | 461 | 77 |
| Slaufrudalur | IISlau-12-2.1 | 30 | 0.06 | 2066 | 10 | 0.04 | 14 | 2.4 | 6 | 2.15 | 57 |  | 208 | 81 | 336 |  | 482 | 80 |
| Slaufrudalur | IISlau-12-4.1 | 17 | 0.78 | 943 | 5.0 | 0.02 | 4 | 1.3 | 3.46 | 1.16 | 31 |  | 101 | 39 | 157 |  | 227 | 39 |
| Slaufrudalur | IISlau-12-5.1 | 13 |  | 5854 | 20 | 0.07 | 115 | 8 | 17 | 3.38 | 167 |  | 602 | 229 | 899 |  | 1289 | 204 |
| Slaufrudalur | IISlau-12-7.1 | 30 | 0.94 | 2102 | 12 | 0.02 | 23 | 2.5 | 6 | 2.16 | 60 |  | 209 | 85 | 330 |  | 475 | 79 |
| Slaufrudalur | IISlau-12-9.1 | 12 | 0.07 | 3990 | 15 | 0.04 | 34 | 5 | 13 | 3.30 | 135 |  | 463 | 168 | 635 |  | 903 | 144 |
| Slaufrudalur | IISlau-12_12.1 | 20 | 4.43 | 4652 | 13 | 0.06 | 17 | 8 | 21 | 6 | 164 | 53 | 499 | 189 | 712 | 131 | 995 | 157 |
| Slaufrudalur | IISlau-12_13.1 | 32 | 4.40 | 2377 | 4.6 | 0.04 | 6 | 3.9 | 10 | 4.52 | 88 | 29 | 290 | 103 | 396 | 76 | 578 | 95 |
| Slaufrudalur | IISlau-12_14.1 | 20 | 4.43 | 4606 | 9 | 0.07 | 28 | 8 | 21 | 6 | 156 | 54 | 542 | 194 | 748 | 133 | 1080 | 172 |
| Slaufrudalur | IISlau-12_15.1 | 23 | 4.26 | 1491 | 6 | 0.02 | 15 | 1.8 | 4.17 | 1.34 | 39 | 15 | 158 | 62 | 267 | 51 | 394 | 62 |
| Slaufrudalur | IISlau-12_16.1 | 19 | 4.53 | 8625 | 20 | 0.09 | 40 | 15 | 45 | 12 | 356 | 104 | 1101 | 378 | 1397 | 242 | 1800 | 273 |
| Slaufrudalur | IISlau-12_17.1 | 18 | 4.32 | 3639 | 18 | 0.06 | 28 | 5 | 13 | 3.47 | 113 | 38 | 397 | 137 | 563 | 104 | 806 | 128 |
| Slaufrudalur | IISlau-12_11.1 | -- | 7 | 1393 | 2.7 | 0.10 | 10 | 1.7 | 4.16 | 1.53 | 36 | 13 | 147 | 53 | 233 | 46 | 363 | 59 |
| Slaufrudalur | IISlau-22_1.1 | 15 | 4.50 | 2266 | 7 | 0.05 | 10 | 4.5 | 10 | 2.49 | 75 | 26 | 267 | 96 | 363 | 67 | 480 | 82 |
| Slaufrudalur | IISlau-22_3.1 | 14 | 4.44 | 7457 | 42 | 0.07 | 45 | 16 | 39 | 12 | 298 | 100 | 977 | 339 | 1253 | 217 | 1550 | 234 |
| Slaufrudalur | IISlau-22_4.1 | 15 | 4.62 | 2381 | 34 | 0.01 | 29 | 3.1 | 8 | 2.40 | 77 | 28 | 294 | 110 | 411 | 73 | 546 | 88 |
| Slaufrudalur | IISlau-22_5.1 | 10 | 4.43 | 2018 | 39 | 0.02 | 33 | 2.3 | 6 | 1.27 | 55 | 21 | 232 | 86 | 342 | 64 | 494 | 76 |
| Slaufrudalur | IISlau-22_6.1 | 11 | 4.28 | 1920 | 29 | 0.02 | 27 | 2.3 | 6 | 1.33 | 56 | 20 | 223 | 85 | 338 | 64 | 487 | 76 |
| Slaufrudalur | IISlau-22_7.1 | 12 | 4.42 | 2058 | 9 | 0.03 | 12 | 4.2 | 9 | 2.12 | 64 | 23 | 241 | 88 | 353 | 65 | 483 | 78 |
| Slaufrudalur | IISlau-22_11.1 | 10 | 2.53 | 1248 | 14 | 0.04 | 14 | 1.0 | 3.29 | 0.72 | 29 | 10 | 116 | 44 | 181 | 30 | 275 | 45 |
| Slaufrudalur | IISlau-22_12.1 | 9 | 2.55 | 4159 | 28 | 0.29 | 31 | 6 | 18 | 4.20 | 140 | 43 | 450 | 158 | 593 | 109 | 745 | 119 |
| Slaufrudalur | IISlau-22_13.1 | 9 | 2.68 | 4994 | 46 | 0.07 | 38 | 7 | 18 | 2.91 | 153 | 51 | 535 | 193 | 768 | 144 | 1020 | 156 |
| Slaufrudalur | IISlau-25-1.1 | 8 | 0.64 | 4395 | 37 | 0.01 | 38 | 9 | 22 | 10 | 182 | 60 | 609 | 190 | 758 | 134 | 924 | 144 |
| Slaufrudalur | IISlau-25-2.1 | 9 | 0.50 | 1550 | 40 | 0.02 | 16 | 1.1 | 2.72 | 0.95 | 27 | 9 | 115 | 40 | 181 | 35 | 259 | 45 |
| Slaufrudalur | IISlau-25-3.1 | 7 | 0.58 | 2721 | 19 | 0.04 | 20 | 2.9 | 8 | 2.67 | 79 | 28 | 314 | 111 | 443 | 82 | 618 | 95 |
| Slaufrudalur | IISlau-25-5.1 | 46 | 1.11 | 3707 | 119 | 0.01 | 72 | 3.6 | 11 | 3.46 | 105 | 42 | 470 | 164 | 654 | 120 | 892 | 131 |
| Slaufrudalur | IISlau-25-6.1 | 3.8 | 9 | 3308 | 817 | 0.03 | 57 | 0.6 | 1.92 | 0.24 | 27 | 17 | 259 | 114 | 591 | 137 | 1189 | 182 |
| Slaufrudalur | IISlau-26-3.1 | 15 | 215 | 3653 | 66 | 1.4 | 100 | 5 | 8 | 0.56 | 79 | 29 | 323 | 130 | 557 | 118 | 1065 | 167 |
| Slaufrudalur | IISlau-26-4.1 | 13 | 102 | 8280 | 181 | 0.18 | 323 | 13 | 24 | 2.23 | 204 | 78 | 843 | 301 | 1281 | 256 | 2072 | 311 |
| Slaufrudalur | IISlau-26-5.1 | 15 | 1.48 | 5892 | 59 | 0.03 | 70 | 9 | 21 | 6 | 185 | 65 | 652 | 221 | 885 | 174 | 1354 | 209 |

---

[51] See **Appendix C.2** for mount names and analysis dates

**Appendix C.3**. Continued

| Intrusion | Grain # | Ti | Fe | Y | Nb | La | Ce | Nd | Sm | Eu | Gd | Tb | Dy | Ho | Er | Tm | Yb | Lu |
|---|---|---|---|---|---|---|---|---|---|---|---|---|---|---|---|---|---|---|
| Slaufrudalur | IISlau-26-6.1 | 18 | 13 | 12752 | 156 | 0.05 | 566 | 23 | 40 | 3.66 | 323 | 114 | 1243 | 439 | 1908 | 403 | 3374 | 510 |
| Slaufrudalur | IISlau-26-7.1 | 15 | 0.60 | 9242 | 188 | 0.04 | 425 | 17 | 30 | 2.95 | 237 | 94 | 981 | 332 | 1418 | 283 | 2245 | 323 |
| Slaufrudalur | IISlau-26_8.1 | 3.2 | 2.46 | 1523 | 3.8 | 0.13 | 7 | 2.7 | 7 | 1.15 | 48 | 15 | 166 | 63 | 259 | 53 | 417 | 71 |
| Slaufrudalur | IISlau-26-1.1 | 16 | 363 | 15263 | 628 | 3.6 | 380 | 58 | 49 | 6 | 422 | 162 | 1698 | 599 | 2354 | 429 | 3156 | 437 |
| Slaufrudalur | IISlau-26-2.1 | -- | 19 | 8365 | 166 | 0.35 | 352 | 15 | 21 | 2.42 | 174 | 65 | 744 | 299 | 1379 | 306 | 2753 | 466 |
| Vesturhorn | IIV-03a-2.1 | 3.6 | 1.62 | 4414 | 45 | 0.13 | 46 | 3.0 | 10 | 2.04 | 116 |  | 430 | 180 | 676 |  | 884 | 136 |
| Vesturhorn | IIV-03a-6.1 | 4.4 | 0.07 | 3585 | 78 | 0.02 | 69 | 2.1 | 8 | 1.34 | 88 |  | 350 | 144 | 561 |  | 749 | 118 |
| Vesturhorn | IIV-03a-8.1 | 4.0 | 0.95 | 1860 | 30 | 0.03 | 32 | 1.0 | 3.32 | 0.84 | 46 |  | 183 | 77 | 300 |  | 418 | 67 |
| Vesturhorn | IIV-03a-9.1 | 6 | 0.23 | 5581 | 168 | 0.03 | 130 | 3.2 | 12 | 1.96 | 139 |  | 494 | 206 | 846 |  | 1151 | 176 |
| Vesturhorn | IIV-03a-10.1 | 8 | 0.29 | 6296 | 31 | 0.14 | 112 | 9 | 21 | 5 | 170 |  | 573 | 236 | 954 |  | 1492 | 241 |
| Vesturhorn | IIV-03a-11.1 | 4.5 | 0.34 | 3604 | 133 | 0.05 | 70 | 1.9 | 7 | 1.84 | 97 |  | 381 | 151 | 571 |  | 726 | 110 |
| Vesturhorn | IIV-03a-12.1 | 4.2 | 2.24 | 2591 | 90 | 0.03 | 60 | 1.4 | 5 | 0.85 | 60 |  | 245 | 101 | 410 |  | 575 | 93 |
| Vesturhorn | IIV-03a-13.1 | 6 | 0.14 | 6693 | 253 | 0.04 | 170 | 3.4 | 15 | 3.26 | 179 |  | 664 | 256 | 1006 |  | 1219 | 177 |
| Vesturhorn | IIV-03a-14.1 | 5 | 0.40 | 3463 | 100 | 0.03 | 89 | 2.2 | 7 | 1.61 | 92 |  | 401 | 148 | 576 |  | 792 | 123 |
| Vesturhorn | IIV-03a-16.1 | 5 | 1.24 | 5539 | 233 | 0.23 | 279 | 3.4 | 12 | 2.53 | 131 |  | 501 | 211 | 839 |  | 1166 | 176 |
| Vesturhorn | IIV-03a-17.1 | 9 | 0.26 | 4847 | 22 | 0.14 | 42 | 11 | 23 | 3.82 | 183 |  | 536 | 197 | 707 |  | 920 | 142 |
| Vesturhorn | IIV-03a-5.1 | 3.6 | 8 | 5168 | 49 | 3.8 | 70 | 8 | 14 | 2.00 | 127 |  | 456 | 192 | 743 |  | 981 | 152 |
| Vesturhorn | IIV-03a-15.1 | 6 | 6 | 3147 | 50 | 36 | 149 | 40 | 19 | 2.60 | 106 |  | 357 | 135 | 500 |  | 679 | 106 |
| Vesturhorn | IIV-15-1.1 | 18 | 0.27 | 1287 | 0.8 | 0.01 | 10 | 2.1 | 5 | 1.63 | 44 | 15 | 144 | 53 | 213 | 38 | 302 | 48 |
| Vesturhorn | IIV-15-2.1 | 20 | 0.30 | 2563 | 1.8 | 0.01 | 15 | 3.3 | 6 | 2.14 | 58 | 21 | 248 | 97 | 426 | 85 | 653 | 106 |
| Vesturhorn | IIV-15-3.1 | 32 | 0.34 | 1277 | 0.8 | 0.01 | 7 | 2.8 | 5 | 1.80 | 41 | 14 | 146 | 49 | 216 | 42 | 339 | 54 |
| Vesturhorn | IIV-15-6.2 | 26 | 0.14 | 510 | 0.8 | 0.01 | 6 | 0.5 | 1.22 | 0.46 | 14 | 5 | 53 | 19 | 81 | 17 | 138 | 23 |
| Vesturhorn | IIV-15-6.1 | 23 | 0.17 | 1134 | 0.8 | 0.01 | 8 | 1.9 | 3.92 | 1.53 | 34 | 11 | 123 | 42 | 173 | 33 | 260 | 41 |
| Vesturhorn | IIV-15-7.1 | 24 | 0.12 | 880 | 0.7 | 0.01 | 6 | 0.7 | 2.44 | 1.23 | 25 | 9 | 97 | 33 | 136 | 26 | 210 | 32 |
| Vesturhorn | IIV-15-10.1 | 25 | 0.20 | 299 | 0.8 | 0.01 | 4 | 0.4 | 1.24 | 0.51 | 12 | 4 | 44 | 16 | 74 | 15 | 119 | 19 |
| Vesturhorn | IIV-15-11.1 | 25 | 0.11 | 1147 | 0.9 | 0.02 | 7 | 1.5 | 3.99 | 1.46 | 34 | 11 | 112 | 39 | 163 | 31 | 234 | 38 |
| Vesturhorn | IIV-15-13.1 | 23 | 4.58 | 227 | 0.7 | 0.06 | 5 | 0.9 | 0.77 | 0.23 | 5 | 2 | 23 | 8 | 41 | 8 | 76 | 13 |
| Vesturhorn | IIV-15-15.1 | 20 | 0.15 | 489 | 0.5 | 0.01 | 8 | 0.4 | 1.05 | 0.48 | 12 | 5 | 50 | 18 | 77 | 15 | 136 | 22 |
| Vesturhorn | IIV-15-16.2 | 20 | 0.25 | 458 | 1.0 | 0.01 | 8 | 0.4 | 0.90 | 0.37 | 10 | 4 | 46 | 17 | 75 | 15 | 126 | 22 |
| Vesturhorn | IIV-15-16.1 | 26 | 0.17 | 968 | 0.8 | 0.01 | 7 | 1.5 | 3.83 | 1.54 | 35 | 11 | 108 | 37 | 156 | 30 | 225 | 37 |
| Vesturhorn | IIV-15-17.1 | 37 | 0.24 | 749 | 1.3 | 0.01 | 6 | 0.8 | 2.01 | 0.84 | 18 | 7 | 71 | 27 | 128 | 27 | 221 | 40 |
| Vesturhorn | IIV-15-18.1 | 30 | 0.31 | 859 | 1.2 | 0.01 | 7 | 0.9 | 2.07 | 0.74 | 20 | 7 | 75 | 30 | 145 | 31 | 270 | 50 |

**Appendix C.3**. Continued

| Intrusion | Grain # | Ti | Fe | Y | Nb | La | Ce | Nd | Sm | Eu | Gd | Tb | Dy | Ho | Er | Tm | Yb | Lu |
|---|---|---|---|---|---|---|---|---|---|---|---|---|---|---|---|---|---|---|
| Vesturhorn | IIV-15-19.2 | 19 | 0.16 | 397 | 0.8 | 0.01 | 7 | 0.3 | 0.83 | 0.39 | 10 | 3 | 38 | 15 | 64 | 14 | 107 | 19 |
| Vesturhorn | IIV-15-19.1 | 25 | 0.23 | 1104 | 0.8 | 0.01 | 8 | 2.3 | 4.39 | 1.60 | 36 | 12 | 118 | 42 | 174 | 34 | 256 | 42 |
| Vesturhorn | IIV-15-19.3 | 10 | 0.27 | 658 | 1.0 | 0.02 | 10 | 0.3 | 0.97 | 0.24 | 12 | 5 | 60 | 24 | 112 | 24 | 192 | 32 |
| Vesturhorn | IIV-16_1.1 | 15 | 4.31 | 10060 | 20 | 0.13 | 168 | 19 | 47 | 14 | 330 | 120 | 1227 | 431 | 1703 | 322 | 2386 | 357 |
| Vesturhorn | IIV-16_2.1 | 14 | 4.42 | 1413 | 3.0 | 0.01 | 13 | 1.7 | 4.68 | 1.59 | 38 | 14 | 149 | 58 | 237 | 47 | 389 | 64 |
| Vesturhorn | IIV-16_3.1 | 17 | 4.41 | 1846 | 3.4 | 0.06 | 12 | 3.5 | 9 | 3.33 | 74 | 26 | 255 | 92 | 381 | 73 | 560 | 94 |
| Vesturhorn | IIV-16_4.1 | 30 | 4.42 | 839 | 2.9 | 0.03 | 7 | 0.9 | 2.52 | 1.07 | 23 | 8 | 91 | 36 | 152 | 32 | 267 | 46 |
| Vesturhorn | IIV-16_5.1 | 23 | 4.48 | 8571 | 17 | 0.10 | 62 | 13 | 34 | 15 | 299 | 102 | 1032 | 367 | 1375 | 256 | 1888 | 280 |
| Vesturhorn | IIV-16_6.1 | 16 | 5 | 1200 | 3.3 | 0.01 | 11 | 1.4 | 3.49 | 1.27 | 29 | 9 | 99 | 44 | 173 | 35 | 272 | 47 |
| Vesturhorn | IIV-16_7.1 | 18 | 4.51 | 1086 | 6 | 0.01 | 11 | 0.9 | 2.14 | 1.01 | 24 | 10 | 112 | 45 | 200 | 41 | 342 | 62 |
| Vesturhorn | IIV-16_8.1 | 15 | 4.56 | 1699 | 8 | 0.01 | 22 | 1.4 | 4.53 | 1.69 | 43 | 17 | 185 | 71 | 306 | 61 | 478 | 78 |
| Vesturhorn | IIV-16_11.1 | 14 | 2.45 | 8076 | 24 | 0.14 | 90 | 14 | 33 | 9 | 290 | 96 | 1013 | 348 | 1409 | 272 | 2002 | 314 |
| Vesturhorn | IIV-16_12.1 | 16 | 2.54 | 1472 | 3.9 | 0.02 | 13 | 1.8 | 5 | 1.76 | 41 | 15 | 158 | 59 | 256 | 51 | 395 | 66 |
| Vesturhorn | IIV-16_13.1 | 27 | 2.33 | 2919 | 6 | 0.07 | 13 | 4.3 | 14 | 5 | 103 | 36 | 355 | 126 | 528 | 105 | 775 | 130 |
| Vesturhorn | IIV-16_14.1 | 15 | 2.55 | 2015 | 3.7 | 0.02 | 14 | 2.5 | 7 | 2.53 | 56 | 21 | 218 | 78 | 324 | 64 | 492 | 80 |
| Vesturhorn | IIV-16_15.1 | 19 | 2.40 | 1774 | 3.3 | 0.02 | 8 | 2.8 | 8 | 2.75 | 59 | 20 | 210 | 73 | 314 | 60 | 461 | 77 |
| Reyðarártindur | IIR-01-1.1 | 82 | 2.11 | 3192 | 65 | 0.02 | 71 | 3.5 | 9 | 0.92 | 88 | 32 | 332 | 126 | 459 | 89 | 672 | 108 |
| Reyðarártindur | IIR-01-4.1 | 12 | 0.18 | 1114 | 9 | 0.01 | 14 | 0.9 | 2.68 | 0.57 | 30 | 14 | 164 | 53 | 272 | 54 | 452 | 75 |
| Reyðarártindur | IIR-01-5.1 | 17 | 7 | 1061 | 8 | 0.03 | 13 | 0.9 | 2.80 | 0.82 | 27 | 10 | 115 | 42 | 177 | 36 | 292 | 49 |
| Reyðarártindur | IIR-01-6.1 | 14 | 0.13 | 1233 | 9 | 0.01 | 14 | 1.1 | 3.15 | 0.84 | 31 | 12 | 132 | 50 | 208 | 41 | 332 | 56 |
| Reyðarártindur | IIR-01-7.1 | 14 | 0.28 | 1254 | 10 | 0.01 | 16 | 1.2 | 2.99 | 0.71 | 31 | 12 | 130 | 48 | 206 | 40 | 335 | 54 |
| Reyðarártindur | IIR-01-8.1 | 30 | 32 | 1256 | 12 | 0.06 | 15 | 1.5 | 3.60 | 0.75 | 34 | 12 | 136 | 51 | 208 | 40 | 342 | 56 |
| Reyðarártindur | IIR-01-9.1 | 10 | 0.61 | 5287 | 14 | 0.05 | 35 | 13 | 22 | 6 | 231 | 94 | 955 | 280 | 1308 | 232 | 1855 | 292 |
| Reyðarártindur | IIR-01-11.1 | 22 | 0.39 | 14575 | 40 | 0.05 | 176 | 58 | 100 | 21 | 709 | 213 | 2022 | 610 | 2213 | 378 | 2702 | 369 |
| Reyðarártindur | IIR-01-12.1 | 20 | 0.61 | 11378 | 299 | 0.03 | 470 | 17 | 45 | 2.05 | 403 | 150 | 1445 | 469 | 1801 | 321 | 2382 | 325 |
| Reyðarártindur | IIR-01-13.1 | 19 | 3.98 | 9513 | 42 | 0.03 | 128 | 22 | 46 | 10 | 373 | 126 | 1231 | 421 | 1624 | 294 | 2169 | 336 |
| Reyðarártindur | IIR-01-14.1 | 13 | 0.61 | 1170 | 11 | 0.02 | 16 | 1.1 | 3.02 | 0.61 | 32 | 12 | 138 | 49 | 211 | 43 | 352 | 57 |
| Reyðarártindur | IIR-01-2.1 | -- | 900 | 4321 | 84 | 0.20 | 56 | 6 | 11 | 2.73 | 102 | 40 | 432 | 169 | 609 | 110 | 783 | 121 |
| Reyðarártindur | IIR-01-3.1 | -- | 111 | 2537 | 18 | 0.09 | 27 | 4.3 | 8 | 1.26 | 75 | 29 | 308 | 107 | 439 | 81 | 673 | 111 |
| Reyðarártindur | IIR-03a-1.1 | 13 | 12 | 13594 | 65 | 0.04 | 263 | 40 | 80 | 5 | 617 | 195 | 1884 | 602 | 2154 | 380 | 2706 | 385 |
| Reyðarártindur | IIR-03a-2.1 | 11 | 2.62 | 8605 | 43 | 0.09 | 125 | 22 | 43 | 2.95 | 328 | 111 | 1080 | 349 | 1303 | 233 | 1706 | 246 |
| Reyðarártindur | IIR-03a-3.1 | 7 | 0.35 | 4797 | 24 | 0.02 | 75 | 8 | 17 | 0.87 | 160 | 58 | 585 | 192 | 748 | 137 | 1029 | 155 |

**Appendix C.3**. Continued

| Intrusion | Grain # | Ti | Fe | Y | Nb | La | Ce | Nd | Sm | Eu | Gd | Tb | Dy | Ho | Er | Tm | Yb | Lu |
|---|---|---|---|---|---|---|---|---|---|---|---|---|---|---|---|---|---|---|
| Reyðarártindur | IIR-03a-4.1 | 12 | 2.94 | 2753 | 32 | 0.01 | 49 | 3.1 | 9 | 0.57 | 79 | 28 | 311 | 107 | 444 | 85 | 628 | 102 |
| Reyðarártindur | IIR-03a-5.1 | 9 | 0.31 | 4608 | 17 | 0.02 | 50 | 9 | 19 | 1.43 | 154 | 57 | 574 | 191 | 751 | 143 | 1040 | 156 |
| Reyðarártindur | IIR-03a-6.1 | 25 | 44 | 13110 | 139 | 0.03 | 298 | 35 | 72 | 4.56 | 547 | 172 | 1675 | 542 | 1984 | 357 | 2569 | 369 |
| Reyðarártindur | IIR-03a-7.1 | 10 | 1.22 | 4903 | 21 | 0.02 | 59 | 11 | 20 | 1.21 | 167 | 57 | 586 | 193 | 746 | 139 | 1046 | 157 |
| Reyðarártindur | IIR-03a-8.1 | 12 | 0.47 | 11061 | 48 | 0.03 | 161 | 26 | 51 | 3.61 | 415 | 138 | 1369 | 438 | 1666 | 297 | 2146 | 311 |
| Reyðarártindur | IIR-03a-9.1 | 14 | 0.47 | 3357 | 43 | 0.02 | 59 | 3.2 | 9 | 0.60 | 92 | 35 | 375 | 129 | 552 | 106 | 809 | 125 |
| Reyðarártindur | IIR-03a-10.1 | 12 | 0.91 | 6872 | 31 | 0.03 | 95 | 16 | 32 | 2.39 | 254 | 86 | 871 | 281 | 1059 | 194 | 1471 | 213 |
| Reyðarártindur | IIR-03a-11.1 | 21 | 0.55 | 7217 | 121 | 0.02 | 181 | 8 | 23 | 1.83 | 240 | 88 | 871 | 289 | 1149 | 212 | 1579 | 238 |
| Reyðarártindur | IIR-03a-14.1 | 12 | 3.85 | 8980 | 40 | 0.03 | 119 | 21 | 43 | 2.90 | 330 | 107 | 1079 | 367 | 1362 | 241 | 1765 | 260 |
| Reyðarártindur | IIR-03a-15.1 | 24 | 0.76 | 7754 | 123 | 0.02 | 192 | 13 | 32 | 2.17 | 281 | 93 | 944 | 314 | 1174 | 219 | 1603 | 228 |
| Reyðarártindur | IIR-03a-16.1 | 22 | 1.29 | 8226 | 114 | 0.03 | 189 | 18 | 37 | 2.47 | 294 | 96 | 965 | 334 | 1210 | 213 | 1582 | 230 |
| Reyðarártindur | IIR-03a-17.1 | 14 | 0.55 | 13920 | 67 | 0.05 | 226 | 42 | 77 | 4.97 | 571 | 188 | 1776 | 565 | 2081 | 365 | 2624 | 370 |
| Reyðarártindur | IIR-03a-18.1 | 11 | 167 | 13850 | 75 | 0.05 | 260 | 35 | 68 | 2.57 | 483 | 165 | 1602 | 510 | 1886 | 339 | 2446 | 351 |
| Reyðarártindur | IIR-13-1.1 | 14 | 6 | 2747 | 15 | 0.03 | 9 | 4.5 | 11 | 6 | 104 | 34 | 332 | 119 | 439 | 80 | 605 | 97 |
| Reyðarártindur | IIR-13-2.1 | -- | 1.67 | 1038 | 5 | 0.12 | 13 | 2.9 | 2.92 | 1.19 | 25 | 9 | 105 | 41 | 178 | 37 | 298 | 50 |
| Reyðarártindur | IIR-13-3.1 | -- | 14 | 868 | 6 | 0.01 | 10 | 0.9 | 2.09 | 0.66 | 21 | 8 | 92 | 33 | 148 | 30 | 243 | 40 |
| Reyðarártindur | IIR-13-4.1 | 15 | 0.21 | 1523 | 5 | 0.01 | 14 | 2.2 | 6 | 1.38 | 50 | 17 | 185 | 63 | 264 | 52 | 407 | 65 |
| Reyðarártindur | IIR-13-5.1 | 15 | 1.44 | 902 | 6 | 0.04 | 10 | 1.1 | 2.36 | 0.66 | 24 | 9 | 100 | 37 | 152 | 31 | 260 | 43 |
| Reyðarártindur | IIR-13-6.1 | 11 | 0.16 | 2648 | 34 | 0.01 | 48 | 2.5 | 6 | 1.25 | 66 | 25 | 284 | 107 | 453 | 87 | 705 | 111 |
| Reyðarártindur | IIR-13-7.1 | 15 | 1.12 | 6171 | 143 | 0.03 | 144 | 7 | 18 | 1.98 | 186 | 69 | 707 | 248 | 986 | 185 | 1474 | 224 |
| Reyðarártindur | IIR-13-8.1 | 16 | 0.21 | 1583 | 4.4 | 0.01 | 14 | 2.5 | 6 | 1.82 | 50 | 19 | 193 | 66 | 269 | 52 | 403 | 66 |
| Reyðarártindur | IIR-13-9.1 | 18 | 0.66 | 1688 | 4.5 | 0.02 | 12 | 2.8 | 6 | 1.76 | 52 | 19 | 200 | 68 | 283 | 52 | 419 | 68 |
| Reyðarártindur | IIR-13-10.1 | 9 | 0.16 | 2701 | 37 | 0.02 | 55 | 2.4 | 6 | 1.11 | 70 | 28 | 303 | 109 | 466 | 92 | 714 | 116 |
| Reyðarártindur | IIR-13-12.1 | 12 | 1.01 | 8691 | 73 | 0.03 | 137 | 15 | 26 | 5 | 257 | 92 | 956 | 365 | 1423 | 272 | 1998 | 320 |
| Reyðarártindur | IIR-13-13.1 | 27 | 0.13 | 4684 | 11 | 0.03 | 14 | 7 | 18 | 7 | 169 | 59 | 583 | 197 | 780 | 148 | 1134 | 177 |
| Reyðarártindur | IIR-13-14.1 | -- | 2.85 | 3466 | 8 | 0.19 | 36 | 10 | 15 | 4.61 | 143 | 47 | 464 | 165 | 634 | 122 | 925 | 147 |
| Reyðarártindur | IIR-13-15.1 | 23 | 0.23 | 2362 | 13 | 0.01 | 10 | 2.6 | 6 | 2.32 | 54 | 20 | 222 | 87 | 364 | 72 | 576 | 99 |
| Reyðarártindur | IIR-13-16.1 | 13 | 0.36 | 987 | 30 | 0.02 | 19 | 0.9 | 2.40 | 0.51 | 25 | 10 | 105 | 41 | 176 | 36 | 313 | 53 |
| Reyðarártindur | IIR-13-17.1 | -- | 1.00 | 3312 | 6 | 0.02 | 15 | 5 | 13 | 5 | 139 | 48 | 505 | 171 | 709 | 134 | 1050 | 168 |
| Reyðarártindur | IIR-13-18.1 | 20 | 0.21 | 6905 | 27 | 0.03 | 41 | 12 | 27 | 10 | 223 | 75 | 749 | 261 | 1006 | 197 | 1535 | 242 |
| Reyðarártindur | IIR-13-19.1 | 25 | 0.18 | 1920 | 2.3 | 0.01 | 8 | 4.3 | 8 | 3.46 | 73 | 25 | 255 | 84 | 358 | 70 | 548 | 85 |
| Sandfell | IISan-01_1.1 | 9 | 4.27 | 2987 | 99 | 0.26 | 44 | 2.6 | 7 | 2.40 | 82 | 33 | 366 | 139 | 587 | 115 | 884 | 142 |

**Appendix C.3**. Continued

| **Intrusion** | **Grain #** | **Ti** | **Fe** | **Y** | **Nb** | **La** | **Ce** | **Nd** | **Sm** | **Eu** | **Gd** | **Tb** | **Dy** | **Ho** | **Er** | **Tm** | **Yb** | **Lu** |
|---|---|---|---|---|---|---|---|---|---|---|---|---|---|---|---|---|---|---|
| Sandfell | IISan-01_2.1 | 6 | 4.62 | 3973 | 34 | 0.21 | 23 | 4.5 | 12 | 3.63 | 109 | 41 | 451 | 172 | 688 | 130 | 1017 | 159 |
| Sandfell | IISan-01_3.1 | 9 | 15 | 3763 | 130 | 6.4 | 78 | 15 | 12 | 3.38 | 106 | 39 | 428 | 165 | 600 | 128 | 963 | 153 |
| Sandfell | IISan-01_4.1 | 9 | 4.65 | 3051 | 101 | 0.01 | 45 | 2.2 | 7 | 2.35 | 76 | 30 | 316 | 131 | 532 | 104 | 774 | 124 |
| Sandfell | IISan-01_5.1 | 10 | 4.60 | 2945 | 88 | 0.33 | 43 | 2.6 | 8 | 2.34 | 71 | 29 | 323 | 126 | 517 | 102 | 809 | 129 |
| Sandfell | IISan-01_6.1 | 8 | 4.49 | 3359 | 106 | 0.03 | 53 | 2.5 | 8 | 2.61 | 83 | 32 | 400 | 147 | 609 | 119 | 920 | 145 |
| Sandfell | IISan-01_7.1 | 8 | 4.42 | 2862 | 81 | 0.03 | 39 | 2.3 | 7 | 2.27 | 71 | 30 | 333 | 126 | 528 | 103 | 799 | 130 |
| Sandfell | IISan-01_8.1 | 6 | 4.53 | 4496 | 45 | 0.04 | 26 | 4.4 | 12 | 3.64 | 114 | 45 | 499 | 195 | 780 | 148 | 1160 | 185 |
| Sandfell | IISan-01_9.1 | 8 | 4.43 | 4236 | 94 | 0.02 | 46 | 3.9 | 11 | 3.64 | 121 | 45 | 502 | 189 | 773 | 148 | 1153 | 186 |
| Sandfell | IISan-01_10.1 | 6 | 4.31 | 1923 | 49 | 0.02 | 23 | 1.6 | 4.64 | 1.69 | 53 | 21 | 231 | 93 | 394 | 74 | 612 | 100 |
| Sandfell | IISan-01_11.1 | 7 | 2.52 | 1441 | 46 | 0.24 | 19 | 1.3 | 3.82 | 1.12 | 34 | 14 | 154 | 61 | 254 | 52 | 411 | 67 |
| Sandfell | IISan-01_12.1 | 6 | 2.55 | 4067 | 39 | 0.08 | 22 | 4.2 | 14 | 3.60 | 130 | 43 | 475 | 173 | 701 | 139 | 1035 | 167 |
| Sandfell | IISan-01_13.1 | 7 | 2.70 | 2254 | 81 | 0.01 | 31 | 1.6 | 6 | 1.65 | 58 | 21 | 236 | 93 | 384 | 77 | 597 | 96 |
| Lýsuskarð | IILYS-07a-1.1 | 14 | 0.23 | 27893 | 753 | 0.28 | 833 | 155 | 255 | 37 | 1494 | 463 | 4283 | 1241 | 4216 | 717 | 4900 | 622 |
| Lýsuskarð | IILYS-07a-2.1 | 15 | 0.22 | 28993 | 670 | 0.31 | 852 | 173 | 245 | 36 | 1414 | 482 | 4317 | 1317 | 4671 | 793 | 5412 | 685 |
| Lýsuskarð | IILYS-07a-3.1 | 9 | 0.19 | 15966 | 913 | 0.07 | 450 | 50 | 95 | 15 | 686 | 249 | 2521 | 777 | 2950 | 519 | 3617 | 463 |
| Lýsuskarð | IILYS-07a-4.1 | 10 | 0.27 | 15889 | 838 | 0.05 | 449 | 46 | 93 | 16 | 668 | 243 | 2334 | 710 | 2467 | 421 | 2852 | 368 |
| Lýsuskarð | IILYS-07a-5.1 | 11 | 0.37 | 28047 | 993 | 0.21 | 892 | 103 | 190 | 35 | 1396 | 439 | 4105 | 1222 | 4177 | 686 | 4599 | 552 |
| Lýsuskarð | IILYS-07a-6.1 | 6 | 0.47 | 5976 | 608 | 0.03 | 153 | 11 | 25 | 4.03 | 209 | 73 | 793 | 267 | 1005 | 181 | 1259 | 166 |
| Lýsuskarð | IILYS-07a-7.1 | 41 | 0.86 | 19768 | 3138 | 0.07 | 1005 | 56 | 120 | 23 | 944 | 309 | 2862 | 822 | 2810 | 457 | 2940 | 343 |
| Lýsuskarð | IILYS-07a-8.1 | 11 | 2.18 | 25707 | 932 | 0.39 | 769 | 100 | 175 | 30 | 1262 | 408 | 3840 | 1103 | 3782 | 618 | 4071 | 474 |
| Lýsuskarð | IILYS-07a-9.1 | 15 | 0.51 | 12120 | 314 | 0.03 | 236 | 27 | 53 | 8 | 436 | 146 | 1510 | 519 | 2109 | 384 | 2938 | 432 |
| Lýsuskarð | IILYS-07a-10.1 | 9 | 0.74 | 21648 | 896 | 0.09 | 778 | 56 | 102 | 18 | 747 | 273 | 2881 | 959 | 3760 | 681 | 4722 | 635 |
| Lýsuskarð | IILYS-07a-11.1 | 13 | 0.61 | 28114 | 679 | 0.27 | 843 | 146 | 230 | 35 | 1409 | 472 | 4276 | 1287 | 4597 | 784 | 5446 | 676 |
| Lýsuskarð | IILYS-07a-12.1 | 14 | 0.27 | 1234 | 35 | 0.01 | 19 | 2.1 | 3.77 | 1.25 | 34 | 13 | 140 | 52 | 225 | 44 | 336 | 58 |
| Lýsuskarð | IILYS-07a-13.1 | 17 | 0.32 | 31131 | 643 | 0.33 | 949 | 154 | 234 | 41 | 1579 | 504 | 4669 | 1393 | 4892 | 824 | 5436 | 689 |
| Lýsuskarð | IILYS-07a-14.1 | 22 | 1.92 | 16613 | 1874 | 0.31 | 775 | 48 | 93 | 18 | 696 | 256 | 2456 | 720 | 2563 | 429 | 2801 | 335 |
| Lýsuskarð | IILYS-07a-19.1 | 17 | 1.83 | 4154 | 89 | 0.64 | 75 | 16 | 22 | 5 | 156 | 50 | 497 | 177 | 658 | 124 | 956 | 150 |
| Lýsuskarð | IILYS-07a-17.1 | -- | 361 | 22036 | 929 | 0.26 | 1677 | 135 | 220 | 31 | 1471 | 554 | 5680 | 1938 | 7772 | 1434 | 10573 | 1499 |
| Lýsuskarð | IILYS-07a-20.1 | -- | 320 | 12547 | 2522 | 0.72 | 512 | 71 | 96 | 17 | 564 | 200 | 1833 | 551 | 1911 | 324 | 2201 | 275 |

**Appendix C.4**. Zircon Trace Element Compositions (ppm), measured *in situ* by SHRIMP-RG (Atomic Number > 71), REE anomalies[52], and estimated model crystallization temperatures[53]

| Sample | Grain # | Hf | Th | U | Eu* | Ce* | Ce/Ce* | Eu/Eu* | Crystallization Temp (ºC) |
|---|---|---|---|---|---|---|---|---|---|
| Slaufrudalur | IISlau-12-1.1 | 7665 | 70 | 118 | 96 | 0.55 | 18 | 0.29 | 892 |
| Slaufrudalur | IISlau-12-2.1 | 7648 | 118 | 141 | 78 | 0.52 | 33 | 0.36 | 949 |
| Slaufrudalur | IISlau-12-4.1 | 8446 | 15 | 37 | 45 | 0.27 | 18 | 0.34 | 877 |
| Slaufrudalur | IISlau-12-5.1 | 11002 | 439 | 390 | 232 | 2.1 | 68 | 0.19 | 841 |
| Slaufrudalur | IISlau-12-7.1 | 7630 | 276 | 236 | 80 | 0.58 | 48 | 0.35 | 948 |
| Slaufrudalur | IISlau-12-9.1 | 8402 | 220 | 268 | 180 | 1.1 | 37 | 0.24 | 831 |
| Slaufrudalur | IISlau-12_12.1 | 8239 | 153 | 219 | 255 | 1.7 | 12 | 0.33 | 895 |
| Slaufrudalur | IISlau-12_13.1 | 7848 | 63 | 92 | 131 | 0.76 | 10 | 0.45 | 956 |
| Slaufrudalur | IISlau-12_14.1 | 8599 | 211 | 257 | 248 | 1.8 | 19 | 0.32 | 896 |
| Slaufrudalur | IISlau-12_15.1 | 8472 | 161 | 166 | 55 | 0.39 | 48 | 0.32 | 910 |
| Slaufrudalur | IISlau-12_16.1 | 8459 | 437 | 406 | 548 | 2.7 | 18 | 0.30 | 888 |
| Slaufrudalur | IISlau-12_17.1 | 9142 | 300 | 321 | 164 | 1.1 | 32 | 0.28 | 881 |
| Slaufrudalur | IISlau-12_11.1 | 9338 | 53 | 90 | 53 | 0.39 | 30 | 0.38 | -- |
| Slaufrudalur | IISlau-22_1.1 | 9556 | 52 | 86 | 119 | 1.1 | 12 | 0.27 | 858 |
| Slaufrudalur | IISlau-22_3.1 | 8141 | 237 | 302 | 468 | 3.6 | 16 | 0.35 | 854 |
| Slaufrudalur | IISlau-22_4.1 | 9072 | 222 | 300 | 106 | 0.64 | 54 | 0.30 | 862 |
| Slaufrudalur | IISlau-22_5.1 | 9986 | 150 | 229 | 77 | 0.51 | 79 | 0.22 | 819 |
| Slaufrudalur | IISlau-22_6.1 | 9852 | 98 | 166 | 79 | 0.48 | 69 | 0.22 | 830 |
| Slaufrudalur | IISlau-22_7.1 | 9396 | 54 | 97 | 101 | 1.1 | 13 | 0.28 | 831 |
| Slaufrudalur | IISlau-22_11.1 | 10963 | 20 | 59 | 42 | 0.15 | 110 | 0.23 | 815 |
| Slaufrudalur | IISlau-22_12.1 | 8487 | 94 | 157 | 215 | 1.2 | 31 | 0.26 | 808 |
| Slaufrudalur | IISlau-22_13.1 | 10005 | 183 | 289 | 225 | 1.4 | 34 | 0.17 | 808 |
| Slaufrudalur | IISlau-25-1.1 | 11096 | 101 | 54 | 272 | 2.0 | 23 | 0.50 | 798 |
| Slaufrudalur | IISlau-25-2.1 | 7703 | 14 | 65 | 37 | 0.25 | 78 | 0.34 | 810 |
| Slaufrudalur | IISlau-25-3.1 | 12474 | 53 | 125 | 106 | 0.57 | 42 | 0.33 | 775 |
| Slaufrudalur | IISlau-25-5.1 | 12391 | 121 | 319 | 144 | 0.65 | 134 | 0.32 | 1009 |
| Slaufrudalur | IISlau-25-6.1 | 16463 | 243 | 859 | 31 | 0.09 | 755 | 0.10 | 720 |
| Slaufrudalur | IISlau-26-3.1 | 16009 | 641 | 765 | 112 | 1.6 | 76 | 0.07 | 859 |
| Slaufrudalur | IISlau-26-4.1 | 15088 | 2349 | 1840 | 304 | 3.9 | 101 | 0.10 | 847 |
| Slaufrudalur | IISlau-26-5.1 | 11516 | 397 | 770 | 271 | 2.1 | 40 | 0.29 | 863 |
| Slaufrudalur | IISlau-26-6.1 | 11836 | 5637 | 3651 | 491 | 7.1 | 97 | 0.10 | 879 |
| Slaufrudalur | IISlau-26-7.1 | 13950 | 2520 | 1865 | 364 | 4.8 | 107 | 0.11 | 864 |
| Slaufrudalur | IISlau-26_8.1 | 9747 | 97 | 160 | 81 | 0.53 | 15 | 0.19 | 705 |
| Slaufrudalur | IISlau-26-1.1 | 11505 | 1188 | 1597 | 622 | 36 | 13 | 0.14 | 868 |
| Slaufrudalur | IISlau-26-2.1 | 10007 | 4516 | 3884 | 261 | 5.3 | 80 | 0.12 | -- |
| Vesturhorn | IIV-03a-2.1 | 10230 | 128 | 255 | 149 | 0.45 | 123 | 0.18 | 716 |
| Vesturhorn | IIV-03a-6.1 | 10106 | 155 | 333 | 112 | 0.29 | 289 | 0.16 | 734 |
| Vesturhorn | IIV-03a-8.1 | 9997 | 57 | 129 | 53 | 0.15 | 259 | 0.21 | 726 |

---

[52] REE anomalies: Ce* and Eu* calculated by logarithmic extrapolation of Sm and Nd, and Nd and Gd, respectively

[53] Model temperatures estimated using the Ti-in-zircon thermometer of Ferry & Watson (2007), see Chapter III, 3.3.b

**Appendix C.4**. Continued

| Sample | Grain # | Hf | Th | U | Eu* | Ce* | Ce/Ce* | Eu/Eu* | Crystallization Temp (ºC) |
|---|---|---|---|---|---|---|---|---|---|
| Vesturhorn | IIV-03a-9.1 | 10212 | 297 | 533 | 179 | 0.44 | 363 | 0.14 | 759 |
| Vesturhorn | IIV-03a-10.1 | 8464 | 542 | 572 | 257 | 2.2 | 63 | 0.27 | 793 |
| Vesturhorn | IIV-03a-11.1 | 9405 | 255 | 435 | 116 | 0.26 | 327 | 0.21 | 736 |
| Vesturhorn | IIV-03a-12.1 | 11544 | 168 | 326 | 78 | 0.20 | 376 | 0.14 | 730 |
| Vesturhorn | IIV-03a-13.1 | 8690 | 457 | 681 | 222 | 0.41 | 505 | 0.19 | 759 |
| Vesturhorn | IIV-03a-14.1 | 10102 | 252 | 361 | 111 | 0.37 | 295 | 0.19 | 750 |
| Vesturhorn | IIV-03a-16.1 | 9677 | 471 | 509 | 171 | 0.52 | 652 | 0.19 | 750 |
| Vesturhorn | IIV-03a-17.1 | 6362 | 284 | 331 | 282 | 2.9 | 18 | 0.18 | 803 |
| Vesturhorn | IIV-03a-5.1 | 10194 | 214 | 367 | 180 | 2.4 | 35 | 0.15 | 715 |
| Vesturhorn | IIV-03a-15.1 | 9904 | 102 | 198 | 193 | 45 | 4 | 0.18 | 755 |
| Vesturhorn | IIV-15-1.1 | 9295 | 215 | 188 | 65 | 0.47 | 27 | 0.33 | 882 |
| Vesturhorn | IIV-15-2.1 | 10413 | 351 | 491 | 83 | 0.92 | 20 | 0.34 | 892 |
| Vesturhorn | IIV-15-3.1 | 9881 | 69 | 99 | 63 | 0.81 | 11 | 0.38 | 956 |
| Vesturhorn | IIV-15-6.2 | 9922 | 24 | 52 | 18 | 0.11 | 62 | 0.34 | 929 |
| Vesturhorn | IIV-15-6.1 | 10332 | 62 | 93 | 50 | 0.51 | 18 | 0.40 | 913 |
| Vesturhorn | IIV-15-7.1 | 10377 | 25 | 47 | 34 | 0.12 | 62 | 0.48 | 919 |
| Vesturhorn | IIV-15-10.1 | 10109 | 22 | 44 | 17 | 0.06 | 74 | 0.41 | 926 |
| Vesturhorn | IIV-15-11.1 | 10475 | 48 | 71 | 51 | 0.29 | 30 | 0.38 | 923 |
| Vesturhorn | IIV-15-13.1 | 10449 | 11 | 27 | 9 | 0.54 | 11 | 0.35 | 915 |
| Vesturhorn | IIV-15-15.1 | 10865 | 44 | 88 | 15 | 0.08 | 115 | 0.41 | 897 |
| Vesturhorn | IIV-15-16.2 | 11605 | 39 | 95 | 13 | 0.07 | 131 | 0.37 | 895 |
| Vesturhorn | IIV-15-16.1 | 10504 | 39 | 66 | 50 | 0.31 | 26 | 0.41 | 928 |
| Vesturhorn | IIV-15-17.1 | 9214 | 31 | 81 | 26 | 0.15 | 45 | 0.42 | 977 |
| Vesturhorn | IIV-15-18.1 | 9268 | 42 | 144 | 28 | 0.19 | 48 | 0.35 | 949 |
| Vesturhorn | IIV-15-19.2 | 11357 | 31 | 73 | 13 | 0.04 | 199 | 0.41 | 888 |
| Vesturhorn | IIV-15-19.1 | 10108 | 64 | 96 | 54 | 0.64 | 15 | 0.39 | 921 |
| Vesturhorn | IIV-15-19.3 | 14230 | 82 | 219 | 15 | 0.04 | 335 | 0.22 | 813 |
| Vesturhorn | IIV-16_1.1 | 8766 | 945 | 727 | 540 | 4.0 | 51 | 0.34 | 861 |
| Vesturhorn | IIV-16_2.1 | 9373 | 38 | 77 | 58 | 0.33 | 49 | 0.36 | 852 |
| Vesturhorn | IIV-16_3.1 | 8795 | 79 | 111 | 112 | 0.71 | 21 | 0.39 | 878 |
| Vesturhorn | IIV-16_4.1 | 8407 | 30 | 63 | 33 | 0.18 | 49 | 0.43 | 947 |
| Vesturhorn | IIV-16_5.1 | 8392 | 440 | 367 | 436 | 2.5 | 30 | 0.46 | 910 |
| Vesturhorn | IIV-16_6.1 | 9036 | 30 | 59 | 43 | 0.28 | 50 | 0.39 | 870 |
| Vesturhorn | IIV-16_7.1 | 9540 | 36 | 77 | 31 | 0.20 | 68 | 0.43 | 880 |
| Vesturhorn | IIV-16_8.1 | 9758 | 103 | 157 | 60 | 0.24 | 114 | 0.37 | 862 |
| Vesturhorn | IIV-16_11.1 | 8999 | 654 | 647 | 422 | 3.1 | 36 | 0.29 | 855 |
| Vesturhorn | IIV-16_12.1 | 9062 | 48 | 79 | 65 | 0.30 | 54 | 0.36 | 866 |
| Vesturhorn | IIV-16_13.1 | 8062 | 105 | 132 | 165 | 0.70 | 22 | 0.41 | 935 |
| Vesturhorn | IIV-16_14.1 | 9237 | 89 | 103 | 87 | 0.45 | 38 | 0.38 | 858 |
| Vesturhorn | IIV-16_15.1 | 8219 | 51 | 78 | 93 | 0.52 | 19 | 0.39 | 887 |
| Reyðarártindur | IIR-01-1.1 | 11985 | 437 | 502 | 125 | 0.67 | 130 | 0.10 | 1100 |
| Reyðarártindur | IIR-01-4.1 | 12154 | 134 | 196 | 39 | 0.15 | 108 | 0.19 | 831 |

**Appendix C.4**. Continued

| Sample | Grain # | Hf | Th | U | Eu* | Ce* | Ce/Ce* | Eu/Eu* | Crystallization Temp (ºC) |
|---|---|---|---|---|---|---|---|---|---|
| Reyðarártindur | IIR-01-5.1 | 11273 | 43 | 92 | 38 | 0.16 | 98 | 0.29 | 872 |
| Reyðarártindur | IIR-01-6.1 | 11153 | 66 | 119 | 43 | 0.21 | 81 | 0.26 | 857 |
| Reyðarártindur | IIR-01-7.1 | 11355 | 68 | 138 | 42 | 0.24 | 82 | 0.22 | 853 |
| Reyðarártindur | IIR-01-8.1 | 11764 | 43 | 107 | 48 | 0.31 | 59 | 0.21 | 947 |
| Reyðarártindur | IIR-01-9.1 | 17277 | 422 | 560 | 308 | 3.8 | 11 | 0.24 | 817 |
| Reyðarártindur | IIR-01-11.1 | 8860 | 704 | 667 | 1152 | 18 | 12 | 0.24 | 905 |
| Reyðarártindur | IIR-01-12.1 | 11271 | 3113 | 2076 | 584 | 3.6 | 160 | 0.05 | 893 |
| Reyðarártindur | IIR-01-13.1 | 10691 | 531 | 597 | 566 | 5.6 | 28 | 0.22 | 890 |
| Reyðarártindur | IIR-01-14.1 | 11266 | 93 | 159 | 42 | 0.23 | 83 | 0.19 | 848 |
| Reyðarártindur | IIR-01-2.1 | 12544 | 128 | 253 | 142 | 1.8 | 37 | 0.25 | -- |
| Reyðarártindur | IIR-01-3.1 | 12062 | 138 | 240 | 107 | 1.2 | 28 | 0.15 | -- |
| Reyðarártindur | IIR-03a-1.1 | 6802 | 883 | 1071 | 961 | 11 | 30 | 0.07 | 845 |
| Reyðarártindur | IIR-03a-2.1 | 7036 | 465 | 1021 | 512 | 6.1 | 25 | 0.08 | 829 |
| Reyðarártindur | IIR-03a-3.1 | 7671 | 300 | 504 | 228 | 2.1 | 44 | 0.05 | 784 |
| Reyðarártindur | IIR-03a-4.1 | 7455 | 190 | 371 | 116 | 0.57 | 106 | 0.06 | 835 |
| Reyðarártindur | IIR-03a-5.1 | 6675 | 231 | 424 | 235 | 2.5 | 25 | 0.08 | 803 |
| Reyðarártindur | IIR-03a-6.1 | 7553 | 1748 | 1431 | 856 | 8.9 | 41 | 0.07 | 922 |
| Reyðarártindur | IIR-03a-7.1 | 6689 | 225 | 413 | 252 | 2.9 | 25 | 0.06 | 820 |
| Reyðarártindur | IIR-03a-8.1 | 7597 | 644 | 781 | 632 | 7.0 | 28 | 0.08 | 833 |
| Reyðarártindur | IIR-03a-9.1 | 7837 | 220 | 386 | 122 | 0.61 | 118 | 0.06 | 851 |
| Reyðarártindur | IIR-03a-10.1 | 7014 | 385 | 534 | 389 | 4.1 | 28 | 0.08 | 838 |
| Reyðarártindur | IIR-03a-11.1 | 7226 | 810 | 1078 | 325 | 1.6 | 139 | 0.07 | 903 |
| Reyðarártindur | IIR-03a-14.1 | 6804 | 516 | 767 | 514 | 5.5 | 27 | 0.07 | 832 |
| Reyðarártindur | IIR-03a-15.1 | 7056 | 856 | 1110 | 408 | 3.0 | 79 | 0.07 | 920 |
| Reyðarártindur | IIR-03a-16.1 | 6358 | 706 | 981 | 452 | 4.5 | 51 | 0.07 | 905 |
| Reyðarártindur | IIR-03a-17.1 | 6645 | 794 | 1005 | 910 | 12 | 23 | 0.07 | 851 |
| Reyðarártindur | IIR-03a-18.1 | 6981 | 915 | 1485 | 784 | 9.5 | 33 | 0.04 | 826 |
| Reyðarártindur | IIR-13-1.1 | 10241 | 36 | 78 | 149 | 0.95 | 12 | 0.53 | 856 |
| Reyðarártindur | IIR-13-2.1 | 9796 | 36 | 77 | 37 | 1.6 | 10 | 0.42 | -- |
| Reyðarártindur | IIR-13-3.1 | 10818 | 29 | 71 | 28 | 0.19 | 64 | 0.31 | -- |
| Reyðarártindur | IIR-13-4.1 | 10289 | 50 | 98 | 74 | 0.46 | 39 | 0.25 | 863 |
| Reyðarártindur | IIR-13-5.1 | 10735 | 24 | 59 | 33 | 0.25 | 50 | 0.27 | 859 |
| Reyðarártindur | IIR-13-6.1 | 12197 | 142 | 258 | 89 | 0.51 | 115 | 0.18 | 828 |
| Reyðarártindur | IIR-13-7.1 | 11068 | 672 | 943 | 251 | 1.4 | 122 | 0.10 | 862 |
| Reyðarártindur | IIR-13-8.1 | 11303 | 51 | 87 | 77 | 0.51 | 33 | 0.31 | 866 |
| Reyðarártindur | IIR-13-9.1 | 10945 | 58 | 90 | 76 | 0.73 | 21 | 0.31 | 883 |
| Reyðarártindur | IIR-13-10.1 | 12607 | 206 | 358 | 90 | 0.50 | 135 | 0.16 | 808 |
| Reyðarártindur | IIR-13-12.1 | 11413 | 630 | 757 | 356 | 4.3 | 39 | 0.20 | 838 |
| Reyðarártindur | IIR-13-13.1 | 9262 | 162 | 231 | 239 | 1.3 | 14 | 0.39 | 933 |
| Reyðarártindur | IIR-13-14.1 | 8807 | 286 | 370 | 199 | 3.9 | 11 | 0.30 | -- |
| Reyðarártindur | IIR-13-15.1 | 9522 | 59 | 137 | 77 | 0.59 | 21 | 0.39 | 911 |
| Reyðarártindur | IIR-13-16.1 | 11497 | 107 | 273 | 34 | 0.17 | 134 | 0.20 | 848 |

**Appendix C.4**. Continued

| Sample | Grain # | Hf | Th | U | Eu* | Ce* | Ce/Ce* | Eu/Eu* | Crystallization Temp (ºC) |
|---|---|---|---|---|---|---|---|---|---|
| Reyðarártindur | IIR-13-17.1 | 9207 | 194 | 235 | 183 | 1.1 | 17 | 0.39 | -- |
| Reyðarártindur | IIR-13-18.1 | 9588 | 281 | 359 | 334 | 2.7 | 19 | 0.41 | 893 |
| Reyðarártindur | IIR-13-19.1 | 9361 | 13 | -- | 105 | 1.2 | 8 | 0.43 | 923 |
| Sandfell | IISan-01_1.1 | 11001 | 239 | 450 | 104 | 0.49 | 109 | 0.30 | 804 |
| Sandfell | IISan-01_2.1 | 10122 | 127 | 248 | 155 | 0.90 | 31 | 0.31 | 756 |
| Sandfell | IISan-01_3.1 | 10768 | 365 | 616 | 156 | 10 | 9 | 0.29 | 799 |
| Sandfell | IISan-01_4.1 | 10525 | 305 | 477 | 103 | 0.35 | 157 | 0.30 | 801 |
| Sandfell | IISan-01_5.1 | 10228 | 171 | 360 | 103 | 0.46 | 116 | 0.30 | 810 |
| Sandfell | IISan-01_6.1 | 10519 | 204 | 417 | 111 | 0.41 | 156 | 0.31 | 792 |
| Sandfell | IISan-01_7.1 | 10407 | 184 | 364 | 95 | 0.40 | 119 | 0.31 | 791 |
| Sandfell | IISan-01_8.1 | 10650 | 155 | 300 | 159 | 0.87 | 36 | 0.30 | 756 |
| Sandfell | IISan-01_9.1 | 10349 | 181 | 400 | 156 | 0.73 | 77 | 0.31 | 790 |
| Sandfell | IISan-01_10.1 | 10475 | 80 | 202 | 68 | 0.30 | 94 | 0.33 | 756 |
| Sandfell | IISan-01_11.1 | 11052 | 55 | 153 | 49 | 0.22 | 106 | 0.30 | 785 |
| Sandfell | IISan-01_12.1 | 10673 | 119 | 265 | 187 | 0.65 | 40 | 0.25 | 757 |
| Sandfell | IISan-01_13.1 | 11057 | 115 | 274 | 80 | 0.22 | 171 | 0.27 | 776 |
| Lýsuskarð | IILYS-07a-1.1 | 8533 | 1731 | 1517 | 2669 | 50 | 20 | 0.18 | 857 |
| Lýsuskarð | IILYS-07a-2.1 | 10686 | 1766 | 1644 | 2550 | 64 | 16 | 0.18 | 864 |
| Lýsuskarð | IILYS-07a-3.1 | 13389 | 1446 | 1454 | 1103 | 14 | 39 | 0.18 | 804 |
| Lýsuskarð | IILYS-07a-4.1 | 11955 | 1242 | 600 | 1079 | 12 | 46 | 0.20 | 820 |
| Lýsuskarð | IILYS-07a-5.1 | 10079 | 2092 | 1826 | 2230 | 30 | 37 | 0.21 | 827 |
| Lýsuskarð | IILYS-07a-6.1 | 11766 | 341 | 691 | 312 | 2.5 | 76 | 0.17 | 761 |
| Lýsuskarð | IILYS-07a-7.1 | 10860 | 4587 | 1114 | 1455 | 14 | 90 | 0.21 | 991 |
| Lýsuskarð | IILYS-07a-8.1 | 12190 | 2000 | 759 | 2032 | 30 | 31 | 0.20 | 823 |
| Lýsuskarð | IILYS-07a-9.1 | 8084 | 620 | 818 | 658 | 7.4 | 39 | 0.16 | 864 |
| Lýsuskarð | IILYS-07a-10.1 | 8265 | 1525 | 2188 | 1192 | 16 | 59 | 0.20 | 810 |
| Lýsuskarð | IILYS-07a-11.1 | 7765 | 1603 | 1549 | 2464 | 49 | 21 | 0.19 | 846 |
| Lýsuskarð | IILYS-07a-12.1 | 8162 | 47 | 104 | 49 | 0.64 | 37 | 0.33 | 853 |
| Lýsuskarð | IILYS-07a-13.1 | 9250 | 1756 | 1632 | 2628 | 54 | 22 | 0.20 | 879 |
| Lýsuskarð | IILYS-07a-14.1 | 10505 | 3166 | 1941 | 1101 | 13 | 73 | 0.21 | 905 |
| Lýsuskarð | IILYS-07a-19.1 | 7313 | 372 | 395 | 252 | 6.1 | 15 | 0.28 | 875 |
| Lýsuskarð | IILYS-07a-17.1 | 14484 | 1286 | 3678 | 2462 | 44 | 47 | 0.17 | -- |
| Lýsuskarð | IILYS-07a-20.1 | 11346 | 3398 | 1027 | 1008 | 28 | 22 | 0.22 | -- |

**Appendix C.5**. Zircon oxygen isotope compositions, measured *in-situ* by SIMS[54]

| Spot Name: | Mount: | Date: | $^{16}$O Measured | $^{16}$O Error | $^{18}$O Measured | $^{18}$O Error | $^{18}$O/$^{16}$O Measured | $^{18}$O/$^{16}$O Error | $^{18}$O/$^{16}$O Corrected | δ$^{18}$O Corrected | Error (1σ) | Total Error (2σ)[55] |
|---|---|---|---|---|---|---|---|---|---|---|---|---|
| **SLAUFRUDALUR** | | | | | | | | | | | | |
| IISlau-12_1.1 | AJP01 | May. '13 | 2.509E+9 | 9.3E+5 | 5.019E+6 | 1.9E+3 | 0.0020007 | 1.5E-7 | 0.0020137 | 4.3 | 0.08 | 0.66 |
| IISlau-12_2.1 | AJP01 | May. '13 | 2.482E+9 | 1.2E+6 | 4.966E+6 | 2.5E+3 | 0.0020008 | 1.9E-7 | 0.0020138 | 4.3 | 0.09 | 0.67 |
| IISlau-12_3.1 | AJP01 | May. '13 | 2.080E+9 | 9.6E+6 | 4.161E+6 | 2.0E+4 | 0.0020006 | 2.2E-7 | 0.0020135 | 4.2 | 0.11 | 0.68 |
| IISlau-12_4.1 | AJP01 | May. '13 | 2.478E+9 | 1.3E+6 | 4.959E+6 | 2.9E+3 | 0.0020012 | 1.3E-7 | 0.0020142 | 4.5 | 0.07 | 0.66 |
| IISlau-12_5.1 | AJP01 | May. '13 | 2.325E+9 | 5.0E+7 | 4.649E+6 | 9.9E+4 | 0.0019990 | 5.2E-7 | 0.0020120 | 3.4 | 0.26 | 0.82 |
| IISlau-12_6.1 | AJP01 | May. '13 | 2.498E+9 | 1.1E+6 | 4.999E+6 | 2.2E+3 | 0.0020007 | 1.1E-7 | 0.0020137 | 4.2 | 0.05 | 0.65 |
| IISlau-12_7.1 | AJP01 | May. '13 | 2.467E+9 | 1.7E+6 | 4.936E+6 | 3.5E+3 | 0.0020005 | 1.2E-7 | 0.0020135 | 4.1 | 0.06 | 0.65 |
| IISlau-12_8.1 | AJP01 | May. '13 | 2.125E+9 | 2.7E+7 | 4.248E+6 | 5.5E+4 | 0.0019991 | 4.3E-7 | 0.0020120 | 3.4 | 0.22 | 0.77 |
| IISlau-12_11.1 | AJP03 | Nov. '13 | 1.813E+9 | 2.1E+6 | 3.649E+6 | 4.3E+3 | 0.0020127 | 1.3E-7 | 0.0020143 | 4.5 | 0.07 | 0.68 |
| IISlau-12_12.1 | AJP03 | Nov. '13 | 1.807E+9 | 5.1E+5 | 3.636E+6 | 1.0E+3 | 0.0020122 | 1.8E-7 | 0.0020138 | 4.3 | 0.09 | 0.69 |
| IISlau-12_13.1 | AJP03 | Nov. '13 | 1.787E+9 | 2.8E+6 | 3.595E+6 | 5.5E+3 | 0.0020119 | 2.3E-7 | 0.0020135 | 4.1 | 0.12 | 0.71 |
| IISlau-12_14.1 | AJP03 | Nov. '13 | 1.791E+9 | 2.8E+6 | 3.605E+6 | 5.7E+3 | 0.0020127 | 1.7E-7 | 0.0020143 | 4.6 | 0.08 | 0.69 |
| IISlau-12_15.1 | AJP03 | Nov. '13 | 1.820E+9 | 1.1E+6 | 3.663E+6 | 2.4E+3 | 0.0020122 | 2.2E-7 | 0.0020138 | 4.3 | 0.11 | 0.70 |
| IISlau-12_16.1 | AJP03 | Nov. '13 | 1.799E+9 | 1.2E+6 | 3.621E+6 | 2.5E+3 | 0.0020126 | 2.1E-7 | 0.0020142 | 4.5 | 0.10 | 0.70 |
| IISlau-12_17.1 | AJP03 | Nov. '13 | 1.805E+9 | 1.9E+6 | 3.633E+6 | 3.7E+3 | 0.0020126 | 2.5E-7 | 0.0020142 | 4.5 | 0.13 | 0.71 |
| IISlau-22_1.1 | AJP03 | Nov. '13 | 1.797E+9 | 2.0E+6 | 3.610E+6 | 4.1E+3 | 0.0020091 | 1.9E-7 | 0.0020107 | 2.8 | 0.09 | 0.69 |
| IISlau-22_3.1 | AJP03 | Nov. '13 | 1.861E+9 | 2.2E+6 | 3.744E+6 | 4.4E+3 | 0.0020119 | 2.0E-7 | 0.0020135 | 4.2 | 0.10 | 0.69 |
| IISlau-22_4.1 | AJP03 | Nov. '13 | 1.866E+9 | 2.0E+6 | 3.752E+6 | 4.2E+3 | 0.0020102 | 2.6E-7 | 0.0020118 | 3.3 | 0.13 | 0.71 |
| IISlau-22_5.1 | AJP03 | Nov. '13 | 1.895E+9 | 2.4E+6 | 3.806E+6 | 4.8E+3 | 0.0020089 | 1.8E-7 | 0.0020105 | 2.6 | 0.09 | 0.69 |
| IISlau-22_6.1 | AJP03 | Nov. '13 | 1.883E+9 | 8.4E+5 | 3.783E+6 | 1.7E+3 | 0.0020093 | 2.4E-7 | 0.0020109 | 2.9 | 0.12 | 0.71 |
| IISlau-22_7.1 | AJP03 | Nov. '13 | 1.881E+9 | 2.1E+6 | 3.779E+6 | 4.2E+3 | 0.0020090 | 2.2E-7 | 0.0020106 | 2.7 | 0.11 | 0.70 |
| IISlau-22_11.1 | AJP02 | Nov. '13 | 1.435E+9 | 4.8E+5 | 2.885E+6 | 8.3E+2 | 0.0020111 | 2.6E-7 | 0.0020128 | 3.8 | 0.13 | 0.72 |
| IISlau-22_12.1 | AJP02 | Nov. '13 | 1.431E+9 | 6.6E+5 | 2.877E+6 | 1.5E+3 | 0.0020104 | 3.5E-7 | 0.0020121 | 3.4 | 0.17 | 0.76 |
| IISlau-22_13.1 | AJP02 | Nov. '13 | 1.398E+9 | 6.4E+6 | 2.808E+6 | 1.3E+4 | 0.0020087 | 2.5E-7 | 0.0020105 | 2.6 | 0.12 | 0.72 |
| IISlau-25_1.1 | AJP04 | Apr. '14 | 4.274E+9 | 4.7E+6 | 8.591E+6 | 9.2E+3 | 0.0020101 | 9.2E-8 | 0.0020117 | 3.3 | 0.05 | 0.30 |
| IISlau-25_2.1 | AJP04 | Apr. '14 | 4.210E+9 | 7.0E+6 | 8.461E+6 | 1.4E+4 | 0.0020095 | 1.3E-7 | 0.0020111 | 3.0 | 0.07 | 0.32 |
| IISlau-25_3.1 | AJP04 | Apr. '14 | 4.219E+9 | 3.7E+6 | 8.487E+6 | 7.3E+3 | 0.0020115 | 1.0E-7 | 0.0020132 | 4.0 | 0.05 | 0.31 |
| IISlau-25_4.1 | AJP04 | Apr. '14 | 4.198E+9 | 4.7E+6 | 8.438E+6 | 9.2E+3 | 0.0020101 | 8.8E-8 | 0.0020118 | 3.3 | 0.04 | 0.30 |
| IISlau-25_5.1 | AJP04 | Apr. '14 | 4.216E+9 | 5.2E+6 | 8.472E+6 | 1.0E+4 | 0.0020097 | 7.5E-8 | 0.0020113 | 3.1 | 0.04 | 0.30 |
| IISlau-25_6.1 | AJP04 | Apr. '14 | 4.155E+9 | 4.8E+6 | 8.347E+6 | 9.8E+3 | 0.0020090 | 9.5E-8 | 0.0020106 | 2.7 | 0.05 | 0.30 |

---

[54] Errors are 1σ unless otherwise noted

[55] Total errors, calculated in quadrature, include propagated analytical and external errors

**Appendix C.5**. Continued

| Spot Name: | Mount: | Date: | $^{16}$O Measured | $^{16}$O Error | $^{18}$O Measured | $^{18}$O Error | $^{18}$O/$^{16}$O Measured | $^{18}$O/$^{16}$O Error | $^{18}$O/$^{16}$O Corrected | δ$^{18}$O Corrected | Error (1σ) | Total Error (2σ) |
|---|---|---|---|---|---|---|---|---|---|---|---|---|
| **SLAUFRUDALUR (continued)** | | | | | | | | | | | | |
| IISlau-26_1.1 | AJP04 | Apr. '14 | 4.147E+9 | 9.2E+6 | 8.330E+6 | 1.8E+4 | 0.0020089 | 1.1E-7 | 0.0020105 | 2.6 | 0.05 | 0.31 |
| IISlau-26_2.1 | AJP04 | Apr. '14 | 4.147E+9 | 6.1E+6 | 8.336E+6 | 1.2E+4 | 0.0020104 | 6.4E-8 | 0.0020121 | 3.4 | 0.03 | 0.29 |
| IISlau-26_3.1 | AJP04 | Apr. '14 | 4.151E+9 | 3.3E+7 | 8.333E+6 | 6.5E+4 | 0.0020076 | 1.3E-7 | 0.0020092 | 2.0 | 0.07 | 0.32 |
| IISlau-26_4.1 | AJP04 | Apr. '14 | 4.061E+9 | 1.9E+7 | 8.140E+6 | 3.7E+4 | 0.0020047 | 1.1E-7 | 0.0020063 | 0.6 | 0.05 | 0.31 |
| IISlau-26_5.1 | AJP04 | Apr. '14 | 4.168E+9 | 9.6E+6 | 8.381E+6 | 1.9E+4 | 0.0020109 | 7.8E-8 | 0.0020126 | 3.7 | 0.04 | 0.30 |
| IISlau-26_6.1 | AJP04 | Apr. '14 | 4.153E+9 | 5.1E+6 | 8.345E+6 | 1.0E+4 | 0.0020096 | 8.9E-8 | 0.0020112 | 3.0 | 0.04 | 0.30 |
| IISlau-26_7.1 | AJP04 | Apr. '14 | 4.129E+9 | 6.0E+6 | 8.301E+6 | 1.2E+4 | 0.0020103 | 7.0E-8 | 0.0020119 | 3.3 | 0.03 | 0.30 |
| **VESTURHORN** | | | | | | | | | | | | |
| IIV-03a_3.1 | AJP01 | May. '13 | 2.298E+9 | 3.2E+6 | 4.593E+6 | 6.2E+3 | 0.0019984 | 1.7E-7 | 0.0020114 | 3.1 | 0.08 | 0.66 |
| IIV-03a_4.1 | AJP01 | May. '13 | 2.427E+9 | 1.4E+6 | 4.853E+6 | 3.0E+3 | 0.0019985 | 1.6E-7 | 0.0020115 | 3.1 | 0.08 | 0.66 |
| IIV-03a_5.1 | AJP01 | May. '13 | 2.382E+9 | 9.1E+5 | 4.767E+6 | 2.0E+3 | 0.0019993 | 1.7E-7 | 0.0020123 | 3.5 | 0.08 | 0.66 |
| IIV-03a_6.1 | AJP01 | May. '13 | 2.365E+9 | 1.0E+6 | 4.731E+6 | 2.2E+3 | 0.0020008 | 1.8E-7 | 0.0020138 | 4.3 | 0.09 | 0.67 |
| IIV-03a_7.1 | AJP01 | May. '13 | 2.400E+9 | 5.3E+6 | 4.796E+6 | 1.1E+4 | 0.0020005 | 1.6E-7 | 0.0020135 | 4.1 | 0.08 | 0.66 |
| IIV-03a_8.1 | AJP01 | May. '13 | 2.451E+9 | 1.5E+6 | 4.906E+6 | 3.1E+3 | 0.0020015 | 1.1E-7 | 0.0020145 | 4.7 | 0.05 | 0.65 |
| IIV-03a_9.1 | AJP01 | May. '13 | 2.457E+9 | 7.4E+5 | 4.917E+6 | 1.4E+3 | 0.0020013 | 1.1E-7 | 0.0020143 | 4.5 | 0.05 | 0.65 |
| IIV-03a_10.1 | AJP01 | May. '13 | 2.439E+9 | 1.5E+6 | 4.881E+6 | 3.1E+3 | 0.0020013 | 1.5E-7 | 0.0020142 | 4.5 | 0.08 | 0.66 |
| IIV-03a_11.1 | AJP01 | May. '13 | 2.438E+9 | 1.8E+7 | 4.877E+6 | 3.5E+4 | 0.0020007 | 4.0E-7 | 0.0020137 | 4.3 | 0.20 | 0.76 |
| IIV-03a_12.1 | AJP01 | May. '13 | 2.436E+9 | 1.3E+6 | 4.878E+6 | 2.7E+3 | 0.0020026 | 1.3E-7 | 0.0020156 | 5.2 | 0.07 | 0.66 |
| IIV-03a_13.1 | AJP01 | May. '13 | 2.182E+9 | 1.4E+7 | 4.364E+6 | 2.9E+4 | 0.0020006 | 3.1E-7 | 0.0020135 | 4.2 | 0.16 | 0.71 |
| IIV-03a_14.1 | AJP01 | May. '13 | 2.485E+9 | 7.7E+5 | 4.973E+6 | 1.8E+3 | 0.0020015 | 2.1E-7 | 0.0020144 | 4.6 | 0.11 | 0.68 |
| IIV-03a_15.1 | AJP01 | May. '13 | 2.451E+9 | 2.5E+6 | 4.907E+6 | 5.1E+3 | 0.0020017 | 1.1E-7 | 0.0020146 | 4.7 | 0.06 | 0.65 |
| IIV-03a_16.1 | AJP01 | May. '13 | 2.474E+9 | 1.6E+6 | 4.952E+6 | 3.2E+3 | 0.0020015 | 1.3E-7 | 0.0020145 | 4.6 | 0.06 | 0.65 |
| IIV-03a_17.1 | AJP01 | May. '13 | 2.490E+9 | 2.1E+6 | 4.990E+6 | 4.3E+3 | 0.0020035 | 1.4E-7 | 0.0020165 | 5.7 | 0.07 | 0.66 |
| IIV-15_1.1 | AJP04 | Apr. '14 | 4.480E+9 | 3.4E+6 | 9.018E+6 | 6.9E+3 | 0.0020128 | 1.0E-7 | 0.0020144 | 4.6 | 0.05 | 0.31 |
| IIV-15_2.1 | AJP04 | Apr. '14 | 4.474E+9 | 4.6E+6 | 9.006E+6 | 9.3E+3 | 0.0020129 | 7.3E-8 | 0.0020145 | 4.7 | 0.04 | 0.30 |
| IIV-15_3.1 | AJP04 | Apr. '14 | 4.449E+9 | 4.8E+6 | 8.953E+6 | 9.7E+3 | 0.0020123 | 1.2E-7 | 0.0020139 | 4.3 | 0.06 | 0.31 |
| IIV-15_3.2 | AJP04 | Apr. '14 | 4.447E+9 | 4.8E+6 | 8.949E+6 | 9.7E+3 | 0.0020125 | 7.0E-8 | 0.0020142 | 4.5 | 0.03 | 0.30 |
| IIV-15_4.1 | AJP04 | Apr. '14 | 4.456E+9 | 3.2E+6 | 8.970E+6 | 6.4E+3 | 0.0020129 | 7.8E-8 | 0.0020145 | 4.7 | 0.04 | 0.30 |
| IIV-15_5.1 | AJP04 | Apr. '14 | 4.458E+9 | 7.8E+6 | 8.966E+6 | 1.6E+4 | 0.0020115 | 5.0E-8 | 0.0020131 | 4.0 | 0.03 | 0.29 |
| IIV-15_6.1 | AJP04 | Apr. '14 | 4.440E+9 | 6.0E+6 | 8.939E+6 | 1.2E+4 | 0.0020125 | 9.9E-8 | 0.0020142 | 4.5 | 0.05 | 0.30 |
| IIV-15_6.2 | AJP04 | Apr. '14 | 4.432E+9 | 4.9E+6 | 8.920E+6 | 9.6E+3 | 0.0020133 | 1.5E-7 | 0.0020150 | 4.9 | 0.07 | 0.32 |
| IIV-15_7.1 | AJP04 | Apr. '14 | 4.441E+9 | 5.5E+6 | 8.939E+6 | 1.1E+4 | 0.0020129 | 8.8E-8 | 0.0020146 | 4.7 | 0.04 | 0.30 |

**Appendix C.5**. Continued

| Spot Name: | Mount: | Date: | $^{16}$O Measured | $^{16}$O Error | $^{18}$O Measured | $^{18}$O Error | $^{18}$O/$^{16}$O Measured | $^{18}$O/$^{16}$O Error | $^{18}$O/$^{16}$O Corrected | δ$^{18}$O Corrected | Error (1σ) | Total Error (2σ) |
|---|---|---|---|---|---|---|---|---|---|---|---|---|
| **VESTURHORN (continued)** | | | | | | | | | | | | |
| IIV-15_8.1 | AJP04 | Apr. '14 | 4.438E+9 | 5.6E+6 | 8.933E+6 | 1.1E+4 | 0.0020128 | 8.4E-8 | 0.0020144 | 4.6 | 0.04 | 0.30 |
| IIV-15_9.1 | AJP04 | Apr. '14 | 4.437E+9 | 5.7E+6 | 8.931E+6 | 1.2E+4 | 0.0020131 | 1.0E-7 | 0.0020147 | 4.7 | 0.05 | 0.30 |
| IIV-15_10.1 | AJP04 | Apr. '14 | 4.454E+9 | 5.1E+6 | 8.960E+6 | 1.0E+4 | 0.0020118 | 1.3E-7 | 0.0020134 | 4.1 | 0.06 | 0.31 |
| IIV-15_11.1 | AJP04 | Apr. '14 | 4.428E+9 | 4.3E+6 | 8.911E+6 | 8.5E+3 | 0.0020125 | 9.2E-8 | 0.0020141 | 4.5 | 0.05 | 0.30 |
| IIV-15_12.1 | AJP04 | Apr. '14 | 4.433E+9 | 6.9E+6 | 8.923E+6 | 1.4E+4 | 0.0020131 | 1.0E-7 | 0.0020147 | 4.7 | 0.05 | 0.31 |
| IIV-15_13.1 | AJP04 | Apr. '14 | 4.434E+9 | 9.9E+6 | 8.925E+6 | 2.0E+4 | 0.0020128 | 8.6E-8 | 0.0020145 | 4.6 | 0.04 | 0.30 |
| IIV-15_14.1 | AJP04 | Apr. '14 | 4.429E+9 | 6.9E+6 | 8.912E+6 | 1.4E+4 | 0.0020123 | 8.3E-8 | 0.0020139 | 4.3 | 0.04 | 0.30 |
| IIV-15_15.1 | AJP04 | Apr. '14 | 4.446E+9 | 6.1E+6 | 8.948E+6 | 1.2E+4 | 0.0020129 | 8.6E-8 | 0.0020145 | 4.6 | 0.04 | 0.30 |
| IIV-15_16.1 | AJP04 | Apr. '14 | 4.419E+9 | 6.6E+6 | 8.895E+6 | 1.3E+4 | 0.0020122 | 9.0E-8 | 0.0020138 | 4.3 | 0.04 | 0.30 |
| IIV-15_16.2 | AJP04 | Apr. '14 | 4.423E+9 | 5.3E+6 | 8.899E+6 | 1.1E+4 | 0.0020127 | 8.0E-8 | 0.0020144 | 4.6 | 0.04 | 0.30 |
| IIV-15_18.1 | AJP04 | Apr. '14 | 4.426E+9 | 4.9E+6 | 8.907E+6 | 1.0E+4 | 0.0020126 | 8.8E-8 | 0.0020142 | 4.5 | 0.04 | 0.30 |
| IIV-15_18.2 | AJP04 | Apr. '14 | 4.407E+9 | 6.5E+6 | 8.870E+6 | 1.3E+4 | 0.0020123 | 7.9E-8 | 0.0020140 | 4.4 | 0.04 | 0.30 |
| IIV-15_19.1 | AJP04 | Apr. '14 | 4.377E+9 | 2.8E+6 | 8.810E+6 | 5.6E+3 | 0.0020128 | 6.7E-8 | 0.0020144 | 4.6 | 0.03 | 0.30 |
| IIV-15_19.2 | AJP04 | Apr. '14 | 4.411E+9 | 4.9E+6 | 8.878E+6 | 9.7E+3 | 0.0020128 | 1.0E-7 | 0.0020144 | 4.6 | 0.05 | 0.30 |
| IIV-15_19.3 | AJP04 | Apr. '14 | 4.328E+9 | 3.9E+6 | 8.707E+6 | 7.9E+3 | 0.0020117 | 7.2E-8 | 0.0020133 | 4.1 | 0.04 | 0.30 |
| IIV-16_1.1 | AJP03 | Nov. '13 | 1.859E+9 | 7.3E+5 | 3.741E+6 | 1.6E+3 | 0.0020127 | 1.6E-7 | 0.0020143 | 4.5 | 0.08 | 0.69 |
| IIV-16_2.1 | AJP03 | Nov. '13 | 1.848E+9 | 2.0E+6 | 3.720E+6 | 4.0E+3 | 0.0020126 | 2.0E-7 | 0.0020142 | 4.5 | 0.10 | 0.70 |
| IIV-16_3.1 | AJP03 | Nov. '13 | 1.851E+9 | 1.8E+6 | 3.727E+6 | 3.6E+3 | 0.0020131 | 1.4E-7 | 0.0020147 | 4.7 | 0.07 | 0.68 |
| IIV-16_4.1 | AJP03 | Nov. '13 | 1.859E+9 | 6.4E+5 | 3.741E+6 | 1.3E+3 | 0.0020120 | 2.0E-7 | 0.0020136 | 4.2 | 0.10 | 0.70 |
| IIV-16_5.1 | AJP03 | Nov. '13 | 1.796E+9 | 3.3E+5 | 3.616E+6 | 7.0E+2 | 0.0020135 | 1.9E-7 | 0.0020151 | 5.0 | 0.10 | 0.69 |
| IIV-16_11.1 | AJP02 | Nov. '13 | 1.405E+9 | 1.9E+6 | 2.824E+6 | 3.7E+3 | 0.0020103 | 2.3E-7 | 0.0020120 | 3.4 | 0.11 | 0.71 |
| IIV-16_12.1 | AJP02 | Nov. '13 | 1.389E+9 | 6.9E+5 | 2.798E+6 | 1.5E+3 | 0.0020136 | 1.8E-7 | 0.0020153 | 5.0 | 0.09 | 0.70 |
| IIV-16_13.1 | AJP02 | Nov. '13 | 1.421E+9 | 1.2E+6 | 2.859E+6 | 2.5E+3 | 0.0020119 | 2.9E-7 | 0.0020137 | 4.2 | 0.14 | 0.74 |
| IIV-16_14.1 | AJP02 | Nov. '13 | 1.398E+9 | 6.8E+5 | 2.813E+6 | 1.2E+3 | 0.0020128 | 2.7E-7 | 0.0020145 | 4.6 | 0.13 | 0.73 |
| IIV-16_15.1 | AJP02 | Nov. '13 | 1.317E+9 | 1.1E+6 | 2.652E+6 | 2.2E+3 | 0.0020142 | 3.3E-7 | 0.0020159 | 5.4 | 0.17 | 0.75 |
| **REYÐARÁRTINDUR** | | | | | | | | | | | | |
| IIR-01_1.1 | AJP04 | Apr. '14 | 4.297E+9 | 7.6E+6 | 8.622E+6 | 1.5E+4 | 0.0020066 | 8.0E-8 | 0.0020082 | 1.5 | 0.04 | 0.30 |
| IIR-01_2.1 | AJP04 | Apr. '14 | 4.232E+9 | 4.9E+6 | 8.495E+6 | 9.6E+3 | 0.0020074 | 1.1E-7 | 0.0020091 | 1.9 | 0.06 | 0.31 |
| IIR-01_3.1 | AJP04 | Apr. '14 | 3.763E+9 | 1.5E+7 | 7.549E+6 | 2.9E+4 | 0.0020061 | 1.6E-7 | 0.0020078 | 1.3 | 0.08 | 0.33 |
| IIR-01_4.1 | AJP04 | Apr. '14 | 4.274E+9 | 6.1E+6 | 8.584E+6 | 1.2E+4 | 0.0020084 | 7.0E-8 | 0.0020101 | 2.4 | 0.03 | 0.30 |
| IIR-01_5.1 | AJP04 | Apr. '14 | 4.247E+9 | 4.8E+6 | 8.525E+6 | 9.5E+3 | 0.0020071 | 1.1E-7 | 0.0020087 | 1.8 | 0.06 | 0.31 |
| IIR-01_6.1 | AJP04 | Apr. '14 | 4.255E+9 | 6.0E+6 | 8.546E+6 | 1.2E+4 | 0.0020086 | 6.9E-8 | 0.0020102 | 2.5 | 0.03 | 0.30 |

**Appendix C.5**. Continued

| Spot Name: | Mount: | Date: | $^{16}$O Measured | $^{16}$O Error | $^{18}$O Measured | $^{18}$O Error | $^{18}$O/$^{16}$O Measured | $^{18}$O/$^{16}$O Error | $^{18}$O/$^{16}$O Corrected | δ$^{18}$O Corrected | Error (1σ) | Total Error (2σ) |
|---|---|---|---|---|---|---|---|---|---|---|---|---|
| **REYÐARÁRTINDUR** | | | | | | | | | | | | |
| IIR-01_7.1 | AJP04 | Apr. '14 | 4.249E+9 | 6.2E+6 | 8.529E+6 | 1.2E+4 | 0.0020072 | 8.4E-8 | 0.0020089 | 1.8 | 0.04 | 0.30 |
| IIR-01_8.1 | AJP04 | Apr. '14 | 3.710E+9 | 1.1E+6 | 7.445E+6 | 2.0E+3 | 0.0020069 | 1.3E-7 | 0.0020085 | 1.7 | 0.06 | 0.32 |
| IIR-01_9.1 | AJP04 | Apr. '14 | 4.186E+9 | 2.6E+6 | 8.418E+6 | 5.3E+3 | 0.0020111 | 1.4E-7 | 0.0020127 | 3.7 | 0.07 | 0.32 |
| IIR-01_10.1 | AJP04 | Apr. '14 | 4.268E+9 | 2.8E+6 | 8.577E+6 | 5.7E+3 | 0.0020096 | 8.0E-8 | 0.0020112 | 3.0 | 0.04 | 0.30 |
| IIR-01_11.1 | AJP04 | Apr. '14 | 4.158E+9 | 9.6E+6 | 8.342E+6 | 1.9E+4 | 0.0020063 | 7.8E-8 | 0.0020079 | 1.3 | 0.04 | 0.30 |
| IIR-01_12.1 | AJP04 | Apr. '14 | 4.029E+9 | 6.5E+6 | 8.082E+6 | 1.3E+4 | 0.0020062 | 7.2E-8 | 0.0020078 | 1.3 | 0.04 | 0.30 |
| IIR-01_13.1 | AJP04 | Apr. '14 | 4.276E+9 | 4.0E+6 | 8.585E+6 | 8.0E+3 | 0.0020076 | 1.2E-7 | 0.0020093 | 2.0 | 0.06 | 0.31 |
| IIR-01_14.1 | AJP04 | Apr. '14 | 4.187E+9 | 3.4E+6 | 8.408E+6 | 6.8E+3 | 0.0020082 | 8.0E-8 | 0.0020098 | 2.3 | 0.04 | 0.30 |
| IIR-03a_1.1 | AJP04 | Apr. '14 | 4.346E+9 | 8.0E+6 | 8.744E+6 | 1.6E+4 | 0.0020118 | 1.3E-7 | 0.0020134 | 4.1 | 0.07 | 0.32 |
| IIR-03a_2.1 | AJP04 | Apr. '14 | 4.475E+9 | 1.4E+7 | 8.993E+6 | 2.7E+4 | 0.0020095 | 9.7E-8 | 0.0020112 | 3.0 | 0.05 | 0.30 |
| IIR-03a_3.1 | AJP04 | Apr. '14 | 4.336E+9 | 3.9E+6 | 8.722E+6 | 7.8E+3 | 0.0020118 | 1.0E-7 | 0.0020134 | 4.1 | 0.05 | 0.30 |
| IIR-03a_4.1 | AJP04 | Apr. '14 | 4.362E+9 | 4.7E+6 | 8.780E+6 | 9.3E+3 | 0.0020131 | 1.0E-7 | 0.0020147 | 4.8 | 0.05 | 0.31 |
| IIR-03a_5.1 | AJP04 | Apr. '14 | 4.362E+9 | 4.7E+6 | 8.780E+6 | 9.4E+3 | 0.0020126 | 6.3E-8 | 0.0020142 | 4.5 | 0.03 | 0.29 |
| IIR-03a_6.1 | AJP04 | Apr. '14 | 4.422E+9 | 8.7E+6 | 8.890E+6 | 1.7E+4 | 0.0020102 | 1.2E-7 | 0.0020118 | 3.3 | 0.06 | 0.31 |
| IIR-03a_7.1 | AJP04 | Apr. '14 | 4.371E+9 | 7.3E+6 | 8.797E+6 | 1.5E+4 | 0.0020128 | 9.3E-8 | 0.0020144 | 4.6 | 0.05 | 0.30 |
| IIR-03a_8.1 | AJP04 | Apr. '14 | 4.341E+9 | 4.4E+6 | 8.736E+6 | 8.8E+3 | 0.0020127 | 1.3E-7 | 0.0020143 | 4.5 | 0.07 | 0.32 |
| IIR-03a_9.1 | AJP04 | Apr. '14 | 4.374E+9 | 5.4E+6 | 8.804E+6 | 1.1E+4 | 0.0020125 | 8.7E-8 | 0.0020141 | 4.5 | 0.04 | 0.30 |
| IIR-03a_10.1 | AJP04 | Apr. '14 | 4.336E+9 | 1.6E+6 | 8.725E+6 | 3.5E+3 | 0.0020123 | 1.2E-7 | 0.0020140 | 4.4 | 0.06 | 0.31 |
| IIR-03a_11.1 | AJP04 | Apr. '14 | 4.211E+9 | 2.6E+6 | 8.473E+6 | 5.2E+3 | 0.0020123 | 9.4E-8 | 0.0020139 | 4.3 | 0.05 | 0.30 |
| IIR-03a_13.1 | AJP04 | Apr. '14 | 4.101E+9 | 4.2E+6 | 8.254E+6 | 8.3E+3 | 0.0020126 | 9.6E-8 | 0.0020142 | 4.5 | 0.05 | 0.30 |
| IIR-03a_14.1 | AJP04 | Apr. '14 | 4.085E+9 | 4.2E+6 | 8.221E+6 | 8.3E+3 | 0.0020127 | 1.1E-7 | 0.0020143 | 4.6 | 0.05 | 0.31 |
| IIR-03a_15.1 | AJP04 | Apr. '14 | 4.132E+9 | 5.0E+6 | 8.314E+6 | 1.0E+4 | 0.0020119 | 1.3E-7 | 0.0020135 | 4.1 | 0.07 | 0.32 |
| IIR-03a_16.1 | AJP04 | Apr. '14 | 4.181E+9 | 8.1E+6 | 8.415E+6 | 1.6E+4 | 0.0020125 | 5.9E-8 | 0.0020142 | 4.5 | 0.03 | 0.29 |
| IIR-03a_17.1 | AJP04 | Apr. '14 | 4.192E+9 | 1.3E+7 | 8.434E+6 | 2.5E+4 | 0.0020119 | 1.1E-7 | 0.0020136 | 4.2 | 0.05 | 0.31 |
| IIR-03a_18.1 | AJP04 | Apr. '14 | 4.297E+9 | 7.1E+6 | 8.641E+6 | 1.4E+4 | 0.0020109 | 1.6E-7 | 0.0020126 | 3.7 | 0.08 | 0.33 |
| IIR-13_1.1 | AJP04 | Apr. '14 | 4.312E+9 | 5.0E+6 | 8.672E+6 | 1.0E+4 | 0.0020112 | 8.1E-8 | 0.0020128 | 3.8 | 0.04 | 0.30 |
| IIR-13_2.1 | AJP04 | Apr. '14 | 4.268E+9 | 2.7E+6 | 8.582E+6 | 5.4E+3 | 0.0020108 | 9.3E-8 | 0.0020125 | 3.6 | 0.05 | 0.30 |
| IIR-13_3.1 | AJP04 | Apr. '14 | 4.311E+9 | 5.7E+6 | 8.658E+6 | 1.1E+4 | 0.0020083 | 7.0E-8 | 0.0020099 | 2.3 | 0.03 | 0.30 |
| IIR-13_4.1 | AJP04 | Apr. '14 | 4.275E+9 | 4.0E+6 | 8.583E+6 | 8.3E+3 | 0.0020077 | 1.2E-7 | 0.0020094 | 2.1 | 0.06 | 0.31 |
| IIR-13_5.1 | AJP04 | Apr. '14 | 4.269E+9 | 3.0E+6 | 8.573E+6 | 6.0E+3 | 0.0020079 | 9.2E-8 | 0.0020096 | 2.2 | 0.05 | 0.30 |
| IIR-13_6.1 | AJP04 | Apr. '14 | 4.283E+9 | 4.1E+6 | 8.616E+6 | 8.3E+3 | 0.0020116 | 1.0E-7 | 0.0020132 | 4.0 | 0.05 | 0.31 |
| IIR-13_7.1 | AJP04 | Apr. '14 | 4.306E+9 | 3.1E+6 | 8.645E+6 | 6.1E+3 | 0.0020077 | 1.3E-7 | 0.0020093 | 2.1 | 0.06 | 0.31 |

**Appendix C.5**. Continued

| Spot Name: | Mount: | Date: | $^{16}$O Measured | $^{16}$O Error | $^{18}$O Measured | $^{18}$O Error | $^{18}$O/$^{16}$O Measured | $^{18}$O/$^{16}$O Error | $^{18}$O/$^{16}$O Corrected | δ$^{18}$O Corrected | Error (1σ) | Total Error (2σ) |
|---|---|---|---|---|---|---|---|---|---|---|---|---|
| **REYÐARÁRTINDUR** | | | | | | | | | | | | |
| IIR-13_8.1 | AJP04 | Apr. '14 | 4.295E+9 | 2.8E+6 | 8.625E+6 | 5.5E+3 | 0.0020083 | 8.5E-8 | 0.0020099 | 2.4 | 0.04 | 0.30 |
| IIR-13_9.1 | AJP04 | Apr. '14 | 4.321E+9 | 4.7E+6 | 8.681E+6 | 9.6E+3 | 0.0020089 | 8.6E-8 | 0.0020105 | 2.7 | 0.04 | 0.30 |
| IIR-13_10.1 | AJP04 | Apr. '14 | 4.315E+9 | 4.2E+6 | 8.665E+6 | 8.3E+3 | 0.0020080 | 1.4E-7 | 0.0020097 | 2.2 | 0.07 | 0.32 |
| IIR-13_11.1 | AJP04 | Apr. '14 | 4.340E+9 | 1.1E+7 | 8.713E+6 | 2.2E+4 | 0.0020078 | 7.4E-8 | 0.0020094 | 2.1 | 0.04 | 0.30 |
| IIR-13_12.1 | AJP04 | Apr. '14 | 4.294E+9 | 4.2E+6 | 8.628E+6 | 8.3E+3 | 0.0020093 | 8.0E-8 | 0.0020110 | 2.9 | 0.04 | 0.30 |
| IIR-13_13.1 | AJP04 | Apr. '14 | 4.299E+9 | 6.0E+6 | 8.646E+6 | 1.2E+4 | 0.0020110 | 9.6E-8 | 0.0020127 | 3.7 | 0.05 | 0.30 |
| IIR-13_14.1 | AJP04 | Apr. '14 | 4.294E+9 | 2.0E+6 | 8.637E+6 | 4.2E+3 | 0.0020115 | 8.7E-8 | 0.0020131 | 3.9 | 0.04 | 0.30 |
| IIR-13_15.1 | AJP04 | Apr. '14 | 4.296E+9 | 5.2E+6 | 8.636E+6 | 1.0E+4 | 0.0020100 | 8.1E-8 | 0.0020116 | 3.2 | 0.04 | 0.30 |
| IIR-13_16.1 | AJP04 | Apr. '14 | 4.231E+9 | 8.3E+6 | 8.492E+6 | 1.7E+4 | 0.0020073 | 8.6E-8 | 0.0020089 | 1.8 | 0.04 | 0.30 |
| IIR-13_17.1 | AJP04 | Apr. '14 | 4.241E+9 | 1.0E+7 | 8.517E+6 | 2.1E+4 | 0.0020082 | 1.1E-7 | 0.0020098 | 2.3 | 0.05 | 0.31 |
| IIR-13_18.1 | AJP04 | Apr. '14 | 4.276E+9 | 5.4E+6 | 8.602E+6 | 1.1E+4 | 0.0020117 | 9.8E-8 | 0.0020134 | 4.1 | 0.05 | 0.30 |
| IIR-13_19.1 | AJP04 | Apr. '14 | 4.249E+9 | 6.0E+6 | 8.551E+6 | 1.2E+4 | 0.0020123 | 6.0E-8 | 0.0020139 | 4.4 | 0.03 | 0.29 |
| IIR-13_20.1 | AJP04 | Apr. '14 | 4.289E+9 | 4.6E+6 | 8.615E+6 | 9.3E+3 | 0.0020085 | 8.5E-8 | 0.0020102 | 2.5 | 0.04 | 0.30 |
| **SANDFELL** | | | | | | | | | | | | |
| IISand-01_1.1 | AJP03 | Nov. '13 | 1.907E+9 | 2.2E+6 | 3.833E+6 | 4.4E+3 | 0.0020095 | 1.5E-7 | 0.0020111 | 2.9 | 0.07 | 0.68 |
| IISand-01_2.1 | AJP03 | Nov. '13 | 1.878E+9 | 7.3E+5 | 3.774E+6 | 1.6E+3 | 0.0020095 | 2.6E-7 | 0.0020111 | 2.9 | 0.13 | 0.71 |
| IISand-01_3.1 | AJP03 | Nov. '13 | 1.817E+9 | 1.4E+6 | 3.645E+6 | 3.0E+3 | 0.0020063 | 1.8E-7 | 0.0020079 | 1.3 | 0.09 | 0.69 |
| IISand-01_4.1 | AJP03 | Nov. '13 | 1.825E+9 | 3.4E+6 | 3.668E+6 | 7.0E+3 | 0.0020099 | 2.3E-7 | 0.0020115 | 3.1 | 0.11 | 0.70 |
| IISand-01_5.1 | AJP03 | Nov. '13 | 1.848E+9 | 1.1E+6 | 3.715E+6 | 2.0E+3 | 0.0020100 | 2.7E-7 | 0.0020116 | 3.2 | 0.13 | 0.72 |
| IISand-01_6.1 | AJP03 | Nov. '13 | 1.744E+9 | 3.3E+5 | 3.505E+6 | 7.5E+2 | 0.0020100 | 1.9E-7 | 0.0020116 | 3.2 | 0.09 | 0.69 |
| IISand-01_7.1 | AJP03 | Nov. '13 | 1.859E+9 | 2.1E+6 | 3.735E+6 | 4.2E+3 | 0.0020095 | 2.1E-7 | 0.0020111 | 2.9 | 0.10 | 0.70 |
| IISand-01_8.1 | AJP03 | Nov. '13 | 1.886E+9 | 2.6E+6 | 3.789E+6 | 5.0E+3 | 0.0020093 | 2.1E-7 | 0.0020110 | 2.9 | 0.10 | 0.70 |
| IISand-01_9.1 | AJP03 | Nov. '13 | 1.976E+9 | 1.4E+6 | 3.968E+6 | 2.7E+3 | 0.0020079 | 1.7E-7 | 0.0020095 | 2.2 | 0.09 | 0.69 |
| IISand-01_10.1 | AJP03 | Nov. '13 | 1.907E+9 | 3.0E+6 | 3.832E+6 | 6.2E+3 | 0.0020098 | 1.9E-7 | 0.0020114 | 3.1 | 0.09 | 0.69 |
| IISand-01_11.1 | AJP02 | Nov. '13 | 1.382E+9 | 1.6E+6 | 2.781E+6 | 3.4E+3 | 0.0020119 | 2.9E-7 | 0.0020137 | 4.2 | 0.14 | 0.74 |
| IISand-01_12.1 | AJP02 | Nov. '13 | 1.380E+9 | 1.5E+6 | 2.775E+6 | 3.0E+3 | 0.0020106 | 1.5E-7 | 0.0020123 | 3.5 | 0.07 | 0.69 |

**Appendix C.5**. Continued

| Spot Name: | Mount: | Date: | $^{16}$O Measured | $^{16}$O Error | $^{18}$O Measured | $^{18}$O Error | $^{18}$O/$^{16}$O Measured | $^{18}$O/$^{16}$O Error | $^{18}$O/$^{16}$O Corrected | δ$^{18}$O Corrected | Error (1σ) | Total Error (2σ) |
|---|---|---|---|---|---|---|---|---|---|---|---|---|
| **REYÐARÁRTINDUR** | | | | | | | | | | | | |
| IIR-13_8.1 | AJP04 | Apr. '14 | 4.295E+9 | 2.8E+6 | 8.625E+6 | 5.5E+3 | 0.0020083 | 8.5E-8 | 0.0020099 | 2.4 | 0.04 | 0.30 |
| IIR-13_9.1 | AJP04 | Apr. '14 | 4.321E+9 | 4.7E+6 | 8.681E+6 | 9.6E+3 | 0.0020089 | 8.6E-8 | 0.0020105 | 2.7 | 0.04 | 0.30 |
| IIR-13_10.1 | AJP04 | Apr. '14 | 4.315E+9 | 4.2E+6 | 8.665E+6 | 8.3E+3 | 0.0020080 | 1.4E-7 | 0.0020097 | 2.2 | 0.07 | 0.32 |
| IIR-13_11.1 | AJP04 | Apr. '14 | 4.340E+9 | 1.1E+7 | 8.713E+6 | 2.2E+4 | 0.0020078 | 7.4E-8 | 0.0020094 | 2.1 | 0.04 | 0.30 |
| IIR-13_12.1 | AJP04 | Apr. '14 | 4.294E+9 | 4.2E+6 | 8.628E+6 | 8.3E+3 | 0.0020093 | 8.0E-8 | 0.0020110 | 2.9 | 0.04 | 0.30 |
| IIR-13_13.1 | AJP04 | Apr. '14 | 4.299E+9 | 6.0E+6 | 8.646E+6 | 1.2E+4 | 0.0020110 | 9.6E-8 | 0.0020127 | 3.7 | 0.05 | 0.30 |
| IIR-13_14.1 | AJP04 | Apr. '14 | 4.294E+9 | 2.0E+6 | 8.637E+6 | 4.2E+3 | 0.0020115 | 8.7E-8 | 0.0020131 | 3.9 | 0.04 | 0.30 |
| IIR-13_15.1 | AJP04 | Apr. '14 | 4.296E+9 | 5.2E+6 | 8.636E+6 | 1.0E+4 | 0.0020100 | 8.1E-8 | 0.0020116 | 3.2 | 0.04 | 0.30 |
| IIR-13_16.1 | AJP04 | Apr. '14 | 4.231E+9 | 8.3E+6 | 8.492E+6 | 1.7E+4 | 0.0020073 | 8.6E-8 | 0.0020089 | 1.8 | 0.04 | 0.30 |
| IIR-13_17.1 | AJP04 | Apr. '14 | 4.241E+9 | 1.0E+7 | 8.517E+6 | 2.1E+4 | 0.0020082 | 1.1E-7 | 0.0020098 | 2.3 | 0.05 | 0.31 |
| IIR-13_18.1 | AJP04 | Apr. '14 | 4.276E+9 | 5.4E+6 | 8.602E+6 | 1.1E+4 | 0.0020117 | 9.8E-8 | 0.0020134 | 4.1 | 0.05 | 0.30 |
| IIR-13_19.1 | AJP04 | Apr. '14 | 4.249E+9 | 6.0E+6 | 8.551E+6 | 1.2E+4 | 0.0020123 | 6.0E-8 | 0.0020139 | 4.4 | 0.03 | 0.29 |
| IIR-13_20.1 | AJP04 | Apr. '14 | 4.289E+9 | 4.6E+6 | 8.615E+6 | 9.3E+3 | 0.0020085 | 8.5E-8 | 0.0020102 | 2.5 | 0.04 | 0.30 |
| **SANDFELL** | | | | | | | | | | | | |
| IISand-01_1.1 | AJP03 | Nov. '13 | 1.907E+9 | 2.2E+6 | 3.833E+6 | 4.4E+3 | 0.0020095 | 1.5E-7 | 0.0020111 | 2.9 | 0.07 | 0.68 |
| IISand-01_2.1 | AJP03 | Nov. '13 | 1.878E+9 | 7.3E+5 | 3.774E+6 | 1.6E+3 | 0.0020095 | 2.6E-7 | 0.0020111 | 2.9 | 0.13 | 0.71 |
| IISand-01_3.1 | AJP03 | Nov. '13 | 1.817E+9 | 1.4E+6 | 3.645E+6 | 3.0E+3 | 0.0020063 | 1.8E-7 | 0.0020079 | 1.3 | 0.09 | 0.69 |
| IISand-01_4.1 | AJP03 | Nov. '13 | 1.825E+9 | 3.4E+6 | 3.668E+6 | 7.0E+3 | 0.0020099 | 2.3E-7 | 0.0020115 | 3.1 | 0.11 | 0.70 |
| IISand-01_5.1 | AJP03 | Nov. '13 | 1.848E+9 | 1.1E+6 | 3.715E+6 | 2.0E+3 | 0.0020100 | 2.7E-7 | 0.0020116 | 3.2 | 0.13 | 0.72 |
| IISand-01_6.1 | AJP03 | Nov. '13 | 1.744E+9 | 3.3E+5 | 3.505E+6 | 7.5E+2 | 0.0020100 | 1.9E-7 | 0.0020116 | 3.2 | 0.09 | 0.69 |
| IISand-01_7.1 | AJP03 | Nov. '13 | 1.859E+9 | 2.1E+6 | 3.735E+6 | 4.2E+3 | 0.0020095 | 2.1E-7 | 0.0020111 | 2.9 | 0.10 | 0.70 |
| IISand-01_8.1 | AJP03 | Nov. '13 | 1.886E+9 | 2.6E+6 | 3.789E+6 | 5.0E+3 | 0.0020093 | 2.1E-7 | 0.0020110 | 2.9 | 0.10 | 0.70 |
| IISand-01_9.1 | AJP03 | Nov. '13 | 1.976E+9 | 1.4E+6 | 3.968E+6 | 2.7E+3 | 0.0020079 | 1.7E-7 | 0.0020095 | 2.2 | 0.09 | 0.69 |
| IISand-01_10.1 | AJP03 | Nov. '13 | 1.907E+9 | 3.0E+6 | 3.832E+6 | 6.2E+3 | 0.0020098 | 1.9E-7 | 0.0020114 | 3.1 | 0.09 | 0.69 |
| IISand-01_11.1 | AJP02 | Nov. '13 | 1.382E+9 | 1.6E+6 | 2.781E+6 | 3.4E+3 | 0.0020119 | 2.9E-7 | 0.0020137 | 4.2 | 0.14 | 0.74 |
| IISand-01_12.1 | AJP02 | Nov. '13 | 1.380E+9 | 1.5E+6 | 2.775E+6 | 3.0E+3 | 0.0020106 | 1.5E-7 | 0.0020123 | 3.5 | 0.07 | 0.69 |

**Appendix C.6**. Zircon Lu-Hf isotope compositions, measured *in-situ* by LA-MC-ICP-MS

| **Spot Name** | **Mount** | **Total Hf Beam (V)** | **$^{176}$Hf/$^{177}$Hf** | **2SE** | **$^{176}$Lu/$^{177}$Hf** | **2SE** | **$^{176}$Yb/$^{177}$Hf** | **2SE** | **$^{178}$Hf/$^{177}$Hf** | **2SE** | **$\varepsilon_{Hf}$** | **2SE** |
|---|---|---|---|---|---|---|---|---|---|---|---|---|
| | | | | | | **SLAUFRUDALUR** | | | | | | |
| IISlau-12_1 | AJP01 | 12.5 | 0.283170 | 4.2E-5 | 0.00175 | 1.3E-4 | 0.0512 | 4.2E-3 | 1.467179 | 4.4E-5 | **13.6** | **1.5** |
| IISlau-12_2 | AJP01 | 10.6 | 0.283112 | 3.0E-5 | 0.00127 | 2.9E-5 | 0.0348 | 9.3E-4 | 1.467157 | 3.5E-5 | **11.5** | **1.1** |
| IISlau-12_7 | AJP01 | 11.5 | 0.283085 | 5.5E-5 | 0.00221 | 6.1E-5 | 0.0639 | 2.1E-3 | 1.467123 | 4.5E-5 | **10.6** | **1.9** |
| IISlau-12_12 | AJP03 | 10.6 | 0.283147 | 5.6E-5 | 0.00273 | 2.6E-4 | 0.0865 | 8.6E-3 | 1.467155 | 4.9E-5 | **12.8** | **2.0** |
| IISlau-12_13 | AJP03 | 12.0 | 0.283115 | 2.8E-5 | 0.00174 | 8.3E-5 | 0.0545 | 3.0E-3 | 1.467187 | 4.2E-5 | **11.7** | **1.0** |
| IISlau-12_14.1 | AJP03 | 11.9 | 0.283086 | 4.9E-5 | 0.00241 | 1.0E-4 | 0.0742 | 2.1E-3 | 1.467101 | 5.0E-5 | **10.6** | **1.7** |
| IISlau-12_15 | AJP03 | 16.1 | 0.283089 | 4.0E-5 | 0.00165 | 5.3E-5 | 0.0528 | 1.2E-3 | 1.467154 | 5.3E-5 | **10.7** | **1.4** |
| IISlau-12_16 | AJP03 | 12.8 | 0.283146 | 3.8E-5 | 0.00370 | 3.7E-4 | 0.1240 | 1.3E-2 | 1.467117 | 3.3E-5 | **12.8** | **1.3** |
| IISlau-12_17 | AJP03 | 14.3 | 0.283148 | 2.7E-5 | 0.00177 | 3.9E-5 | 0.0560 | 1.3E-3 | 1.467168 | 3.8E-5 | **12.8** | **1.0** |
| IISlau-22_1 | AJP03 | 14.2 | 0.283086 | 4.3E-5 | 0.00152 | 3.0E-5 | 0.0479 | 8.5E-4 | 1.467120 | 4.7E-5 | **10.6** | **1.5** |
| IISlau-22_3 | AJP03 | 13.3 | 0.283133 | 3.2E-5 | 0.00473 | 1.3E-4 | 0.1599 | 2.6E-3 | 1.467166 | 3.8E-5 | **12.3** | **1.1** |
| IISlau-22_5 | AJP03 | 15.1 | 0.283105 | 2.9E-5 | 0.00115 | 3.7E-5 | 0.0367 | 7.3E-4 | 1.467166 | 3.3E-5 | **11.3** | **1.0** |
| IISlau-22_6 | AJP03 | 14.6 | 0.283099 | 4.8E-5 | 0.00196 | 1.2E-4 | 0.0627 | 3.3E-3 | 1.467113 | 5.0E-5 | **11.1** | **1.7** |
| IISlau-22_7 | AJP03 | 11.6 | 0.283056 | 4.0E-5 | 0.00205 | 1.3E-4 | 0.0642 | 3.6E-3 | 1.467140 | 4.4E-5 | **9.6** | **1.4** |
| IISlau-22_12 | AJP02 | 18.3 | 0.283135 | 5.1E-5 | 0.00081 | 8.3E-5 | 0.0245 | 2.8E-3 | 1.467235 | 4.3E-5 | **12.4** | **1.8** |
| IISlau-22_14 | AJP03 | 12.8 | 0.283015 | 5.4E-5 | 0.00228 | 2.4E-4 | 0.0701 | 6.2E-3 | 1.467120 | 6.0E-5 | **8.1** | **1.9** |
| IISlau-22_15 | AJP03 | 13.9 | 0.283145 | 3.3E-5 | 0.00287 | 2.9E-4 | 0.0990 | 1.1E-2 | 1.467162 | 3.7E-5 | **12.7** | **1.2** |
| IISlau-25_3.1 | AJP04 | 9.4 | 0.283115 | 3.7E-5 | 0.00159 | 3.1E-5 | 0.0519 | 1.2E-3 | 1.467130 | 3.8E-5 | **11.7** | **1.3** |
| | | | | | | **VESTURHORN** | | | | | | |
| IIV-03a_2 | AJP01 | 14.6 | 0.283165 | 2.6E-5 | 0.00306 | 2.2E-4 | 0.0948 | 7.4E-3 | 1.467134 | 3.4E-5 | **13.4** | **0.9** |
| IIV-03a_4 | AJP01 | 18.8 | 0.283206 | 4.3E-5 | 0.00179 | 9.4E-5 | 0.0503 | 2.1E-3 | 1.467200 | 5.1E-5 | **14.9** | **1.5** |
| IIV-03a_6 | AJP01 | 13.8 | 0.283184 | 3.0E-5 | 0.00246 | 2.6E-4 | 0.0748 | 7.7E-3 | 1.467182 | 3.6E-5 | **14.1** | **1.1** |
| IIV-03a_8 | AJP01 | 21.9 | 0.283144 | 4.3E-5 | 0.00249 | 1.8E-4 | 0.0769 | 5.4E-3 | 1.467179 | 5.4E-5 | **12.7** | **1.5** |
| IIV-03a_10 | AJP01 | 12.9 | 0.283122 | 3.4E-5 | 0.00240 | 8.6E-5 | 0.0703 | 2.1E-3 | 1.467156 | 3.5E-5 | **11.9** | **1.2** |
| IIV-03a_11 | AJP01 | 16.1 | 0.283129 | 2.9E-5 | 0.00192 | 3.8E-5 | 0.0607 | 1.3E-3 | 1.467152 | 3.2E-5 | **12.1** | **1.0** |
| IIV-03a_12 | AJP01 | 19.7 | 0.283178 | 3.2E-5 | 0.00227 | 7.4E-5 | 0.0689 | 2.4E-3 | 1.467171 | 3.0E-5 | **13.9** | **1.1** |
| IIV-03a_13 | AJP01 | 16.2 | 0.283160 | 3.3E-5 | 0.00308 | 2.9E-4 | 0.0975 | 9.3E-3 | 1.467186 | 3.6E-5 | **13.2** | **1.2** |
| IIV-03a_14 | AJP01 | 19.9 | 0.283153 | 2.8E-5 | 0.00233 | 8.1E-5 | 0.0713 | 2.6E-3 | 1.467148 | 2.9E-5 | **13.0** | **1.0** |
| IIV-03a_19 | AJP01 | 16.0 | 0.283248 | 3.7E-5 | 0.00499 | 8.6E-4 | 0.1500 | 2.6E-2 | 1.467194 | 5.3E-5 | **16.4** | **1.3** |

**Appendix C.6**. Continued

| Spot Name | Mount | Total Hf Beam (V) | $^{176}$Hf/$^{177}$Hf | 2SE | $^{176}$Lu/$^{177}$Hf | 2SE | $^{176}$Yb/$^{177}$Hf | 2SE | $^{178}$Hf/$^{177}$Hf | 2SE | $\varepsilon_{Hf}$ | 2SE |
|---|---|---|---|---|---|---|---|---|---|---|---|---|
| | | | | | | **VESTURHORN (Continued)** | | | | | | |
| IIV-15_2.1 | AJP04 | 18.2 | 0.283137 | 2.6E-5 | 0.00167 | 1.9E-5 | 0.0475 | 5.2E-4 | 1.467161 | 3.4E-5 | **12.4** | **0.9** |
| IIV-15_3.1 | AJP04 | 16.3 | 0.283156 | 2.4E-5 | 0.00104 | 1.3E-4 | 0.0300 | 3.9E-3 | 1.467172 | 3.2E-5 | **13.1** | **0.8** |
| IIV-15_4.1 | AJP04 | 19.5 | 0.283147 | 2.5E-5 | 0.00058 | 1.7E-5 | 0.0168 | 5.9E-4 | 1.467167 | 3.0E-5 | **12.8** | **0.9** |
| IIV-15_6.1 | AJP04 | 15.9 | 0.283090 | 2.9E-5 | 0.00097 | 5.6E-5 | 0.0276 | 1.5E-3 | 1.467160 | 3.2E-5 | **10.8** | **1.0** |
| IIV-15_7.1 | AJP04 | 17.2 | 0.283090 | 2.7E-5 | 0.00065 | 4.2E-5 | 0.0180 | 1.1E-3 | 1.467140 | 4.2E-5 | **10.8** | **1.0** |
| IIV-15_9.1 | AJP04 | 15.8 | 0.283148 | 1.9E-5 | 0.00092 | 5.8E-5 | 0.0249 | 1.8E-3 | 1.467147 | 2.9E-5 | **12.8** | **0.7** |
| IIV-15_10.1 | AJP04 | 10.9 | 0.283171 | 4.2E-5 | 0.00061 | 3.8E-5 | 0.0174 | 9.2E-4 | 1.467182 | 4.5E-5 | **13.6** | **1.5** |
| IIV-15_11.1 | AJP04 | 17.4 | 0.283126 | 2.6E-5 | 0.00061 | 9.0E-6 | 0.0174 | 3.0E-4 | 1.467163 | 4.2E-5 | **12.0** | **0.9** |
| IIV-15_15.1 | AJP04 | 16.6 | 0.283117 | 2.2E-5 | 0.00074 | 3.9E-5 | 0.0206 | 1.1E-3 | 1.467156 | 3.1E-5 | **11.7** | **0.8** |
| IIV-15_16.1 | AJP04 | 16.5 | 0.283128 | 1.9E-5 | 0.00079 | 2.2E-5 | 0.0219 | 4.9E-4 | 1.467165 | 2.9E-5 | **12.1** | **0.7** |
| IIV-15_17.1 | AJP04 | 17.3 | 0.283127 | 2.5E-5 | 0.00043 | 1.2E-5 | 0.0117 | 3.2E-4 | 1.467160 | 2.8E-5 | **12.1** | **0.9** |
| IIV-15_18.1 | AJP04 | 16.1 | 0.283131 | 1.8E-5 | 0.00104 | 5.5E-6 | 0.0264 | 1.7E-4 | 1.467146 | 3.3E-5 | **12.2** | **0.6** |
| IIV-15_19.1 | AJP04 | 16.7 | 0.283119 | 1.8E-5 | 0.00084 | 2.9E-5 | 0.0230 | 7.6E-4 | 1.467161 | 2.7E-5 | **11.8** | **0.6** |
| IIV-15_19.2 | AJP04 | 18.7 | 0.283136 | 1.7E-5 | 0.00048 | 9.3E-6 | 0.0131 | 2.4E-4 | 1.467168 | 2.8E-5 | **12.4** | **0.6** |
| IIV-16_1 | AJP03 | 15.7 | 0.283167 | 3.0E-5 | 0.00593 | 2.9E-5 | 0.1876 | 3.0E-4 | 1.467191 | 3.1E-5 | **13.5** | **1.1** |
| IIV-16_2 | AJP03 | 14.0 | 0.283124 | 2.9E-5 | 0.00242 | 6.5E-5 | 0.0727 | 2.0E-3 | 1.467143 | 3.4E-5 | **12.0** | **1.0** |
| IIV-16_3.1 | AJP03 | 11.7 | 0.283161 | 3.9E-5 | 0.00299 | 2.2E-4 | 0.0897 | 6.6E-3 | 1.467132 | 4.9E-5 | **13.3** | **1.4** |
| IIV-16_4 | AJP03 | 13.7 | 0.283115 | 3.1E-5 | 0.00148 | 1.2E-4 | 0.0427 | 3.6E-3 | 1.467169 | 3.9E-5 | **11.7** | **1.1** |
| IIV-16_7 | AJP03 | 12.4 | 0.283109 | 3.1E-5 | 0.00198 | 1.1E-4 | 0.0586 | 3.1E-3 | 1.467162 | 4.4E-5 | **11.4** | **1.1** |
| IIV-16_9 | AJP03 | 15.2 | 0.283095 | 4.4E-5 | 0.00286 | 3.0E-4 | 0.0879 | 9.6E-3 | 1.467160 | 4.1E-5 | **11.0** | **1.6** |
| IIV-16_10 | AJP03 | 14.6 | 0.283159 | 3.1E-5 | 0.00117 | 1.8E-4 | 0.0344 | 5.9E-3 | 1.467143 | 4.5E-5 | **13.2** | **1.1** |
| IIV-16_13 | AJP02 | 15.6 | 0.283140 | 2.8E-5 | 0.00205 | 9.4E-5 | 0.0604 | 3.2E-3 | 1.467147 | 3.6E-5 | **12.5** | **1.0** |
| | | | | | | **LÝSUSKARÐ** | | | | | | |
| IILys-07a_12.1 | AJP04 | 6.3 | 0.283063 | 5.0E-5 | 0.00155 | 1.1E-4 | 0.0472 | 3.8E-3 | 1.467196 | 4.9E-5 | **9.8** | **1.8** |
| IILys-07a_14.1 | AJP04 | 15.2 | 0.283130 | 4.4E-5 | 0.00461 | 2.0E-4 | 0.1845 | 7.8E-3 | 1.467158 | 3.8E-5 | **12.2** | **1.6** |
| IILys-07a_23.1 | AJP04 | 14.7 | 0.283117 | 4.7E-5 | 0.00613 | 2.2E-4 | 0.2346 | 8.5E-3 | 1.467181 | 4.5E-5 | **11.7** | **1.7** |
| IILys-07a_24.1 | AJP04 | 13.0 | 0.283037 | 4.2E-5 | 0.00667 | 5.3E-4 | 0.2530 | 1.9E-2 | 1.467086 | 4.5E-5 | **8.9** | **1.5** |

**Appendix C.6**. Continued

| **Spot Name** | **Mount** | **Total Hf Beam (V)** | **$^{176}$Hf/$^{177}$Hf** | **2SE** | **$^{176}$Lu/$^{177}$Hf** | **2SE** | **$^{176}$Yb/$^{177}$Hf** | **2SE** | **$^{178}$Hf/$^{177}$Hf** | **2SE** | **$\varepsilon_{Hf}$** | **2SE** |
|---|---|---|---|---|---|---|---|---|---|---|---|---|
| **REYÐARÁRTINDUR** | | | | | | | | | | | | |
| IIR-13_19.1 | AJP04 | 13.4 | 0.283127 | 3.6E-5 | 0.00177 | 5.2E-5 | 0.0504 | 1.6E-3 | 1.467159 | 3.9E-5 | **12.1** | **1.3** |
| IIR-13_20.1 | AJP04 | 11.8 | 0.283082 | 4.0E-5 | 0.00175 | 5.3E-5 | 0.0522 | 1.9E-3 | 1.467131 | 4.4E-5 | **10.5** | **1.4** |
| **SANDFELL** | | | | | | | | | | | | |
| IISand-01_4 | AJP03 | 14.8 | 0.283122 | 3.6E-5 | 0.00260 | 1.8E-4 | 0.0789 | 4.9E-3 | 1.467105 | 4.7E-5 | **11.9** | **1.3** |
| IISand-01_5 | AJP03 | 15.1 | 0.283102 | 5.3E-5 | 0.00328 | 8.6E-4 | 0.1120 | 3.2E-2 | 1.467104 | 4.6E-5 | **11.2** | **1.9** |
| IISand-01_7 | AJP03 | 16.5 | 0.283153 | 3.3E-5 | 0.00212 | 1.5E-5 | 0.0647 | 5.1E-4 | 1.467123 | 3.5E-5 | **13.0** | **1.2** |
| IISand-01_10 | AJP03 | 16.2 | 0.283187 | 3.0E-5 | 0.00216 | 2.0E-4 | 0.0745 | 7.9E-3 | 1.467181 | 2.9E-5 | **14.2** | **1.1** |
| IISand-01_11 | AJP02 | 15.4 | 0.283177 | 2.3E-5 | 0.00225 | 8.2E-5 | 0.0667 | 2.6E-3 | 1.467123 | 3.1E-5 | **13.8** | **0.8** |
| IISand-01_13 | AJP02 | 16.3 | 0.283174 | 2.1E-5 | 0.00156 | 8.8E-5 | 0.0448 | 2.1E-3 | 1.467192 | 3.5E-5 | **13.7** | **0.7** |
| IISand-01_14 | AJP03 | 16.4 | 0.283168 | 5.2E-5 | 0.00373 | 2.9E-4 | 0.1250 | 1.3E-2 | 1.467149 | 4.4E-5 | **13.5** | **1.8** |
| IISand-01_15L | AJP03 | 19.9 | 0.283220 | 3.9E-5 | 0.00256 | 2.6E-5 | 0.0802 | 7.8E-4 | 1.467198 | 4.6E-5 | **15.4** | **1.4** |

# APPENDIX D

# ADDITIONAL DATA NOT DISCUSSED IN THIS DISSERTATION

**Appendix D.1**. Whole-rock Hf isotope compositions, measured by Solution MC-ICP-MS

| Sample | $^{176}$Hf/$^{177}$Hf | 2σ | $^{178}$Hf/$^{177}$Hf | 2σ | $^{180}$Hf/$^{177}$Hf | 2σ | $\varepsilon_{Hf}$ | 2σ |
|---|---|---|---|---|---|---|---|---|
| **Austurhorn Intrusive Complex** | | | | | | | | |
| IA-NS-2 | 0.283140 | ± 7 | 1.467182 | ± 11 | 1.886801 | ± 26 | 12.6 | ± 0.3 |
| IA-NS-4b | 0.283141 | ± 7 | 1.467173 | ± 12 | 1.886785 | ± 23 | 12.6 | ± 0.2 |
| IA-NS-6 | 0.283161 | ± 8 | 1.467184 | ± 16 | 1.886733 | ± 32 | 13.3 | ± 0.3 |
| IA-NS-7 | 0.283182 | ± 6 | 1.467189 | ± 10 | 1.886814 | ± 16 | 14.0 | ± 0.2 |
| IA-NS-9 | 0.283157 | ± 8 | 1.467171 | ± 18 | 1.887282 | ± 34 | 13.2 | ± 0.3 |
| IA-G-1 | 0.283138 | ± 6 | 1.467179 | ± 10 | 1.886861 | ± 21 | 12.5 | ± 0.2 |
| IA-G-3 | 0.283134 | ± 8 | 1.467159 | ± 14 | 1.887068 | ± 28 | 12.3 | ± 0.3 |
| IA-G-5 | 0.283128 | ± 7 | 1.467163 | ± 15 | 1.886663 | ± 22 | 12.1 | ± 0.3 |
| **Slaufrudalur Intrusive Complex** | | | | | | | | |
| IISlau-25 | 0.283132 | ± 7 | 1.467169 | ± 12 | 1.886809 | ± 23 | 12.3 | ± 0.2 |
| IISlau-42 | 0.283133 | ± 6 | 1.467177 | ± 12 | 1.886804 | ± 22 | 12.3 | ± 0.2 |
| IISlau-22 | 0.283135 | ± 6 | 1.457181 | ± 11 | 1.886855 | ± 22 | 12.4 | ± 0.2 |
| IISlau-26 | 0.283133 | ± 7 | 1.467181 | ± 10 | 1.886892 | ± 20 | 12.3 | ± 0.2 |
| IISlau-12 | 0.283129 | ± 6 | 1.467163 | ± 10 | 1.886790 | ± 18 | 12.2 | ± 0.2 |

**Appendix D.2**. Whole-rock Nd isotope compositions, measured by Solution MC-ICP-MS

| **Sample** | **$^{143}$Nd/$^{144}$Nd** | **2σ** | **$^{145}$Nd/$^{144}$Nd** | **2σ** | **$^{148}$Nd/$^{144}$Nd** | **2σ** | **$^{150}$Nd/$^{144}$Nd** | **2σ** | **$\varepsilon_{Nd}$** | **2σ** |
|---|---|---|---|---|---|---|---|---|---|---|
| **Austurhorn Intrusive Complex** | | | | | | | | | | |
| IA-NS-2 | 0.51298 | ±9 | 0.348393 | ±7 | 0.242086 | ±5.7 | 0.236870 | ±8.1 | 6.8 | ± 0.2 |
| IA-NS-4b | 0.51298 | ±9 | 0.348412 | ±6 | 0.241586 | ±6.0 | 0.236432 | ±9.1 | 6.8 | ± 0.2 |
| IA-NS-6 | 0.51298 | ±8 | 0.348417 | ±6 | 0.241576 | ±9.0 | 0.236433 | ±10.0 | 6.8 | ± 0.2 |
| IA-NS-7 | 0.51299 | ±8 | 0.348424 | ±6 | 0.241571 | ±6.1 | 0.236420 | ±7.2 | 7.1 | ± 0.2 |
| IA-NS-9 | 0.51301 | ±10 | 0.348422 | ±6 | 0.241555 | ±8.0 | 0.236418 | ±9.0 | 7.3 | ± 0.2 |
| IA-G-1 | 0.51300 | ±9 | 0.348414 | ±7 | 0.241568 | ±5.5 | 0.236430 | ±8.5 | 7.3 | ± 0.2 |
| IA-G-3 | 0.51300 | ±6 | 0.348415 | ±5 | 0.241558 | ±7.0 | 0.236483 | ±10.0 | 7.3 | ± 0.1 |
| IA-G-5 | 0.51301 | ±10 | 0.348416 | ±6 | 0.241566 | ±7.6 | 0.236415 | ±10.4 | 7.4 | ± 0.2 |
| **Slaufrudalur Intrusive Complex** | | | | | | | | | | |
| IISlau-25 | 0.51303 | ±8 | 0.348324 | ±7 | 0.241580 | ±4.7 | 0.236426 | ±7.5 | 7.8 | ± 0.2 |
| IISlau-42 | 0.51303 | ±8 | 0.348417 | ±7 | 0.241589 | ±5.7 | 0.236447 | ±7.7 | 7.8 | ± 0.2 |
| IISlau-22 | 0.51303 | ±9 | 0.348420 | ±7 | 0.241560 | ±5.3 | 0.236415 | ±7.7 | 7.8 | ± 0.2 |
| IISlau-26 | 0.51301 | ±9 | 0.348418 | ±5 | 0.241596 | ±6.4 | 0.236447 | ±9.4 | 7.5 | ± 0.2 |
| IISlau-12 | 0.51303 | ±11 | 0.348429 | ±8 | 0.241570 | ±6.3 | 0.236430 | ±10.5 | 7.9 | ± 0.2 |

**Appendix D.3**. Whole-rock Pb isotope compositions, measured by Solution MC-ICP-MS

| Sample | $^{206}Pb/^{204}Pb$ | 2σ | $^{207}Pb/^{204}Pb$ | 2σ | $^{208}Pb/^{204}Pb$ | 2σ | $^{207}Pb/^{206}Pb$ | 2σ | $^{208}Pb/^{206}Pb$ | 2σ |
|---|---|---|---|---|---|---|---|---|---|---|
| **Austurhorn Intrusive Complex** | | | | | | | | | | |
| IA-NS-2 | 18.4630 | ±8 | 15.4795 | ±9 | 38.174 | ±2 | 0.83841 | ±1 | 2.06759 | ±6 |
| IA-NS-4b | 18.4965 | ±7 | 15.4945 | ±7 | 38.165 | ±2 | 0.83769 | ±1 | 2.06334 | ±5 |
| IA-NS-7 | 18.5147 | ±9 | 15.4827 | ±9 | 38.171 | ±3 | 0.83625 | ±2 | 2.06165 | ±7 |
| IA-NS-9 | 18.5265 | ±6 | 15.4857 | ±5 | 38.168 | ±1 | 0.83587 | ±1 | 2.06017 | ±4 |
| IA-G-1 | 18.4495 | ±6 | 15.4796 | ±5 | 38.142 | ±2 | 0.83902 | ±1 | 2.06736 | ±4 |
| IA-G-5 | 18.2859 | ±7 | 15.4614 | ±6 | 37.966 | ±2 | 0.84555 | ±1 | 2.07624 | ±3 |
| **Slaufrudalur Intrusive Complex** | | | | | | | | | | |
| IISlau-25 | 18.5526 | ±6 | 15.4930 | ±5 | 38.255 | ±1 | 0.83509 | ±1 | 2.06195 | ±3 |
| IISlau-42 | 18.5517 | ±6 | 15.4909 | ±5 | 38.254 | ±1 | 0.83502 | ±1 | 2.06205 | ±3 |
| IISlau-22 | 18.6238 | ±7 | 15.4950 | ±7 | 38.291 | ±2 | 0.83201 | ±1 | 2.05603 | ±5 |
| IISlau-26 | 18.5442 | ±5 | 15.4900 | ±3 | 38.236 | ±1 | 0.83530 | ±1 | 2.06186 | ±3 |
| IISlau-12 | 18.5307 | ±6 | 15.4915 | ±5 | 38.237 | ±1 | 0.83599 | ±1 | 2.06342 | ±3 |

# REFERENCES

Anders, E., Grevesse, N., 1989. Abundances of the elements: Meteoritic and solar. *Geochimica et Cosmochimica Acta* 53:197-214.

Anderson, A.T., Davis, A.M., Lu, F.Q., 2000. Evolution of Bishop Tuff rhyolitic magma based on melt and magnetite inclusions and zoned phenocrysts. *Journal of Petrology* 41, 449-473.

Arth, J.G., 1976. Behavior of trace-elements during magmatic processes - summary of theoretical models and their applications. *Journal of Research of the US Geological Survey* 4, 41-47.

Bachmann, O., Dungan, M.A., Bussy, F., 2005. Insights into shallow magmatic processes in large silicic magma bodies: the trace element record in the Fish Canyon magma body, Colorado. *Contributions to Mineralogy and Petrology* 149: 338-349.

Bachmann, O., Bergantz, G.W., 2004. On the origin of crystal-poor rhyolites: Extracted from batholithic crystal mushes. *Journal of Petrology* 45, 1565-1582.

-, 2008. Rhyolites and their Source Mushes across Tectonic Settings. *Journal of Petrology* 49, 2277-2285.

Bachmann, O., Dungan, M.A., Bussy, F., 2005. Insights into shallow magmatic processes in large silicic magma bodies: the trace element record in the Fish Canyon magma body, Colorado. *Contributions to Mineralogy and Petrology* 149, 338-349.

Bacon, C.R., Druitt, T.H., 1988. Compositional evolution of the zoned calcalkaline magma chamber of Mount Mazama, Crater Lake, Oregon. *Contributions to Mineralogy and Petrology* 98, 224-256.

Barth, A.P., Wooden, J.L., 2010. Coupled elemental and isotopic analyses of polygenetic zircons from granitic rocks by ion microprobe, with implications for melt evolution and the sources of granitic magmas. *Chemical Geology* 277, 149-159.

Bea, F., Pereira, M.D., Stroh, A., 1994. Mineral leucosome trace-element partitioning in a peraluminous migmatite (a laser ablation-ICP-MS study). *Chemical Geology* 117, 291-312.

Belousova, E.A., Griffin, W.L., O'Reilly, S.Y., Fisher, N.I., 2002. Igneous zircon: trace element composition as an indicator of source rock type. *Contributions to Mineralogy and Petrology* 143: 602–622.

Beswick, A.E., 1965. A Study of the Slaufrudalur Granophyre Intrusion, South-East Iceland [Ph.D. thesis, unpub.]: Imperial College, London, 284 p.

Bindeman, I.N., Valley, J.W., 2001. Low-delta O-18 rhyolites from Yellowstone: Magmatic evolution based on analyses of zircons and individual phenocrysts. *Journal of Petrology* 42, 1491-1517.

Bindeman, I., 2006. The secretes of supervolcanoes: Microscopic crystals of volcanic ash are revealing surprising clues about the world's most devastating eruptions. *Scientific American*, 294(**6**): 36-43.

-, 2008. Oxygen Isotopes in Mantle and Crustal Magmas as Revealed by Single Crystal Analysis. Minerals, Inclusions and Volcanic Processes 69, 445-478.

Bindeman, I., Fu, B., Kita, N., Valley, J., 2008a. Origin and evolution of Yellowstone silicic magmatism based on ion microprobe analysis of isotopically-zoned zircons. *Journal of Petrology* 49: 163-193.

Bindeman, I., Gurenko, A., Sigmarsson, O., Chaussidon, M., 2008b. Oxygen isotope heterogeneity and disequilibria of olivine crystals in large volume Holocene basalts from Iceland: Evidence for magmatic digestion and erosion of Pleistocene hyaloclastites. *Geochimica Et Cosmochimica Acta* 72, 4397-4420.

Bindeman, I.N., Schmitt, A.K., Evans, D.A.D., 2010. Limits of hydrosphere-lithosphere interaction: Origin of the lowest-known delta O-18 silicate rock on Earth in the Paleoproterozoic Karelian rift. *Geology* 38, 631-634.

Bindeman, I., Gurenko, A., Carley, T., Miller, C., Martin, E., Sigmarsson, O., 2012. Silicic magma petrogenesis in Iceland by remelting of hydrothermally altered crust based on oxygen isotope diversity and disequilibria between zircon and magma with implications for MORB. *Terra Nova* 24, 227-232.

Bindeman, I.N., Serebryakov, N.S., Schmitt, A.K., Vazquez, J.A., Guan, Y., Azimov, P.Y., Astafiev, B.Y., Palandri, J., Dobrzhinetskaya, L., 2014. Field and microanalytical isotopic investigation of ultradepleted in O-18 Paleoproterozoic "Slushball Earth" rocks from Karelia, Russia. *Geosphere* 10, 308-339.

Black, L.P., Kamo, S.L., Allen, C.M., Davis, D.W., Aleinikoff, J.N., Valley, J.W., Mundil, R., Campbell, I.H., Korsch, R.J., Williams, I.S., Foudoulis, C., 2004. Improved $^{206}$Pb/$^{238}$U microprobe geochronology by the monitoring of a trace-element-related matrix effect; SHRIMP, ID-TIMS, ELA-ICP-MS and oxygen isotope documentation for a series of zircon standards. Chemical *Geology* 205, 115-140.

Blake, D.H., 1966. Net-veined complex of Austurhorn intrusion southeastern Iceland. *Journal of Geology* 74, 891-907.

-, 1970. Geology of the Alftafjördur volcano, a Tertiary volcanic centre in South-Eastern Iceland. *Scientia Islandica* 2: 43-63.

Blichert-Toft, J., Chauvel, C., Albarède, F., 1997. Separation of Hf and Lu for high-precision isotope analysis of rock samples by magnetic sector-multiple collector ICP-MS. *Contributions to Mineralogy and Petrology* 127: 248-260.

Blundy, J., Wood, B., 1994. Prediction of crystal-melt partition-coefficients from elastic-moduli. *Nature* 372, 452-454.

-, 2003. Partitioning of trace elements between crystals and melts. *Earth and Planetary Science Letters* 210, 383-397.

Blundy, J.D., Robinson, J.A.C., Wood, B.J., 1998. Heavy REE are compatible in clinopyroxene on the spinel lherzolite solidus. *Earth and Planetary Science Letters* 160, 493-504.

Boehnke, P., Watson, E.B., Trail, D., Harrison, T.M., Schmitt, A.K., 2013. Zircon saturation re-visited. *Chemical Geology* 351: 324-334.

Bouvier, A., Vervoort, J.D., Patchett, P.J., 2008. The Lu–Hf and Sm–Nd isotopic composition of CHUR: Constraints from unequilibrated chondrites and implications for the bulk composition of terrestrial planets. *Earth and Planetary Science Letters* 273: 48-57.

Bryan S.E., Peate I.U., Peate D.W., Self S., Jerram D.A., Mawby M.R., Marsh J.S., Miller J.A., 2010. The largest volcanic eruptions on Earth. *Earth Science Reviews* **102**(3-4): 207-229.

Burchardt, S., Tanner, D., Krumbholz, M., 2011. The Slaufrudalur pluton, southeast Iceland: An example of shallow magma emplacement by coupled cauldron subsidence and magmatic stoping. *Geological Society of America Bulletin* 124(1-2): 213-227.

Cargill, H.K., Hawkes, L, Ledeboer, J.A., 1928. The major intrusions of south-eastern Iceland. *Quarterly Journal of the Geological Society of London* 84: 505-539.

Carley, T.L., Miller, C.F., Wooden, J.L., Bindeman, I.N., Barth, A.P., 2011. Zircon from historic eruptions in Iceland: reconstructing storage and evolution of silicic magmas. *Mineralogy and Petrology* 102, 135-161.

Carley, T.L., Miller, C.F., Wooden, J.L., Padilla, A.J., Schmitt, A.K., Economos, R.C., Bindeman, I.N., Jordan, B.T., 2014. Iceland is not a magmatic analog for the Hadean: Evidence from the zircon record. *Earth and Planetary Science Letters* 405, 85-97.

Carmody, R.W., 1991. The Slaufrudalur Stock of Southeast Iceland: Geology, Geochemistry and Petrogenesis [Ph.D. thesis, unpub.]: Johns Hopkins University, Baltimore, 392 p.

Cavosie, A.J., Valley, J.W., Wilde, S.A., Edinburgh Ion Microprobe, F., 2006. Correlated microanalysis of zircon: Trace element, $\delta^{18}O$, and U-Th-Pb isotopic constraints on the igneous origin of complex > 3900 Ma detrital grains. *Geochimica Et Cosmochimica Acta* 70, 5601-5616.

Charreteur, G., Tegner, C., Haase, K., 2013. Multiple ways of producing intermediate and silicic rocks within Thingmúli and other Icelandic volcanoes. *Contributions to Mineralogy and Petrology* 166, 471-490.

Cherniak, D.J., Hanchar, J.M., Watson, E.B., 1997a. Diffusion of tetravalent cations in zircon. *Contributions to Mineralogy and Petrology* 127: 383-390.

-, 1997b. Rare-earth diffusion in zircon. *Chemical Geology* 134: 289-301.

Cherniak, D.J., and Watson, E.B., 2000. Pb diffusion in zircon. *Chemical Geology* 172: 5-24.

-, 2003. Diffusion in zircon. In: Hanchar, J.M., Hoskin, P.W.O. (Eds.), *Zircon*. Reviews in Mineralogy and Geochemistry, vol. 53. Mineralogical Society of America, Washington DC, pp. 113–143.

-, 2007. Ti diffusion in zircon. *Chemical Geology* 242: 470-483.

Claiborne, L.L., Miller, C.F., Walker, B.A., Wooden, J.L., Mazdab, F.K., Bea, F., 2006. Tracking magmatic processes through Zr/Hf ratios in rocks and Hf and Ti zoning in zircons: An example from the Spirit Mountain batholith, Nevada. *Mineralogical Magazine* 70, 517-543.

Claiborne, L.L., Miller, C.F., Flanagan, D.M., Clynne, M.A., Wooden, J.L., 2010a. Zircon reveals protracted magma storage and recycling beneath Mount St. Helens. *Geology* 38(**11**): 1011–1014.

Claiborne, L.L., Miller, C.F., Wooden, J.L., 2010b. Trace element composition of igneous zircon: a thermal and compositional record of the accumulation and evolution of a large silicic batholith, Spirit Mountain, Nevada. *Contributions to Mineralogy and Petrology* 160: 511–531.

Coleman, D.S., Gray, W., Glazner, A.F., 2004. Rethinking the emplacement and evolution of zoned plutons: geochronologic evidence for incremental assembly of the Tuolumne intrusive suite, California. *Geology* 32(**5**): 433–436.

Colombini, L.L., Miller, C.F., Gualda, G.A.R., Wooden, J.L., Miller, J.S., 2011. Sphene and zircon in the Highland Range volcanic sequence (Miocene, southern Nevada, USA): elemental partitioning, phase relations, and influence on evolution of silicic magma. *Mineralogy and Petrology* 102, 29-50.

Corfu, F., Hanchar, J.M., Hoskin, P.W.O., Kinny, P., 2003. Atlas of zircon textures. In: Hanchar, J.M., Hoskin, P.W.O. (Eds.), *Zircon*. Reviews in Mineralogy and Geochemistry, vol. 53. Mineralogical Society of America, Washington DC, pp. 469-500.

Dall'Agnol, R., Ramo, O.T., de Magalhaes, M.S., Macambira, M.J.B., 1999. Petrology of the anorogenic, oxidised Jamon and Musa granites, Amazonian Craton: implications for the genesis of Proterozoic A-type granites. *Lithos* 46, 431-462.

Darling, J., Storey, C., Hawkesworth, C., 2009. Impact melt sheet zircons and their implications for the Hadean crust. *Geology* 37(**10**): 927-930.

Deering, C.D., Bachmann, O., 2010. Trace element indicators of crystal accumulation in silicic igneous rocks. *Earth and Planetary Science Letters* 297, 324-331.

Drew, D.L., Bindeman, I.N., Watts, K.E., Schmitt, A.K., Fu, B., McCurry, M., 2013. Crustal-scale recycling in caldera complexes and rift zones along the Yellowstone hotspot track: O and Hf isotopic evidence in diverse zircons from voluminous rhyolites of the Picabo volcanic field, Idaho. *Earth and Planetary Science Letters* 381, 63-77.

Duffield, W.A., Bacon, C.R., Delaney, P.T., 1986. Deformation of poorly consolidated sediment during shallow emplacement of basaltic sill, Coso Range, California. *Bulletin of Volcanology* 48: 97-107.

Eiler, J.M., Gronvold, K., Kitchen, N., 2000. Oxygen isotope evidence for the origin of chemical variations in lavas from Theistareykir volcano in Iceland's northern volcanic zone. *Earth and Planetary Science Letters* 184, 269-286.

Elders, W.A., Frioleifsson, G.O., Zierenberg, R.A., Pope, E.C., Mortensen, A.K., Guomundsson, A., Lowenstern, J.B., Marks, N.E., Owens, L., Bird, D.K., Reed, M., Olsen, N.J., Schiffman, P., 2011. Origin of a rhyolite that intruded a geothermal well while drilling at the Krafla volcano, Iceland. *Geology* 39, 231-234.

Elhlou, S., Belousova, E., Griffin, W.L., Pearson, N.J., O'Reilly, S.Y., 2006. Trace element and isotopic composition of GJ red zircon standard by laser ablation. *Geochimica et Cosmochimica Acta* 70(18) Supplement (Abstract)

Ewart, A., Griffin, W.L., 1994. Application of proton-microprobe data to trace-element partitioning in volcanic-rocks. *Chemical Geology* 117, 251-284.

Ferry, J.M., Watson, E.B., 2007. New thermodynamic models and revised calibrations for the Ti-in-zircon and Zr-in-rutile thermometers. *Contributions to Mineralogy and Petrology* 154: 429–437.

Fisher, C.M., Hanchar, J.M., Samson, S.D., Dhuime, B., Blichert-Toft, J., Vervoort, J.D., Lam, R., 2011. Synthetic zircon doped with hafnium and rare earth elements: A reference material for in situ hafnium isotope analysis. *Chemical Geology* 286, 32-47.

Fisher, C.M., Vervoort, J.D., Hanchar, J.M., 2014. Guidelines for reporting zircon Hf isotopic data by LA-MC-ICPMS and potential pitfalls in the interpretation of these data. *Chemical Geology* 363, 125-133.

Flinter, B.H., 1959. The magnetic separation of some alluvial minerals in Malaya. *The American Mineralogist* 44(**7-8**): 738-751.

Fohey-Breting, N., Barth, A., Wooden, J., Mazdab, F., Carter, C., Schermer, E., 2010. Relationship of voluminous ignimbrites to continental arc plutons: Petrology of Jurassic ignimbrites and contemporaneous plutons in southern California. *Journal of Volcanology and Geothermal Research* 189: 1–11.

Frost, T.J. Mahood, G.A., 1987. Field, chemical, and physical constraints on mafic-felsic magma interaction in the Lamarck Granodiorite, Sierra Nevada, California. *Geological Society of America Bulletin* 99: 272-291.

Fu, B., Page, F.Z., Cavosie, A.J., Fournelle, J., Kita, N.T., Lackey, J.S., Wilde, S.A., Valley, J.W., 2008. Ti-in-zircon thermometry: applications and limitations. *Contributions to Mineralogy and Petrology* 156: 197-215.

Furman, T., Meyer, P.S., Frey, F.A., 1992a. Evolution of Icelandic central volcanoes: evidence from the Austurhorn intrusion, southeastern Iceland. *Bulletin of Volcanology* 55: 45-62.

Furman, T., Frey, F.A., Meyer, P.S., 1992b. Petrogenesis of evolved basalts and rhyolites at Austurhorn, southeastern Iceland: the role of fractional crystallization. *Journal of Petrology* 33: 1405-1445.

Gaetani, G.A., Grove, T.L., 1995. Partitioning of rare-earth elements between clinopyroxene and silicate melt - crystal-chemical controls. *Geochimica Et Cosmochimica Acta* 59, 1951-1962.

Gale, N.H., Moorbath, S., Simons, J., Walker, G.P.L., 1966. K-Ar ages of acid intrusive rocks from Iceland. *Earth and Planetary Science Letters* 1: 284-288.

Genske, F.S., Beier, C., Haase, K.M., Turner, S.P., Krumm, S., Brandl, P.A., 2013. Oxygen isotopes in the Azores islands: Crustal assimilation recorded in olivine. *Geology* 41, 491-494.

Ghiorso, M.S., Gualda, G.A.R., 2013. A method for estimating the activity of titania in magmatic liquids from the compositions of coexisting rhombohedral and cubic iron–titanium oxides. *Contributions to Mineralogy and Petrology* 165: 73-81.

Glazner, A.F., Bartley, J.M., Coleman, D.S., Gray, W., Taylor, R.Z., 2004. Are plutons assembled over millions of years by amalgamation from small magma chambers? *GSA Today* 14: 4–11.

Glazner, A.F., Coleman, D.S., Bartley, J.M., 2008. The tenuous connection between high-silica rhyolites and granodiorite plutons. *Geology* 36, 183-186.

Griffin, W.L., Powell, W.J., Pearson, N.J., O'Reilly, S.Y., 2008. Appendix A2; GLITTER; data reduction software for laser ablation ICP-MS. Short Course Series - Mineralogical Association of Canada, 40, 308-311.

Grimes, C.B., John, B.E., Kelemen, P.B., Mazdab, F.K., Wooden, J.L., Cheadle, M.J., Hanghøj, K., Schwartz, J.J., 2007. Trace element chemistry of zircons from oceanic crust: A method for distinguishing detrital zircon provenance. *Geology* 35, 643-646.

Gualda, G.A.R., Cook, D.L., Chopra, R., Qin, L.P., Anderson, A.T., Rivers, M., 2004. Fragmentation, nucleation and migration of crystals and bubbles in the Bishop Tuff rhyolitic magma. *Transactions of the Royal Society of Edinburgh-Earth Sciences* 95, 375-390.

Gualda, G.A.R., Pamukcu, A.S., Claiborne, L.L., Rivers, M.L., 2010. Quantitative 3D petrography using X-ray tomography 3: Documenting accessory phases with differential absorption tomography. *Geosphere* 6, 782-792.

Gunnarsson, B., Marsh, B.D., Taylor, H.P., 1998. Generation of Icelandic rhyolites: silicic lavas from the Torfajokull central volcano. *Journal of Volcanology and Geothermal Research* 83, 1-45.

Gurenko, A.A., Bindeman, I.N., Sigurdsson, I.A., 2015. To the origin of Icelandic rhyolites: insights from partially melted leucocratic xenoliths. *Contributions to Mineralogy and Petrology* 169: 49.

Guppy, E.M., Hawkes, L., 1925. A composite dyke from Eastern Iceland. *Quarterly Journal of the Geological Society* 81: 325-340.

Halliday, A.N., Davidson, J.P., Hildreth, W., Holden, P., 1991. Modeling the petrogenesis of high Rb/Sr silicic magmas. *Chemical Geology* 92, 107-114.

Hanchar, J.M., Miller, C.F., 1993. Zircon zonation patterns as revealed by cathodoluminescence and backscattered electron images - implications for interpretation of complex crustal histories. *Chemical Geology* 110, 1-13.

Harper, B.E., Miller, C.F., Koteas, G.C., Cates, N.L., Wiebe, R.A., Lazzareschi, D.S., Cribb, J.W., 2004. Granites, dynamic magma chamber processes and pluton construction: the Aztec Wash pluton, Eldorado Mountains, Nevada, USA. *Transactions of the Royal Society of Edinburgh: Earth Sciences* 95: 277–295.

Hattori, K., Muehlenbachs, K., 1982. Oxygen isotope ratios of the Icelandic crust. *Journal of Geophysical Research* 87, 6559-6565.

Hawkes, L., Hawkes, L.K., 1932. The Sandfell laccolith and 'Dome of Elevation'. *Quarterly Journal of the Geologic Society* 89: 379-400.

Hawkesworth, C.J. Kemp, A.I.S., 2006. Evolution of the continental crust. *Nature* (Reviews) 443: 811-817.

Hayden, L.A., Watson, E.B., Wark, D.A., 2008. A thermobarometer for sphene (titanite). *Contributions to Mineralogy and Petrology* 155: 529-540.

Hollis, J.A., Van Kranendonk, M.J., Cross, A.J., Kirkland, C.L., Armstrong, R.A., Allen, C.M., 2014. Low delta O-18 zircon grains in the Neoarchean Rum Jungle Complex, northern Australia: An indicator of emergent continental crust. *Lithosphere* 6, 17-25.

Hoskin, P.W.O., Ireland, T.R., 2000. Rare earth element chemstry of zircon and its use as a provenance indicator. *Geology* 28(**7**): 627-630.

-, 2004. Trace-element composition of hydrothermal zircon and the alteration of Hadean zircon from the Jack Hills, Australia. *Geochimica et Cosmochimica Acta* 69(**3**): 637-648.

Hoskin, P.W.O., Schaltegger, U., 2003. The composition of zircon and igneous and metamorphic petrogenesis. In: Hanchar, J.M., Hoskin, P.W.O. (Eds.), *Zircon*. Reviews in Mineralogy and Geochemistry, vol. 53. Mineralogical Society of America, Washington DC, pp. 27–62.

Jónasson, K., 2007. Silicic volcanism in Iceland: Composition and distribution within the active volcanic zones. *Journal of Geodynamics* 43, 101-117.

Kemp, A.I.S., Hawkesworth, C.J., Foster, G.L., Paterson, B.A., Woodhead, J.D., Hergt, J.M., Gray, C.M., Whitehouse, M.J., 2007. Magmatic and crustal differentiation history of granitic rocks from Hf-O isotopes in zircon. *Science* 315(**5814**): 980-983.

Kinney, P.D., Maas, R., 2003. *Lu-Hf and Sm-Nd isotope systems in zircon*. In: Hanchar, J.M., Hoskin, P.W.O. (Eds.), *Zircon*. Reviews in Mineralogy and Geochemistry, vol. 53. Mineralogical Society of America, Washington DC, pp. 327–385.

Kurosawa, M., Jackson, S.E., Sueno, S., 2002. Trace element analysis of NIST SRM 614 and 616 glass reference materials by laser ablation microprobe-inductively coupled plasma-mass spectrometry. *Geostandards Newsletter-the Journal of Geostandards and Geoanalysis* 26, 75-84.

Leeman, W.P., Phelps, D.W., 1981. Partitioning of rare-earths and other trace-elements between sanidine and coexisting volcanic glass. *Journal of Geophysical Research* 86, 193-199.

Lipman, P.W., 2007. Incremental assembly and prolonged consolidation of Cordilleran magma chambers: Evidence from the Southern Rocky Mountain volcanic field. *Geosphere* 3(**1**): 42-70.

Loomis, T.P., Welber, P.W., 1982. Crystallization processes in the Rocky Hill granodiorite pluton, California: an interpretation based on compositional zoning of plagioclase. *Contributions to Mineralogy and Petrology* 81: 230–239.

Ludwig, K.R., 2008. Unpublished - SQUID 2 data reduction program. Berkeley Geochronology Center: http://www.bgc.org/isoplot_etc/squid.html.

Luhr, J.F., Carmichael, I.S.E., 1980. Colima Volcanic Complex, Mexico .1. Post-caldera andesites from Volcan Colima. *Contributions to Mineralogy and Petrology* 71, 343-372.

Maclennan, J., McKenzie, D., Grönvold, K., Shimizu, N., Eiler, J.M., Kitchen, N., 2003. Melt mixing and crystallization under Theistareykir, northeast Iceland. *Geochemistry Geophysics Geosystems* 4, 40.

Mahon, K.I., 1996. The New "York" Regression: Application of an Improved Statistical Method to Geochemistry. *International Geology Review* 38: 293-303.

Mahood, G., Hildreth, W., 1983. Large partition-coefficients for trace-elements in high-silica rhyolites. *Geochimica Et Cosmochimica Acta* 47, 11-30.

Marsh, B.D., Gunnarsson, B., Congdon, R., Carmody, R., 1991. Hawaiian basalt and Icelandic rhyolite: indicators of differentiation and partial melting. *Geologische Rundschau* 80, 481-510.

Marsh, B.D., 2006. Dynamics of magmatic systems. *Elements* 2: 287-292.

Marshall, L.A., Sparks, R.S.J., 1984. Origin of some mixed magma net-veined ring intrusions. *Journal of the Geological Society of London* 141: 171-182.

Martin, E., Sigmarsson, O., 2005. Trondhjemitic and granitic melts formed by fractional crystallization of an olivine tholeiite from Reykjanes Peninsula, Iceland. *Geological Magazine* 142, 651-658.

-, 2007. Crustal thermal state and origin of silicic magma in Iceland: the case of Torfajökull, Ljósufjöll and Snaefellsjökull volcanoes. *Contributions to Mineralogy and Petrology* 153, 593-605.

-, 2010. Thirteen million years of silicic magma production in Iceland: Links between petrogenesis and tectonic settings. *Lithos* 116, 129-144.

Martin, E., Paquette, J.L., Bosse, V., Ruffet, G., Tiepolo, M., Sigmarsson, O., 2011. Geodynamics of rift-plume interaction in Iceland as constrained by new $^{40}Ar/^{39}Ar$ and in situ U-Pb zircon ages. *Earth and Planetary Science Letters* 311, 28-38.

Mattson, S.R., Vogel, T.A., Wilband, J.T., 1986. Petrochemistry of the silicic-mafic complexes at Vesturhorn and Austurhorn, Iceland: evidence for zoned stratified magma. *Journal of Volcanology and Geothermal Research* 28, 197-223.

Mazdab, F.K., Wooden, J.L., 2006. Trace element analysis in zircon by ion microprobe (SHRIMP-RG): Technique and applications. *Geochimica et Cosmochimica Acta* 70(18): A405-A405.

McDowell, S.M., Miller, C.F., Mundil, R., Ferguson, C.A., Wooden, J.L., 2014. Zircon evidence for a ~200 k.y. supereruption-related thermal flare-up in the Miocene southern Black Mountains, western Arizona, USA. *Contributions to Mineralogy and Petrology* 168: 1031.

Michael, P.J., 1983. Chemical differentiation of the Bishop Tuff and other high-silica magmas through crystallization processes. *Geology* 11, 31-34.

-, 1988. Partition coefficients for rare-Earth elements in mafic minerals of high silica rhyolites - the importance of accessory mineral inclusions. *Geochimica Et Cosmochimica Acta* 52, 275-282.

Miller, C.F., Mittlefehldt, D.W., 1984. Extreme fractionation in felsic magma chambers - a product of liquid-state diffusion or fractional crystallization? *Earth and Planetary Science Letters* 68, 151-158.

Miller, C.F., Wark, D.A., 2008. Supervolcanoes and their explosive supereruptions. *Elements* 4: 11-16.

Moorbath, S., Sigurdsson, H., Goodwin, R., 1968. K-Ar ages of the oldest exposed rocks in Iceland. *Earth and Planetary Science Letters* 4: 197-205.

Morel, M.L.A., Nebel, O., Nebel-Jacobsen, Y.J., Miller, J.S., Vroon, P.Z., 2008. Hafnium isotope characterization of the GJ-1 zircon reference material by solution and laser-ablation MC-ICPMS. *Chemical Geology* 255: 231-235.

Muehlenbachs, K., Anderson, A.T., Sigvaldason, G.E., 1974. Low-$O^{18}$ basalts from Iceland. *Geochimica Et Cosmochimica Acta* 38(4), 577-588.

Nagasawa, H., 1970. Rare earth concentrations in zircons and apatites and their host dacites and granites. *Earth and Planetary Science Letters* 9, 359-&.

Nash, W.P., Crecraft, H.R., 1985. Partition coefficients for trace-elements in silicic magmas. *Geochimica Et Cosmochimica Acta* 49, 2309-2322.

Onuma, N., Higuchi, H., Wakita, H., Nagasawa, H., 1968. Trace element partition between 2 pyroxenes and host lava. *Earth and Planetary Science Letters* 5, 47-&.

Padilla, A.J., Miller, C.F., Bindeman, I.N., Economos, R.C., Carley, T.L., Banik, T.J., Schmitt, A.K., 2014. Generating the world's lowest magmatic zircon $\delta^{18}O$: Melting of intensely hydrothermally altered sources at Austurhorn Intrusive Complex, SE Iceland. *Geological Society of America Abstracts with Programs* Vol. 46, No. 6, p.199 (Abstract)

Padilla, A.J., Miller, C.F., Carley, T.L., Economos, R.C., Schmitt, A.K., Coble, M.A., Wooden, J.L., Fisher, C.M., Hanchar, J.M., (*in review*). Elucidating the magmatic history of the Austurhorn Silicic Intrusive Complex (SE Iceland) using zircon elemental and isotopic geochemistry and geochronology. *Submitted to Contributions to Mineralogy and Petrology*.

Pamukcu, A.S., Gualda, G.A.R., Anderson, A.T., 2012. Crystallization stages of the Bishop Tuff magma body recorded in crystal textures in pumice clasts. *Journal of Petrology* 53(**3**): 589-609.

Pamukcu, A.S., Carley, T.L., Gualda, G.A.R., Miller, C.F., Ferguson, C.A., 2013. The Evolution of the Peach Spring Giant Magma Body: Evidence from Accessory Mineral Textures and Compositions, Bulk Pumice and Glass Geochemistry, and Rhyolite-MELTS Modeling. *Journal of Petrology* 54, 1109-1148.

Pamukcu, A.S., Gualda, G.A.R., Ghiorso, M.S., Miller, C.F., McCracken, R.G., 2015. Phase-equilibrium geobarometers for silicic rocks based on rhyolite-MELTS-Part 3: Application to the Peach Spring Tuff (Arizona-California-Nevada, USA). *Contributions to Mineralogy and Petrology* 169, 17.

Patchett, P.J., Tatsumoto, M., 1980. A routine high-precision method for Lu-Hf isotope geochemistry and chronology. *Contributions to Mineralogy and Petrology* 75: 263-267.

Pearce, N.J.G., Perkins, W.T., Westgate, J.A., Gorton, M.P., Jackson, S.E., Neal, C.R., Chenery, S.P., 1997. A compilation of new and published major and trace element data for NIST SRM 610 and NIST SRM 612 glass reference materials. *Geostandards Newsletter-the Journal of Geostandards and Geoanalysis* 21, 115-144.

Peate, D.W., Breddam, K., Barker, J.A., Kurz, M.D., Barker, A.K., Prestvik, T., Grassineau, N., Skovgaard, A.C., 2010. Compositional characteristics and spatial distribution of enriched Icelandic mantle components. *Journal of Petrology* 51(**7**): 1447-1475.

Pope, E.C., Bird, D.K., Arnorsson, S., 2013. Evolution of low-O-18 Icelandic crust. *Earth and Planetary Science Letters* 374, 47-59.

Prowatke, S., Klemme, S., 2006. Rare earth element partitioning between titanite and silicate melts: Henry's law revisited. *Geochimica Et Cosmochimica Acta* 70, 4997-5012.

Rampino, M.R., Ambrose, S.H., 2000. Volcanic winter in the Garden of Eden: the Toba supereruption and the late Pleistocene human population crash. *Geological Society of America Special Papers* 345: 71-82.

Reimink, J.R., Chacko, T., Stern, R.A., Heaman, L.M., 2014. Earth's earliest evolved crust generated in an Iceland-like setting. *Nature Geoscience* 7, 529-533.

Robinson, D.M., Miller, C.F., 1999. Record of magma chamber processes preserved in accessory mineral assemblages, Aztec Wash pluton, Nevada. *American Mineralogist* 84: 1346-1353.

Robock, A., 2002. The climatic aftermath. *Science* 295: 1242-1244.

Roobol, M.J., 1974. The geology of the Vesturhorn Intrusion, SE Iceland. *Geological Magazine* 111(4): 273-368.

Rosenblum, S., 1958. Magnetic susceptibilities of minerals in the Frantz isodynamic magnetic separator. *The American Mineralogist* 43(1-2): 170-173.

Ross, J.G., Mussett, A.E., 1976. $^{40}$Ar/$^{39}$Ar dates for spreading rates in eastern Iceland. *Nature* 259(5538): 36-38.

Ruprecht, P., Bachmann, O., 2010. Pre-eruptive reheating during magma mixing at Quizapu volcano and the implications for the explosiveness of silicic arc volcanoes. *Geology* 38(10): 919-922.

Rudnick, R.L., 1995. Making continental crust. *Nature* (Reviews) 378:571-578.

Sano, Y., Terada, K., Fukuoka, T., 2002. High mass resolution ion microprobe analysis of rare earth elements in silicate glass, apatite and zircon: lack of matrix dependency. *Chemical Geology* 184, 217-230.

Schattel, N., Portnyagin, M., Golowin, R., Hoernle, K., Bindeman, I., 2014. Contrasting conditions of rift and off-rift silicic magma origin on Iceland. *Geophysical Research Letters* 41, 5813-5820.

Schnetzler, C.C., Philpotts, J.A., 1970. Partition coefficients of rare-earth elements between igneous matrix material and rock-forming mineral phenocrysts-2. *Geochimica Et Cosmochimica Acta* 34, 331.

Severs, M.J., Beard, J.S., Fedele, L., Hanchar, J.M., Mutchler, S.R., Bodnar, R.J., 2009. Partitioning behavior of trace elements between dacitic melt and plagioclase, orthopyroxene, and clinopyroxene based on laser ablation ICPMS analysis of silicate melt inclusions. *Geochimica Et Cosmochimica Acta* 73, 2123-2141.

Shane, P., Smith, V.C., Nairn, I., 2008. Millenial timescale resolution of rhyolite magma recharge at Tarawera volcano: insights from quartz chemistry and melt inclusions. *Contributions to Mineralogy and Petrology* 156: 397-411.

Shannon, R.D., 1976. Revised Effective Ionic Radii and Systematic Studies of Interatomic Distances in Halides and Chalcogenides. *Acta Crystallographica* (1976), A32, 751-767.

Sigmarsson, O., Hémond, C., Condomines, M., Fourcade, S., Oskarsson, N., 1991. Origin of silicic magma in Iceland revealed by Th isotopes. *Geology* 19, 621-624.

Sigmarsson, O., Steinthórsson, S., 2007. Origin of Icelandic basalts: A review of their petrology and geochemistry. *Journal of Geodynamics* 43, 87-100.

Sisson, T.W., 1994. Hornblende-melt trace-element partitioning measured by ion microprobe. *Chemical Geology* 117, 331-344.

Sparks, S.R.J., Sigurdsson, H., Wilson, L., 1977. Magma mixing: a mechanism for triggering acid explosive eruptions. *Nature* 267: 315-318.

Stix, J., Gorton, M.P., 1990. Variations in trace element partition coefficients in sanidine in the Cerro Toledo rhyolite, Jemez Mountains, New Mexico: effects of composition, temperature, and volatiles. *Geochimica Et Cosmochimica Acta* 54, 2697-2708.

Streck, M.J., 2002. Partial melting to produce high-silica rhyolites of a young bimodal suite: compositional constraints among rhyolites, basalts, and metamorphic xenoliths from the Harney Basin, Oregon. *International Journal of Earth Sciences* 91, 583-593.

Streck, M.J., Grunder, A.L., 1997. Compositional gradients and gaps in high-silica rhyolites of the Rattlesnake Tuff, Oregon. *Journal of Petrology* 38, 133-163.

Thirlwall, M.F., Gee, M.A.M., Lowry, D., Mattey, D.P., Murton, B.J., Taylor, R.N., 2006. Low $\delta^{18}O$ in the Icelandic mantle and its origins: Evidence from Reyjanes Ridge and Icelandic lavas. *Geochimica Et Cosmochimica Acta* 70, 993-1019.

Thorarinsson, S.B., Tegner, C., 2009. Magma chamber processes in central volcanic systems of Iceland: constraints from layered gabbro of the Austurhorn intrusive complex. *Contributions to Mineralogy and Petrology* 158: 223-244.

Thordarson, T., Self, S., 2003. Atmospheric and environmental effects of the 1783–1784 Laki eruption: A review and reassessment. *Journal of Geophysical Research* 108(**D1**): 411.

Thordarson, T., Larsen, G., 2007. Volcanism in Iceland in historical time: Volcano types, eruption styles and eruptive history. *Journal of Geodynamics* 43, 118-152.

Trail, D., Mojzsis, S.J., Harrison, T.M., Schmitt, A.K., Watson, E.B., Young, E.D., 2007. Constraints on Hadean zircon protoliths from oxygen isotopes, Ti-thermometry, and rare earth elements. *Geochemistry Geophysics Geosystems* 8, 22.

Trail, D., Watson, E.B., Tailby, N.D., 2011. The oxidation state of Hadean magmas and implications for early Earth's atmosphere. *Nature* 480, 79-U238.

-, 2012. Ce and Eu anomalies in zircon as proxies for the oxidation state of magmas. *Geochimica Et Cosmochimica Acta* 97, 70-87.

Trail, D., Tailby, N.D., Lanzirotti, A., Newville, M., Thomas, J.B., Watson, E.B., 2015. Redox evolution of silicic magmas: Insights from XANES measurements of Ce valence in Bishop Tuff zircons. *Chemical Geology* 402, 77-88.

Troll, V.R., Sachs, P.M., Schmincke, H.U., Sumita, M., 2003. The REE-Ti mineral chevkinite in comenditic magmas from Gran Canaria, Spain: a SYXRF-probe study. *Contributions to Mineralogy and Petrology* 145, 730-741.

Upton, B.G.J., Wright, J.B., 1961. Intrusions of Gabbro and Graonphyre in the Snaefellsness, Western Iceland. *Geological magazine* vol. XCVIII (**6**): 488-492.

Valley, J.W., Kinny, P.D., Schulze, D.J., Spicuzza, M.J., 1998. Zircon megacrysts from kimberlite: oxygen isotope variability among mantle melts. *Contributions to Mineralogy and Petrology* 133, 1-11.

Valley, J.W., 2003. Oxygen isotopes in zircon. In: Hanchar, J.M., Hoskin, P.W.O. (Eds.), *Zircon*. Reviews in Mineralogy and Geochemistry, vol. 53. Mineralogical Society of America, Washington DC, pp. 343-385.

Vernon, R.H., 1984. Microgranitoid enclaves in granites - globules of hybrid magma quenched in a plutonic environment. *Nature* 309(**5967**): 438-439.

Walker, B.A. Jr., Miller, C.F., Claiborne, L.L., Wooden, J.L., Miller, J.S., 2007. Geology and geochronology of the Spirit Mountain batholith, southern Nevada: Implications for timescales and physical processes of batholith construction. *Journal of Volcanology and Geothermal Research* 167: 239-262.

Walker, G.P.L., 1960. Zeolite zones and dike distribution in relation to the structure of the basalts of eastern Iceland. *Journal of Geology* 68: 515-527.

-, 1963. The Breiddalur central volcano, eastern Iceland. *Quaternary Journal of the Geological Society of London* 119: 29-63.

-, 1964. Geological investigations in eastern Iceland. *Bulletin of Volcanology* 27: 1- 15.

-, 1966. Acid volcanic rocks in Iceland. *Bulletin of Volcanology* 29: 375-402.

Walker, G.P.L., Skelhorn, P.R., 1966. Some associations of acid and basic igneous rocks. *Earth-Science Reviews* 2: 93-109.

Wark, D.A., Miller, C.F., 1993. Accessory mineral behavior during differentiation of a granite suite: monazite, xenotime and zircon in the Sweetwater Wash pluton, Southeastern California, USA. *Chemical Geology* 110, 49-67.

Wark, D.A., Hildreth, W., Spear, F.S., Cherniak, D.J., Watson, E.B., 2007. Pre-eruption recharge of the Bishop magma system. *Geology* 35(**3**): 235-238.

Watson, E.B., 1976. Two-liquid partition coefficients: experimental data and geochemical implications. *Contributions to Mineralogy and Petrology* 56, 119-134.

-, 1980. Some experimentally determined zircon-liquid partition coefficients for the rare earth elements. *Geochimica Et Cosmochimica Acta* 44, 895-897.

Watson, E.B., Cherniak, D.J., 1997. Oxygen diffusion in zircon. *Earth & Planetary Science Letters* 148(**3-4**): 527-544.

Watson, E.B., Harrison, T.M., 2005. Zircon thermometer reveals minimum melting conditions on earliest Earth. *Science* 308(**5723**): 841-844.

Watson, E.B., Wark, D.A., Thomas, J.B., 2006. Crystallization thermometers for zircon and rutile. *Contributions to Mineralogy and Petrology* 151: 413-433.

Watts, K., Leeman, W., Bindeman, I., Larson, P., 2010. Supereruptions of the Snake River Plain: Two-stage derivation of low-18O rhyolites from normal-18O crust as constrained by Archean xenoliths. *Geology* 38: 503-506.

Wiebe, R.A., Collins, W.J., 1998. Depositional features and stratigraphic sections in granitic plutons: implications for the emplacement and crystallization of granitic magma. *Journal of Structural Geology* 20(**9/10**): 1273-1289.

Wiebe, R.A., Blair, K.D., Hawkins, D.P. Sabine, C.P., 2002. Mafic injections, in situ hybridization, and crystal accumulation in the Pyramid Peak granite, California. *Geological Society of America Bulletin* 114: 909–20.

Wiebe, R.A., Hawkins, D.P., 2004. Multiple replenishments in an evolving silicic magma chamber: the Vinalhaven intrusive complex, Maine, USA. *Geochimica et Cosmochimica Acta* 68(**11S**): A672.

Wiebe, R.A., Manon, M.R., Hawkins, D.P., McDonough, W.F., 2004. Late-stage mafic injection and thermal rejuvenation of the Vinalhaven Granite, Coastal Maine. *Journal of Petrology* 45(**11**): 2133-2153.

Wiebe, R.A., Wark, D.A., Hawkins, D.P., 2007. Insights from quartz cathodoluminescence zoning into crystallization of the Vinalhaven granite, coastal Maine. *Contributions to Mineralogy and Petrology* 154: 439-453.

Wones, D.R., 1989. Significance of the assemblage titanite + magnetite + quartz in granitic rocks. *American Mineralogist* 74, 744-749.

Wood., B.J., Blundy, J.D., 2001. The effect of cation charge on crystal-melt partitioning of trace elements. *Earth & Planetary Science Letters* 188: 59-71.

Woodhead, J.D., Hergt, J.M., 2005. A preliminary appraisal of seven natural zircon reference materials for in situ Hf isotope determination. *Geostandards and Geoanalytical Research* 29(2): 183-195.

Wotzlaw, J.F., Bindeman, I.N., Schaltegger, U., Brooks, C.K., Naslund, H.R., 2012. High-resolution insights into episodes of crystallization, hydrothermal alteration and remelting in the Skaergaard intrusive complex. *Earth and Planetary Science Letters* 355, 199-212.

Zellmer, G.F., Rubin, K.H., Grönvold, K., Jurado-Chichay, Z., 2008. On the recent bimodal magmatic processes and their rates in the Torfajökull-Veidivötn area, Iceland. *Earth and Planetary Science Letters* 269, 387-397.

Zheng, Y.F., 1993. Calculation of oxygen isotope fractionation in anhydrous silicate minerals. *Geochimica Et Cosmochimica Acta* 57, 1079-1091.

Zheng, Y.F., Wu, Y.B., Chen, F.K., Gong, B., Li, L., Zhao, Z.F., 2004. Zircon U-Pb and oxygen isotope evidence for a large-scale O-18 depletion event in igneous rocks during the neoproterozoic. *Geochimica Et Cosmochimica Acta* 68, 4145-4165.